Geophysics

سرفصل ها

- کلیات
- روش گرانی
- روش مغناطیسی
- روش های الکتریکی
- روش های لرزه ای
  - تئوری لرزه انکساری
  - تئوری لرزه بازتابی
  - تفسیر داده های لرزه ای

Remote sensing

Constraining the Earth's sub-surface with observations at the surface

Geophysical techniques measure physical phenomena:

- **Gravity**
- **Magnetism**
- **Elastic waves**
- **Electricity**
- **Electromagnetic waves**

Which are sensitive to sub-surface physical properties:

- **Density**
- **Magnetic susceptibility**
- **Seismic wave velocity and density**
- **Resistivity**
- **Conductance/inductance/permitivity**

Active and passive

Passive

Measure naturally occurring phenomena

- **Gravity field**
- **Magnetic field**
- **Seismic arrivals - earthquakes**

Active

Transmit a signal into the subsurface and record what comes back

- **Seismic arrival – explosions**
- **Electrical current**
- **Electromagnetic waves**

Geophysical methods

Method	**Measured parameter**	**“Operative” physical property**	**Application**
Gravity	Spatial variations in the strength of the gravitational field of the Earth	Density	Fossil fuels Bulk mineral deposits Construction
Magnetic	Spatial variations in the strength of the geomagnetic field	Magnetic susceptibility and remanence	Fossil fuels Metalliferous mineral deposits Construction
Seismic	Travel times of reflected/refracted seismic waves	Seismic velocity (and density)	Fossil fuels Bulk mineral deposits Construction
Electromagnetic (SeaBed Logging)	Response to electromagnetic radiation	Electric conductivity/resistivity and inductance	Fossil fuels Metalliferous mineral deposits
Electrical -Resistivity -Self potential	 Earth resistance Electrical potentials	 Electrical conductivity Electrical conductivity	Widely used
Radar	Travel times of reflected radar pulses	Dielectric constant	Environmental Construction

Planning a survey

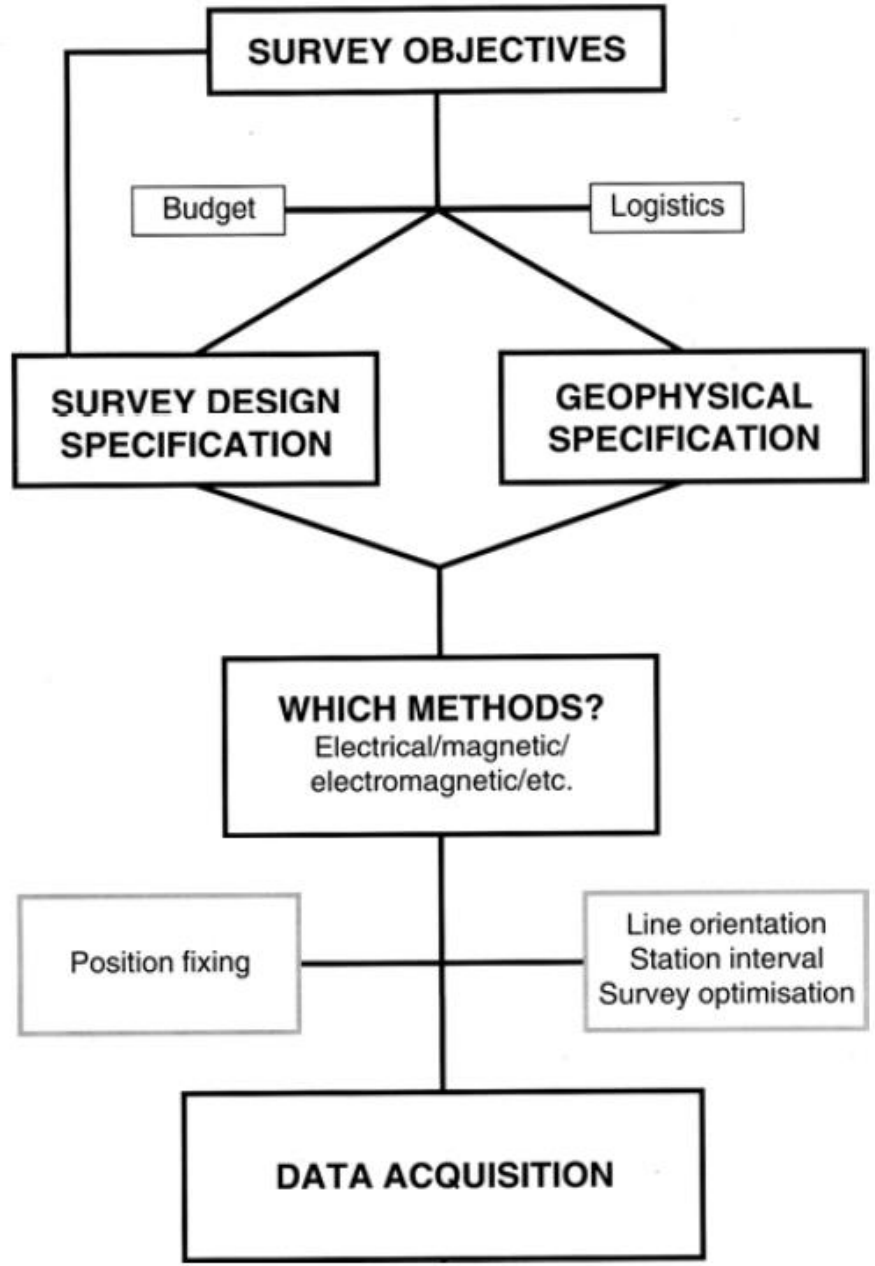

Target identification

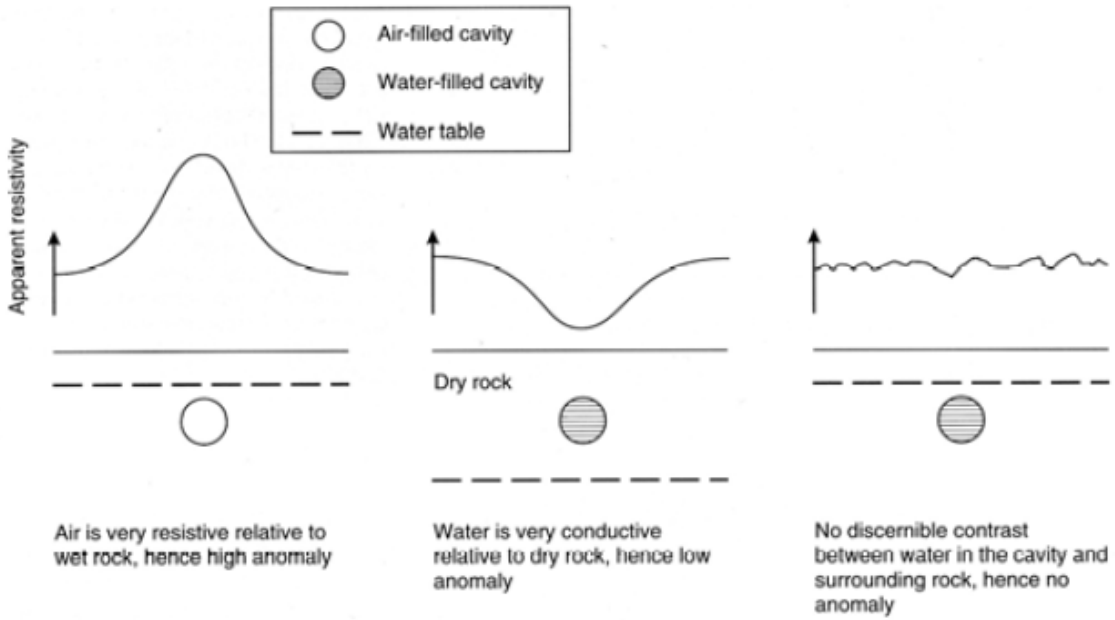

Figure 1.5 Contrasts in physical properties from different geological targets give rise to a geophysical target. When there is no contrast, the target is undetectable geophysically

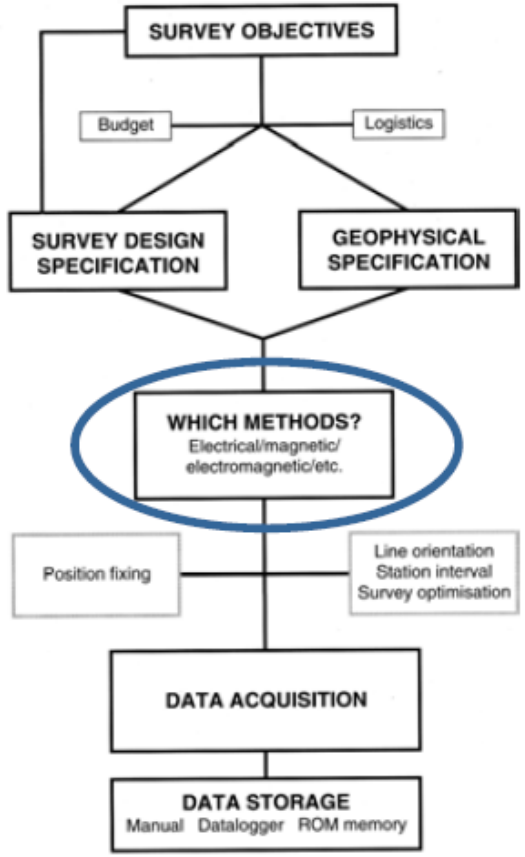

Techniques and targets

Geophysical Method	Dependent physical property	Hydrocarbon exploration (coal, oil, gas)	Regional geologic study (>100s km2)	Exploration/development of mineral deposits	Engineering site investigations	Hydrogeological investigations	Detection of subsurface cavities	Mapping leachate and contamination plumes	Location of buried metallic objects	Archaeogeophysics	Forensic geophysics
Gravity	Density	**P**	**P**	s	s	s	s			s	
Magnetic	Susceptibility	**P**	**P**	**P**	s		m		**P**	**P**	
Seismic refraction	Elastic moduli, density	**P**	**P**	m	**P**	s	s				
Seismic reflection	Elastic moduli, density	**P**	**P**	m	s	s	m				
Resistivity	Resistivity	m	m	**P**	**P**	**P**	**P**	**P**	s	**P**	m
Spontaneous potential	Potential differences			**P**	m	**P**	m	m	m		
Induced polarization	Resistivity, capacitance	m	m	**P**	m	s	m	m	m	m	m
Electromagnetic (EM)	Conductance, inductance	s	**P**	**P**	**P**	**P**	**P**	**P**	**P**	**P**	m
EM - VLF	Conductance, inductance	m	m	**P**	m	s	s	s	m	m	
EM – Ground penetrating radar	Permitivity, conductivity			m	**P**	**P**	**P**	s	**P**	**P**	**P**
Magneto-telluric	Resistivity	s	**P**	**P**	m	m					

P – primary method; s – secondary; m – maybe sometimes

Profiling vs. mapping

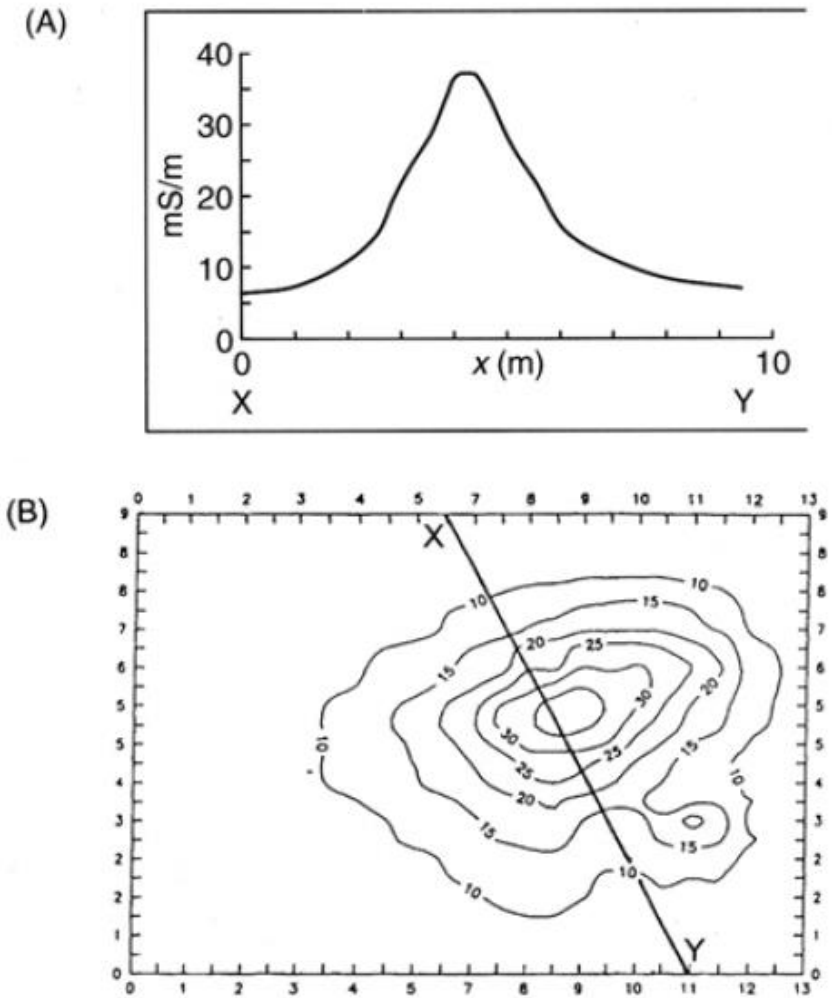

What is the nature of the target?

- **2D or 3D?**
- **Preliminary site evaluation necessary?**

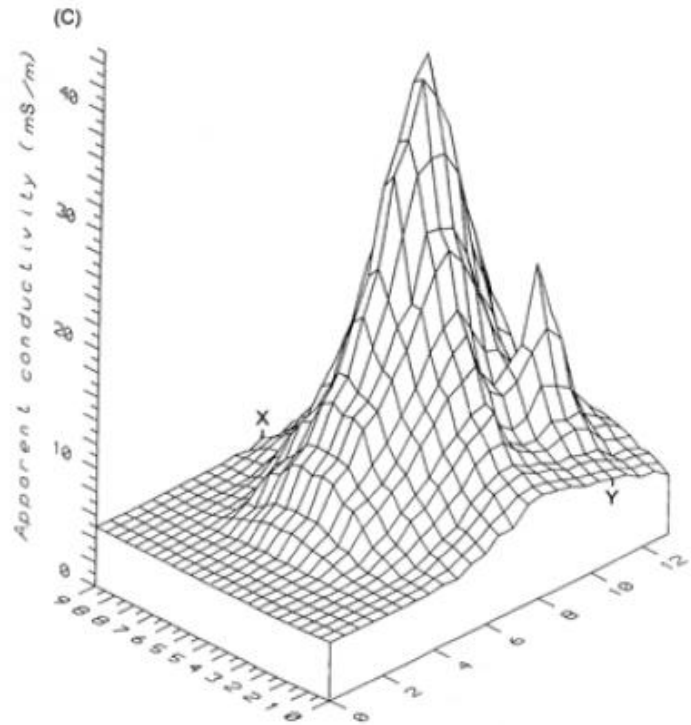

Station spacing

Must ensure that spacing is sufficient to sample anticipated signal

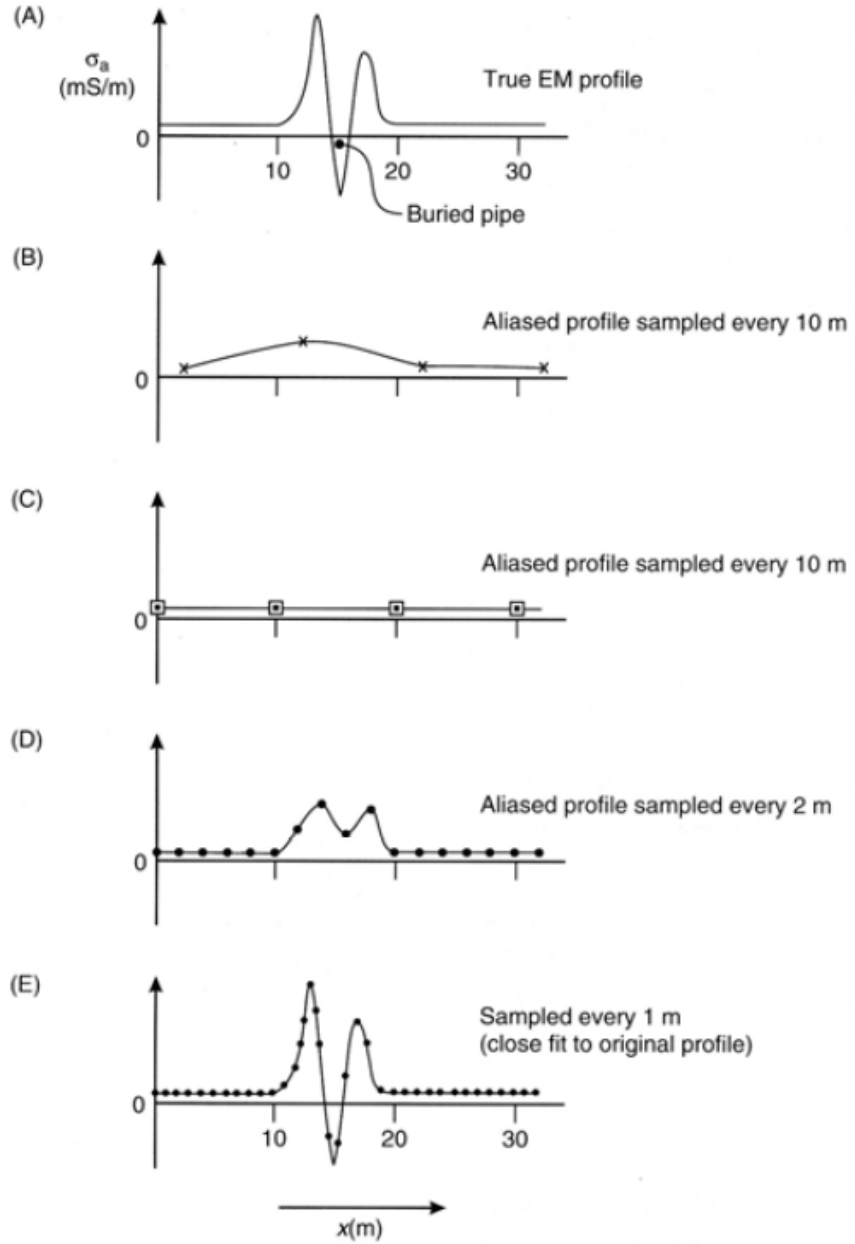

Multiple methods

...to improve uniqueness and cross-check interpretations

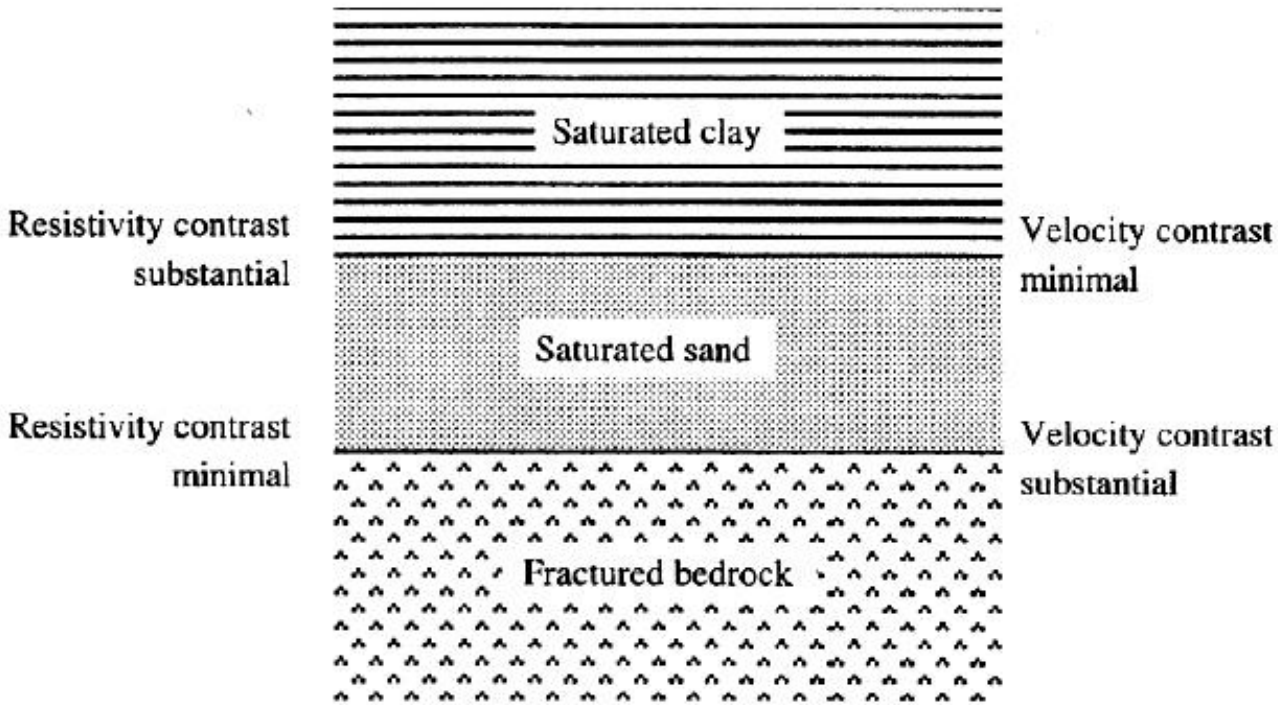

Figure 1-1 Determining the thickness of a confined aquifer by using both seismic refraction and electrical resistivity.

Gravity

- Gravity surveying measures spatial variations in the Earth's gravitational field caused by differences in the *density* of sub-surface rocks
- In fact, it measures the variation in the *accelaration* due to gravity
- It is expressed in so called *gravity anomalies* (in milligal, 10^{-5} ms^{-2}), measured in respect to a reference level, usually the *geoid*
- Gravity is a scalar

Gravity: Newton's Law of Gravitation

- Newton's Universal Law of Gravitation for small masses, m_1 and m_2 separated by a distance r, at the earth surface:

$$\textbf{Attractive force, } F = G\frac{m_1 m_2}{r^2}$$

- With G ('big gee') is the Universal Gravitational Constant: 6.67x10-11 $m^3/kg^1 \cdot s^2$

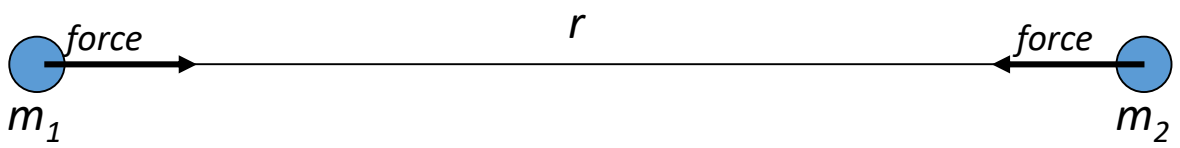

Gravity: Earth

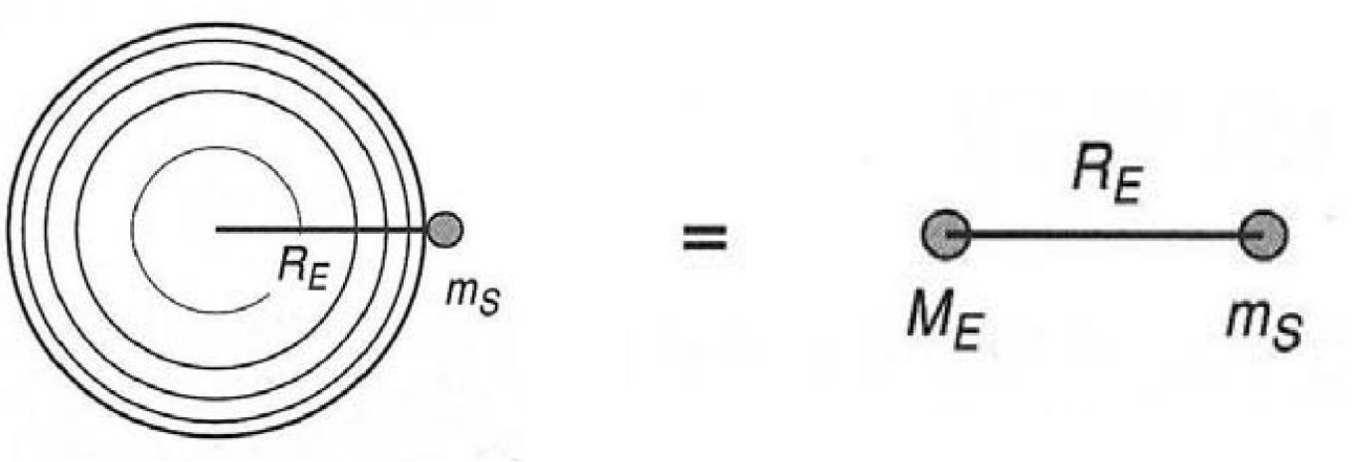

$$F_E = \frac{G \times M_E \times m_s}{R_E^2} = m_s g \rightarrow g = \frac{G \times M_E}{R_E^2}$$

- Spherical
- Non-rotating
- Homogeneous

→ g ('little gee') is constant!

Gravity

- Non-spherical → Ellipse of rotation
- Rotating → Centrifugal forces
- Non-homogeneous
  - Subsurface heterogeneities
  - Lateral density differences in the Earth

→ g (’little gee’) is NOT constant

Gravity units

- 1 mGal = 10 g.u. = 10^{-5} m/s^2 ~ 10^{-6}·g

Gravity anomalies

The Gravity anomaly is positive if the body is more dense than its surroundings, negative if less

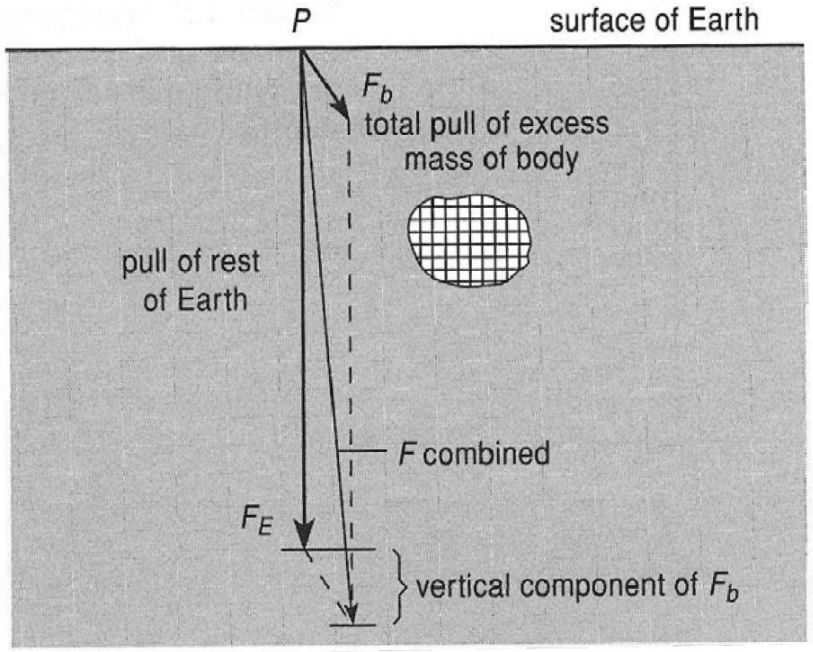

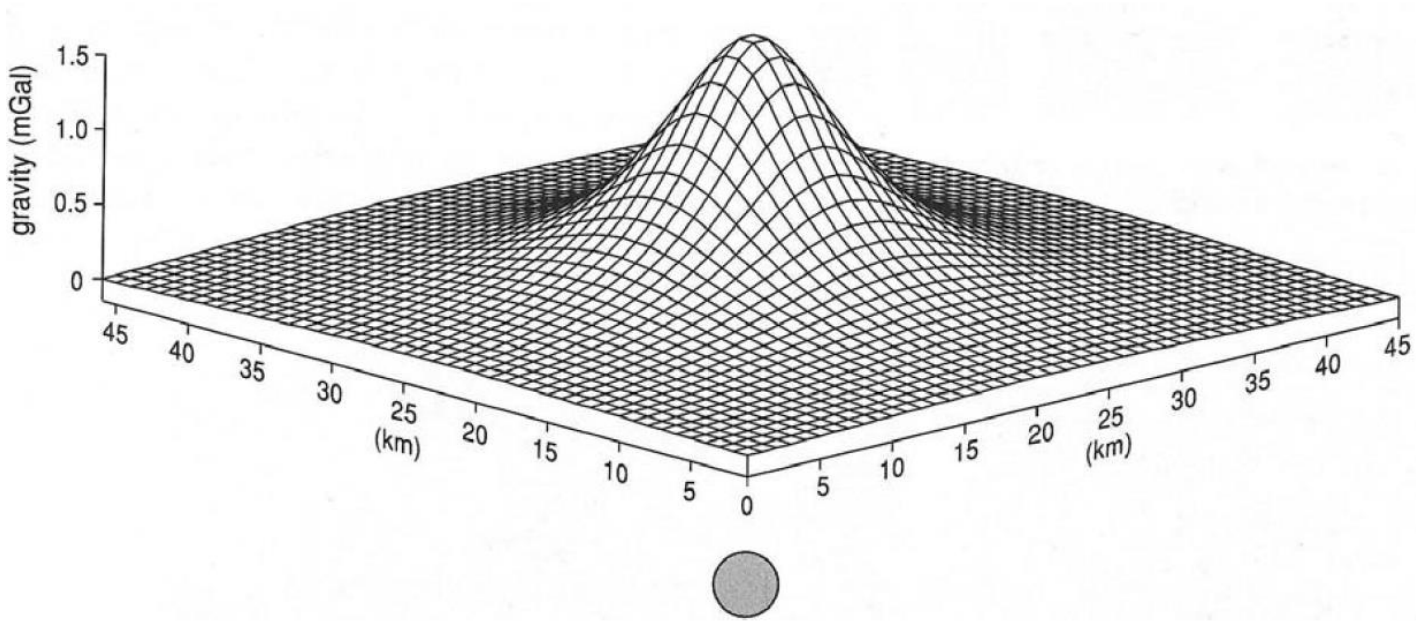

Gravity is a scalar: the combined pull has approx. The same direction as the Earth pull; we measure therefore only the size, or magnitude, of *g*

Gravity anomalies of specific bodies

sphere & horizontal cylinder at different depths

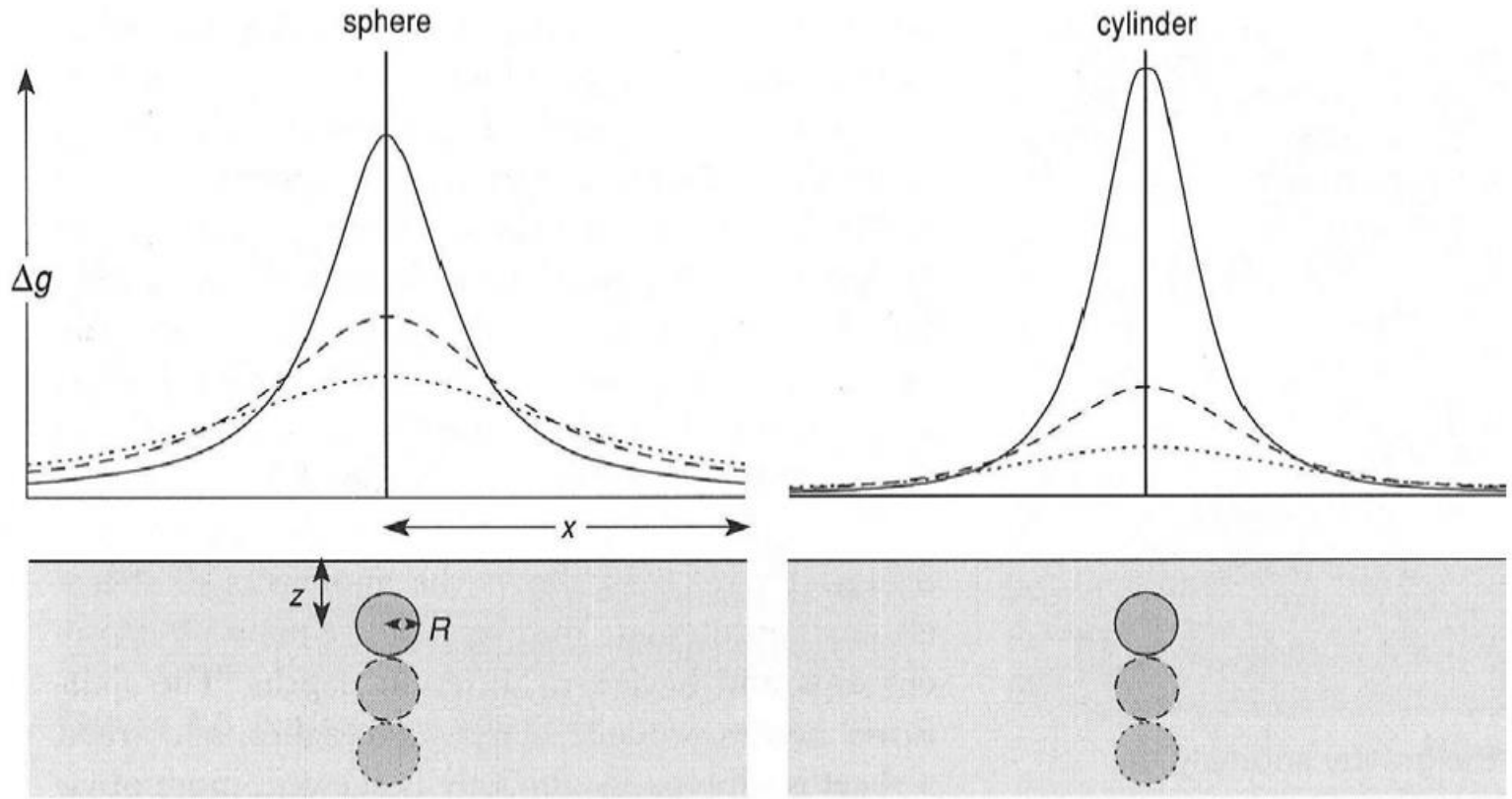

Gravity anomalies of specific bodies

sheets (dykes or veins)

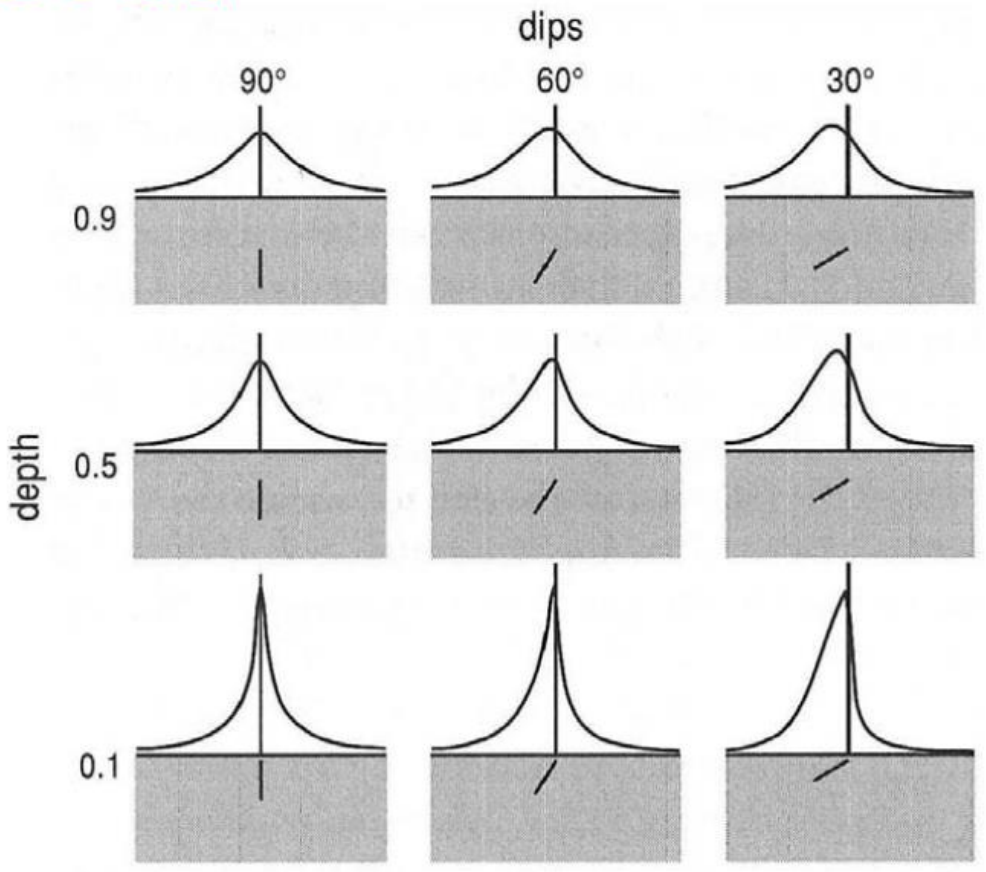

Measurements of Gravity

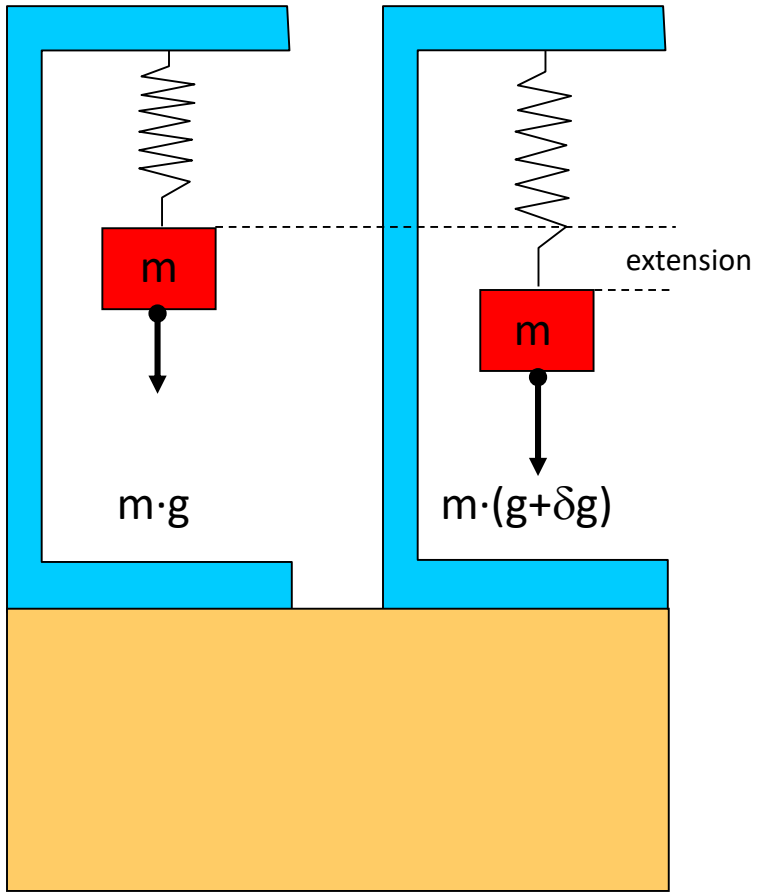

- Spring or Beam
- Corrections
  - Instrumental drift
  - Latitude (due to Earth rotation)
  - Elevation
    - Free-air correction
    - Bouguer correction
    - Terrain correction
  - Tidal
  - Eötvös (due to measurements on moving vehicles)

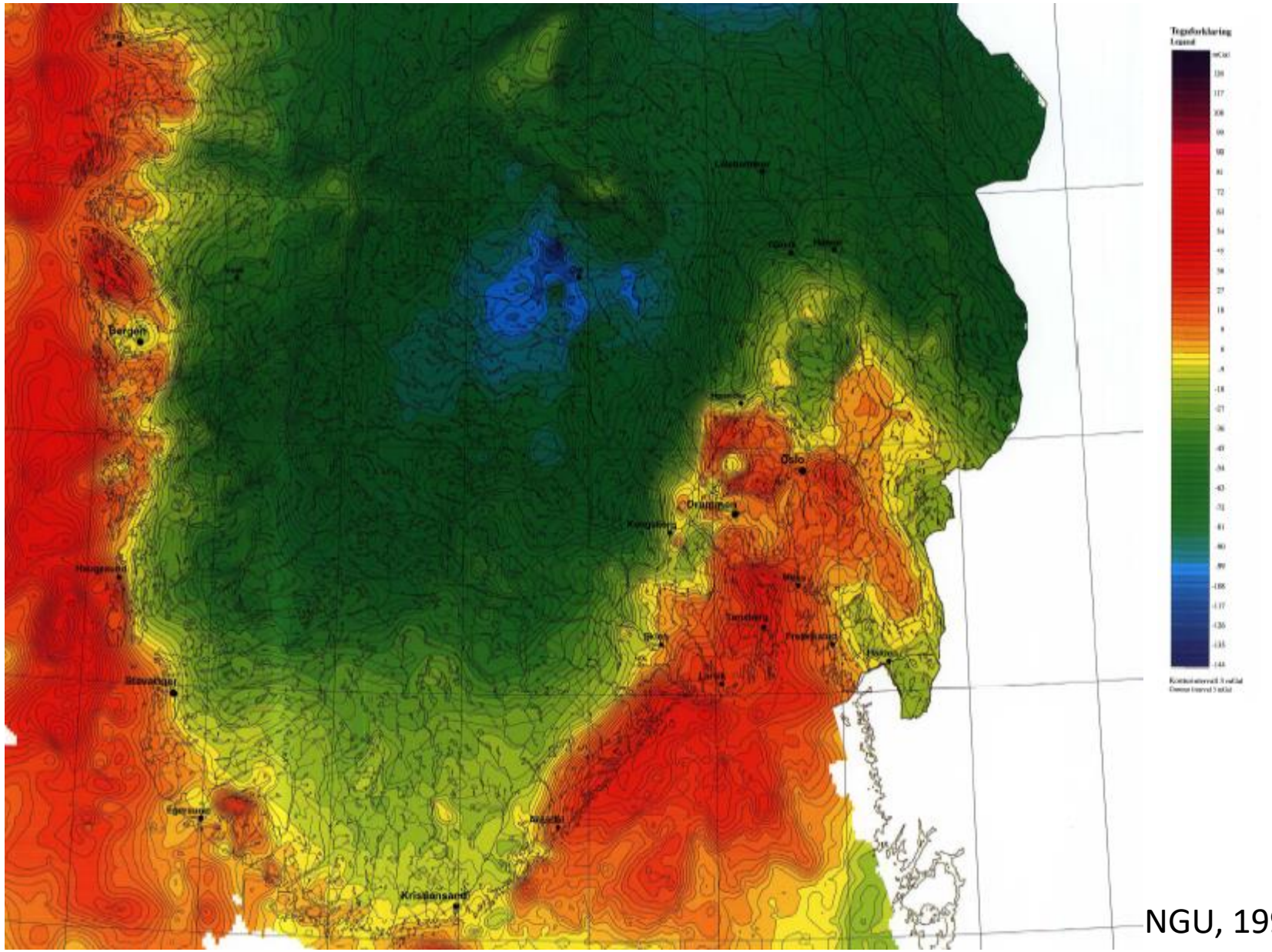

NGU, 1992

Magnetics

- Magnetic surveying aims to investigate the subsurface geology by measuring the strength or intensity of the Earth's magnetic field.
- Lateral variation in *magnetic susceptibility* and *remanence* give rise to spatial variations in the magnetic field
- It is expressed in so called *magnetic anomalies*, i.e. deviations from the Earth's magnetic field.
- The unit of measurement is the *tesla* (T) which is volts·s·m^{-2} In magnetic surveying the *nanotesla* is used (1nT = 10^{-9} T)
- The magnetic field is a vector
- Natural magnetic elements: iron, cobalt, nickel, gadolinium
- Ferromagnetic minerals: magnetite, ilmenite, hematite, pyrrhotite

- → Magnetic surveying depends on the target producing a **magnetic anomaly by locally modifying the Earth's magnetic field**
- → the relationship of the anomaly to its source is **more complex than for gravity**
- → for as well as depending on the *source's shape* and *magnetic properties*, it also depends on its **orientation**, the **latitude** at which the anomaly occurs and if it has a **remanent magnetisation** (as is usual) upon its history

the measured **total field** derives from **adding together** the *field of the body* and the *Earth's field*:
vector addition of strengths and directions

Buried: short, but powerful dipole

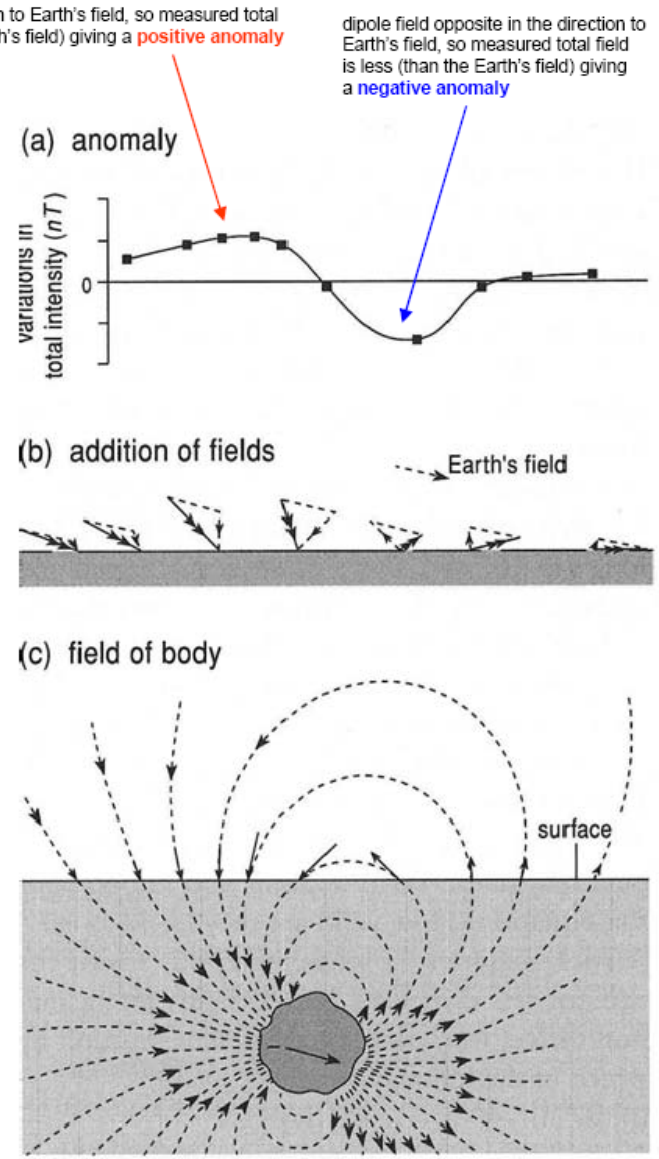

Remanent & Induced Magnetisations

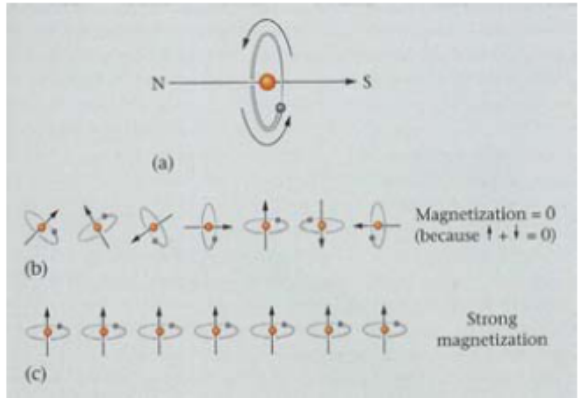

remanent magnetisation: the ability to retain magnetisation in the absence of a field or in the presence of a different magnetic field

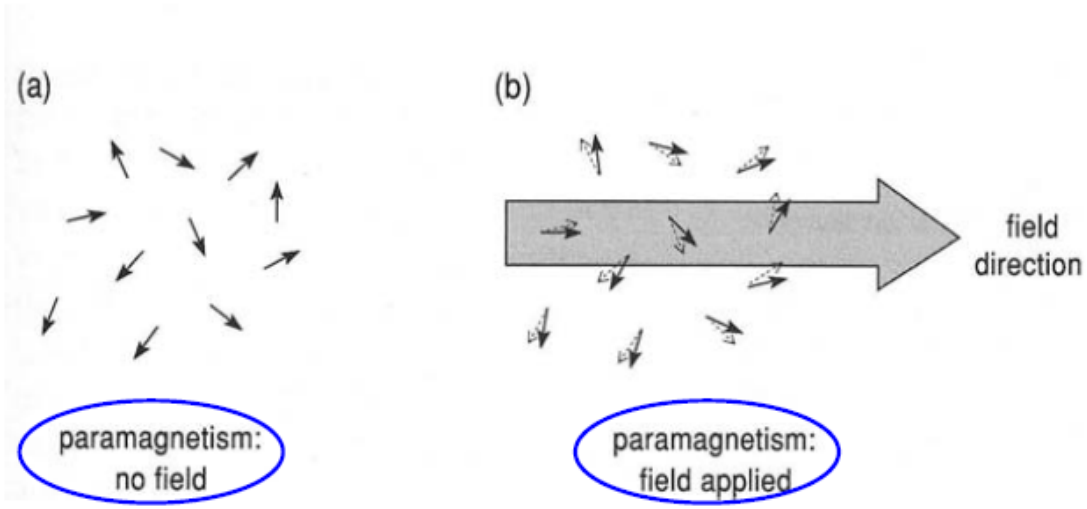

alignment and hence magnetisation disappears as soon as the field is removed

directions of the magnetisations of the magnetic atoms spontaneous align
[iron materials & its compounds, e.g. magnetite]

Magnetic susceptibility (χ): the ability of a rock to become temporarily magnetised while a magnetic field is applied to it

paramagnetic materials → become magnetised only when the field is present
ferromagnetic materials → increase their magnetisation while a field is applied

} this temporary magnetisation is called **induced magnetisation**

strength of the magnetic field

$$M_i = \chi \times H$$

induced magnetization = susceptibility × field

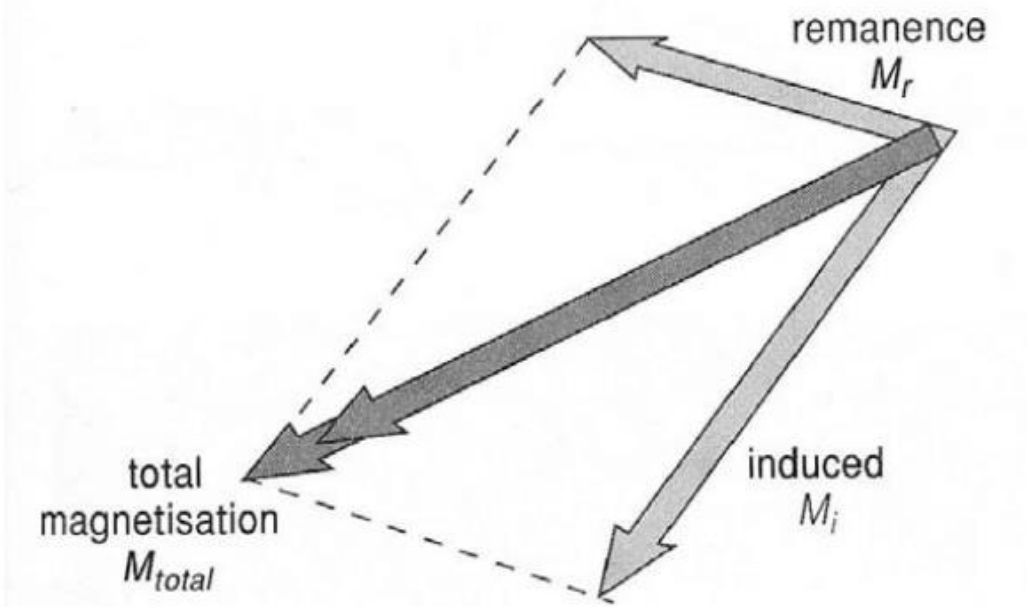

Rock type	Susceptibility (rationalised SI units)
Sediments	
chalk	c. 0
limestone	0.00001-0.025*
salt	–0.00001
sandstone	0–0.2
shale	0.0006–0.02
Igneous and metamorphic	
basalt	0.0005–0.18
gabbro	0.0008–0.08
gneiss	0–0.003
granite	0.00002–0.05
peridotite	0.09–0.2
rhyolite	0.0002–0.04
serpentinite	0.003–0.08
slate	0–004
Other	
water, ice	–0.000009

*Ranges, which are from several sources, are approximate.

Magnetic Data Acquisition

Land surveys

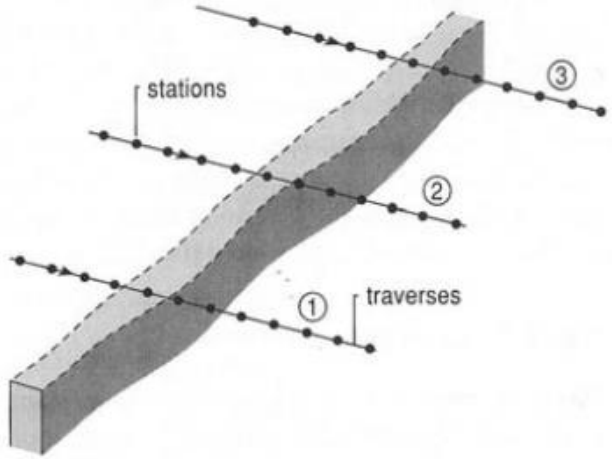

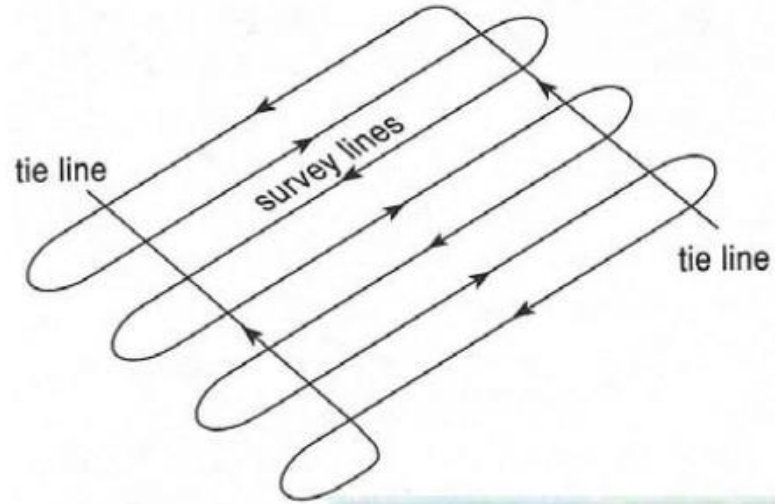

Aeromagnetic surveys

- covers large and, otherwise, inaccessible areas
- looses in resolution [due to the height of the plane]

Magnetic anomalies of simple shaped bodies

1. The field of a dipole

the field of each pole is found separately and then added

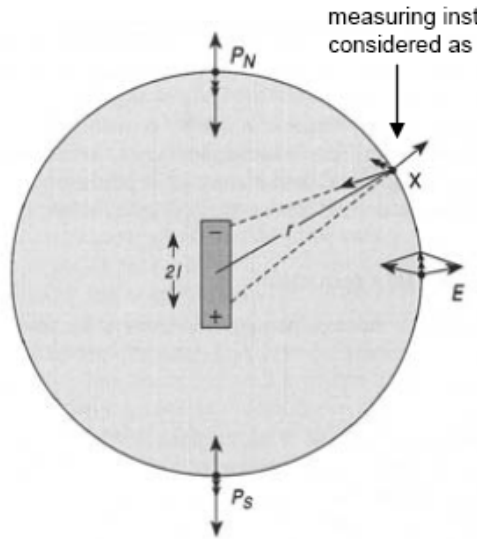

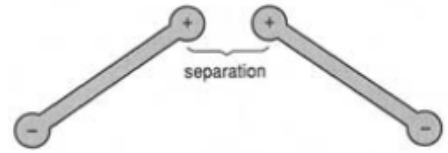

magnets with isolated poles

a magnetic body is thought of as being made of **+/- magnetic poles**

$$\underset{\text{inclination}}{\tan I} = 2 \underset{\text{latitude}}{\tan \lambda}$$

2. Anomaly of a dipole, or small body

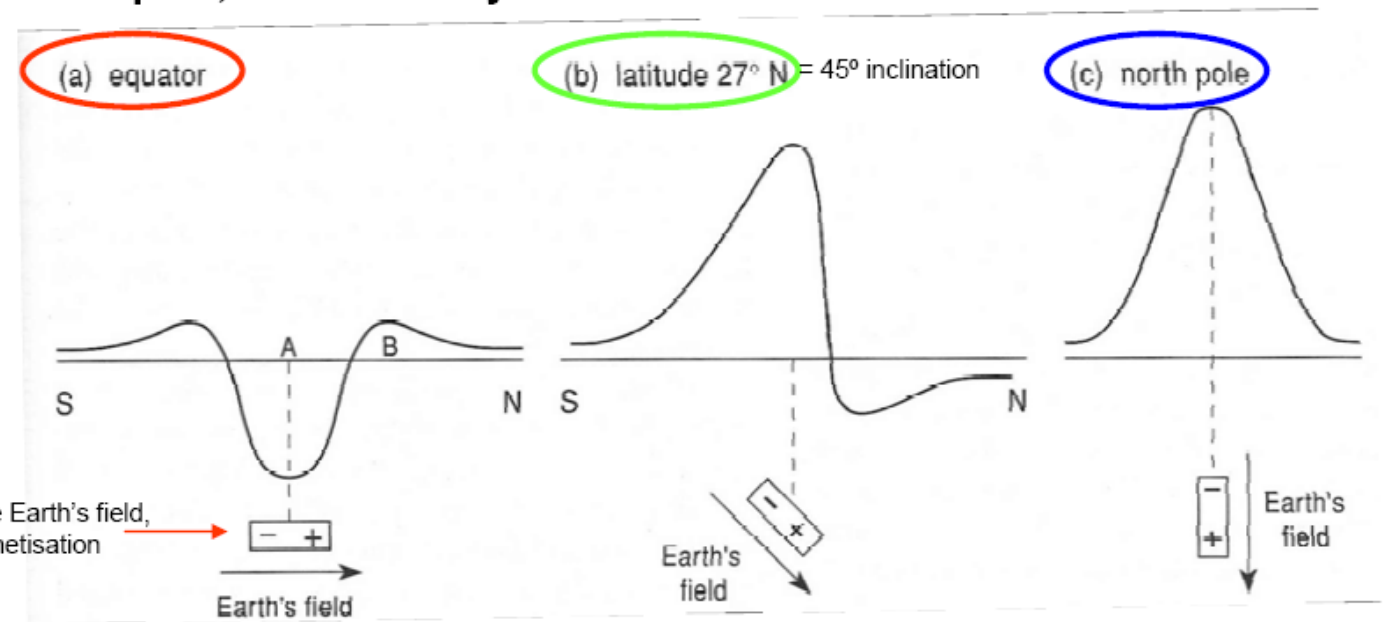

dipole aligned with the Earth's field, i.e. only induced magnetisation

Depth of a magnetic body

similar with gravity:

- ***the shallower a body, the sharper & larger the anomaly***
- ***the deeper the body the broader the anomaly***

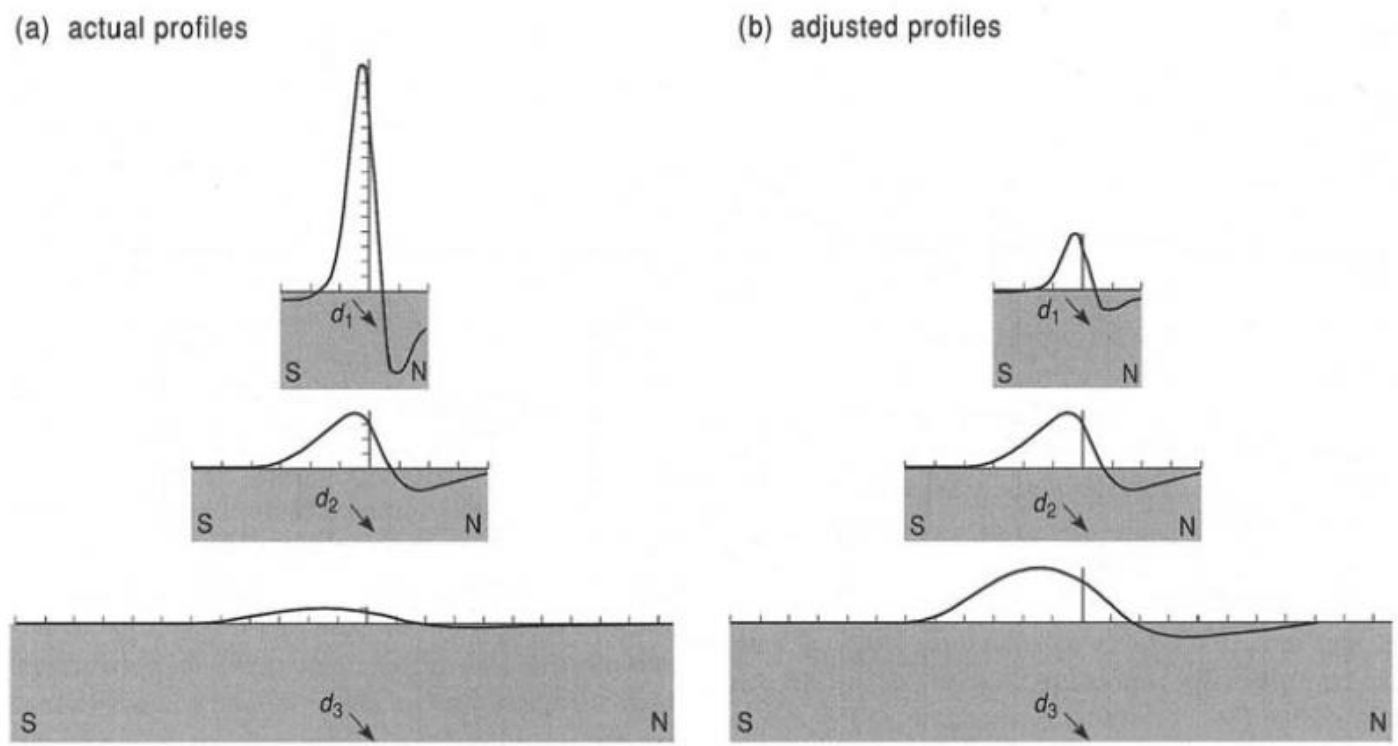

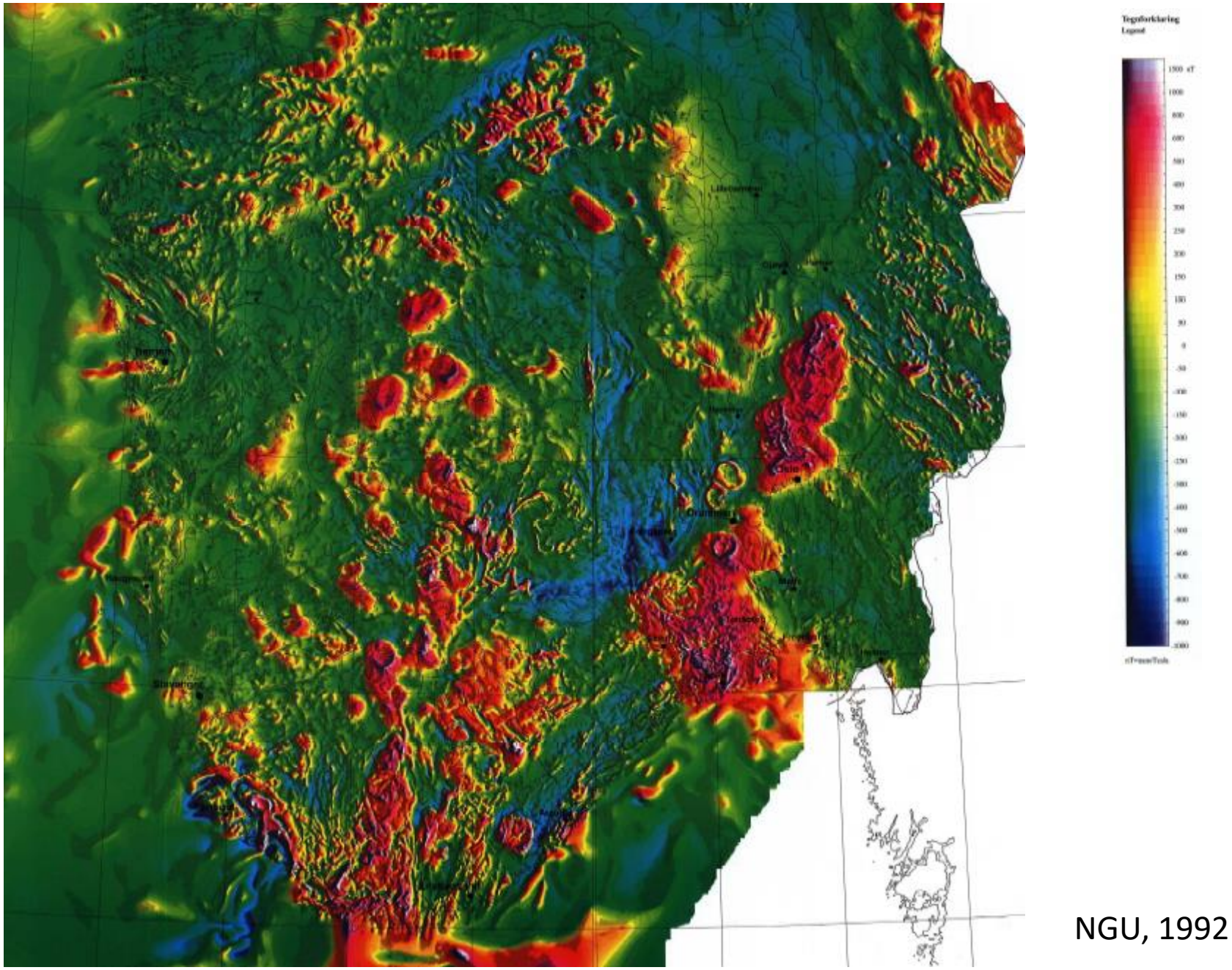
Tegnforklaring
Legend
1500 nT
1000
800
600
500
400
300
250
200
150
100
50
0
-50
-100
-150
-200
-250
-300
-400
-500
-600
-700
-800
-900
-1000
nTesseTesla

NGU, 1992

Electromagnetics

Electromagnetic methods use the response of the ground to the propagation of incident alternating electromagnetic waves, made up of two orthogonal vector components, an electrical intensity (E) and a magnetizing force (H) in a plane perpendicular to the direction of travel

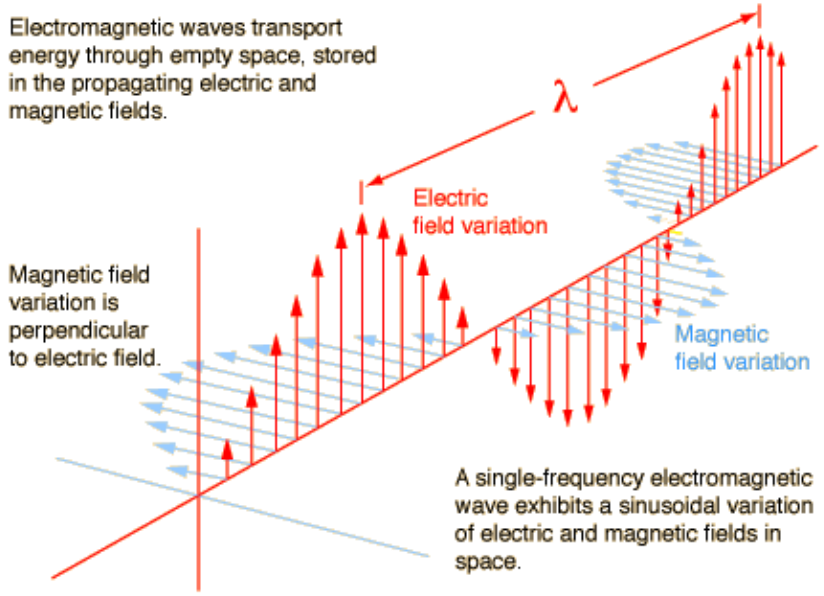

Electromagnetics

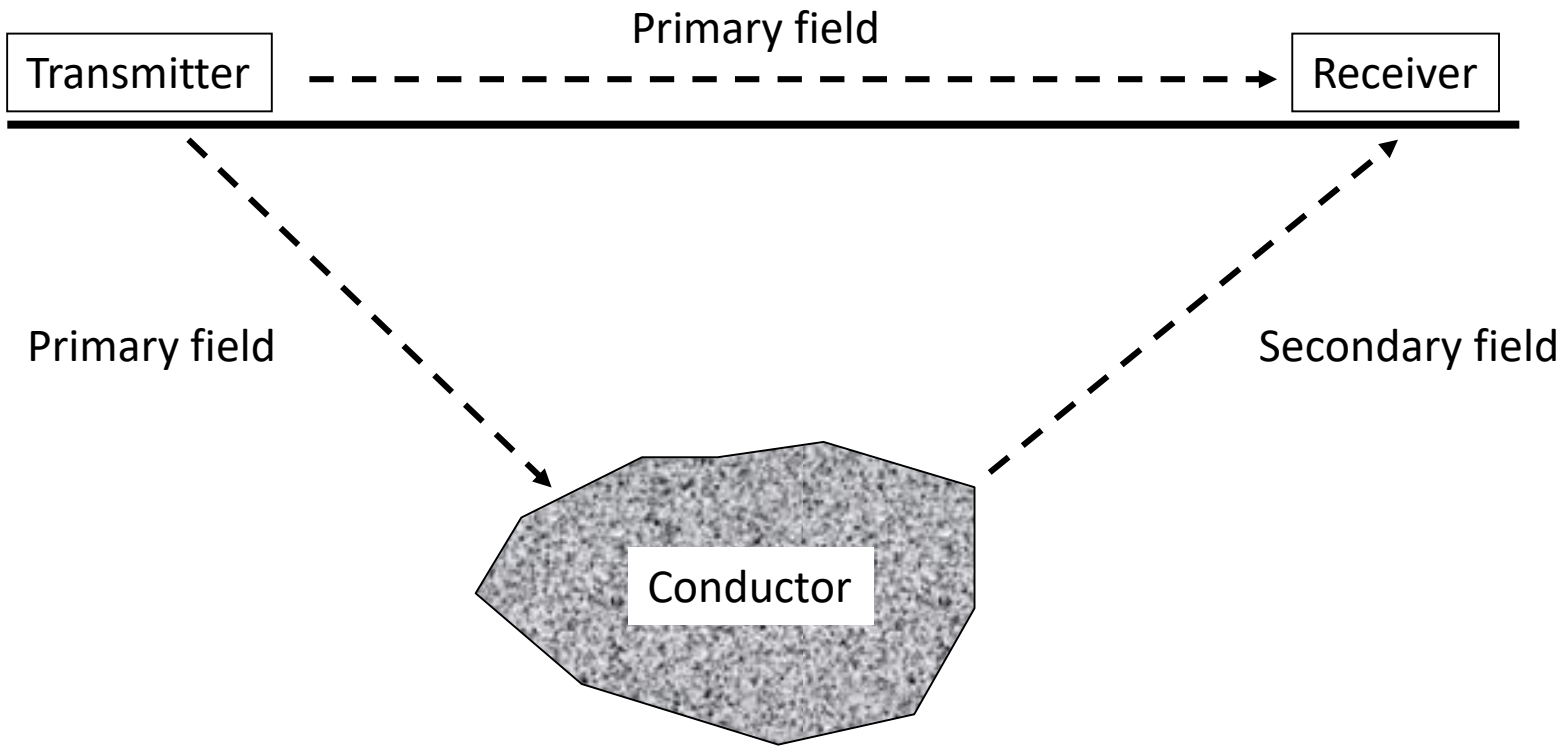

Electromagnetic anomaly = Primary Field – Secondary Field

Electromagnetics – Sea Bed Logging

SBL is a marine electromagnetic method that has the ability to map the subsurface resistivity remotely from the seafloor.

The basis of SBL is the use of a mobile horizontal electric dipole (HED) source transmitting a low frequency electromagnetic signal and an array of seafloor electric field receivers.

A hydrocarbon filled reservoir will typically have high resistivity compared with shale and a water filled reservoirs.

SBL therefore has the unique potential of distinguishing between a hydrocarbon filled and a water filled reservoir

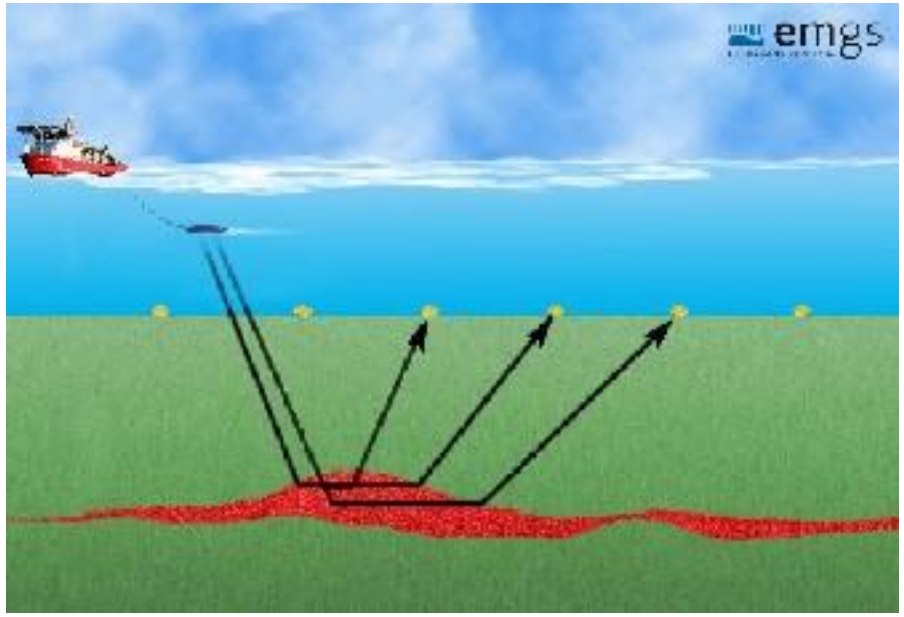

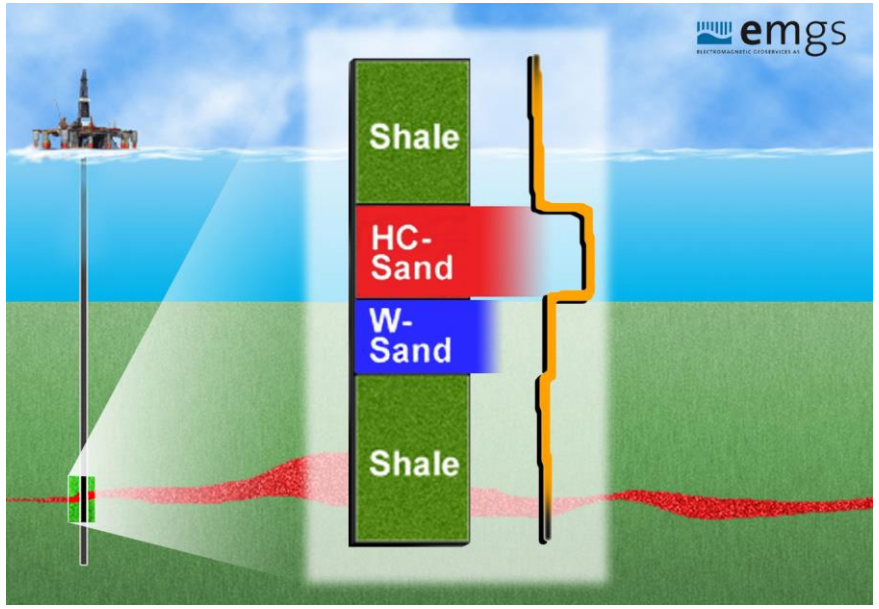

Reflection Seismology

- Principle of reflection seismology
  - What is reflection seismology
  - Seismic wave propagation
  - Acquisition – collecting seismic data
  - Prosessing
- Limitations and Pitfalls
  - Resolution (Horizontal and Vertical)
  - Velocity Effects (Seismic velocities – Depth Conversion)
  - Geometrical Effects (Migration)
  - Seismic Modelling (Synthetic seismograms)
- 2D vs. 3D seismic reflection

Reflection Seismology

Reflection Seismology

- → most important tool for **2D/3D mapping of subsurface**
  [reveals layering, structural features such as faulting & folding]
- → extensively used by the **oil & gas industry** to search for hydrocarbon fields

Reflection seismology can be considered as *echo or depth sounding* &
it is easier performed at **sea** than on **land**

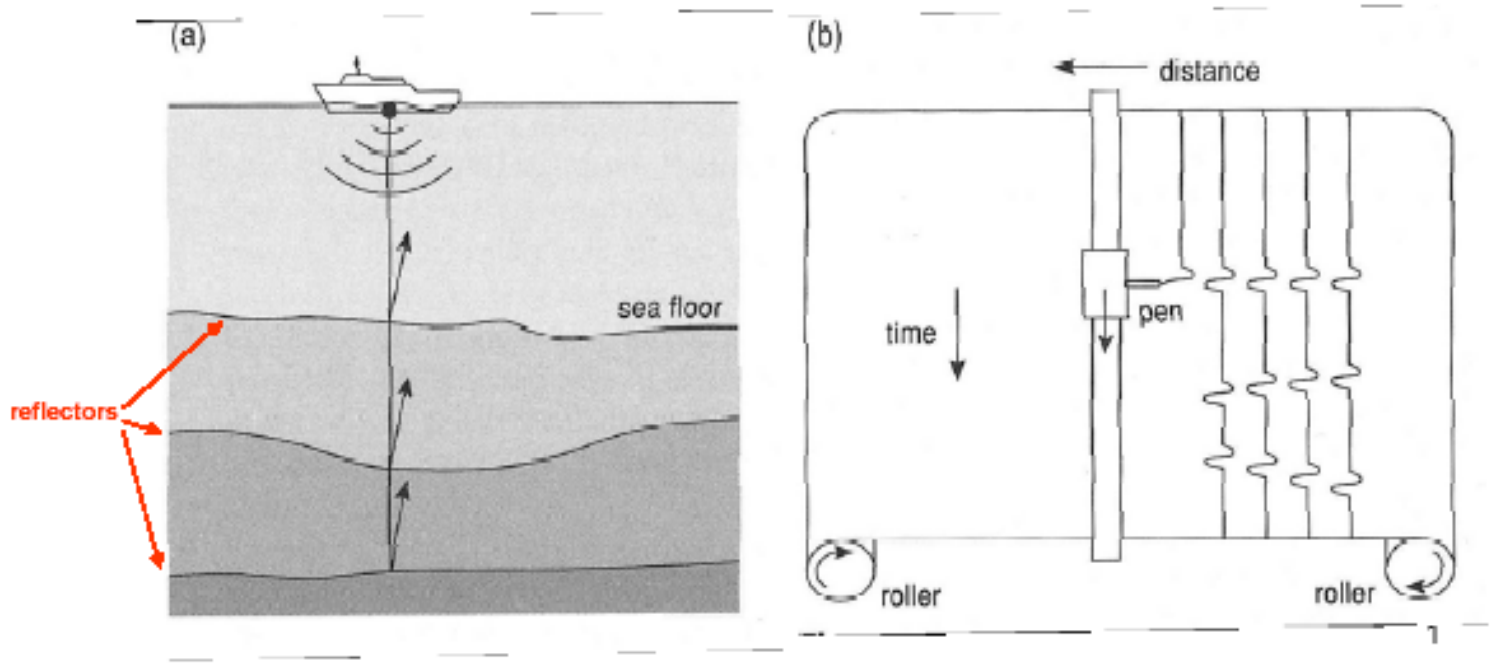

Reflection Seismology

Reflection seismics output: seismic section (seismic reflection profile)

vertical scale not in depth (m),
but in **two-way travel-time (TWT, sec)**:
the time it takes the ray *to reach the reflector & return back*

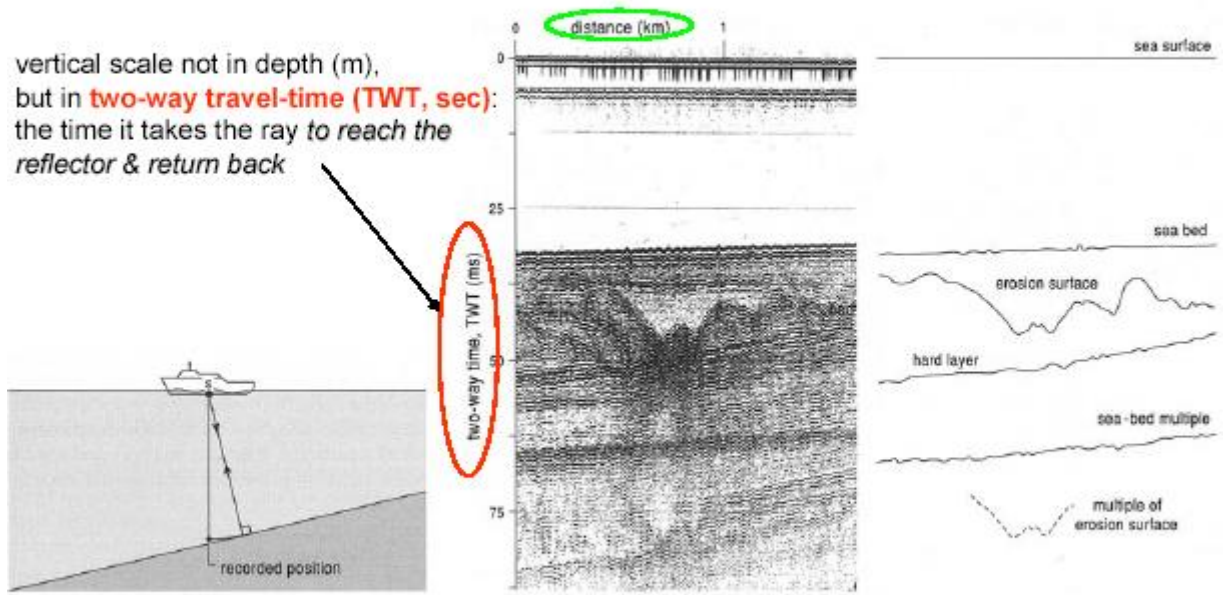

one of the problems: reflections may not come directly below the source, since they reflect at right angle to the interface, but the recording takes no account of this

Reflection Seismology

Seismic waves can be considered both as energy distributed along wave fronts, and as rays. In an isotropic (same velocity in all directions) and homogeneous medium the energy will propagate spherically from the source.

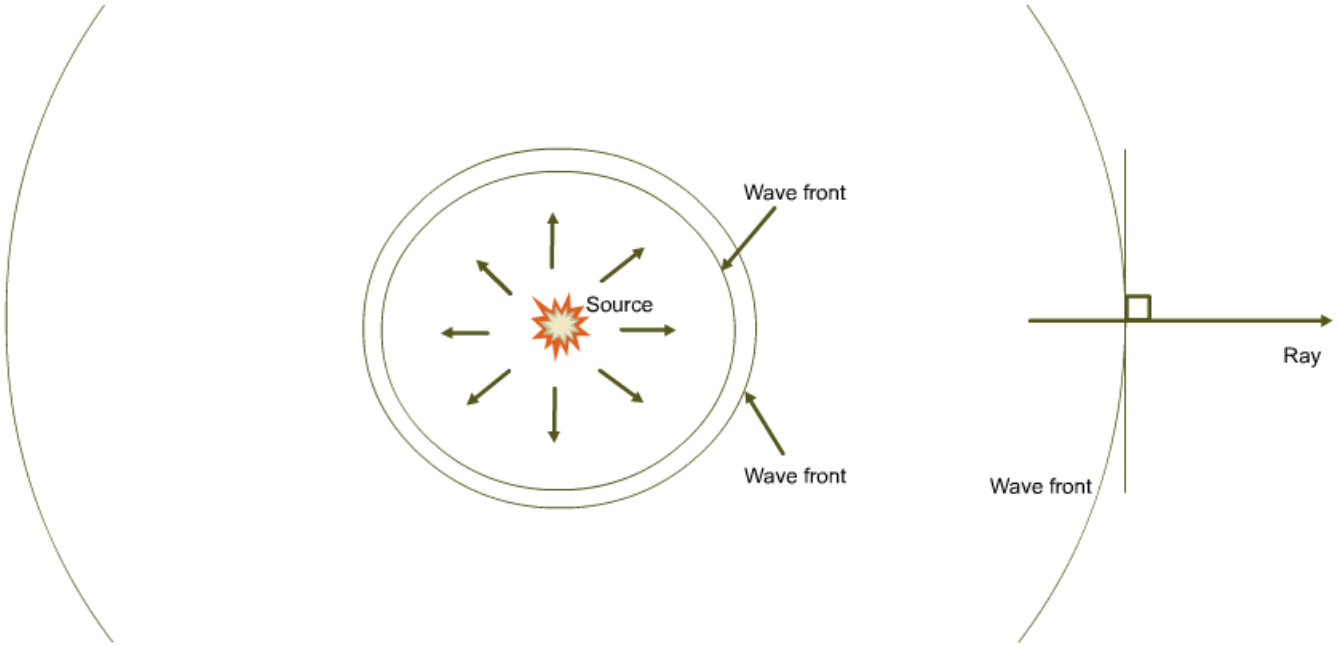

The seismic wave along one wave front has always the same phase. At large distance from the source the wave front is close to planar, and the wave is called a plane wave.

The seismic ray points in the direction of propagation and is perpendicular to the wave front in isotropic media

Reflection Seismology

The amplitude of a seismic waves decays due to spherical spreading, as the energy in the wave is distributed along a wave front increasing steadily in size, absorption, which is friction in the rock as the wave propagates, and reflections and P-S conversions at each interface.

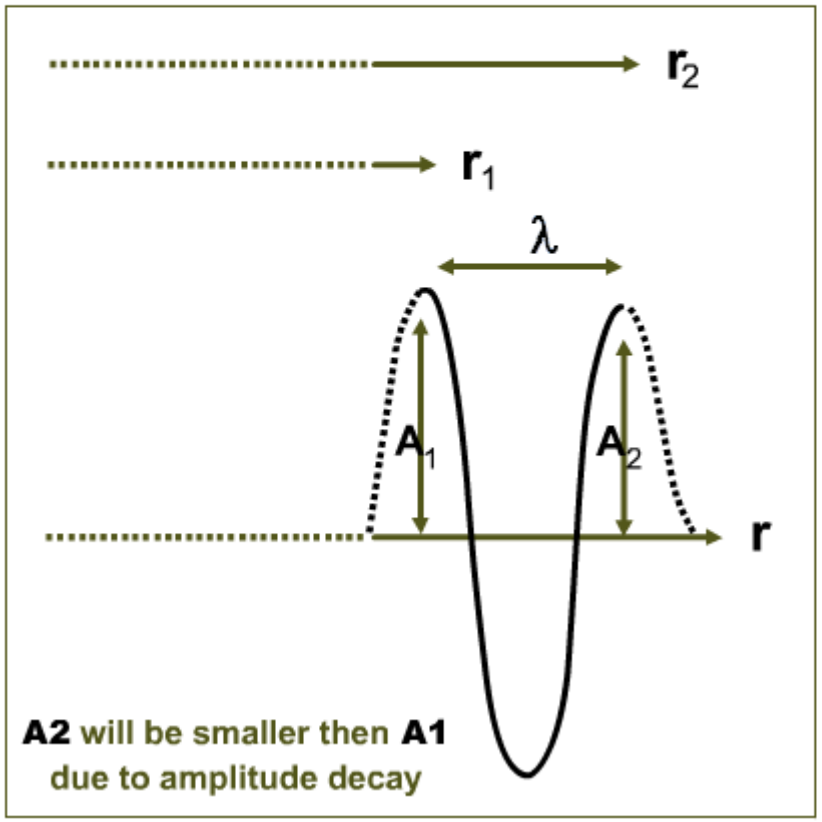

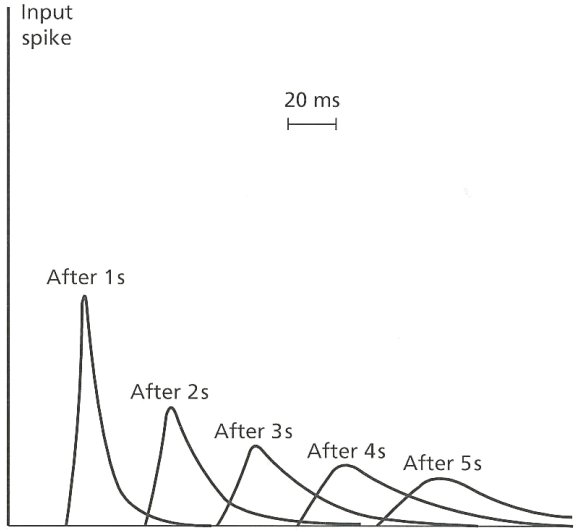

- Spherical spreading
- Absorption
- Transmission/conversion

Reflection Seismology

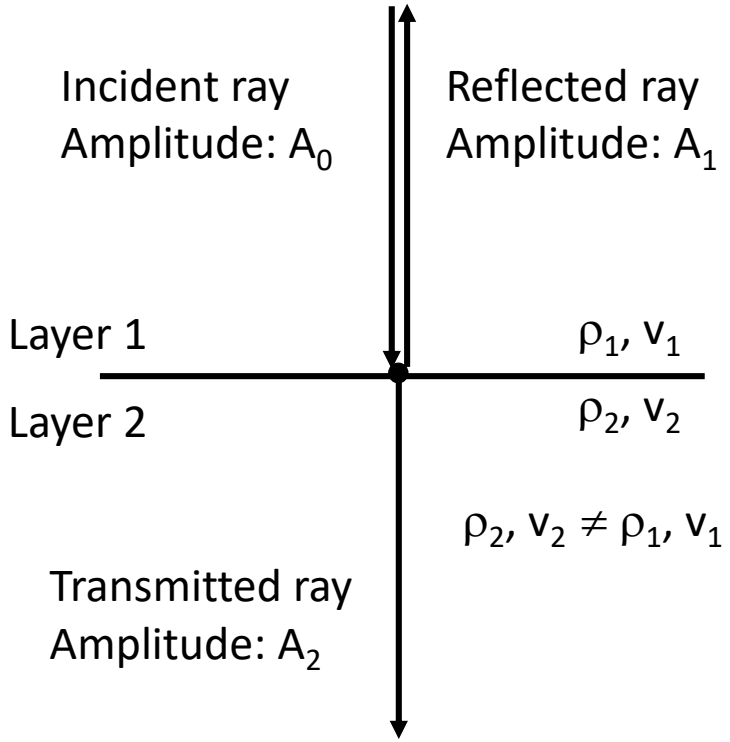

Acoustic Impedance: $Z = \rho \cdot v$

Reflection Coefficient: $R = A_1/A_0$

$$R = \frac{\rho_2 v_2 - \rho_1 v_1}{\rho_2 v_2 + \rho_1 v_1} = \frac{Z_2 - Z_1}{Z_2 + Z_1}$$

Transmission Coefficient: $T = A_2/A_0$

$$T = \frac{2\rho_1 v_1}{\rho_2 v_2 + \rho_1 v_1}$$

$-1 \leq R \leq 1$

$R = 0$ → All incident energy transmitted ($Z_1 = Z_2$) → no reflection

$R = -1$ or $+1$ → All incident energy reflected → strong reflection

$R < 0$ → Phase change (180°) in reflected wave

Reflection Seismology

reflected energy: R^2
transmitted energy: T^2

$R^2 + T^2 = 1$

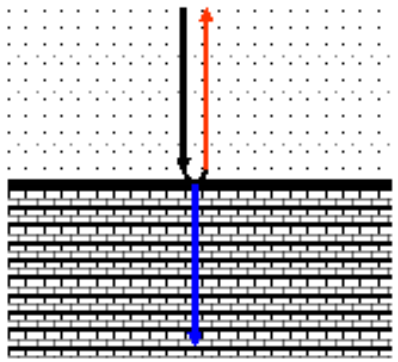

Table 7.1 Seismic velocities and densities either side of an interface

Rock	Range of velocity, v_p	Range of density, ρ
Upper layer: sandstone	2 to 6 km/sec	2.05 to 2.55 Mg/m³
Lower layer: limestone	2 to 6 km/sec	2.60 to 2.80 Mg/m³

$$R = \frac{(2.80 \times 6) - (2.05 \times 2)}{(2.80 \times 6) + (2.05 \times 2)} = 0.608$$

& reflected energy = $0.608^2 = 0.37$

(strong reflector with 37% of energy reflected)

If top & lower layers have the same acoustic impedance then:

$$R = \frac{(2.64 \times 3) - (2.40 \times 3.3)}{(2.64 \times 3) + (2.40 \times 3.3)} = 0$$

- meaning that although there is a lithological boundary there is no seismic reflector
- rare to have similar acoustic impedance [more common weak reflection]
- geological interface # seismic interface

Reflection Seismology

The angle with which the reflected wave departs from an interface is equal to the incoming angle.

teta r = teta i

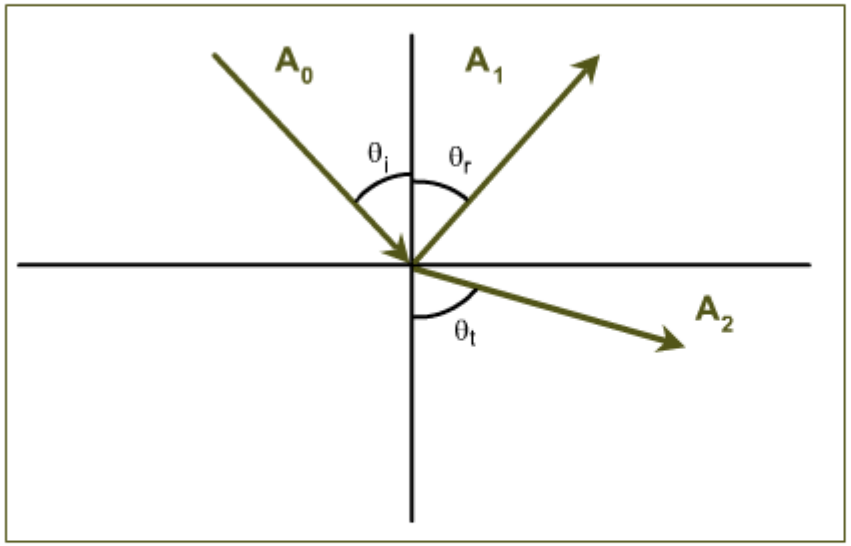

The transmitted wave is refracted according to Snell's law…… .

Snell's Law

$$\frac{\sin\theta_t}{V_t} = \frac{\sin\theta_i}{V_i} \qquad \frac{\sin\theta_r}{V_r} = \frac{\sin\theta_i}{V_i}$$

When the transmitted wave propagates along the interface, the incoming angle is called critical angle, and the transmitted wave is called head wave. In case of a velocity gradient in the layer, the wave will 'dive' within this layer (diving wave).

Reflection Seismology

SEISMIC TRACE (REFLECTION SEISMOGRAM)

Seismic trace:
amplified oscillographic recording of each detector (geo-/ hydro-phone)

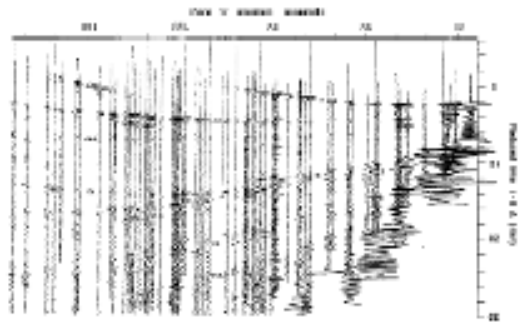

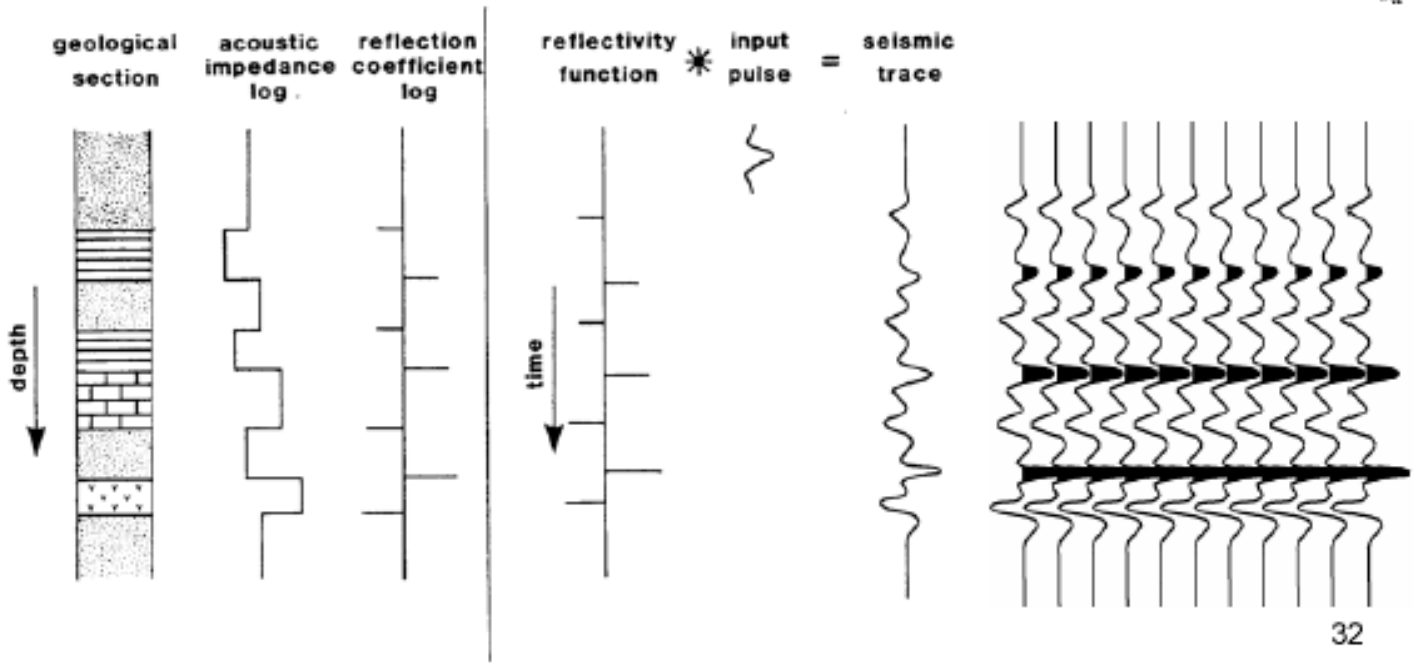

Processing – CMP - CSG

Common Shot Gather and Common Mid-Point are two essential terms used in seismic processing. Look at the animations below to understand how it works.

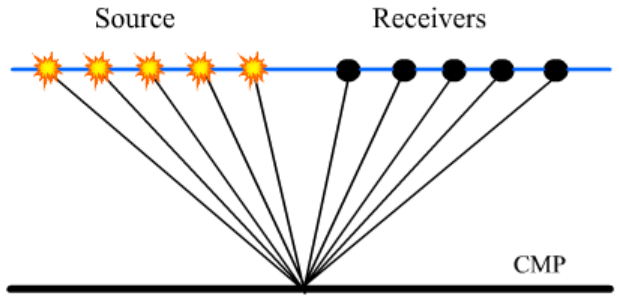

CMP animation

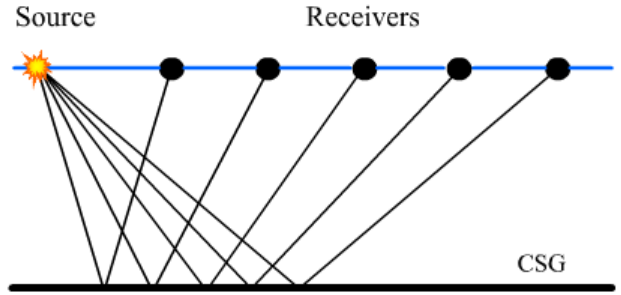

CSG animation

CSG: Common Shot Gather, all seismic traces recorded from one shot.

CMP: Common Mid-Point Gather, all seismic traces from subsequent shots rearranged in order to map the same point; the mid point between shot and receiver.

Processing – NMO

The figure shows an example of a CMP-gather, containing reflections from two reflectors recorded by four channels (assuming straight ray-paths). The figure shows that increasing the shot-receiver distance, increases the travel-time. The difference between (assumed) vertical two-way travel-time and observed travel-time is called normal-move-out (NMO).

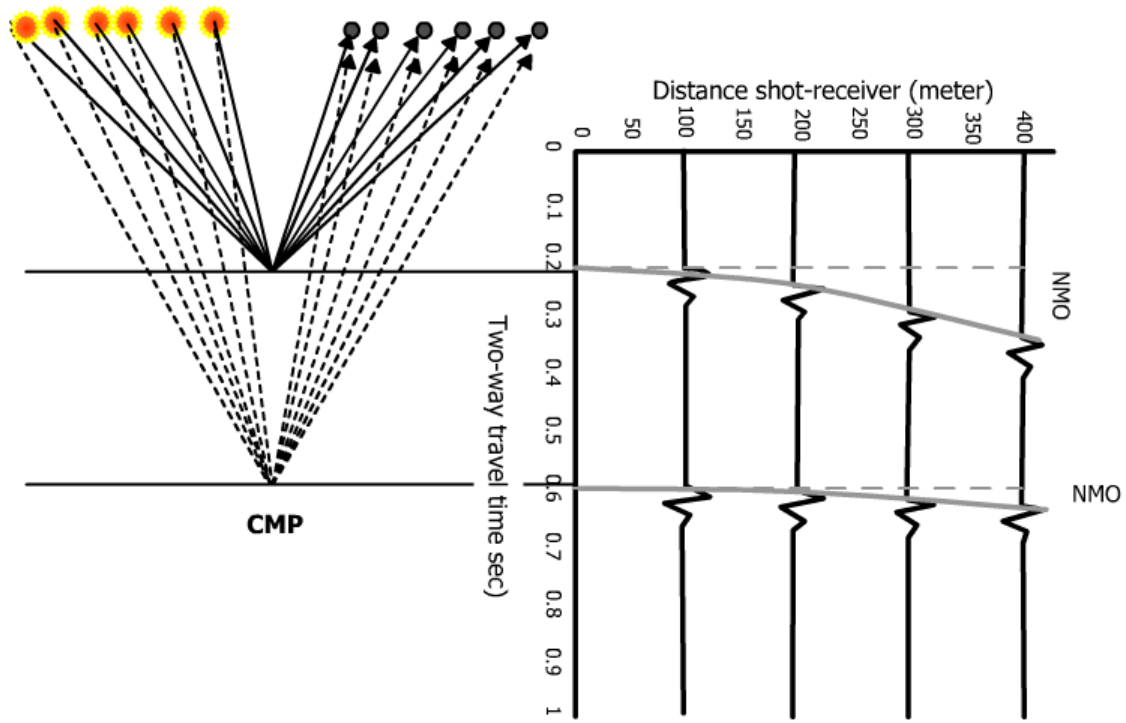

Processing – Stacking

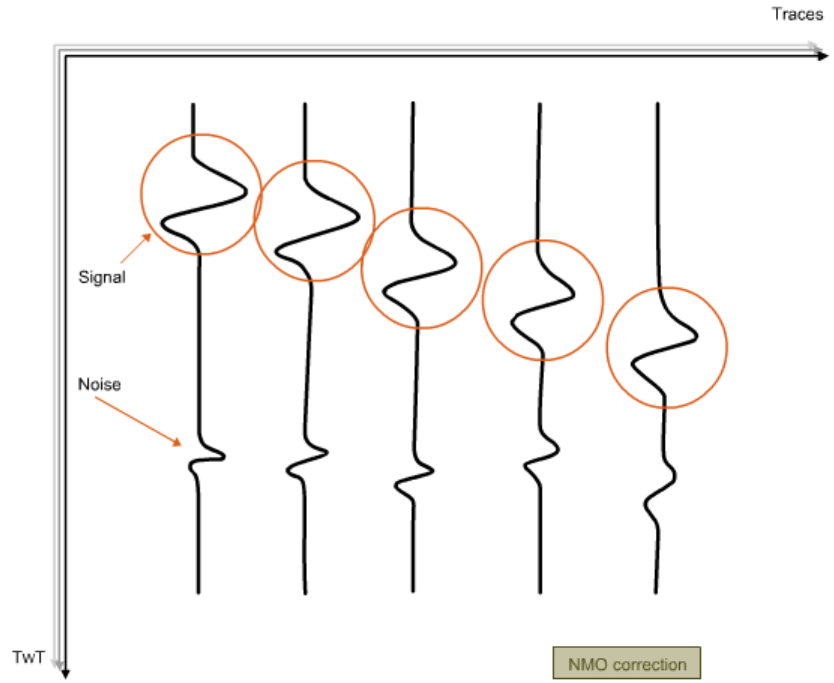

NMO correction

Processing – Stacking

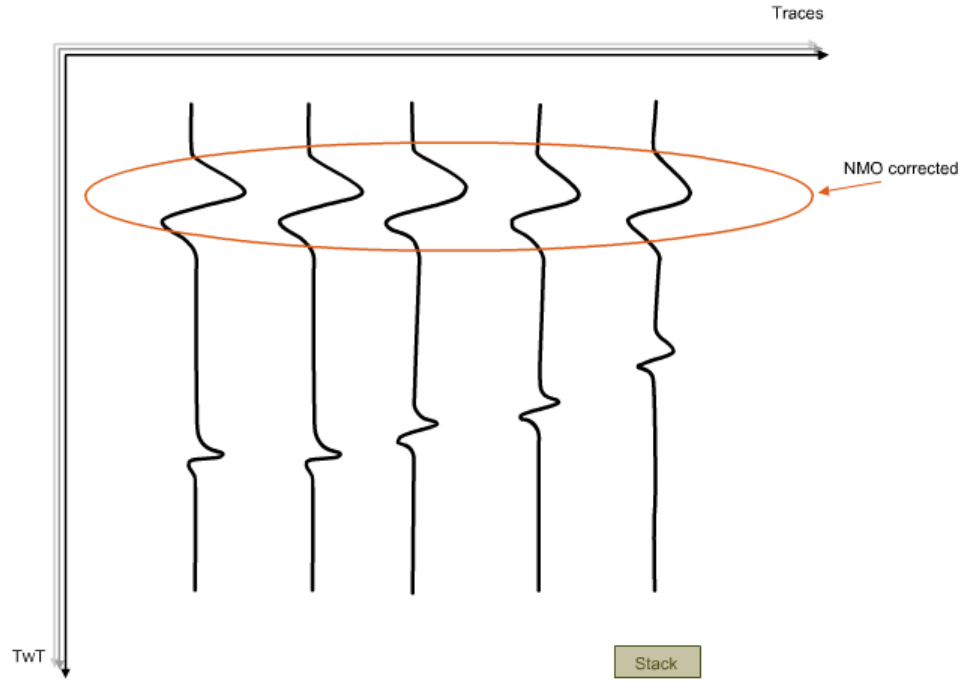

Processing – Stacking

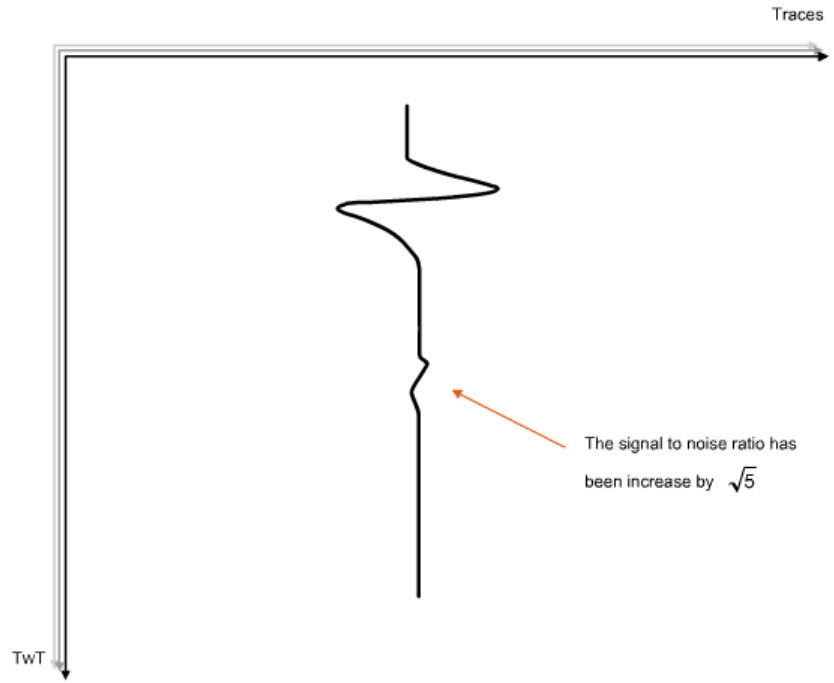

Reflection Seismology

- SEISMIC PROSESSING
  - The objective of seismic prosessing is to enhance the signal-to-noise ration by means of e.g. filtering

Reflection Seismology

- Limitations and Pitfalls
  - Interference
  - Horizontal and Vertical Resolution
  - Velocity Effects
  - Geometrical Effects
  - Multiples

INTERFERENCE

Reflection Seismology

Interference

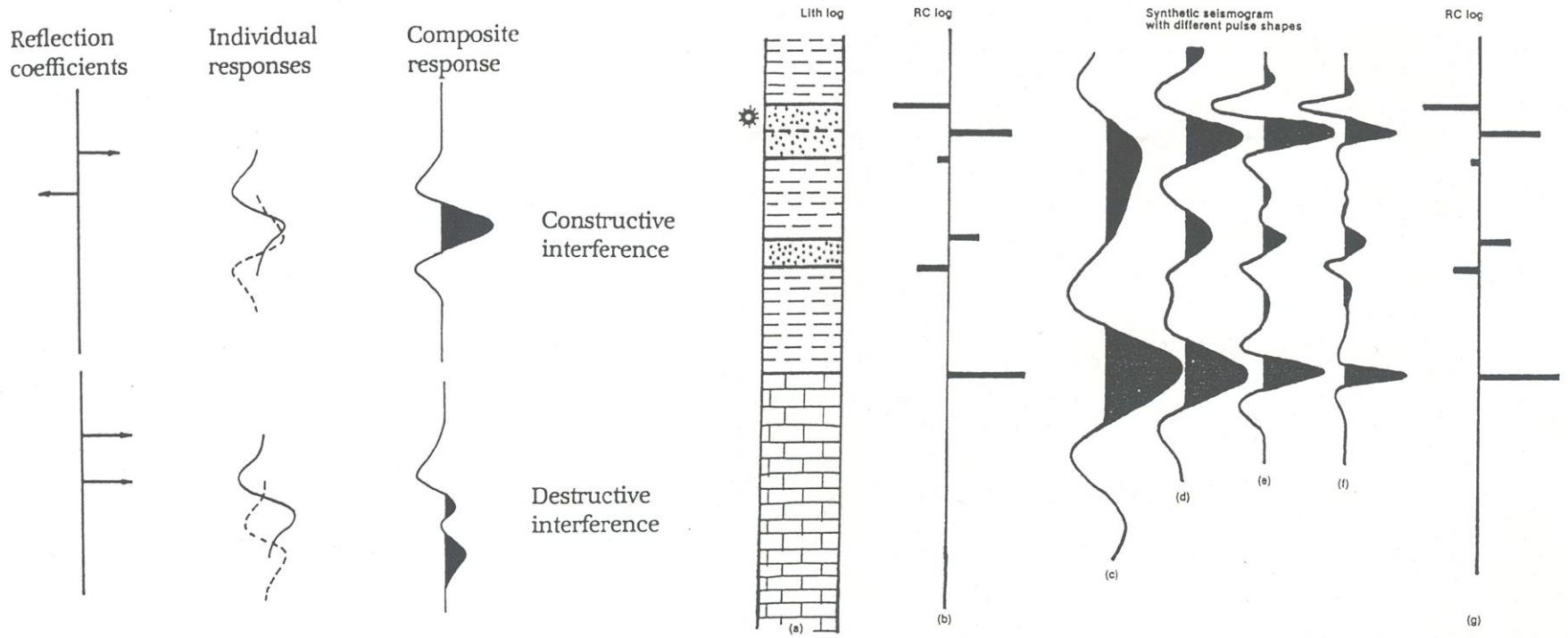

Reflection Seismology

Interference

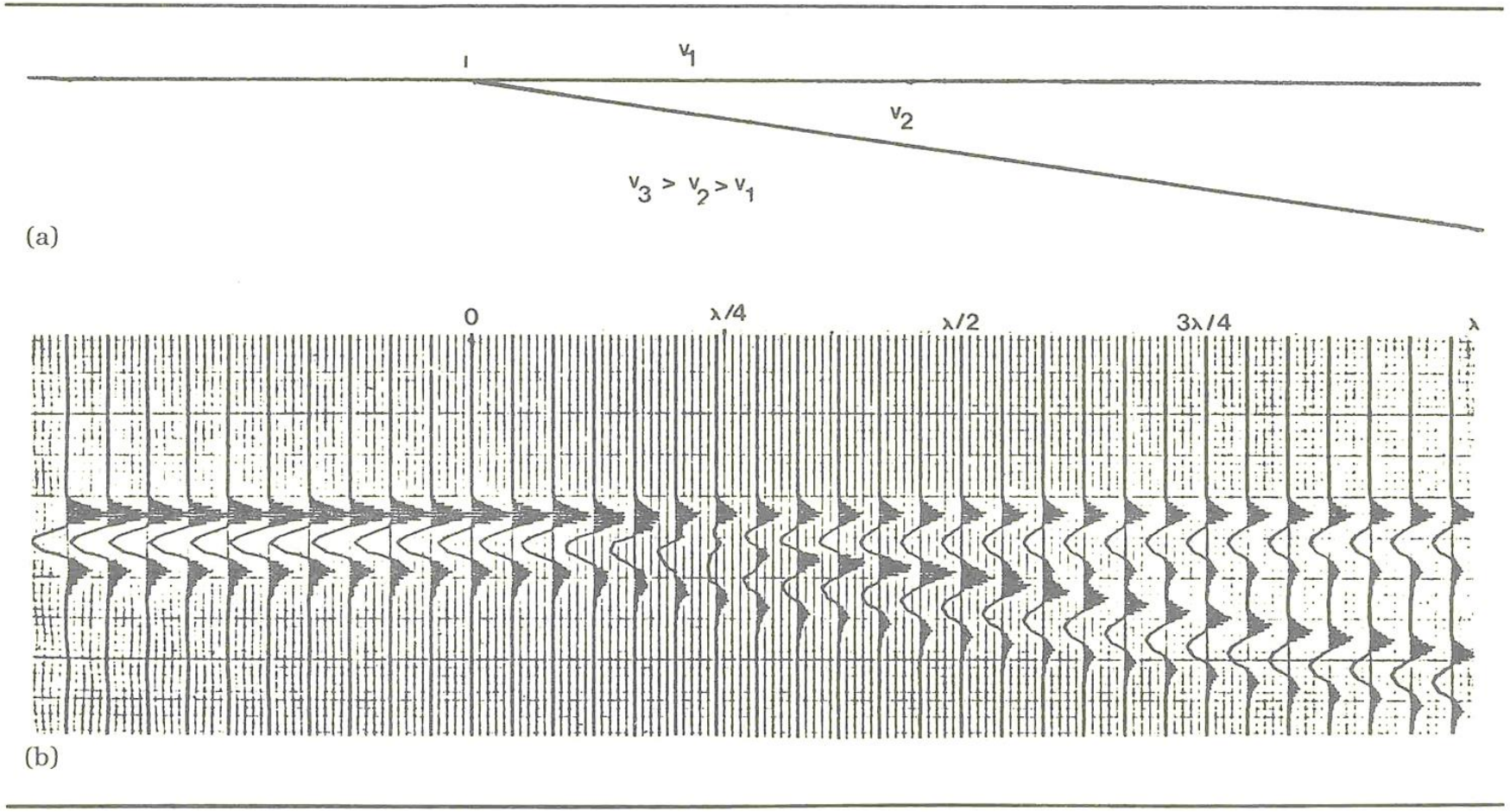

VERTICAL RESOLUTION

Reflection Seismology

Wavelength increases

Frequency decreases

with depth

Reduced vertical resolution

f	v	λ	λ/4	z
100 Hz	2 km/s	20 m	5 m	~250 m
40 Hz	4 km/s	100 m	25 m	~2250 m

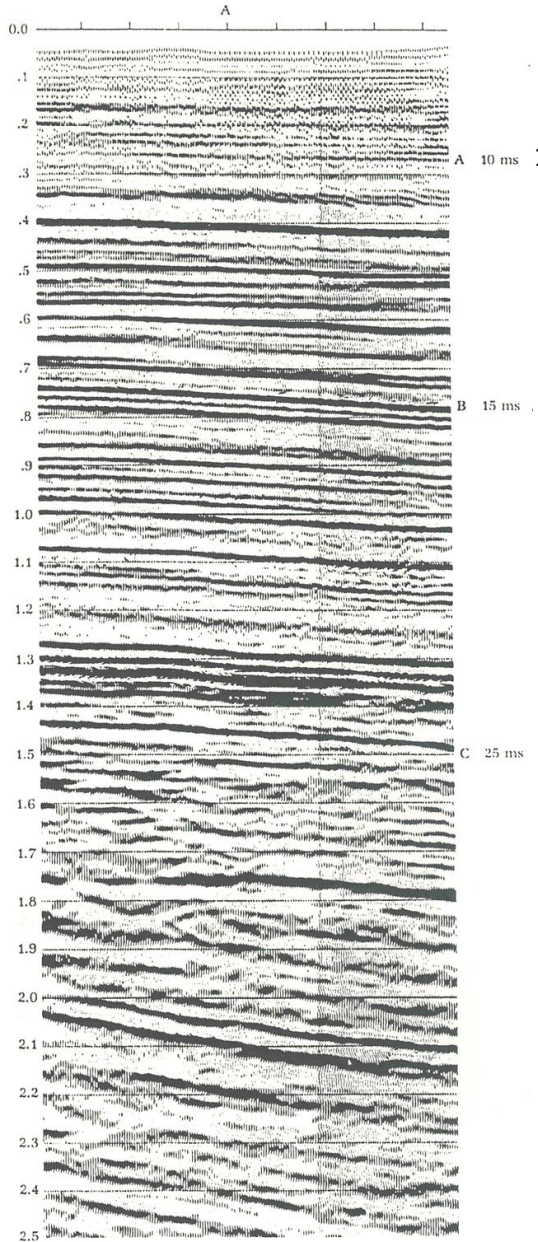

100 Hz

67 Hz

40 Hz

Reflection Seismology

Table 1-1. Typical Limits of Visibility and Separability for a range of geologic situations.

			Age of rocks		VERY YOUNG	YOUNG	MEDIUM	OLD	VERY OLD
			Depth of target		VERY SHALLOW	SHALLOW	MEDIUM	DEEP	VERY DEEP
			Formation Velocity (m/s)		1600	2000	3500	5000	6000
			Predominant Frequency (Hz)		70	50	35	25	20
			Wavelength (m)	λ	23	40	100	200	300
			LIMIT OF SEPARABILITY	$\frac{\lambda}{4}$	**6**	**10**	**25**	**50**	**75**
LIMIT OF VISIBILITY	Poor S/N	e.g.	Water sand poor data	$\sim\frac{\lambda}{8}$	**3**	**5**	**13**	**25**	**38**
	Moderate S/N	e.g.	Water or oil sand fairly good data	$\sim\frac{\lambda}{12}$	**2**	**3**	**8**	**17**	**25**
	High S/N	e.g.	Gas sand good data	$\sim\frac{\lambda}{20}$	**1**	**2**	**5**	**10**	**15**
	Outstanding S/N	e.g.	Gas sand excellent data	$\sim\frac{\lambda}{30}$	**<1**	**1**	**3**	**7**	**10**

units are meters

(Brown 1999)

HORIZONTAL RESOLUTION

Reflection Seismology

Horizontal Resolution

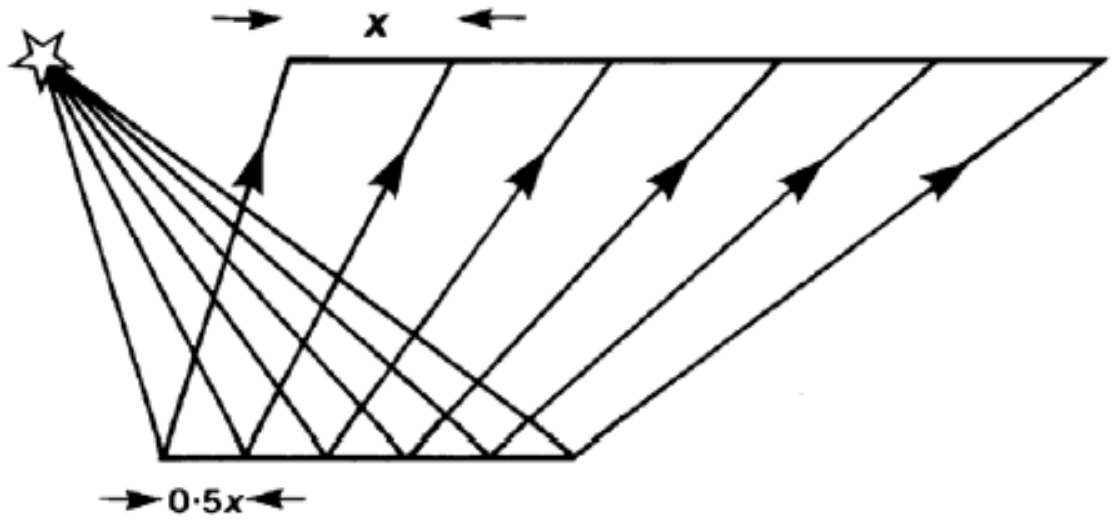

Horizontal Resolution = half the detector spacing

Reflection Seismology

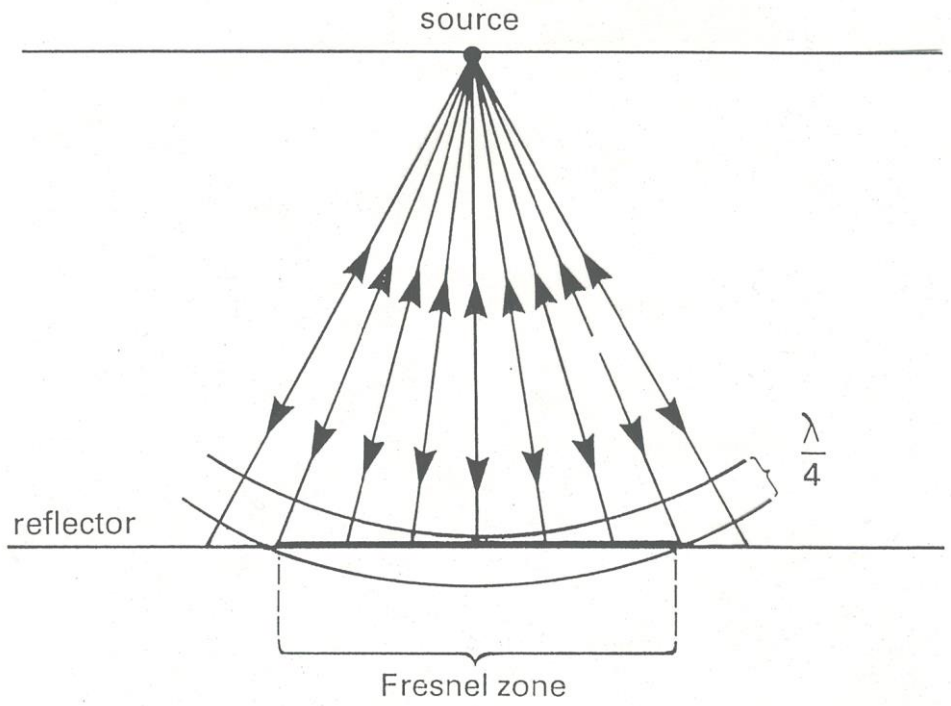

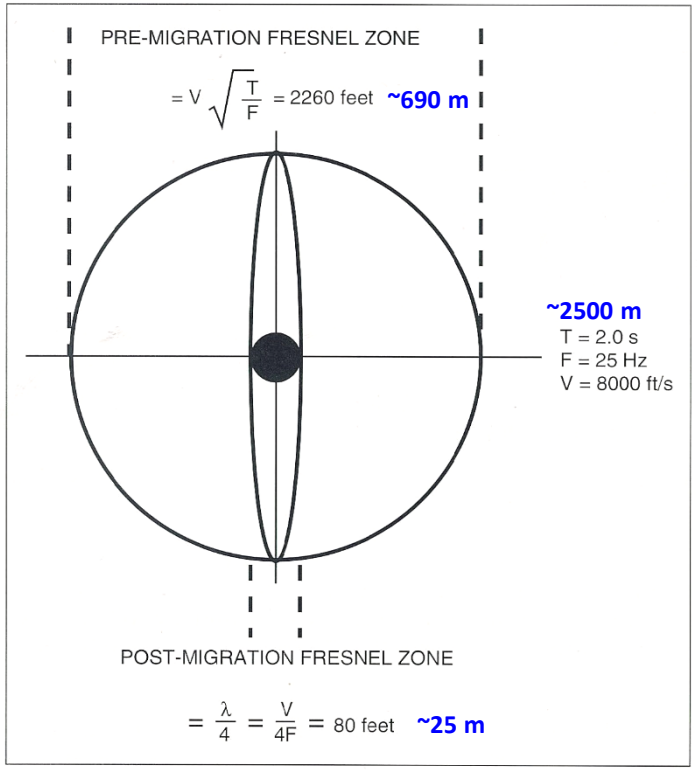

Reflection Seismology

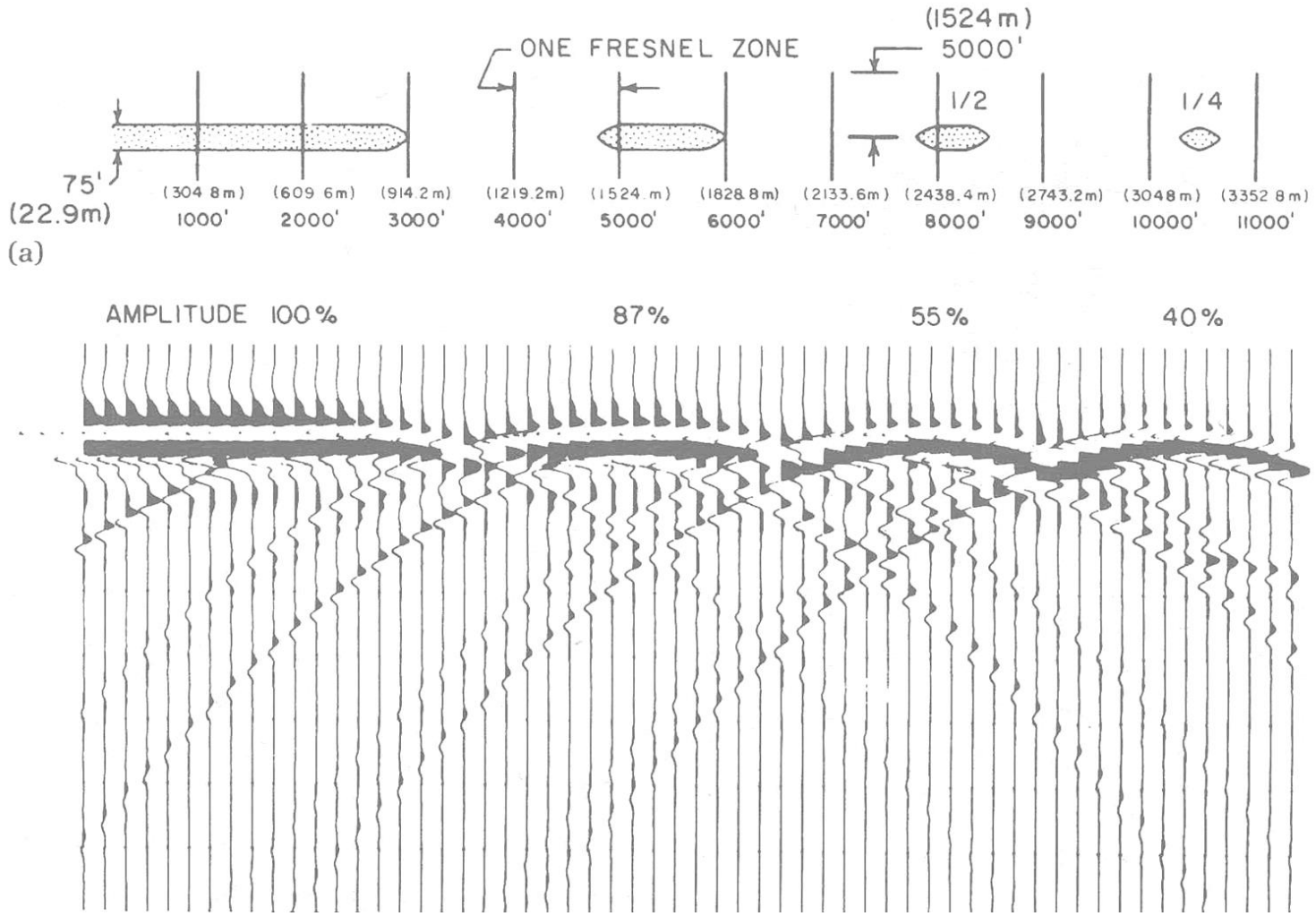

GEOMETRICAL EFFECTS

Reflection Seismology

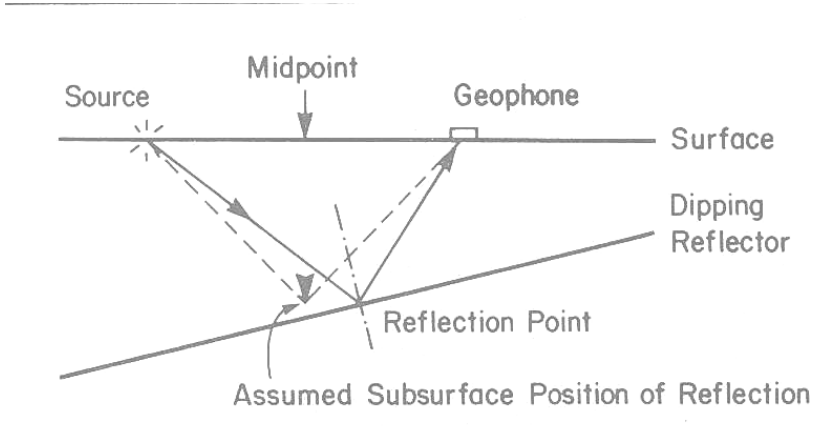

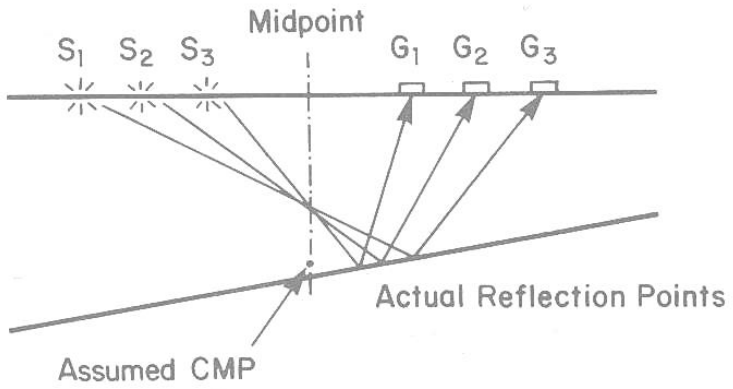

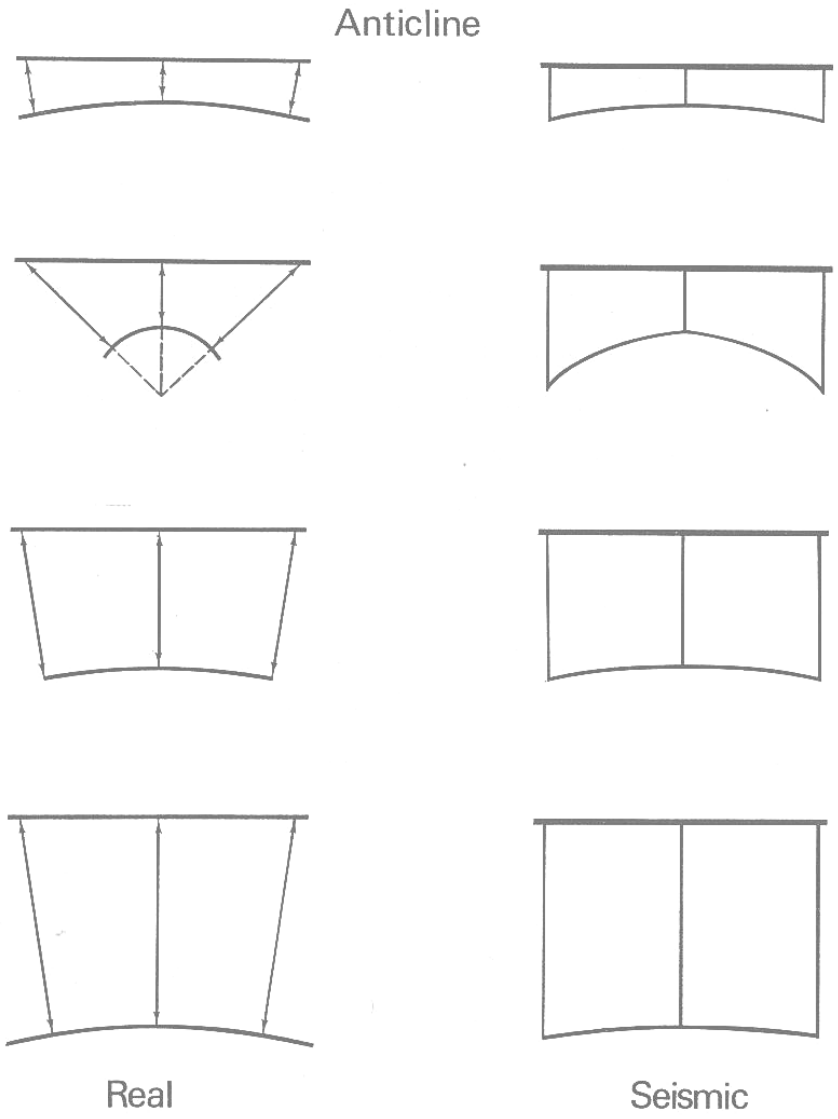
Anticline
Real
Seismic

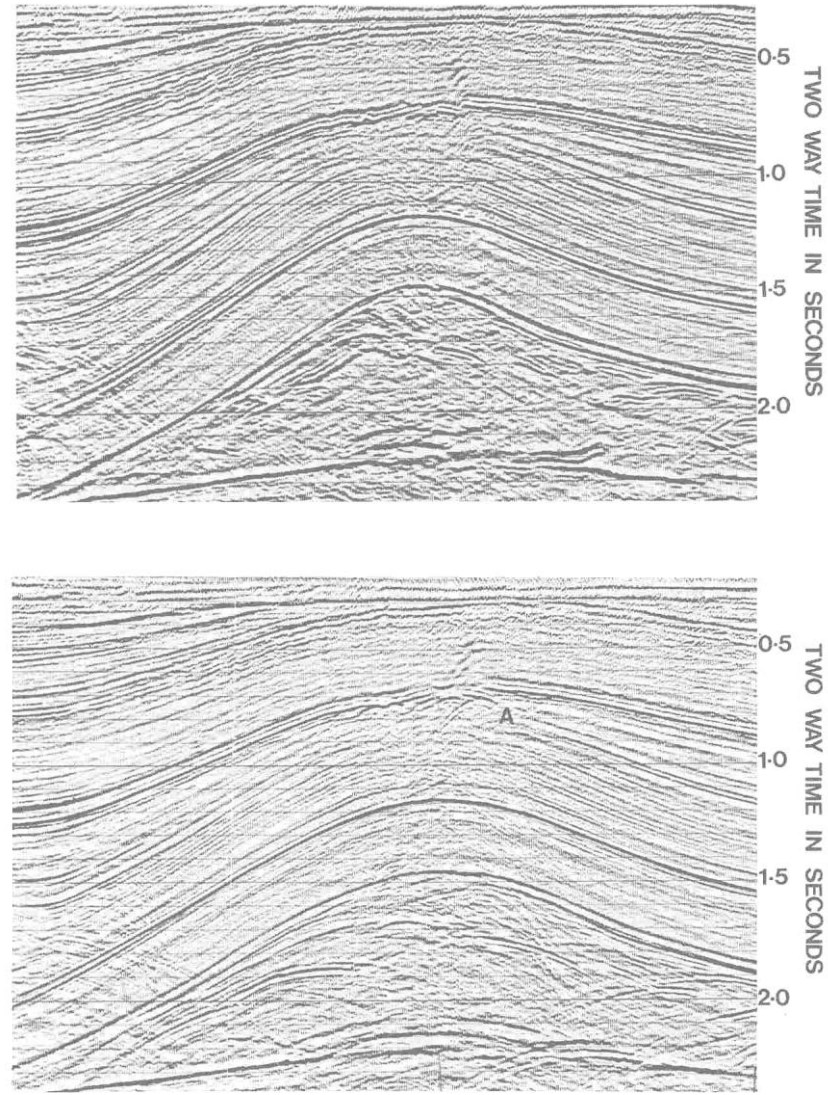
0·5
1·0
1·5
2·0
TWO WAY TIME IN SECONDS
A
0·5
1·0
1·5
2·0
TWO WAY TIME IN SECONDS

Synclines

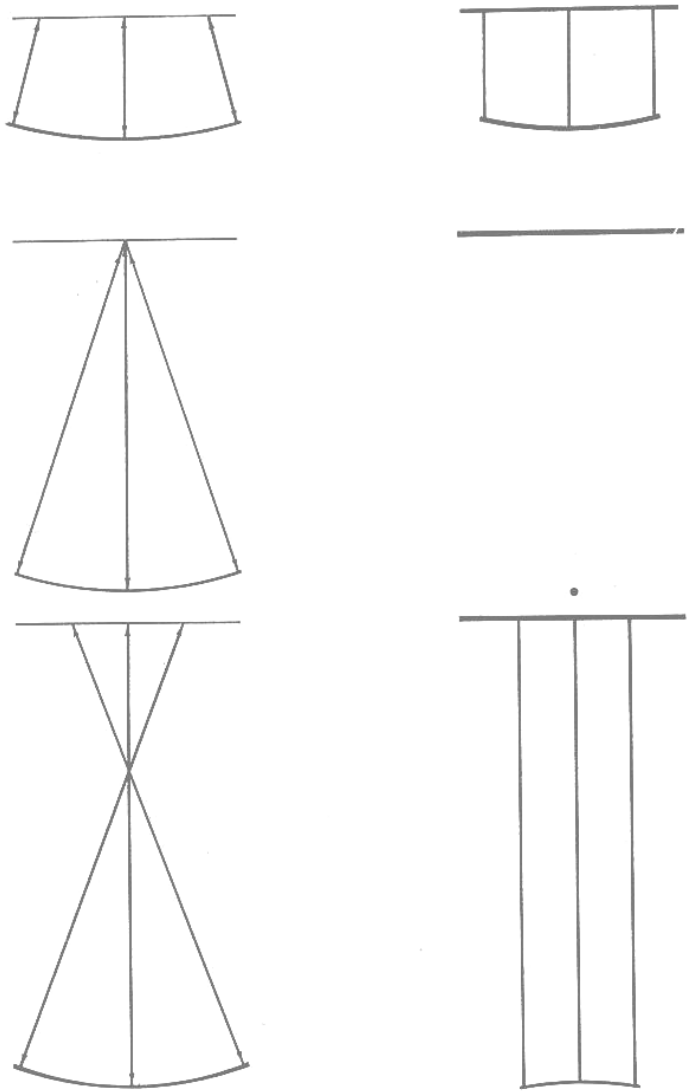

Real

Seismic

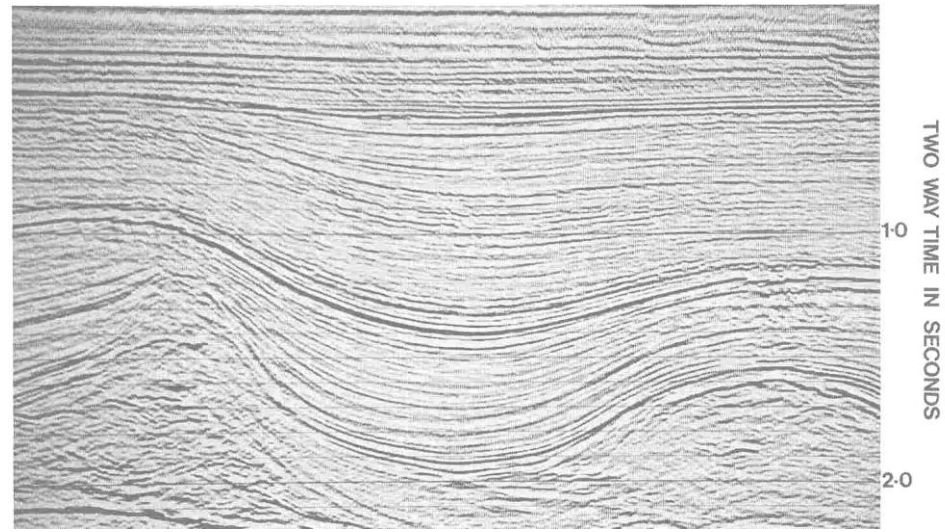

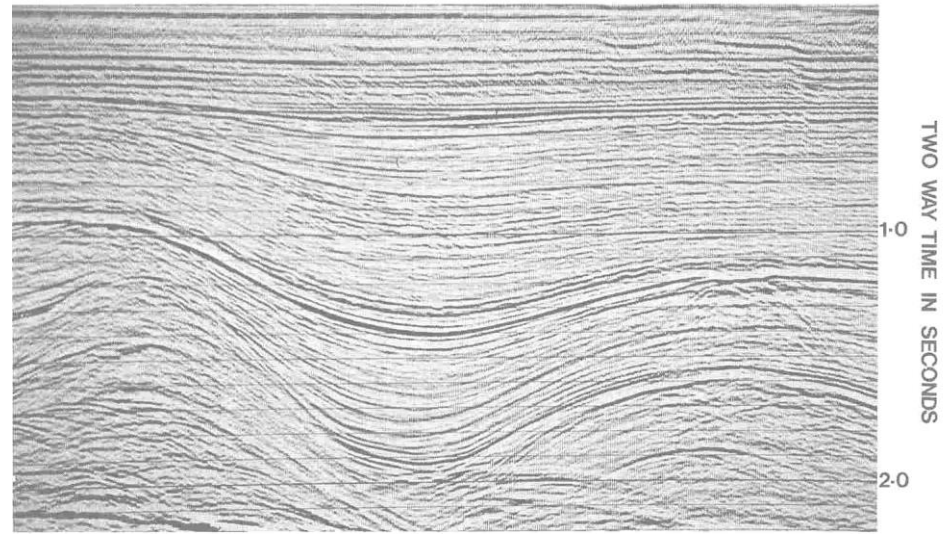

VELOCITY EFFECTS

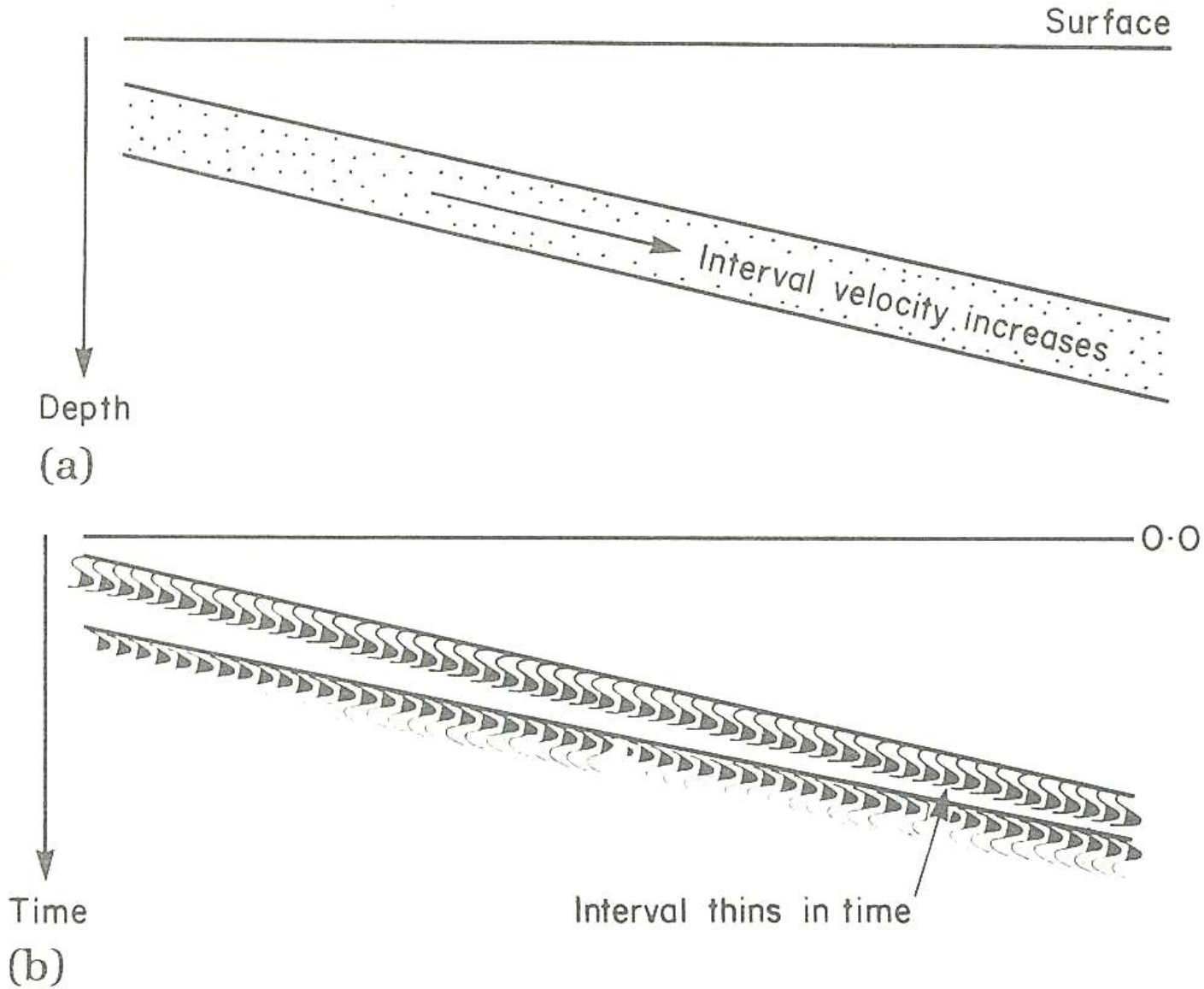
Surface
Interval velocity increases
Depth
(a)
0·0
Time
Interval thins in time
(b)

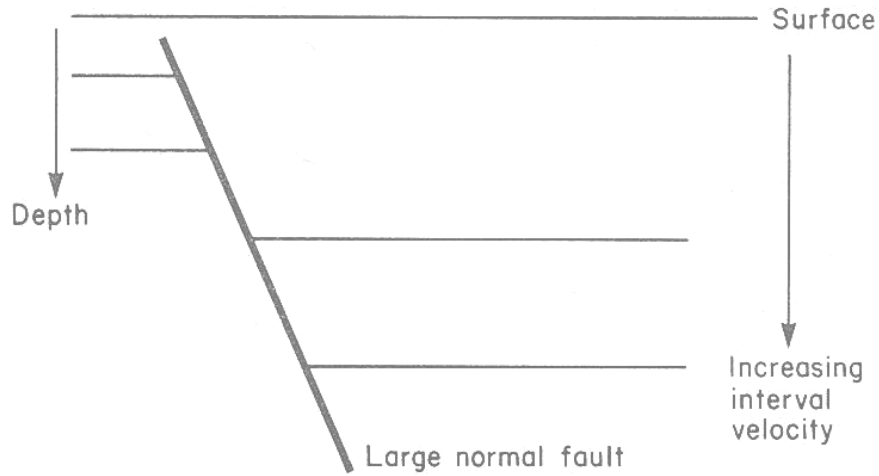
Surface
Depth
Increasing
interval
velocity
Large normal fault

(a)

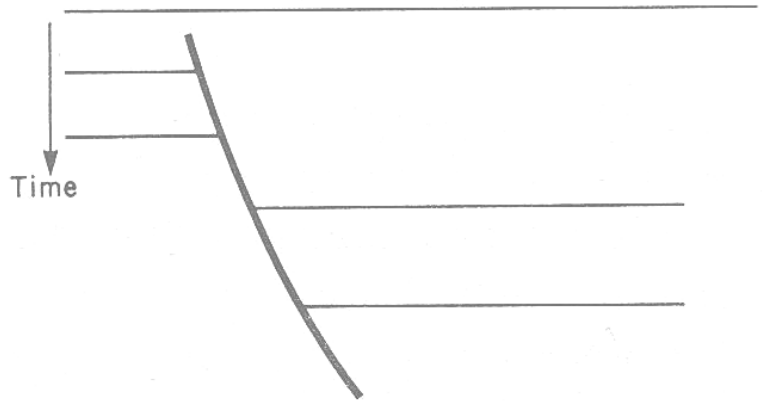
Time

(b)

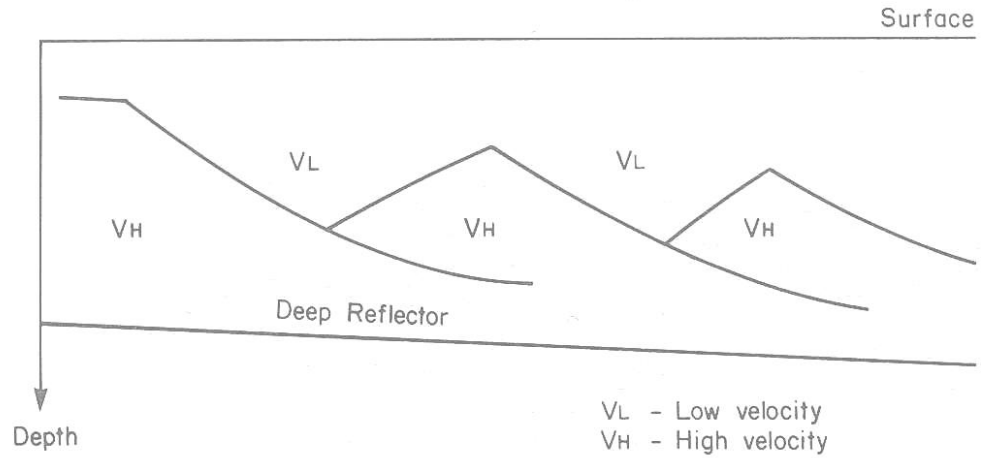
Surface
VL
VL
VH
VH
VH
Deep Reflector
Depth
VL - Low velocity
VH - High velocity

(a)

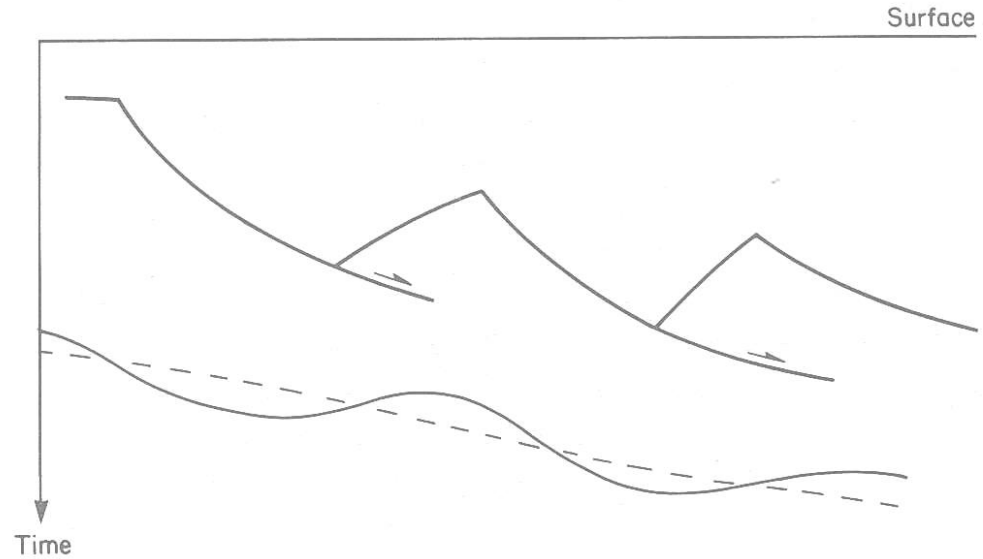
Surface
Time

(b)

MULTIPLES

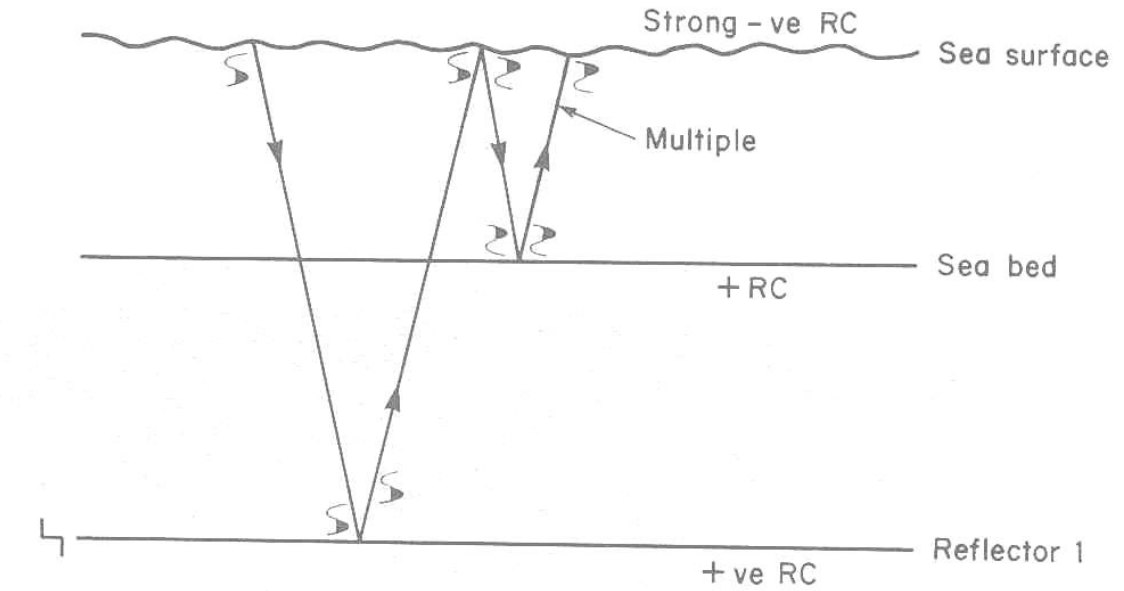
Strong – ve RC
Sea surface
Multiple
Sea bed
+ RC
Reflector 1
+ ve RC

(a)

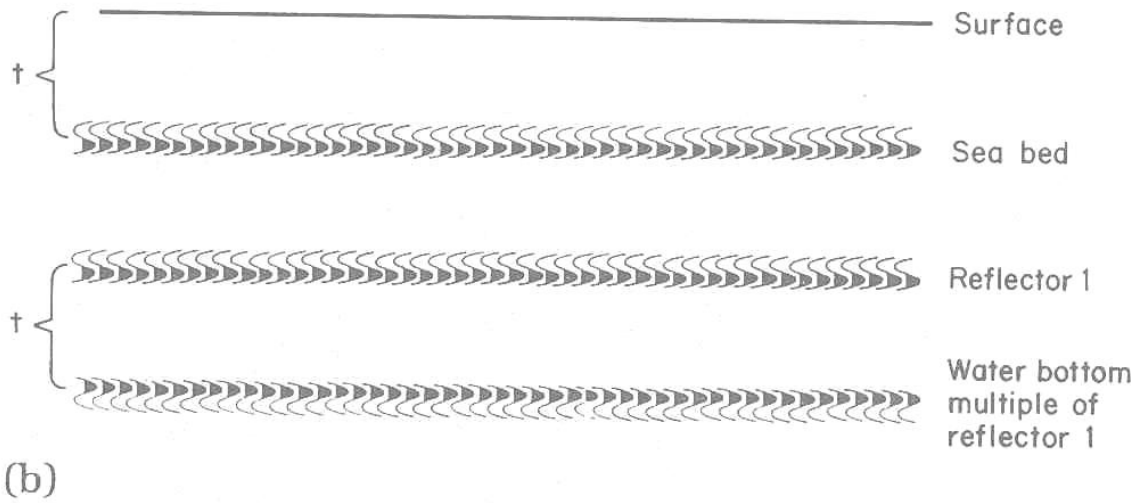
Surface
t
Sea bed
Reflector 1
t
Water bottom
multiple of
reflector 1

(b)

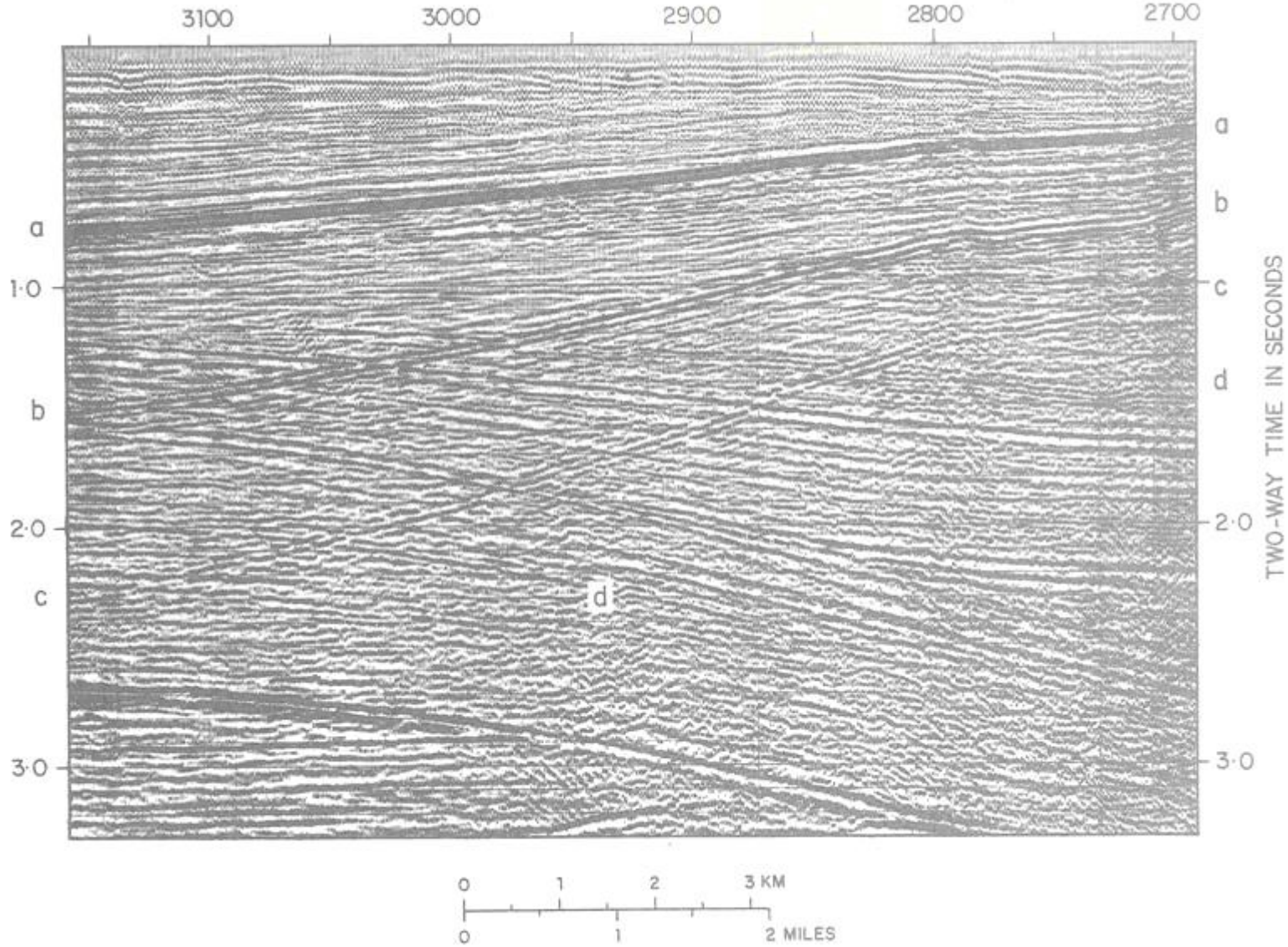
3100
3000
2900
2800
2700
a
b
c
d
1·0
2·0
3·0
TWO-WAY TIME IN SECONDS
0 1 2 3 KM
0 1 2 MILES

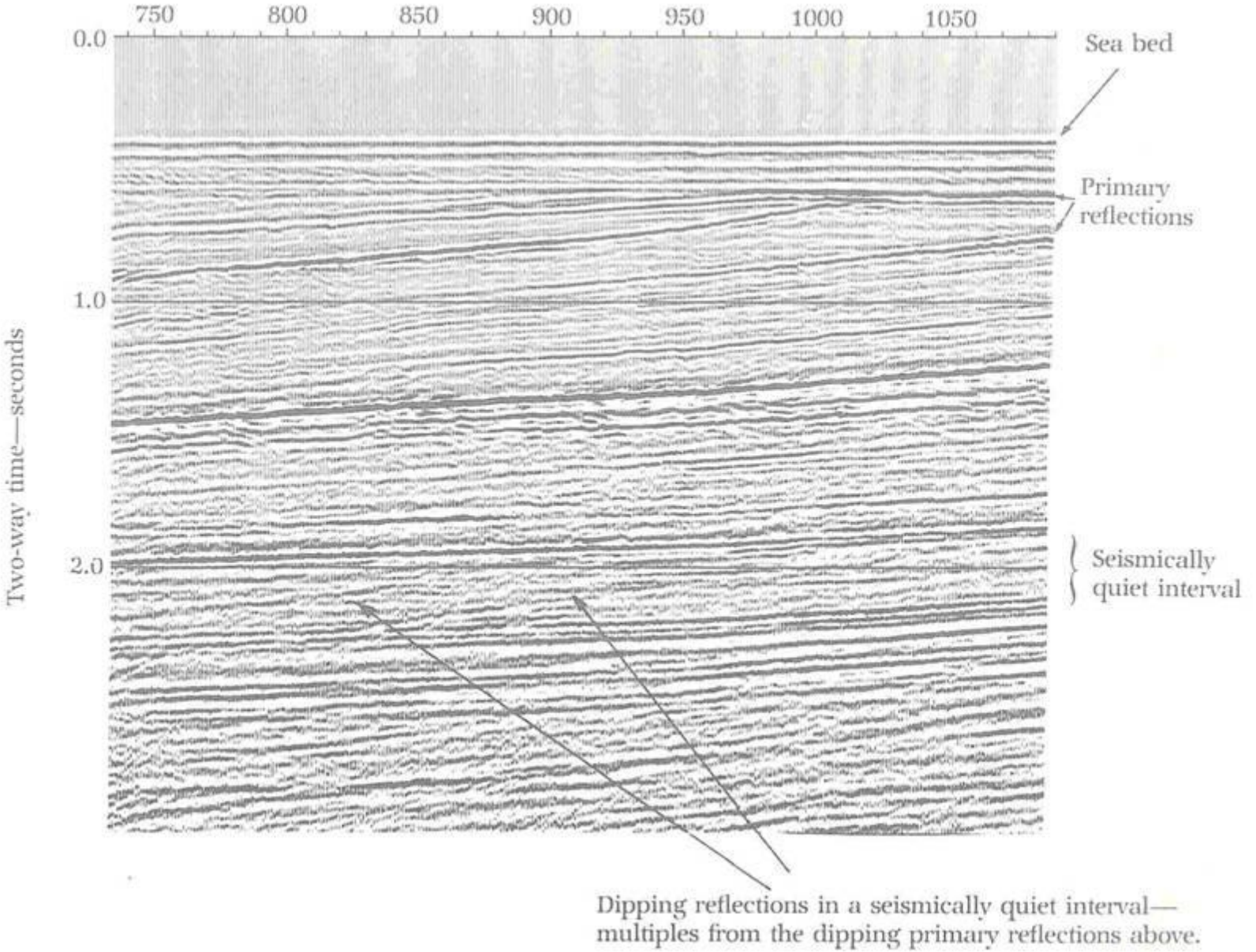
750
800
850
900
950
1000
1050
0.0
1.0
2.0
Two-way time—seconds
Sea bed
Primary reflections
Seismically quiet interval
Dipping reflections in a seismically quiet interval—multiples from the dipping primary reflections above.

Gravity survey

Seismic survey

انواع امواج الاستیک:

اگر پوسته زمین را یک محیط کاملاً الاستیک فرض کنیم (به غیر از مجاورت چشمه که تغییر پلاستیک داریم) موج صوتی عبوری ، موج الاستیک نامیده می شود.
امواج الاستیک را بر اساس نحوه ارتعاش ذرات و انتشار آنها ، طبقه بندی می کنند:

۱- موج پیکری (موج فشاری، برشی)
۲- موج سطحی (موج ریلی، لاو)

REFLECTION COEFFICIENTS

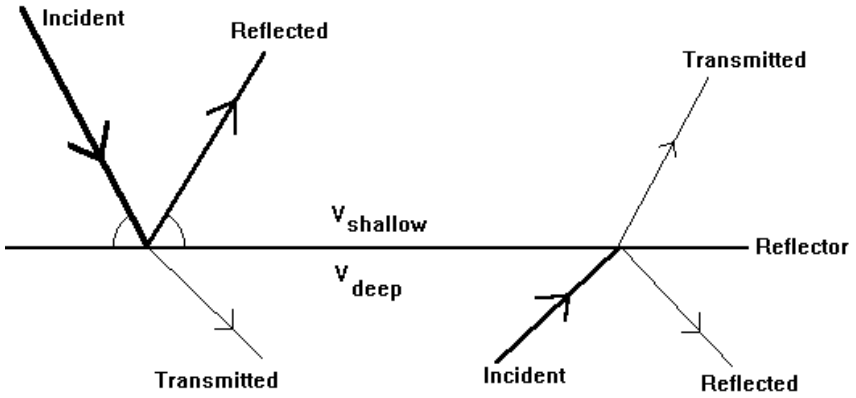

سرعت انتشار امواج به نوع لایه ها بستگی دارد.

Seismic Waves

- Body
  - P
  - S
- Surface
  - Love
  - Rayleigh

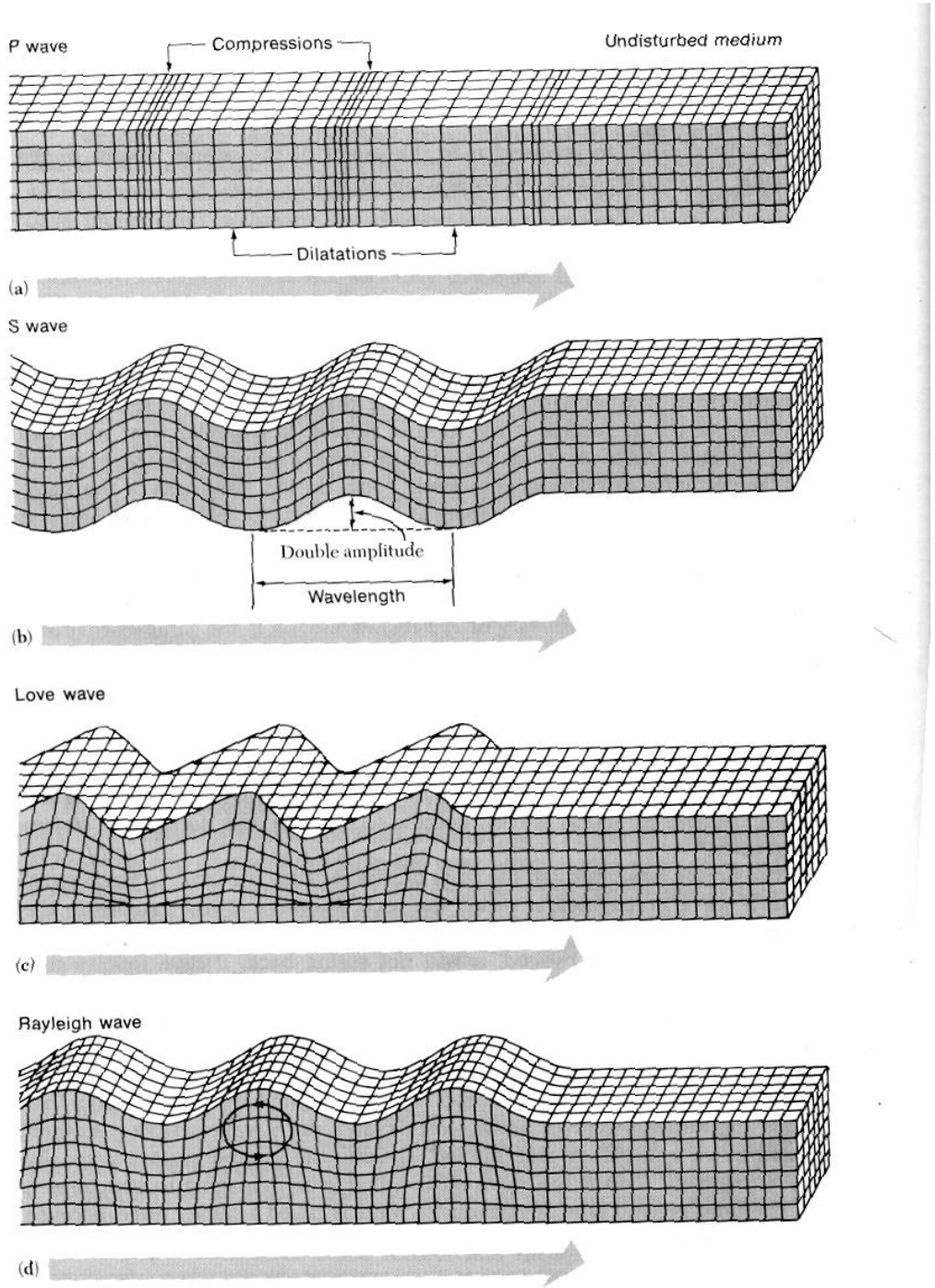

1- موج فشاری ، اولیه
(P- wave)

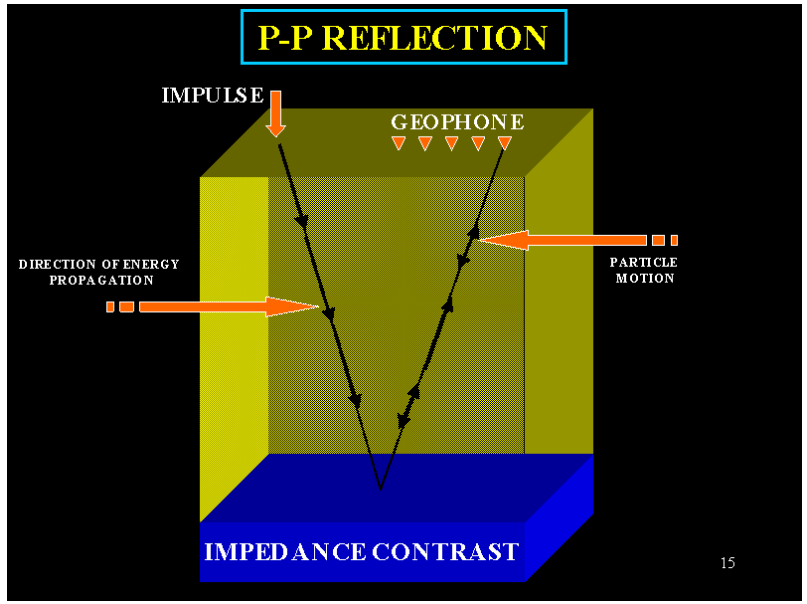

-جهت ارتعاش ذرات در این موج ، در جهت انتشار موج است.
-سرعت موج P تابعی از مدول برشی (rigidity) و چگالی محیط (density) می باشد .

-سرعت موج P در سنگهای سخت بین ۲۵۰۰ – ۷۰۰۰ متر بر ثانیه و در سنگهای نرم و متخلخل بین ۳۰۰- ۵۰۰ متر بر ثانیه است.

-در روی خشکی ، منبع انرژی (shot) باعث انتشار امواجی در هوا می شود (air wave)که به آن (air blast) گویند. این امواج می توانند جبهه موج ثانویه را در سطح لایه ایجاد کند که به آن air – coupled wave می گویند. این موج با سرعت حدود ۳۵۰ متر بر ثانیه حرکت می کند که سرعتی کمتر از موج فشاری دارد. سرعت air wave به دما و رطوبت بستگی دارد و بین ۴۰۰- ۳۰۰ متر بر ثانیه تغییر می کند.

P-Wave

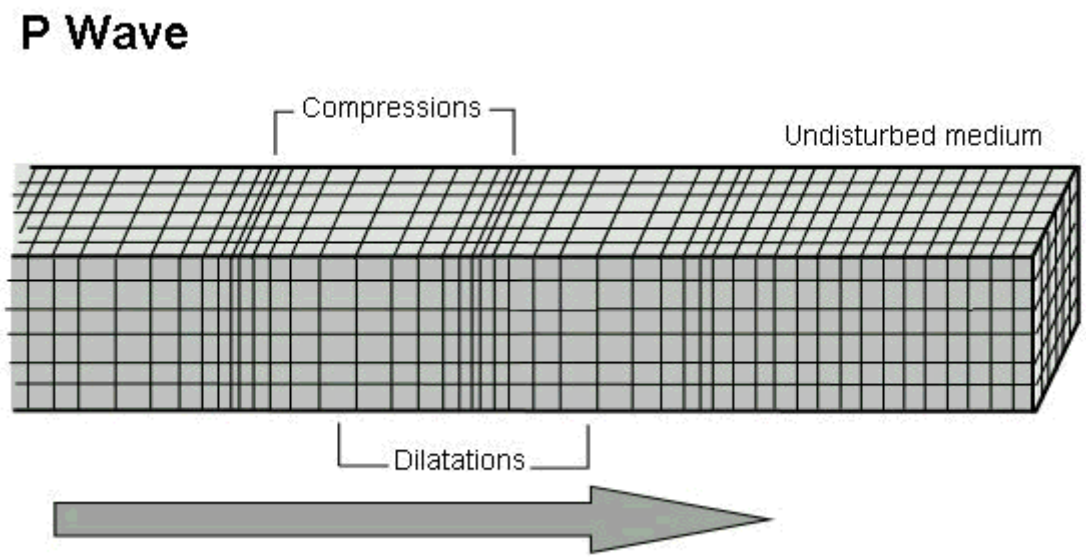

۲- موج برشی ، ثانویه
(S- wave)

-حرکت ذره برای موج برشی بر جهت انتشار آن عمود است.

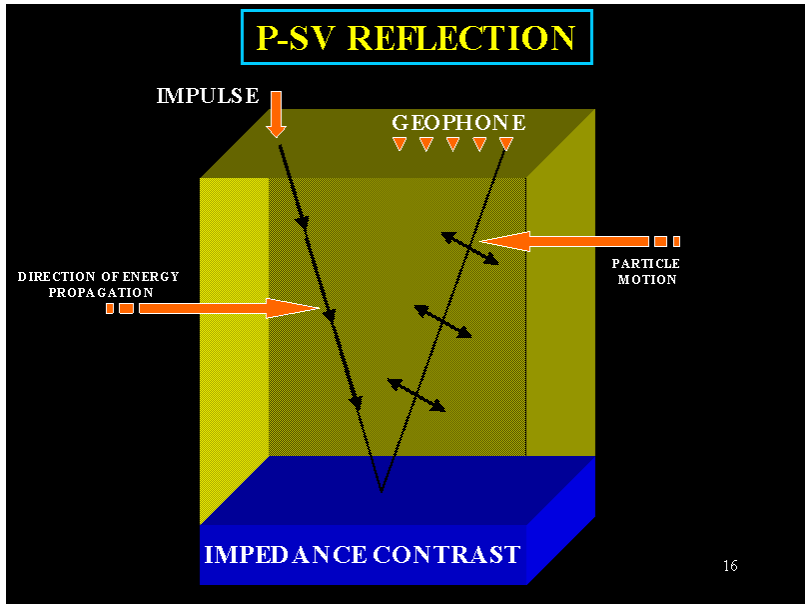

سرعت موج برشی تابعی از مقاومت محیط در برابر تنش برشی می باشد. به طور تخمینی، سرعت موج S، نصف سرعت موج P است . در سیالات مانند آب، بعلت آنکه تنش وکرنش برشی وجود ندارد، موج S نمی تواند منتشر شود.
به همین علت رکوردهای دریایی ، نسبت S/N بالاتری نسبت به داده های خشکی دارند.
بخشی از این مسئله مربوط به آن است که موج S نمی تواند در آب تولید شود و توسط گیرنده ها دریافت شود و تمام رسیدها مربوط به موج فشاری می باشد. رکوردهای خشکی معمولاً تلفیقی از امواج فشاری و برشی هستند. سرعت موج برشی می تواند در اثر لایه بندی و شکستگی تغییر کند. مثلاً برای سنگ لایه بندی شده که شکستگی های آن با سیال پر شده است ، مقاومت در برابر نیروی برشی بیشتر شده (نسبت به سنگ هموژن) به عبارت دیگر شکستگی ها درجه حرکت برشی ذرات را محدود می کنند.

S-Wave

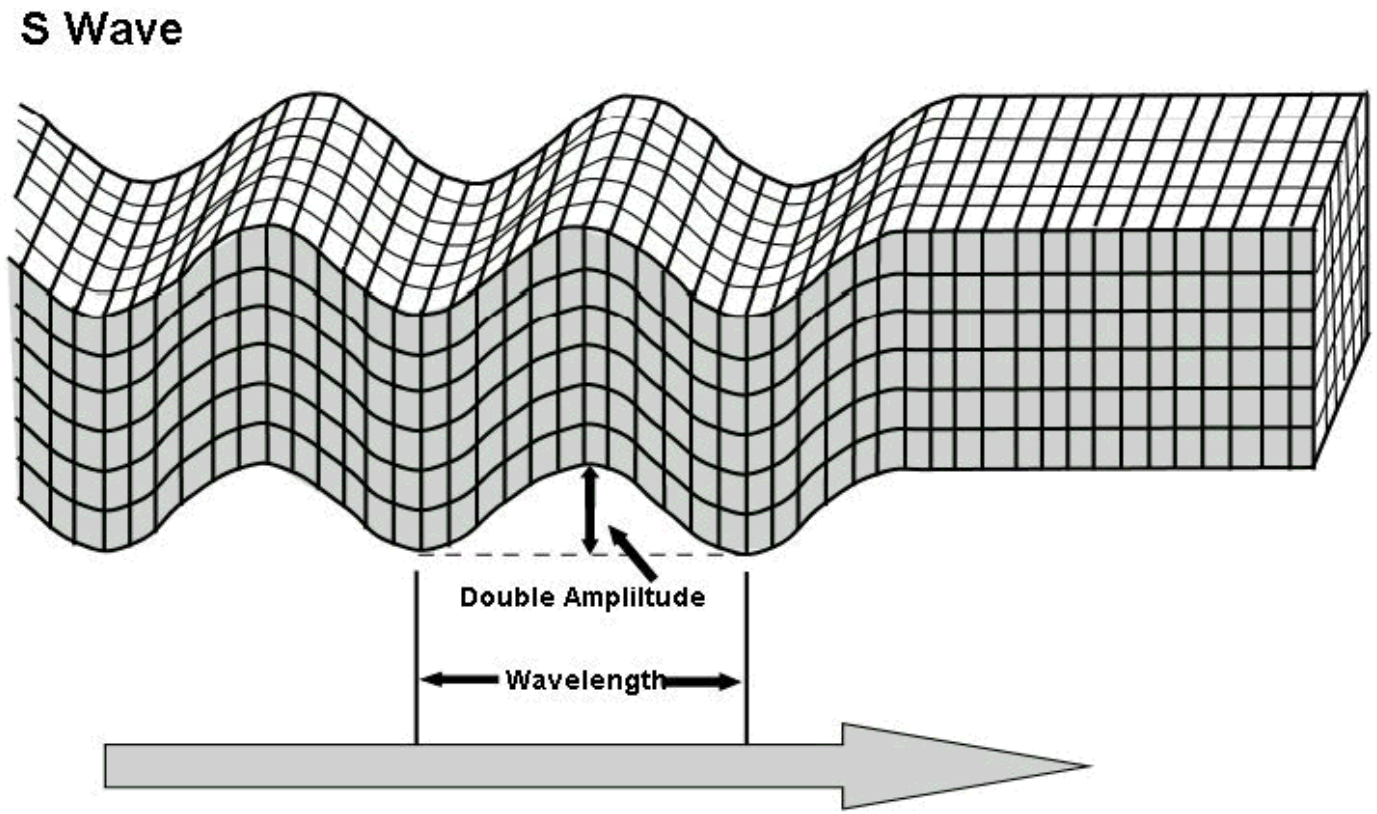

Soil Properties from Wave Velocity

- Shear Modulus $G = \rho . V_s^2$

  ρ: Density of soil

- Constrained Modulus, $M = \rho . V_p^2$

- Young's Modulus, $E = \dfrac{\rho V_s^2 \left(3V_p^2 - 4V_s^2\right)}{V_p^2 - V_s^2}$

- Poisson's Ratio, $\nu = \dfrac{V_p^2 - 2V_s^2}{2\left(V_p^2 - V_s^2\right)}$

Seismic Wave Speeds

Material	P wave Velocity (m/s)	S wave Velocity (m/s)
Air	332	
Water	1400-1500	
Petroleum	1300-1400	
Steel	6100	3500
Concrete	3600	2000
Granite	5500-5900	2800-3000
Basalt	6400	3200
Sandstone	1400-4300	700-2800
Limestone	5900-6100	2800-3000
Sand (Unsaturated)	200-1000	80-400
Sand (Saturated)	800-2200	320-880
Clay	1000-2500	400-1000
Glacial Till (Saturated)	1500-2500	600-1000

Wave Velocities in Geomaterials

Material	Velocity (ft/sec)	
	Compression Waves	Shear Waves
ROCK		
Agglomerate	5 000–6 000	—
Anhydrite, gypsum	11 500–21 400	—
Basalt		
Sound	18 300–21 100	10 500
Weathered and fractured	9 000–14 000	—
Chalk		
Above groundwater	6 000–13 000	—
Below groundwater	8 000	—
Conglomerate	7 920–8 000	—
Diabase	19 700	—
Diorite	19 100	10 100
Dolomite	10 700–20 200	—
Dunite	24 400–28 400	12 500–14 400
Gabbro	21 300	11 200
Granite		
Sound	13 100–20 000	6 900–10 800
Highly weathered	10 500	—
Decomposed	1 540–2 200	—
Granodiorite	15 000–15 800	10 200
Greenstone	13 300–16 100	—
Limestone		
Hard	16 400–20 200	9 500–10 700
Soft	5 600–13 900	—
Salt	14 400–21 400	—
Phyllite	10 000–11 000	—
Sandstone	4 620–14 200	—
Shale		
Hard	9 000–15 400	—
Soft or weathered	2 600–8 000	—

Material	Velocity (ft/sec)	
	Compression Waves	Shear Waves
SOIL		
Alluvium	1 640–6 600	—
Clay	3 000–9 200	—
Glacial deposits		
Moraine		
Dry	2 500–5 000	—
Saturated	5 000–7 000	—
Till	5 600–7 400	—
Gravel	1 500–3 000	—
Sand	4 600–8 400	—
Sand, cemented	2 800–3 200	—
Sand, loose	5 940	1 650
Talus, loose rock	1 250–2 500	—
Top soil		
Dry	600–900	—
Wet	1 000–2 500	—
OTHER		
Ice	12 050	—
Water, fresh	4 700–5 500	—
Water, salt	4 800–5 000	—

Sources: Clark (1966); Dobrin (1976); Jakosky (1950); U.S. Army Corps of Engineers (1979).

موج سطحی Surface wave :

در روی خشکی ، سنگهای سطحی هوازده شده و به صورت یک لایه هوازده (weathering layer) یا لایه کم سرعت LVL در می آید. بدان علت است که موج P با سرعت پائین در آن منتشر می شود. همچنین موج سطحی از مرز بین هوا و زمین عبور می کند.
با رفتن به عمق ارتعاش ذرات امواج سطحی با دامنه کاهش یافته و جهت نوسان آن نیز معکوس می شود.

L-Wave

- **Love Waves**
- The first kind of surface wave is called a **Love wave**, named after A.E.H. Love, a British mathematician who worked out the mathematical model for this kind of wave in 1911.
- It's the fastest surface wave and moves the ground from side-to-side.

L-Wave

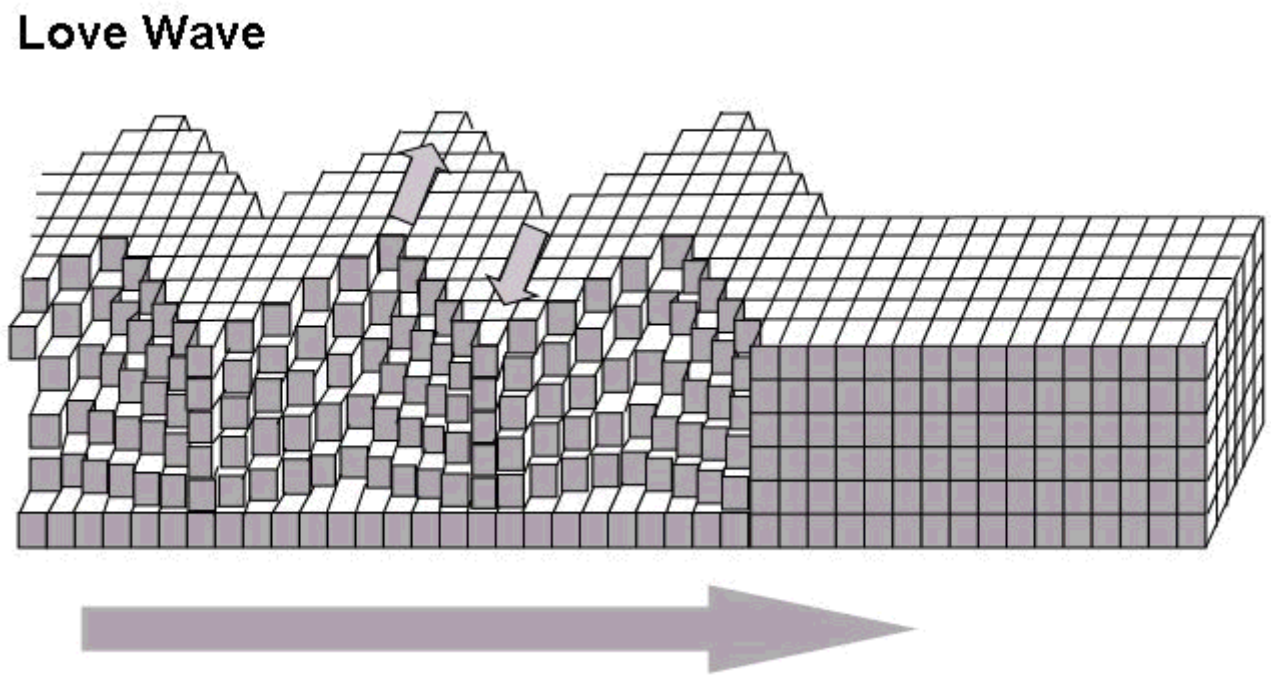

Rayleigh Waves

- **Rayleigh Waves**
- The other kind of surface wave is the **Rayleigh wave**, named for John William Strutt, Lord Rayleigh, who mathematically predicted the existence of this kind of wave in 1885.
- A Rayleigh wave rolls along the ground just like a wave rolls across a lake or an ocean. Because it rolls, it moves the ground up and down, and side-to-side in the same direction that the wave is moving.
- Most of the shaking felt from an earthquake is due to the Rayleigh wave, which can be much larger than the other waves.

Rayleigh Waves

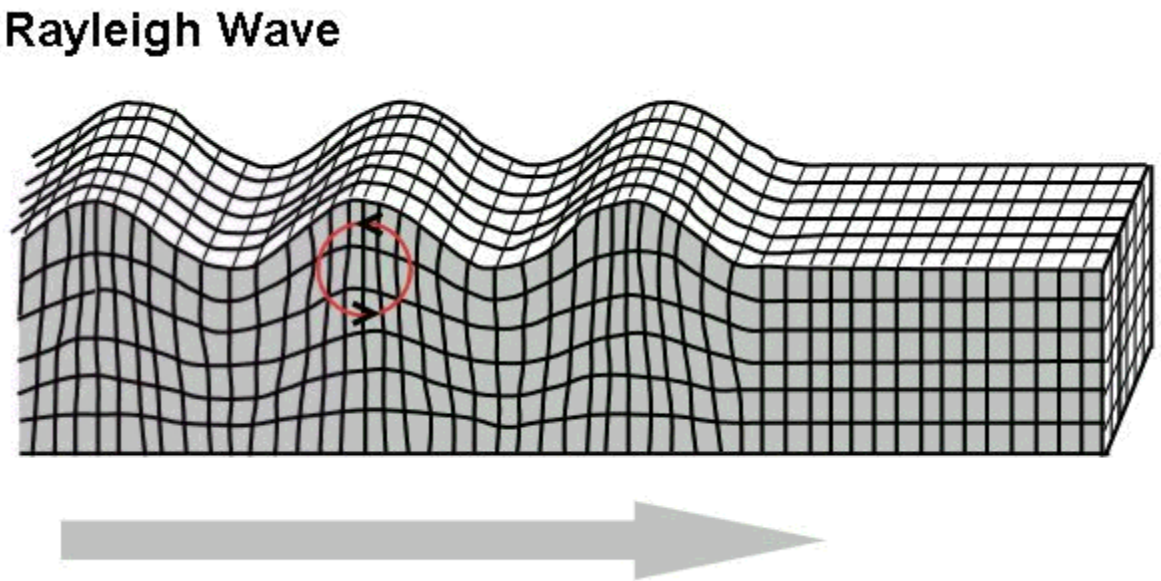

GROUND-ROLL

1. SURFACE WAVES $(0 < V_{Ray1} < \beta)$
2. AIR WAVES (Land case)

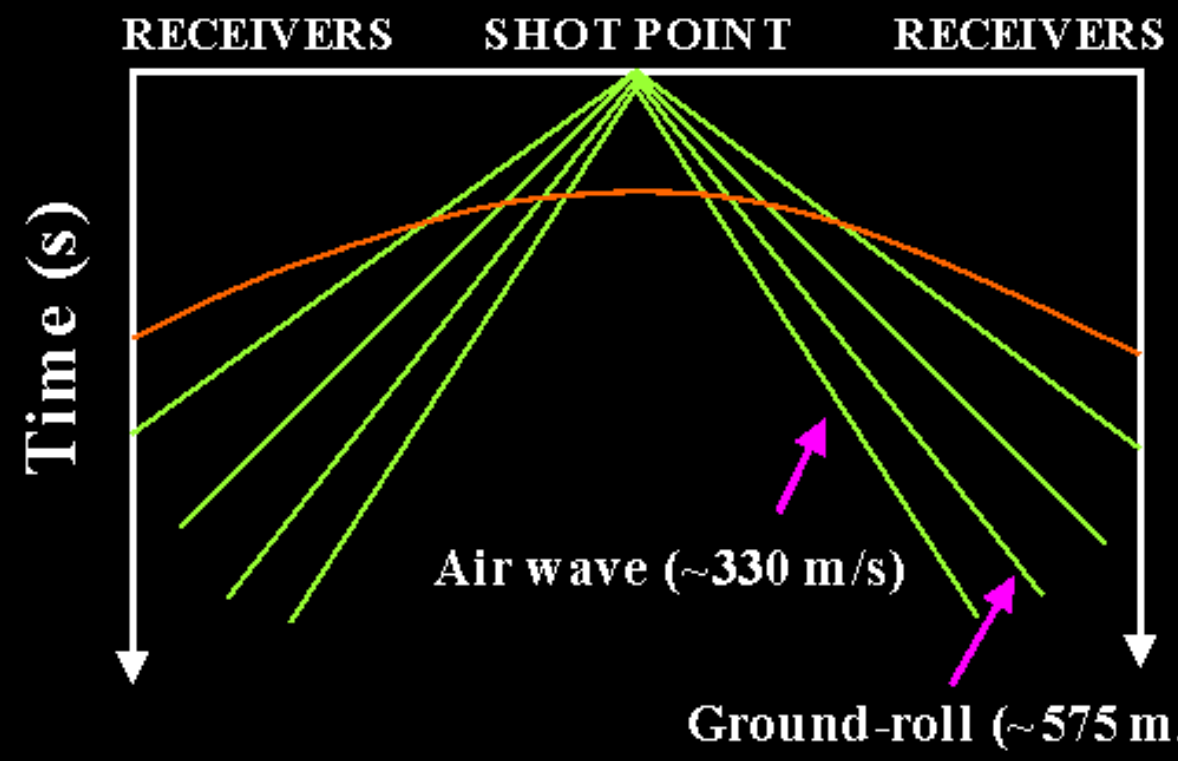

99

Snell's Law

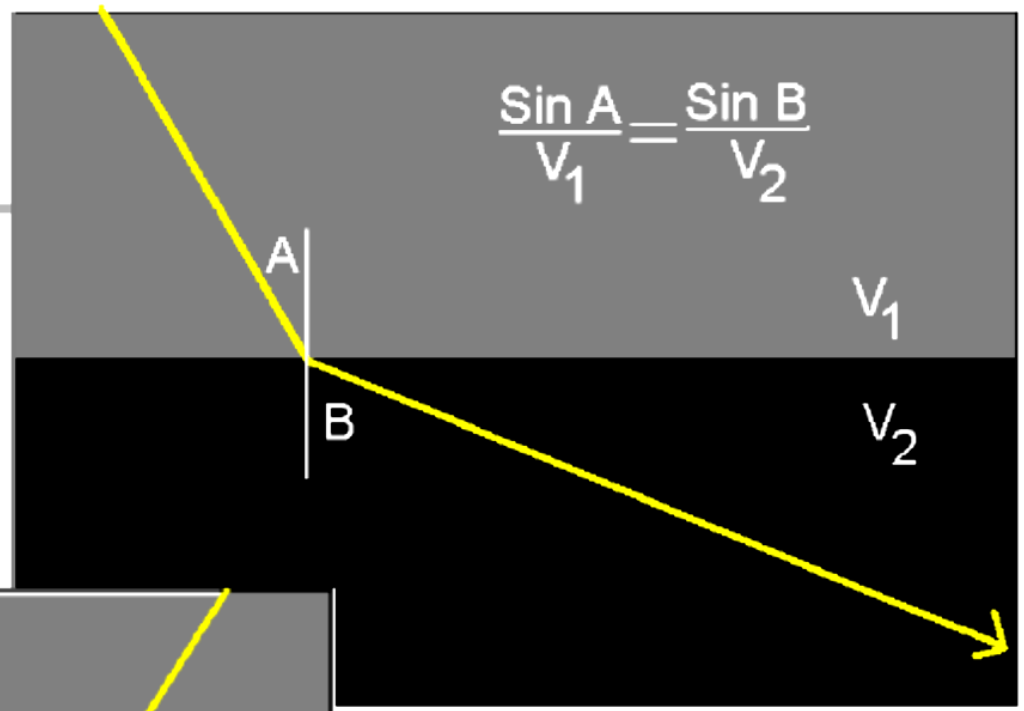

Critical Angle of Refraction

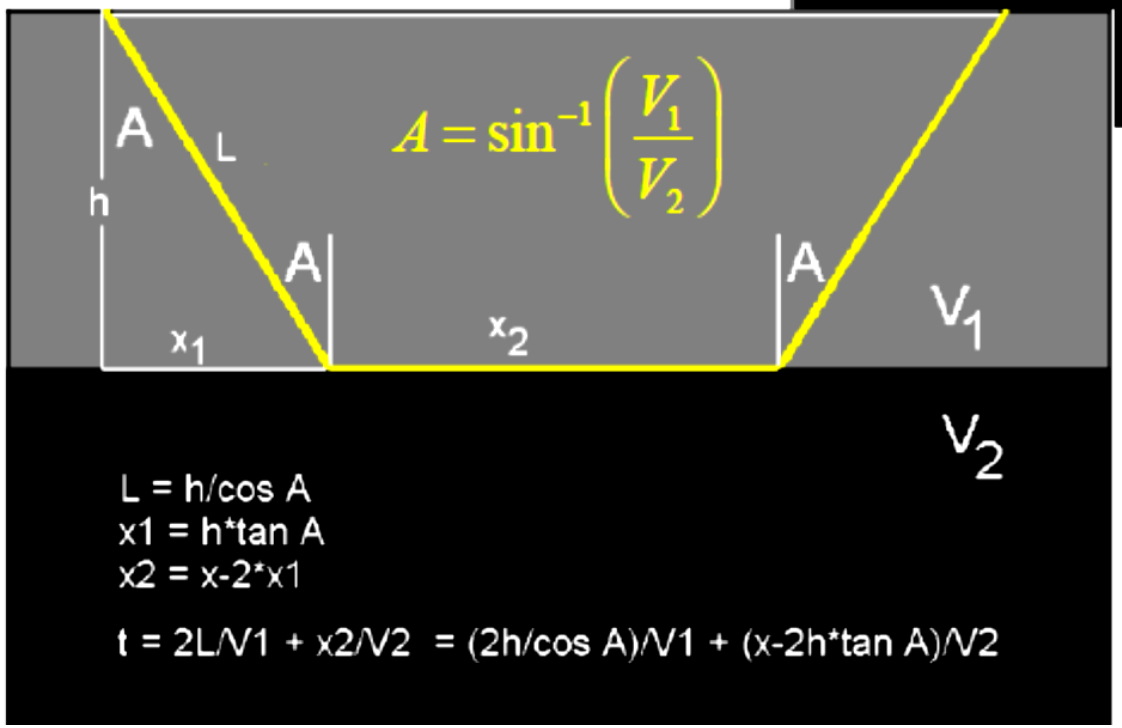

L = h/cos A
x1 = h*tan A
x2 = x-2*x1

t = 2L/V1 + x2/V2 = (2h/cos A)/V1 + (x-2h*tan A)/V2

21

تبدیل امواج :

در مرز لایه ها ، بخشی از موج بازتاب شده و بخشی عبور می کند. بر اساس خواص الاستیک مرز لایه بندی، موج P یا موج S می توانند به یکدیگر تبدیل شوند یا به امواج دیگر.

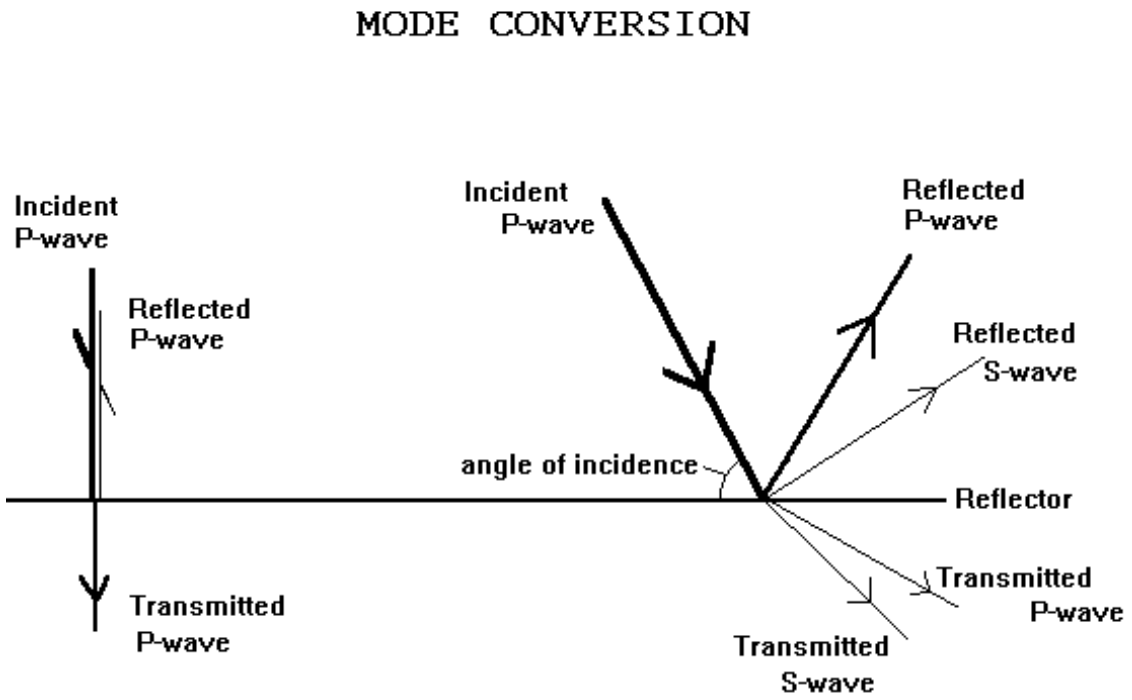

کاهش انرژی لرزه ای :

دامنه موج به صورت عکس فاصله از چشمه ، کاهش پیدا می کند.

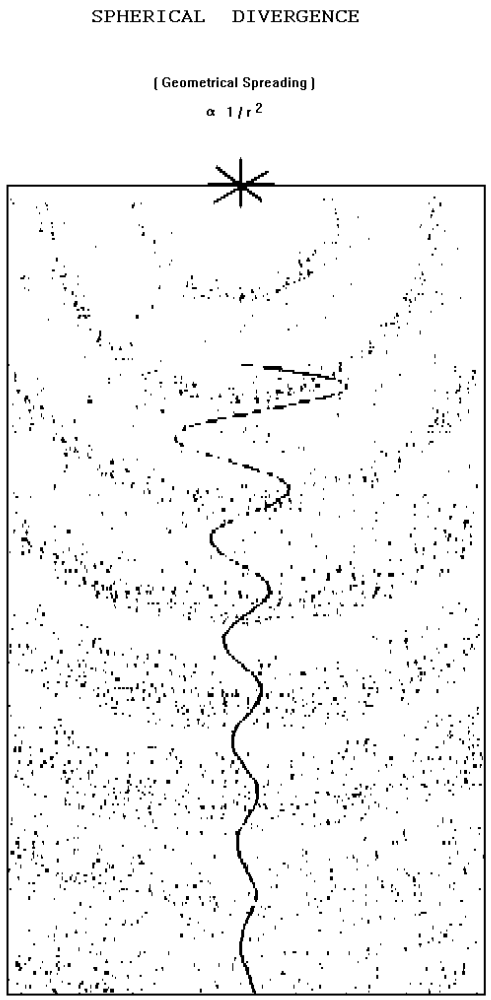

دسته بندی امواج لرزه ای:

- DIRECT
- REFLECTED, DIFFRACTED WAVES
- REFRACTED

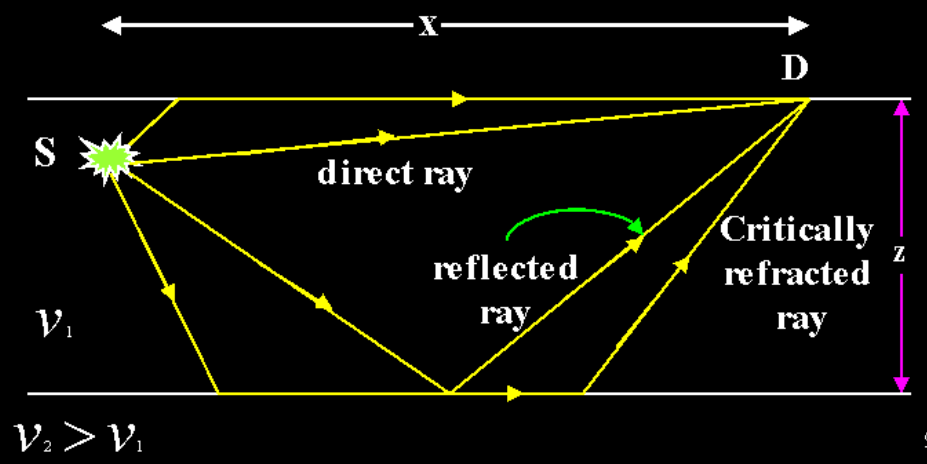

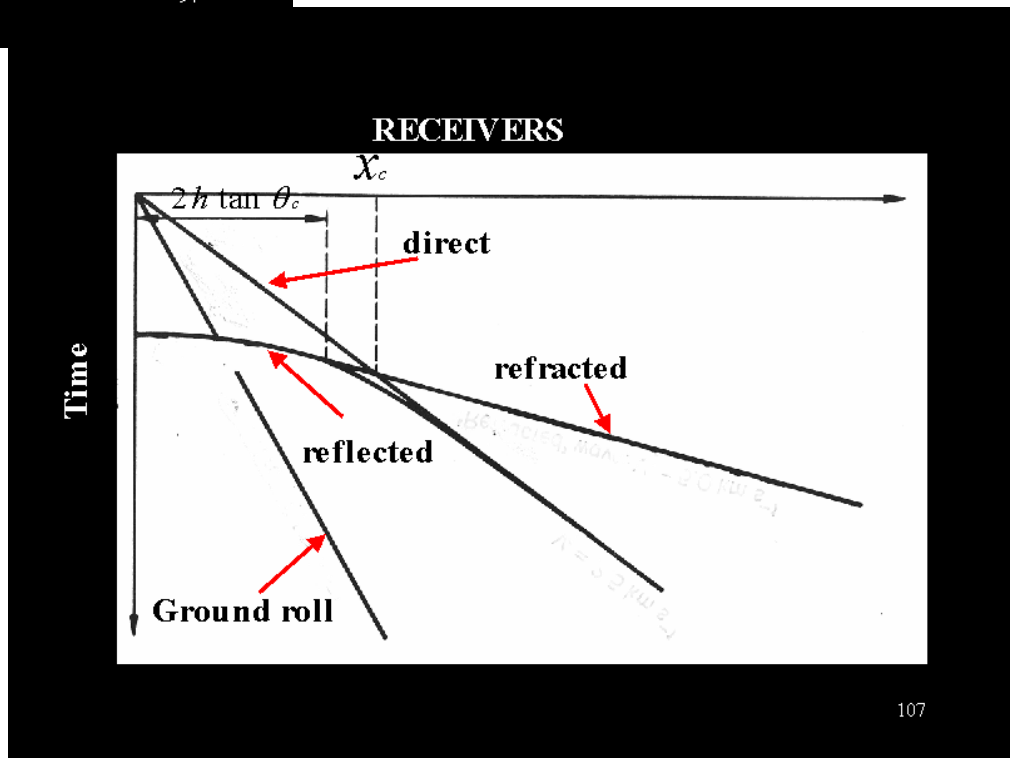

Seismic Methods

- Seismic Reflection Method
- Seismic Refraction Method
- Cross-Hole Test
- Down Hole Test & Up-Hole Test
- Spectral Analysis of Surface Wave (SASW)

Seismic Refraction Method

Depths less than ~ 30 m

Cost Effective as compared to Reflection method (<3to5 times)

Used for computation of layer thickness of soil

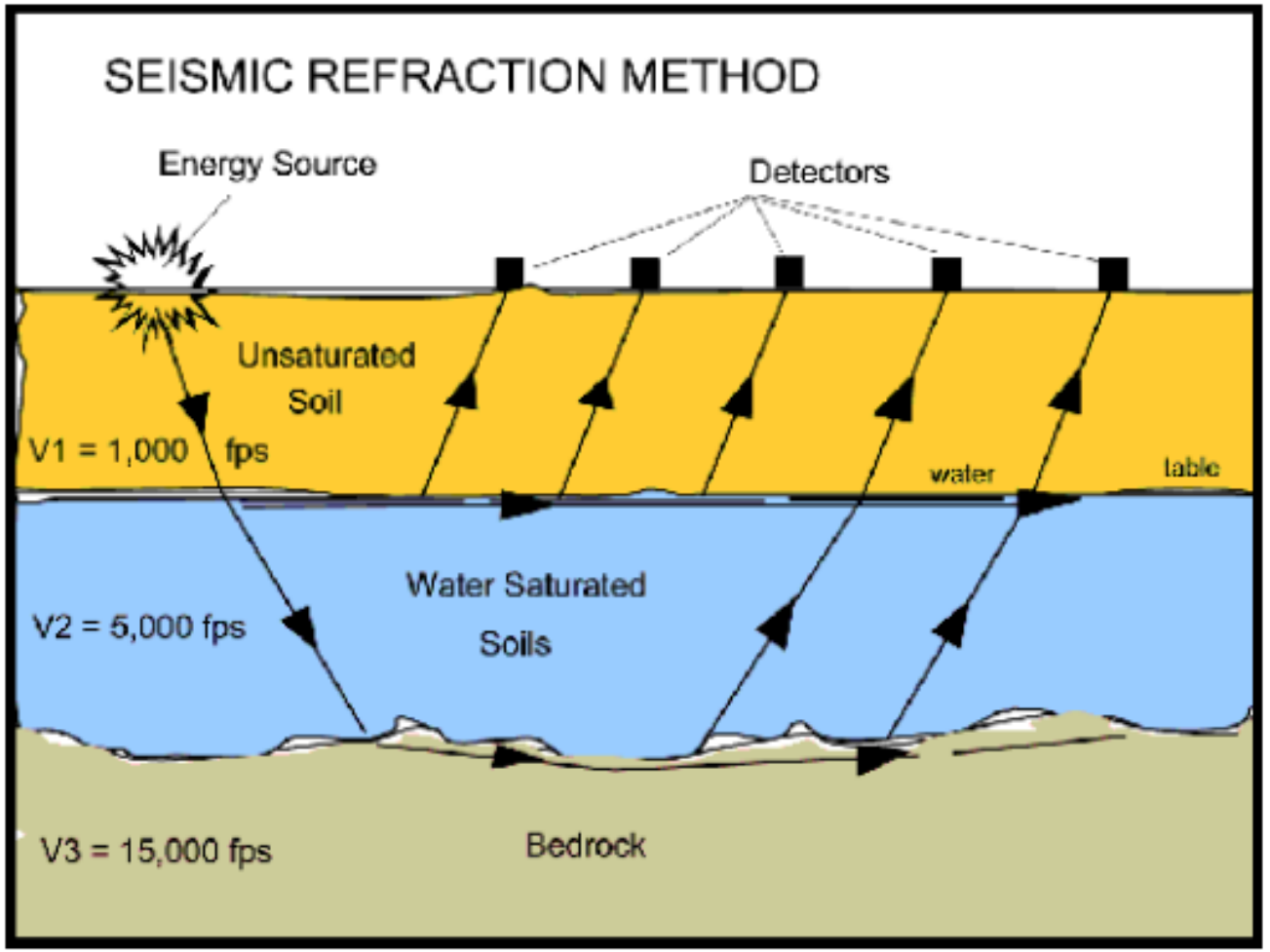

Seismic Reflection Method

Depths greater than ~15 m

Particularly suited to marine applications (e.g. lakes, rivers, oceans, etc.)

The inability of water to transmit shear waves makes collection of high quality reflection data possible even at very shallow depths that would be impractical to impossible on land.

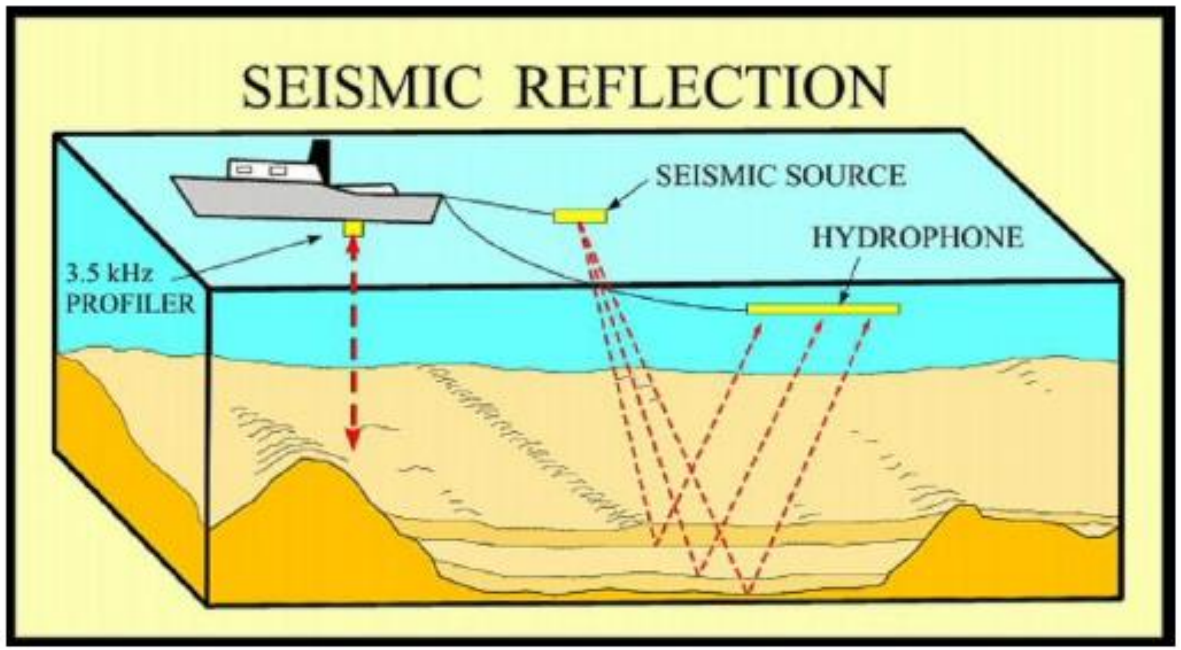

28

Differences in *Seismic Reflection* and *Seismic Refraction* Method

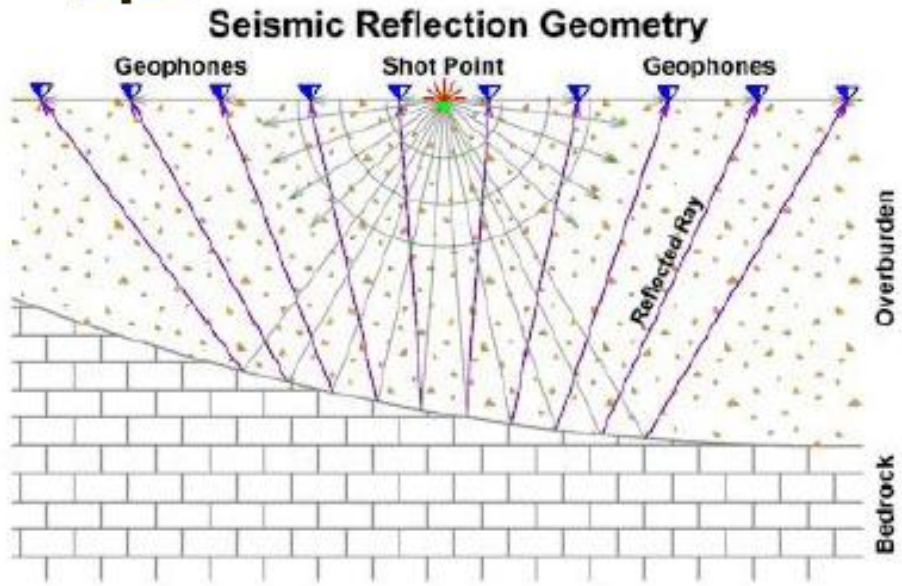

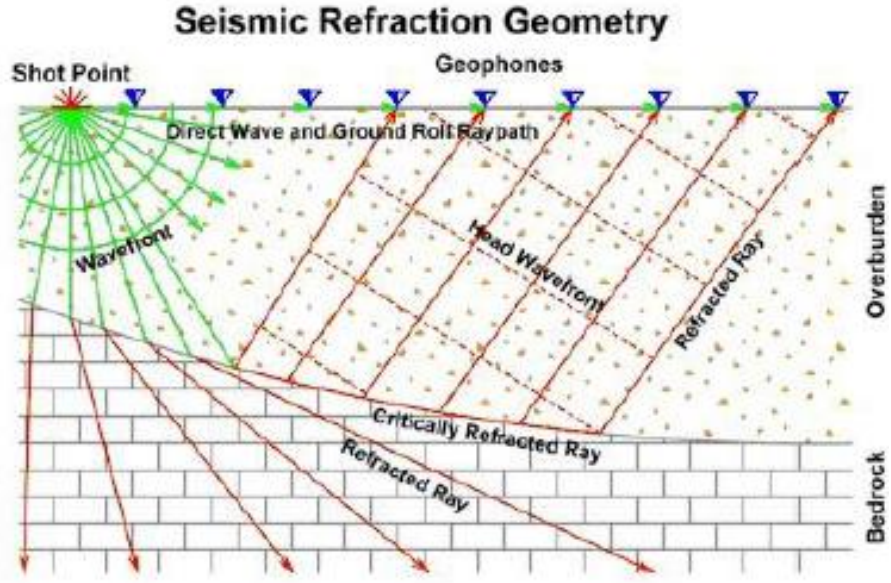

Seismic Reflection uses field equipment similar to seismic refraction, but field and data processing procedures are employed to maximize the energy reflected along near vertical ray paths by subsurface density contrasts.

Seismic Refraction involves measuring the travel time of the component of seismic energy which travels down to the top of rock (or other distinct density contrast), is refracted along the top of rock, and returns to the surface.

Cross-Hole Test

Sensors are placed at one elevation in one or more boring. Source is triggered in another boring at the same elevation.

S wave travels horizontally from source to receiving hole, and the arrivals of S waves are noted

Shear wave velocity (Vs) is calculated by dividing the distance between the bore holes and the travel time.

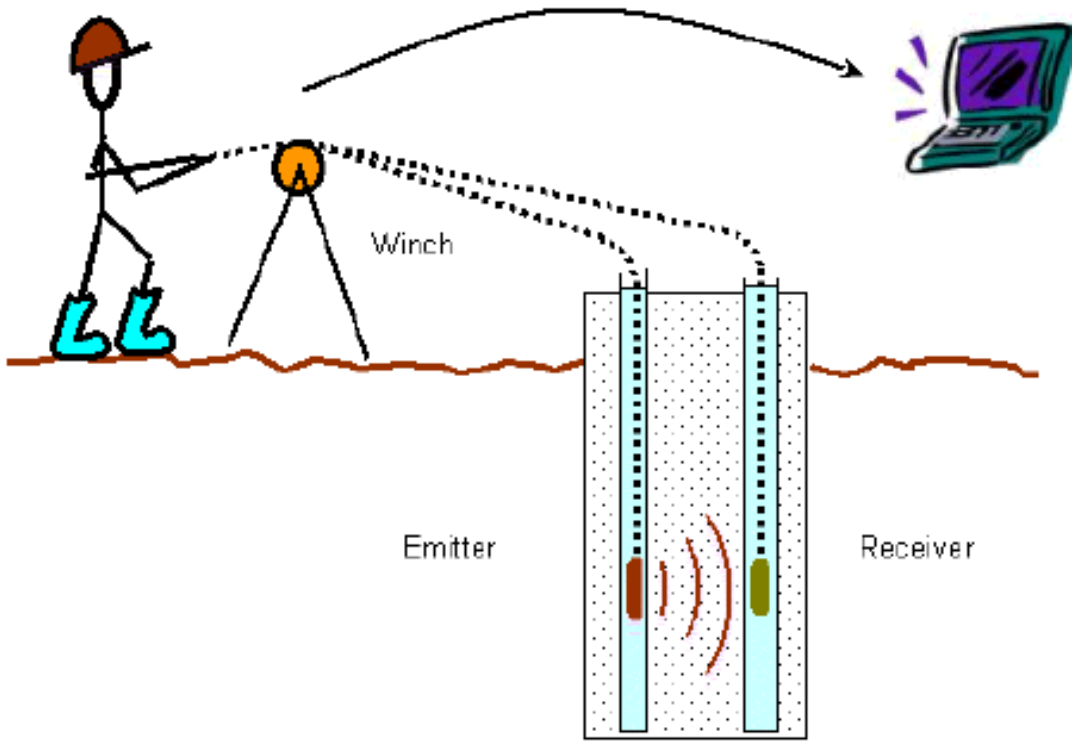

Cross-Hole Test

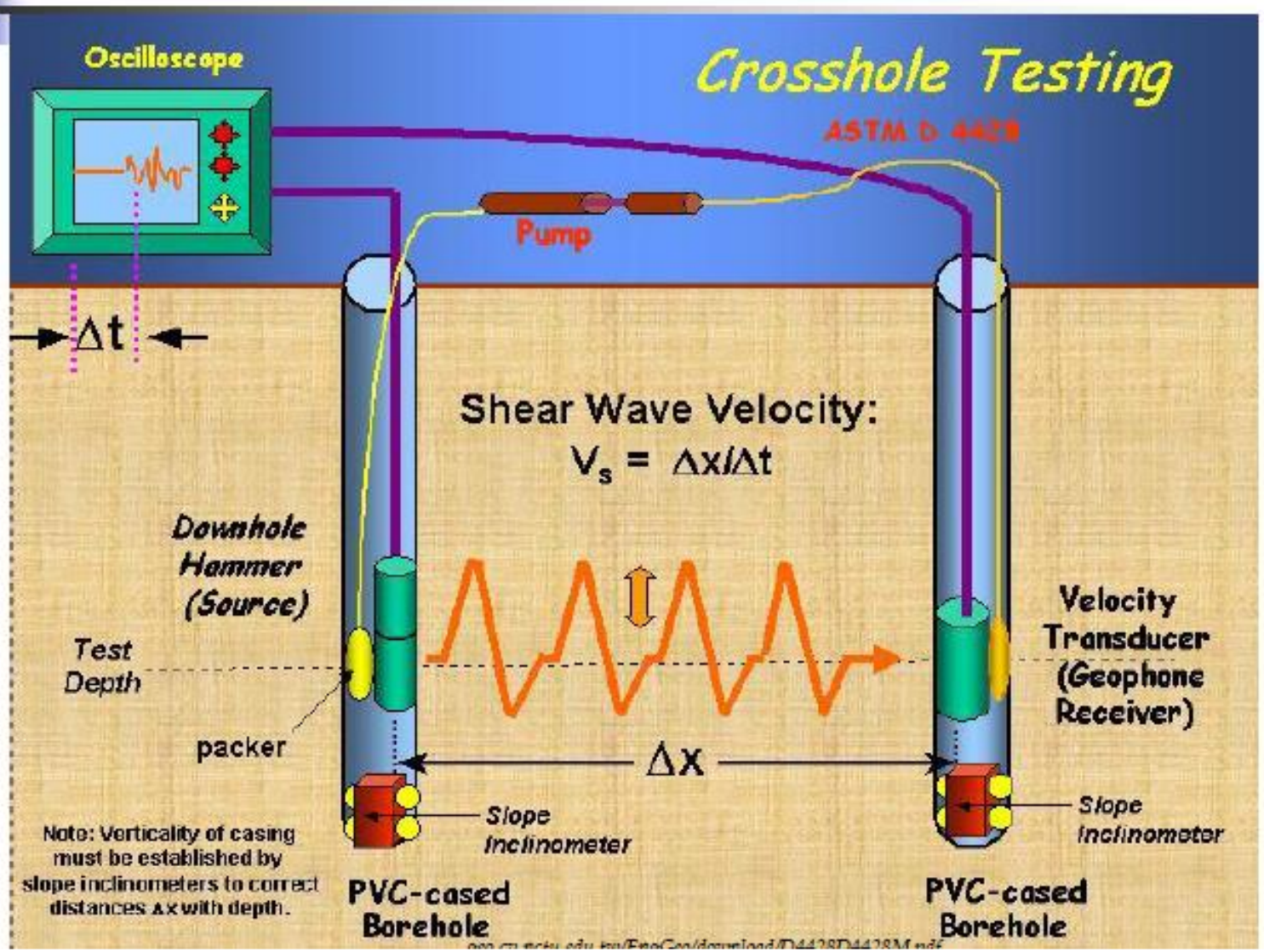

Cross-Hole Record

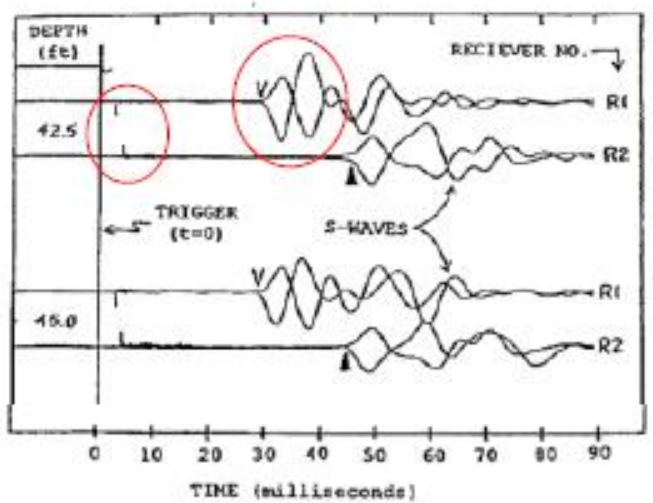

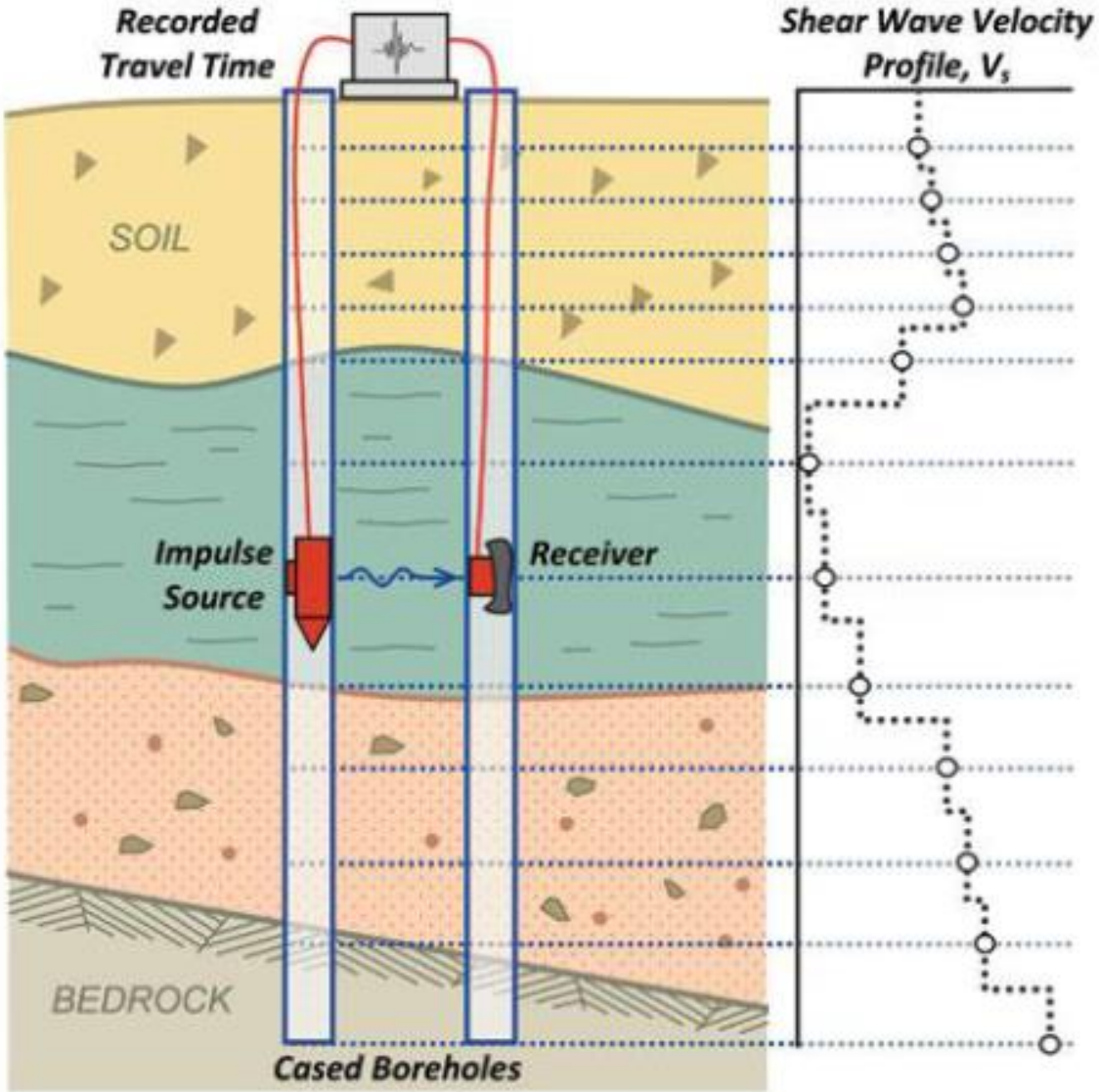

http://www.structuremag.org/article.aspx?articleID=994

Down Hole Test

Sensors are placed at **various depths in the boring**. Source is located above the receivers, at the ground surface.

Only one bore hole is required.

A source rich in S wave should be used (P wave travels faster than S wave)

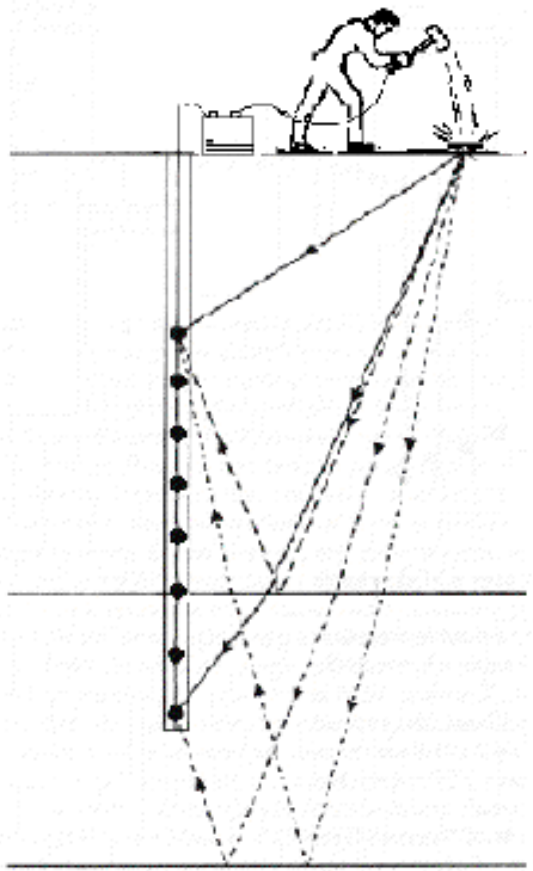

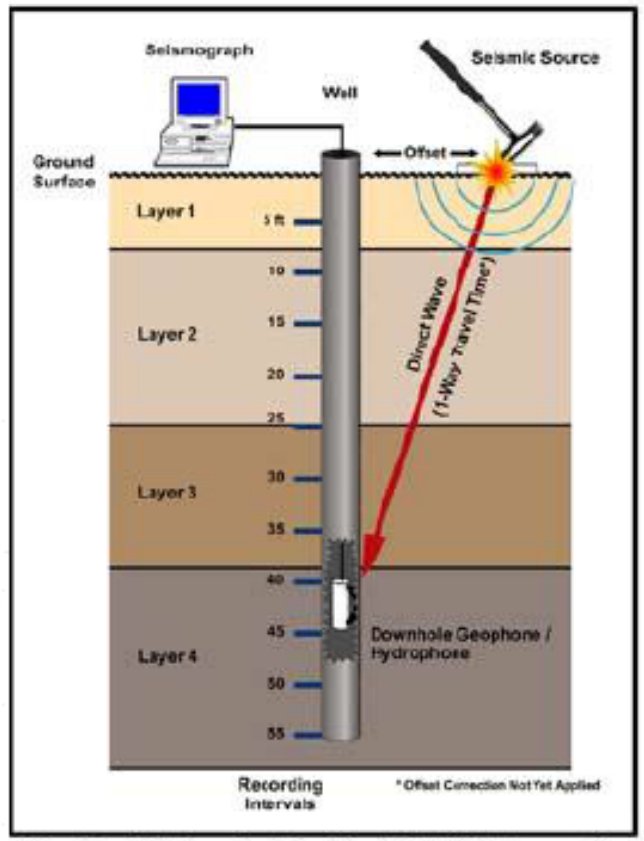

Vertical Seismic Profile (VSP) Schematic

Up-Hole method: source of energy is deep in boring and the receiver is at the ground surface

http://www.geophysics.co.uk/mets3.html

Seismic Cone Penetration Test (SCPT)
A Down-Hole Test

Seismic cone is pushed into the ground

Shear wave is generated at the top and the time required for the shear wave to reach the seismometer in the cone is measured

Computer in the SCPT rig collects and processes all the data & shear wave velocity is measured

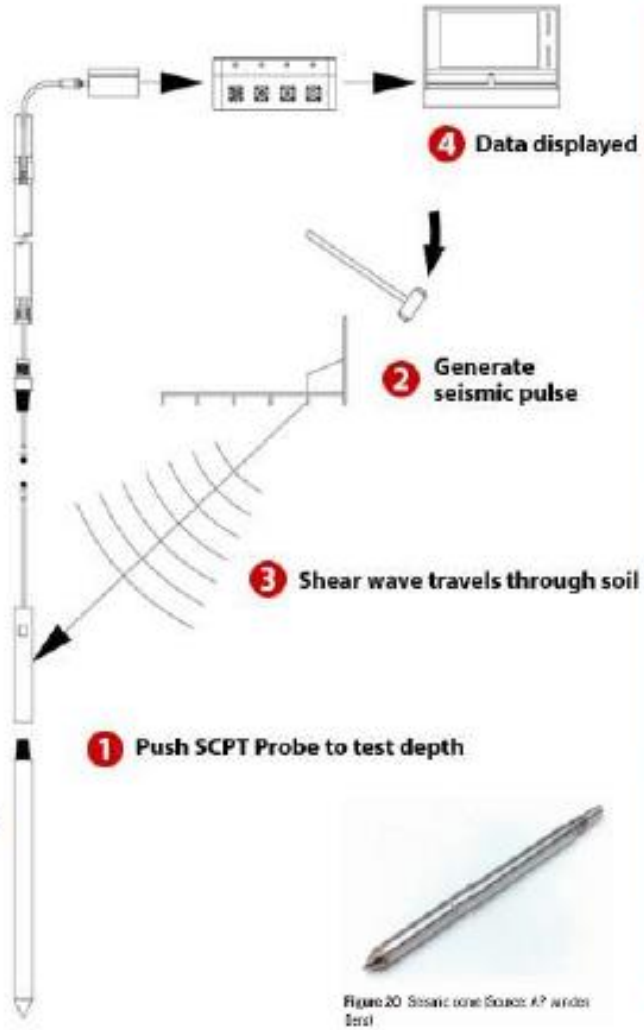

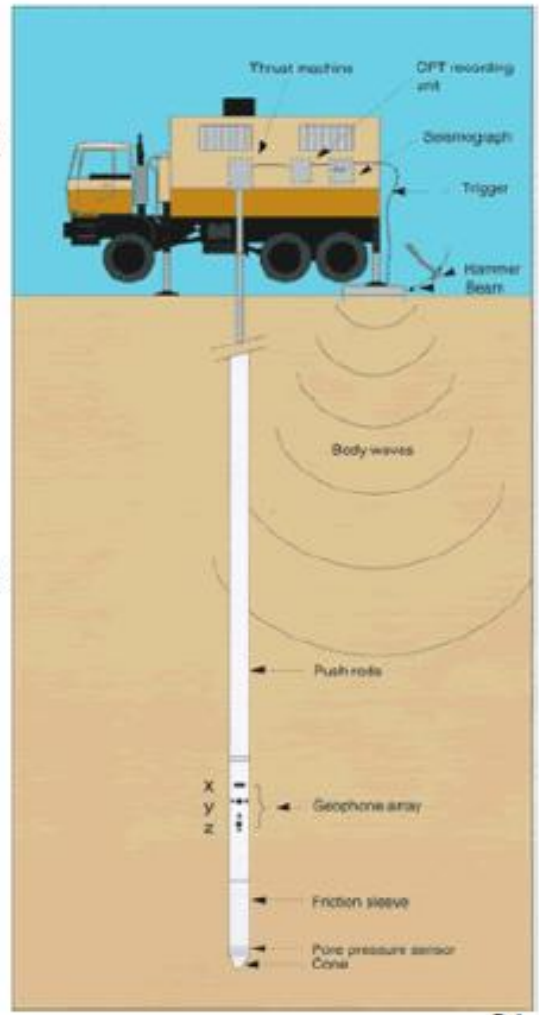

Figure 20 Seismic cone (Source: AP winder test)

Down-Hole Test Record

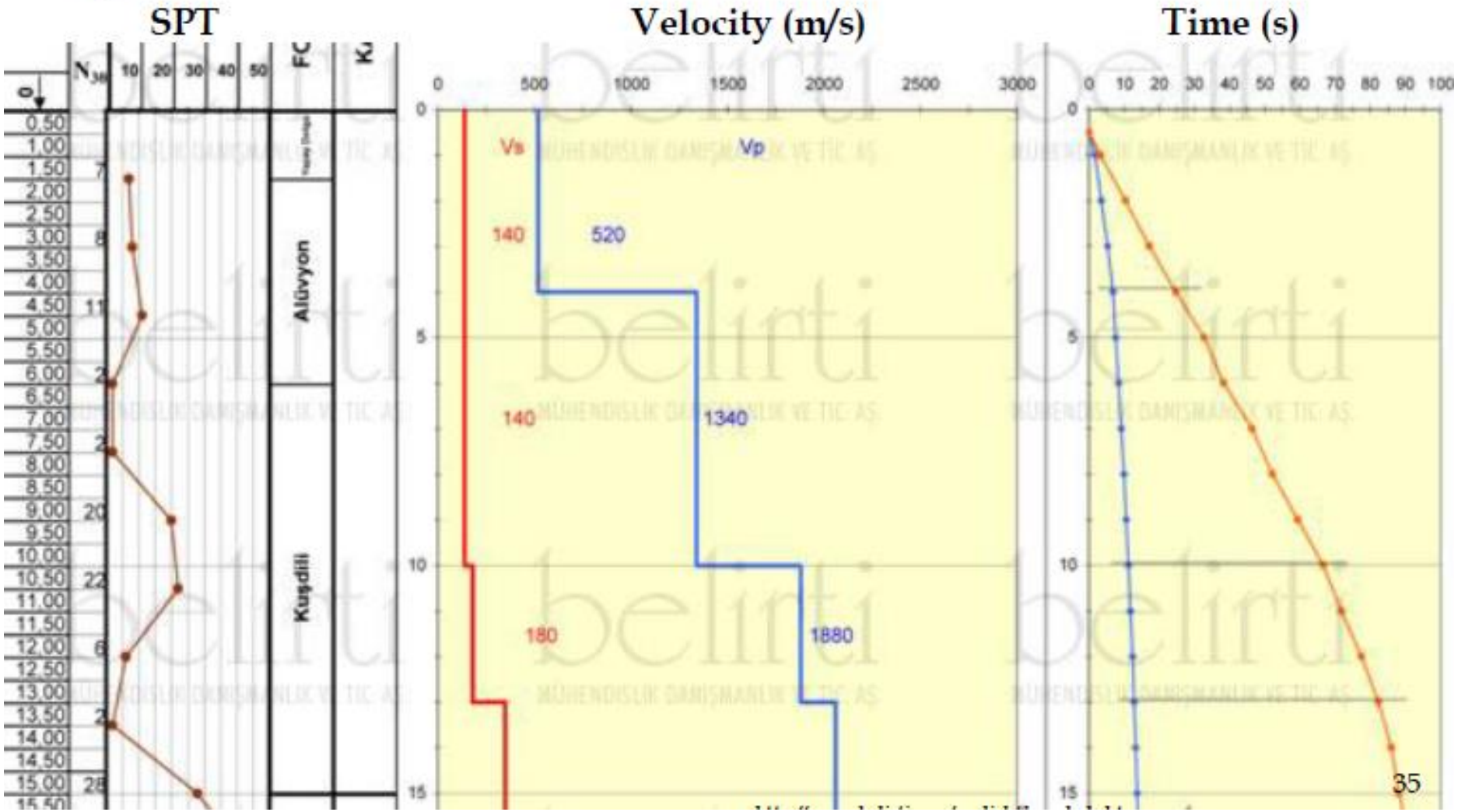

SASW Test

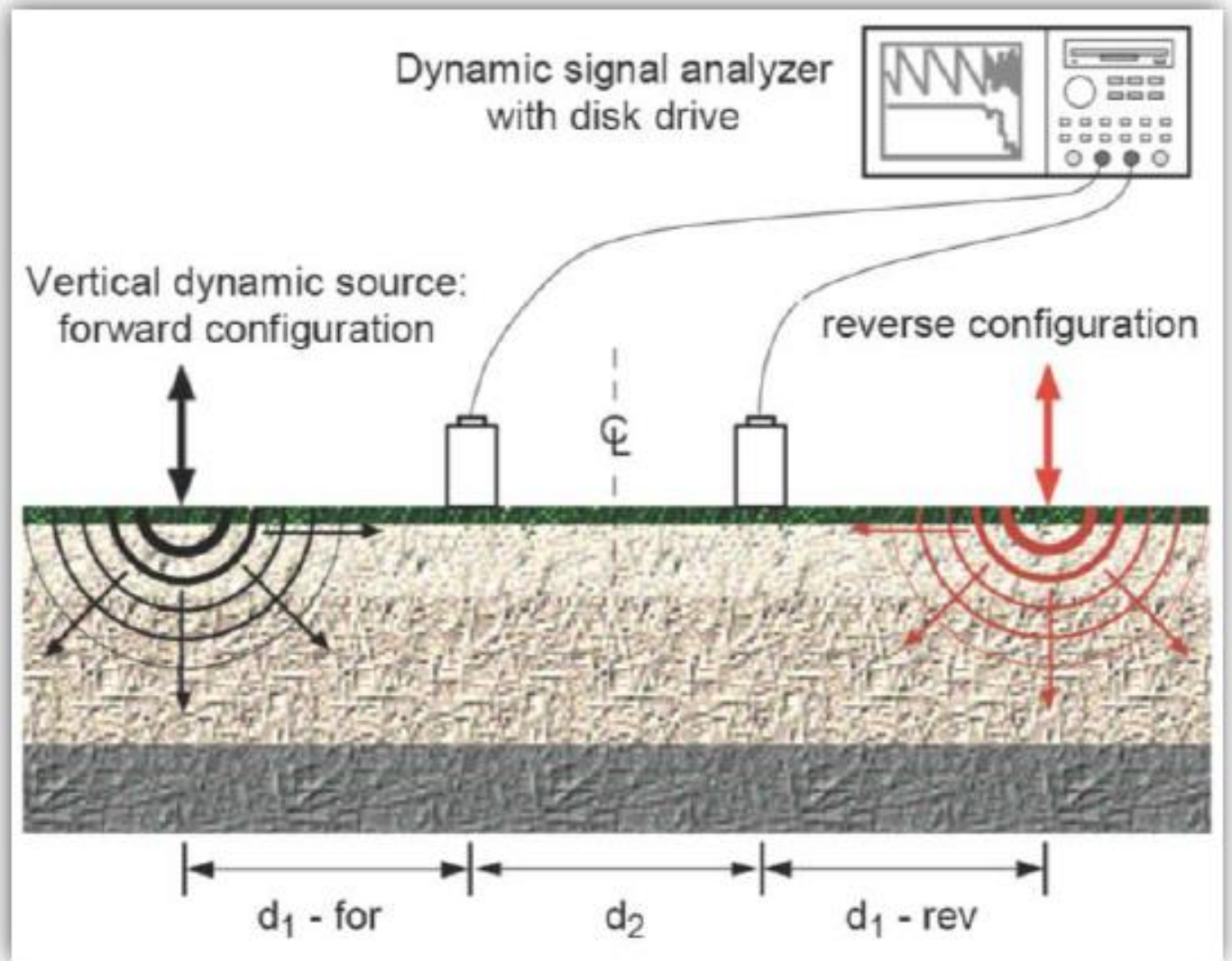
Dynamic signal analyzer
with disk drive
Vertical dynamic source:
forward configuration
reverse configuration
℄
d_1 - for
d_2
d_1 - rev

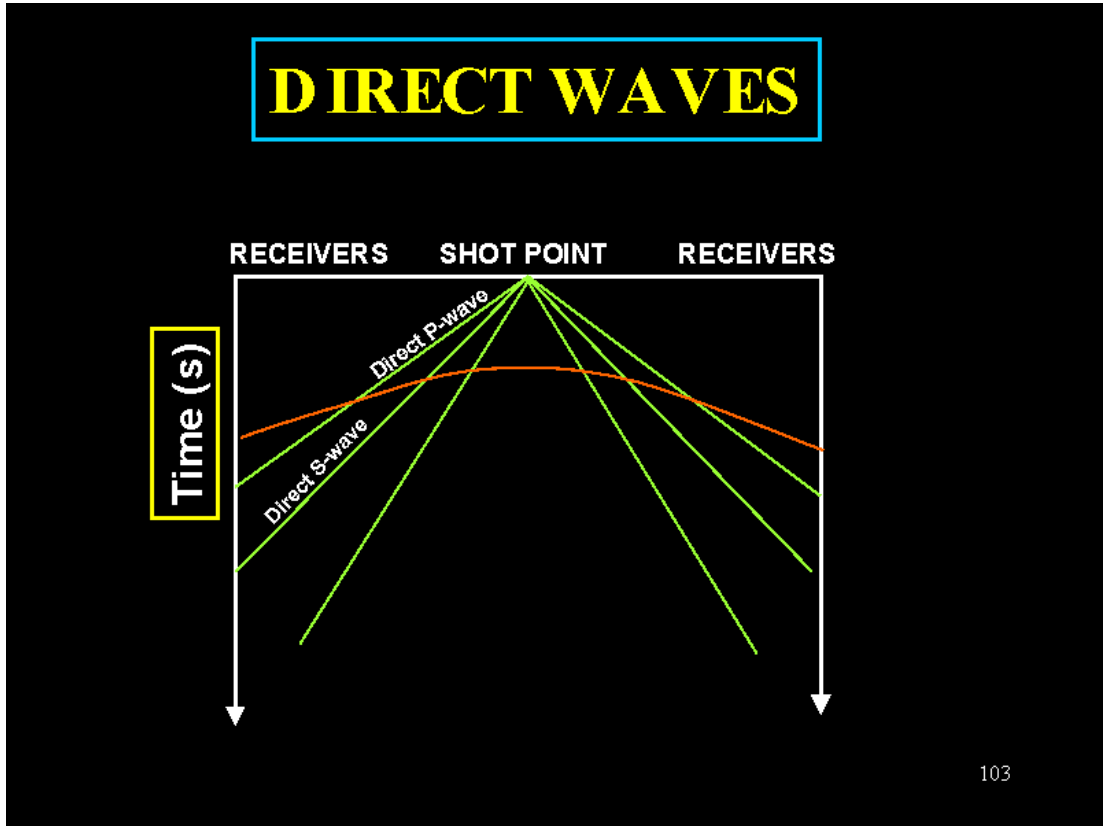

موج مستقیم

امواج مستقیم (Direct wave)

بخشی از انرژی لرزه ای که از لایه مجاور با هوا حرکت می کند، موج مستقیم نامیده می شود و سرعت آن معادل با سرعت لایه سطحی است که از میان آن عبور می کند. در برداشتهای دریایی، موج مستقیم برای تعیین سرعت موج در آب (حدود ۱۵۰۰ متر بر ثانیه) بکار می روند.

DIRECT WAVES

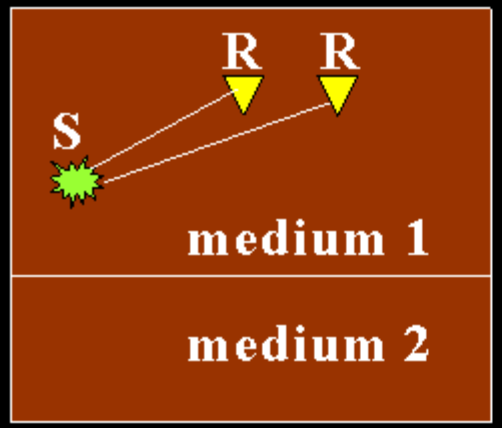

1. PROPAGATE IN THE WATER OR THROUGH THE FIRST LAYER IN LAND.
2. IT DIRECTLY GOES FROM SOURCE TO RECEIVER WITHOUT HITTING ANY REFLECTORS OR DIFFRACTORS.

3. $d = x_r - x_s$: distance from source to receiver.

v: velocity of water or first layer in land.

$$t_P = \frac{d}{V_P}; \; t_S = \frac{d}{V_S}$$

102

Refraction Seismic Survey

موج شکست مرزی

Head wave ، بخشی از جبهه موج اولیه هستند که به طرف سطح پائین لایه هوازده حرکت می کنند و در سطح پائین لایه هوازده شکسته می شوند (تحت زاویه بحرانی) و دوباره به سطح زمین بر می گردند. این امواج همان امواج شکست مرزی (refraction) هستند.

$$h_1 = \frac{t_i}{2} \frac{v_2 v_1}{\left(v_2^{\,2} - v_1^{\,2}\right)^{\frac{1}{2}}}$$

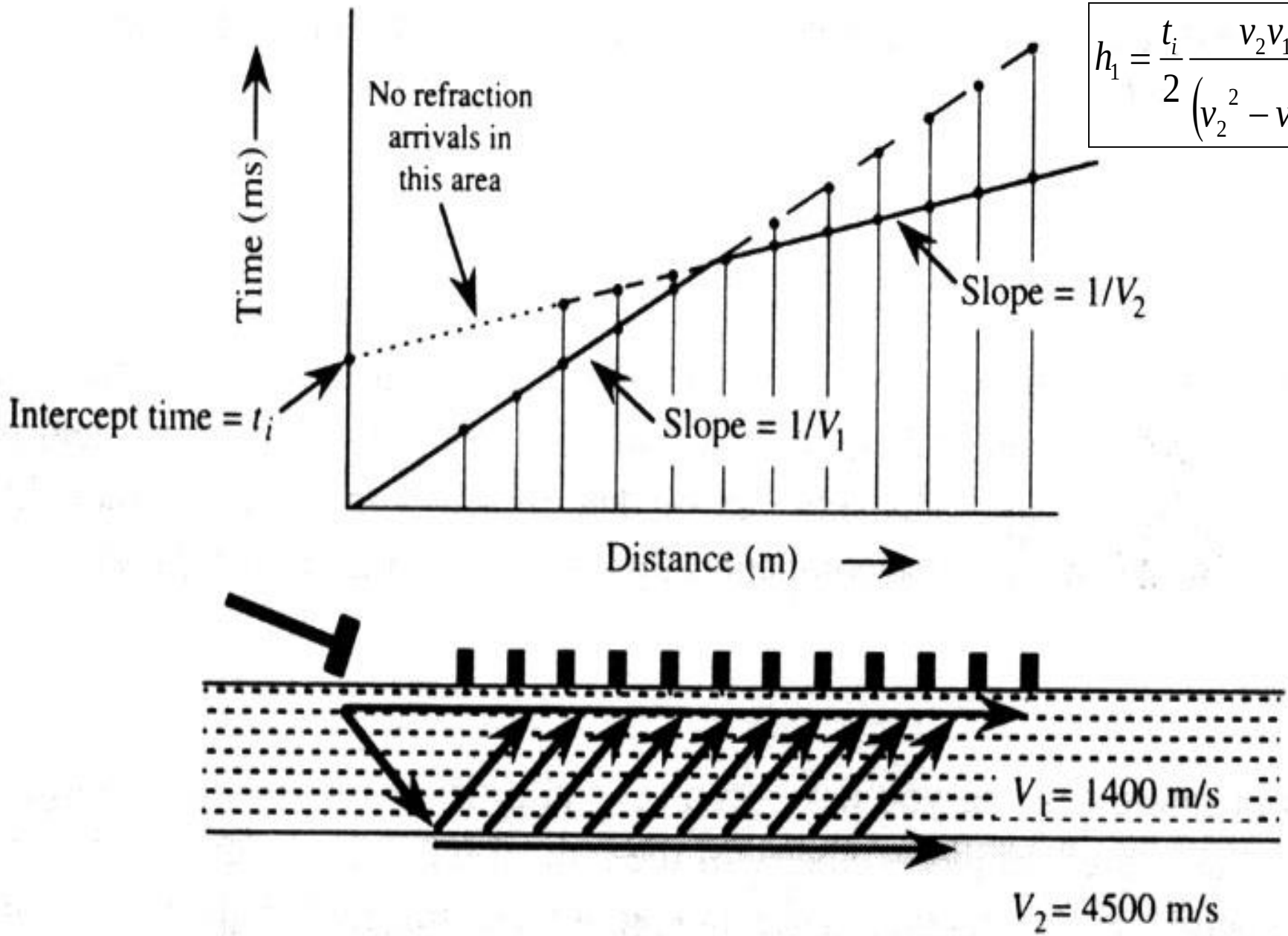

CRITICAL ANGLE

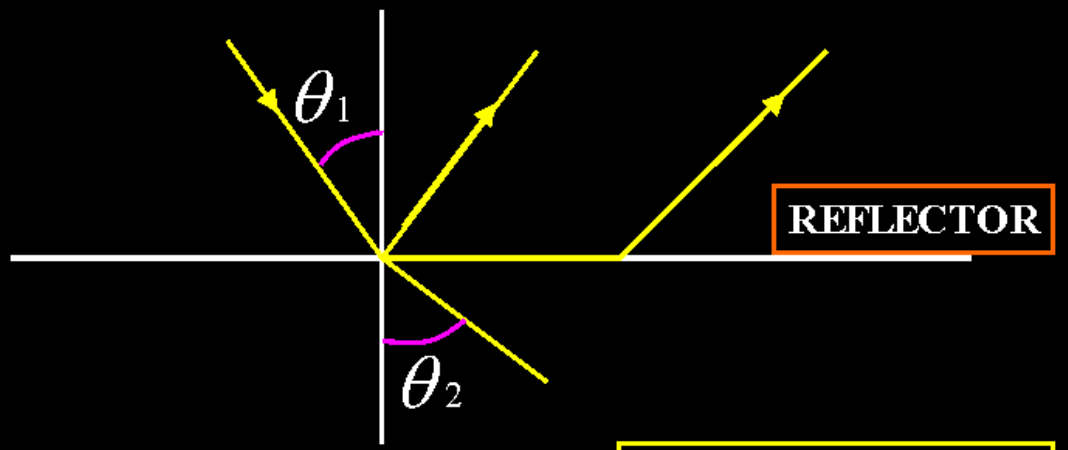

CRIT

if V

As $\theta_2 \rightarrow$

Si

$$\frac{\sin\theta_c}{V_{P1}} = \frac{\sin 90}{V_{P2}} = \frac{1}{V_{P2}}$$

$$\theta_c = \sin^{-1}\left(\frac{V_{P1}}{V_{P2}}\right)_{23}$$

22

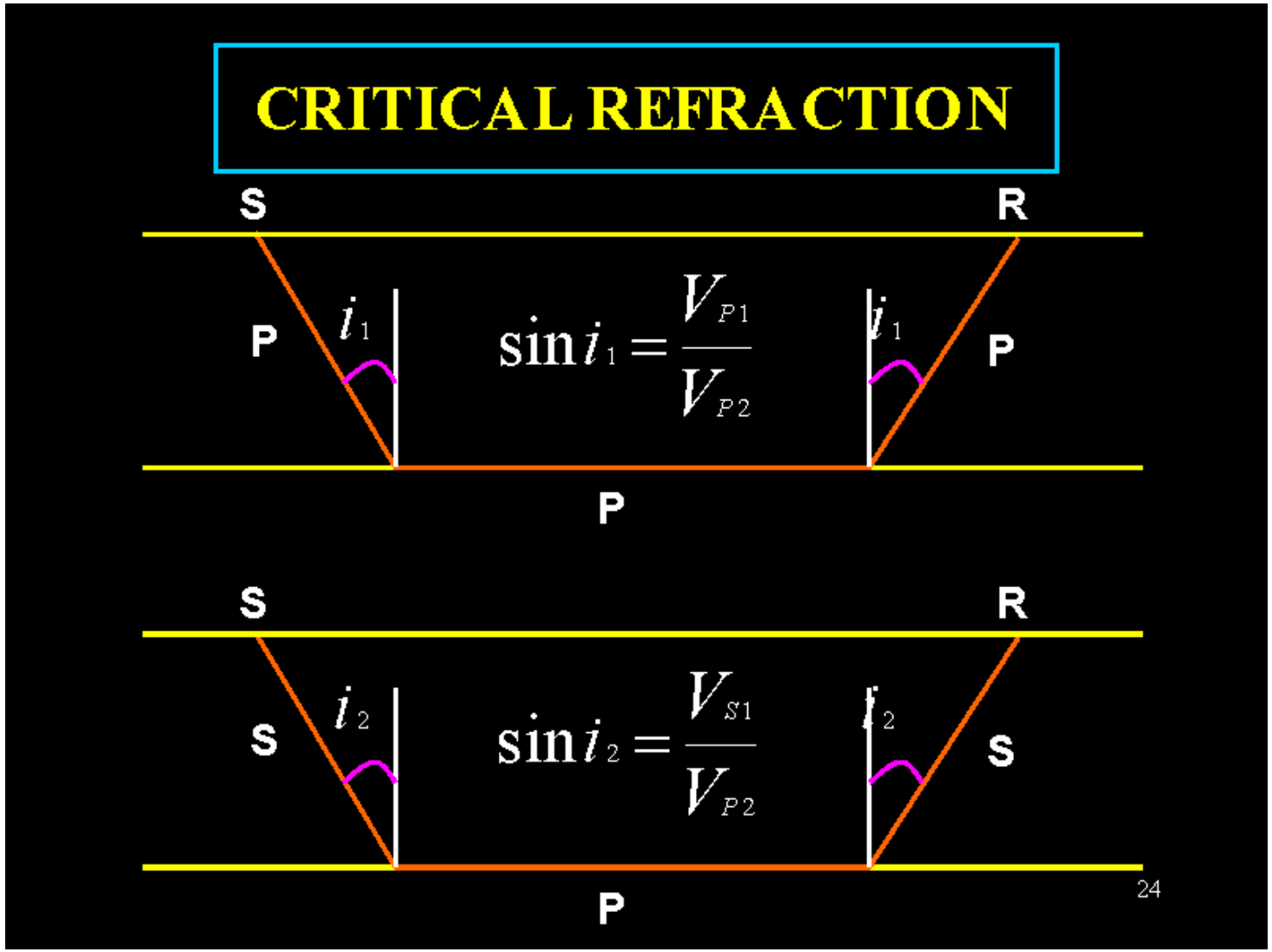
CRITICAL REFRACTION
S
R
P
i_1
$\sin i_1 = \frac{V_{P1}}{V_{P2}}$
i_1
P
P
S
R
S
i_2
$\sin i_2 = \frac{V_{S1}}{V_{P2}}$
i_2
S
P
24

Two horizontal layers

$$T_{SA} = T_{BD} = \frac{z}{Cos\theta}\frac{1}{V_1}$$

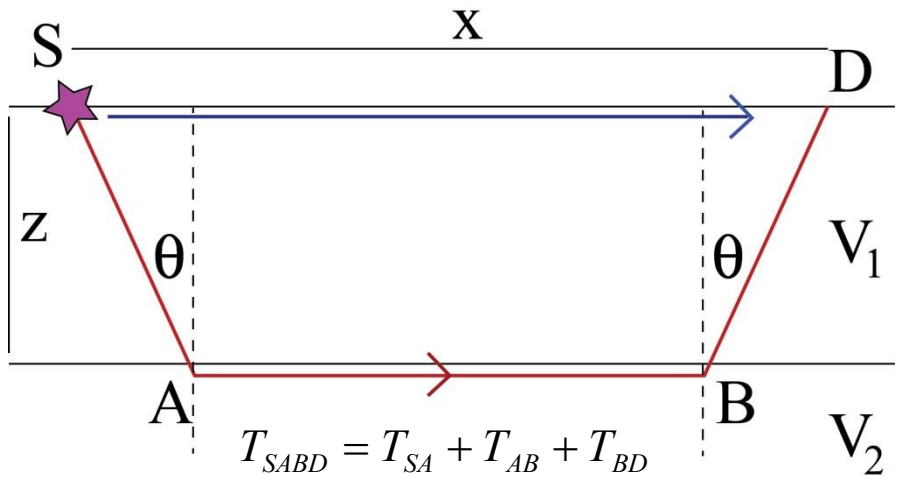

$$x = AB + 2\tan\theta z$$

$$T_{SABD} = \frac{2z}{\mathrm{Cos}\theta}\frac{1}{V_1} + \frac{x - 2\tan\theta z}{V_2} = \frac{x}{V_2} + 2z\left(\frac{1}{\mathrm{Cos}\theta V_1} - \frac{\tan\theta}{V_2}\right) = \frac{x}{V_2} + \frac{2z}{\mathrm{Cos}\theta V_1}\left(1 - \frac{V_1\mathrm{Sin}\theta}{V_2}\right) = \frac{x}{V_2} + \frac{2z}{\mathrm{Cos}\theta V_1}\left(1 - \mathrm{Sin}^2\theta\right)$$

$$T_{SABD} = \frac{x}{V_2} + 2\frac{z\mathrm{Cos}\theta}{V_1}$$

$$\mathrm{Sin}\theta = \frac{V_1}{V_2}, \qquad \mathrm{Cos}\theta = \sqrt{\left(1 - \mathrm{Sin}^2\theta\right)} = \sqrt{\left(1 - \left(\frac{V_1}{V_2}\right)^2\right)}$$

$$T_{SABD} = \frac{x}{V_2} + \frac{2z}{V_1V_2}\left(V_2^2 - V_1^2\right)^{1/2}$$

This is the travel time of the refracted wave. The refracted wave propagates along a buried interface at the velocity of the lower medium. They are normally the first phases to arrive at a receiver and hence are called head waves.

Time-Distance Plot

At the the cross-over distance, x_{cros}, travel times of the direct and refracted arrivals are equal.

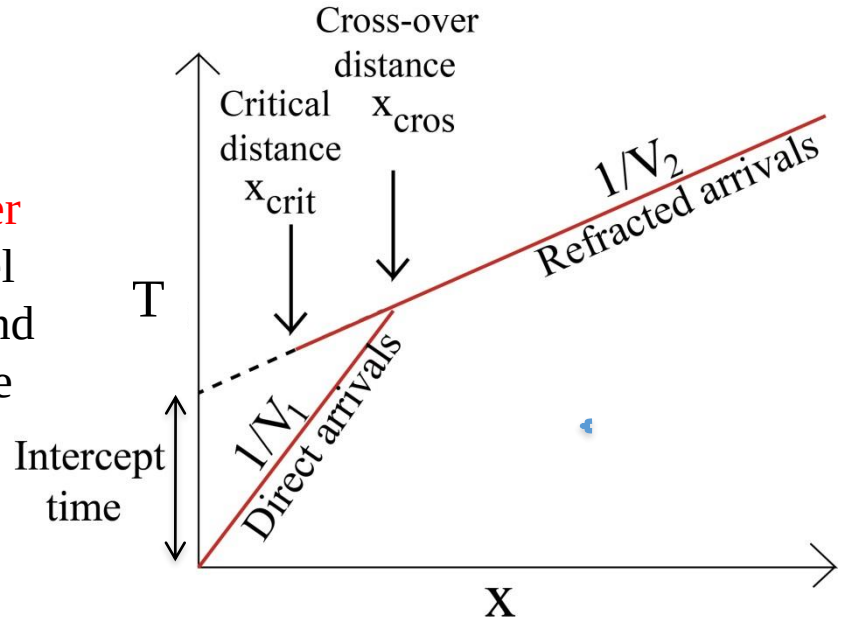

$$\frac{x_{cros}}{V_1} = \frac{x_{cros}}{V_2} + \frac{2z}{V_1 V_2}(V_2^2 - V_1^2)^{1/2}$$

$$x_{cros} = 2z\left[\frac{V_2 + V_1}{V_2 - V_1}\right]^{1/2}$$

The thickness of the upper of the two layers, z, can be determined from the cross-over distance and the velocities or the intercept time and the velocities.

$$z = \frac{1}{2}\left[\frac{V_2 - V_1}{V_2 + V_1}\right]^{1/2} x_{cros}$$

$$\text{Intercept time} = \frac{2z}{V_1 V_2}(V_2^2 - V_1^2)^{1/2}$$

Multiple layers

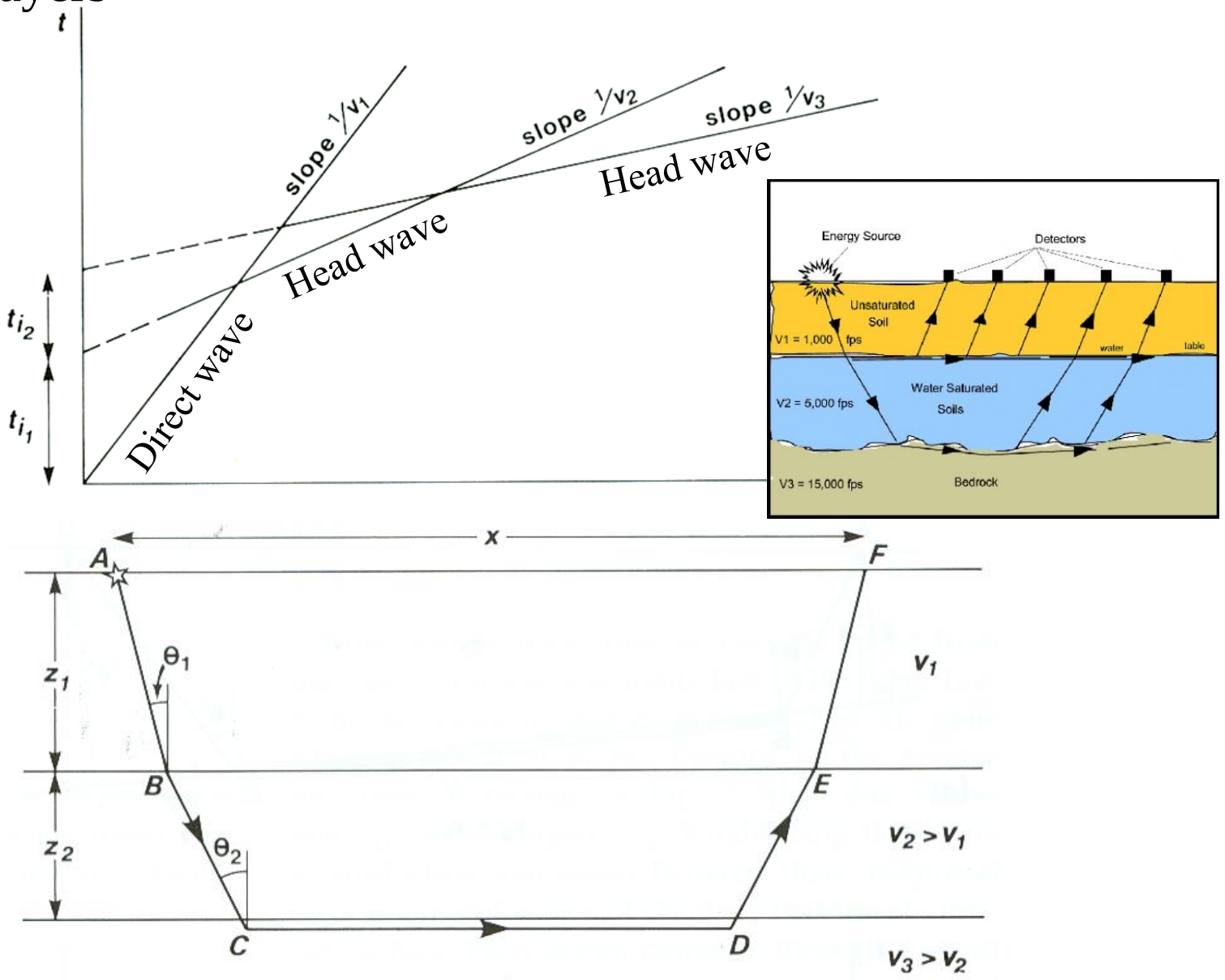

ABCDEF is the refracted ray path through the bottom layer of a three layer model. The travel time curve for the direct and two head waves are shown above.

$$T_{SD} = \frac{x}{V_2} + 2\frac{z\mathrm{Cos}\theta}{V_1}, \qquad V_2 = \frac{V_1}{\mathrm{Sin}\theta}$$

By analogy:

$$T_{ABCDEF} = \frac{x}{V_3} + 2\frac{z_1\mathrm{Cos}\theta_1}{V_1} + 2\frac{z_2\mathrm{Cos}\theta_2}{V_2}$$

The velocity V_3 can be estimated from the slope of the second head wave. V_1 and V_2 can be estimated from the direct and first head wave and z_1 and z_2 from the intercept times

$$T_n = \frac{x}{V_n} + \sum_{i=1}^{n-1} \frac{2z_i\mathrm{Cos}\theta_i}{V_i}$$

where

$$\theta_i = \sin^{-1}\left(\frac{V_i}{V_n}\right)$$

This gives the travel time, T_n of a ray critically refracted along the top surface of the n th horizontal layer

Mendips field data

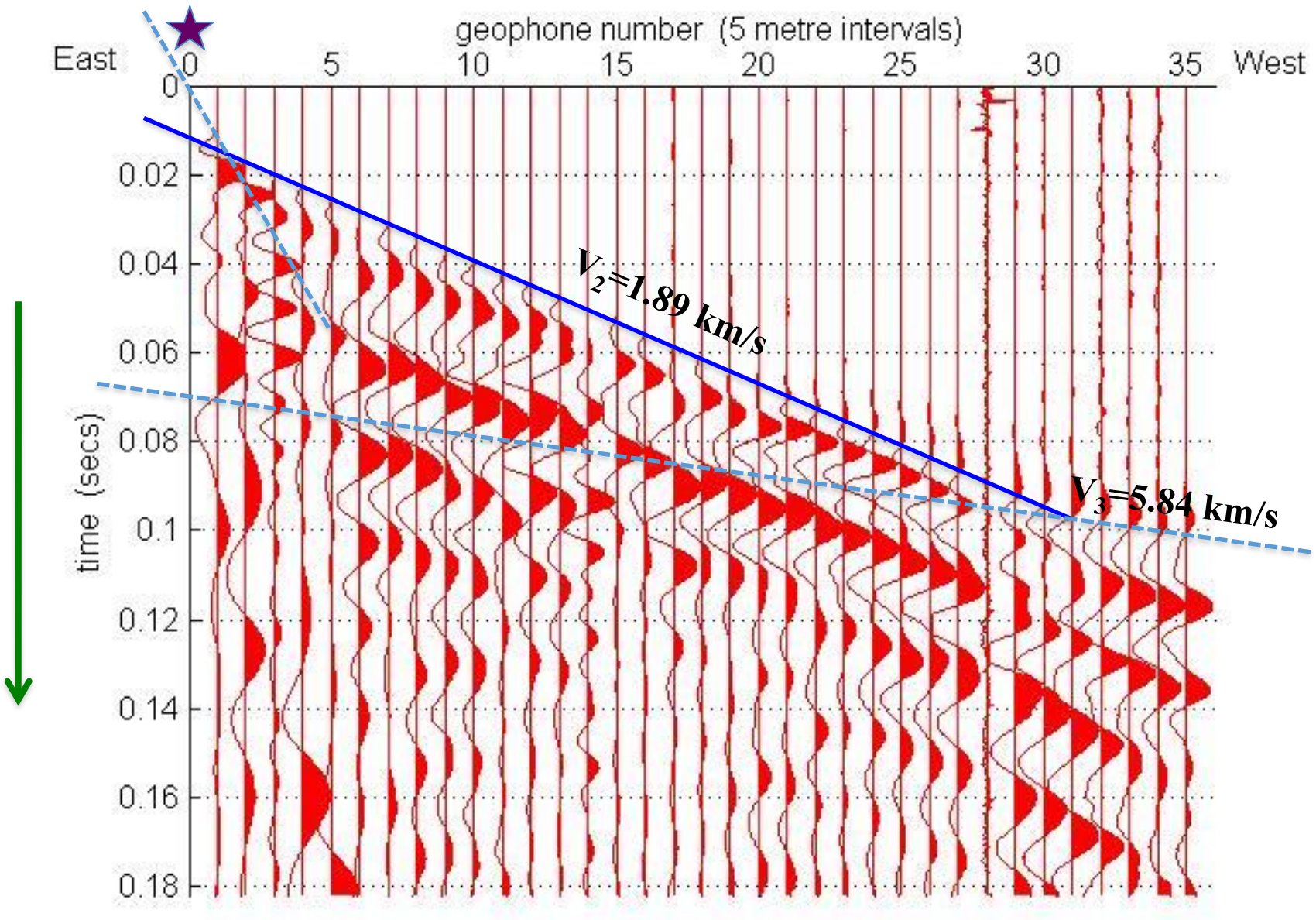

Dipping layers

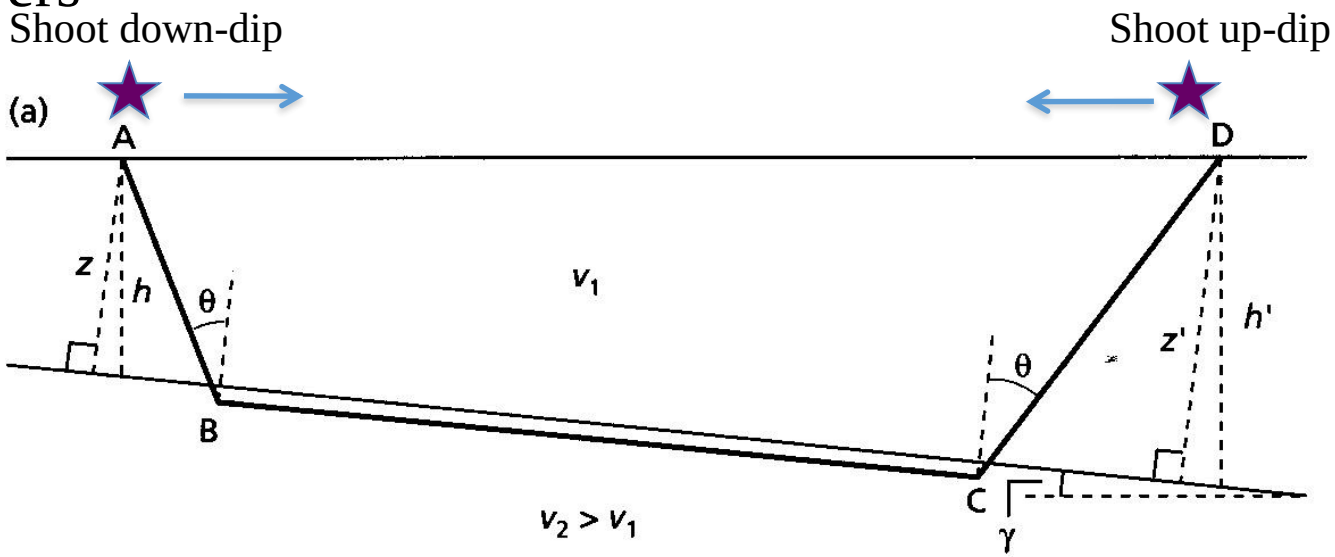

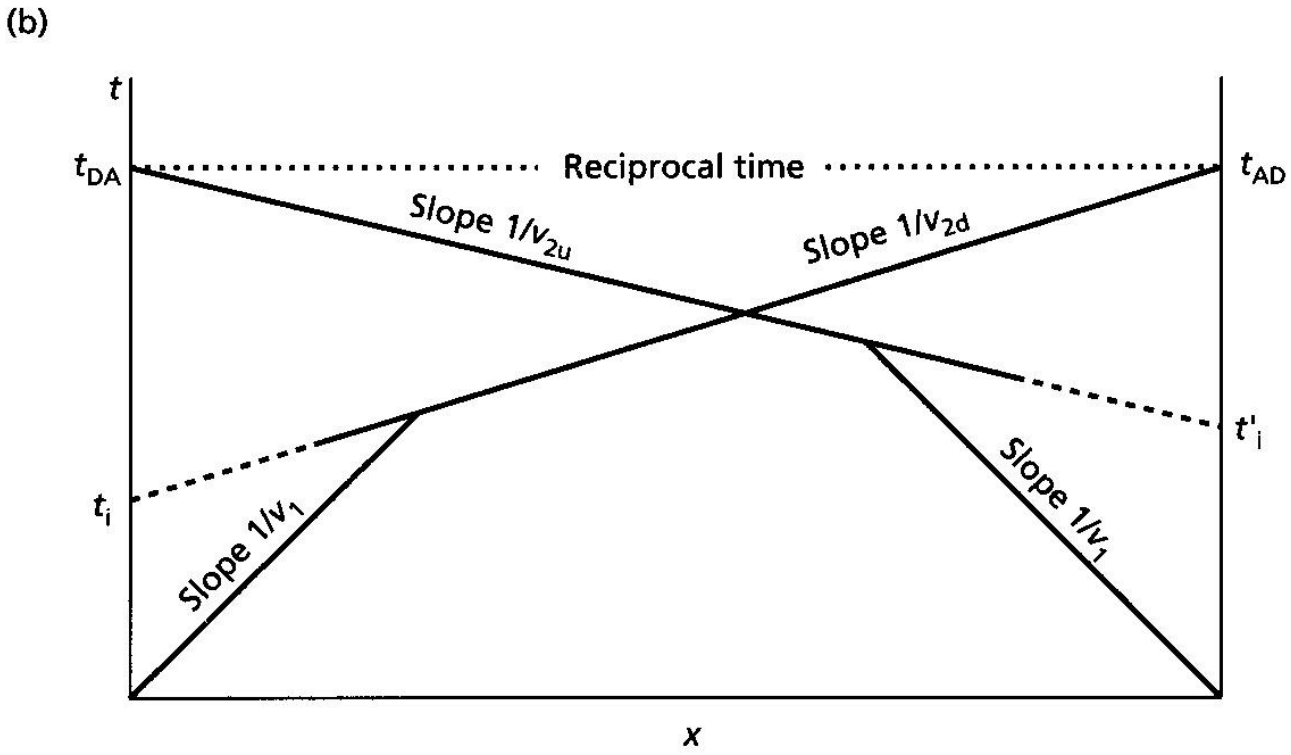

Down-dip: $$t_2(x) = \frac{x\sin(\theta+\gamma)}{v_1} + \frac{2z\cos\theta}{v_1}$$

Up-dip: $$t_2'(x) = \frac{x\sin(\theta-\gamma)}{v_1} + \frac{2z'\cos\theta}{v_1}$$

$$\theta = \frac{1}{2}(\sin^{-1}(V_1/V_{2d}) + \sin^{-1}(V_1/V_{2u}))$$

$$\gamma = \frac{1}{2}(\sin^{-1}(V_1/V_{2d}) - \sin^{-1}(V_1/V_{2u}))$$

$$t_i = 2z\cos\theta/V_1$$

$$z = V_1 t_i/2\cos\theta, \qquad z' = V_1 t_i'/2\cos\theta$$

$$h = z/\cos\gamma, \qquad h' = z'/\cos\gamma$$

θ and γ can be estimated from the velocities V_1, V_{2u} and V_{2d} and hence z and z' and h and h' calculated.

See Keary & Brooks (Chap 5) + Practical 4

Offsets in the travel time Vs. distance plot for head waves from opposite sides of a fault

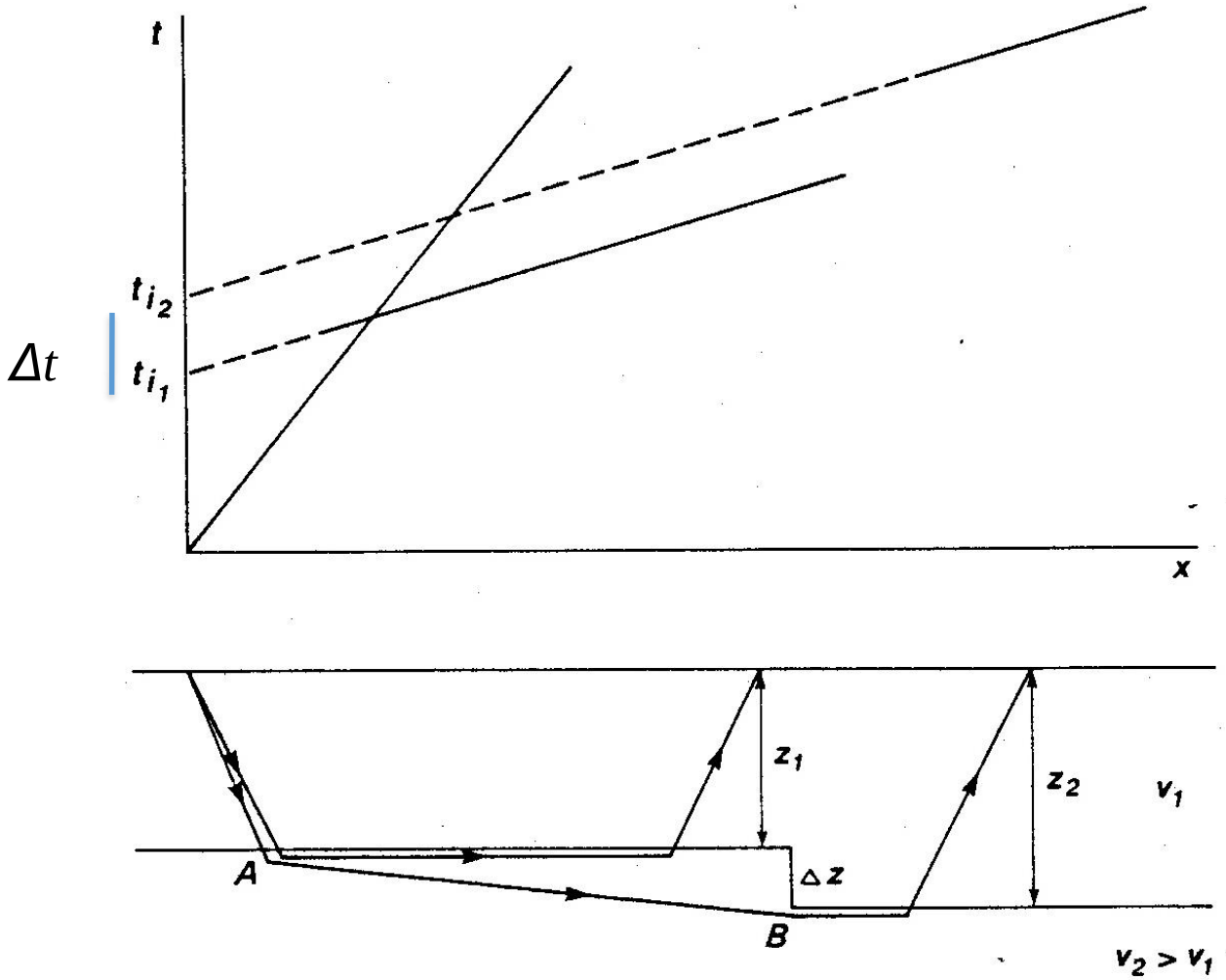

The throw on the fault, Δz, can be calculated from the travel time offset, Δt

$$\Delta z = \Delta t \frac{V_1 V_2}{(V_2^2 - V_1^2)^{1/2}}$$

Note: Valid only for small throws cf. refractor depth.

Thin and low velocity layers

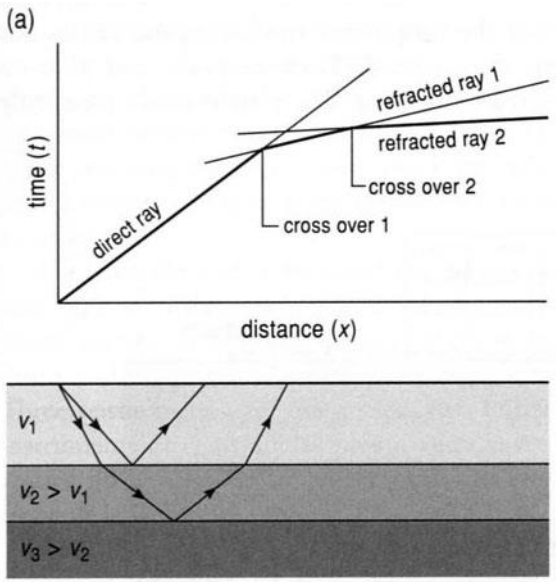

A thin layer that does not generate a head wave that is a first arrival

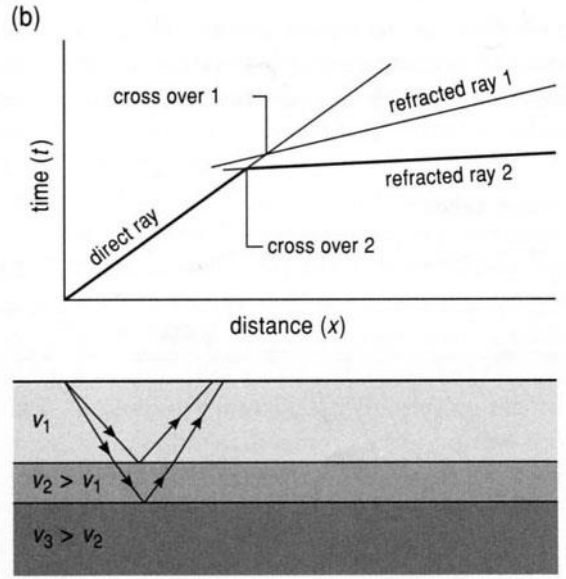

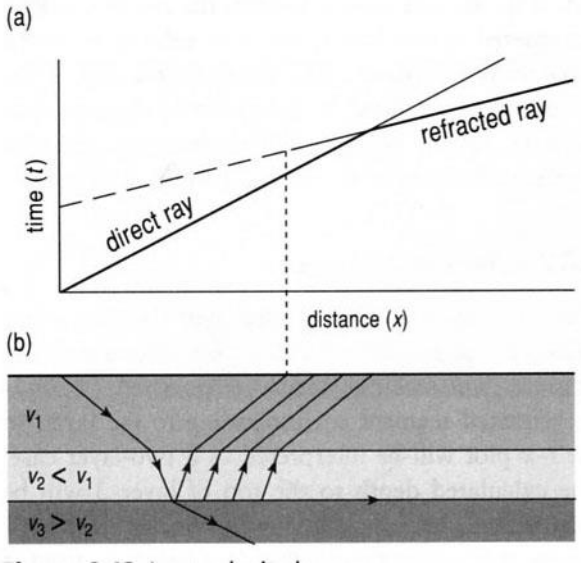

A low velocity layer that does not generate a head wave

Non-planar refractor geometry

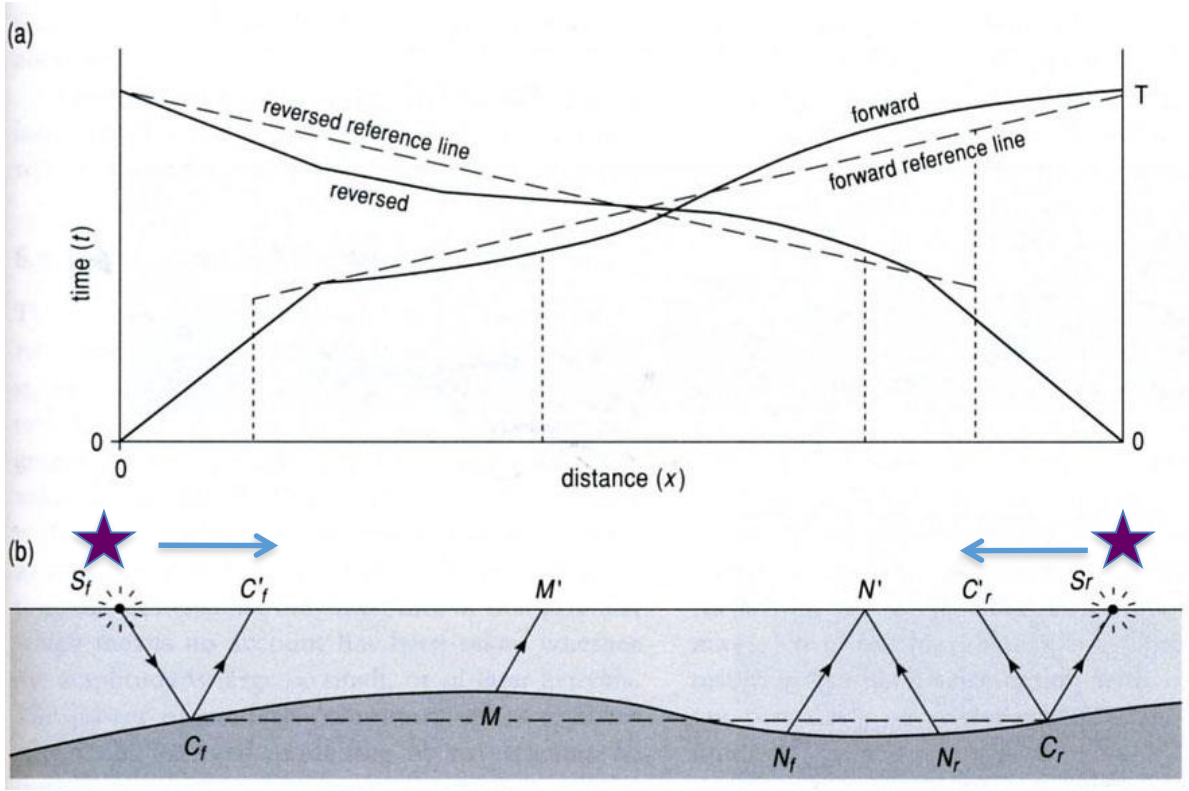

Reference (dashed lines) show the planar case

M (e.g.) is nearer the surface than the reference interface, the actual travel time to *M'* plots below the reference line. Conversely, that for *N'* is above it. These observations can be quantified using the concept of delay time.

تمرین ۲

- در مطالعه لرزه نگاری شکست مرزی روی دو لایه تخت با فصل مشترک شیبدار، ابتدا از یک شلیک مستقیم جلوبب (S1) استفاده شده است. با توجه به نمودارهای زمان – فاصله، سرعت لایه اول ۲.۲ کیلومتر بر ثانیه و سرعت ظاهری افق انکساری در جهت فروشیب برابر ۴ کیلومتر بر ثانیه است. در مرحله بعد نقطه شلیک S1 و ژئوفون ها ۱۵۰ متر به طرف جلو جا به جا شده که در این حال زمان ورود جبهه امواج شکست مرزی به هر ژئوفون ۵ میلی ثانیه افزایش یافته است. با توجه به اطلاعات داده شده، شیب و سرعت واقعی افق انکساری را محاسبه کنید. اگر زمان قطع نمودار زمان – فاصله موج شکست مرزی با محور زمان در شلیک اول (S1) برابر ۲۰ میلی ثانیه باشد، عمق قائم افق انکساری در زیر نقطه S1 چه مقدار است.

تمرین ۳

- داده های شکست مرزی زیر از یک خط برداشت به طول ۲۷۵ متر بدست آمده است. با استفاده از روش به علاوه و منهای هاگدرون داده ها را تفسیر کرده و اطلاعات ممکن در خصوص سطح دو لایه را بدست آورید.

شلیک جلویی		شلیک عقبی	
فاصله ژئوفون از نقطه شلیک (m)	زمان (ms)	فاصله ژئوفون از نقطه شلیک (m)	زمان (ms)
۱۲.۵۰	۶.۰۰	۱۲.۵۰	۶.۰۰
۲۵.۰۰	۱۲.۵	۲۵.۰۰	۱۲.۵
۳۷.۵۰	۱۹.۰۰	۳۷.۵۰	۱۷.۰
۵۰.۰۰	۲۵.۰	۵۰.۰۰	۱۹.۵
۷۵.۰۰	۳۷.۰	۷۵.۰۰	۲۵.۰
۱۰۰.۰۰	۴۲.۵	۱۰۰.۰۰	۳۰.۵
۱۲۵.۰۰	۴۸.۵	۱۲۵.۰۰	۳۷.۵
۱۵۰.۰۰	۵۳.۰	۱۵۰.۰۰	۴۵.۵
۱۷۵.۰۰	۵۷.۰	۱۷۵.۰۰	۵۲.۰
۲۰۰.۰۰	۶۱.۵	۲۰۰.۰۰	۵۹.۰
۲۲۵.۰۰	۶۶.۰	۲۲۵.۰۰	۶۵.۵
۲۵۰.۰۰	۷۱.۰	۲۵۰.۰۰	۷۱.۰
۲۷۵.۰۰	۷۶.۵	۲۷۵.۰۰	۷۶.۵

۳- موج بازتابی

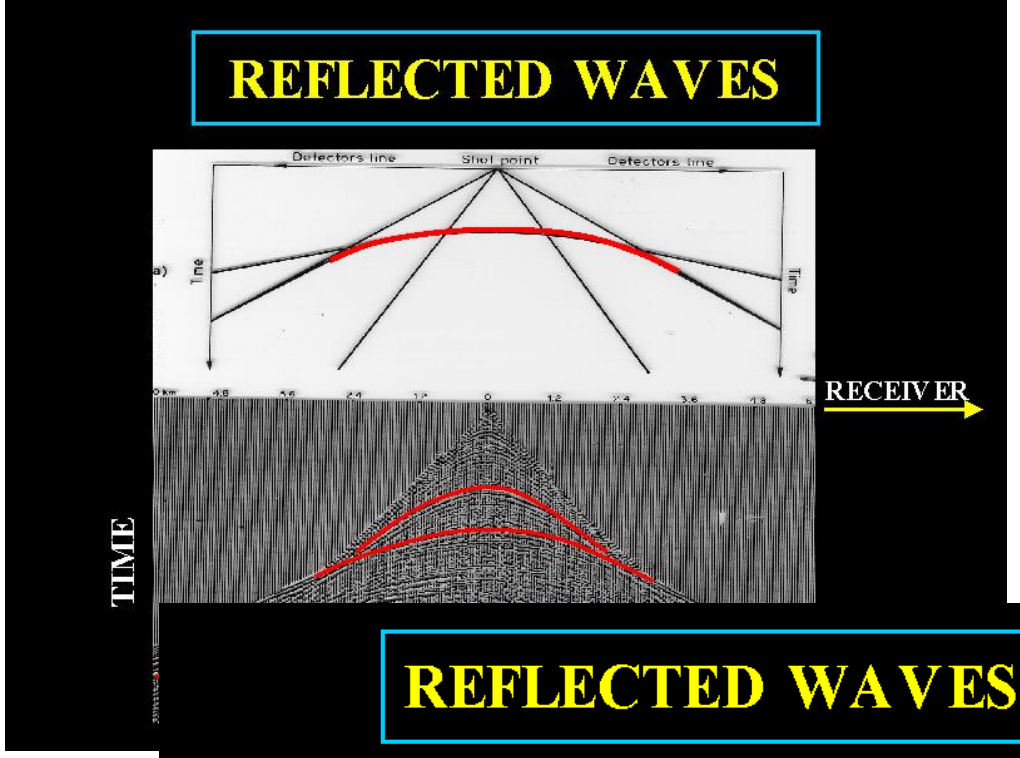

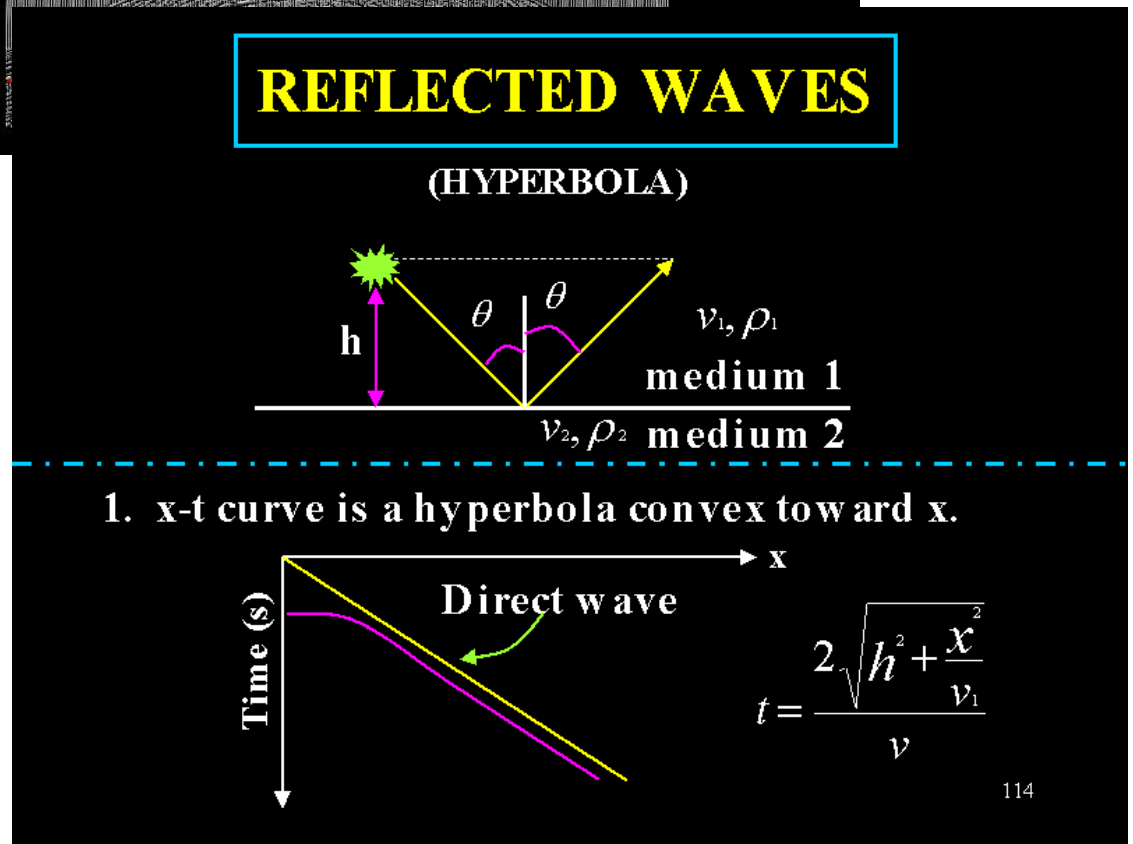

Convolution

- A mathematical operator which computes the “amount of overlap” between two functions. Can be thought of as a general moving average
- Discrete domain:

$$(f * g)(m) = \sum_n f(n)g(m-n)$$

- Continuous domain:

$$(f * g)(t) = \int f(t-\tau)g(\tau)\,d\tau$$

Discrete domain

- Basic steps
  1. Flip (reverse) one of the digital functions.
  2. Shift it along the time axis by one sample.
  3. Multiply the corresponding values of the two digital functions.
  4. Summate the products from step 3 to get one point of the digital convolution.
  5. Repeat steps 1-4 to obtain the digital convolution at all times that the functions overlap.

- Example

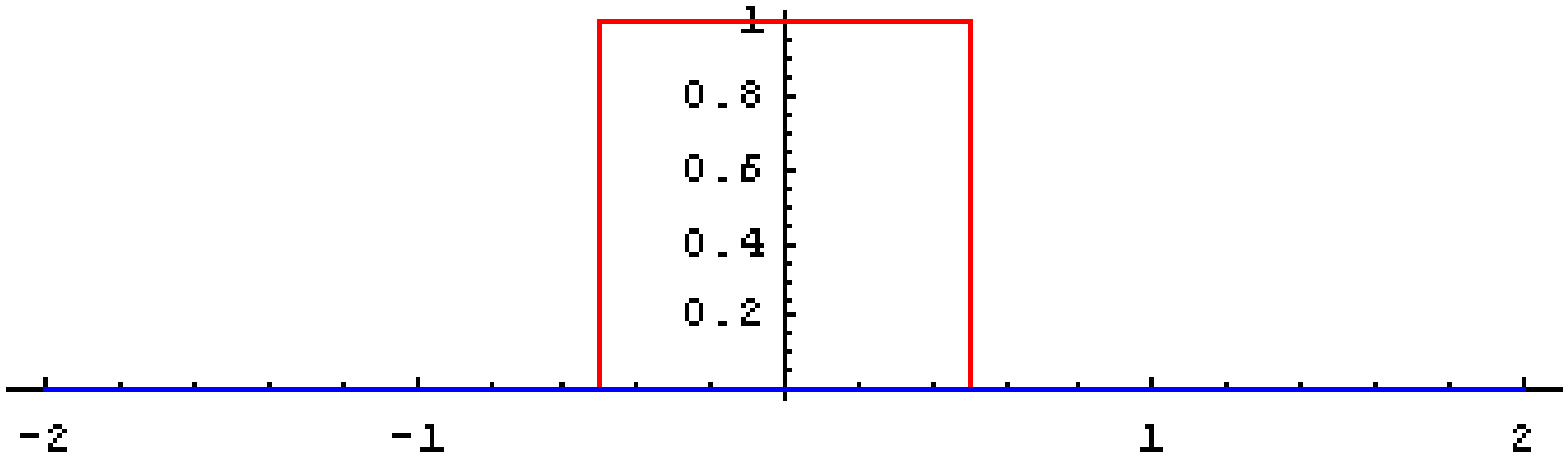
1
0.8
0.6
0.4
0.2
-2
-1
1
2

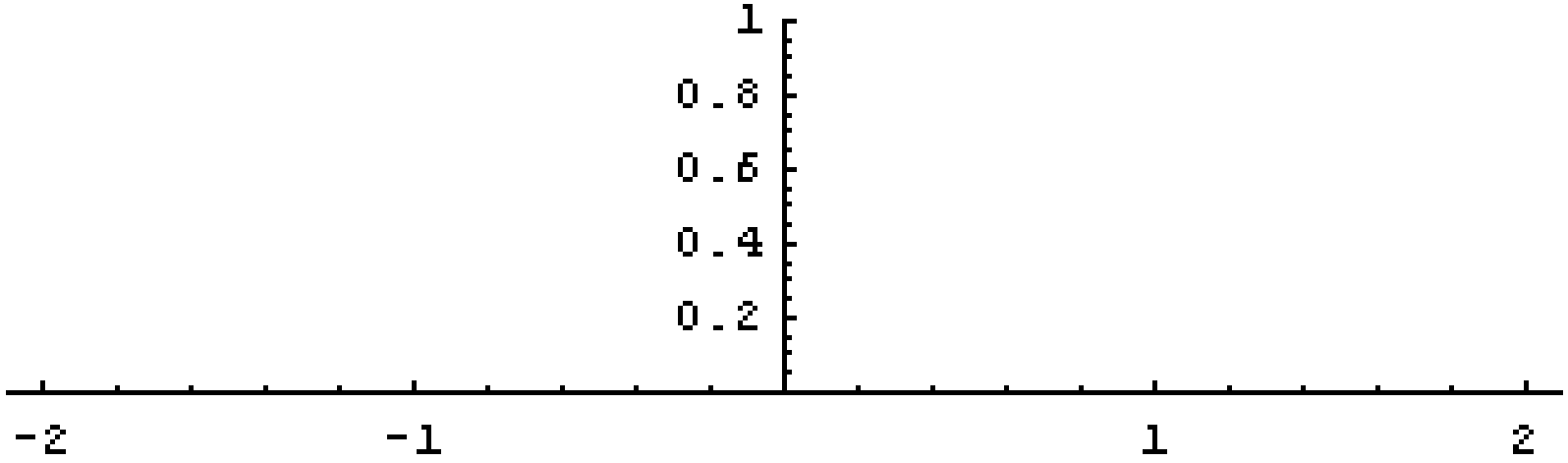
1
0.8
0.6
0.4
0.2
-2
-1
1
2

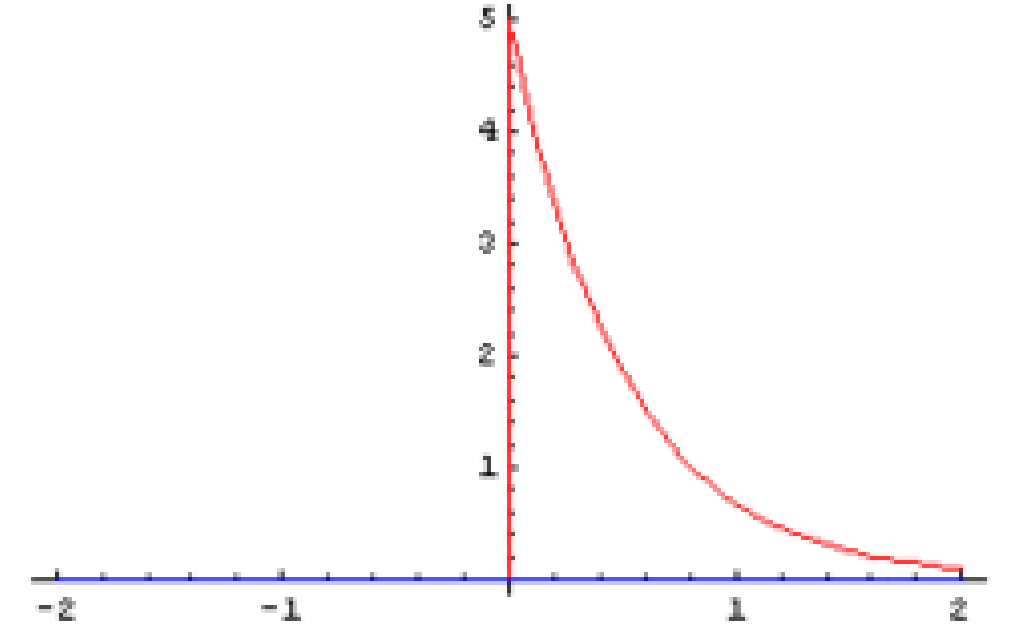
5
4
3
2
1
-2
-1
1
2

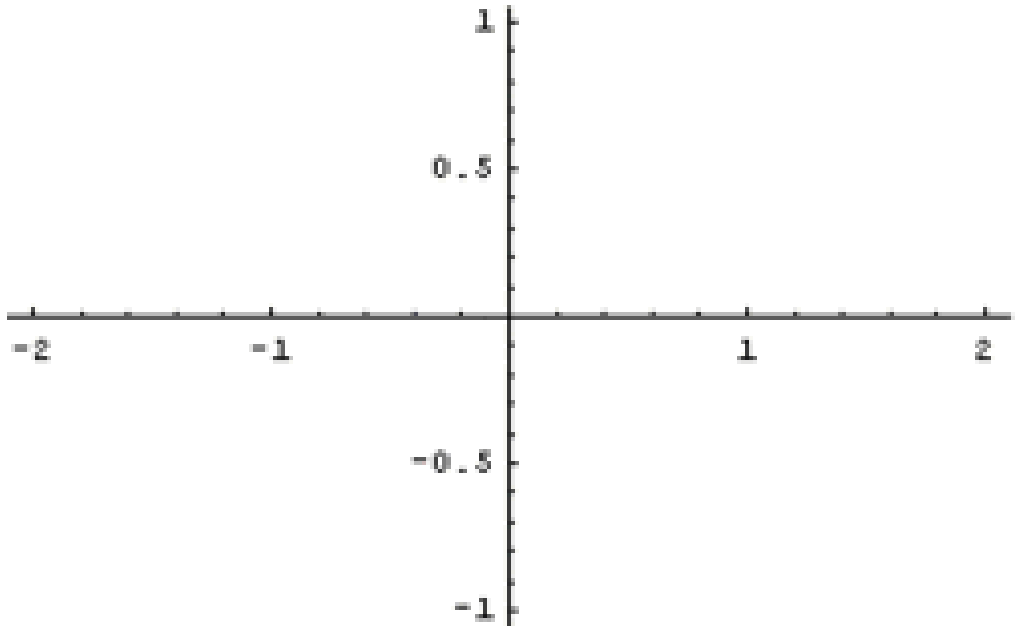
1
0.5
-0.5
-1
-2
-1
1
2

Continuous domain example

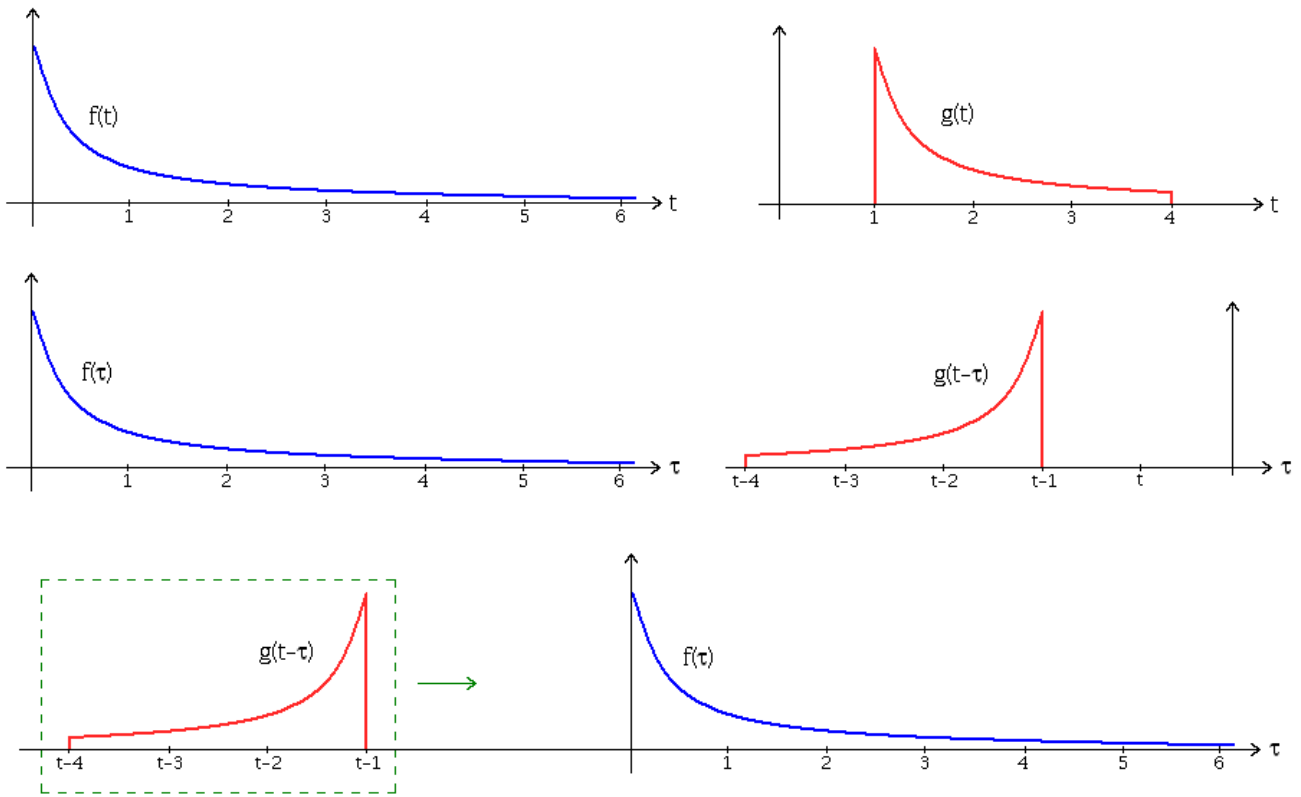

Continuous domain example

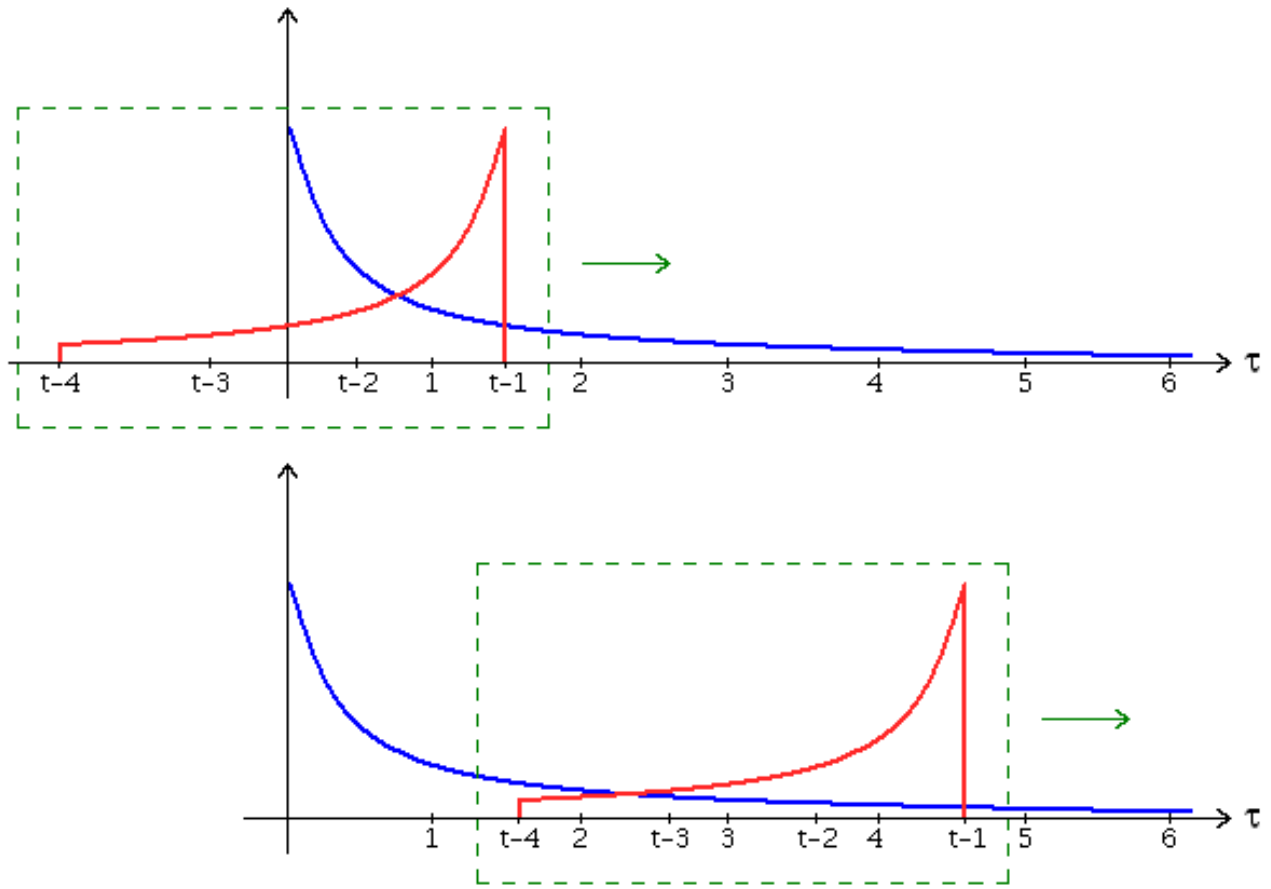

LTI (Linear Time-Invariant) Systems

- Convolution can describe the effect of an LTI system on a signal
- Assume we have an LTI system H, and its impulse response h[n]
- Then if the input signal is x[n], the output signal is y[n] = x[n] * h[n]

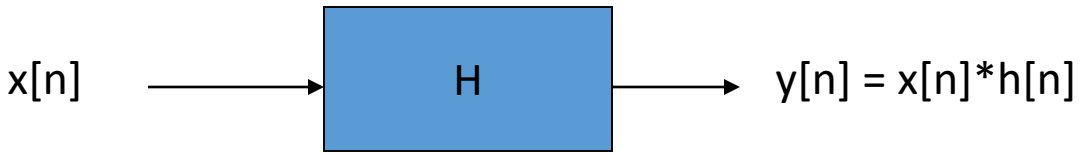

Mathematics of Waves

- Periodic phenomena occur everywhere
  - vision, sound, electronic communication, etc.

- In order to manipulate physical world, we need mathematical tools

Fourier Series

- Any reasonable function can be expressed as a (infinite) linear combination of sines and cosines

$F(t) = a_0 + a_1\cos(\omega t) + b_1\sin(\omega t) +$
$a_2\cos(2\omega t) + b_2\sin(2\omega t) + \ldots$

=

$$\sum_{n=0}^{\infty} (a_n \cos(n\omega t) + b_n \sin(n\omega t))$$

F(t) is a periodic function with

$$\omega = \frac{2\pi}{T}$$

Reasonable?

- F(t) is a periodic function with

$$\omega = \frac{2\pi}{T}$$

- must satisfy certain other conditions
  - finite number of discontinuities within T
  - finite average within T
  - finite number of minima and maxima

Calculate Coefficients

$$F(t) = \sum_{n=0}^{\infty} (a_n \cos(n\omega t) + b_n \sin(n\omega t))$$

$$a_0 = \frac{\int_0^T f(t)dt}{T}$$

$$a_k = \frac{2}{T}\int_0^T f(t)\cos(k\omega t)dt \qquad b_k = \frac{2}{T}\int_0^T f(t)\sin(k\omega t)dt$$

Example

- F(t) = square wave, with T=1.0s ( )

$$\omega = \frac{2\pi}{1.0}$$

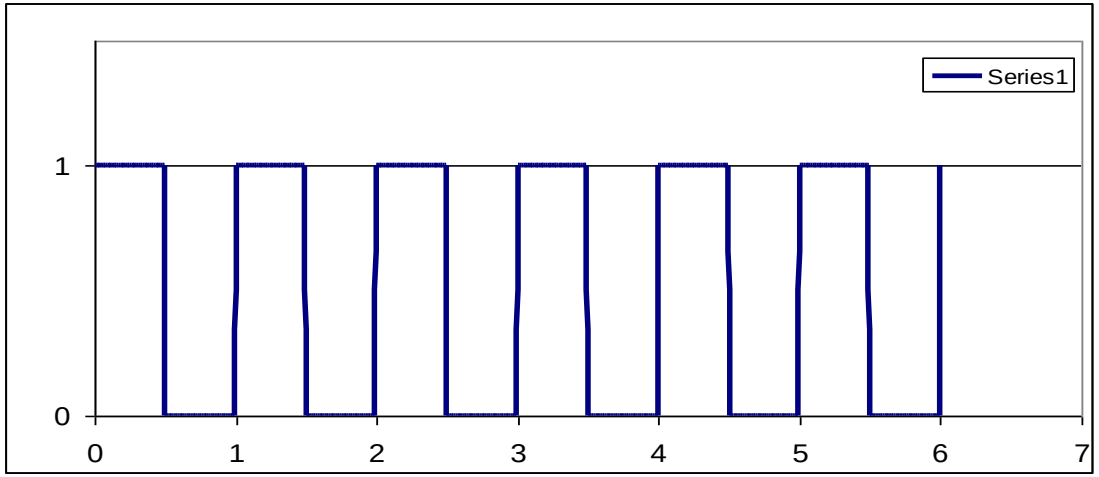

Example

$$F(t) \approx \frac{4}{\pi} \sin \omega t$$

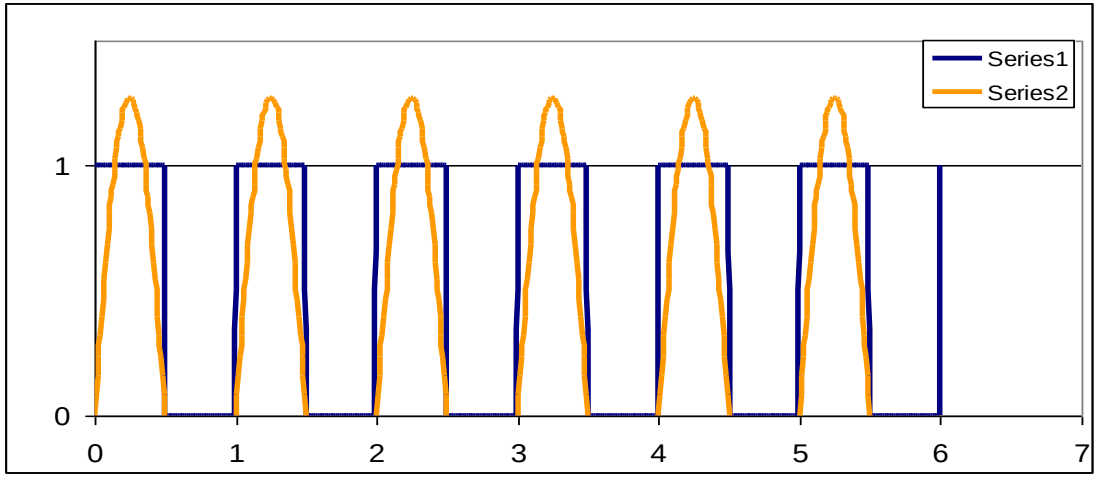

Example

$$F(t) \approx \frac{4}{\pi}\sin \omega t + \frac{4}{3\pi}\sin 3\omega t + \frac{4}{5\pi}\sin 5\omega t$$

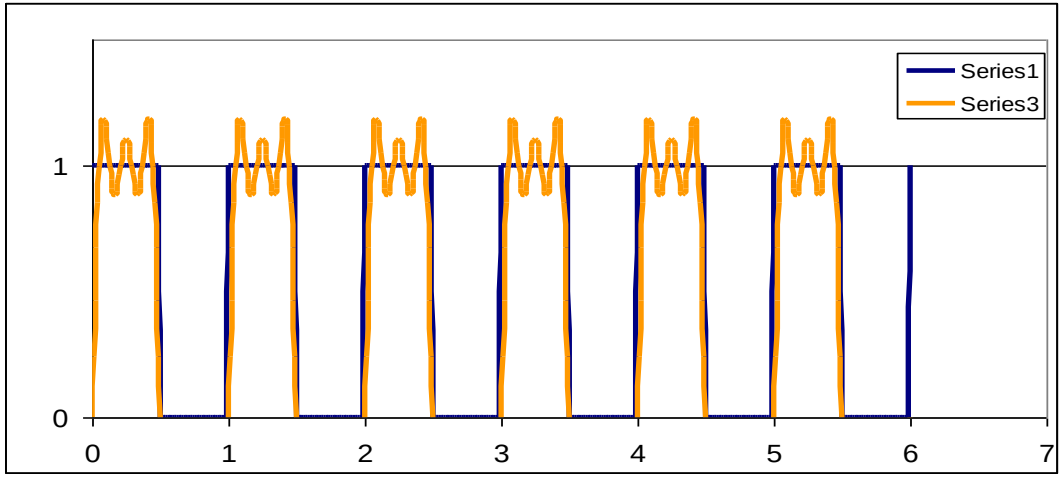

Example

- What if
  - T = .01s;
  - T = .05s;
  - T = 50s;

$$F(t) \approx \frac{4}{\pi}\sin \omega t + \frac{4}{3\pi}\sin 3\omega t + \frac{4}{5\pi}\sin 5\omega t$$

$$F(t) \approx \frac{4}{\pi}\sin \omega t + \frac{4}{3\pi}\sin 3\omega t + \frac{4}{5\pi}\sin 5\omega t$$

$$F(t) \approx \frac{4}{\pi}\sin \omega t + \frac{4}{3\pi}\sin 3\omega t + \frac{4}{5\pi}\sin 5\omega t$$

Time vs. Frequency Domain

- Time

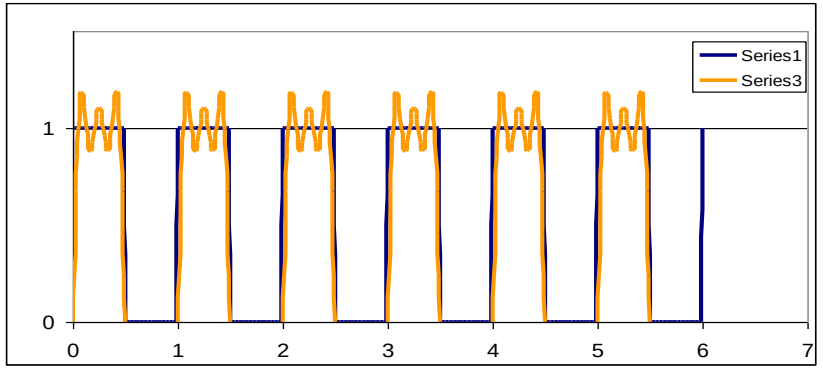

- Frequency

$$F(t) \approx \frac{4}{\pi}\sin \omega t + \frac{4}{3\pi}\sin 3\omega t + \frac{4}{5\pi}\sin 5\omega t$$

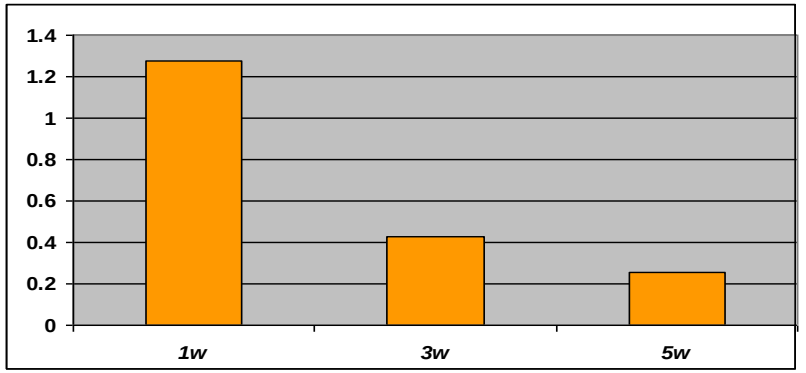

Why Frequency Domain?

- Allows efficient representation of a good approximation to the original function
- Makes filtering easy
- Note that convolution in the time domain is equivalent to multiplication in the frequency domain (and vice versa)
  - When you are faced with a difficult convolution (or multiplication), you can switch domains and do the complement operation

Fourier Family

Type of Transform	Example Signal
Fourier Transform *signals that are continious and aperiodic*	
Fourier Series *signals that are continious and periodic*	
Discrete Time Fourier Transform *signals that are discrete and aperiodic*	
Discrete Fourier Transform *signals that are discrete and periodic*	

Discrete Fourier Transform

- Rarely have closed form equation for F(t)

- Must sample at periodic intervals
  - generates a series of numeric values
  - apply transform to a time window of values
  - N = number of sample points
  - x[ ] contains sample points

DFT Notation

- c_k[i] and s_k [i] are the cosine and sine waves, each N points in length
  - c_k is cosine wave for amplitude in *ReX*[k]
  - s_k is sine wave for amplitude in *ImX*[k]
- k refers to the frequency of the wave
  - usually between 0 and N/2

$$c_k[i] = \cos(2\pi k i / N)$$

$$s_k[i] = \sin(2\pi k i / N)$$

Complex exponentials

- Alternatively, we can use complex exponentials
- Euler's formula: $e^{iw} = \cos(w) + i*\sin(w)$

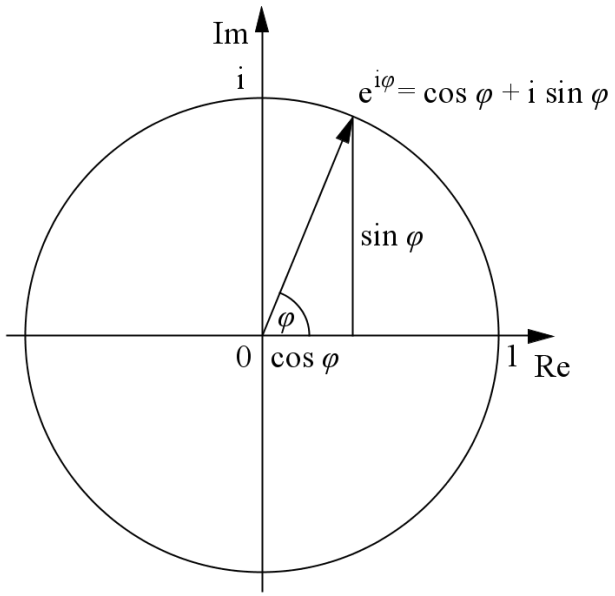

Calculate DFT

- Separate sinusoids

$$\mathrm{Re}\, X[k] = \sum_{i=0}^{N-1} x[i] \cos(2\pi k i / N)$$

$$\mathrm{Im}\, X[k] = -\sum_{i=0}^{N-1} x[i] \sin(2\pi k i / N)$$

- Complex exponentials

$$X_k = \sum_{n=0}^{N-1} x_n e^{-\frac{2\pi i}{N} k n} \qquad k = 0, \ldots, N-1$$

Calculate Inverse DFT

- Coefficients first need to be normalized

$$\mathrm{Re}\,\overline{X}[k] = \frac{\mathrm{Re}\,X[k]}{N/2} \qquad \mathrm{Im}\,\overline{X}[k] = -\frac{\mathrm{Im}\,X[k]}{N/2}$$

- With two special cases

$$\mathrm{Re}\,\overline{X}[0] = \frac{\mathrm{Re}\,X[0]}{N} \qquad \mathrm{Re}\,\overline{X}[N/2] = \frac{\mathrm{Re}\,X[N/2]}{N}$$

Calculate Inverse DFT

- Corresponding points within the basis function contribute to each input value
  - Equation uses the normalized coefficients
- Result is exactly equal to original data (within rounding error), ie IDFT(DFT(x[n])) = x[n]

$$x[i] = \sum_{k=0}^{N/2} \mathrm{Re}\,\overline{X}[k] \cos(2\pi k i / N) + \sum_{k=0}^{N/2} \mathrm{Im}\,\overline{X}[k] \sin(2\pi k i / N)$$

$$x_n = \frac{1}{N} \sum_{k=0}^{N-1} X_k e^{\frac{2\pi i}{N} kn} \qquad n = 0, \ldots, N-1.$$

DCT (Discrete Cosine Transform)

- DCT is very similar to DFT
  - Sine wave + phase shift equals cosine wave
  - N coefficients of cosine basis functions
  - Advantage: Result is purely real
  - Most common is “Type II”
  - Used in JPEG and MPEG

$$X_k = \sum_{n=0}^{N-1} x_n \cos\left[\frac{\pi}{N}\left(n + \frac{1}{2}\right)k\right]$$

FFT (Fast Fourier Transform)

- FFT is an efficient algorithm for computing the DFT
  - Naïve method for DFT requires $O(N^2)$ operations
  - FFT uses divide and conquer to break up problem into many 2-point DFT's (which are easy to compute)
  - 2-point DFT: $\mathbf{X}[0] = x[0] + x[1]$

    $\mathbf{X}[1] = x[0] - x[1]$
  - $\log_2 N$ stages, O(N) operations per stage => O(N log N) total operations
  - Ideally, want N to be a power of 2 or close to a power of 2

4-point FFT “butterfly” diagram

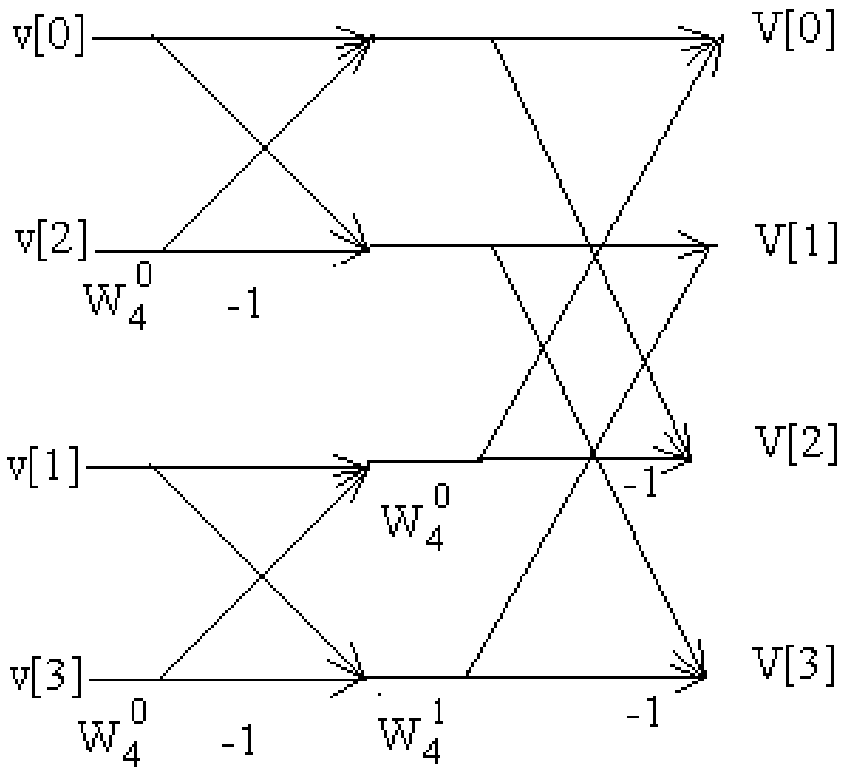

Fourier Transform

- Definitions:

$$X(\omega) = \int_{-\infty}^{\infty} x(t) e^{-i\omega t}\, dt \qquad x(t) = \frac{1}{2\pi} \int_{-\infty}^{\infty} X(\omega) e^{i\omega t}\, d\omega$$

$$X(f) = \int_{-\infty}^{\infty} x(t) e^{-i2\pi ft}\, dt \qquad x(t) = \int_{-\infty}^{\infty} X(f) e^{i2\pi ft}\, df$$

- Can be difficult to compute =>

  Often rely upon table of transforms

Delta function

- Definition:

$$\delta(x) = \begin{cases} \infty, & x = 0 \\ 0, & x \neq 0 \end{cases} \qquad \int_{-\infty}^{\infty} \delta(x)\, dx = 1. \qquad \int_{-\infty}^{\infty} f(x)\, \delta(x)\, dx = f(0)$$

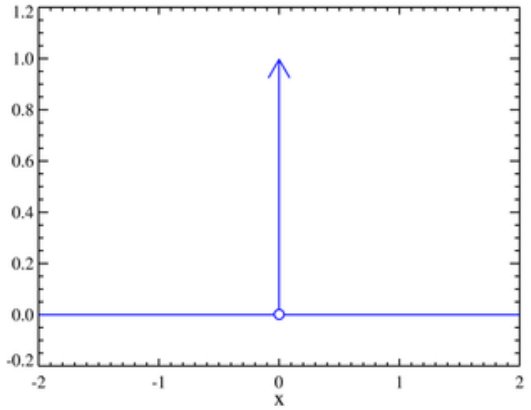

- Often, the result of the Fourier Transform needs to be expressed in terms of the delta function

Fourier Transform pairs

- $\Leftrightarrow$

$$\mathcal{F}_x\left[\sin\left(2\pi k_0 x\right)\right](k) \qquad \frac{1}{2} i\left[\delta\left(k+k_0\right)-\delta\left(k-k_0\right)\right],$$

- $\Leftrightarrow$

$$\mathcal{F}_x\left[\cos\left(2\pi k_0 x\right)\right](k) \qquad \frac{1}{2}\left[\delta\left(k-k_0\right)+\delta\left(k+k_0\right)\right],$$

- $\Leftrightarrow$

$$\mathcal{F}_x[1](k) \qquad \delta(k),$$

- There is a duality in all transform pairs

Basic Filters: Basic Concepts

Filtering is an important computation process in Geophysics that can be divided in two principal categories:

Natural filtering. It is produced when an observation or record is deformed or affected by the media characteristics.

Artificial filtering. It is produced by the observer when the observation or phenomena is recorded. In general, the record will be constituted a complex mixture of several components that will be necessary to separate (or filter), for a subsequent analysis.

Basic Filters: Basic Definition

A filter operates converting an input signal x(t) to an output signal y(t):

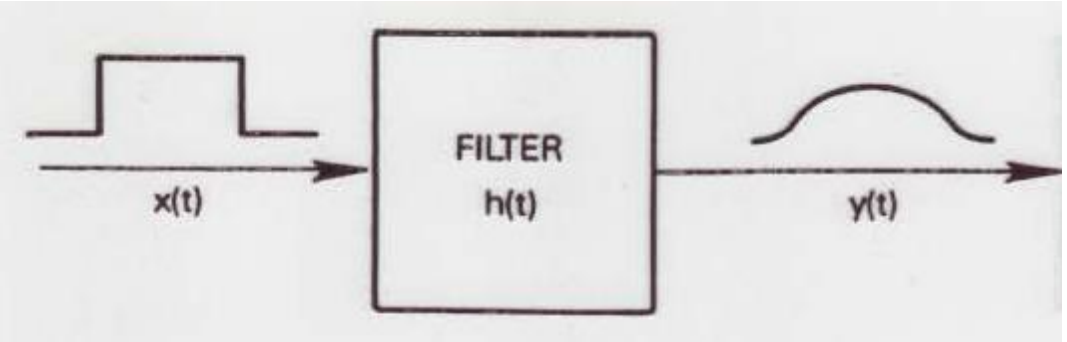

where h(t) is determined by the system properties. This general definition of a filter must be restricted to apply the spectral analysis, performed by the FFT. For it, the system given by h(t) must satisfy the fundamental properties listed below (bath, 1974).

Basic Filters: Fundamental Properties

Property of linearity. The differential equations of the system are linear equations. Thus, the system is a linear system:

$$f(t) = a_n f_n(t) \rightarrow g(t) = a_n g_n(t)$$

$$f(t) = \sum_n a_n f_n(t) \rightarrow g(t) = \sum_n a_n g_n(t)$$

$$\text{when } f_n(t) \rightarrow g_n(t)$$

The system is stationary. The differential equations of the system have constant coefficients. Then, the system properties are time independent.

$$f(t-\tau) \rightarrow g(t-\tau) \quad \text{when} \quad f(t) \rightarrow g(t)$$

Basic Filters: Convolution Formula

When a filter satisfy the properties above mentioned, the output signal g(t) can be computed by the convolution formula (bath, 1974):

$$g(t) = \int_{-\infty}^{\infty} f(\tau)h(t-\tau)d\tau$$

$$g(t) = f(t) * h(t) \quad \leftrightarrow \quad G(\omega) = F(\omega) \cdot H(\omega)$$

$$|G(\omega)| = |F(\omega)| \cdot |H(\omega)| \qquad \Phi_G(\omega) = \Phi_F(\omega) + \Phi_H(\omega)$$

amplitude spectrum phase spectrum

F(ω) = input-signal spectrum ,, H(ω) = filter-response spectrum
G(ω) = output-signal spectrum

Basic Filters: Distortions

Amplitude-distorting filters. When the amplitude spectrum of a filter is not a constant, this filter produces distortions in the amplitude spectrum of the output signal (bath, 1974).

Phase-distorting filters. When the phase spectrum of a filter is not zero, this filter produces distortions in the amplitude spectrum of the output signal. The output signal will be displaced on time respect to the input signal (bath, 1974).

No-distorting filters. When the amplitude spectrum of a filter is a constant and the phase spectrum is zero, this filter doesn’t produce distortions in the amplitude spectrum of the output signal (bath, 1974).

Basic Filters: Low-pass Filter

When the amplitude spectrum of a filter is written as (bath, 1974):

$$|H(\omega)| = 0 \quad \text{for } |\omega| > \alpha$$

This filter is a *low-pass* filter. The effects of this kind of filter can be observed by using of the program SPECTRUM.

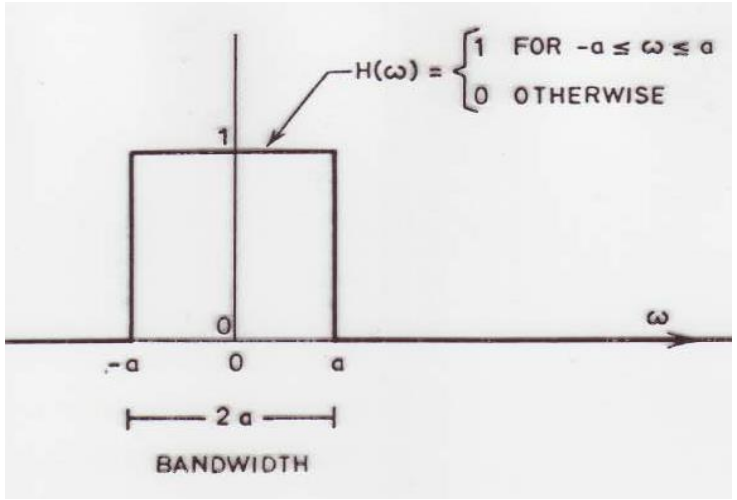

Basic Filters: High-pass Filter

When the amplitude spectrum of a filter is written as (bath, 1974):

$$|H(\omega)| = 0 \quad \text{for } |\omega| < \alpha$$

This filter is a *high-pass* filter. The effects of this kind of filter can be observed by using of the program SPECTRUM.

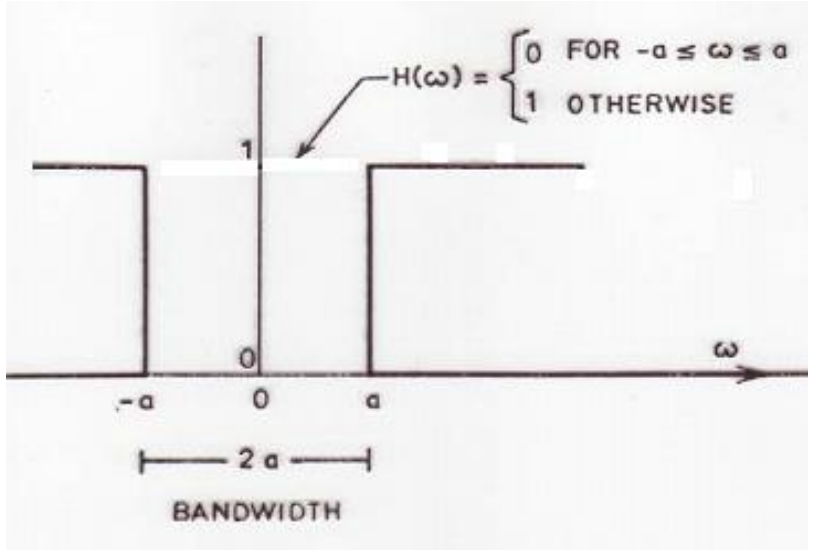

Basic Filters: Band-pass Filter

When the amplitude spectrum of a filter is written as (bath, 1974):

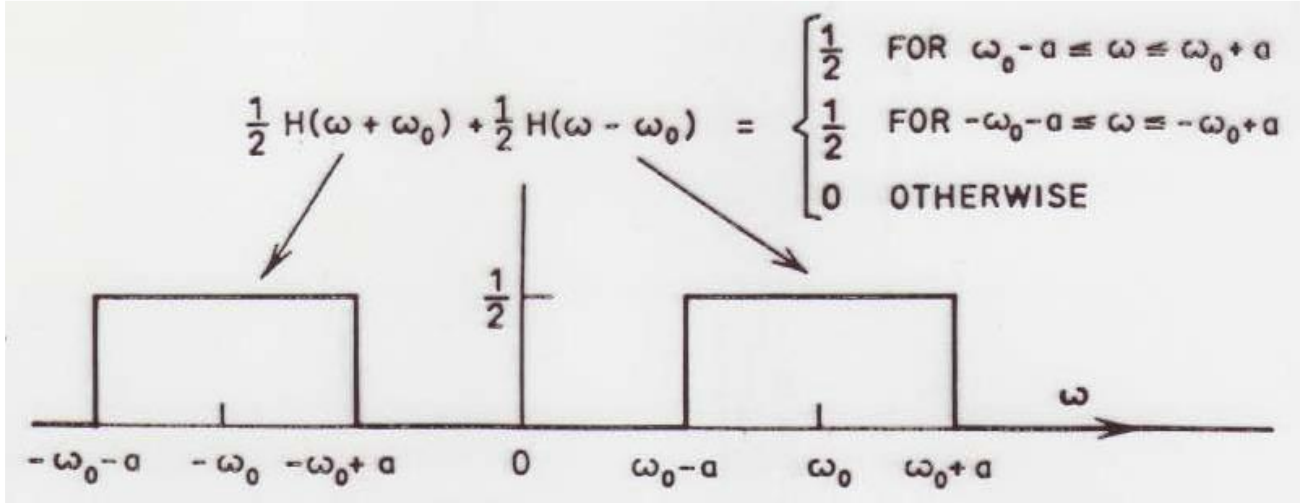

This filter is a *band-pass* filter. The effects of this kind of filter can be observed by using of the program SPECTRUM.

Basic Filters: Instrumental Response

The problem arisen in the recording of a physical phenomena is well illustrated below. The instrument used to perform this record distorts the original true-signal x(t) given the output signal y(t).

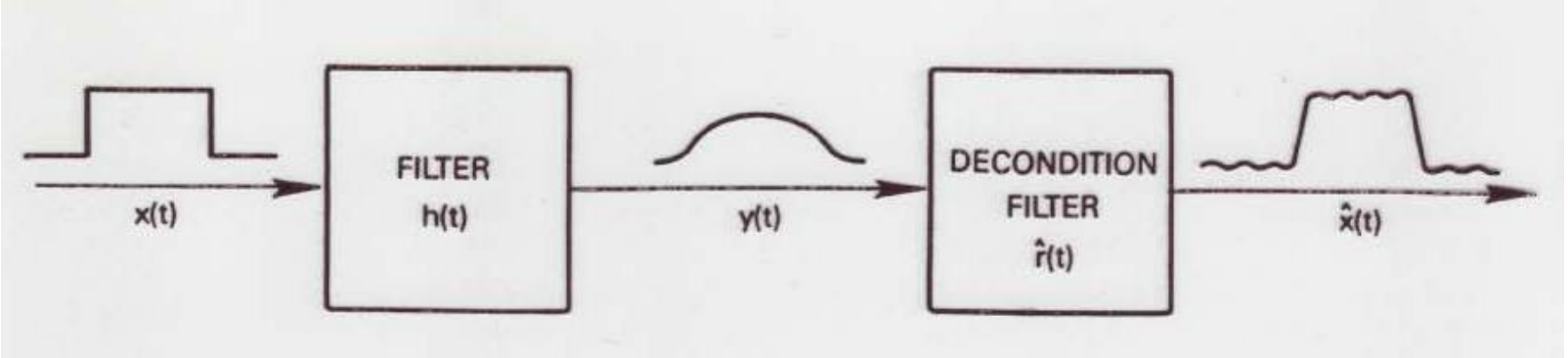

For this reason, a further process called *deconvolution* must be performed to recover the input signal x(t). Unfortunately, the input signal x(t) is never recovered *completely*. Thus, the signal recovered by the *decondition filter* is not *exactly* equal to x(t). Nevertheless, if the deconvolution process is well done, the recovered signal can be used instead of the original signal x(t), with a small error (Brigham, 1988).

Basic Filters: Instrumental Response

The distortions produced by the instrument give the output signal g(t). This *perturbed* signal g(t) is the convolution of the *true* signal f(t) and the *system response* h(t), written as

$$g(t) = \int_{-\infty}^{\infty} f(\tau)h(t-\tau)d\tau$$

$$g(t) = f(t) * h(t) \quad \leftrightarrow \quad G(\omega) = F(\omega) \cdot H(\omega)$$

$$|G(\omega)| = |F(\omega)| \cdot |H(\omega)|$$
$$\Phi_G(\omega) = \Phi_F(\omega) + \Phi_H(\omega)$$

$$\rightarrow$$

$$|F(\omega)| = |G(\omega)| / |H(\omega)|$$
$$\Phi_F(\omega) = \Phi_G(\omega) - \Phi_H(\omega)$$

When the *true spectrum* F(ω) is computed from the *output spectrum* G(ω) and the *instrumental spectrum* H(ω), the *original true-signal* f(t) is recovered computing the FFT backward applied to the true spectrum F(ω).

Basic Filters: Instrumental Response

The *instrumental response* or spectrum H(ω) is always known for the instrument used in the recording of the input signal f(t). In the case of seismological instruments, the *amplitude* and *phase* of H(ω) are plotted below for two typical seismographs.

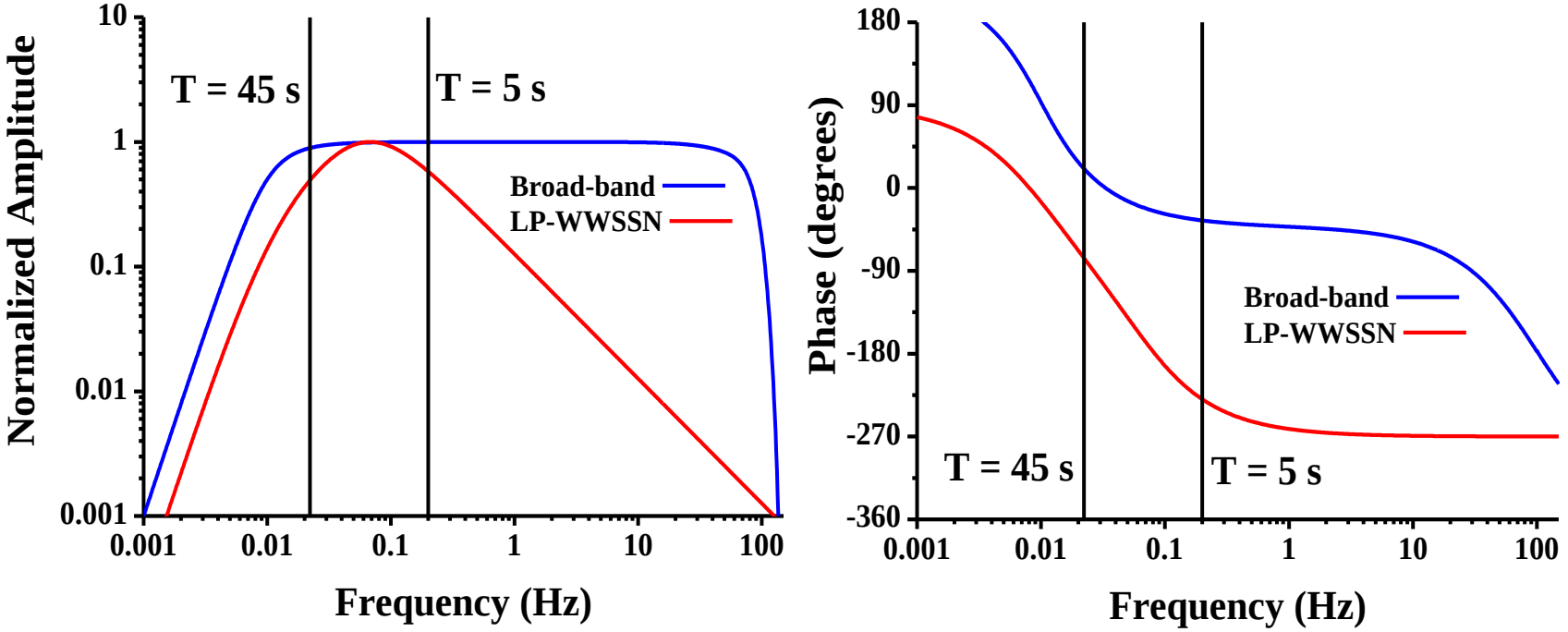

Basic Filters: Instrumental Response

The *instrumental response* or spectrum H(ω) will produce distortions on the amplitude and phase of the signal recorded. The figure presented below shows as the *true amplitude and phase* can be recovered, after the instrumental correction performed for the *LP-WWSSN* instrument.

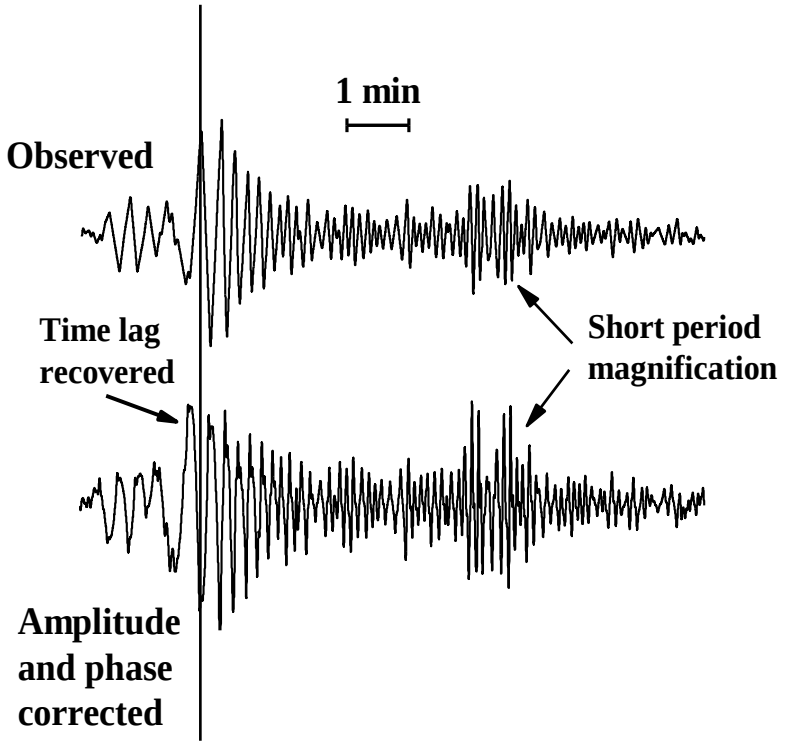

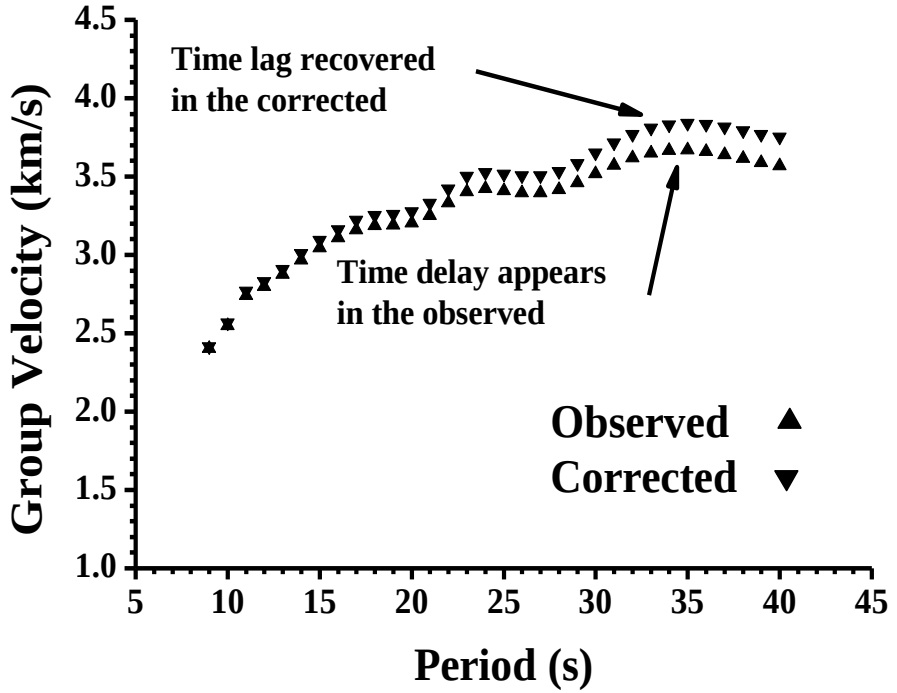

Basic Filters: Instrumental Response

The *instrumental response* or spectrum H(ω) will produce distortions on the amplitude and phase of the signal recorded. The figure presented below shows as the *true amplitude and phase* can be recovered, after the instrumental correction performed for the *broad-band* instrument.

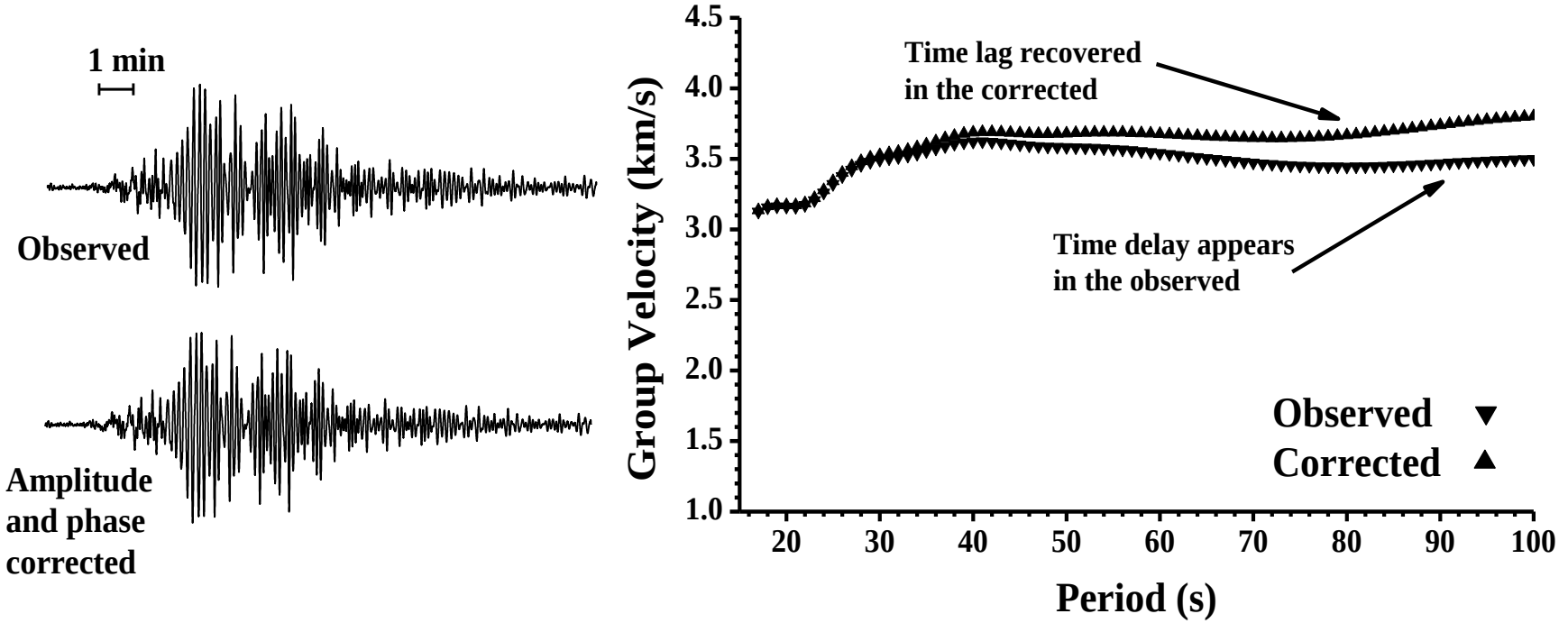

Basic Filters: References

Bath M. (1974). *Spectral Analysis in Geophysics*. Elsevier, Amsterdam.

Brigham E. O. (1988). *The Fast Fourier Transform and Its Applications*. Prentice Hall, New Jersey.

Basic Filters: Web Pages

http://airy.ual.es/www/series.htm

http://airy.ual.es/www/spectrum.htm

http://airy.ual.es/www/spectrum2D.htm

Filtering Geophysical Data: Be careful!

- Filtering: basic concepts
- Seismogram examples, high-low-bandpass filters
- The crux with causality
- Windowing seismic signals
  - Various window functions
  - Multitaper approach
  - Wavelets (principle)

Scope: Understand the effects of filtering on time series (seismograms). Get to know frequently used windowing functions.

Why filtering

1. Get rid of unwanted frequencies
2. Highlight signals of certain frequencies
3. Identify harmonic signals in the data
4. Correcting for phase or amplitude characteristics of instruments
5. Prepare for down-sampling
6. Avoid aliasing effects

A seismogram

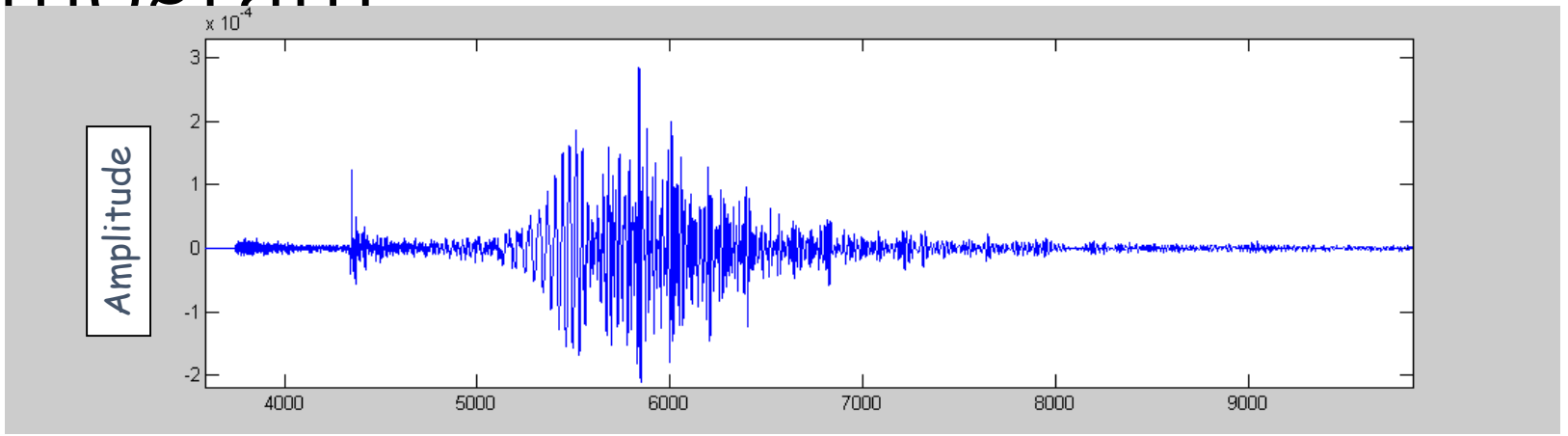

Time (s)

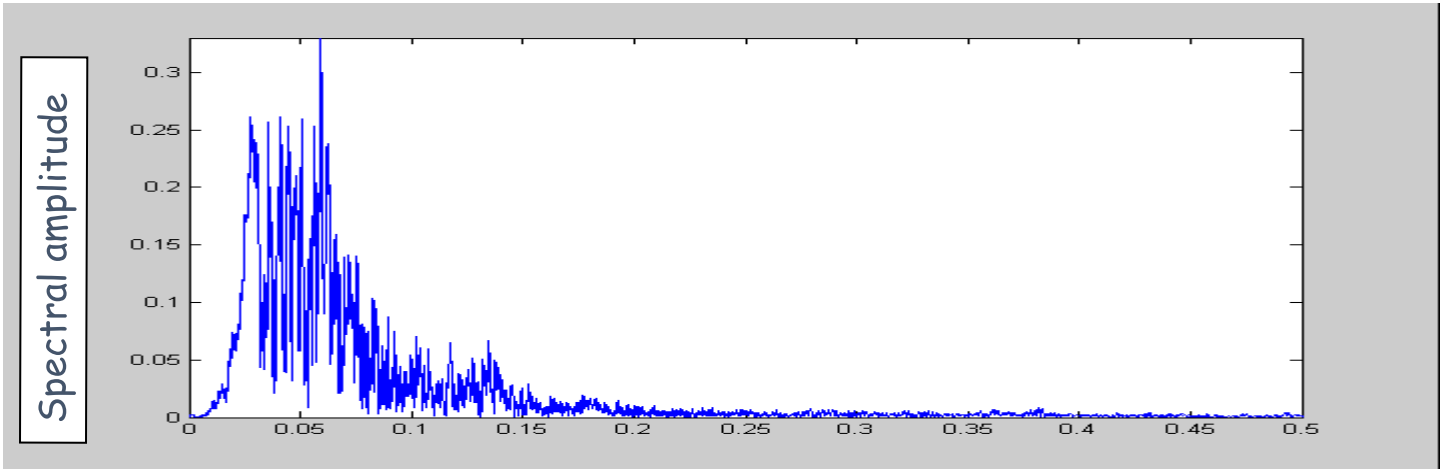

Frequency (Hz)

Digital Filtering

Often a recorded signal contains a lot of information that we are not interested in (noise). To get rid of this noise we can apply a filter in the frequency domain.

The most important filters are:

- High pass: cuts out low frequencies
- Low pass: cuts out high frequencies
- Band pass: cuts out both high and low frequencies and leaves a band of frequencies
- Band reject: cuts out certain frequency band and leaves all other frequencies

Cutoff frequency

the **cutoff or corner frequency** is the frequency either above which or below which the power output of a circuit, such as a line, amplifier, or filter, is reduced to 1/2 of the passband power; the half-power point. This is equivalent to a voltage (or amplitude) reduction to 70.7% of the passband. This happens to be close to $-3dB$, and the cutoff frequency is frequently referred to as the $-3dB$ point. It is also referred to as the knee frequency, due to a frequency response curve's physical appearance.

Cut-off and slopes in spectra

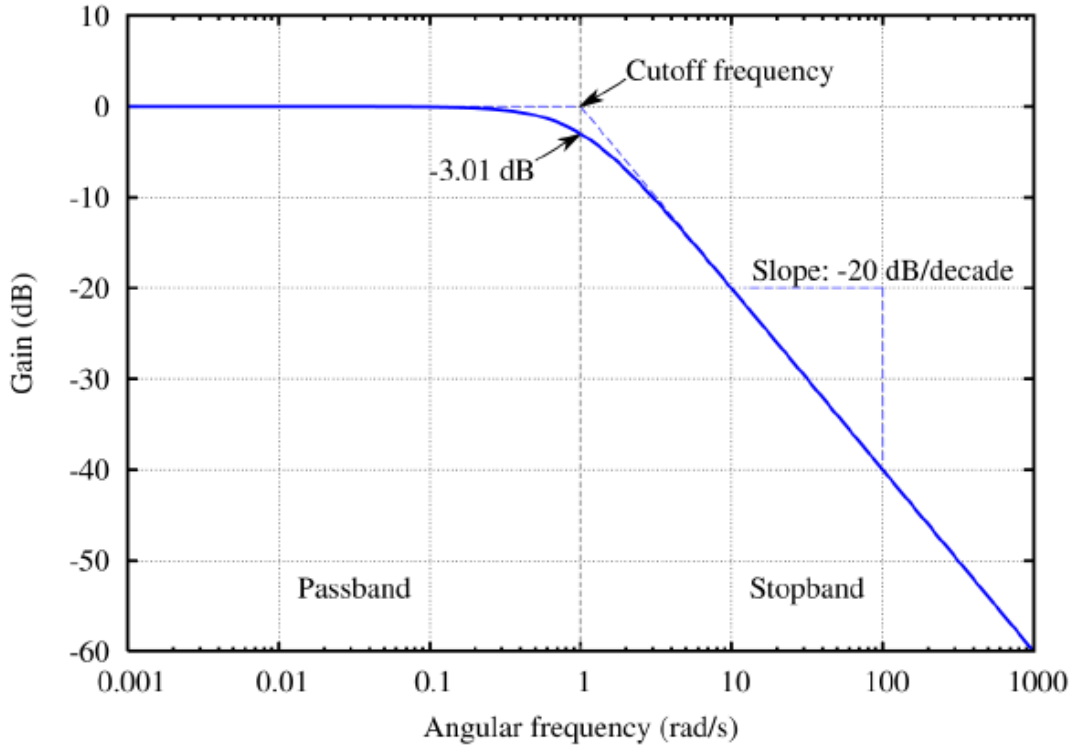

Figure 5.2: Amplitude response of a highpass Butterworth filter, showing the passband, stopband and the cutoff frequency. (The slope $-20dB$ per decade is the same as $-6dB$ per octave, equivalent to a slope of $-s^1$ [as one order of magnitude in amplitude is equal to $20db$].)

Digital Filtering

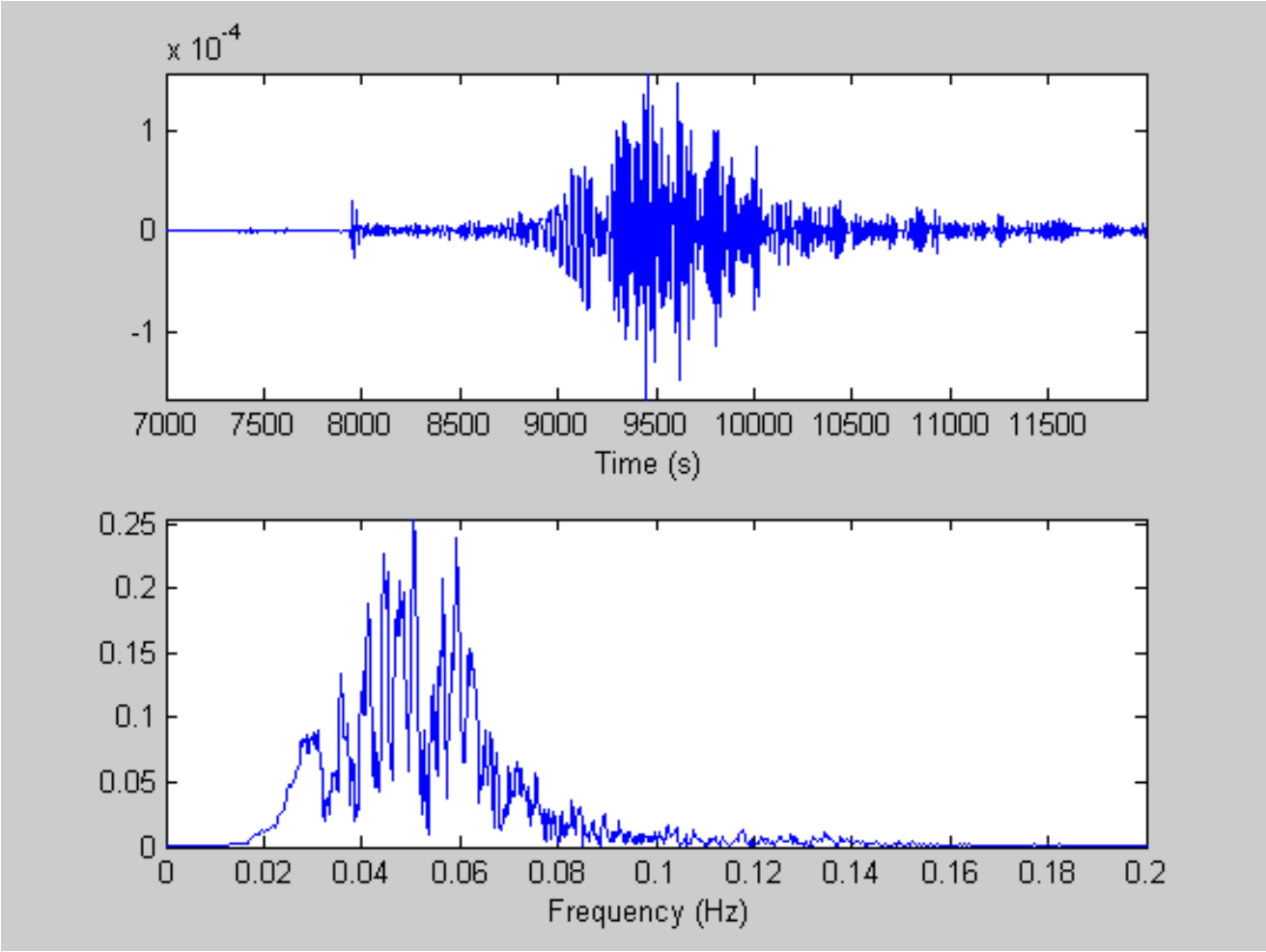

Low-pass filtering

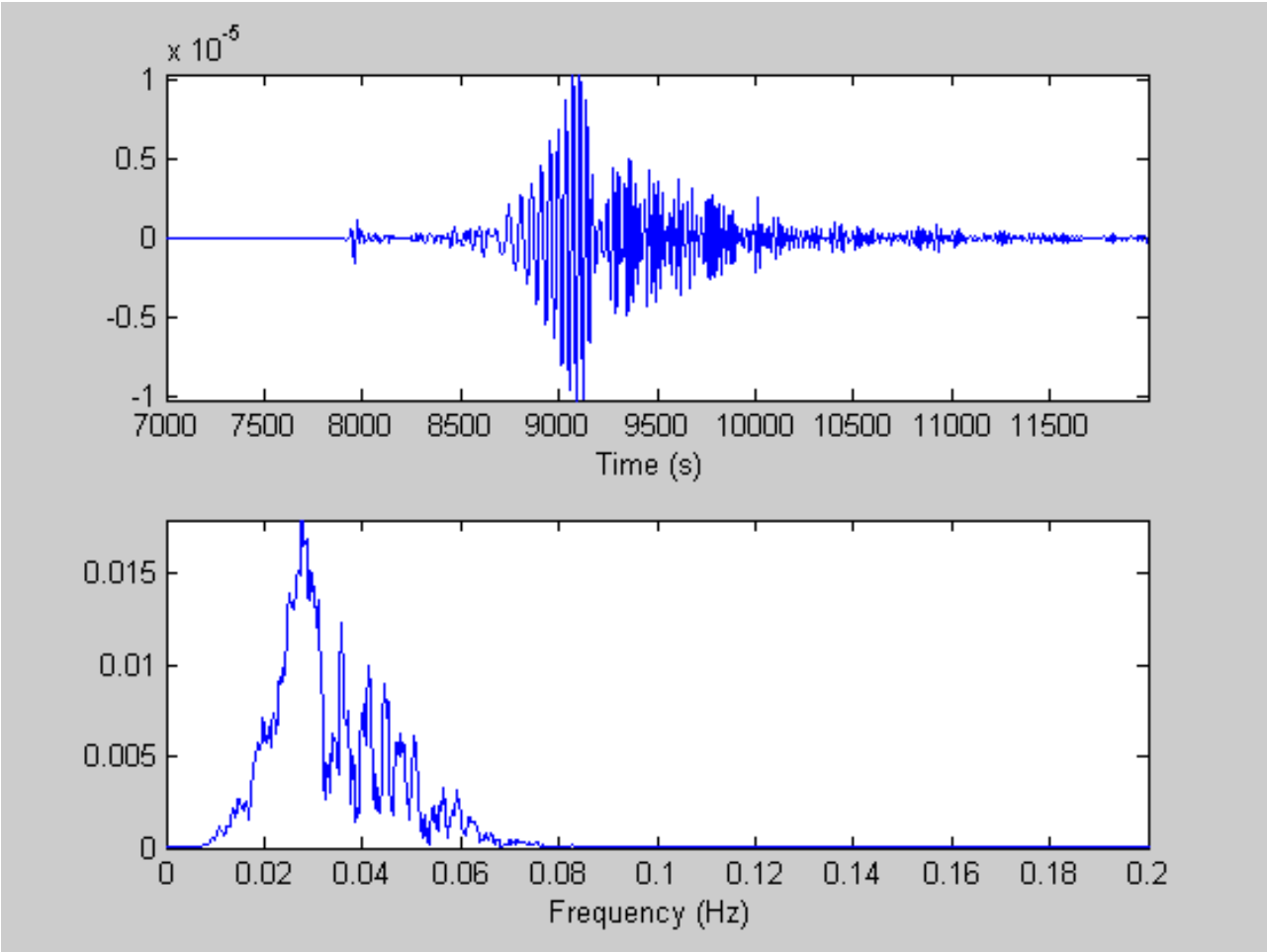

Lowpass filtering

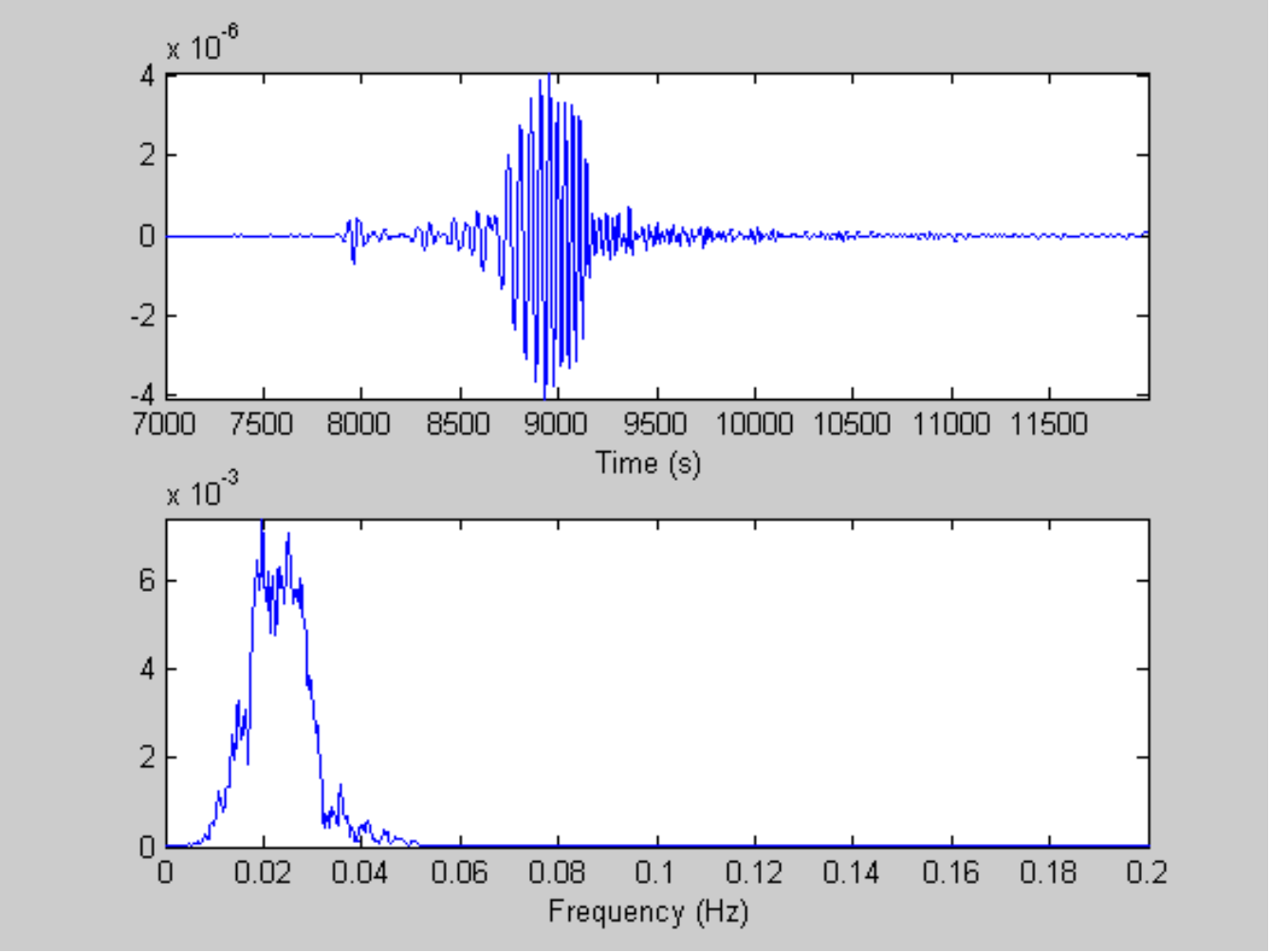

High-pass filter

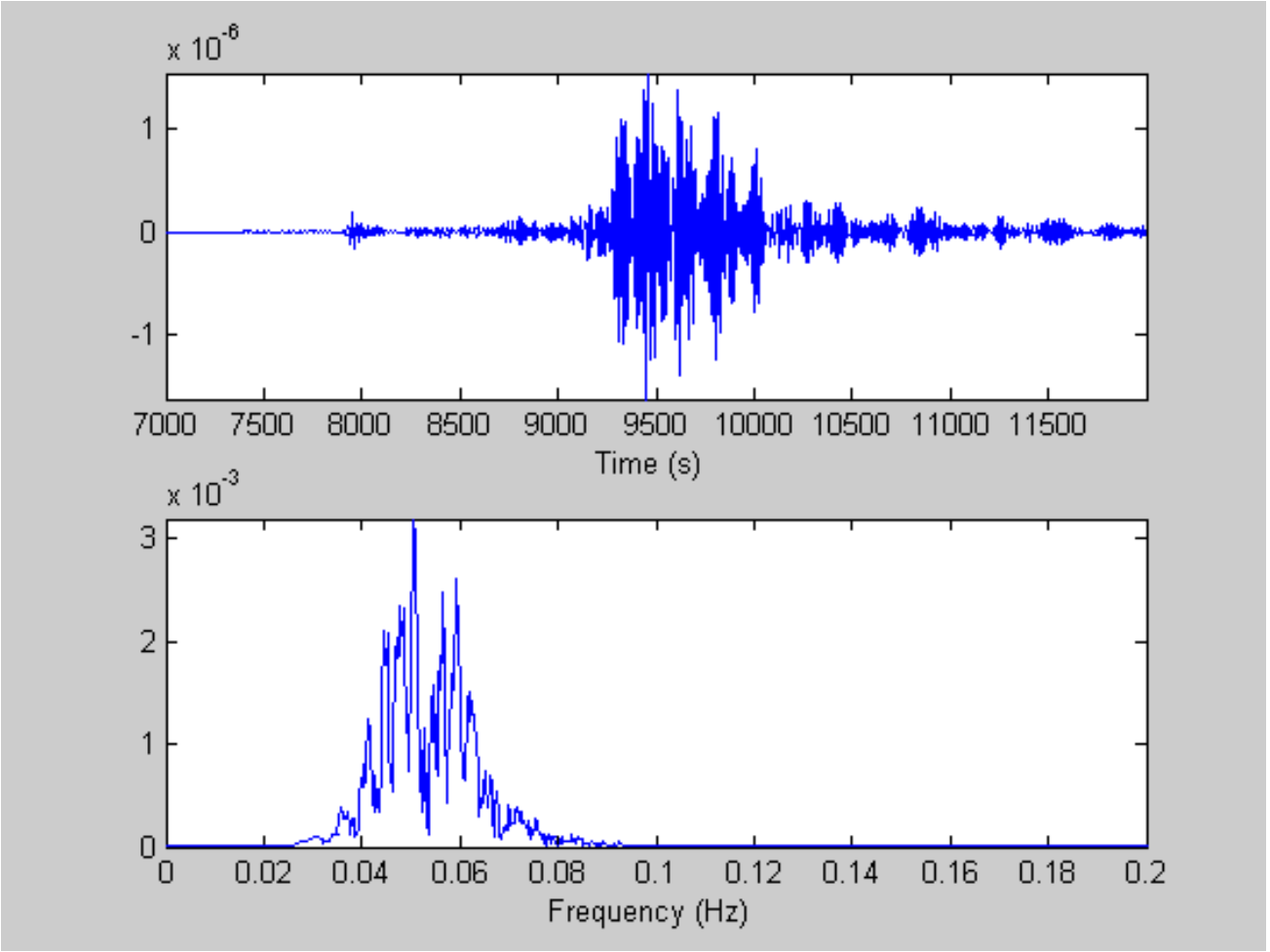

Band-pass filter

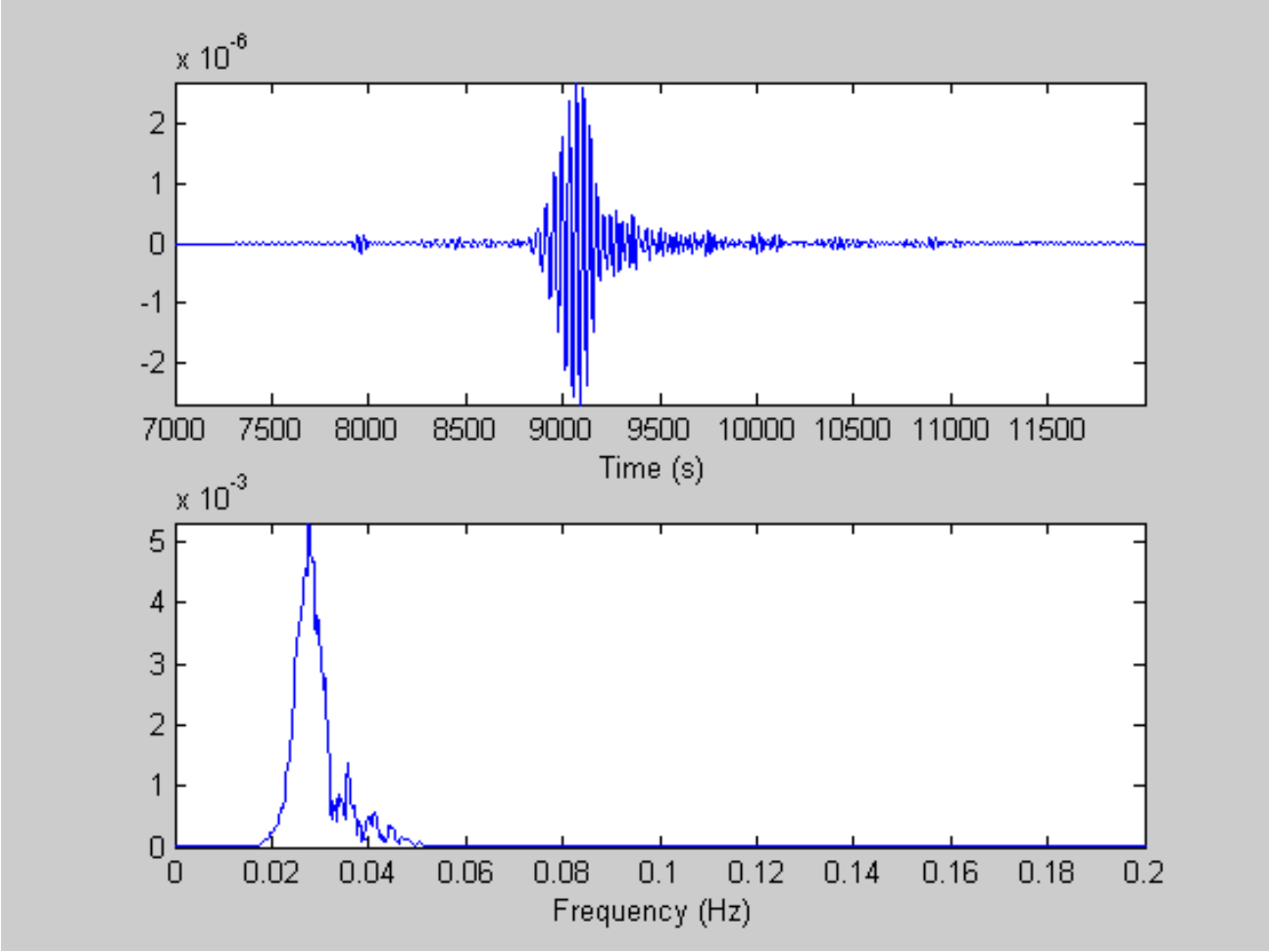

The simplemost filter

The simplemost filter gets rid of all frequencies above a certain cut-off frequency (low-pass), „box-car“

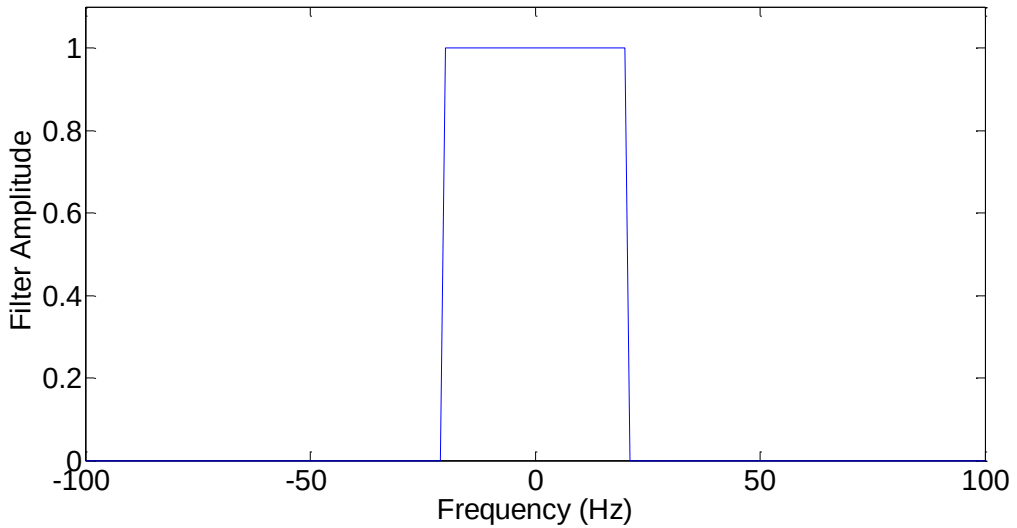

$$H_L(\omega) = \begin{cases} 1 & if \quad |\omega| \le \omega \\ 0 & if \quad |\omega| > \omega_0 \end{cases}$$

The simplemost filter

… and its brother
… (high-pass)

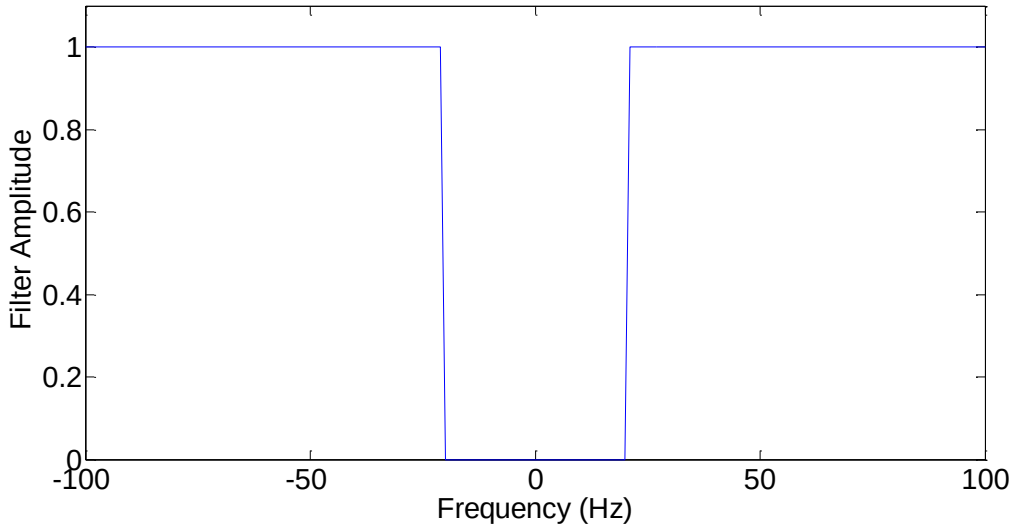

$$H_H(\omega) = 1 - H_L(\omega) = \begin{cases} 1 & if \quad |\omega| > \omega \\ 0 & if \quad |\omega| \le \omega_0 \end{cases}$$

… let‘s look at the consequencse

$$f(t) = \frac{1}{\sqrt{2\pi}} \int_{-\infty}^{\infty} F(k) e^{-ik\omega} dt$$

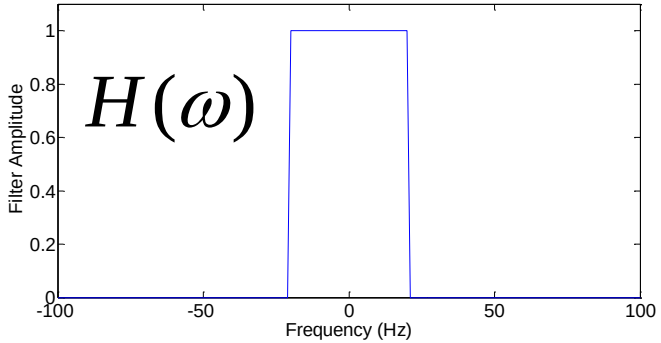

$$f^{filt}(t) = \frac{1}{\sqrt{2\pi}} \int_{-\infty}^{\infty} H(\omega) F(\omega) e^{-ik\omega} dt$$

… but what does H(ω) look like in the time domain … remember the convolution theorem?

… surprise …

$$h(t) = \frac{1}{\sqrt{2\pi}} \int_{-\infty}^{\infty} H(\omega) e^{-ik\omega} dt$$

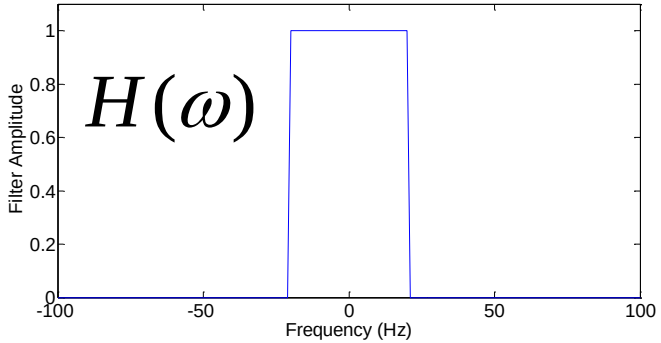

Zero phase and causal filters

Zero phase filters can be realised by

- Convolve first with a chosen filter
- Time reverse the original filter and convolve again
- First operation multiplies by $F(\omega)$, the 2nd operation is a multiplication by $F^*(\omega)$
- The net multiplication is thus $|F(w)|^2$
- These are also called two-pass filters

The Butterworth Filter (Low-pass, 0-phase)

$$\left|F_L(\omega)\right| = \frac{1}{1+(\omega/\omega_c)^{2n}}$$

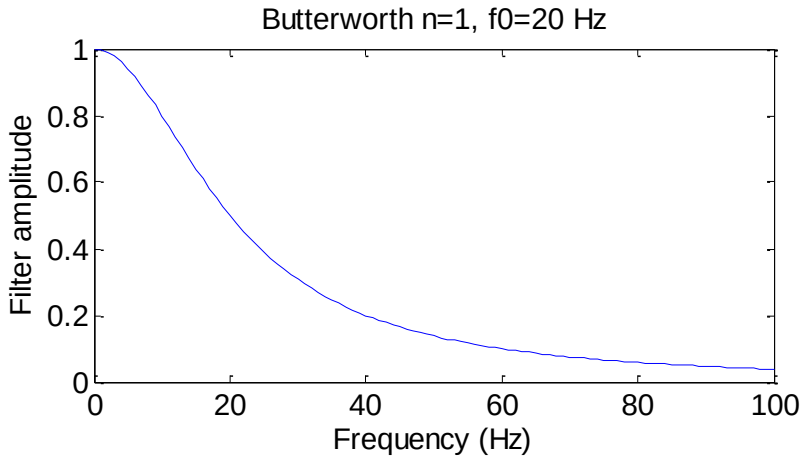

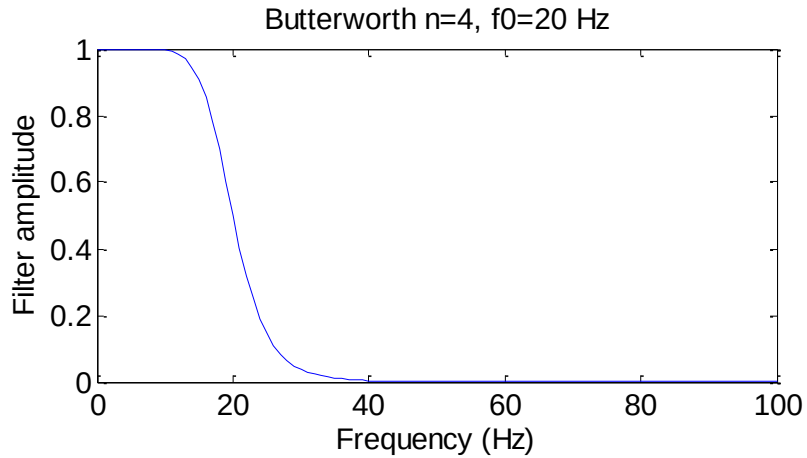

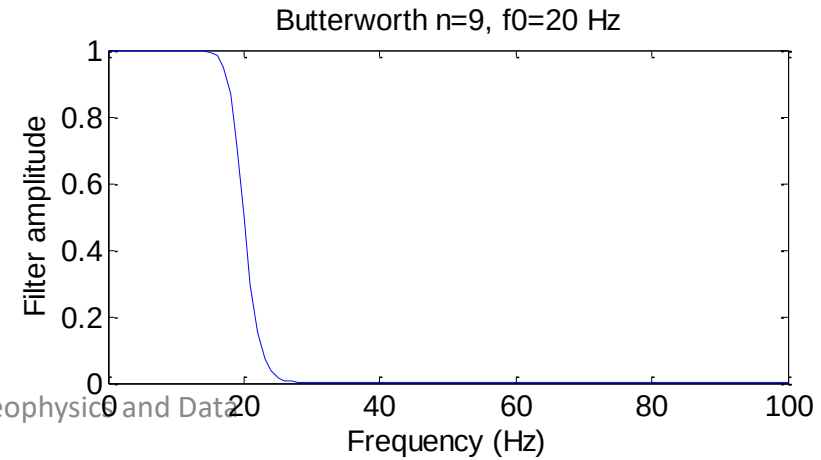

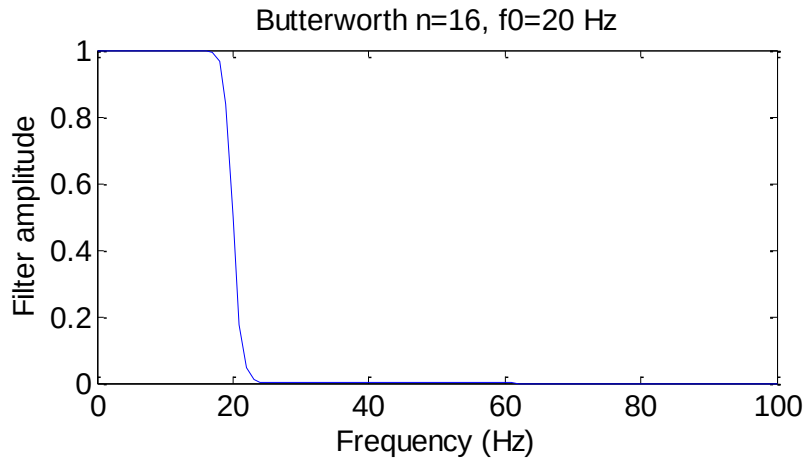

… effect on a spike …

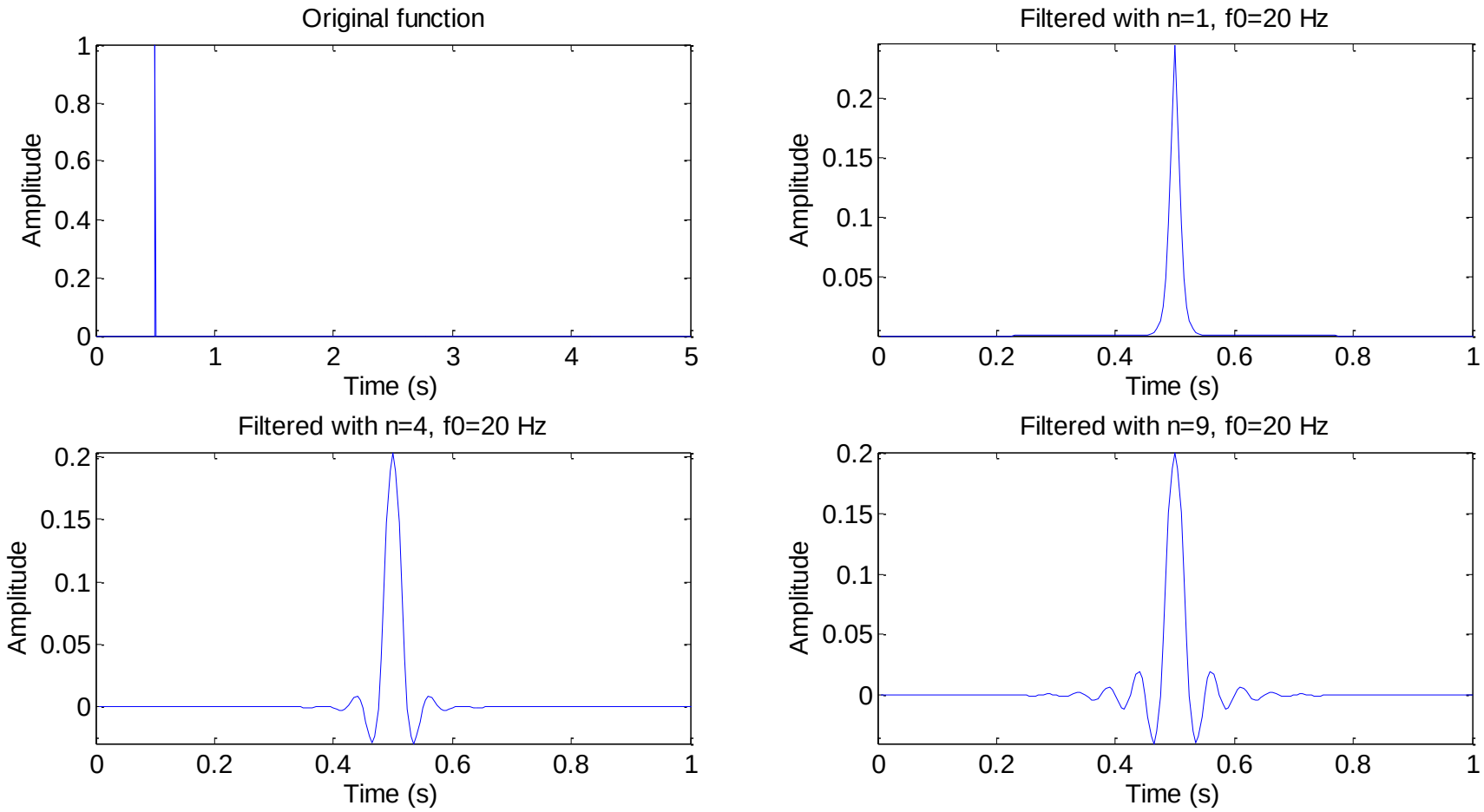

… on a seismogram …

… varying the order …

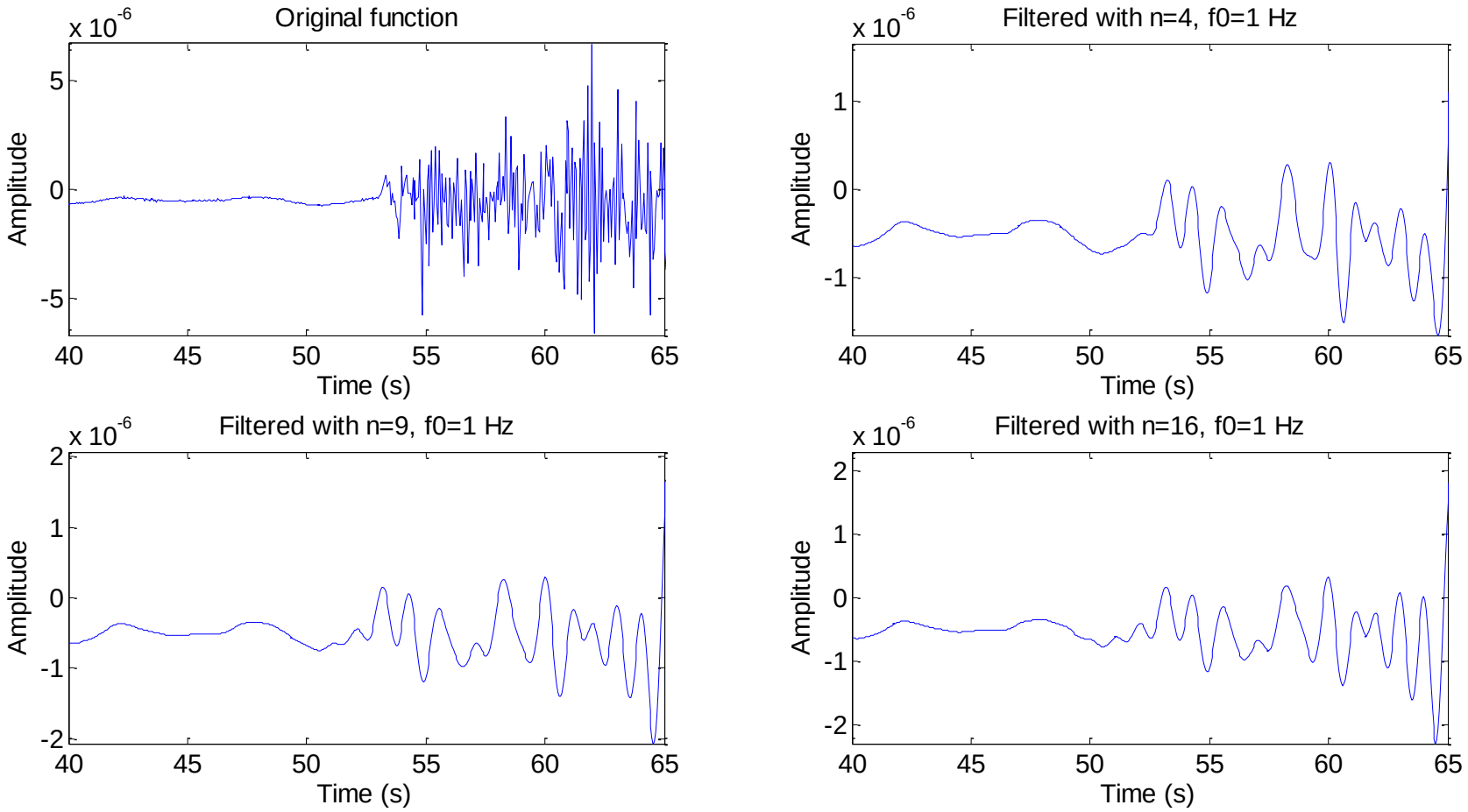

… on a seismogram …

… varying the cut-off frequency…

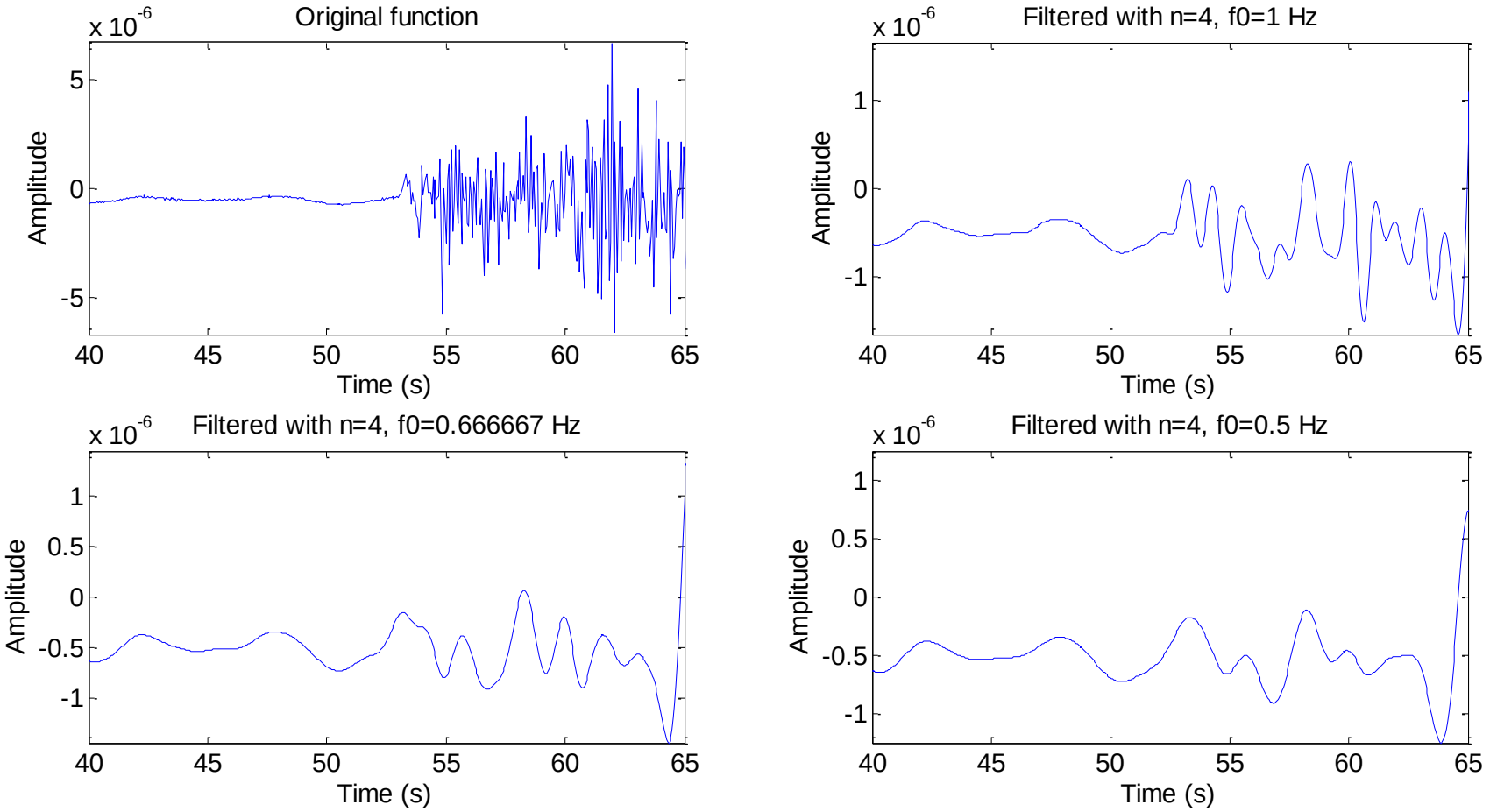

The Butterworth Filter (High-Pass)

$$\left|F_H(\omega)\right| = 1 - \frac{1}{1+(\omega/\omega_c)^{2n}}$$

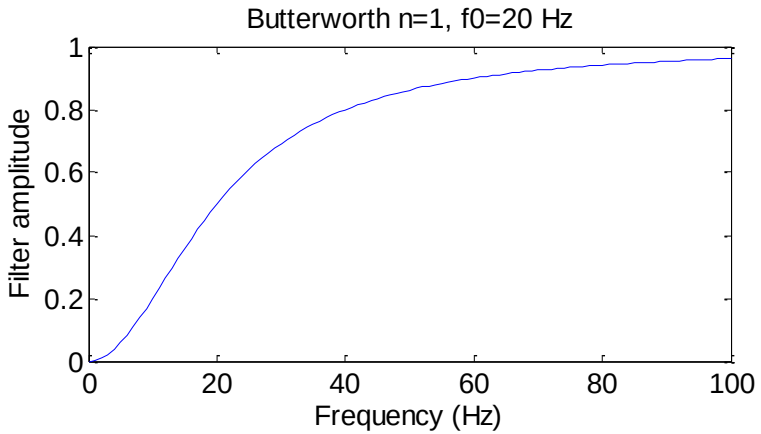

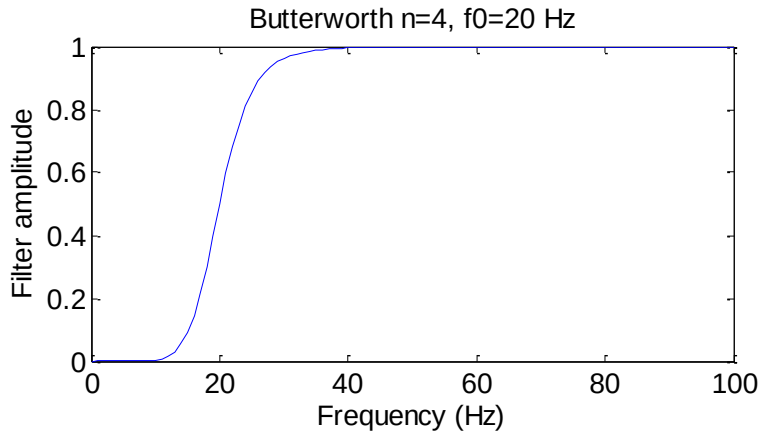

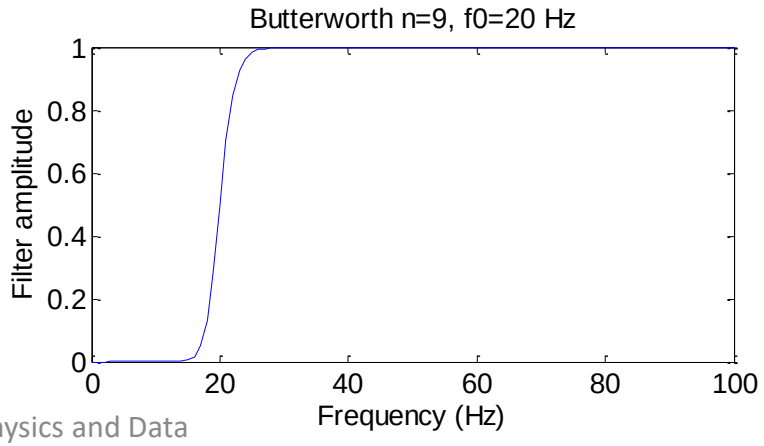

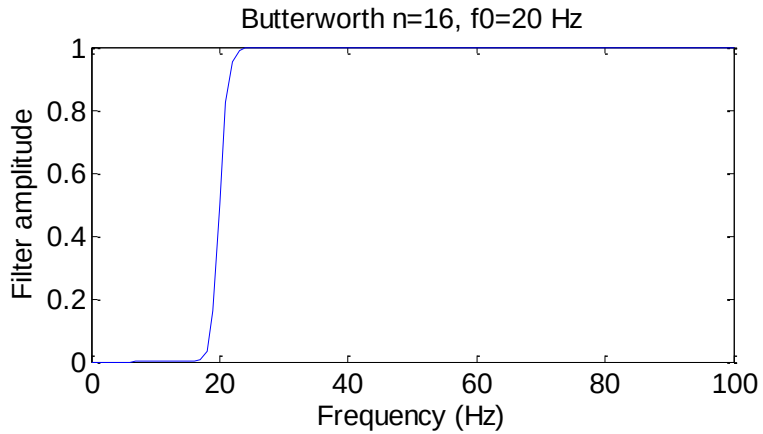

… effect on a spike …

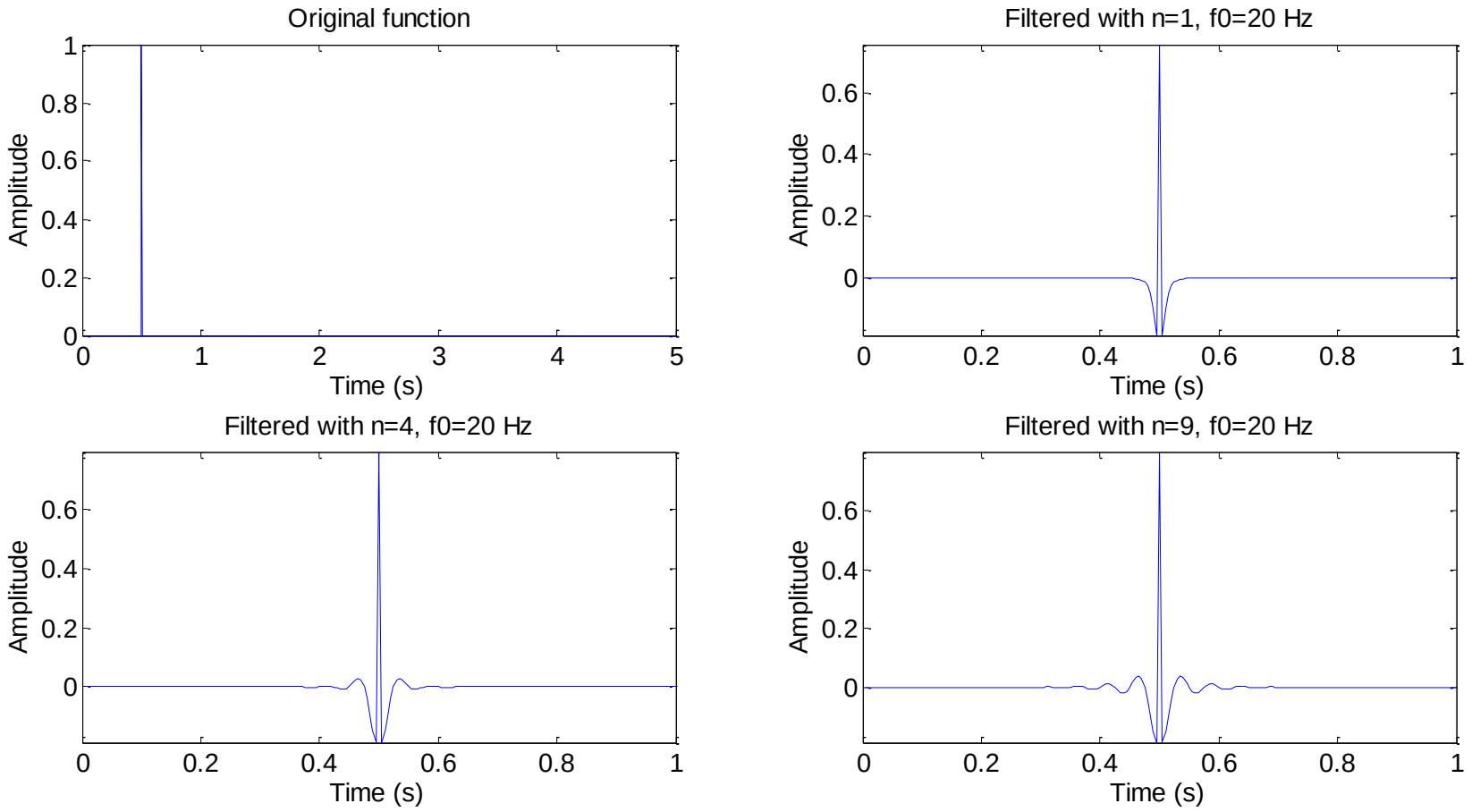

… on a seismogram …

… varying the order …

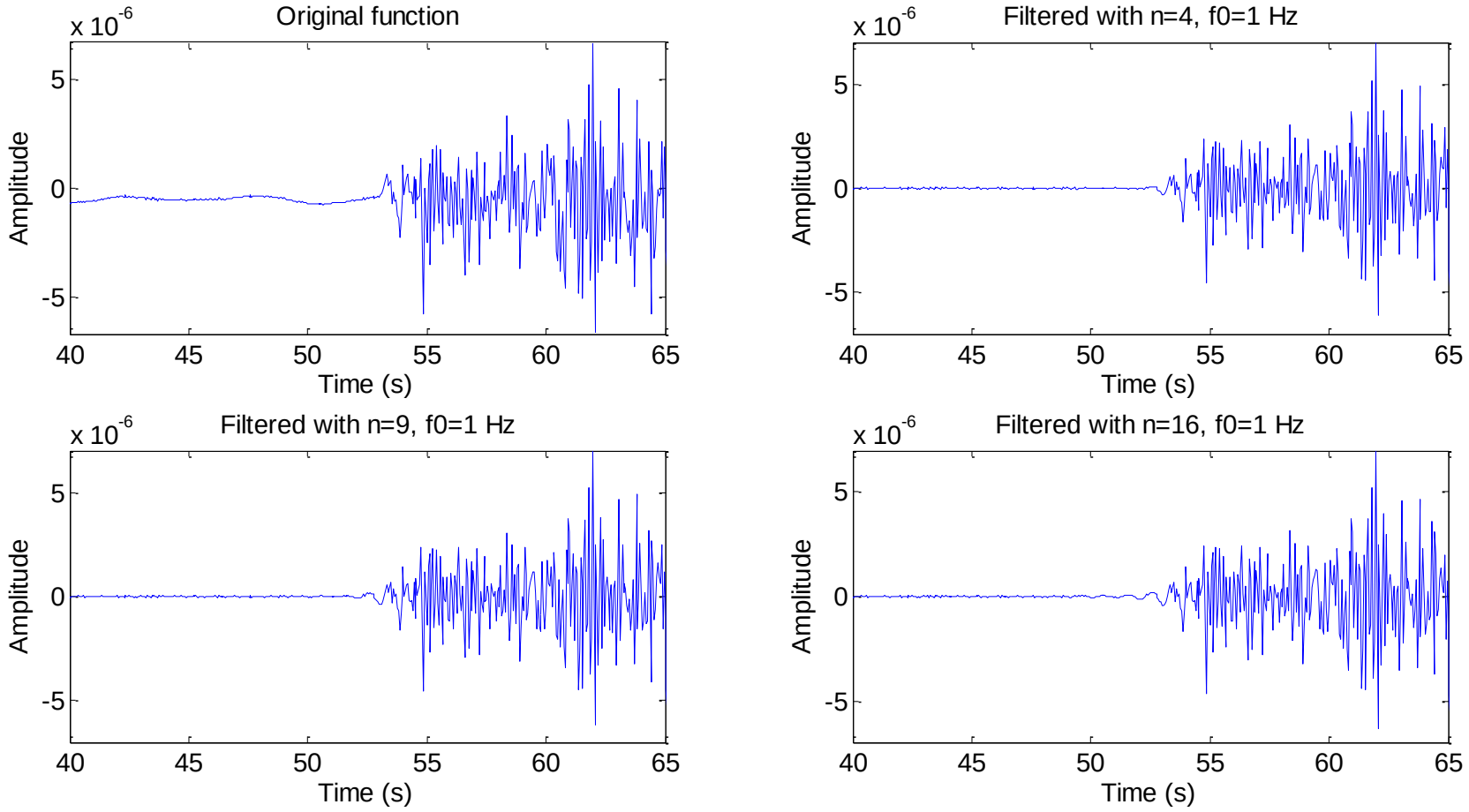

… on a seismogram …

… varying the cut-off frequency…

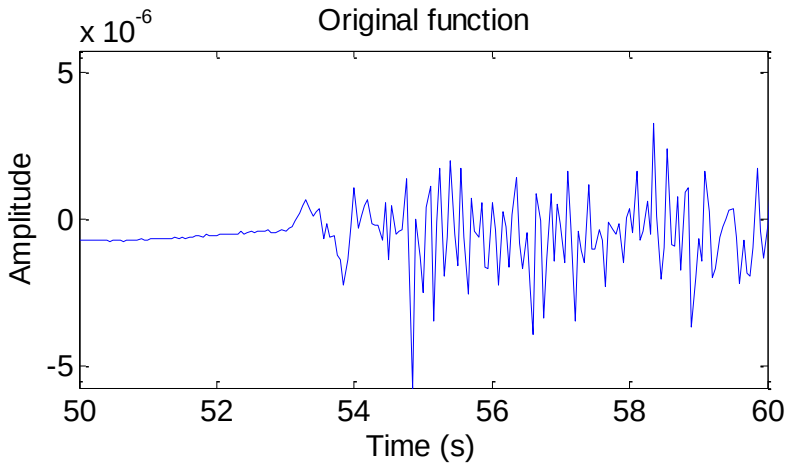

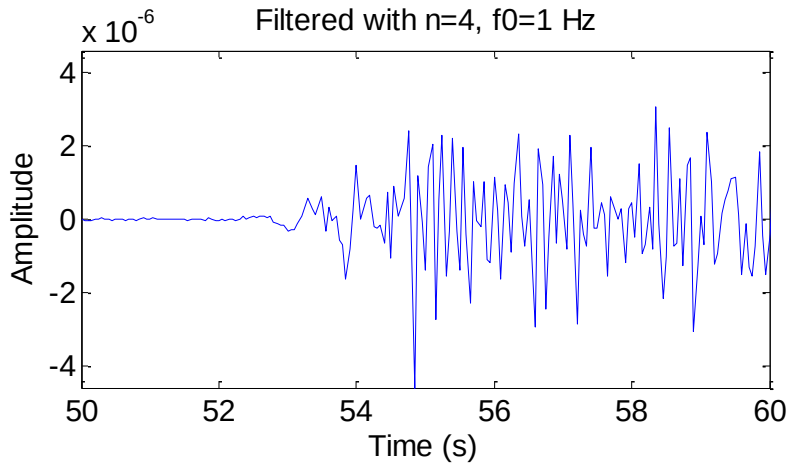

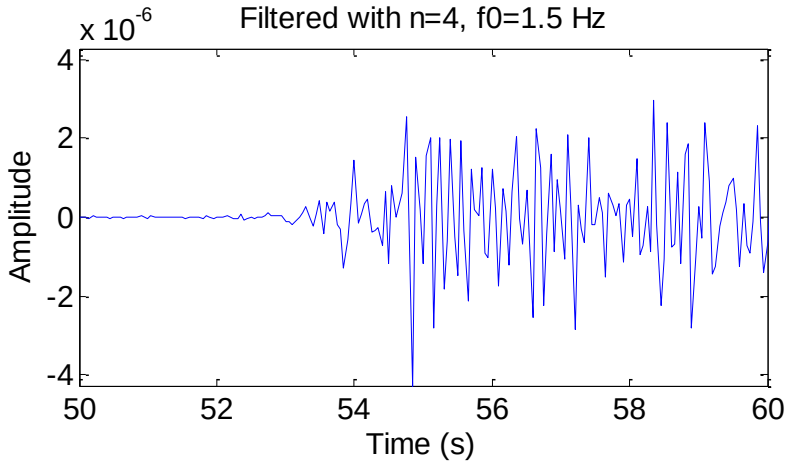

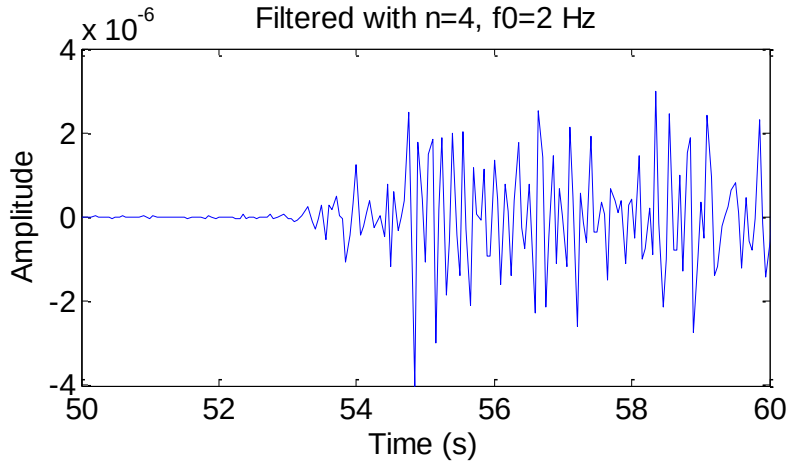

The Butterworth Filter (Band-Pass)

$$\left|F_{BP}(\omega)\right| = 1 - \frac{1}{1+\left[(\omega-\omega_b)/\Delta\omega\right]^{2n}}$$

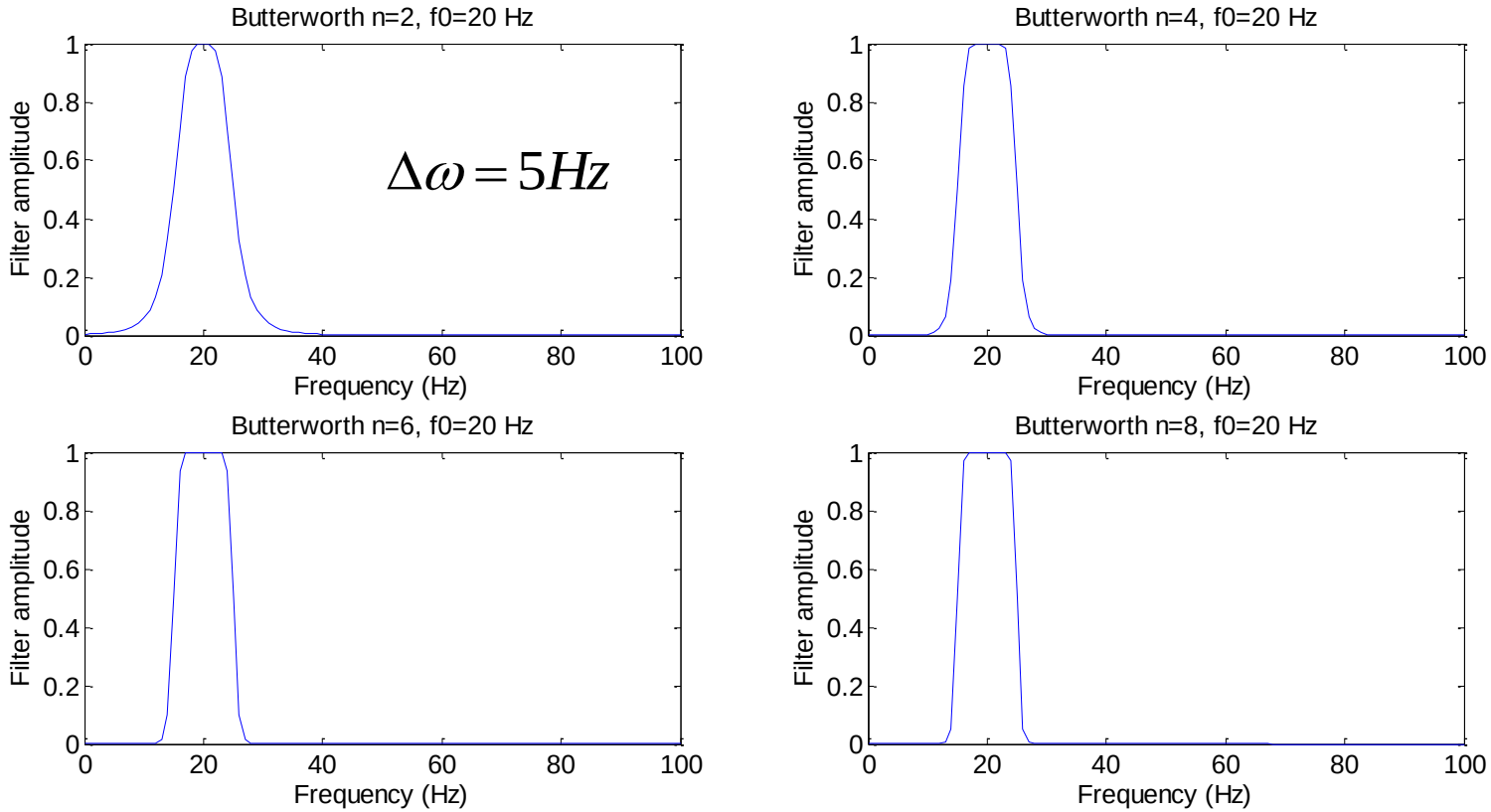

… effect on a spike …

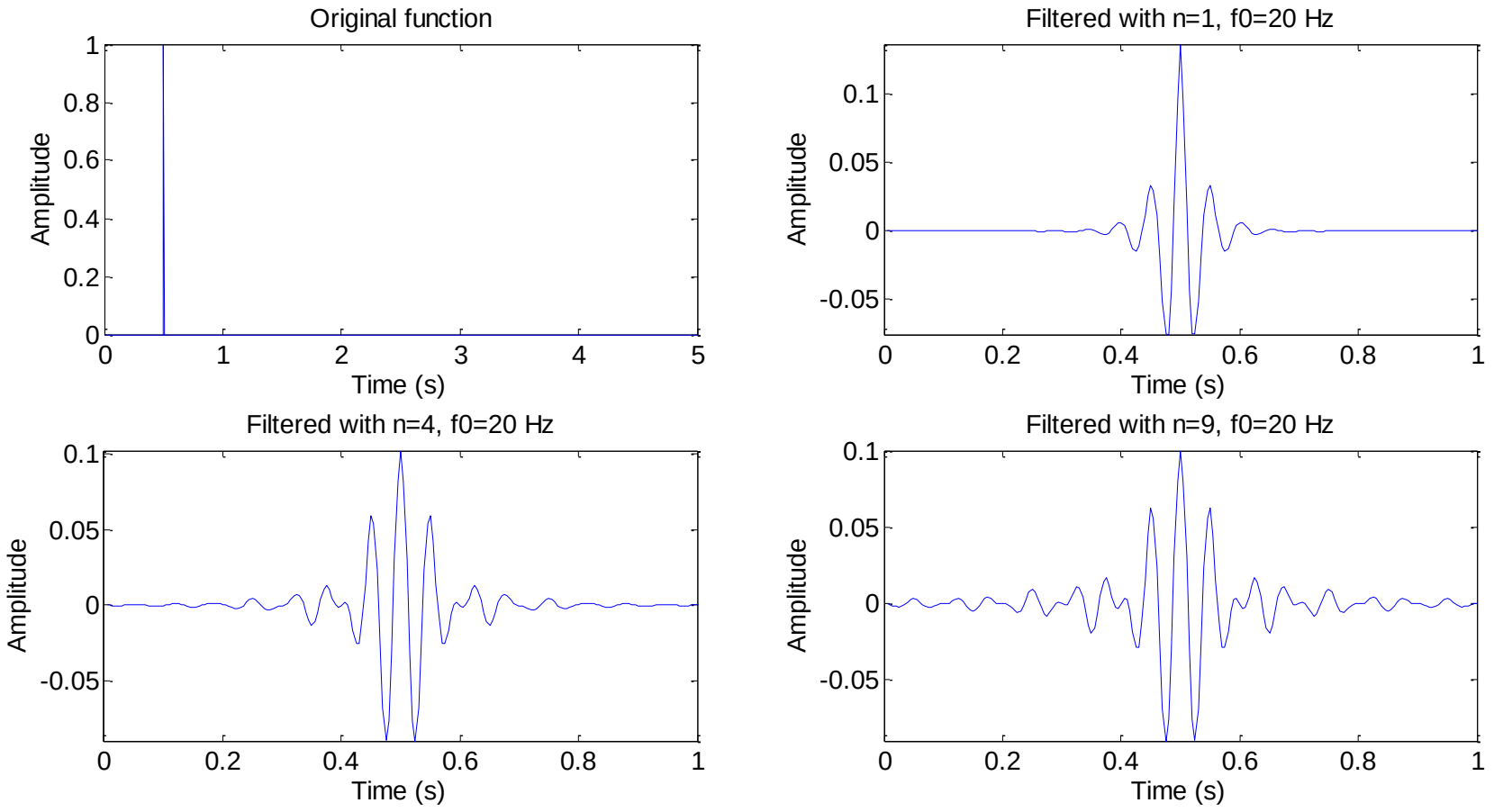

… on a seismogram …

… varying the order …

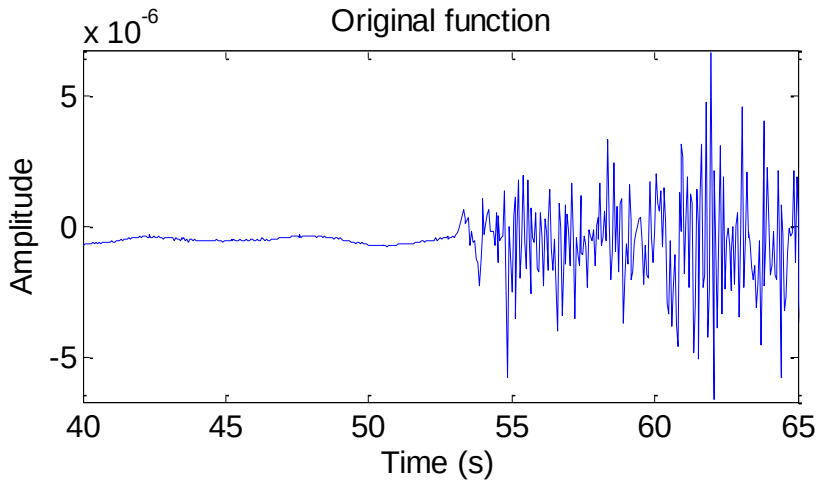

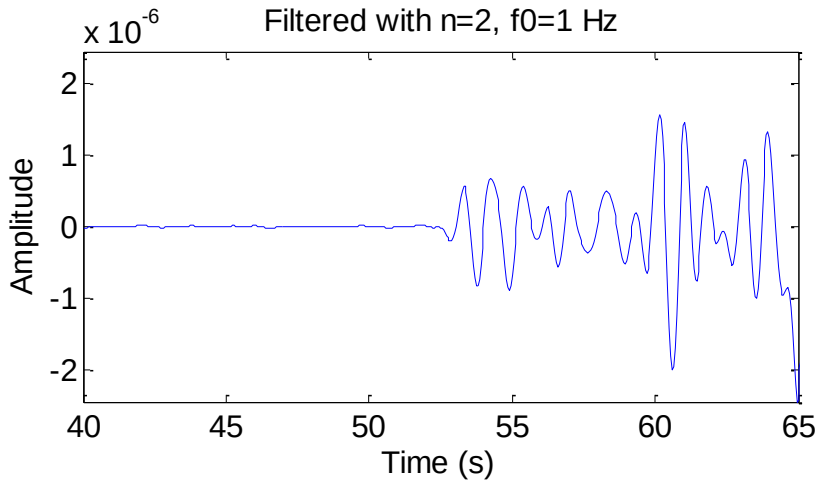

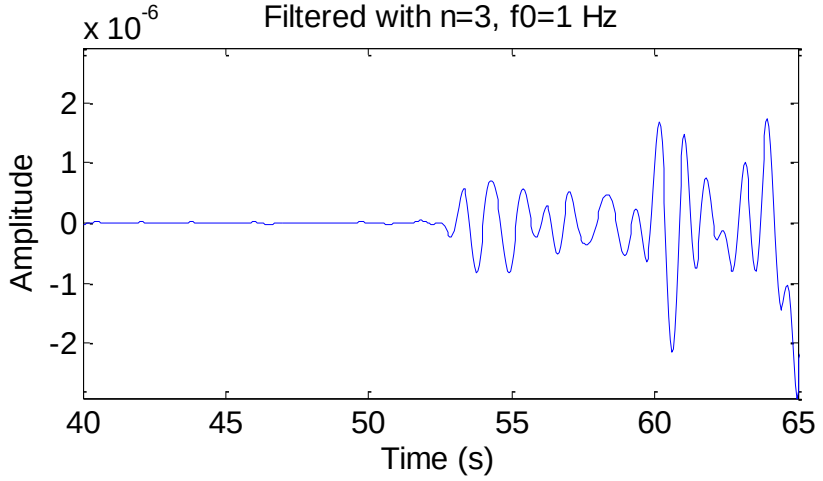

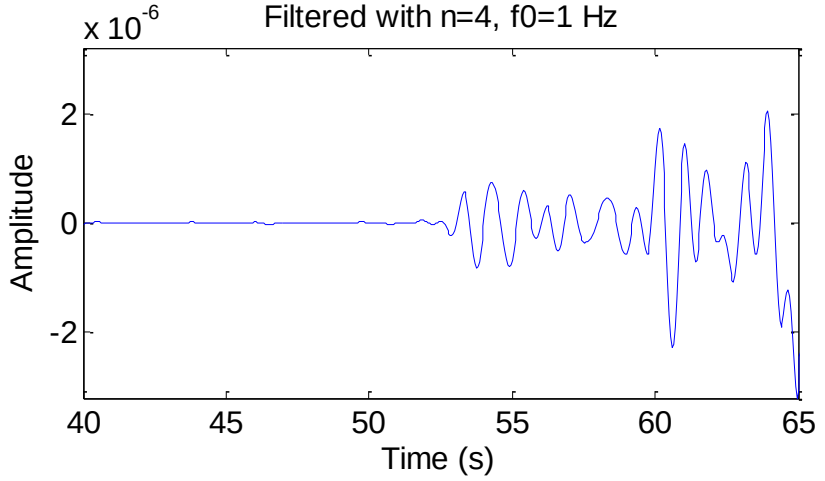

… on a seismogram …

… varying the cut-off frequency…

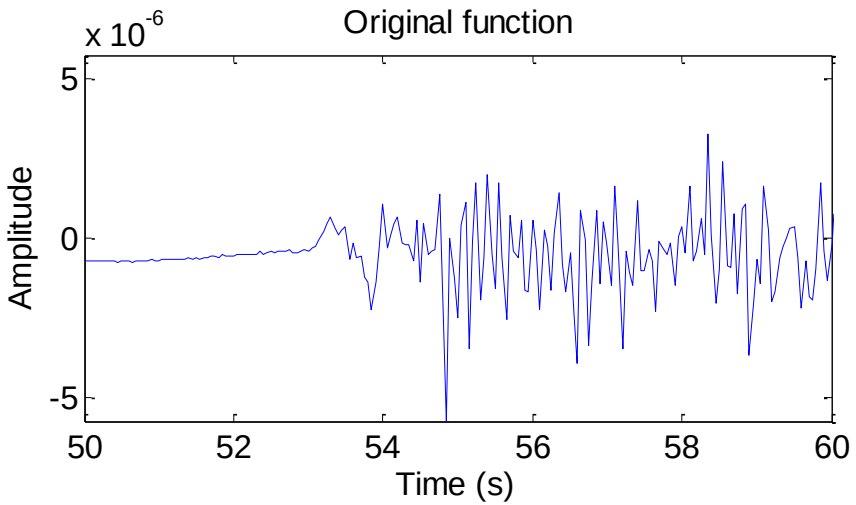

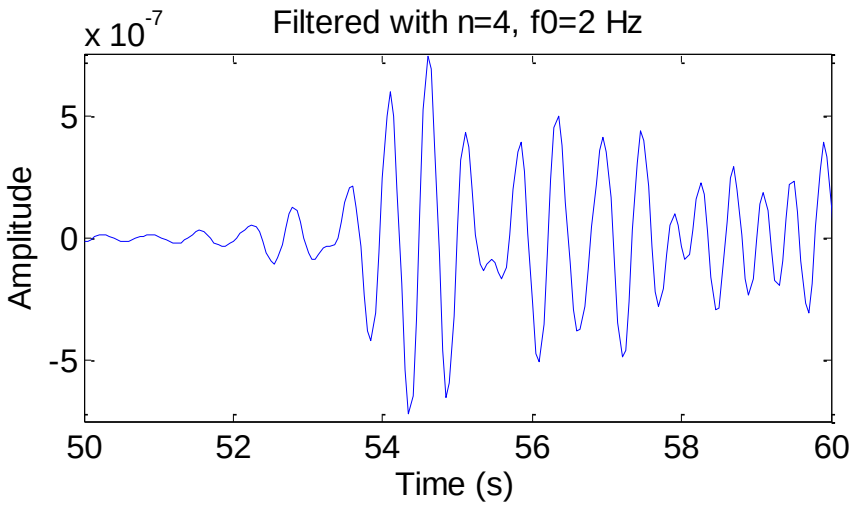

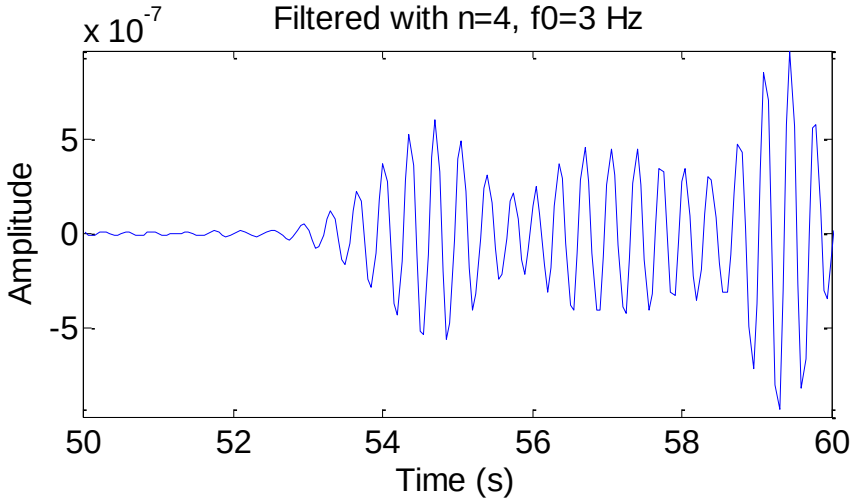

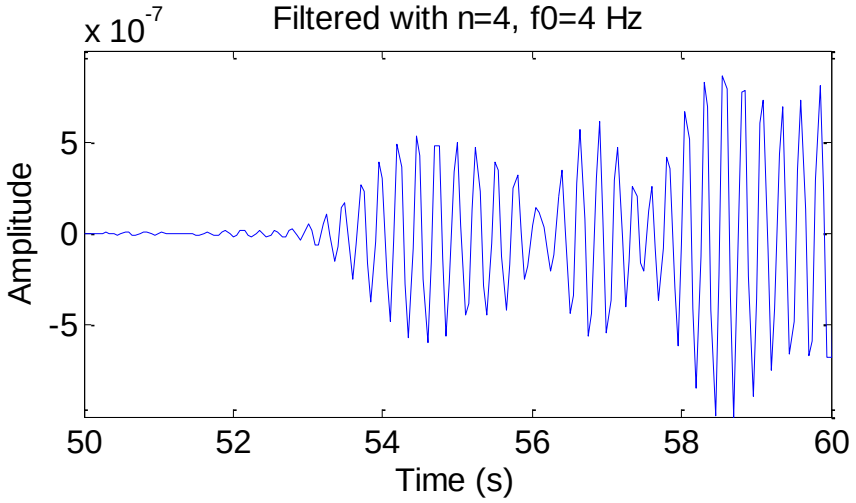

Zero phase and causal filters

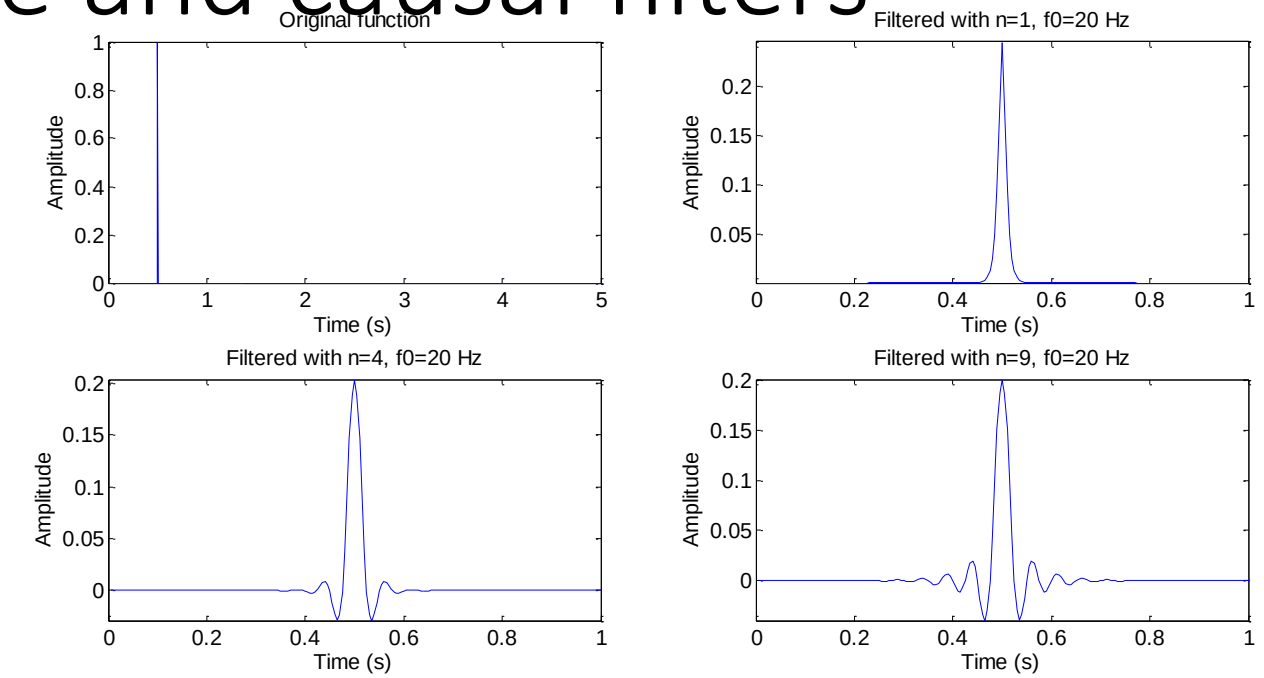

When the phase of a filter is set to zero (and simply the amplitude spectrum is inverted) we obtain a **zero-phase filter**. It means a peak will not be shifted.

Such a filter is **acausal**. Why?

Butterworth Low-pass (20 Hz) on spike

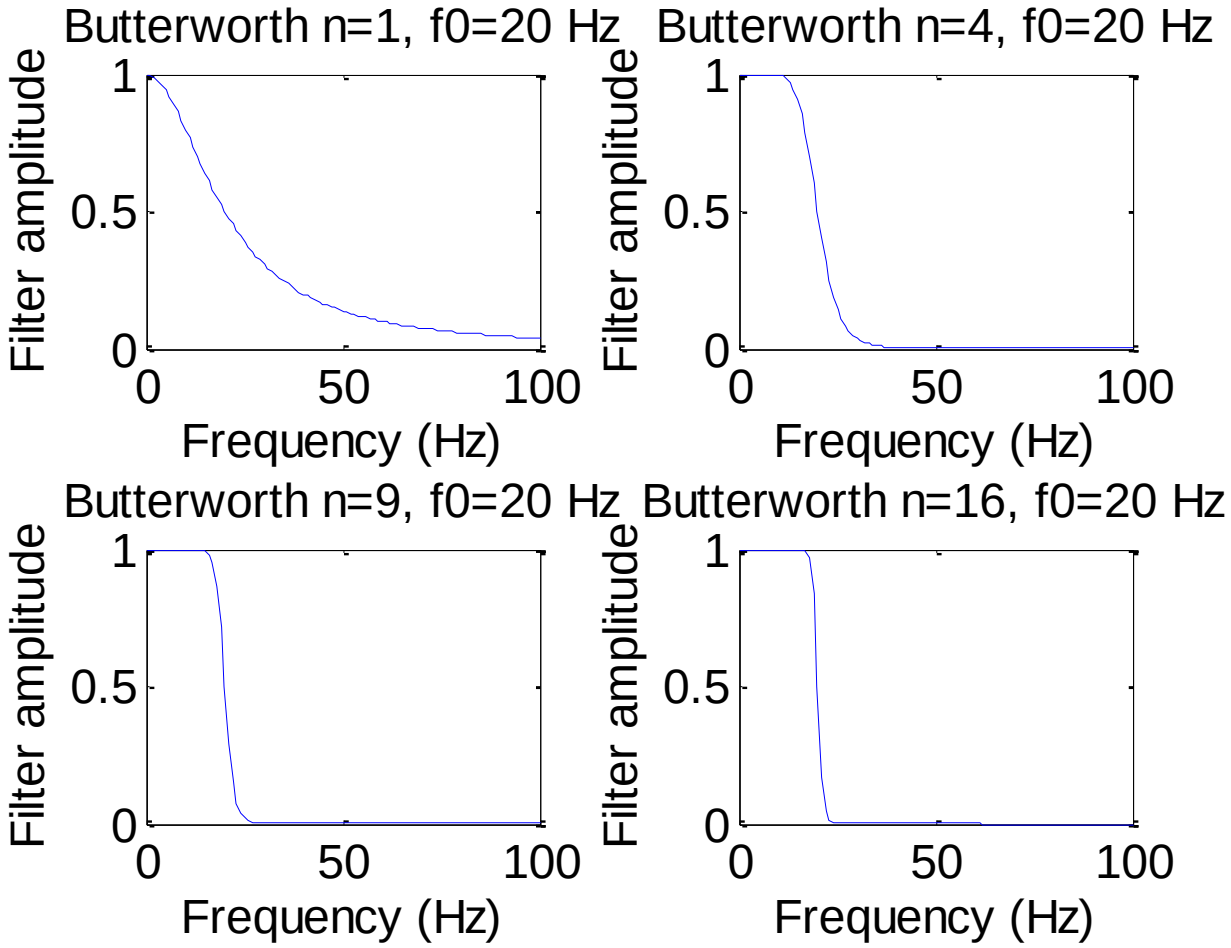

(causal) Butterworth Low-pass (20 Hz) on spike

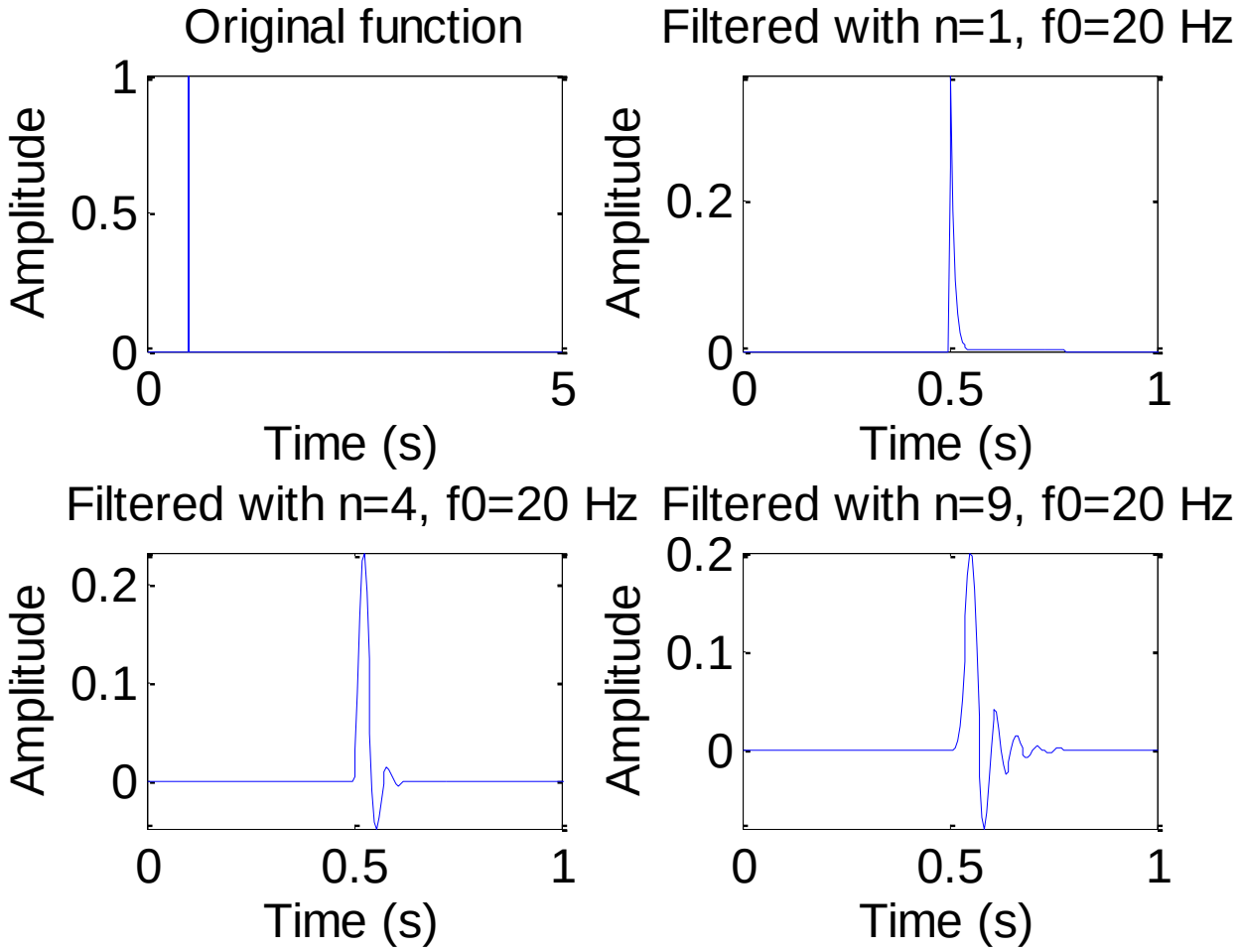

Butterworth Low-pass (20 Hz) on data

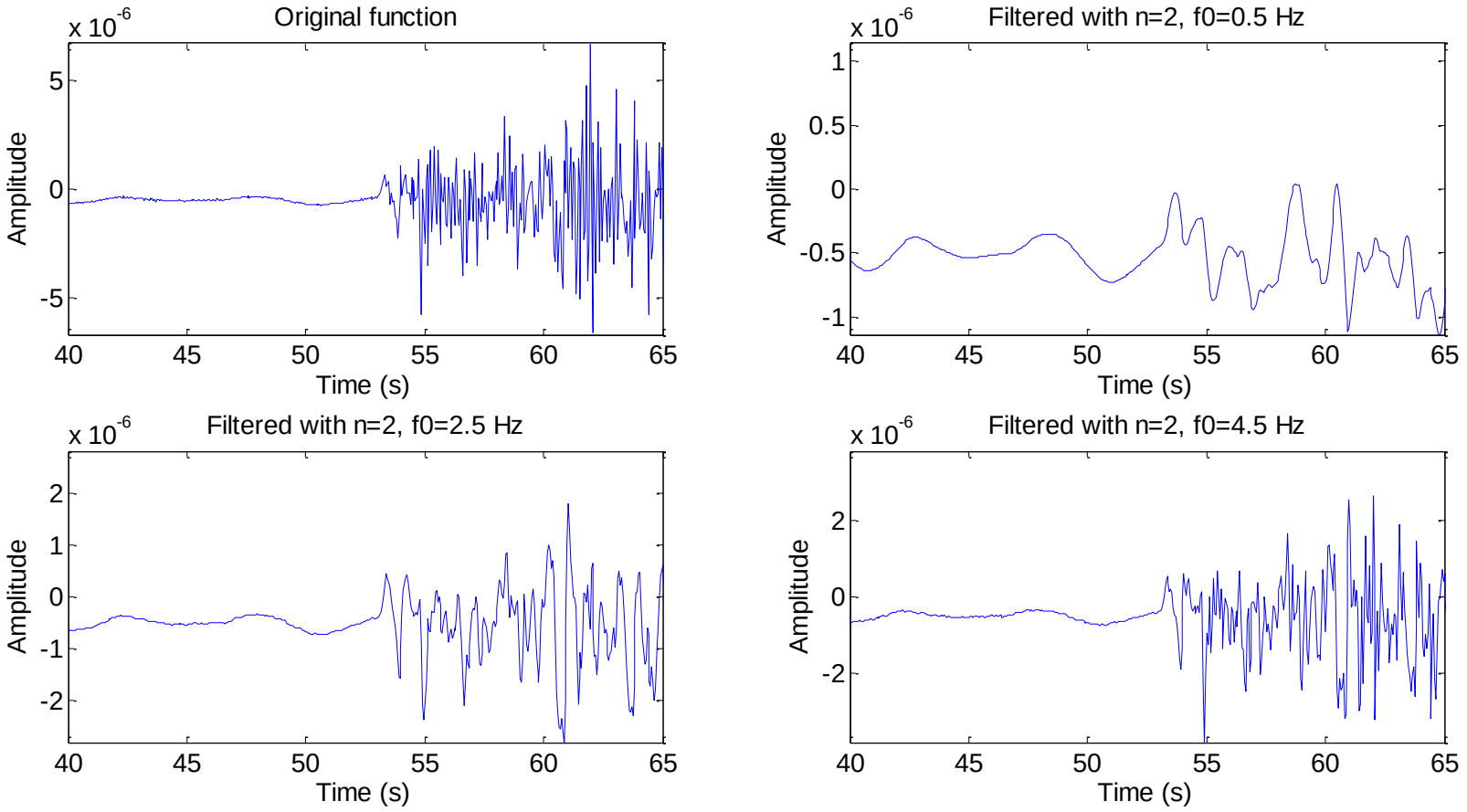

Other windowing functions

- So far we only used the Butterworth filtering window
- In general if we want to extract time windows from (permanent) recordings we have other options in the time domain.
- The key issues are
  - Do you want to preserve the main maxima at the expense of side maxima?
  - Do you want to have as little side lobes as posible?

Example

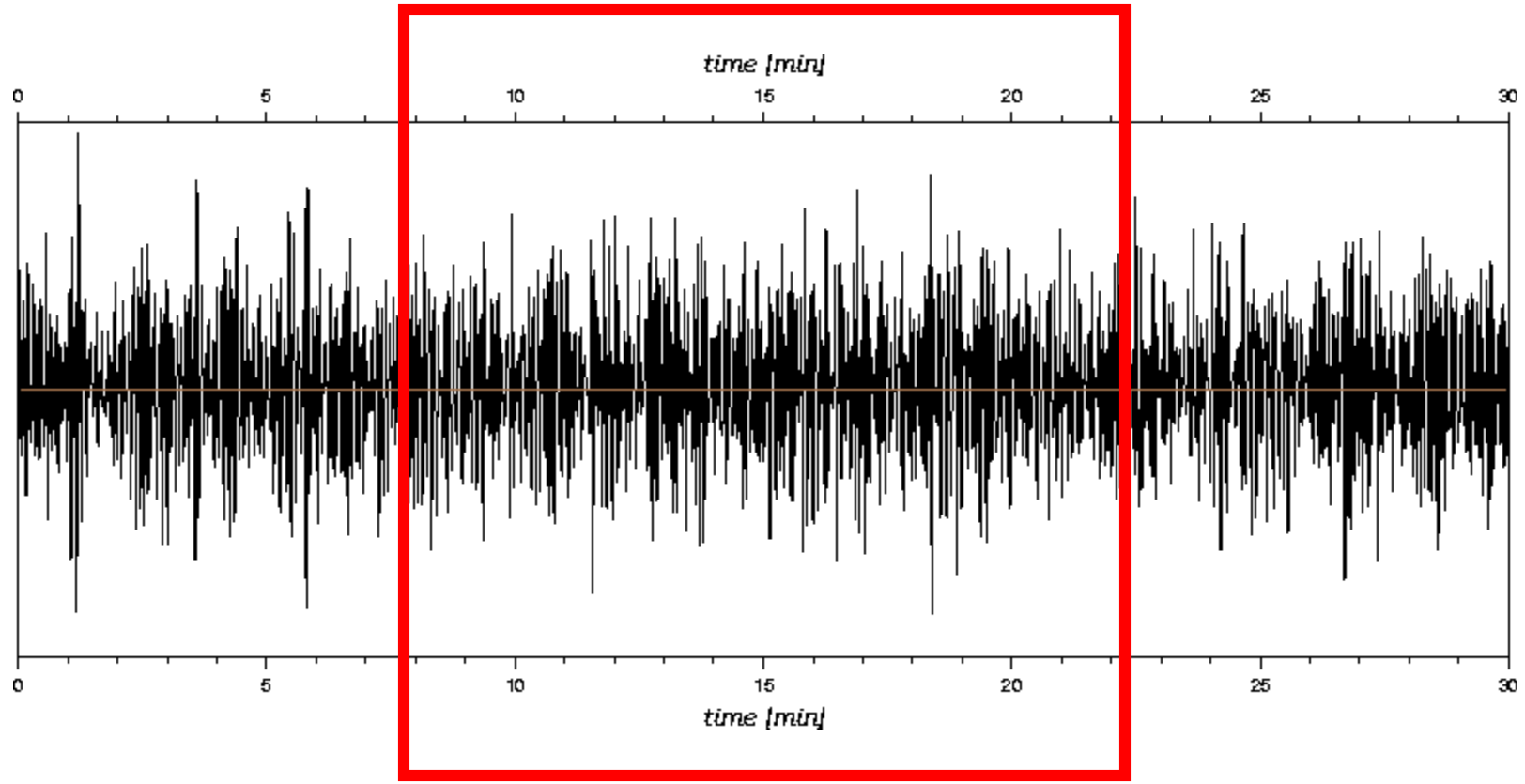

Possible windows

Plain box car (arrow stands for Fourier transform):

$$w_R(t) = \begin{cases} 1, & |t| \le M \\ 0, & |t| > M \end{cases} \Rightarrow \qquad W_R(f) = 2M \frac{\sin 2\pi f M}{2\pi f M}$$

Bartlett

$$w_R(t) = \begin{cases} 1 - \dfrac{|t|}{M}, & |t| \le M \\ 0, & |t| > M \end{cases} \Rightarrow \qquad W_B(f) = M \left(\frac{\sin 2\pi f M}{\pi f M} \right)^2$$

Possible windows

Hanning

$$w_H(t) = \left\{ \begin{array}{ll} \frac{1}{2}(1+\cos\frac{\pi t}{M}), & |t| \le M \\ 0, & |t| > M \end{array} \right\} \Rightarrow \qquad W_H(f) = M \frac{\sin 2\pi f M}{2\pi f M} \frac{1}{1-(2\pi f M)^2}$$

The spectral representations of the boxcar, Bartlett (and Parzen) functions are:

$$W(f) = \left(\frac{\sin 2\pi f M}{2\pi f M} \right)^n \qquad n = 1,2,4; \qquad M = T/2$$

Examples

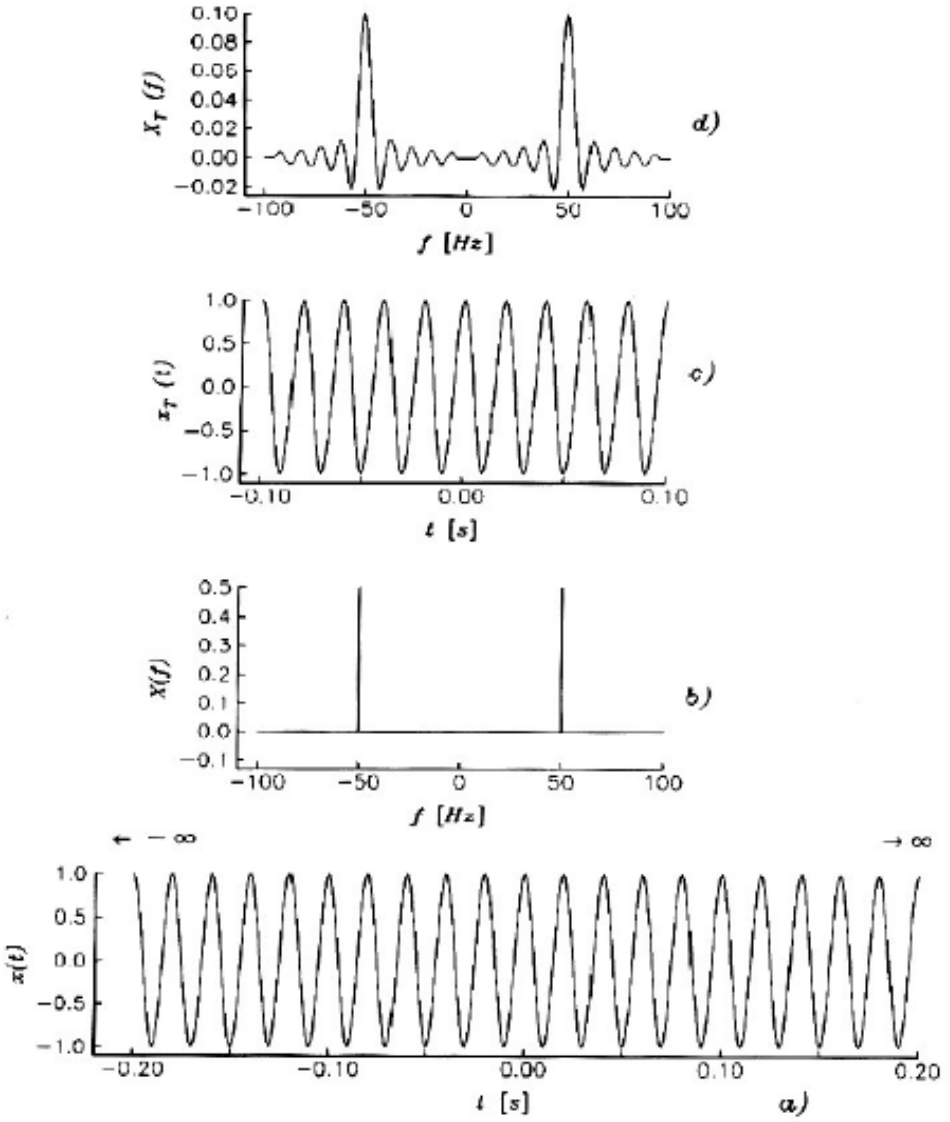
0.10
0.08
0.06
0.04
0.02
0.00
−0.02
$X_T(f)$
−100
−50
0
50
100
f [Hz]
d)
1.0
0.5
0.0
−0.5
−1.0
$x_T(t)$
−0.10
0.00
0.10
t [s]
c)
0.5
0.4
0.3
0.2
0.1
0.0
−0.1
$X(f)$
−100
−50
0
50
100
f [Hz]
b)
$t \to -\infty$
$\to \infty$
1.0
0.5
0.0
−0.5
−1.0
$x(t)$
−0.20
−0.10
0.00
0.10
0.20
t [s]
a)

Examples

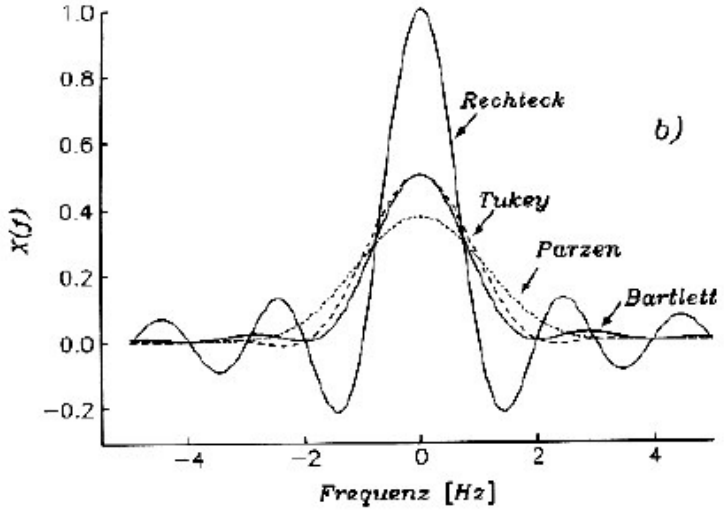
1.0
0.8
0.6
0.4
0.2
0.0
−0.2
X(f)
Rechteck
b)
Tukey
Parzen
Bartlett
−4
−2
0
2
4
Frequenz [Hz]

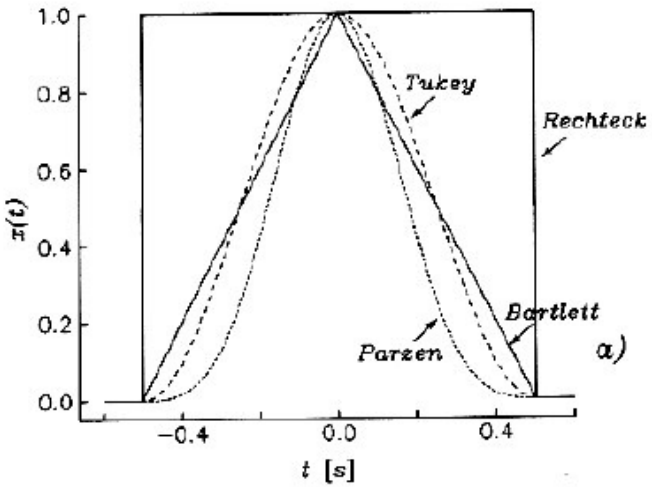
1.0
0.8
0.6
0.4
0.2
0.0
x(t)
Tukey
Rechteck
Bartlett
Parzen
a)
−0.4
0.0
0.4
t [s]

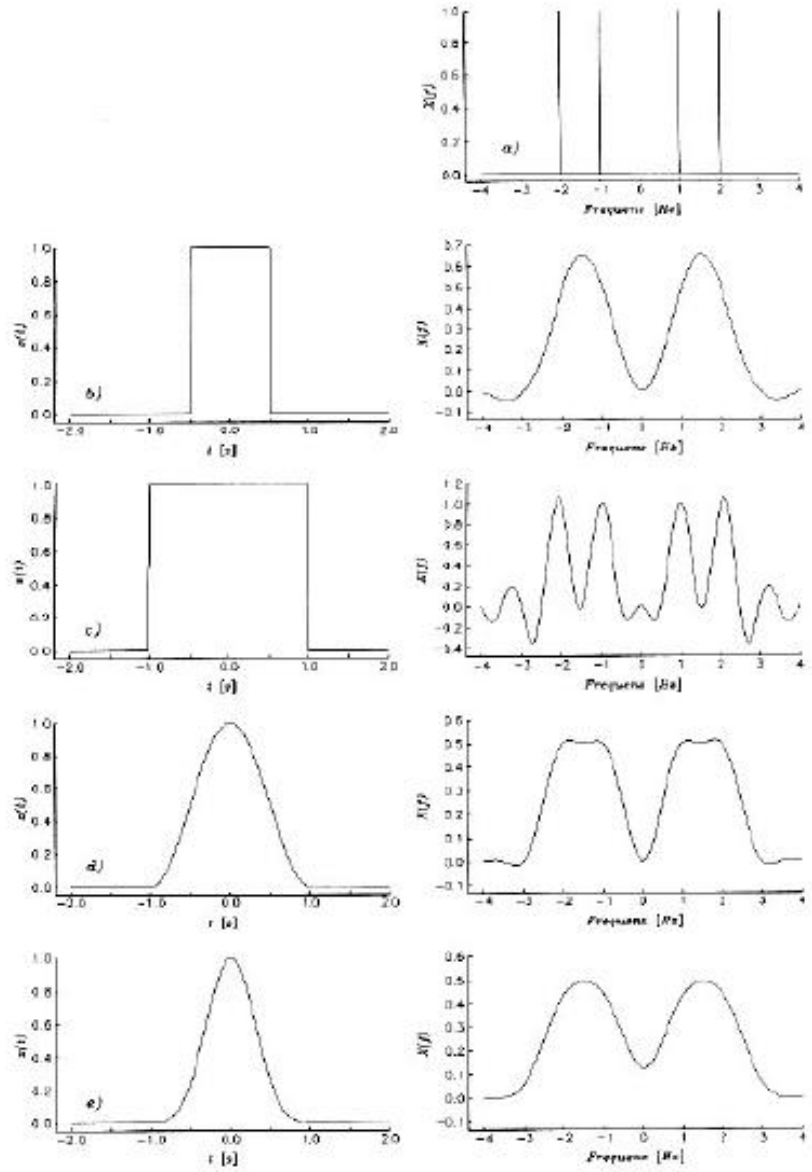

The Gabor transform: t-f misfits

phase information:

- can be measured reliably
- ± linearly related to Earth structure
- physically interpretable

amplitude information:

- hard to measure (earthquake magnitude often unknown)
- non-linearly related to structure

$$\hat{u}(\omega, t) := G(u) = \frac{1}{\sqrt{2\pi}} \int_{-\infty}^{\infty} u(\tau)\, g(\tau - t)\, e^{-i\omega\tau}\, d\tau$$

[t-ω representation of synthetics, u(t)]

$$\hat{u}_0(\omega, t) := G(u_0) = \frac{1}{\sqrt{2\pi}} \int_{-\infty}^{\infty} u_0(\tau)\, g(\tau - t)\, e^{-i\omega\tau}\, d\tau$$

[t-ω representation of data, $u_0(t)$]

The Gabor time window

The Gaussian time windows is given by

$$g_\sigma(t) = \frac{1}{2\sqrt{\pi\sigma}} e^{-\frac{t^2}{4\sigma}}$$

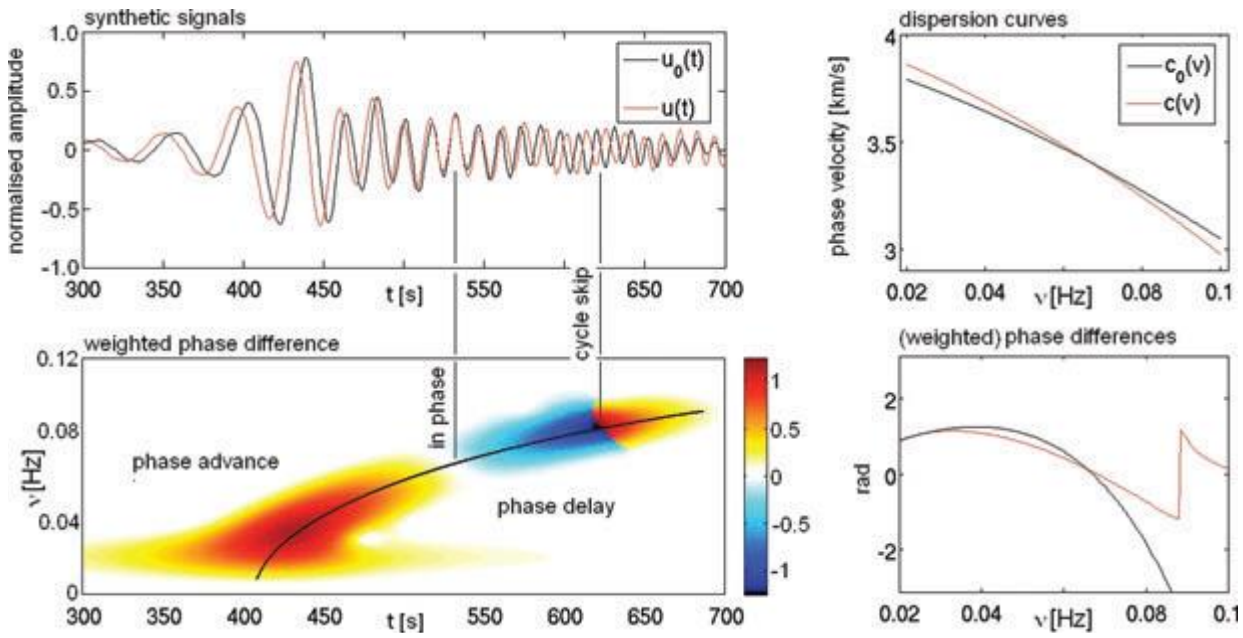

Exam

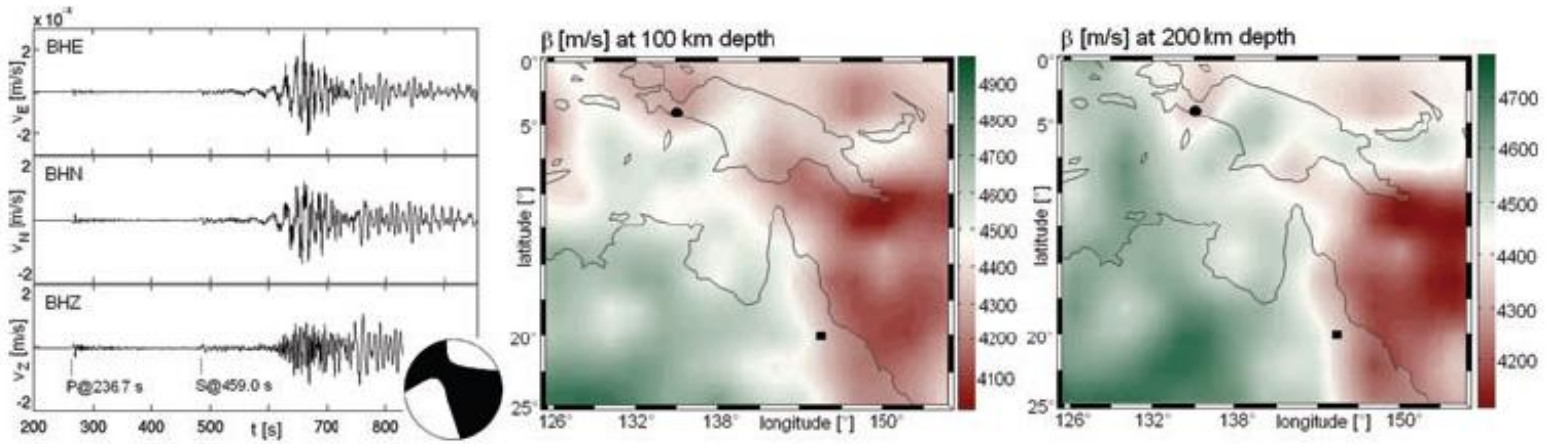

Figure 3. Left-hand panel: unprocessed velocity seismograms of the West Irian event (1993 June 12) recorded at the permanent station CTAO, located in NW Australia. The CMT solution is visualized in the lower right-hand panel of the BHZ channel recording. Central panel: model of the *S*-wave velocity β at the depth of 100 km. The maximum lateral variations $\Delta\beta$ reach 10 per cent of the background value. The source and receiver locations are plotted as a circle (•) and a square (****), respectively. Right-hand panel: the same as in the central one but at the depth of 200 km. The lateral variations are smaller than at 100 km depth and finally vanish below 350 km.

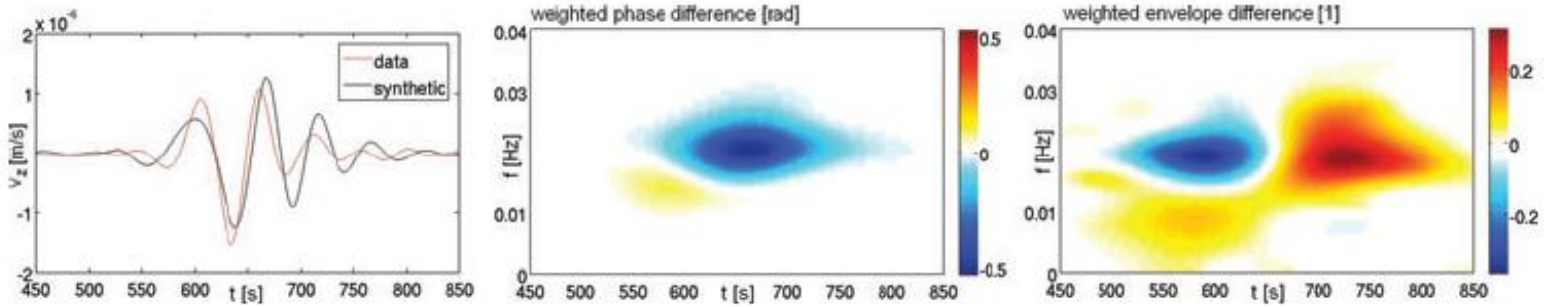

Figure 4. Left-hand panel: comparison of vertical-component surface wave trains, low-pass filtered with a cut-off frequency of 0.02 Hz (50 s). The synthetic is plotted in black and the data in red. Centre panel: weighted phase difference in time–frequency space. Both positive and negative phase differences are observable. Right-hand panel: weighted envelope difference in time–frequency space.

Multitaper

Goal: *„obtaining a spectrum with little or no bias and small uncertainties“.* problem comes down to finding the right tapering to reduce the bias (i.e, spectral leakage).

In principle we seek:

$$\hat{S}(f) = \left| \sum_{t=0}^{N-1} x(t) a(t)\, e^{-2\pi i f t} \right|^2,$$

where $a(t)$ is a series of weights called a taper.

This section follows Prieto eet al., GJI, 2007. Ideas go back to a paper by Thomson (1982).

Multi-taper Principle

$$\hat{S}(f) = \left| \sum_{t=0}^{N-1} x(t)a(t)\, e^{-2\pi i f t} \right|^2$$

- Data sequence x is multiplied by a set of orthgonal sequences (tapers)
- We get several single periodograms (spectra) that are then averaged
- The averaging is not even, various weights apply
- Tapers are constructed to optimize resistance to spectral leakage
- Weighting designed to generate smooth estimate with less variance than with single tapers

Spectrum estimates

We start with

$$\hat{S}(f) = |Y(f)|^2 = \left| \sum_{t=0}^{N-1} x(t)a(t)\, e^{-2\pi i f t} \right|^2$$

with

$$\sum_{t=0}^{N-1} |a(t)|^2 = 1 \qquad A(f) = \sum_{t=0}^{N-1} a(t)\, e^{-2\pi i f t}$$

To maintain total power.

Condition for optimal tapers

N is the number of points, W is the resolution bandwith (frequency increment)

$$\lambda(N, W) = \frac{\int_{-W}^{W} |A(f)|^2 \, \mathrm{d}f}{\int_{-\frac{1}{2}}^{\frac{1}{2}} |A(f)|^2 \, \mathrm{d}f}$$

One seeks to maximize λ the fraction of energy in the interval (–W,W). From this equation one finds a‘s by an eigenvalue problem -> Slepian function

Slepian functions

The tapers (Slepian functions) in time and frequency domains

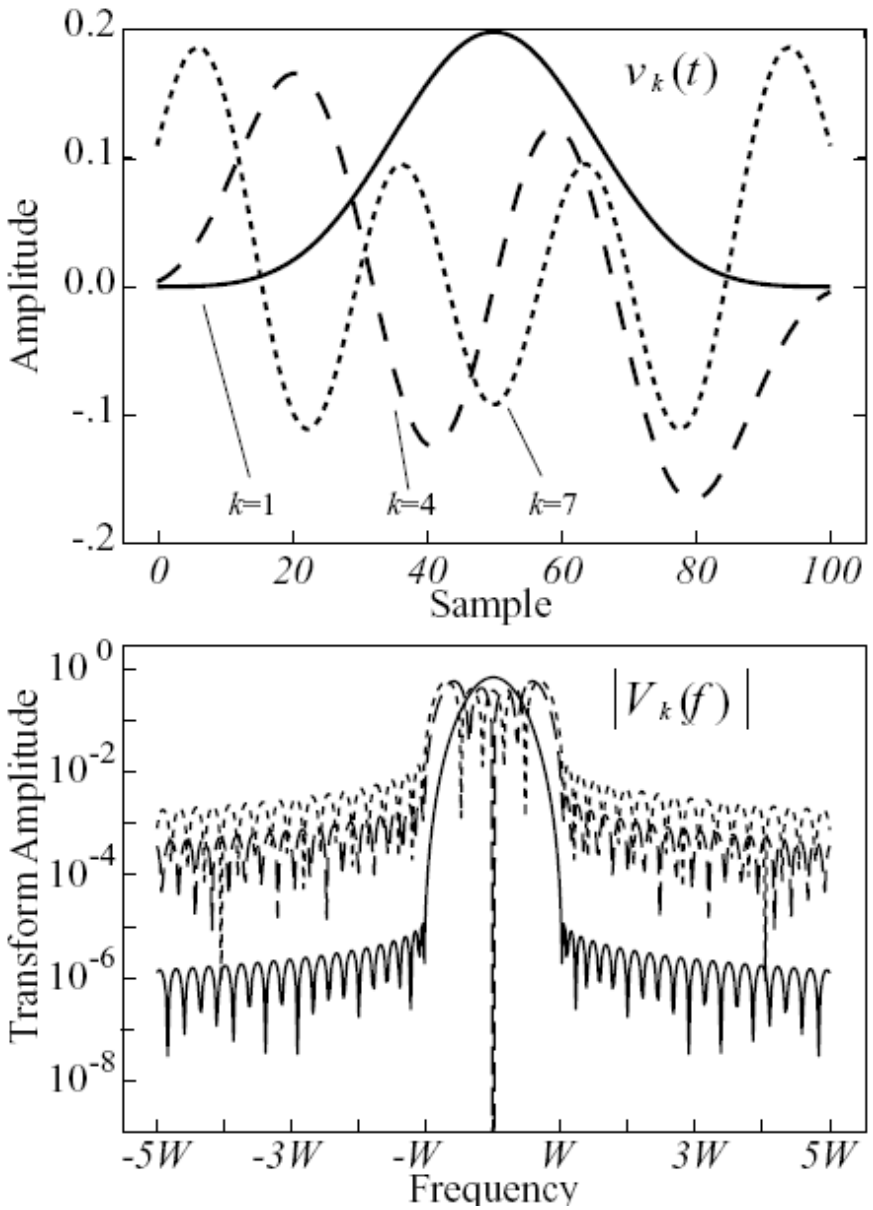

Final assembly

The objective of this method is to estimate the spectrum $S(f)$ by using K of the Slepian sequences to obtain the *k eigencomponents*:

$$Y_k(f) = \sum_{t=0}^{N-1} x(t) v_k(t) e^{-2\pi i f t}$$

Slepian sequences (tapers)

and a set of K eigenspectra as in (7):

$$\hat{S}_k(f) = |Y_k(f)|^2$$

from which we can form the mean spectrum

$$\bar{S}(f) = \frac{1}{K} \sum_{k=1}^{K} \hat{S}_k(f).$$

Final averaging of spectra

Example

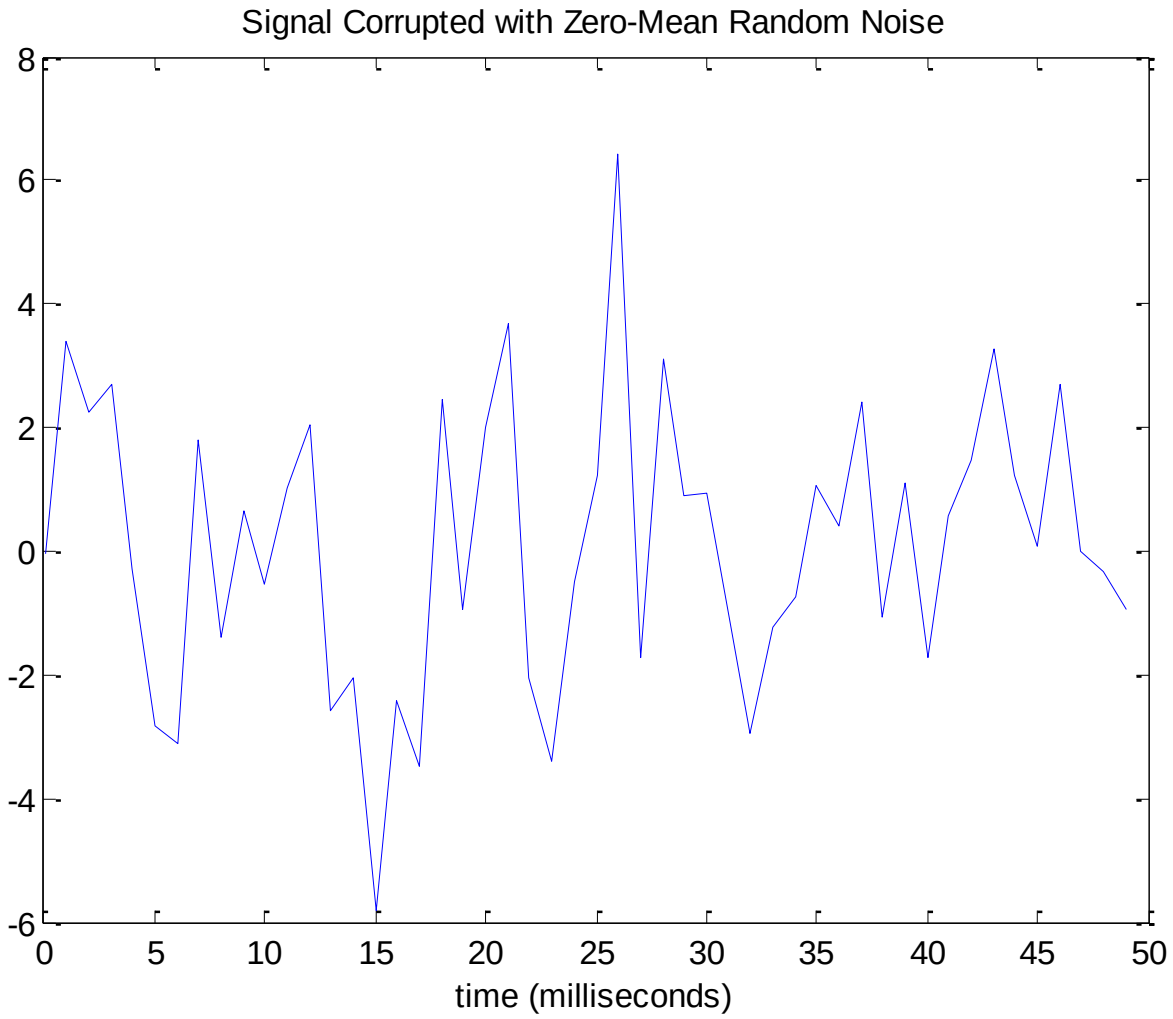
Signal Corrupted with Zero-Mean Random Noise
8
6
4
2
0
-2
-4
-6
0
5
10
15
20
25
30
35
40
45
50
time (milliseconds)

Classical Periodogram

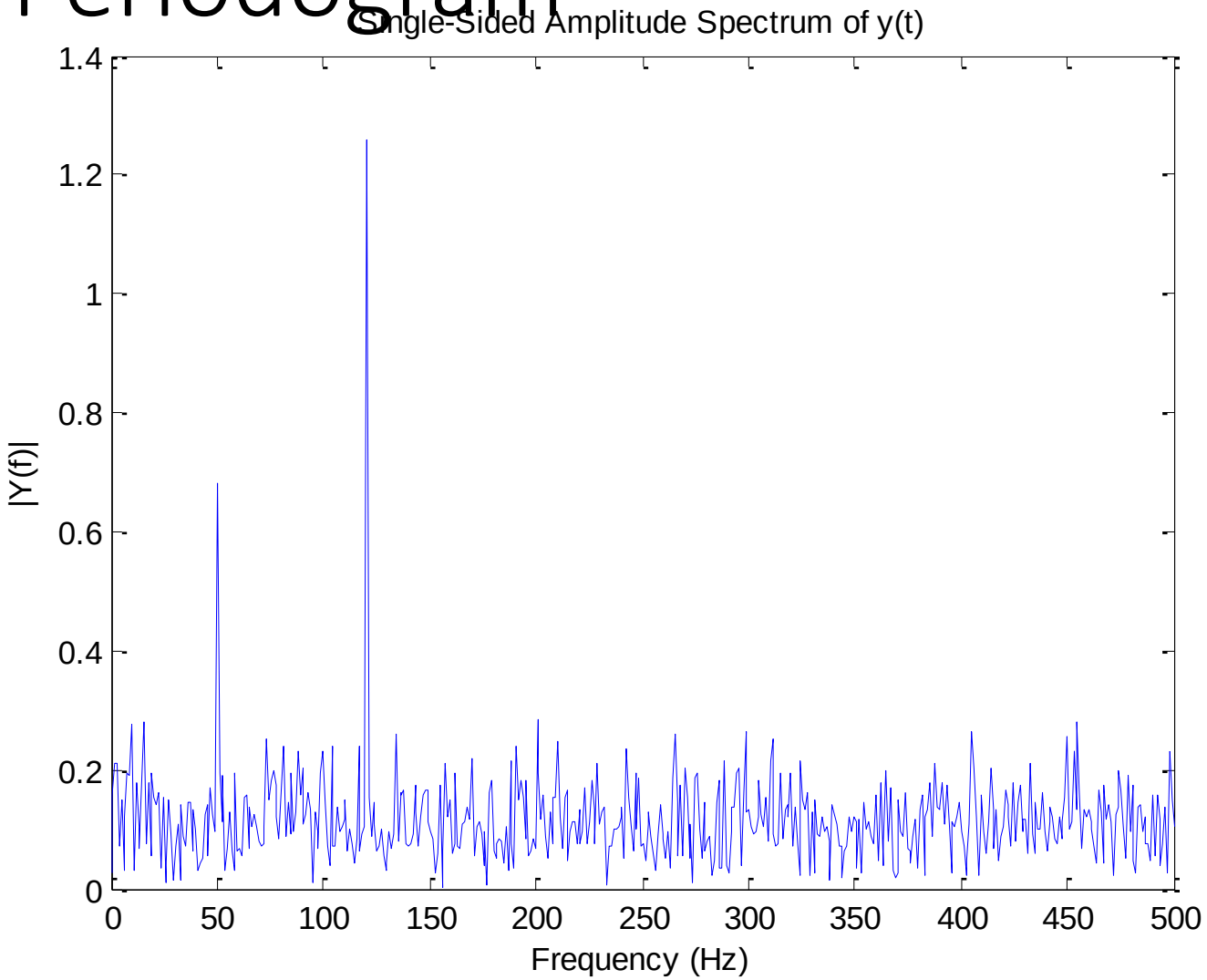

… and its power …

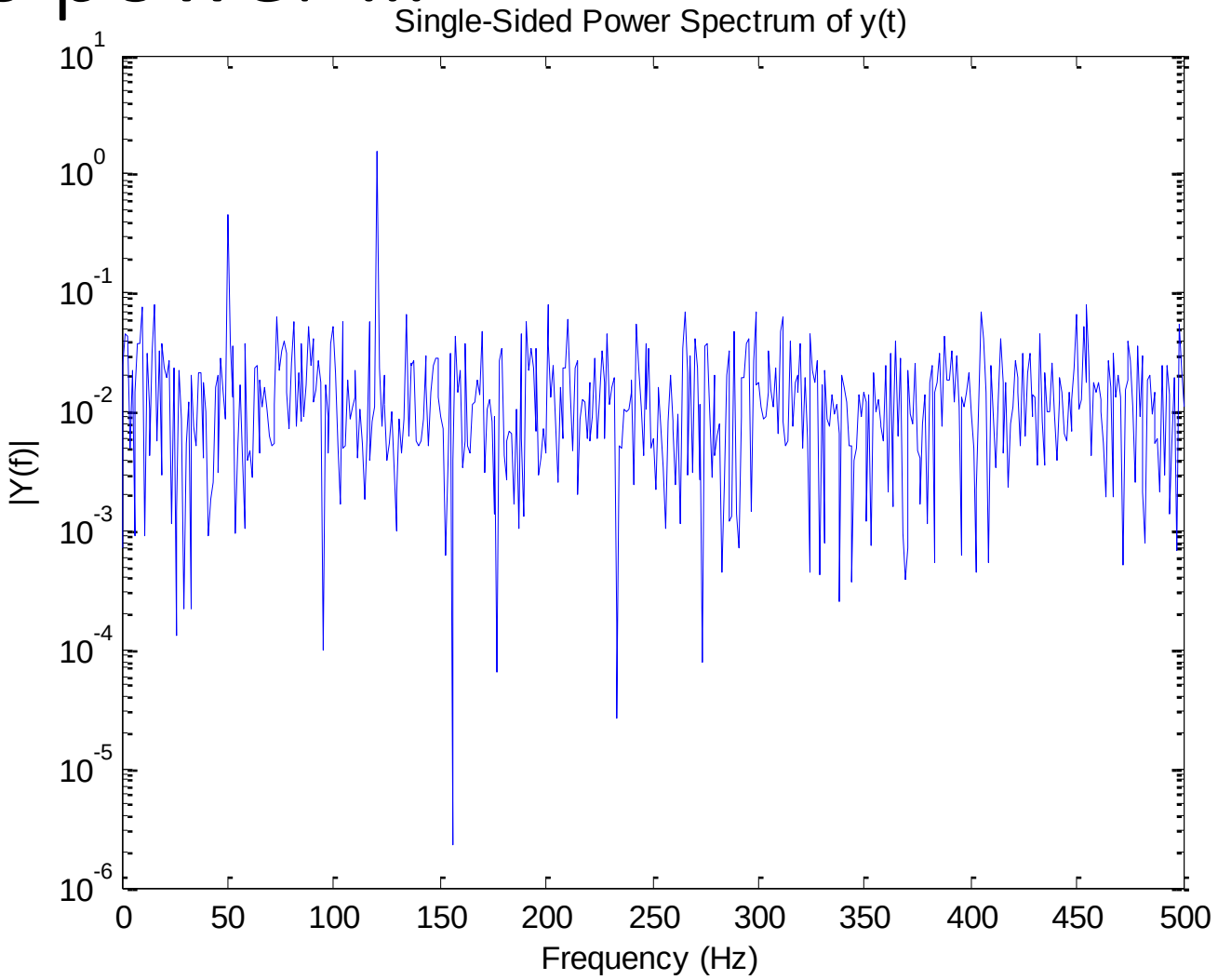

… multitaper spectrum …

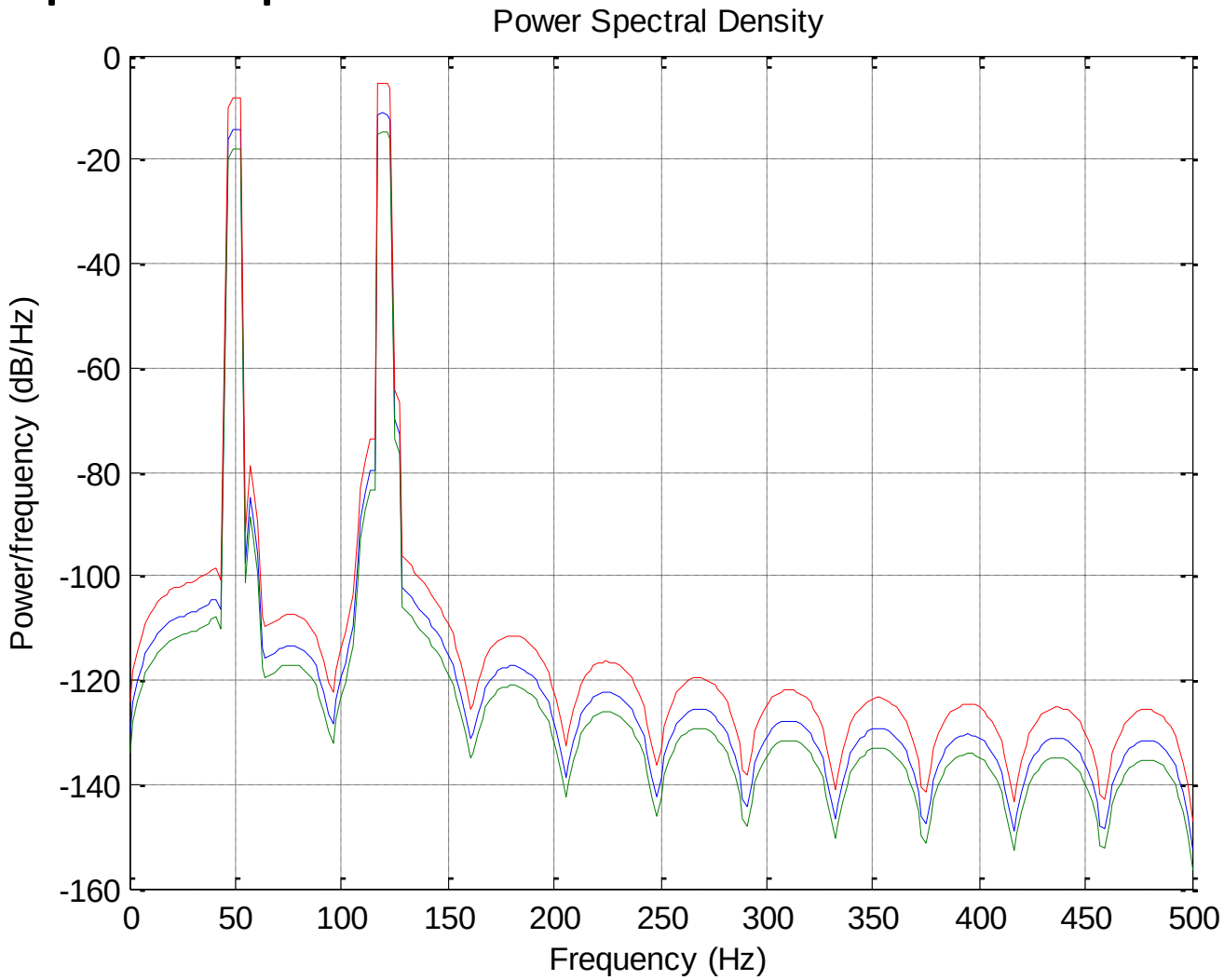

Wavelets – the principle

Motivation:

- Time-frequency analysis
- Multi-scale approach
- „when do we hear what frequency?“

Continuous vs. local basis functions

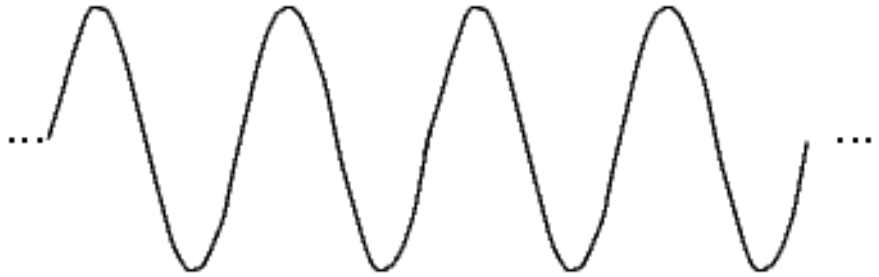

Sine Wave

Wavelet (db10)

$$F(\omega) = \int_{-\infty}^{\infty} f(t) e^{-j\omega t} dt$$

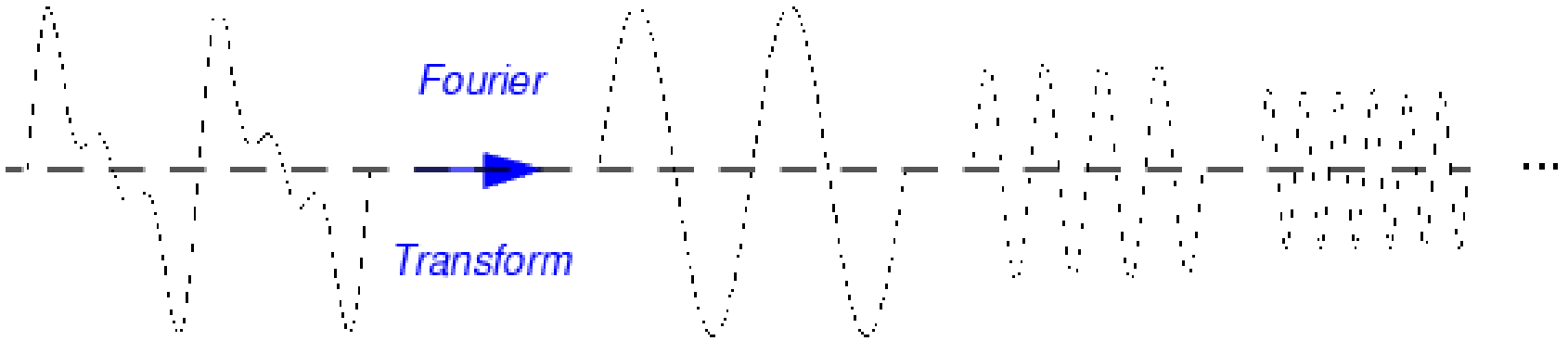

Signal

Constituent sinusoids of different frequencies

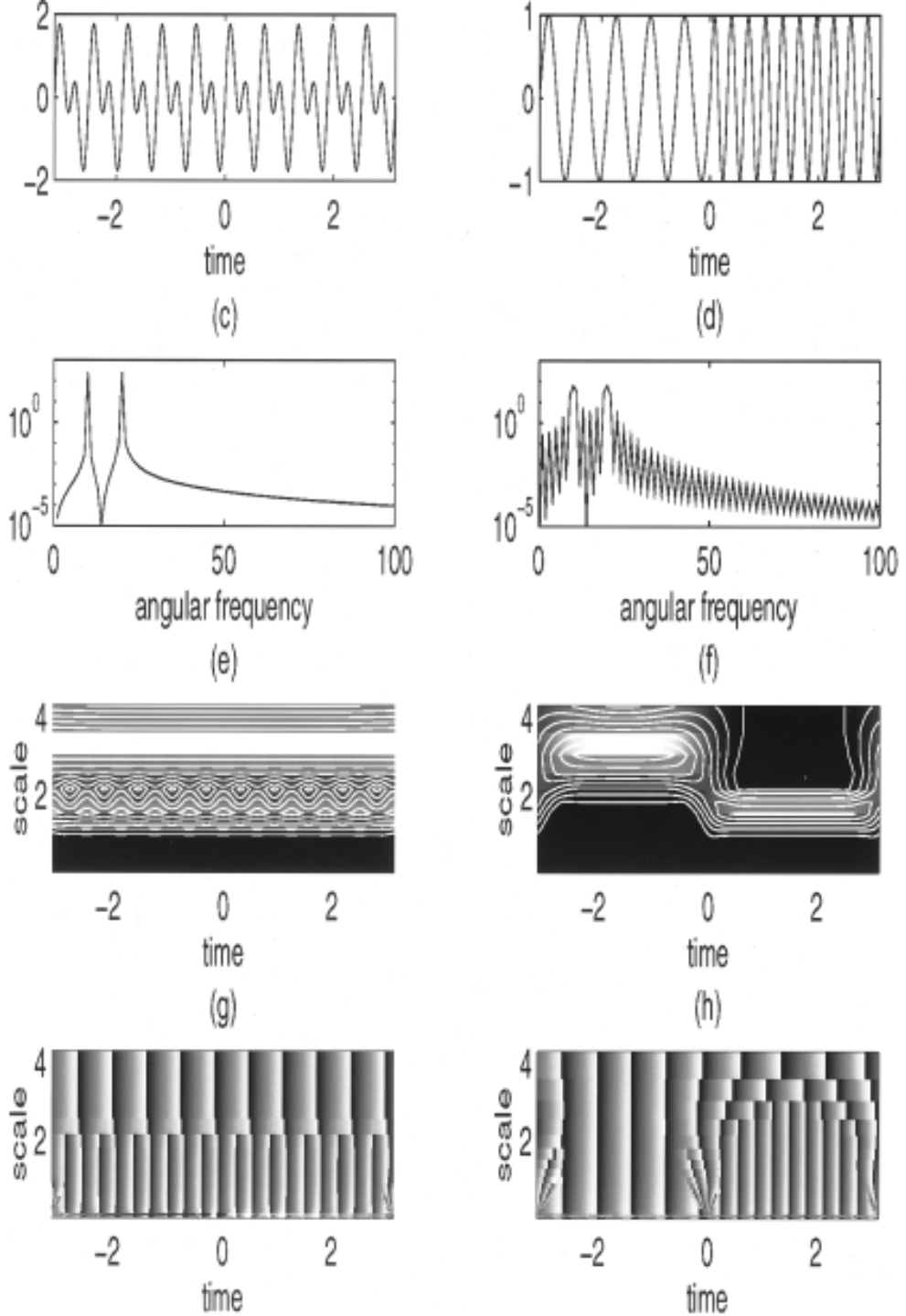

Figure 1. Spectral and wavelet analysis of two signals. The first signal (Figure 1a) consists of superposition of two frequencies (sin $10t$ and sin $20t$), and the second (Figure 2b) consists of the same two frequencies, each applied separately over half of the signal duration. Figures 1c and 1d show the Fourier spectra of the signals (i.e., $|f(\omega)|^2$ versus ω) for Figures 1a and 1b, respectively. Figures 1e and 1f show the magnitude of their wavelet transforms, and Figures 1g and 1h show the phase of their wavelet transforms (using Morlet wavelet). Notice the instability in calculation of phase at small scales where the modulus of wavelet transforms is very small.

Some maths

A wavelet can be defined as

$$\Psi^{a,b}(t) = |a|^{-1/2}\Psi\left(\frac{t-b}{a}\right)$$

With the transform pair:

$$W_\Psi(f)(a,b) = \frac{1}{\sqrt{a}}\int_{-\infty}^{\infty} f(t)\Psi\left(\frac{x-b}{a}\right)dt$$

$$f(t) = C_\Psi \int_{-\infty}^{\infty}\int_{-\infty}^{\infty} \left\langle f, \Psi^{a,b}\right\rangle \Psi^{a,b}(t)a^{-2}dadb$$

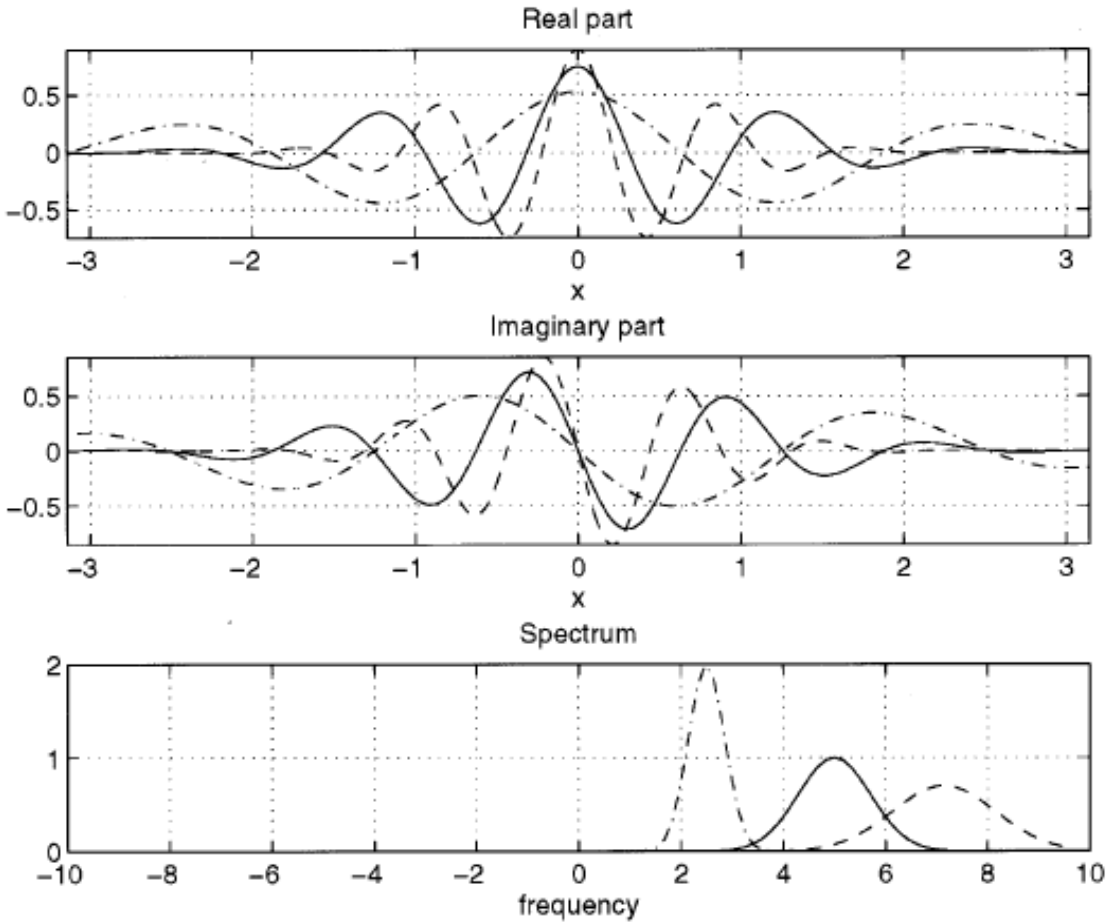

Figure 4. Real and imaginary parts of the Morlet wavelet ($\omega_0 = 5$) and its Fourier spectrum for different scales: $\lambda < 1$ (dashed lines), $\lambda = 1$ (solid lines), and $\lambda > 1$ (dash-dotted lines). Notice the effect of dilation on the wavelet and the corresponding change in its Fourier spectrum. When the wavelet dilates, its Fourier transform contracts, and vice versa. Also notice that the Fourier transform of the Morlet wavelet is supported entirely on the positive-frequency axis.

Resulting wavelet representation

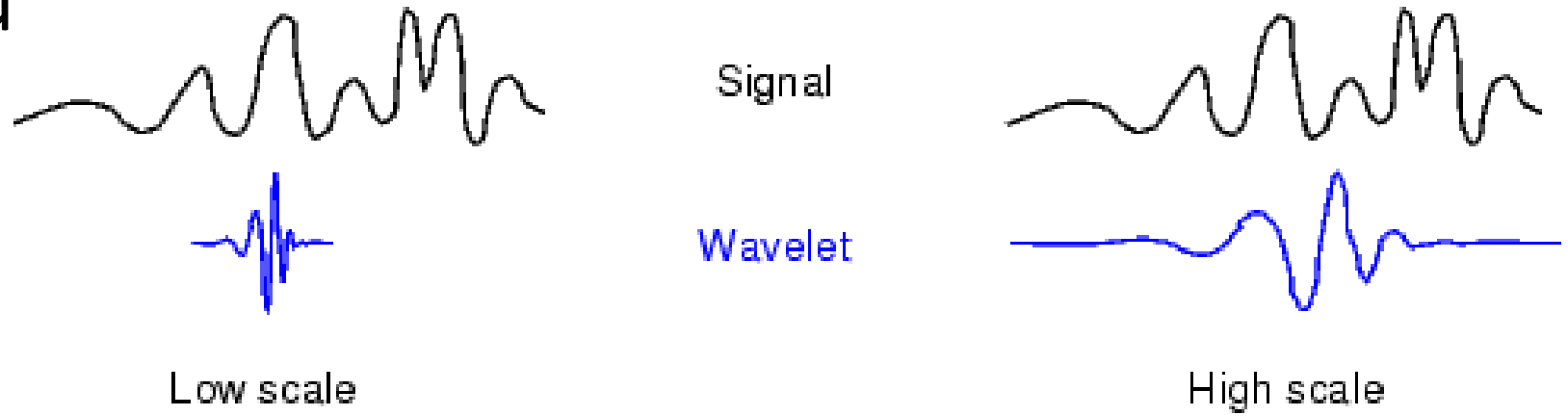

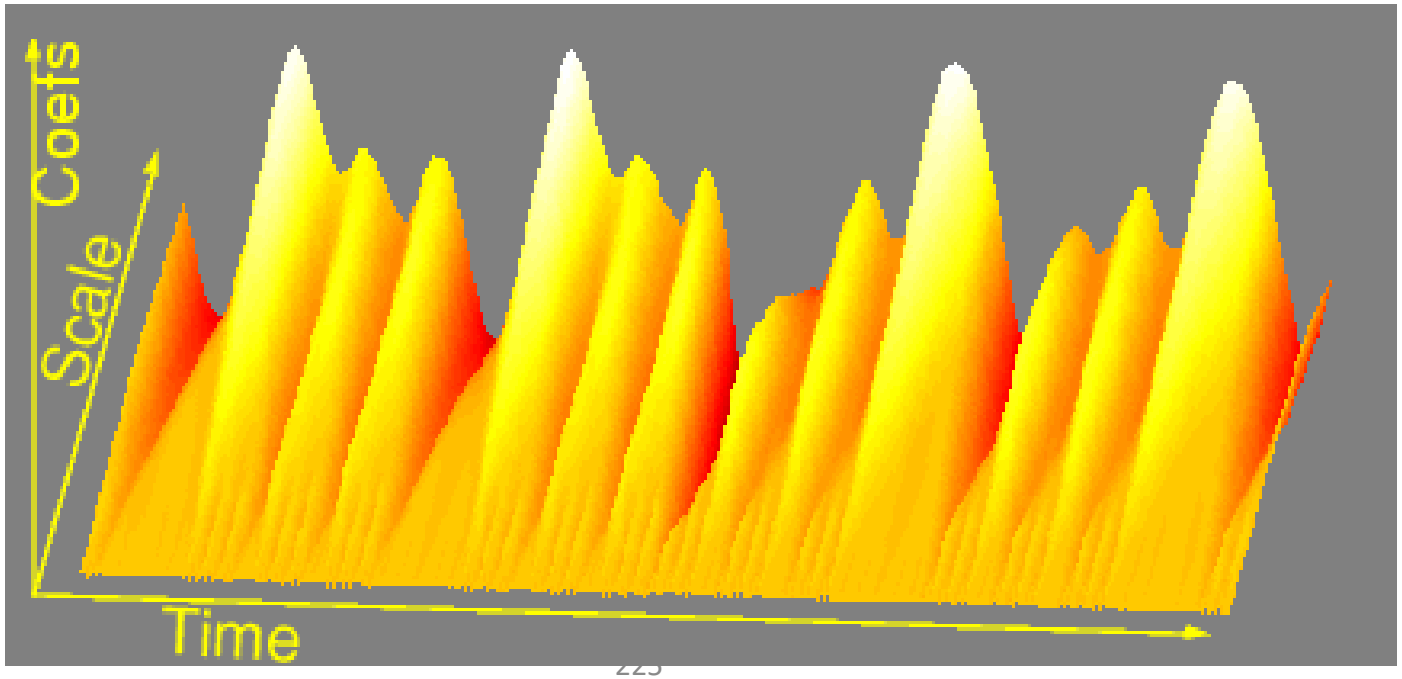

Shifting and scaling

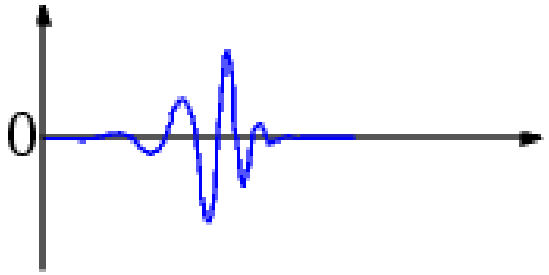

Wavelet function
$\psi(t)$

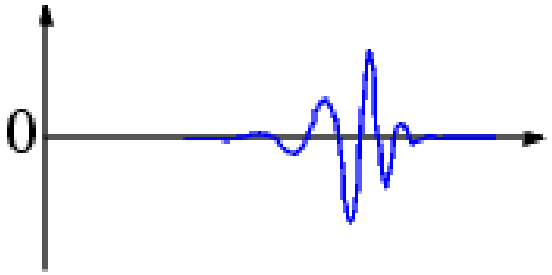

Shifted wavelet function
$\psi(t-k)$

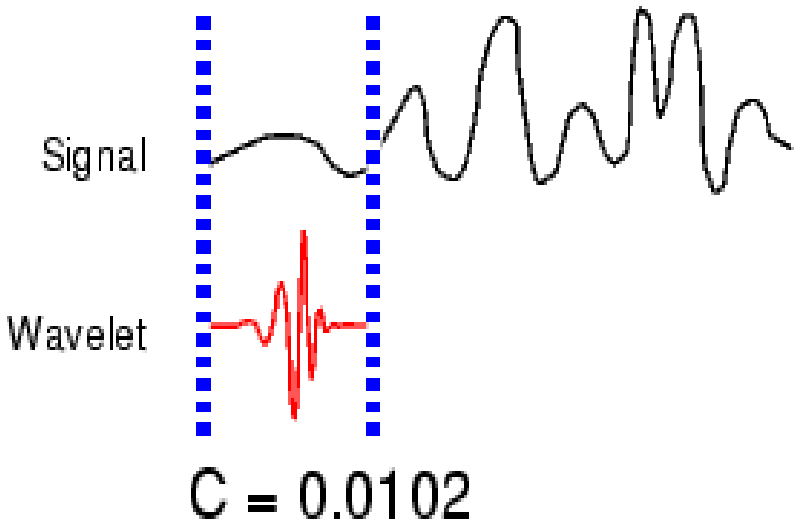

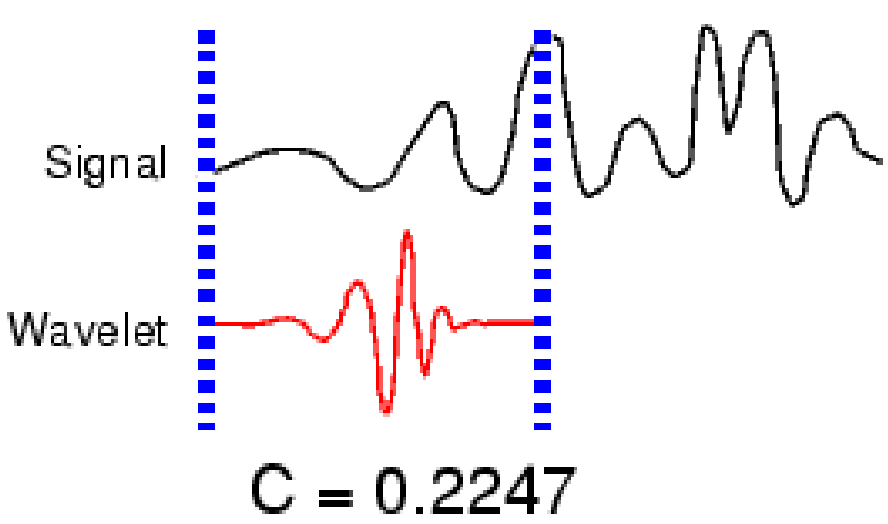

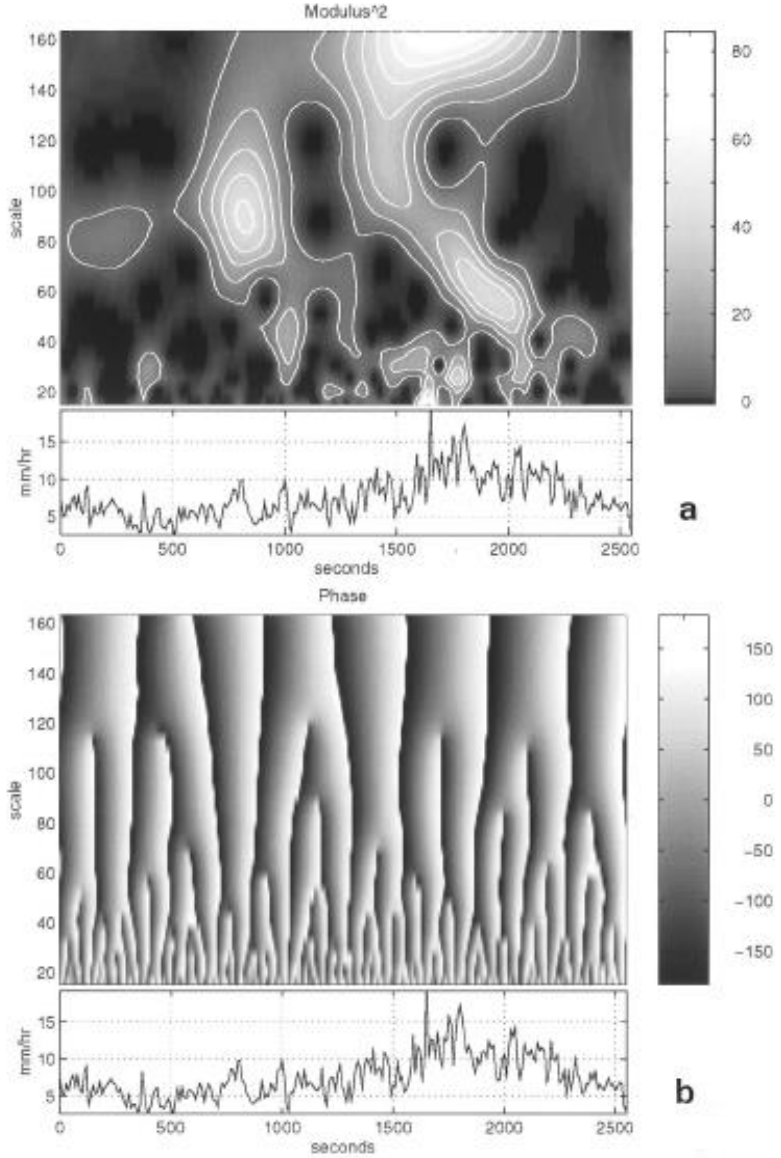

Figure 5. Analysis of temporal rainfall using the Morlet wavelet. The data were collected every 10 s on May 3, 1990, over Iowa City, Iowa, using an optical rain gage. (a) Square of the modulus or scalogram, that is, $|Wf(\lambda, t)|^2$, and (b) phase of $Wf(\lambda, t)$. The rainfall intensity is shown at the bottom of each figure. The scalogram clearly shows the presence of multiscale features and also some embedding of small-scale features within large-scale features. The phase plot shows the convergence of lines of constant phase to singularities (see discussion in text). (Reprinted by permission of Academic Press.)

Application to seismograms

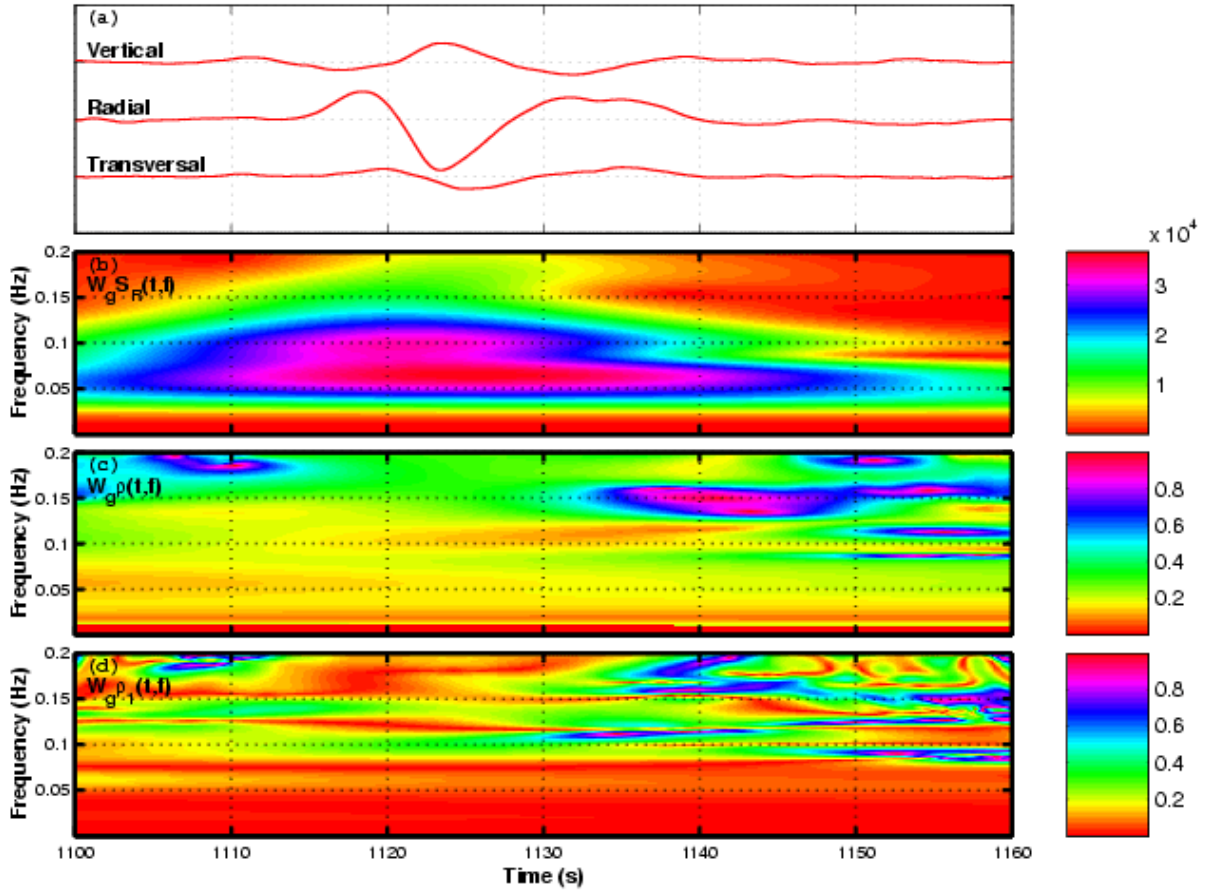

http://users.math.uni-potsdam.de/~hols/DFG1114/projectseis.html

Graphical comparison

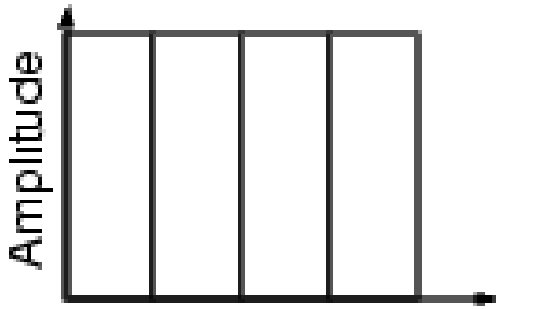

Time Domain (Shannon)

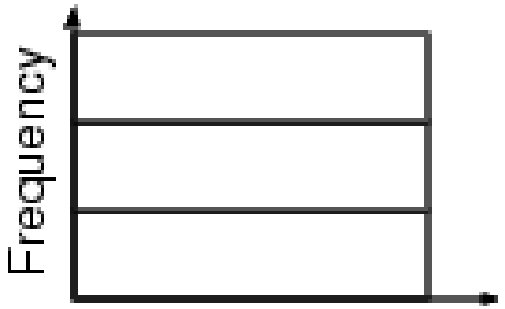

Frequency Domain (Fourier)

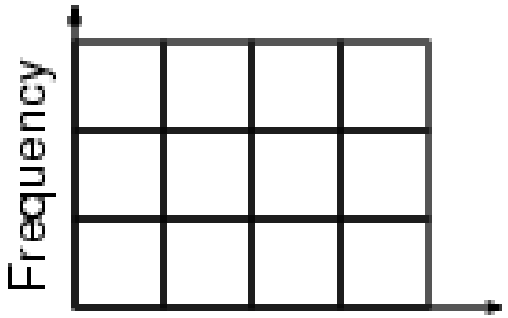

STFT (Gabor)

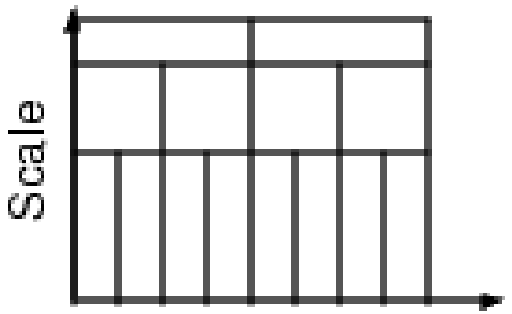

Wavelet Analysis

Summary

- Filtering is not necessarily straight forward, even the fundamental operations (LP, HP, BP, etc) require some thinking before application to data.
- The form of the filter decides upon the changes to the waveforms of the time series you are filtering
- For seismological applications filtering might drastically influence observables such as travel times or amplitudes
- „Windowing“ the signals in the right way is fundamental to obtain the desired filtered sequence

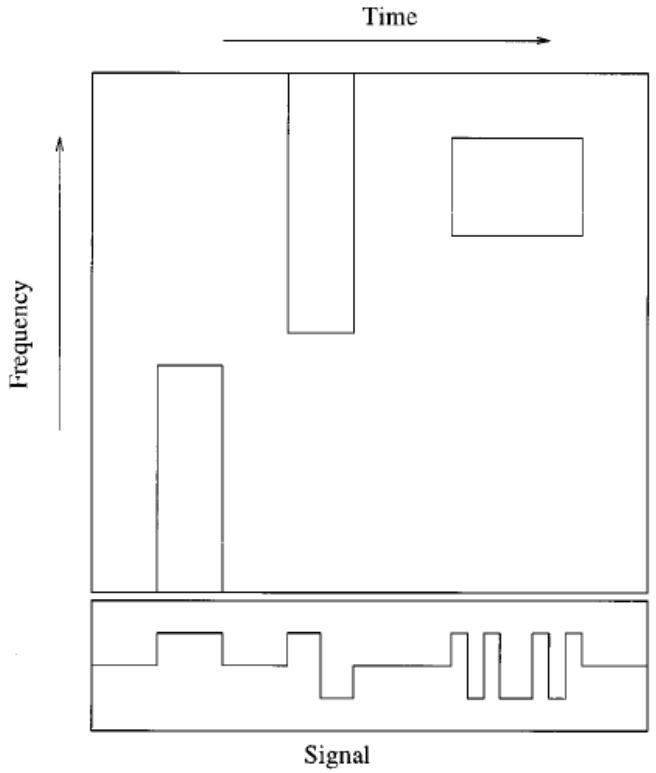

Figure 3. Schematic of time-frequency plane decomposition using wavelet packets.

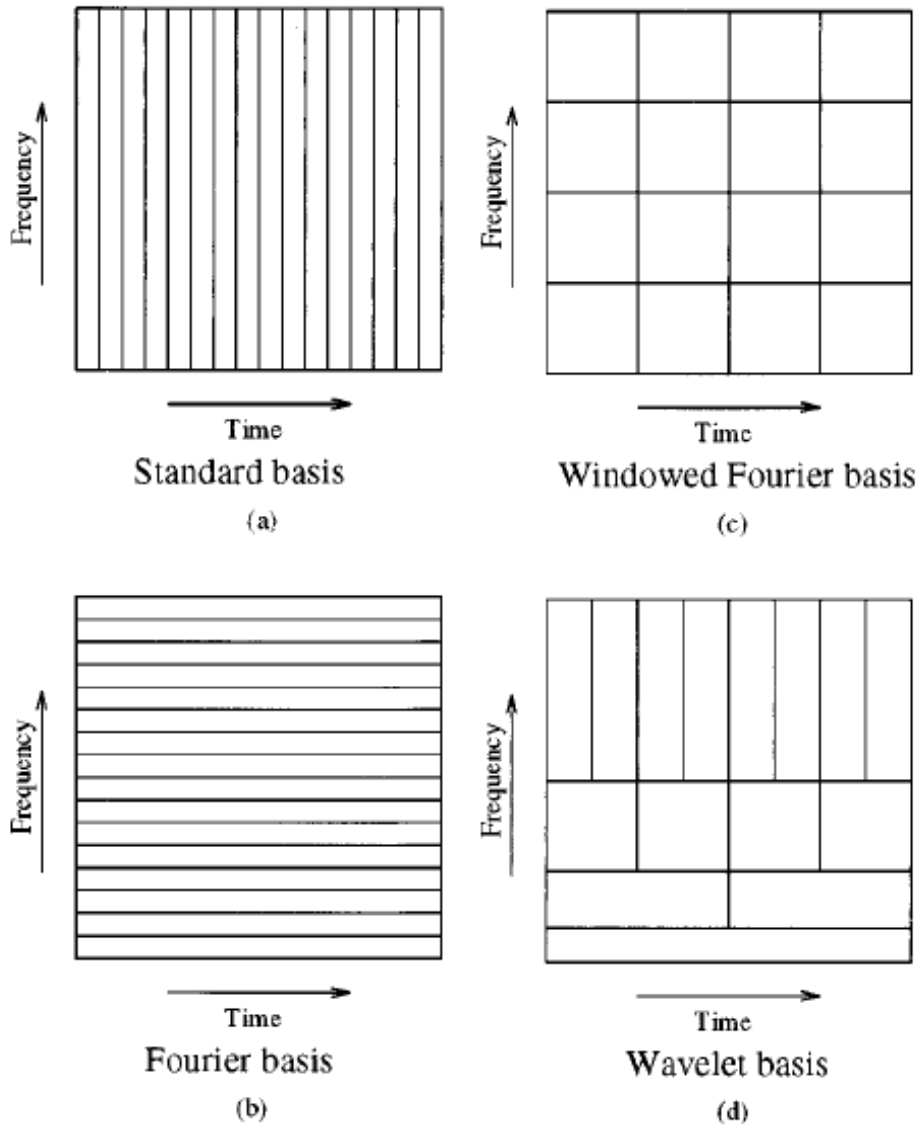

Signal Processing

Mike Doggett

Staffordshire University

CORRELATION

- **Introduction**
- **Correlation Function – Continuous-Time Functions**
- **Auto Correlation and Cross Correlation Functions**
- **Correlation Coefficient**
- **Correlation – Discrete-Time Signals**
- **Correlation of Digital Signals**

INTRODUCTION

Correlation techniques are widely used in signal processing with many applications in telecommunications, radar, medical electronics, physics, astronomy, geophysics etc . . .. .

Correlation has many useful properties, giving for example the ability to:

- Detect a wanted signal in the presence of noise or other unwanted signals.
- Recognise patterns within analogue, discrete-time or digital signals.
- Allow the determination of time delays through various media, eg free space, various materials, solids, liquids, gases etc . . .

- Correlation is a comparison process.

- The correlation betweeen two functions is a measure of their similarity.

- The two ‘functions’ could be very varied. For example fingerprints: a fingerprint expert can measure the correlation between two sets of fingerprints.

- This section will consider the correlation of signals expressed as functions of time. The signals could be continuous, discrete time or digital.

- When measuring the correlation between two functions, the result is often expressed as a correlation coefficient, ρ, with ρ in the range –1 to +1.

$\rho = -1$ $\rho = 0$ $\rho = +1$

Similar but opposite **No similarity** **Exactly similar**

- **Correlation involves multiplying, ‘sliding’ and integrating**

- **Consider 2 functions**

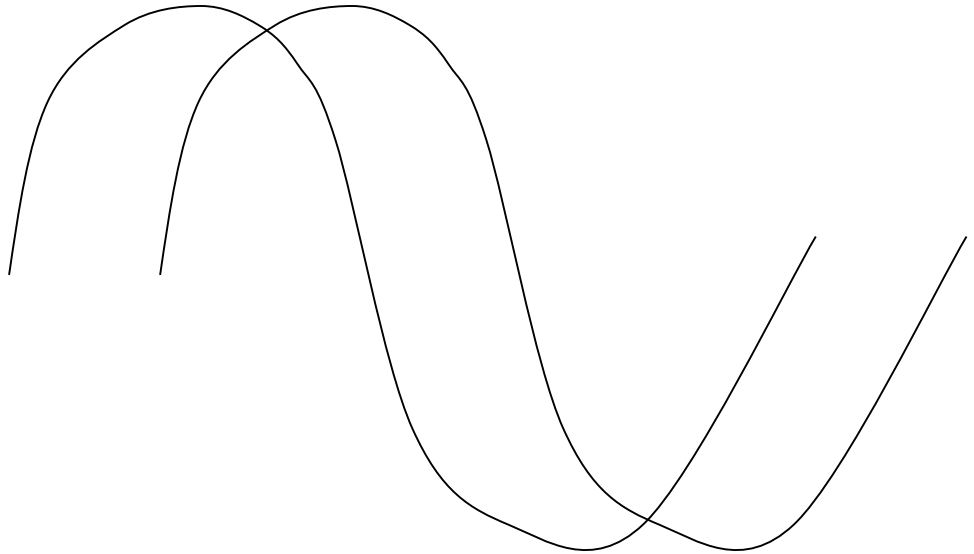

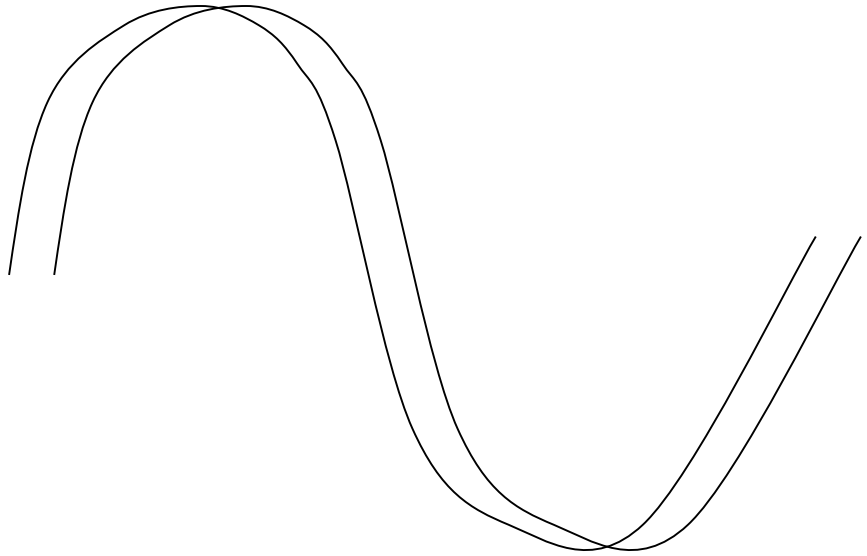

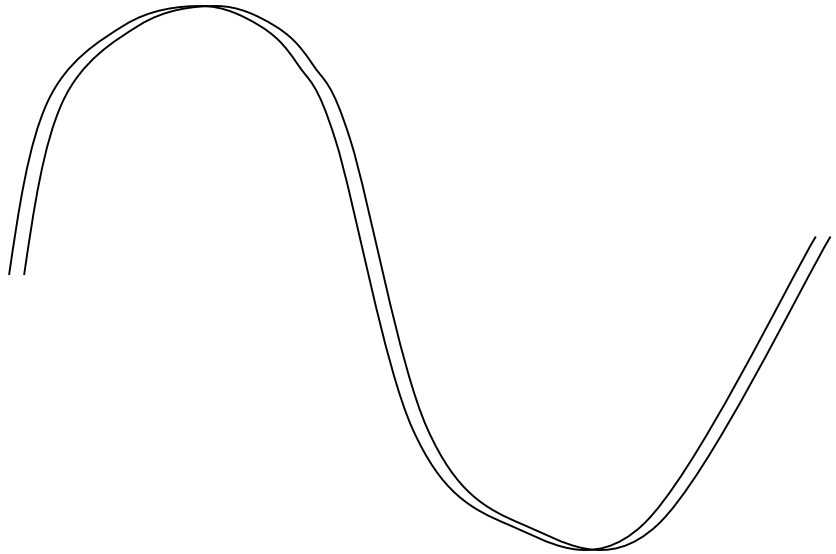

- **Consider 2 more functions**

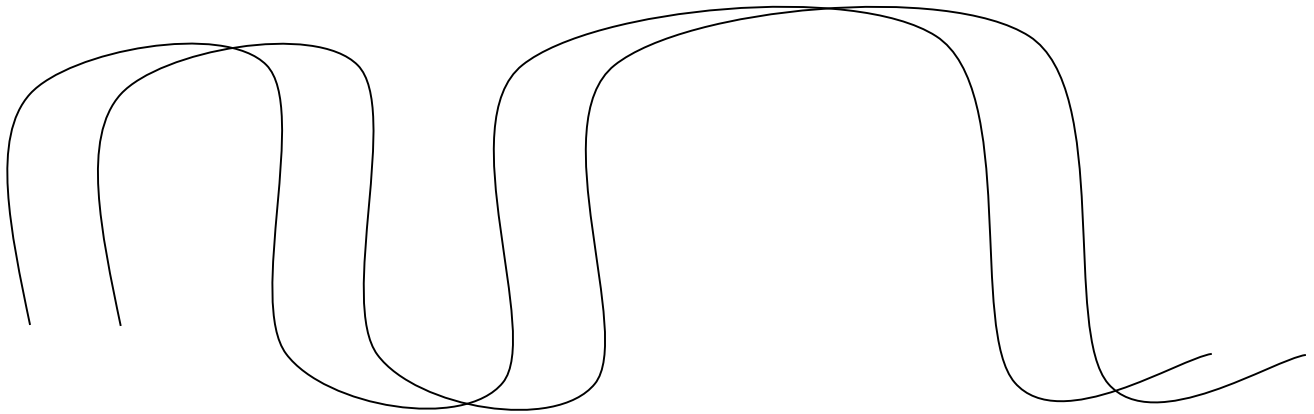

- **Consider 2 more functions**

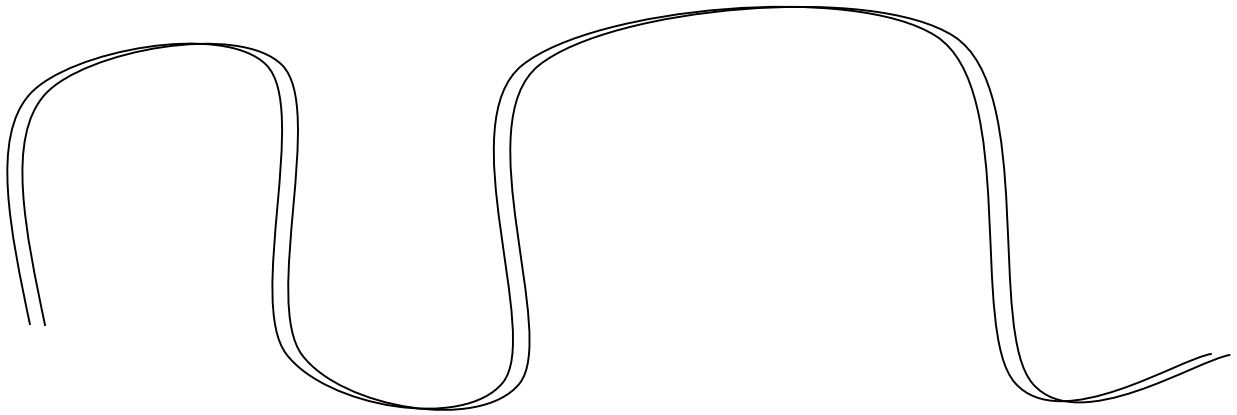

CONVOLUTION

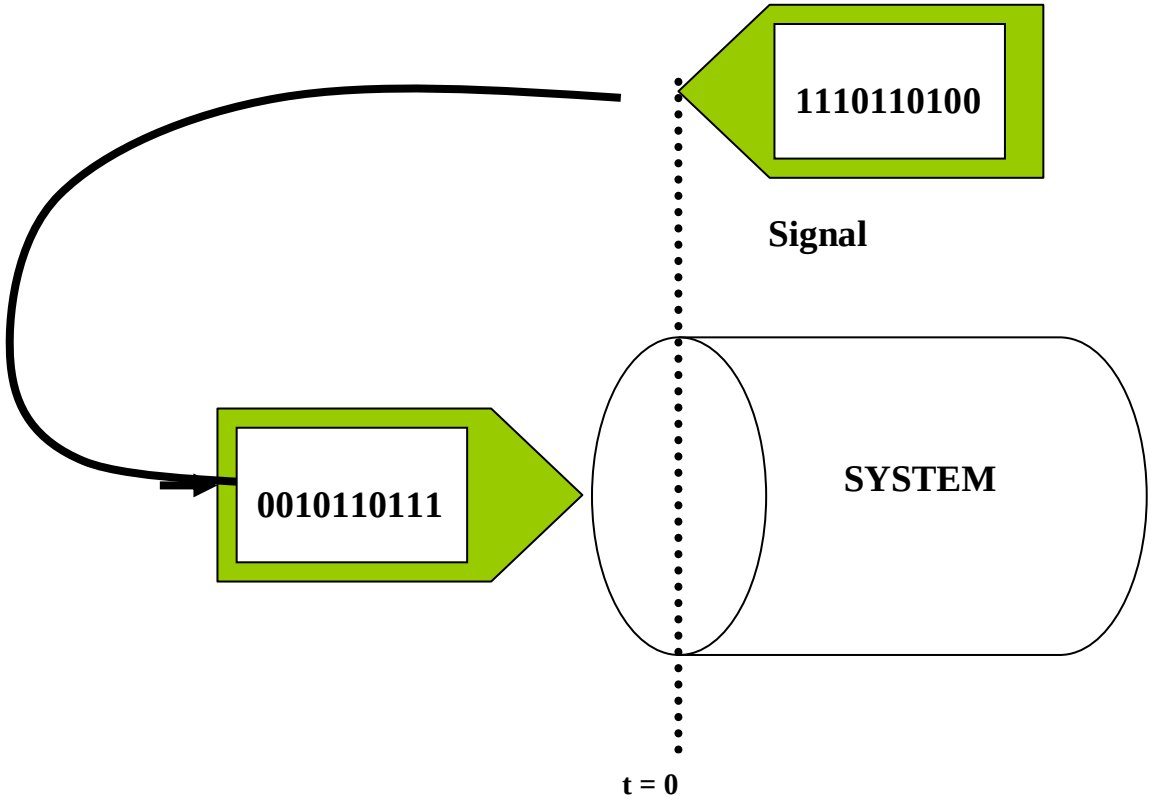

- **CORRELATION FUNCTION – CONTINUOUS TIME FUNCTIONS**
- Consider two continuous functions of time, $v_1(t)$ and $v_2(t)$. The functions may be random or deterministic.
- The correlation or similarity between these two functions measured over the interval T is given by:

$$R_{12}(\tau) = \lim_{T \to \infty} \frac{1}{T} \int_{\frac{-T}{2}}^{\frac{T}{2}} v_1(t) v_2(t-\tau) dt$$

- The functions may be deterministic or random.

- R12(τ) is the correlation function and is a measure of the similarity between the functions v1(t) and v2(t).

- The measure of correlation is a function of a new variable, τ, which represents a time delay or time shift between the two functions.

- Note that correlation is determined by multiplying one signal, v1(t), by another signal shifted in time, v2(t-τ), and then finding the integral of the product,

- Thus correlation involves multiplication, time shifting (or delay) and integration.

- The integral finds the average value of the product of the two functions, averaged over a long time ($T \to \infty$) for non-periodic functions.

- For periodic functions, with period T, the correlation function is given by:

$$R_{12}(\tau) = \frac{1}{T} \int_{\frac{-T}{2}}^{\frac{T}{2}} v_1(t) v_2(t-\tau) dt$$

- The correlation process is illustrated below:

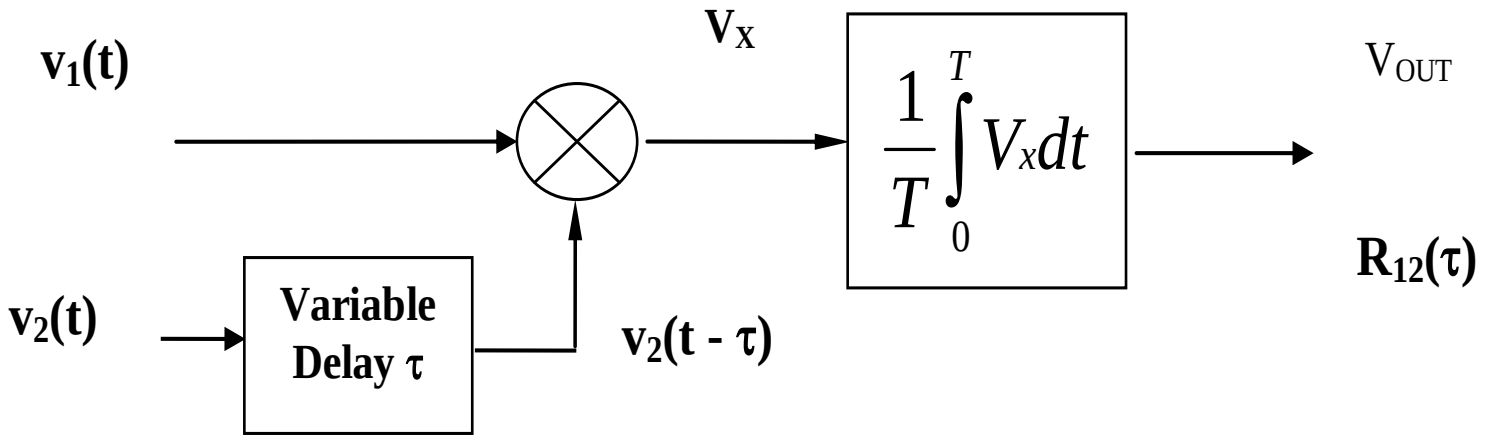

- As previously stated:

$$R_{12}(\tau) = \frac{1}{T}\int_{\frac{-T}{2}}^{\frac{T}{2}} v_1(t)v_2(t-\tau)dt$$

- The output $R_{12}(\tau)$ is the correlation between the two functions as a function of the delay τ.

- The correlation at a particular value of τ would be solved by solving $R_{12}(\tau)$,

AUTO CORRELATION AND CROSS CORRELATION FUNCTIONS

- **Auto Correlation**
- In auto correlation a signal is compared to a time delayed version of itself. This results in the Auto Correlation Function or ACF.
- Consider the function v(t), (which in general may be random or deterministic).

- The ACF, R(τ) , is given by

$$R(\tau) = \frac{1}{T} \int_{\frac{-T}{2}}^{\frac{T}{2}} v(t)v(t-\tau)dt$$

- Of particular interest is the ACF when $\tau = 0$, and v(t) represents a voltage signal:

$$R(0) = \frac{1}{T} \int_{\frac{-T}{2}}^{\frac{T}{2}} v(t)^2 \, dt$$

- R(0) represents the mean square value or normalised average power in the signal v(t)

- **Cross Correlation**
- In cross correlation, two ‘separate’ signals are compared, eg the functions v1(t) and v2(t) previously discussed.

- The CCF is

$$R_{12}(\tau) = \frac{1}{T} \int_{\frac{-T}{2}}^{\frac{T}{2}} v_1(t) v_2(t-\tau) dt$$

- **Diagrams for ACF and CCF**
- **Auto Correlation Function, ACF**

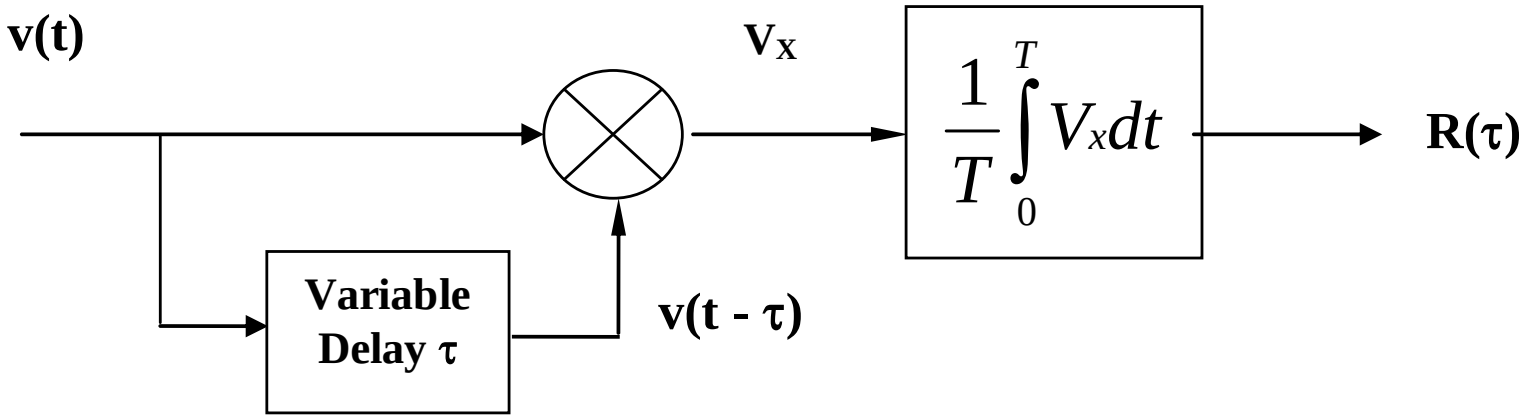

- **Note, if the input is v1(t) the output is R11(τ)**
- **if the input is v2(t) the output is R22(τ)**

- **Cross Correlation Function, CCF**

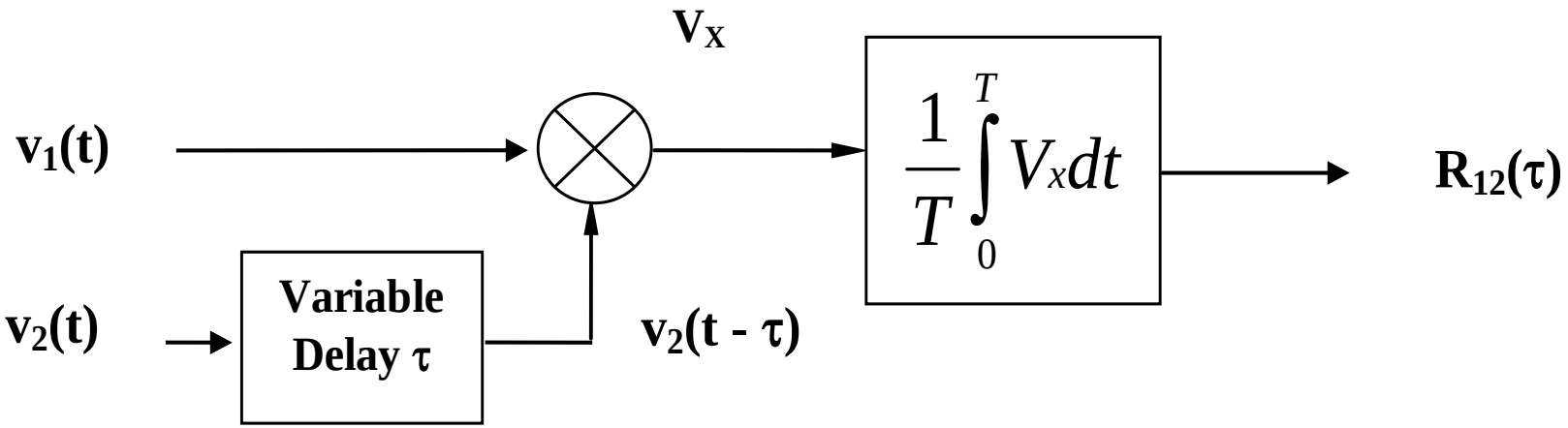

- **CORRELATION COEFFICIENT**
- The correlation coefficient, ρ, is the normalised correlation function.

- For cross correlation (ie the comparison of two separate signals), the correlation coefficient is given by:

$$\rho = \frac{R_{12}(\tau)}{\sqrt{R_{11}(0).R_{22}(0)}}$$

- Note that $R_{11}(0)$ and $R_{22}(0)$ are the mean square values of the functions $v_1(t)$ and $v_2(t)$ respectively.

- For auto correlation (ie the comparison of a signal with a time delayed version of itself), the correlation coefficient is given by:

$$\rho = \frac{R(\tau)}{\sqrt{R(0).R(0)}} = \frac{R(\tau)}{R(0)}$$

- For signals with a zero mean value, ρ is in the range $-1 < \rho < +1$

- If ρ = +1 then the are equal (Positive correlation).
- If ρ = 0, then there is no correlation, the signals are considered to be orthogonal.
- If ρ = -1, then the signals are equal and opposite (negative correlation)

- **EXAMPLES OF CORRELATION – CONTINUOUS TIME FUNCTIONS**

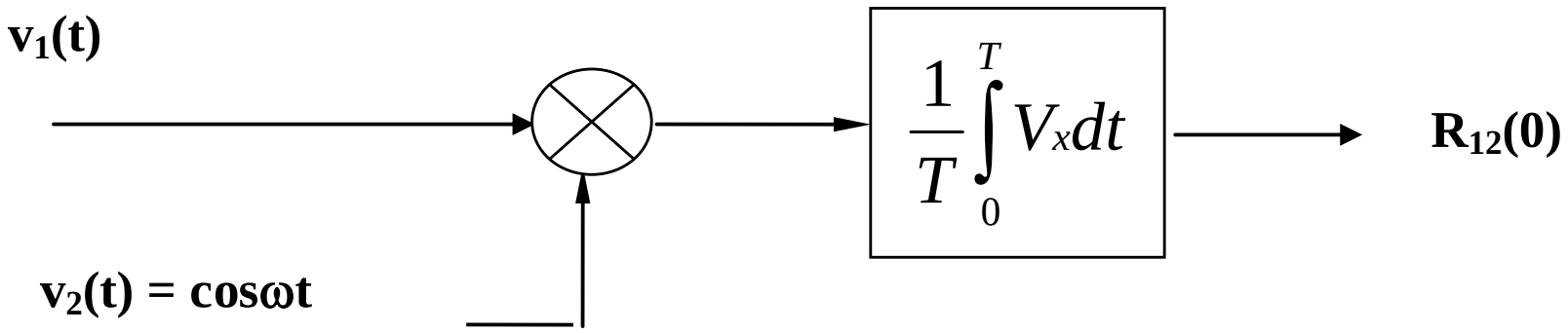

- The above may be used for the demodulation of PSK/PRK (Phase Shift Keying / Phase Reversal Keying) signals.

- For PSK/PRK, the input signal is $v1(t) = d(t)\cos\omega t$, d(t) = +V for data 1's and d(t) = -V for data 0's.

- The second function, $v2(t) = \cos\omega t$, is the carrier signal.

- Analyse the above process to determine the output R12(0) for the inputs given.

Interpretation of Seismic

polarity of waveform

1. In electricity,

   voltage = current × resistance,

   which in acoustic terms is equivalent to

   pressure = particle velocity × acoustic impedance.

2. In electricity,

   power = current × voltage,

   which in acoustic terms is equivalent to

   intensity = particle velocity × pressure,

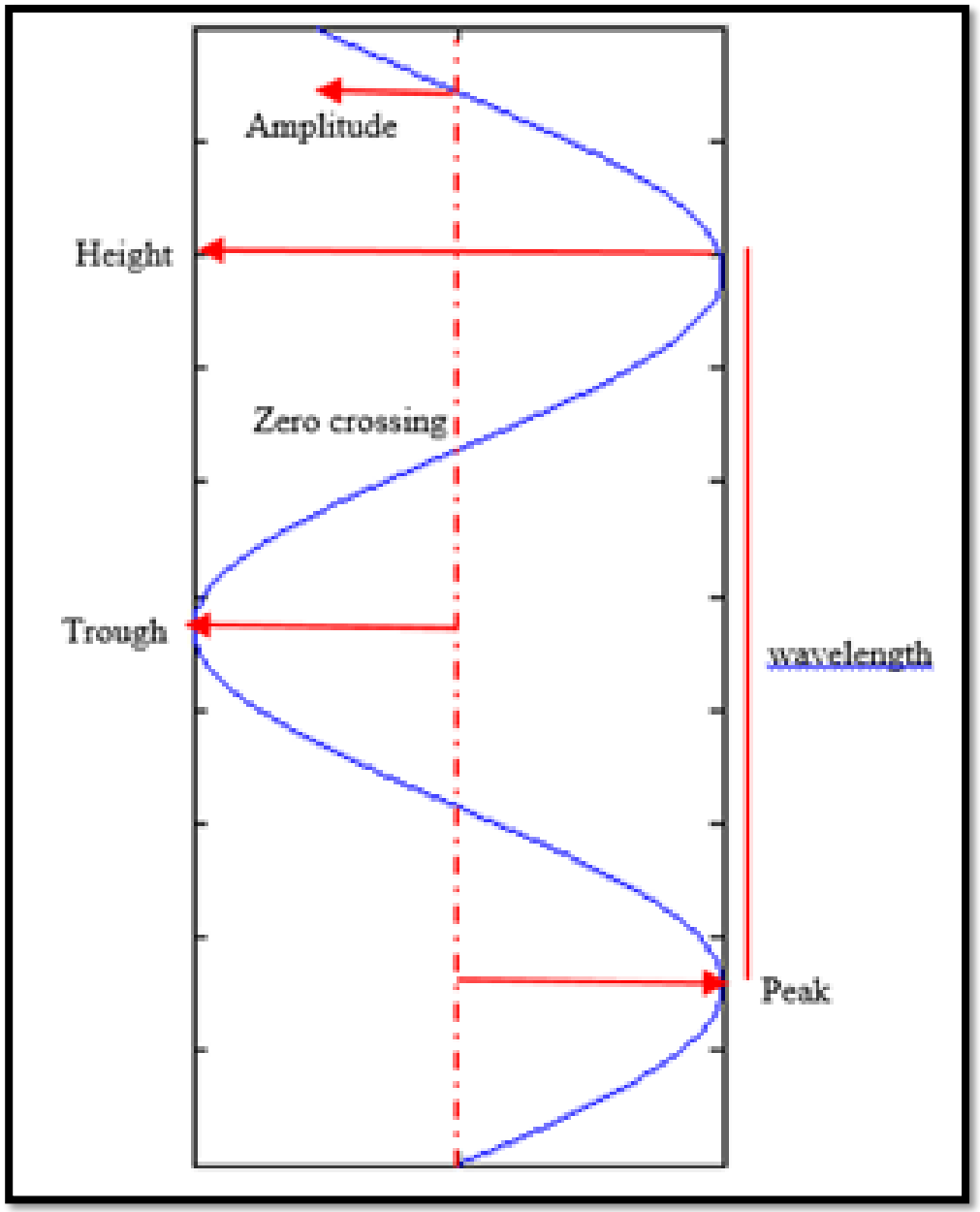
Amplitude
Height
Zero crossing
Trough
wavelength
Peak

The strength of a reflection generated at a boundary can be quantified in terms of the boundary's reflection coefficient (*RC*); at normal incidence this is

$$RC = \frac{Z_2 - Z_1}{Z_2 + Z_1}, \qquad (2.2)$$

where

Z_1 = acoustic impedance in the upper layer.
Z_2 = acoustic impedance in the lower layer.

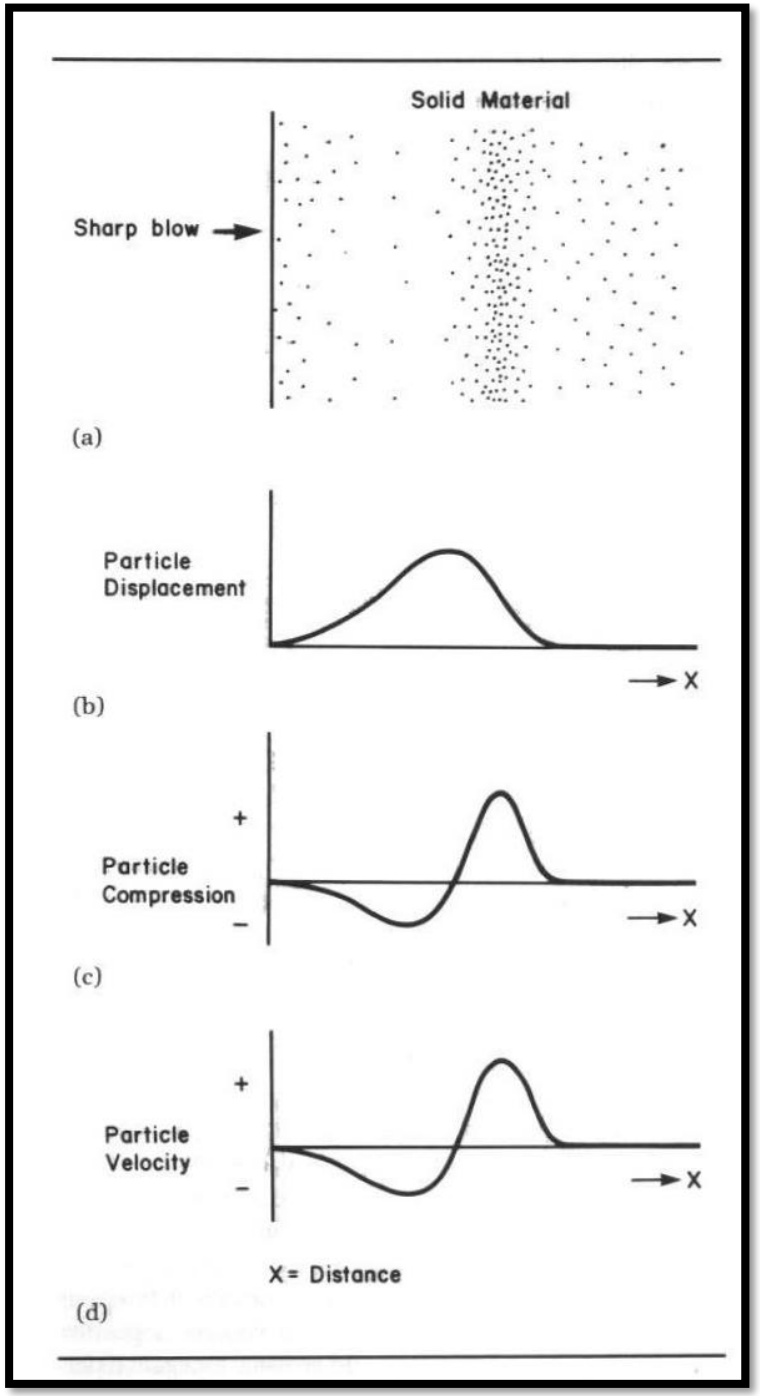

FIGURE 2.3 *Response of particle compression and particle velocity to the passage of a compressional wave.* (a) *Diagrammatic representation of particle spacing in a solid material a few milliseconds after being struck by a sharp blow.* (b) *The maximum particle displacement corresponds with the propagating compressional wave.* (c) *The particle compression is at a maximum in the propagating wave and a minimum in the rarefactional area behind the compression wave.* (d) *The particle velocity is positive (i.e., forward) in the compressional part of the wave and negative (i.e., in a backward direction) in the rarefactional part of the wave. The waveforms for particle compression and particle velocity are identical. After Anstey, 1977, by permission of IHRDC Press.*

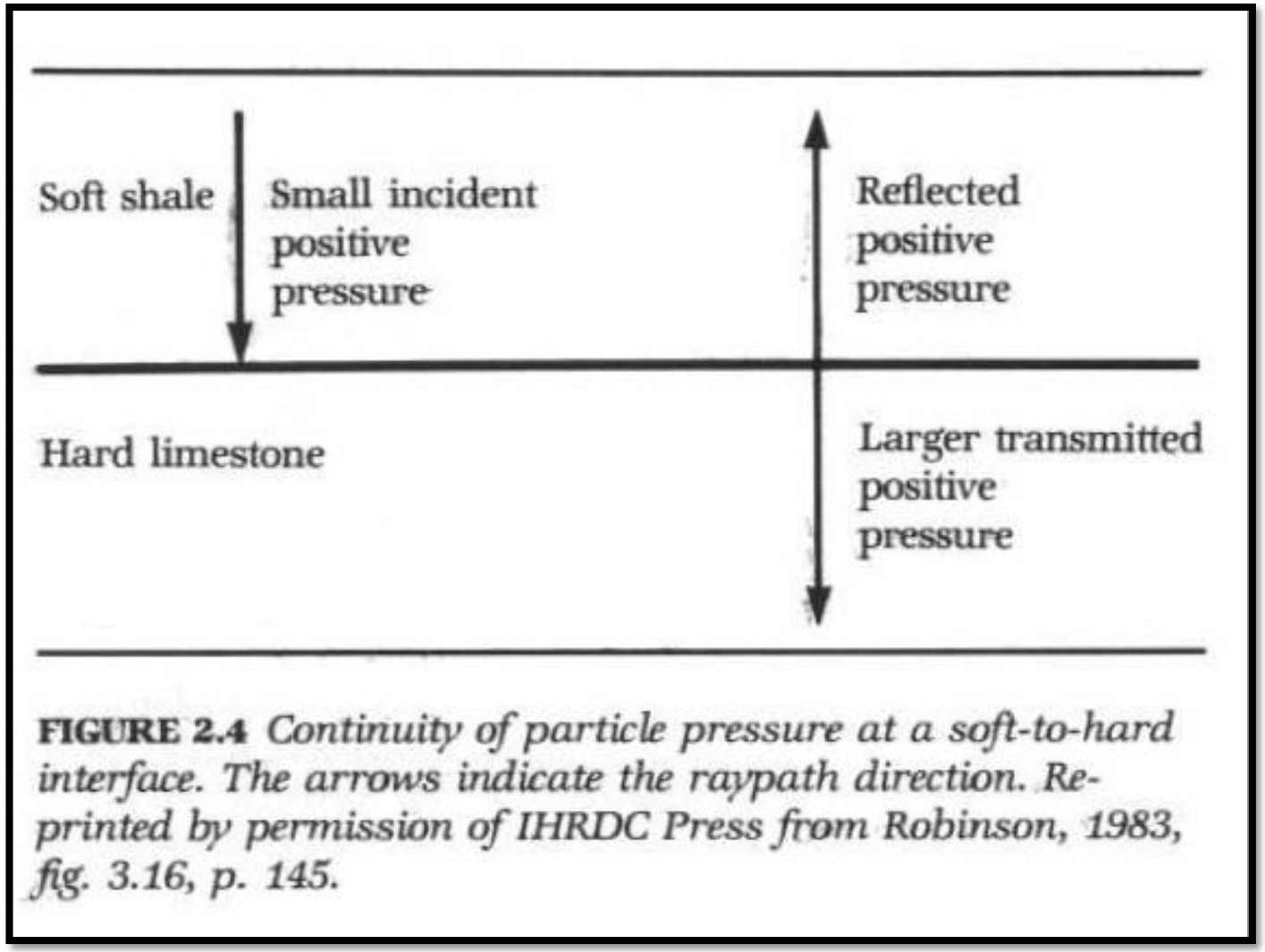

FIGURE 2.4 *Continuity of particle pressure at a soft-to-hard interface. The arrows indicate the raypath direction. Reprinted by permission of IHRDC Press from Robinson, 1983, fig. 3.16, p. 145.*

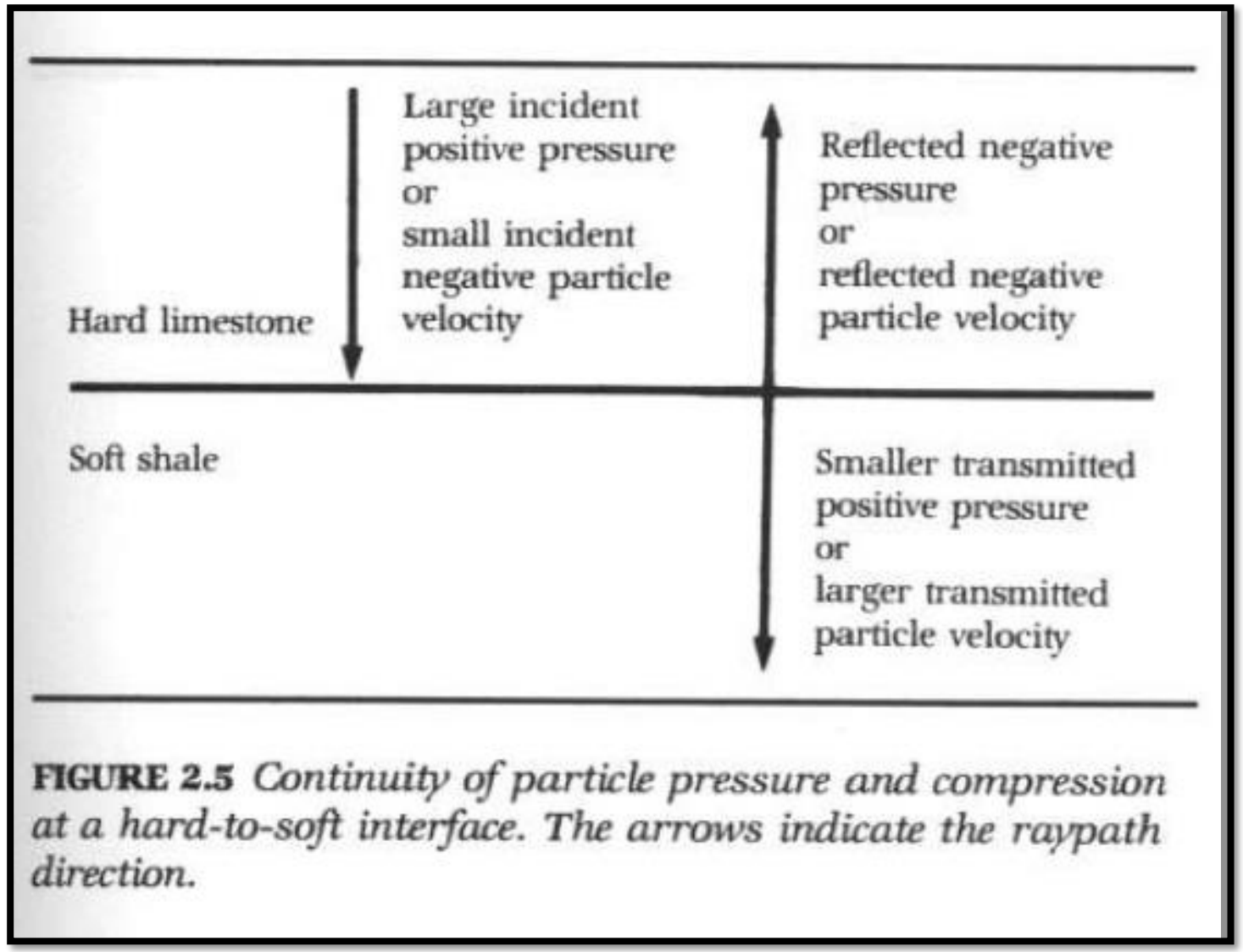

FIGURE 2.5 *Continuity of particle pressure and compression at a hard-to-soft interface. The arrows indicate the raypath direction.*

1. A positive seismic signal produces a positive acoustic pressure on a hydrophone in water or an upward initial motion on a geophone on land.
2. A positive seismic signal is recorded as a negative number on a tape, a negative deflection (downswing) on a monitor record, and a trough (white) on a seismic section.

Using this convention, in a seismic section displayed with SEG normal polarity we would expect:

A reflecting boundary to appear as a trough in the seismic trace if $Z_2 > Z_1$

A reflecting boundary to appear as a peak in the seismic trace if $Z_2 < Z_1$

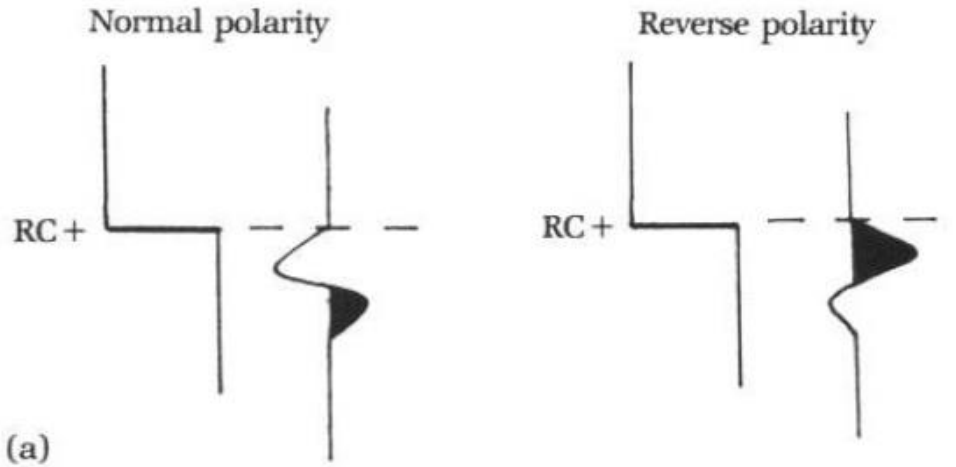

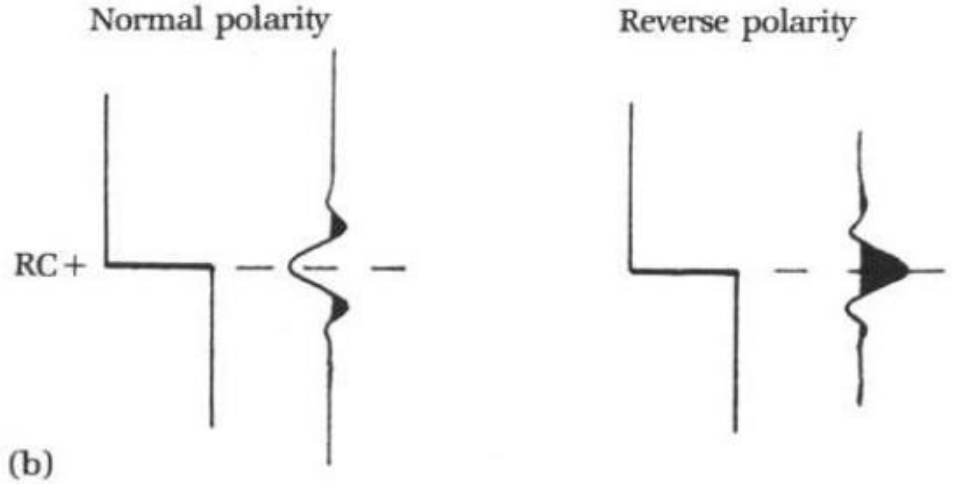

FIGURE 2.6 *Examples of idealized normal and reverse polarity for* (a) *minimum- and* (b) *zero-phase wavelets at an acoustic-impedance boundary with a positive reflection coefficient.*

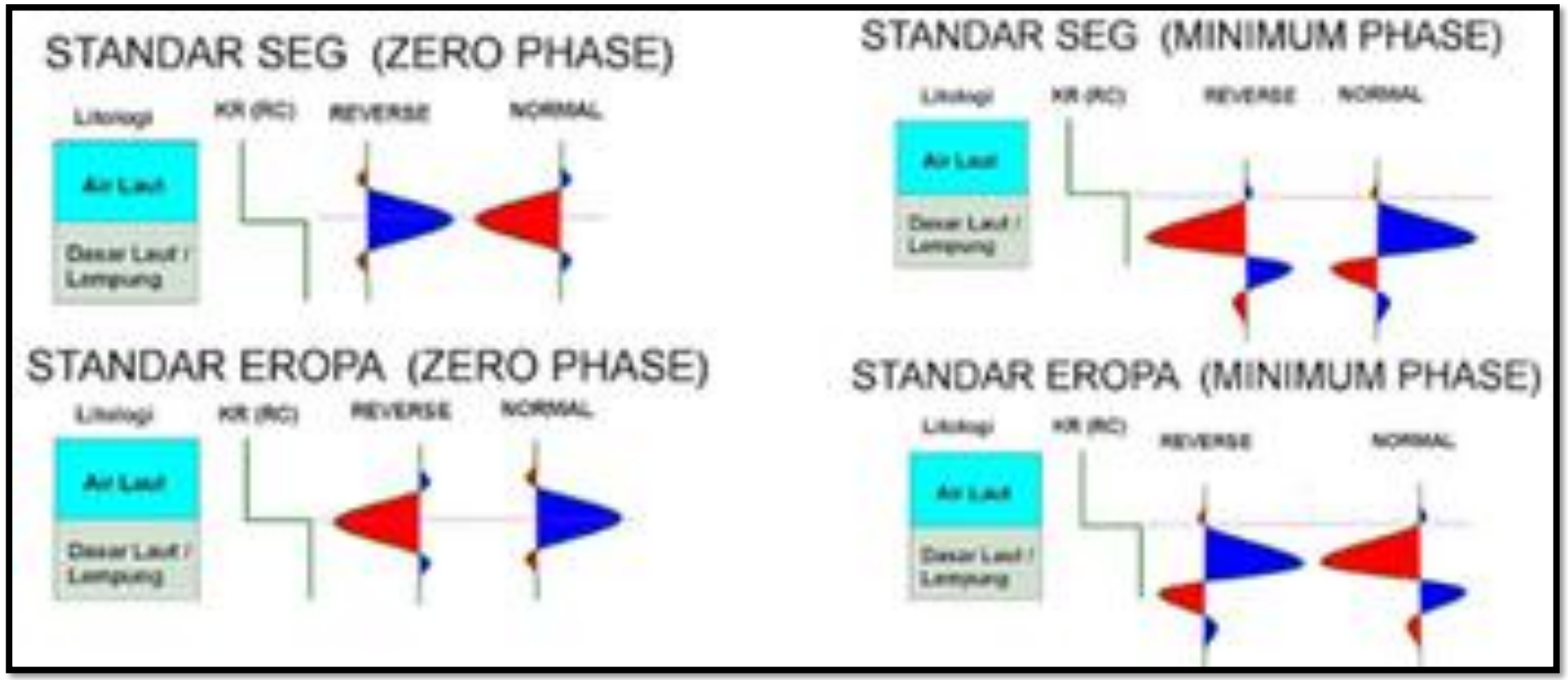
STANDAR SEG (ZERO PHASE)
Litologi
KR (RC)
REVERSE
NORMAL
Air Laut
Dasar Laut / Lempung
STANDAR SEG (MINIMUM PHASE)
Litologi
KR (RC)
REVERSE
NORMAL
Air Laut
Dasar Laut / Lempung
STANDAR EROPA (ZERO PHASE)
Litologi
KR (RC)
REVERSE
NORMAL
Air Laut
Dasar Laut / Lempung
STANDAR EROPA (MINIMUM PHASE)
Litologi
KR (RC)
REVERSE
NORMAL
Air Laut
Dasar Laut / Lempung

1. Given the same amplitude spectrum, a zero-phase signal is always shorter and always has greater amplitude than the equivalent minimum-phase signal; it therefore has a greater signal/noise ratio.
2. The maximum amplitude of zero-phase signals always coincides with the theoretical reflectivity spike. The maximum amplitude of a minimum-phase signal is delayed with reference to the reflectivity spike.

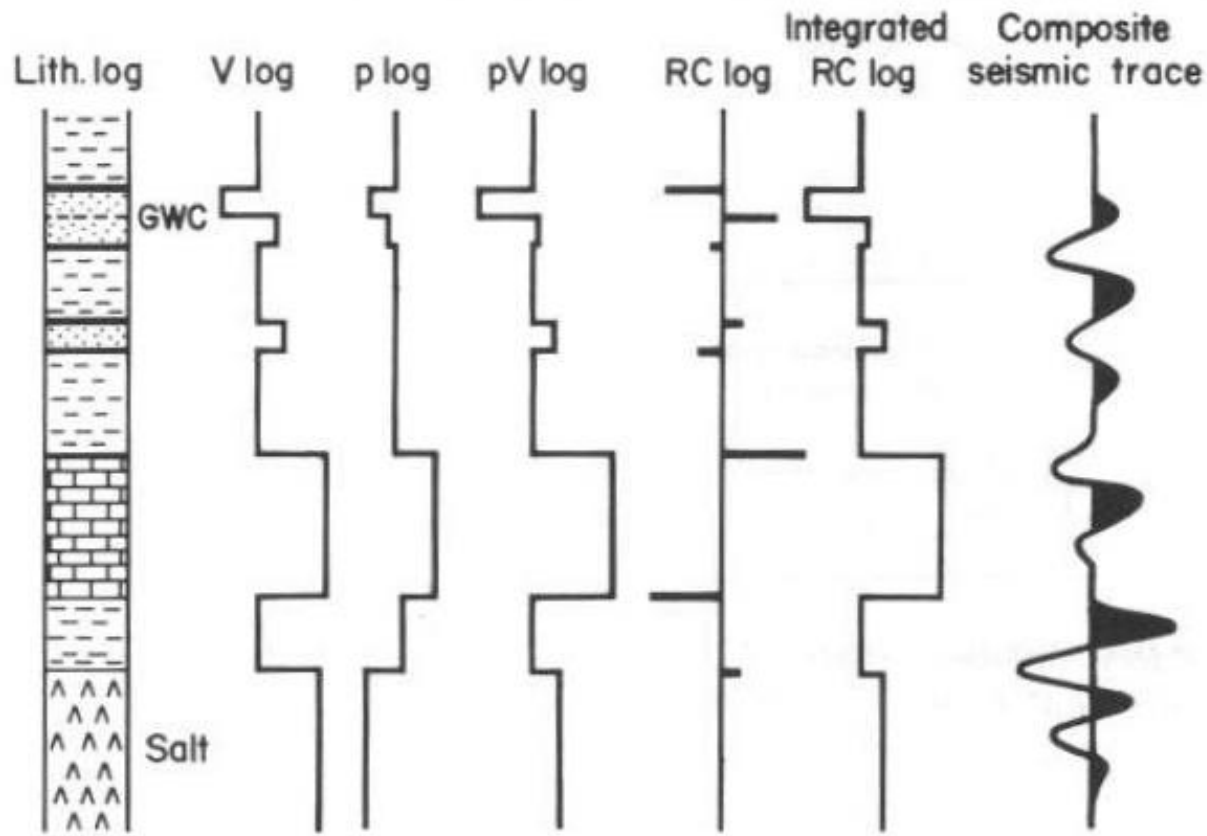
Lith. log
V log
p log
pV log
RC log
Integrated RC log
Composite seismic trace
GWC
Salt

FIGURE 2.7 *The derivation of the reflection coefficient log and the resulting composite trace for a minimum-phase, normal-polarity (SEG) wavelet. The lithological sequence shown at the left consists of: a basal salt section overlain by a thick shale, massive limestone, and a shale sequence containing two sands. The lower sand is water saturated, while the upper sand contains gas overlying water-saturated sand. The velocity is shown under* V *log; with high velocity in the salt and limestone, a velocity in the water-wet sands slightly higher than in the shales, and a major depression of velocity in the gas sand. The density log is shown under* ρ *log. The salt density is very low, and the porosity in the lower sand causes the density to be coincident with that of the shales. The density in the gas sand is depressed. The acoustic-impedance log, shown under* ρV *log, is the product of velocity and density. For most lithologies it has similar form to the* V *log, excepting cases where velocity and density change in opposite directions. This occurs in the upper water sand, and is not significant; but in the salt the changes in velocity and density almost cancel. The reflection coefficients of the acoustic-impedance boundaries are shown under* RC *log, which shows the sign and expected strength of reflections. A composite seismic trace that would be produced by convolving a minimum-phase, normal-polarity (SEG) wavelet with the* RC *log is shown. The integrated* RC *log shows the effect of making a running sum of all values in a moving window down the* RC *log; this restores the* ρV *log. After Anstey, 1980a, and Robinson, 1983, by permission of IHRDC Press.*

significant velocity increase at the top of the salt. If we were to rely solely on velocity as an indicator of acoustic impedance, we would expect the boundary to generate a strong reflection. However, the density shows a significant decrease from the claystones into the salt—a change in the opposite direction to that of the velocity. As acoustic impedance is the product of velocity and density, the changes in velocity and density largely cancel each other to produce only a small change in acoustic impedance at the top of the salt. A reflection from the top salt will be much weaker than we would have expected had we based our expectations of reflection strength on the velocity increase.

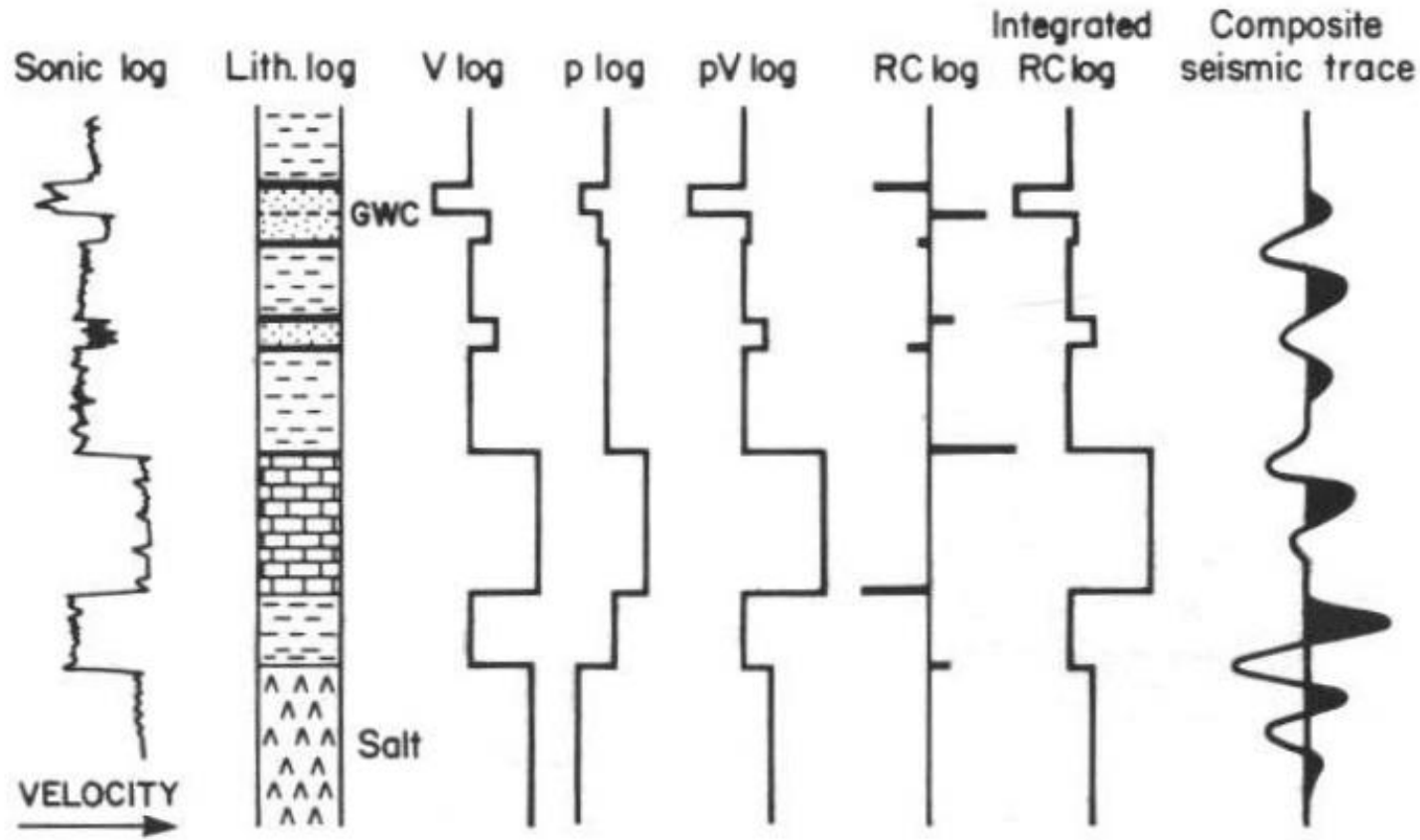

FIGURE 2.9 *Diagram showing the difference in resolution between a wireline sonic log and a seismic trace. After Anstey,*

Interference

contrast. The composite trace cannot be interpreted simply, as there is not a straightforward one-to-one relationship between the seismic trace and the acoustic boundaries. Because the seismic pulse is longer than the separation between some of these contrasts, the reflections interfere.

Interference always occurs when the reflections from different reflectors overlap. Interference is controlled by the length of seismic pulse in milliseconds and the spacing of acoustic-impedance boundaries in time, which is a function of the interval velocity.

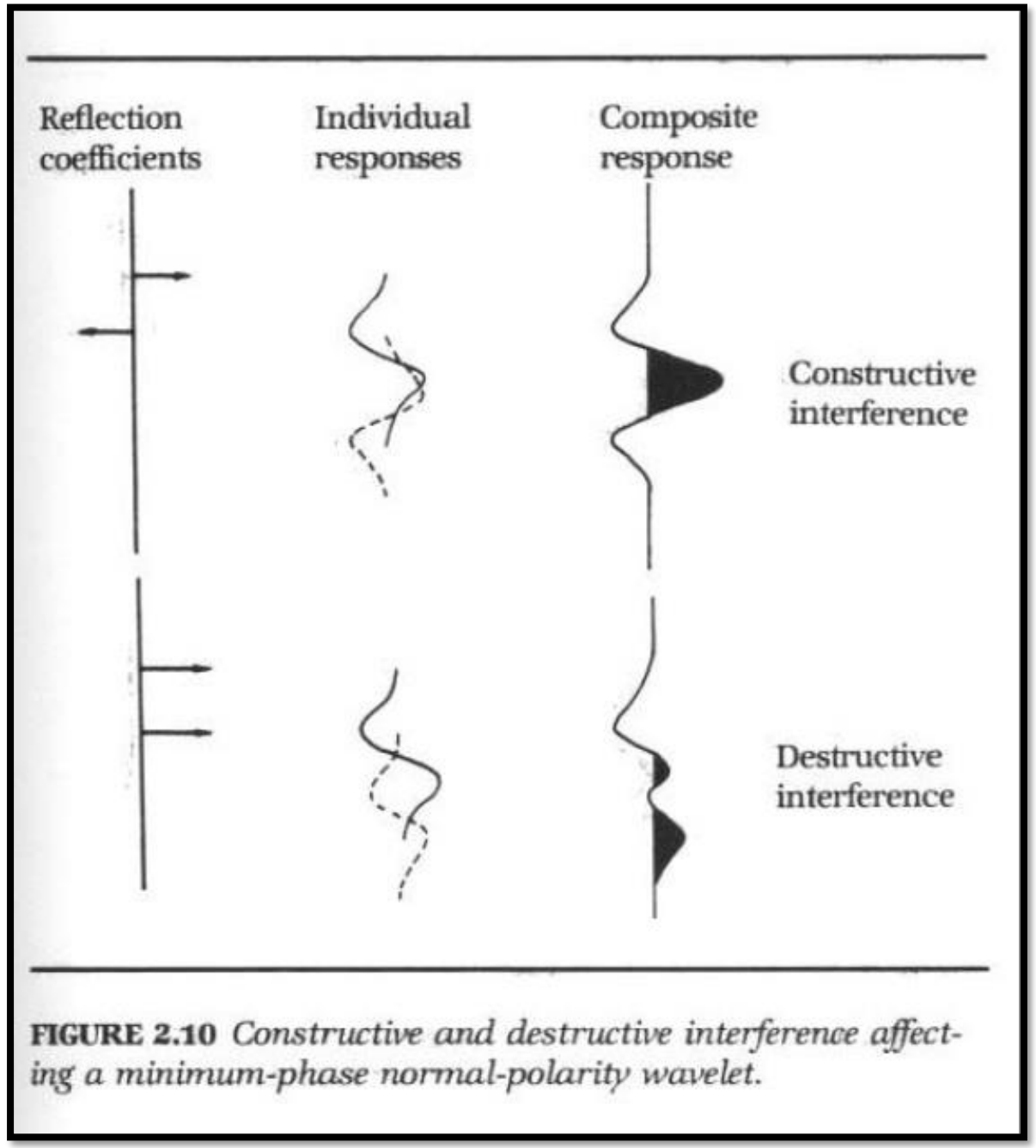

FIGURE 2.10 *Constructive and destructive interference affecting a minimum-phase normal-polarity wavelet.*

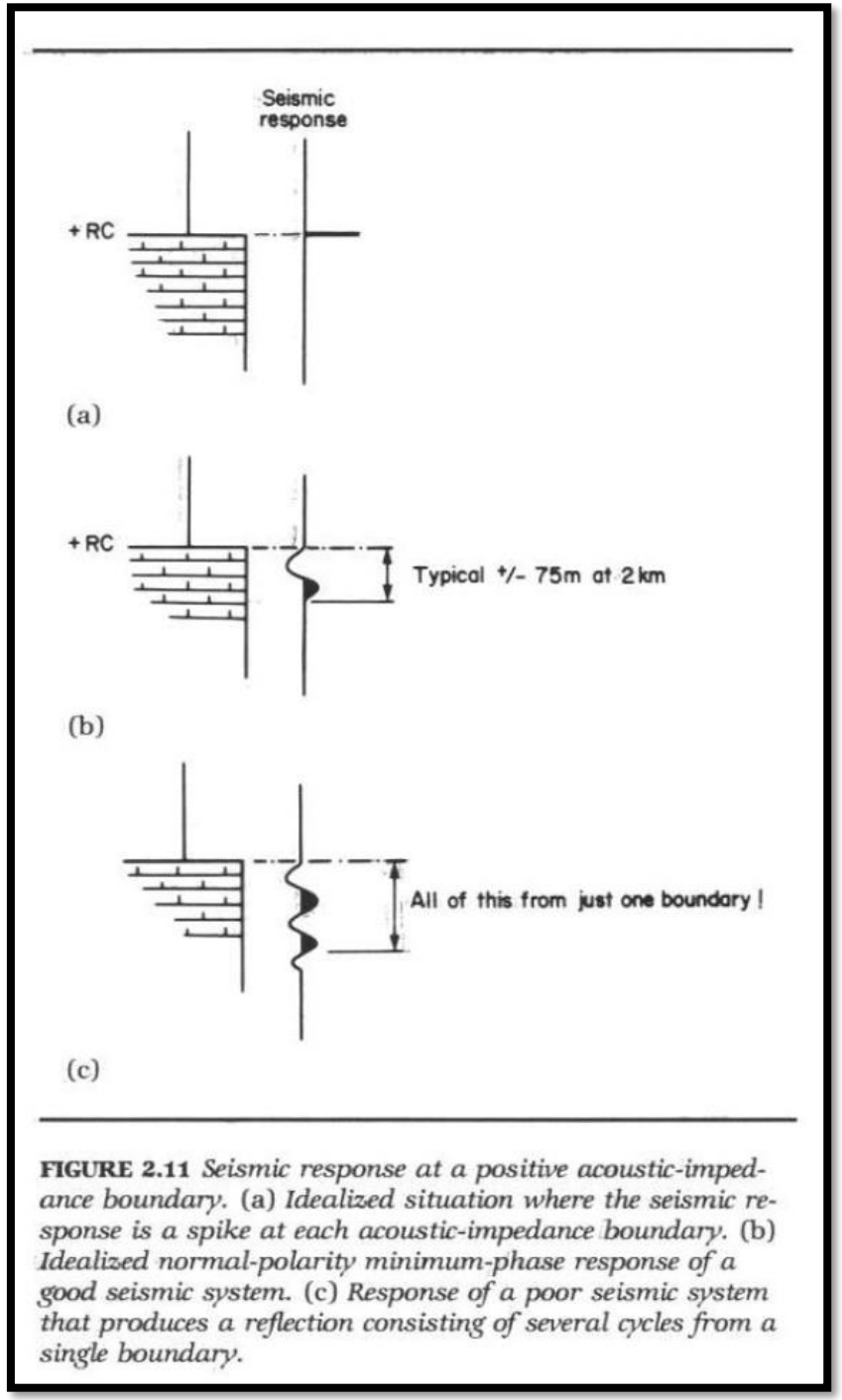

FIGURE 2.11 *Seismic response at a positive acoustic-impedance boundary.* (a) *Idealized situation where the seismic response is a spike at each acoustic-impedance boundary.* (b) *Idealized normal-polarity minimum-phase response of a good seismic system.* (c) *Response of a poor seismic system that produces a reflection consisting of several cycles from a single boundary.*

The length of the seismic pulse is critical. Ideally, the pulse would be a spike whose reflections would be similar spikes of lesser amplitude (fig. 2.11a); particle motion would be instantaneous and wavelength infinitesimal; and we would have almost perfect resolution. Typically, however, the input pulse consists of one or two peaks and one or two troughs and has a duration (length in the seismic section) of 20–100 ms (fig. 2.11b). The fact that the wavelet often comprises several cycles (follow half-cycles) rather than the desired spike, means that a single reflecting horizon can generate a reflection consisting of the primary event followed immediately by one or more follow half-cycles (fig. 2.11c). This can give a false impression of interbedding.

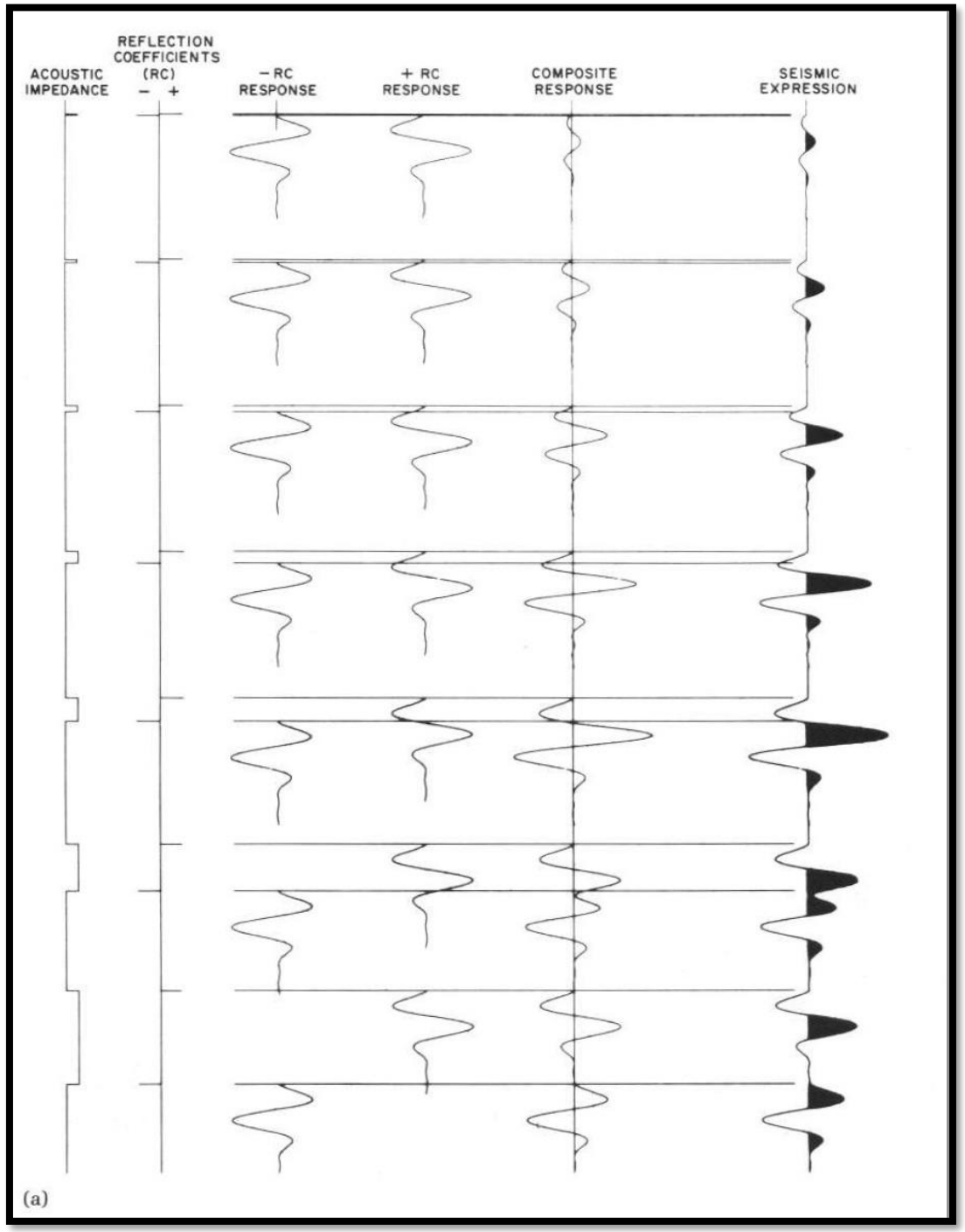
ACOUSTIC IMPEDANCE
REFLECTION COEFFICIENTS (RC)
− +
− RC RESPONSE
+ RC RESPONSE
COMPOSITE RESPONSE
SEISMIC EXPRESSION
(a)

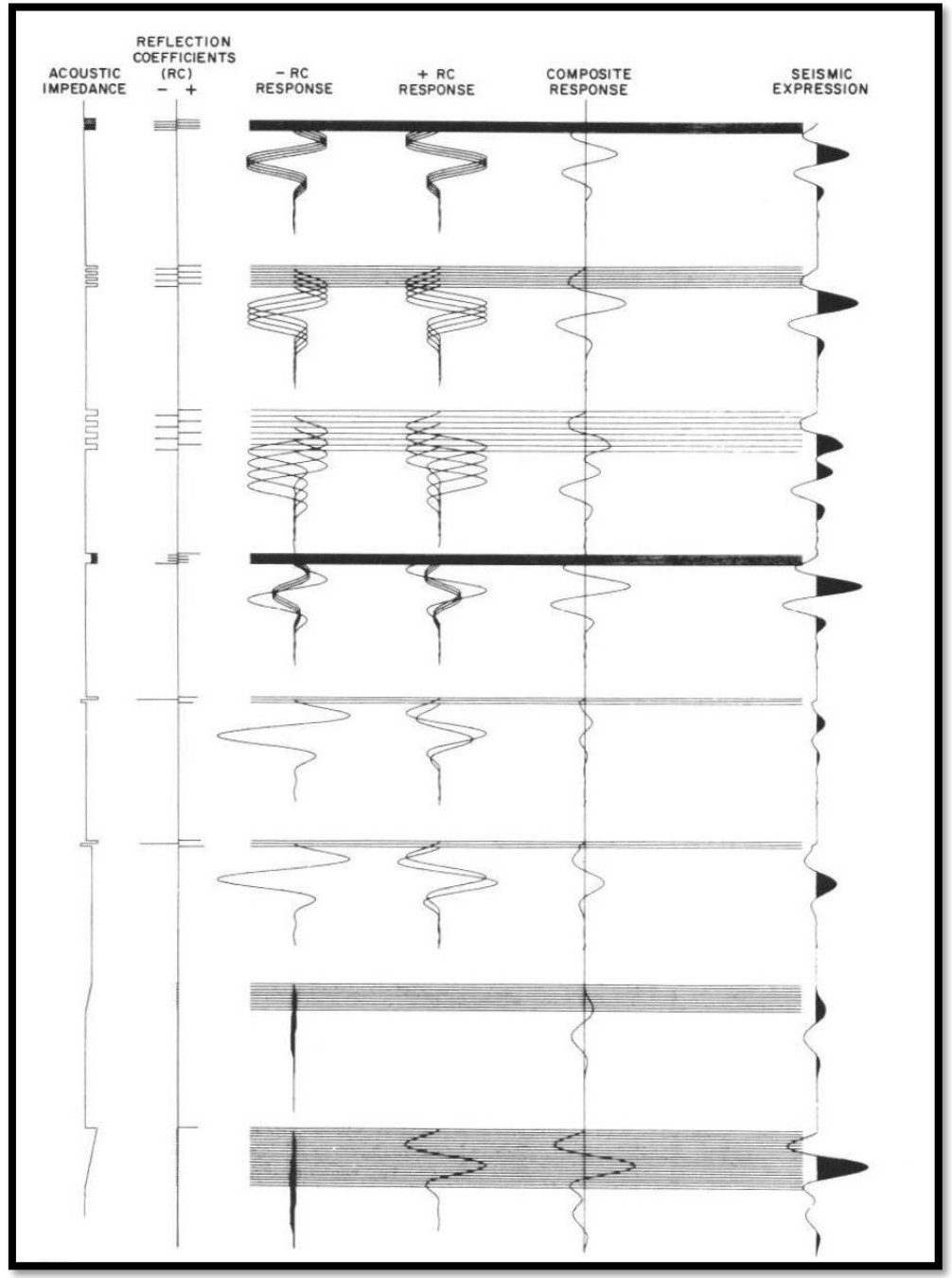
ACOUSTIC IMPEDANCE
REFLECTION COEFFICIENTS (RC)
− +
− RC RESPONSE
+ RC RESPONSE
COMPOSITE RESPONSE
SEISMIC EXPRESSION

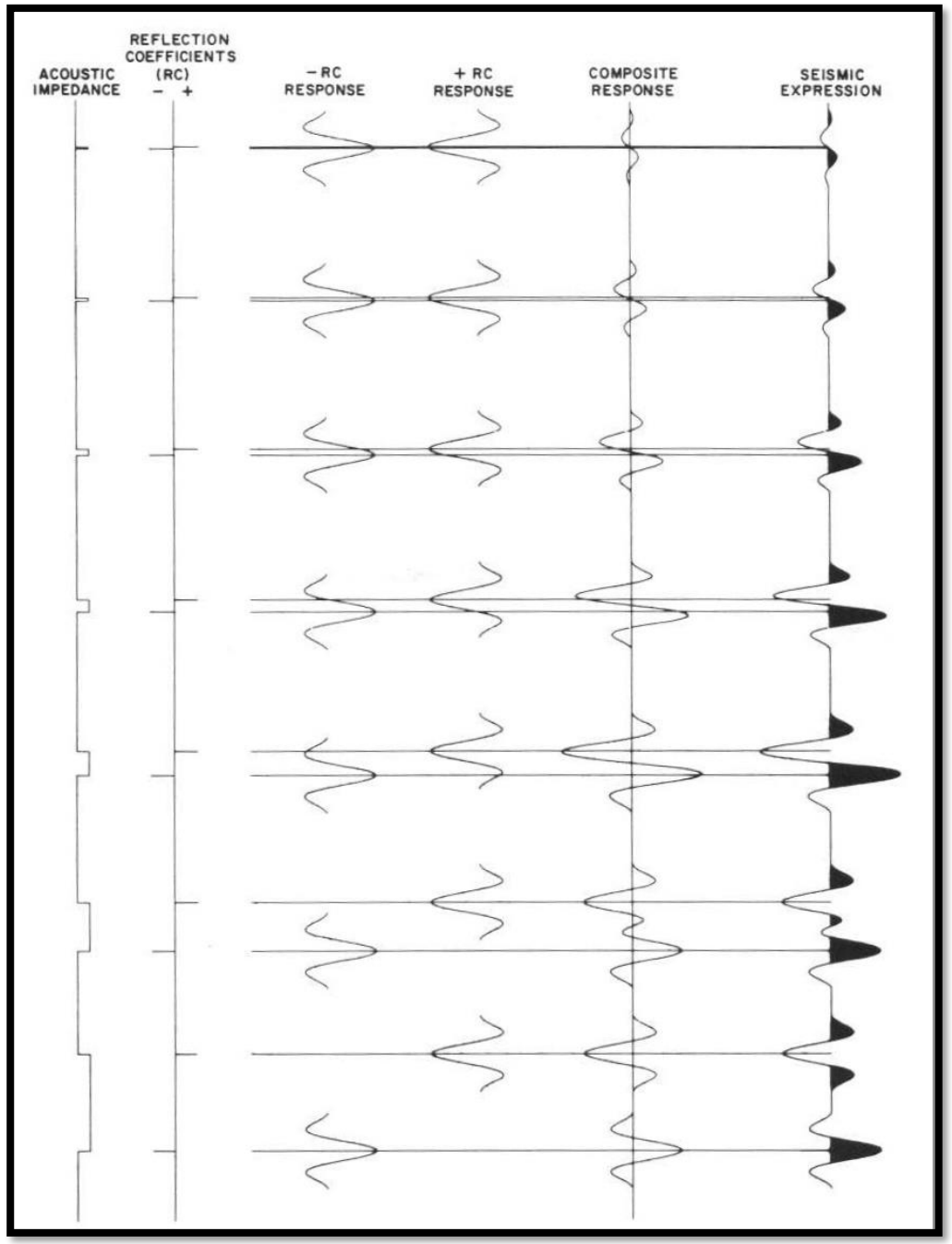
ACOUSTIC IMPEDANCE
REFLECTION COEFFICIENTS (RC)
− +
− RC RESPONSE
+ RC RESPONSE
COMPOSITE RESPONSE
SEISMIC EXPRESSION

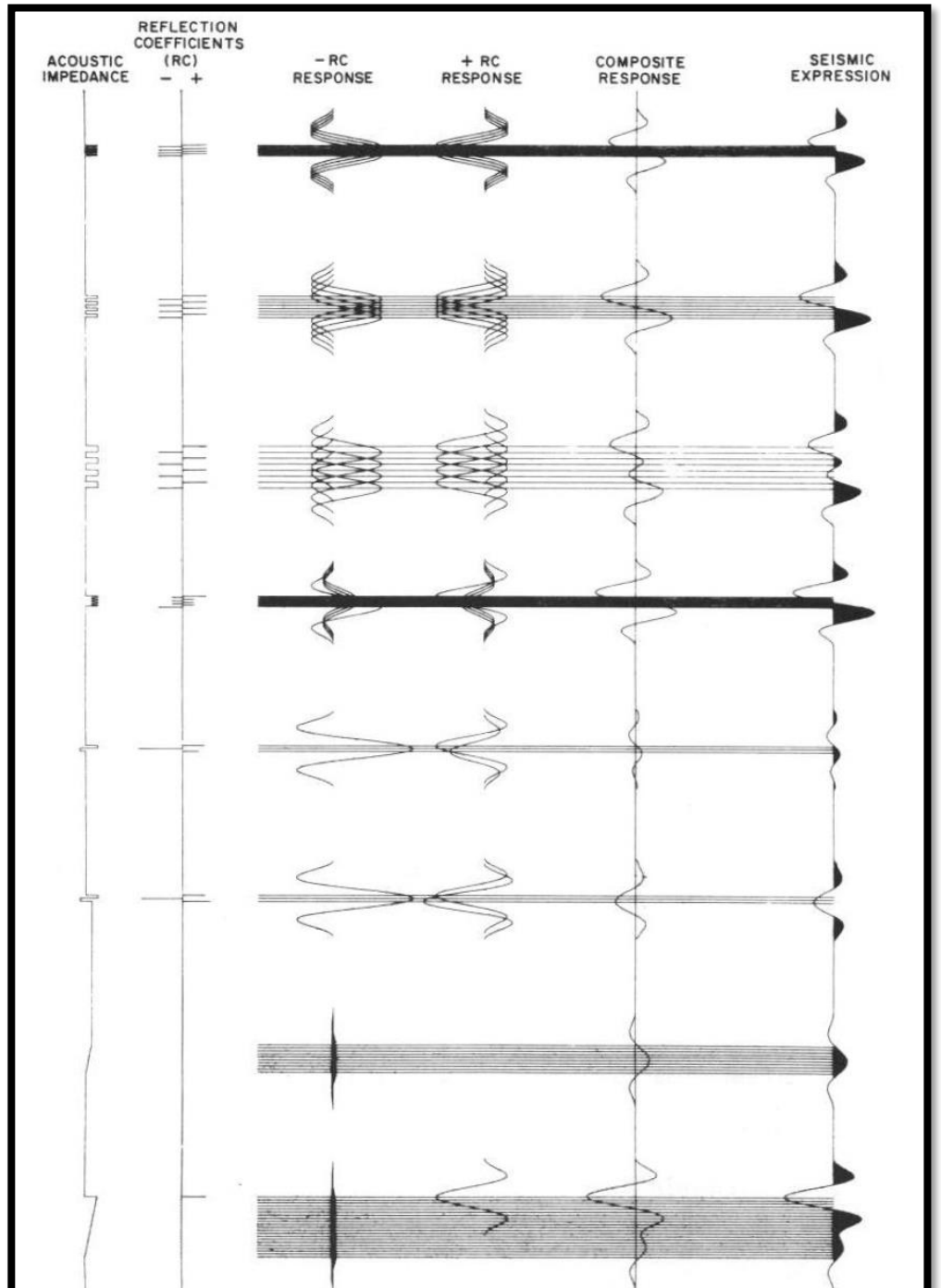
ACOUSTIC IMPEDANCE
REFLECTION COEFFICIENTS (RC)
– +
– RC RESPONSE
+ RC RESPONSE
COMPOSITE RESPONSE
SEISMIC EXPRESSION

Vertical Resolution

1. How thick must a bed or unit be before there is no interference between the reflections from acoustic-impedance contrasts at the unit's top and base?
2. How thin can a bed or unit be before its top and base are no longer resolvable?

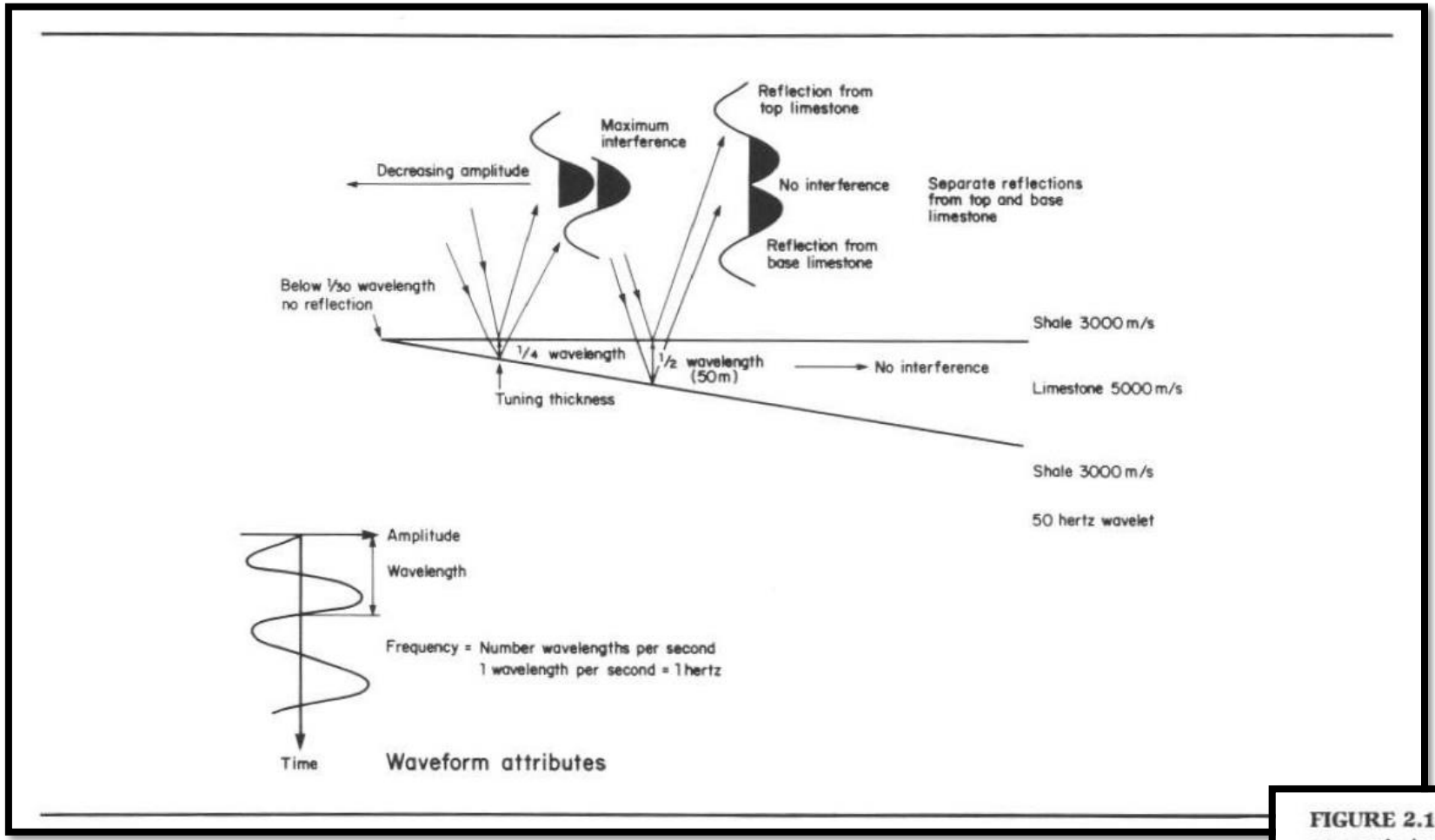

FIGURE 2.14 *Interference effects associated with a high acoustic-impedance wedge encased in lower acoustic-impedance shale. The limestone must be thicker than half the seismic wavelength for no interference between reflections from its top and base. Maximum interference and amplitude of the resulting reflection occurs at a limestone thickness equivalent to one quarter of the seismic wavelength—the tuning thickness. For limestone thicknesses below one-quarter wavelength, the reflection remains the same shape but decreases in amplitude. Once the limestone is about one-thirtieth wavelength or less, reflections from the top and base effectively cancel and there is no detectable seismic response.*

In the shallow section where velocities are usually low and frequencies are high, wavelengths of around 40 m are common, with a corresponding resolvable thickness of 10 m and a detectable limit of bed thickness to produce a reflection of about 1.3 m. Deeper in the section, where velocities are higher and frequencies lower, these resolvable and detectable limits are higher. In the example above, for example, with a velocity of 5000 m/s and a frequency of 20 Hz, the resolvable and detectable limits are 62.5 m and 8.3 m, respectively. It is difficult to determine directly from the seismic trace the wavelength of the seismic pulse in meters. However, if the wavelet's period and the inter-

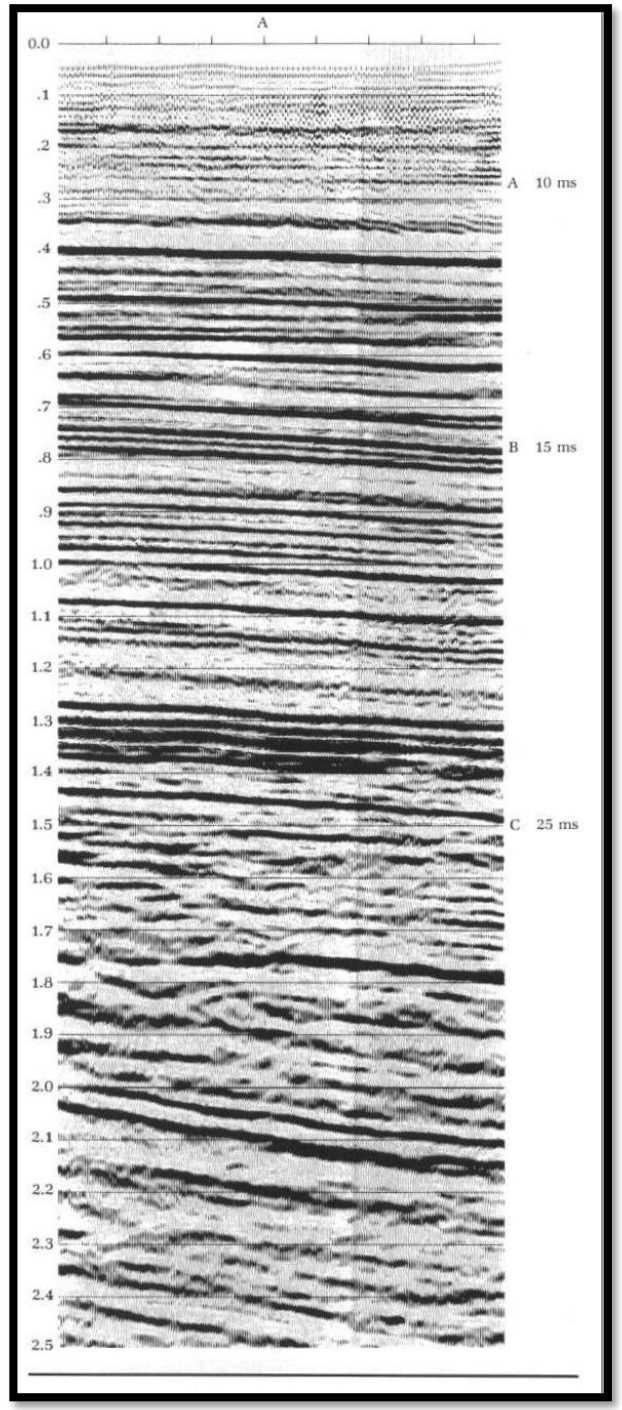

FIGURE 2.15 *Estimating the dominant frequency or period of the seismic wavelet from a seismic section. Isolated high-amplitude, continuous reflections should be chosen to reduce the risk of interference effects. It is assumed that on minimum-phase processed sections, individual reflections consist of a lead and follow half-cycles (the first and second half-cycles). Zero-phase data is assumed to have a waveform consisting of lead and follow half-cycles symmetric about a higher-amplitude central peak or trough. The dominant frequency is Hertz = 1/period(s). The seismic section here is processed to produce a minimum-phase waveform and is displayed with reverse polarity (SEG).*

Reflection A: duration 12 ms; frequency 83 Hz
Reflection B: duration 15 ms; frequency 67 Hz
Reflection C: duration 25 ms; frequency 40 Hz

The estimated frequencies should always be calculated for several reflections in a particular time range and the estimates compared with the time-variant filter (TVF) limits given in the seismic section label. The estimated value must fall within the range of the time-variant filter.

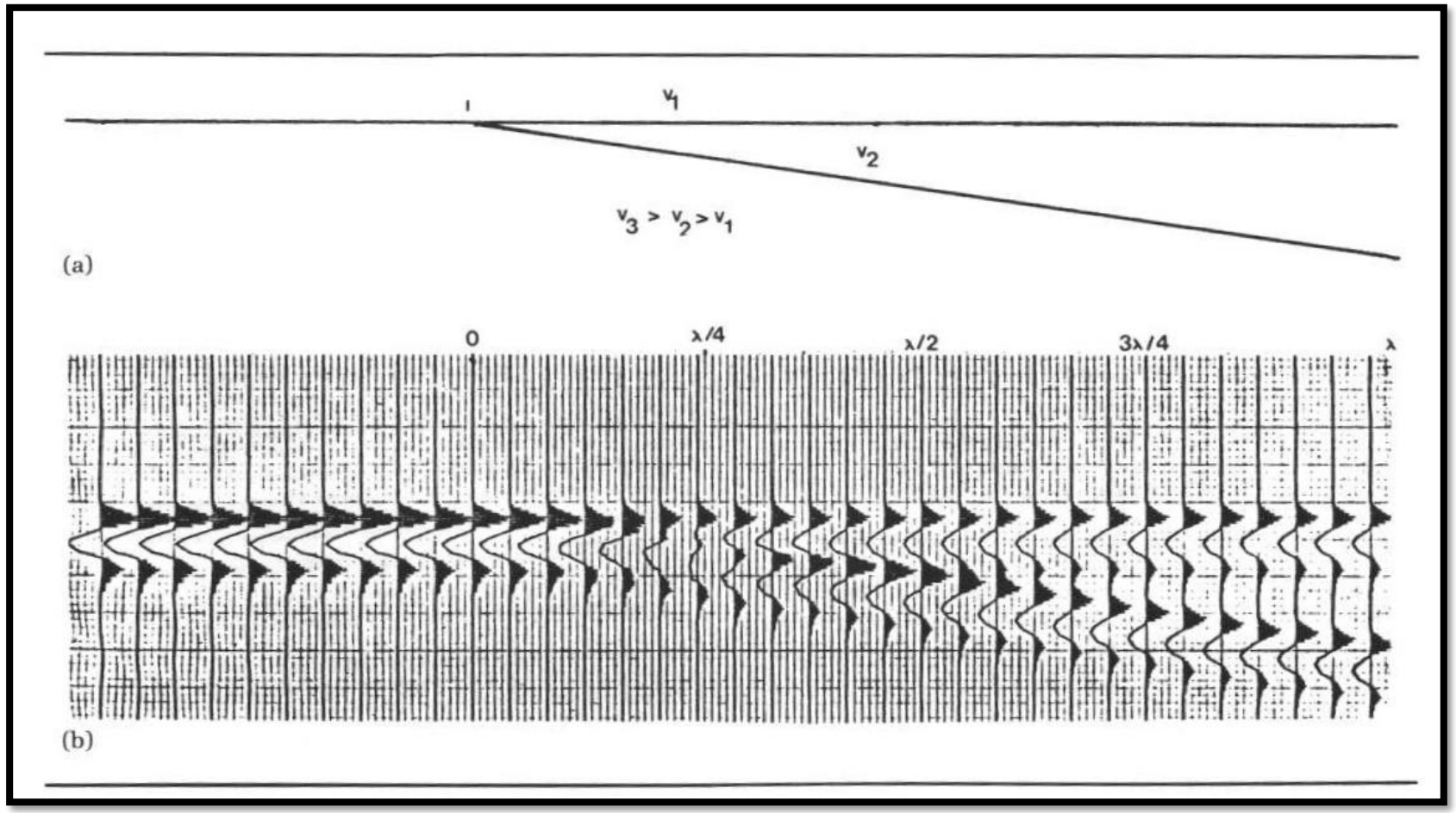

FIGURE 2.16 *Reflection from a wedge of acoustic impedance intermediate in magnitude between that of the over- and underlying units. The thickness of the wedge is indicated as a fraction of the dominant wavelength. Note that there is still a reflection beyond the limit of the wedge due to the contrast in acoustic impedance between the over- and underlying layers.* (a) *Model.* (b) *Seismic section. Reprinted by permission of the EAEG from Sheriff, 1975, fig. 6.9, p. 128.*

Horizontal Resolution

able area of the reflector surface. The resulting reflection is actually produced from a circular zone of quite large diameter. The extent of the area producing the reflection is known as the *Fresnel zone*. This is the portion of the reflector from which energy returns to the geophone or hydrophone within a half-cycle (i.e., one-quarter wavelength) after the onset of the reflection. Contributions from this zone sum constructively to produce a reflection (fig. 2.18). On an unmigrated section, horizontal resolution is determined by the size of the Fresnel zone.

Figure 2.19 shows a model of Fresnel effects. The model shows a continuous bed to the left and three isolated units with lateral extents expressed in terms of Fresnel zones. Each unit thins and pinches out over a shorter distance. The model indicates the following predicted responses:

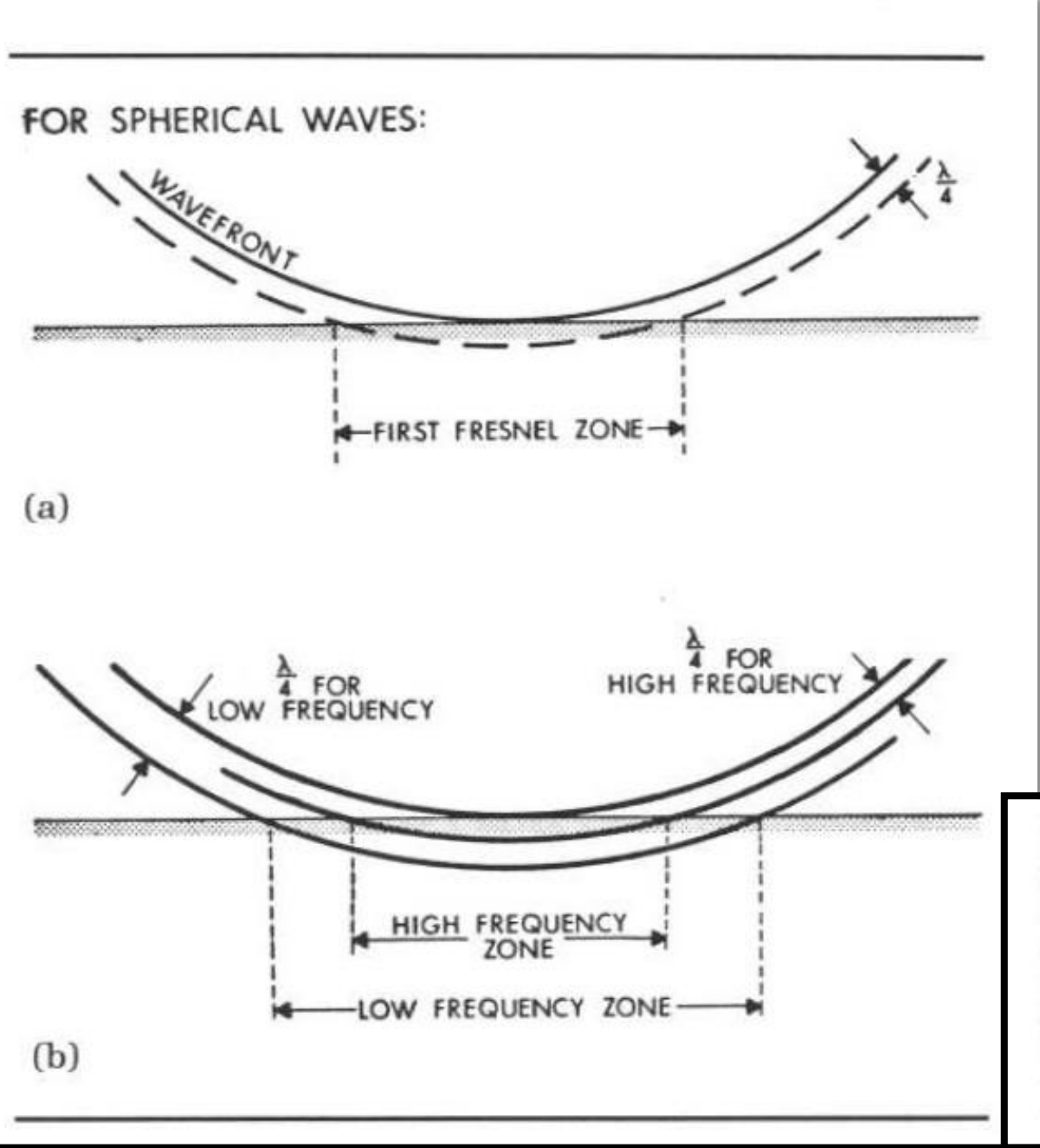

FIGURE 2.18 *Fresnel zone.* (a) *The first energy to reach a geophone from a plane reflector is from the point where the reflector is first tangent to the wavefront. The area of the reflector that produces the reflection is limited by the area that the wavefront one-quarter wavelength later makes with the reflector. The energy arriving within this interval sums constructively to produce the reflection.* (b) *The Fresnel zone is larger for low-frequency components than for high-frequency ones. Reprinted by permission of the AAPG from Sheriff, 1977, fig. 7, p. 11.*

The magnitude of Fresnel zones can be approximated from the relationship

$$rf = \frac{V}{2}\sqrt{\frac{t}{f}} \qquad (2.5)$$

where

rf = radius of the Fresnel zone.
V = average velocity.
t = two-way time in seconds.
f = dominant frequency in hertz.

For example, a reflection at 1.7 seconds with a 35-Hz component corresponds to a Fresnel-zone radius of 275 m (equivalent to an area of 0.237 km^2), for an average veloc-

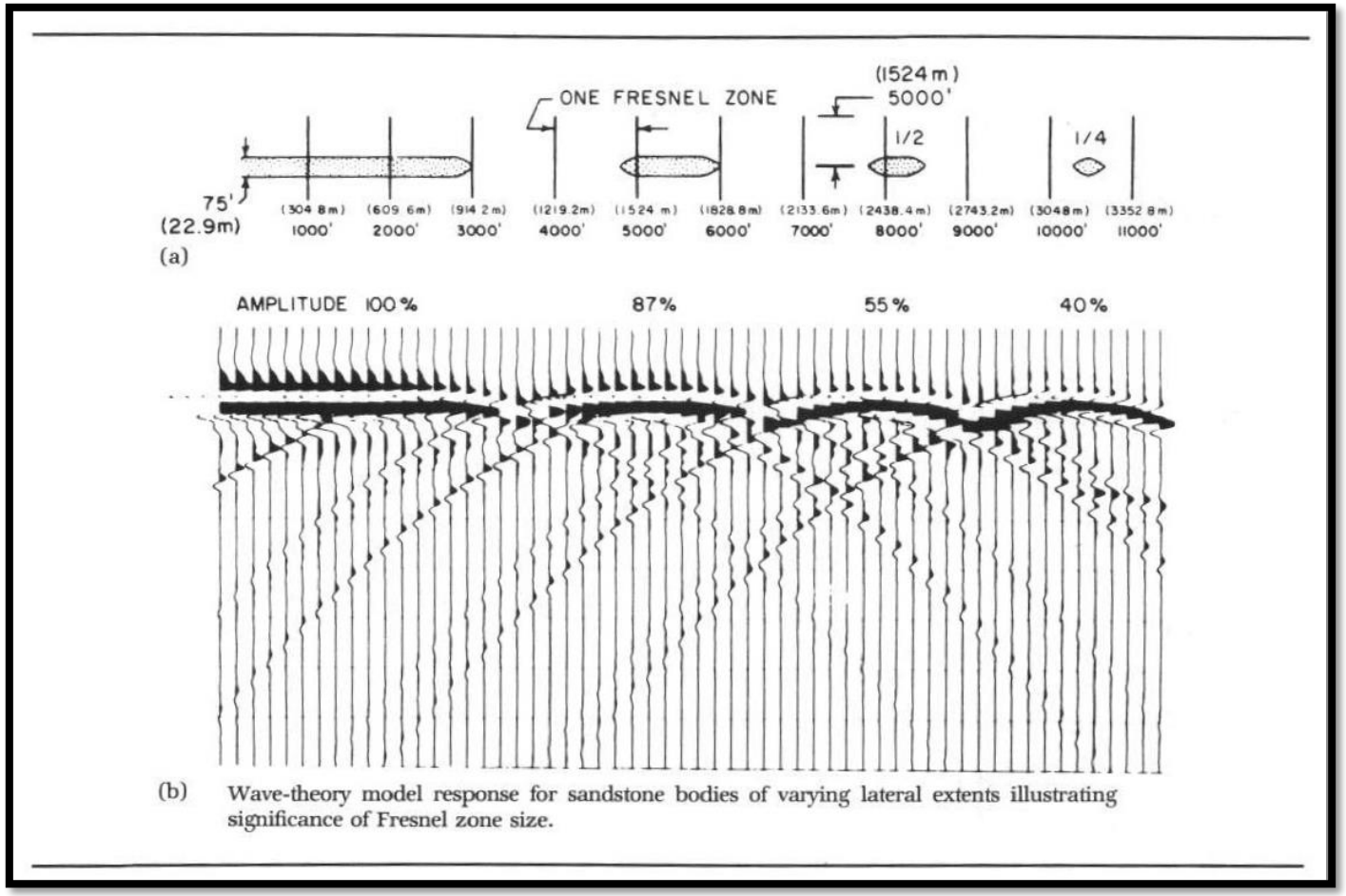

Wave-theory model response for sandstone bodies of varying lateral extents illustrating significance of Fresnel zone size.

FIGURE 2.19 *Reflections from reflectors of varying limited extents.* (a) *Cross-section of model: vertical lines are spaced at the Fresnel-zone size.* (b) *Seismic section over the model. The peak amplitudes of the four reflections are, respectively, 100%, 87%, 55%, and 40%. Reprinted by permission of the AAPG from Meckel and Nath, 1977, fig. 5, p. 421; after Neidell and Poggiagliolmi, 1977.*

1. A diffraction is associated with each bed termination.
2. The amplitude of each diffraction decays rapidly away from its apex.
3. The diffractions show polarity reversed on opposing limbs.
4. The gaps between the units are largely masked by the diffractions.
5. A unit of only ½ Fresnel zone produces a seismic response that is indistinguishable from a diffraction from a point source. Even with a width of one Fresnel zone the seismic response can only be distinguished with difficulty from that of a simple diffraction.

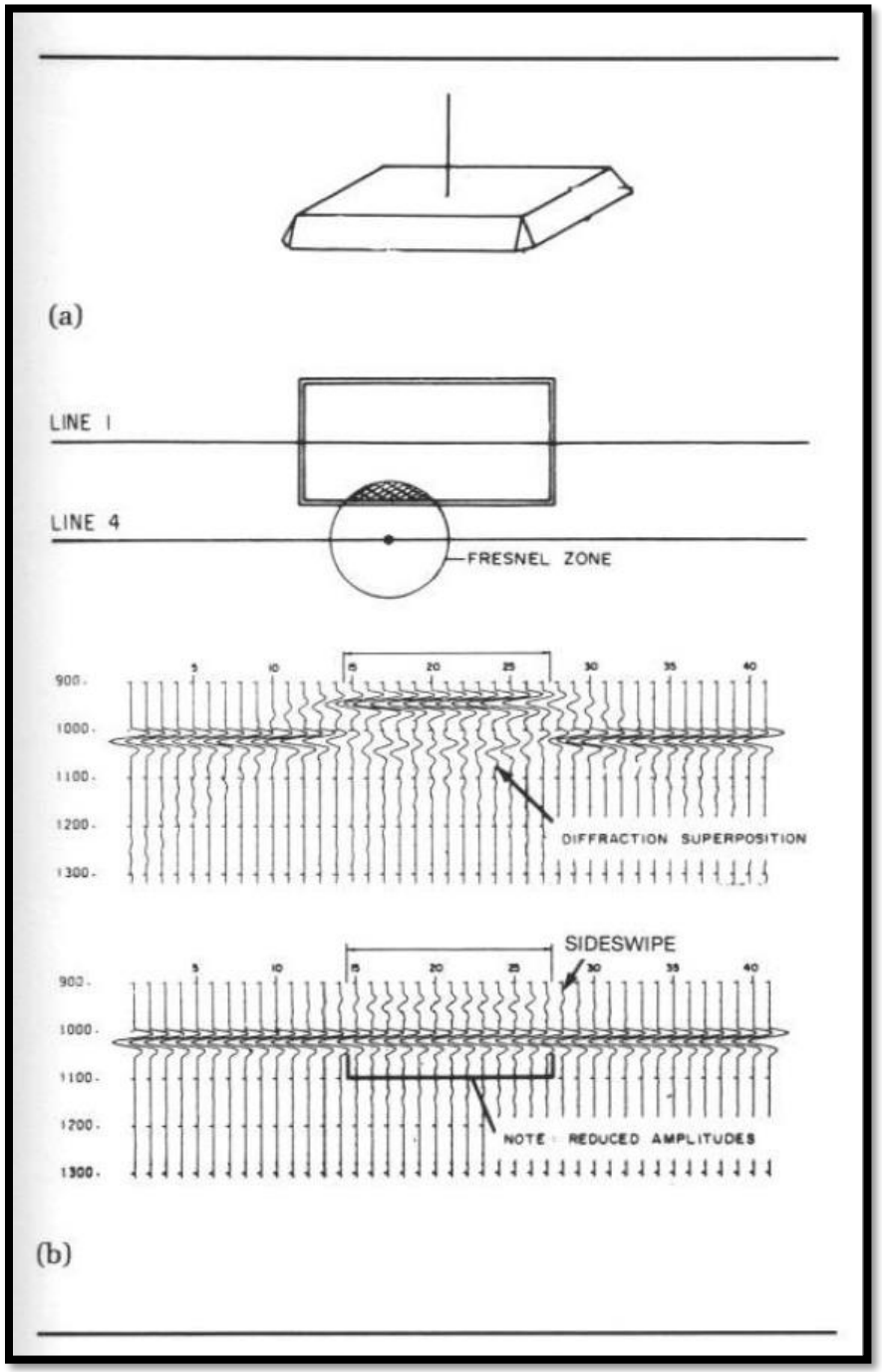

FIGURE 2.20 *Reflections from a box model.* (a) *Isometric diagram of the model; the length:width:height:depth ratios are 10:5:1:10.* (b) *Plan showing Fresnel-zone dimensions relative to box dimensions. Line 1 passes over the box. Line 4 passes to the side of the box, but close enough for part of the Fresnel zone to impinge on the box. Reprinted by permission of IHRDC Press from Sheriff, 1980a; after Neidell and Poggiagliolmi, 1977.*

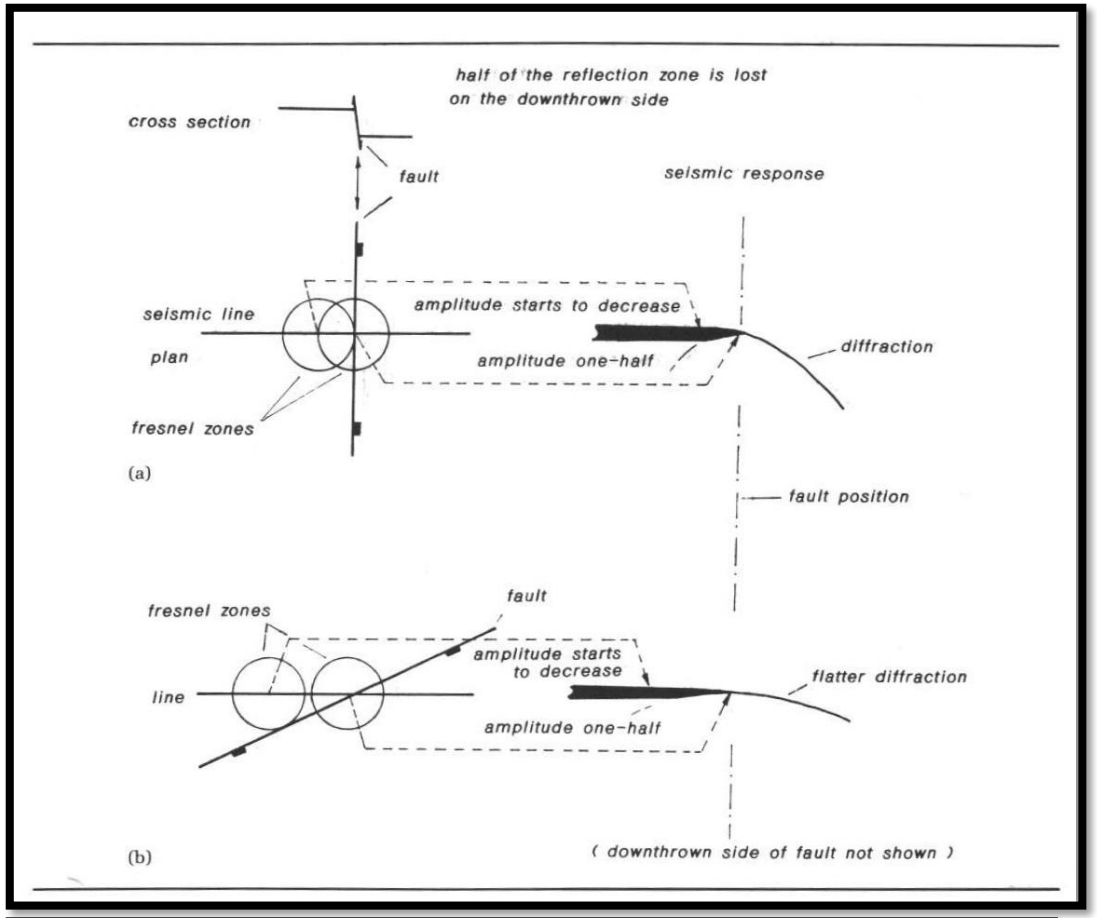

FIGURE 2.21 *Effect of Fresnel zones on reflection amplitude near to a fault.* (a) *Fault perpendicular to the seismic line that juxtaposes a reflector against material of constant acoustic impedance. Reflection amplitude is constant until the Fresnel zone passes over the fault. Reflection amplitude decreases and reaches half of its former value when the center of the Fresnel zone is coincident with the fault.* (b) *Fault oblique to the seismic line. The decrease in reflection amplitude is spread over a larger portion of the seismic line. After Anstey, 1980a, by permission of IHRDC Press.*

The effect of Depth

Velocity tends to increase with depth due to compaction and diagenetic effects. Frequency decreases due to attenuation of the seismic wave—there is an almost constant fractional energy loss per cycle of the seismic wave; and higher frequencies are attenuated more than lower frequencies for a particular path length. From this we can conclude that with increasing depth vertical and lateral resolution decreases, and interference effects become more pronounced as the pulse length increases (due to lower frequency). The loss of frequency with depth makes it less likely that a bed's thickness will exceed the minimum one-quarter wavelength for potential resolution

boundaries. Figure 2.22 illustrates how the seismic response varies with depth, even for the same pair of lithologies. Limestone is overlain by clay, producing a large positive reflection coefficient in the shallow subsurface. The seismic wavelet here is also of relatively high frequency and the seismic response is a sharp, high-amplitude reflection. As the lithologies become more deeply buried, the clay compacts and converts to shale and the limestone gradually reduces in porosity. Acoustic impedance increases for both lithologies—but at a greater rate in the shale. This results in a real decrease in acoustic-impedance contrast with increasing burial. By the time the shale and limestone are buried to 5000 m or more, the difference in acoustic impedance may not be especially large. The decrease in acoustic-impedance contrast results in gradually weaker reflections from the same lithology pair with increasing depth. The reflections not only become weaker; they also change their shape. The Earth preferentially attenuates the higher frequency part of the seismic signal with increasing traveltime, resulting in a gradual increase in wavelength with depth. This wavelength increase changes the shape of the reflection (fig. 2.22).

Figure 2.23 shows the effect of different wavelet length (frequency) on interference effects. Looked at in another way, the four seismic traces shown in figure 2.23 could be used to model the seismic response for the lithological column *a* at different burial depths. At the shallowest depth, *f*, in figure 2.23 the seismic response has the highest frequency, but this decreases with depth resulting in poorer resolution. Responses *e*, *d*, and *c* would represent the changing waveform as frequency decreases with increasing burial.

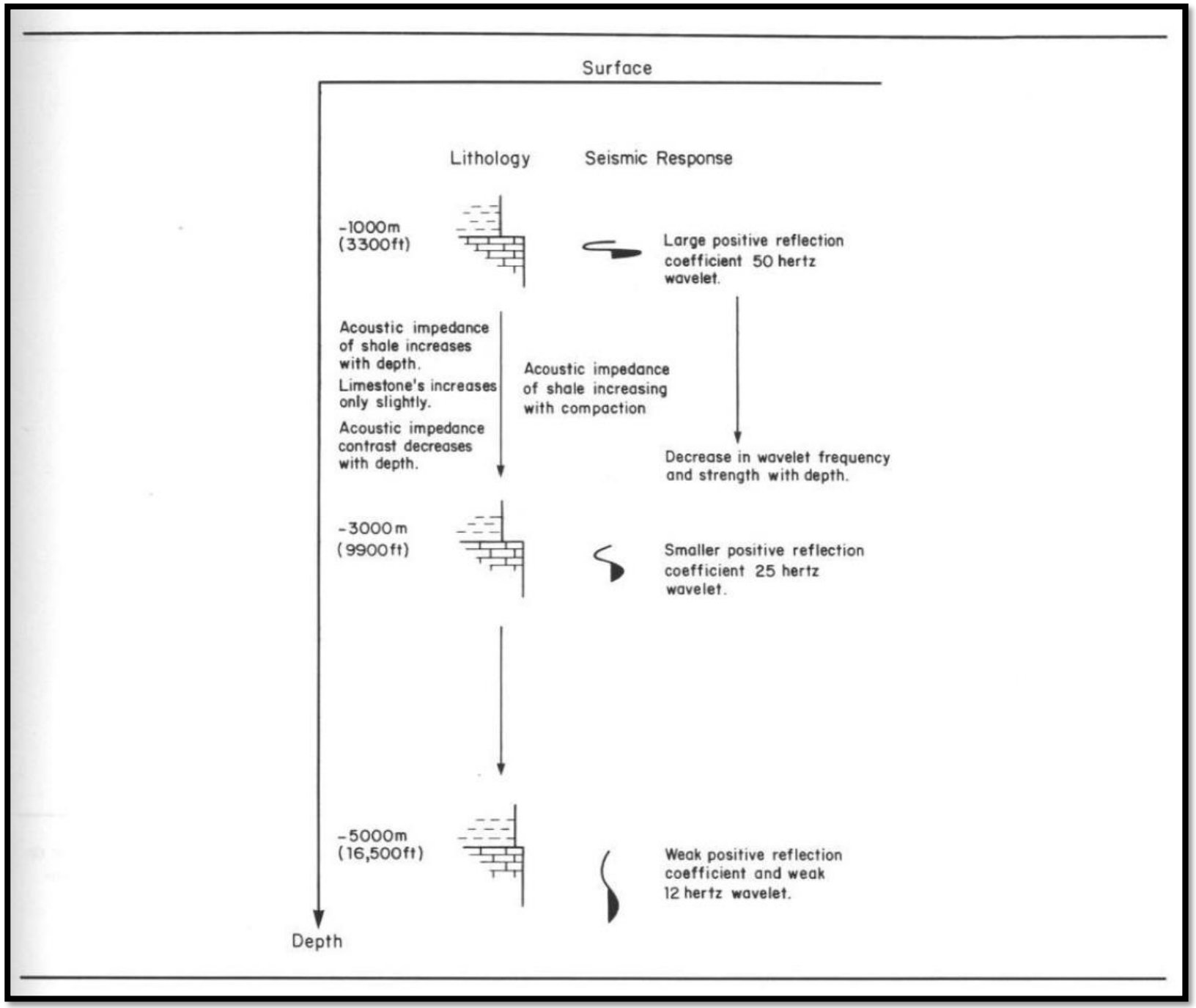
Surface
Lithology
Seismic Response
-1000m
(3300ft)
Large positive reflection coefficient 50 hertz wavelet.
Acoustic impedance of shale increases with depth.
Limestone's increases only slightly.
Acoustic impedance contrast decreases with depth.
Acoustic impedance of shale increasing with compaction
Decrease in wavelet frequency and strength with depth.
-3000m
(9900ft)
Smaller positive reflection coefficient 25 hertz wavelet.
-5000m
(16,500ft)
Weak positive reflection coefficient and weak 12 hertz wavelet.
Depth

FIGURE 2.22 *Sketch showing the effect of increasing depth, through changes in acoustic impedance and seismic-wavelet frequency, on the seismic response from an acoustic-impedance contrast between clay and limestone. The effects of burial, especially compaction, affect clays more than limestone. Although both show an overall increase in acoustic impedance with depth, the rate of increase is greater in the claystones. This results in weaker reflections with depth. The Earth attenuates the seismic signal, preferentially removing the higher frequency components. The gradual loss of frequency with depth changes the wavelength and shape of the seismic wavelet. The combined effect of decreasing frequency and acoustic-impedance contrasts produces a change from shallow, strong, sharp reflections to weak, long reflections at depth.*

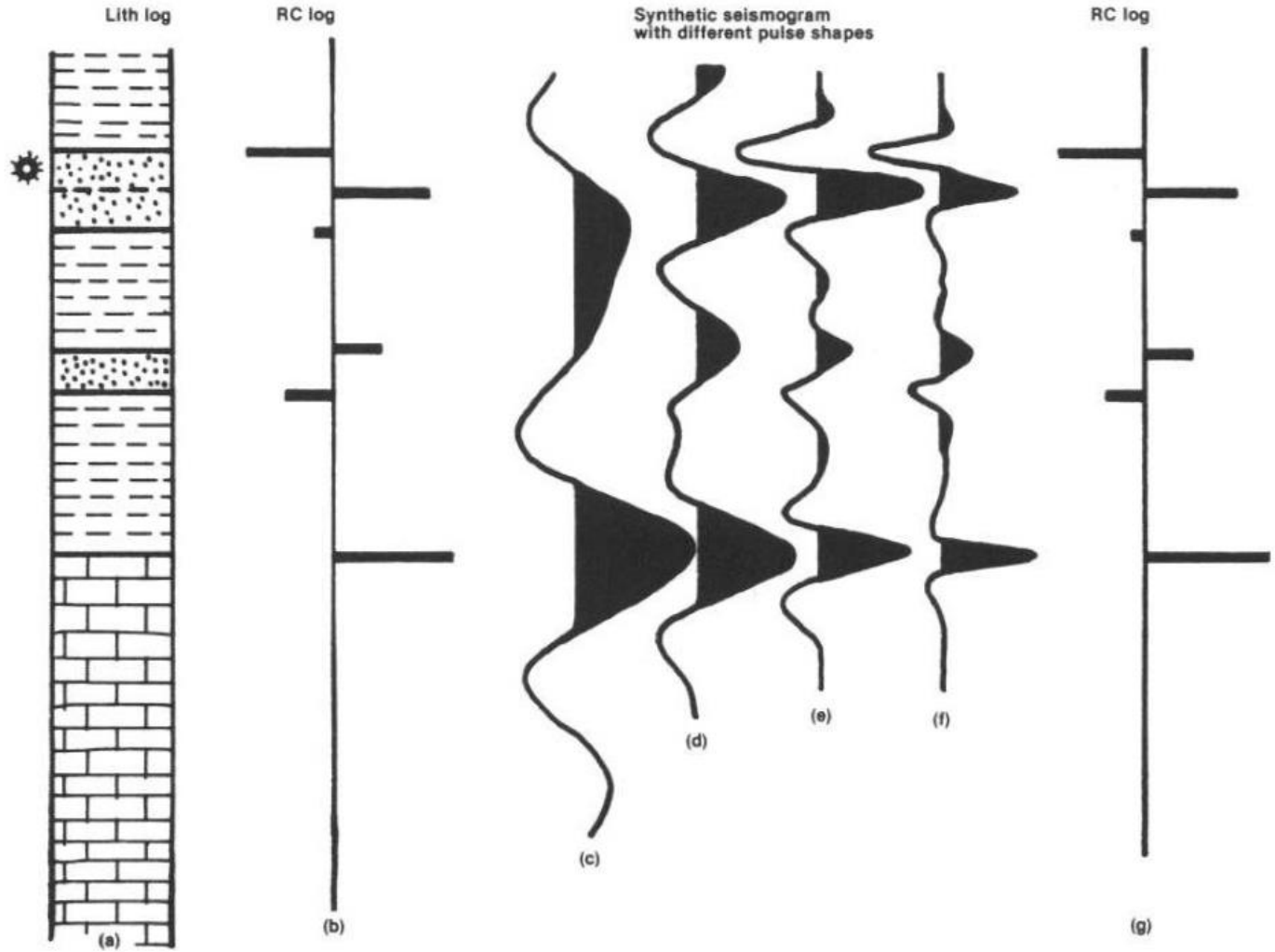

FIGURE 2.23 *The effect of wavelet frequency on the seismic response. Reprinted by permission of IHRDC Press from Anstey, 1980a.*

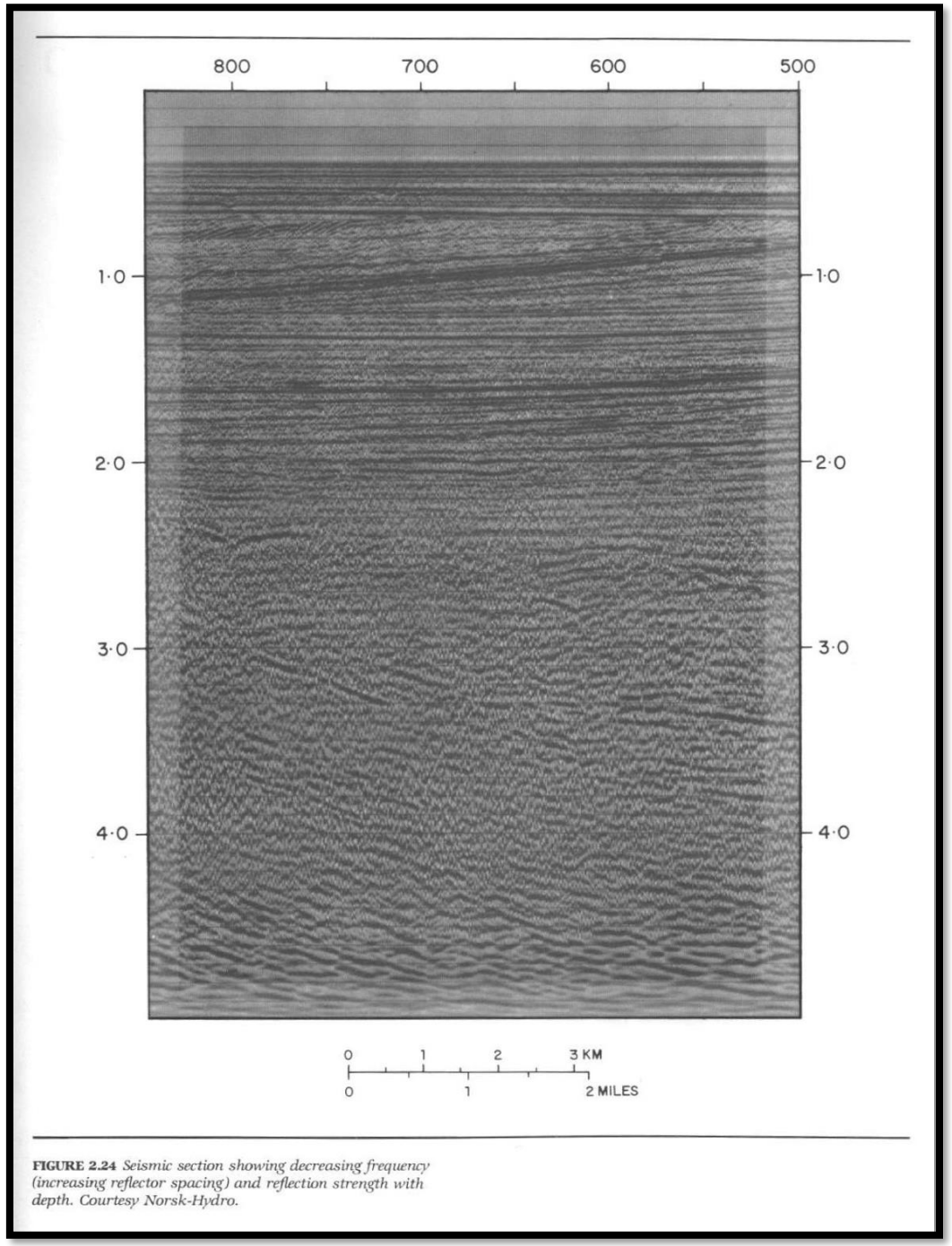

FIGURE 2.24 *Seismic section showing decreasing frequency (increasing reflector spacing) and reflection strength with depth. Courtesy Norsk-Hydro.*

NMO

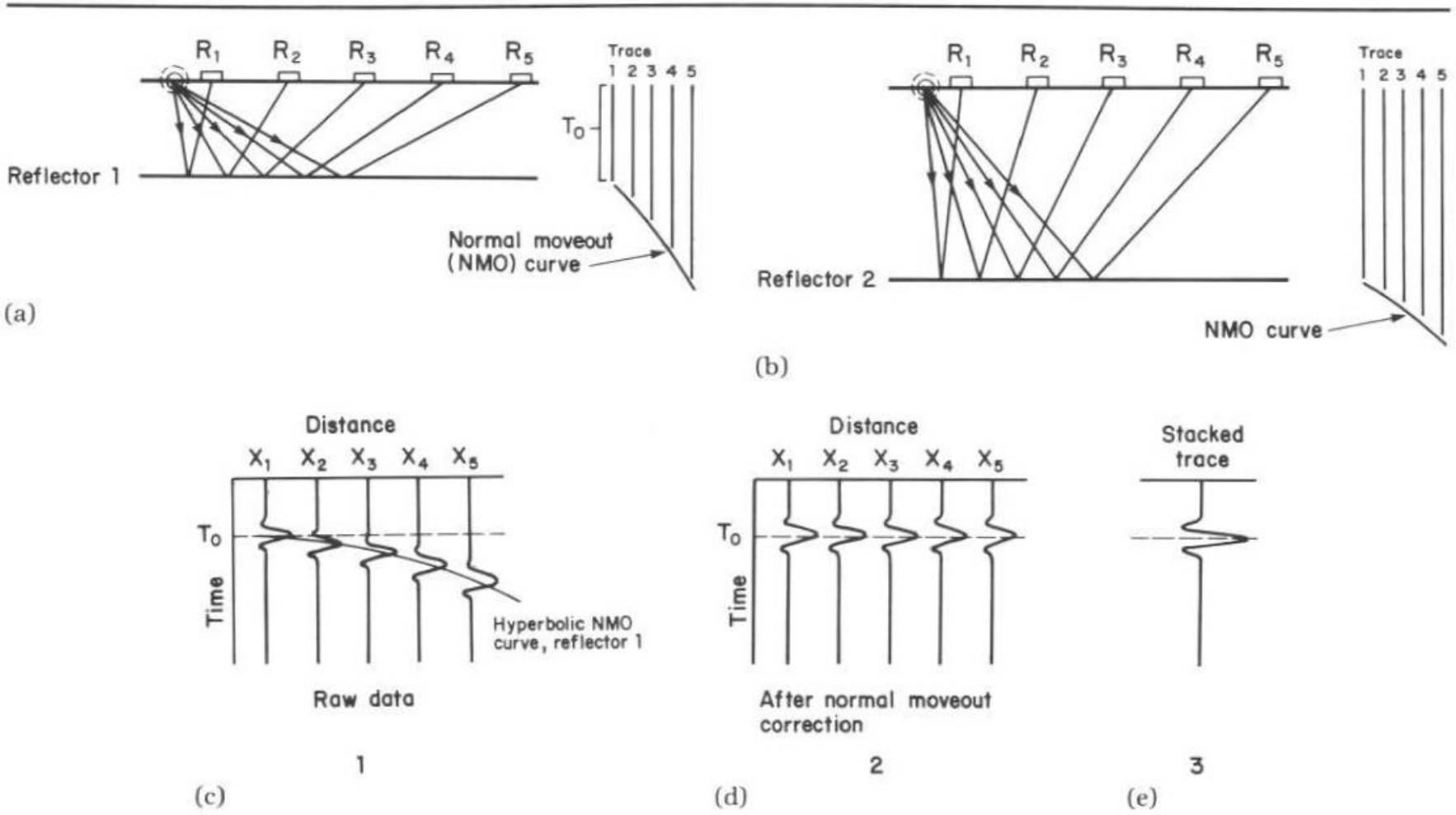
R1 R2 R3 R4 R5
Trace
1 2 3 4 5
T0
Reflector 1
Normal moveout
(NMO) curve
(a)
R1 R2 R3 R4 R5
Trace
1 2 3 4 5
Reflector 2
NMO curve
(b)
Distance
X1 X2 X3 X4 X5
T0
Time
Hyperbolic NMO
curve, reflector 1
Raw data
1
(c)
Distance
X1 X2 X3 X4 X5
T0
Time
After normal moveout
correction
2
(d)
Stacked
trace
3
(e)

Static Correction

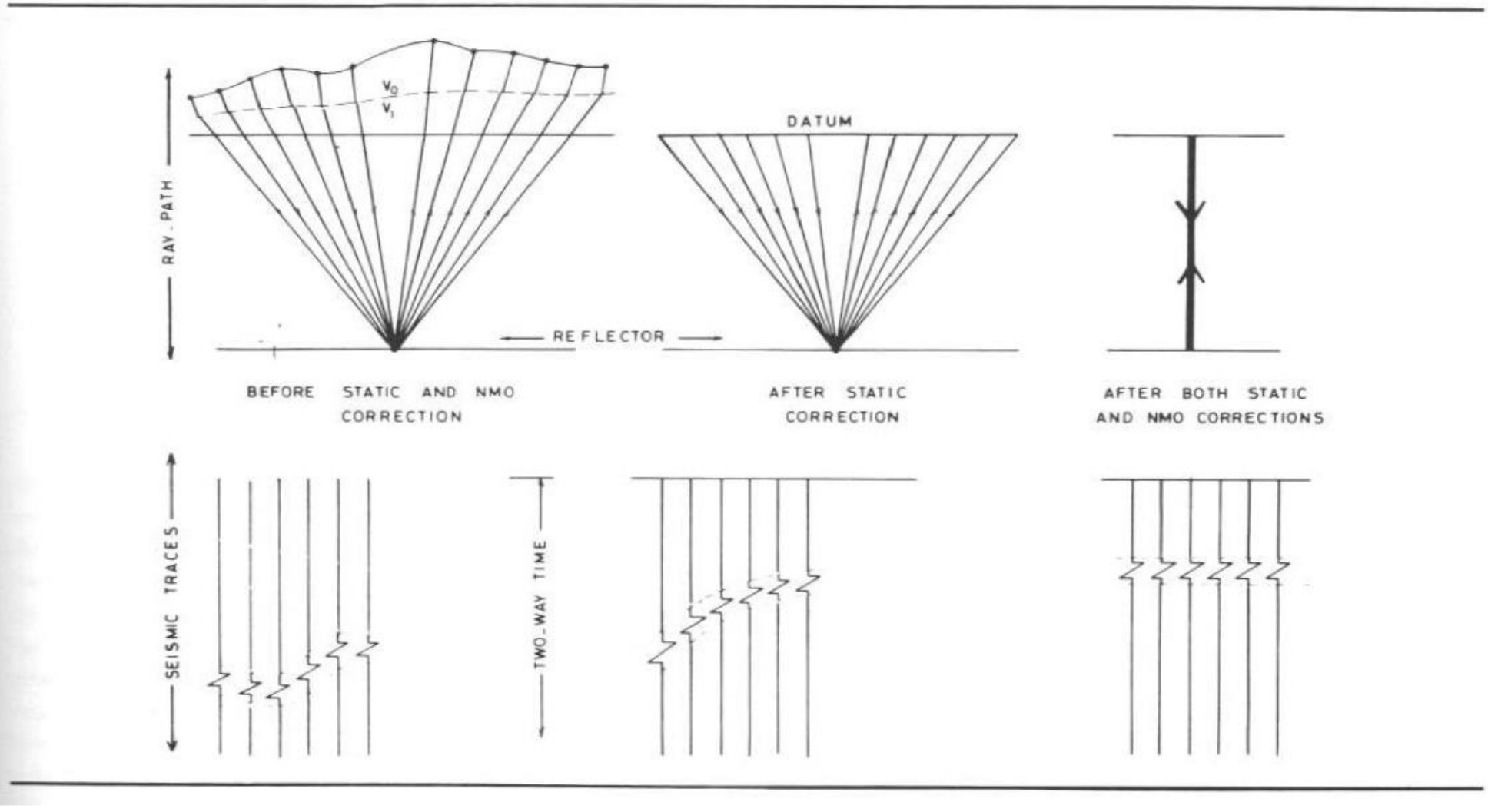

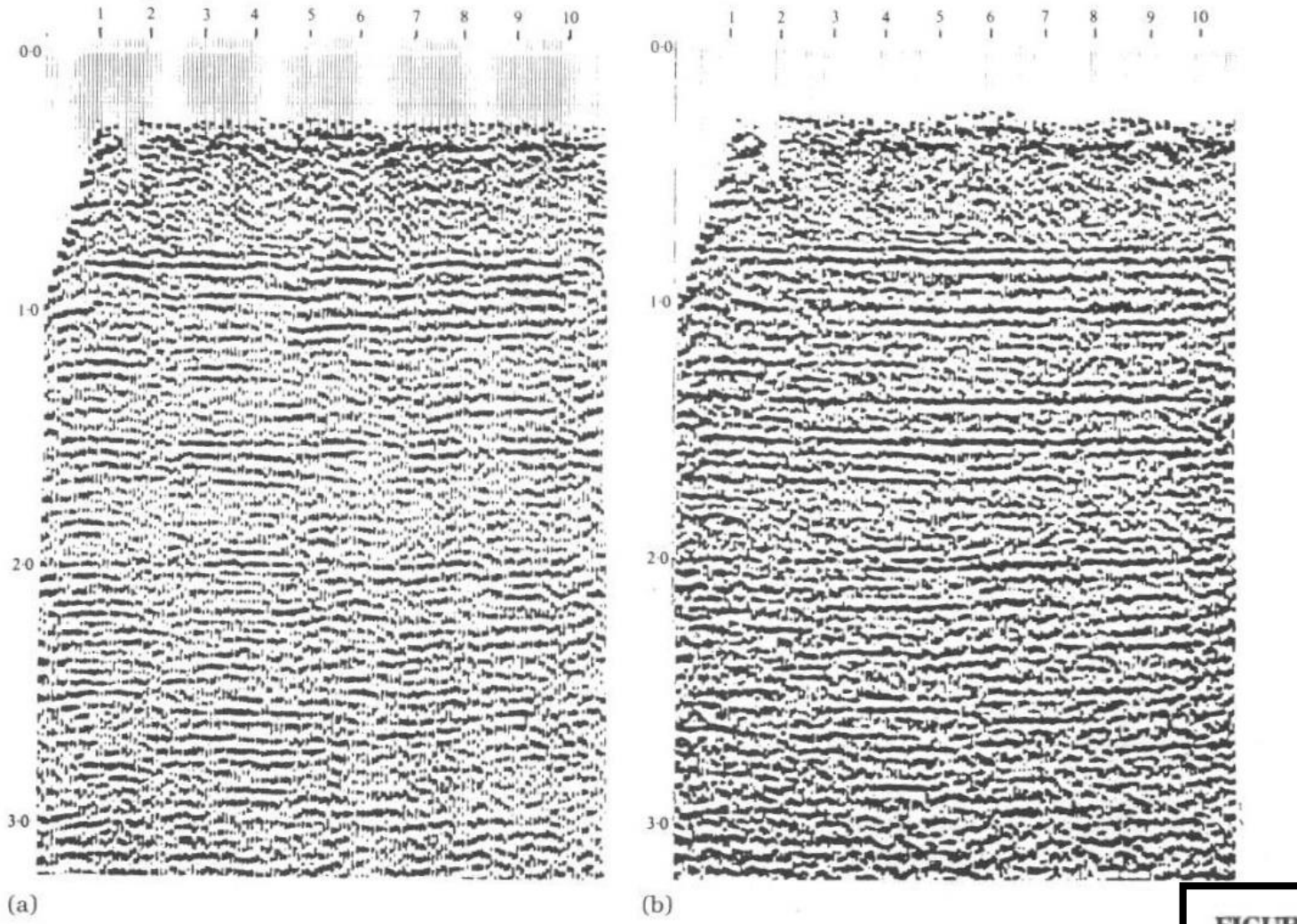

FIGURE 3.5 *Static corrections applied to a seismic section to eliminate the effects of variations in elevation, weathering thickness, or weathering velocity.* (a) *Before static corrections, the reflections appear discontinuous and the entire section is noisy.* (b) *After static corrections. Reprinted by permission of Cambridge University Press from Telford et al., 1976.*

Multiples

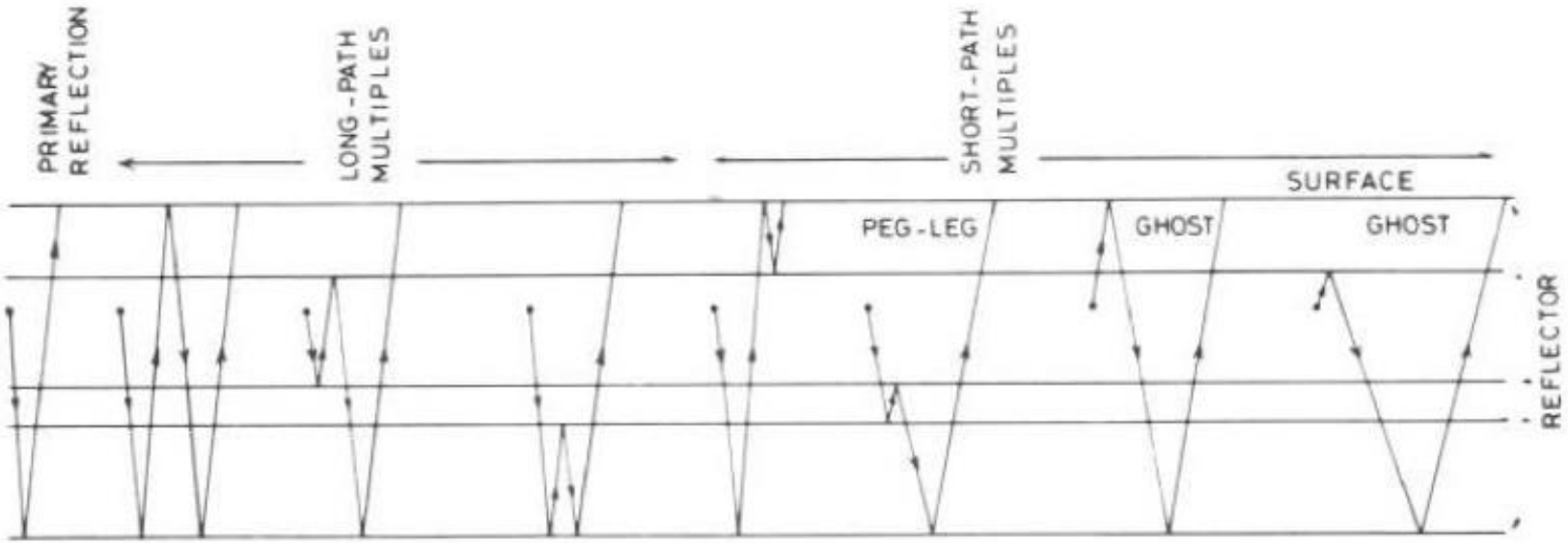
PRIMARY REFLECTION
LONG-PATH MULTIPLES
SHORT-PATH MULTIPLES
SURFACE
PEG-LEG
GHOST
GHOST
REFLECTOR

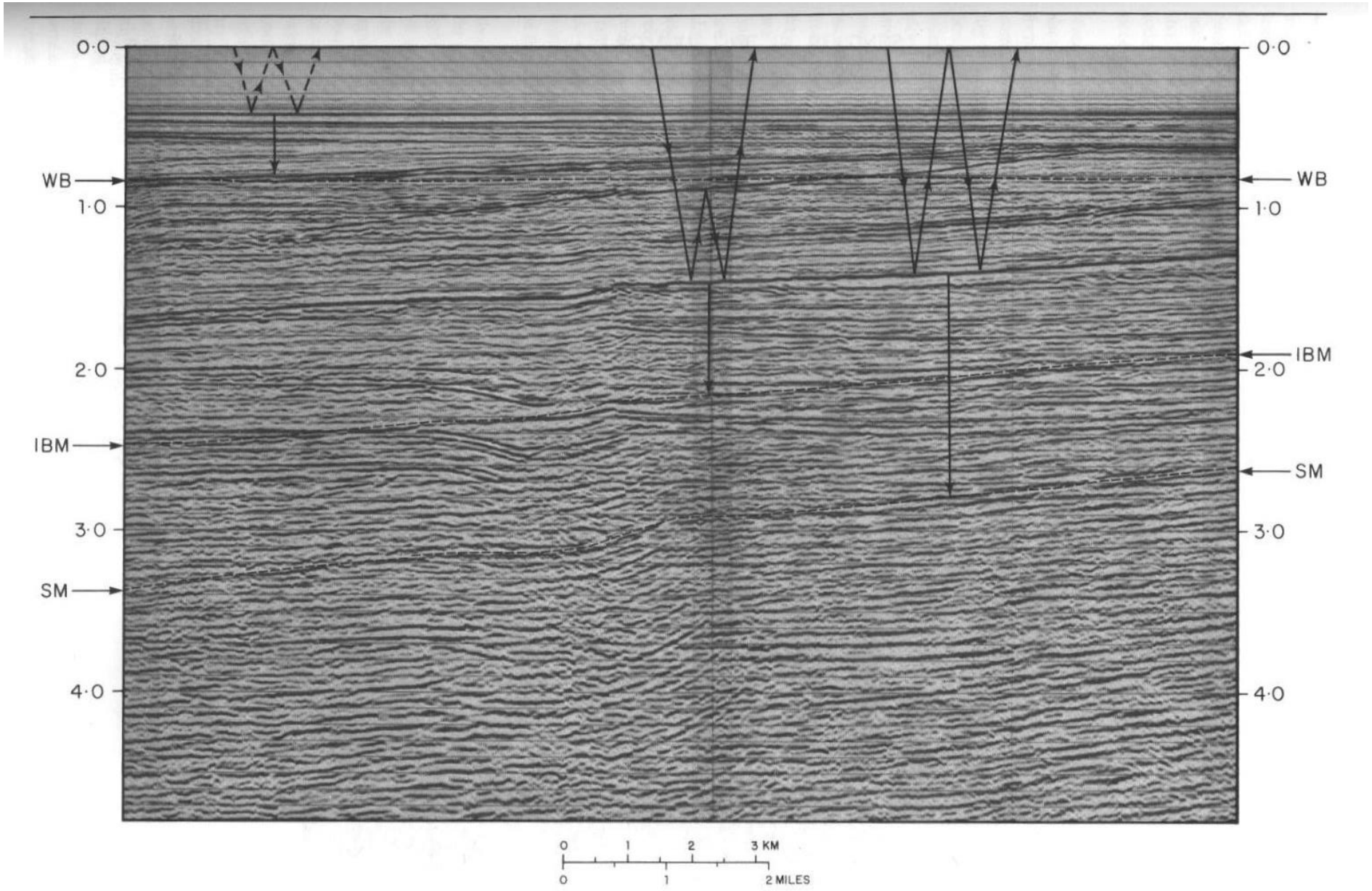

FIGURE 3.10 *A seismic section with a "good" set of multiples.* SM, *simple multiple;* WB, *water-bottom multiple;* IBM, *interbed multiple. Courtesy Société Nationale Elf Aquitaine.*

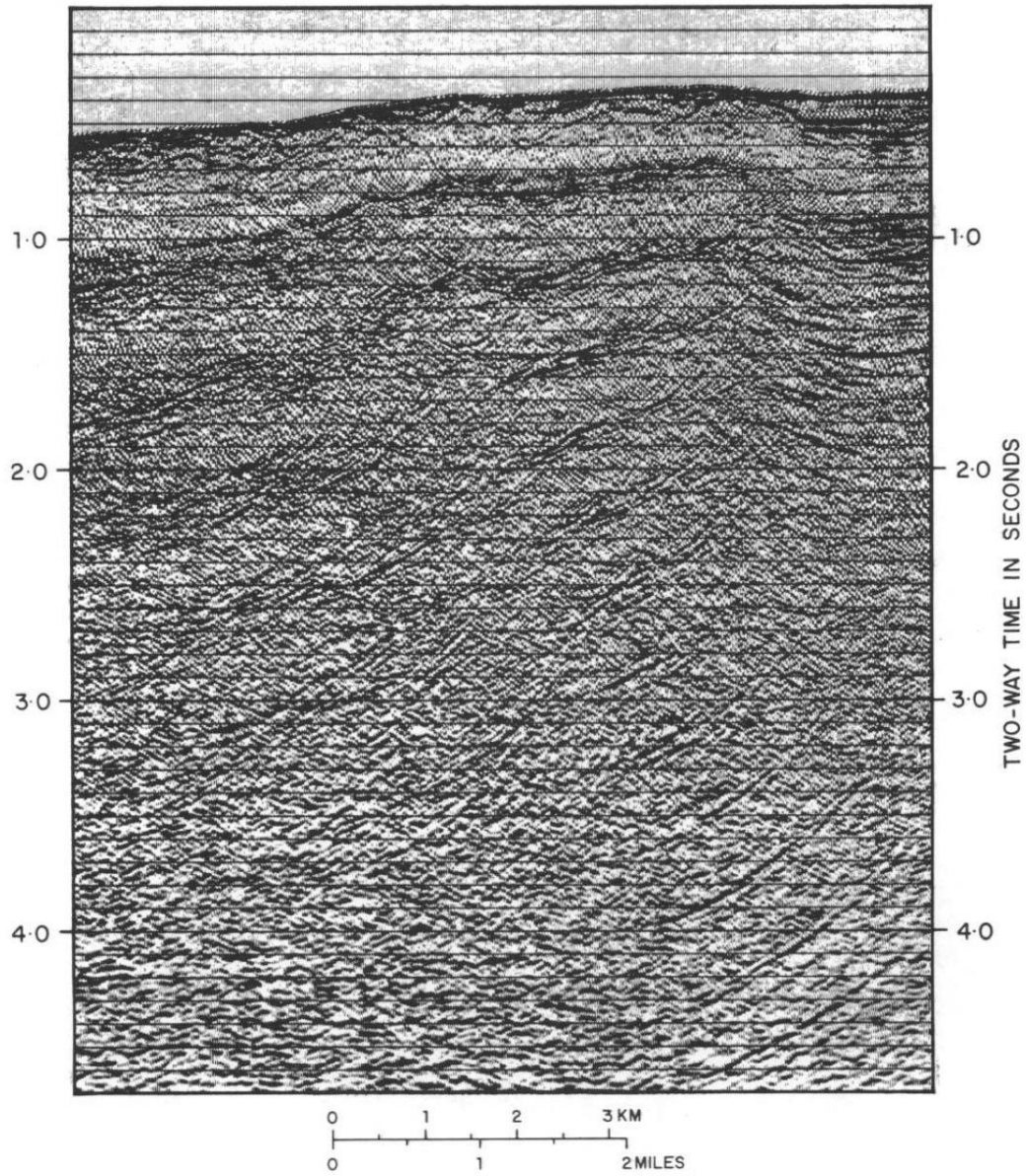

FIGURE 3.11 *Seismic section, with crystalline basement outcropping at the sea floor, showing water-bottom multiples. The water-bottom multiple is repeated 12 times. Note: The section has been migrated, and this has caused the dipping parts of the multiple to be moved in an updip direction. Courtesy Saga Petroleum.*

Multiples can be divided into two main categories: long-path and short-path. Long-path multiples have travel paths that are long compared with primary reflections from the same deep interfaces; and, therefore, appear as separate reflections. Short-path multiples arrive so soon after the primary reflection from the same interface that they interfere with, and add tails to, the primary reflection, and thus change the waveshape but do not necessarily appear as a separate event.

multiples. Stacking and deconvolution are the two main lines of attack.

Stacking, the combining of the recorded traces after they have been corrected for normal moveout, is the main, and best, form of attack, especially against long-path multiples. Figure 3.9 illustrates how stacking attacks multiples. Velocities for shallower reflections are smaller than

Deconvolution is the next line of attack. It is used mainly against short-path multiples and works by combining the recorded trace with another specially designed trace (operator), which will remove or attenuate repetitions and compress the wavelet. Deconvolution is a time series analysis operation which attempts to undo the filter effects (e.g., attenuation, reverberation, etc.) of the Earth on the propagating wavelet. Deconvolution is used to sharpen the seismic pulse and attenuate multiples. There are many different types of deconvolution and a detailed discussion of the topic is beyond the scope of this book. However, two types are relatively common:

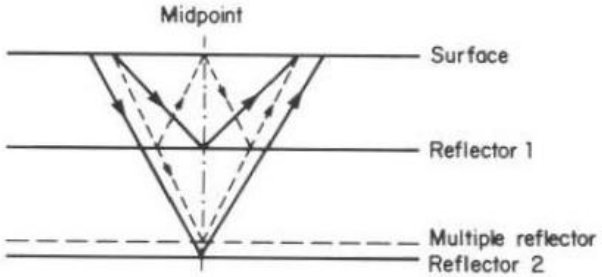
Midpoint
Surface
Reflector 1
Multiple reflector
Reflector 2

(a)

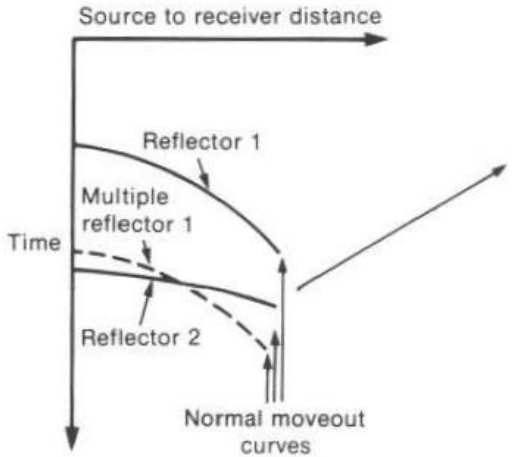
Source to receiver distance
Reflector 1
Multiple
reflector 1
Time
Reflector 2
Normal moveout
curves

(b)

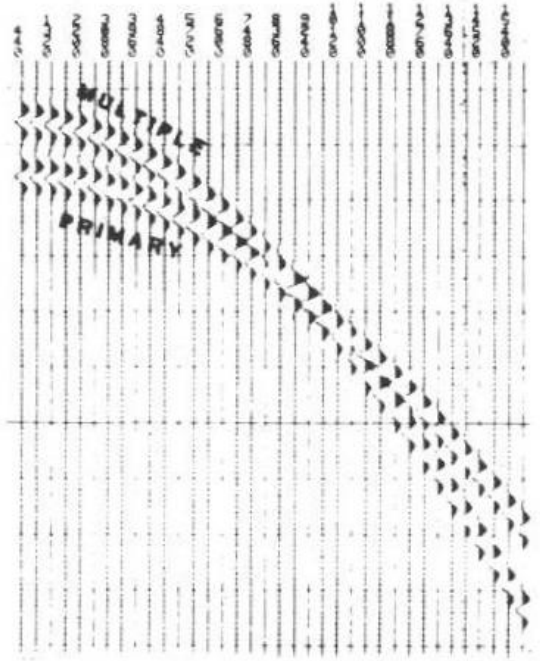
MULTIPLE
PRIMARY

(c)

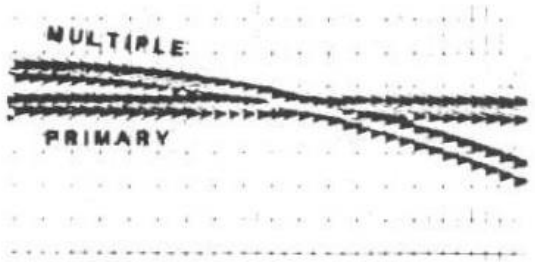
MULTIPLE
PRIMARY

(d)

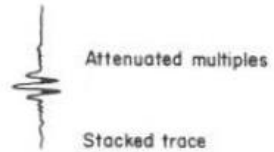
Attenuated multiples
Stacked trace

(e)

FIGURE 3.9 *Removal of multiples by CMP stacking:* (a) *Cross-section showing two reflectors and multiple of the upper reflector.* (b) *Time versus offset diagram showing the NMO curves for reflections from reflectors 1 and 2 and the multiple of reflector 1. The NMO curve for reflection 2 is flatter than that of reflection 1. The multiple of reflection 1 has the same NMO curves as the reflection and crosscuts the flatter NMO curve of reflection 2.* (c) *A common midpoint gather for the multiple and reflection 2 shown in* (b). (d) *The CMP gather after normal moveout correction: Reflection 2 has been corrected, bringing the reflection to the same time on all of the traces. The multiple is overcorrected and has a residual moveout.* (e) *The stacked trace: The primary has been reinforced and the multiple attenuated. Reprinted by permission of IHRDC Press from Sengbush, 1983.*

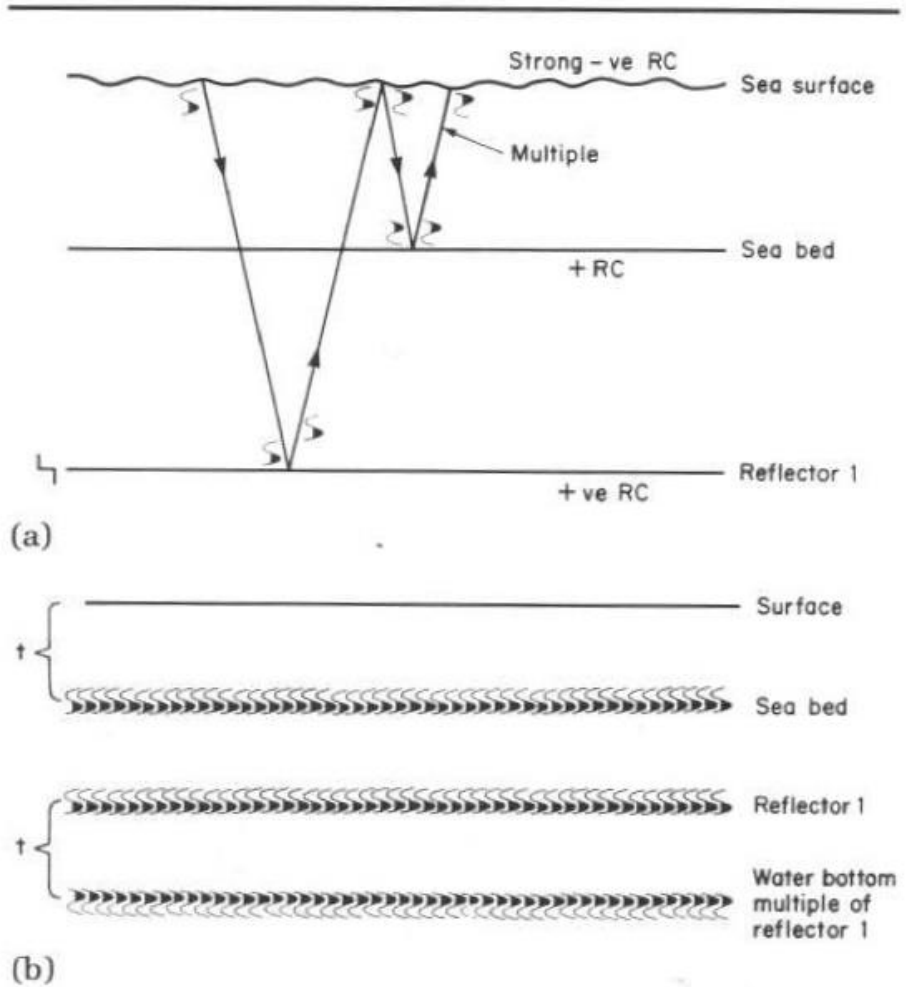

FIGURE 3.12 *Water-bottom multiples.* (a) *Geological model.* (b) *Seismic expression (SEG normal polarity). The strong negative reflection coefficient of the air/water interface causes a polarity reversal of the downgoing multiple reflection. The positive sea-bed reflection coefficient does not affect the reflection polarity; therefore, the recorded multiple reflection is opposite in polarity to that of the primary reflection.*

Multiples from Dipping Reflectors. When the primary reflector is dipping and the surface layer is flat, the multiple reflection will show twice the angle of dip; since, at any given point, the multiple is twice as deep as the primary event (fig. 3.13). The exaggerated dip of multiple reflections is characteristic and can often be useful in discriminating multiples from deeper primary reflections. The primary reflection (a) in figure 3.14 has a positive reflection coefficient and dips from right to left. The first simple multiple (b) has twice the dip and reversed polarity. The third multiple (c) has three times the dip of (a). The reflection quality of the multiple (c) is too poor to demonstrate a polarity reversal. It should have the same polarity as the primary reflection (a). Remnants of a fourth multiple (d) can just be seen. Simple multiples are most likely to be a problem when especially strong reflectors are present.

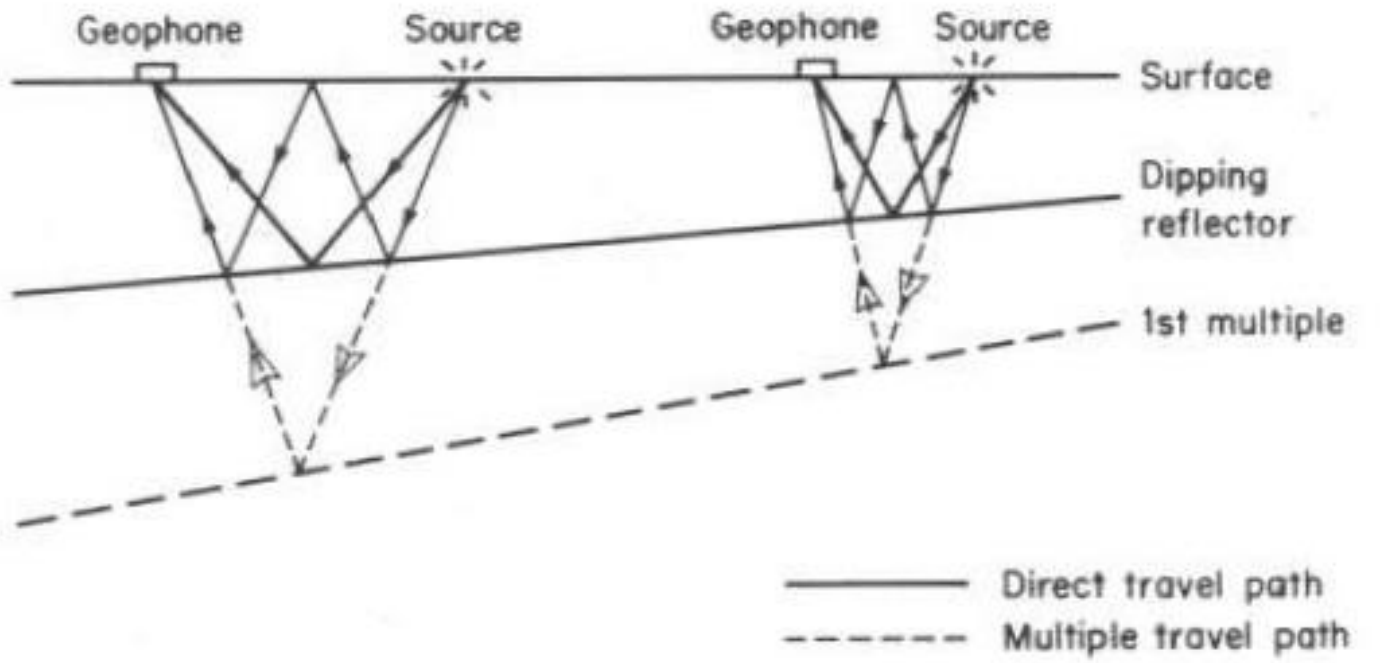

FIGURE 3.13 *Diagram showing how the multiple of a dipping reflector has twice the dip.*

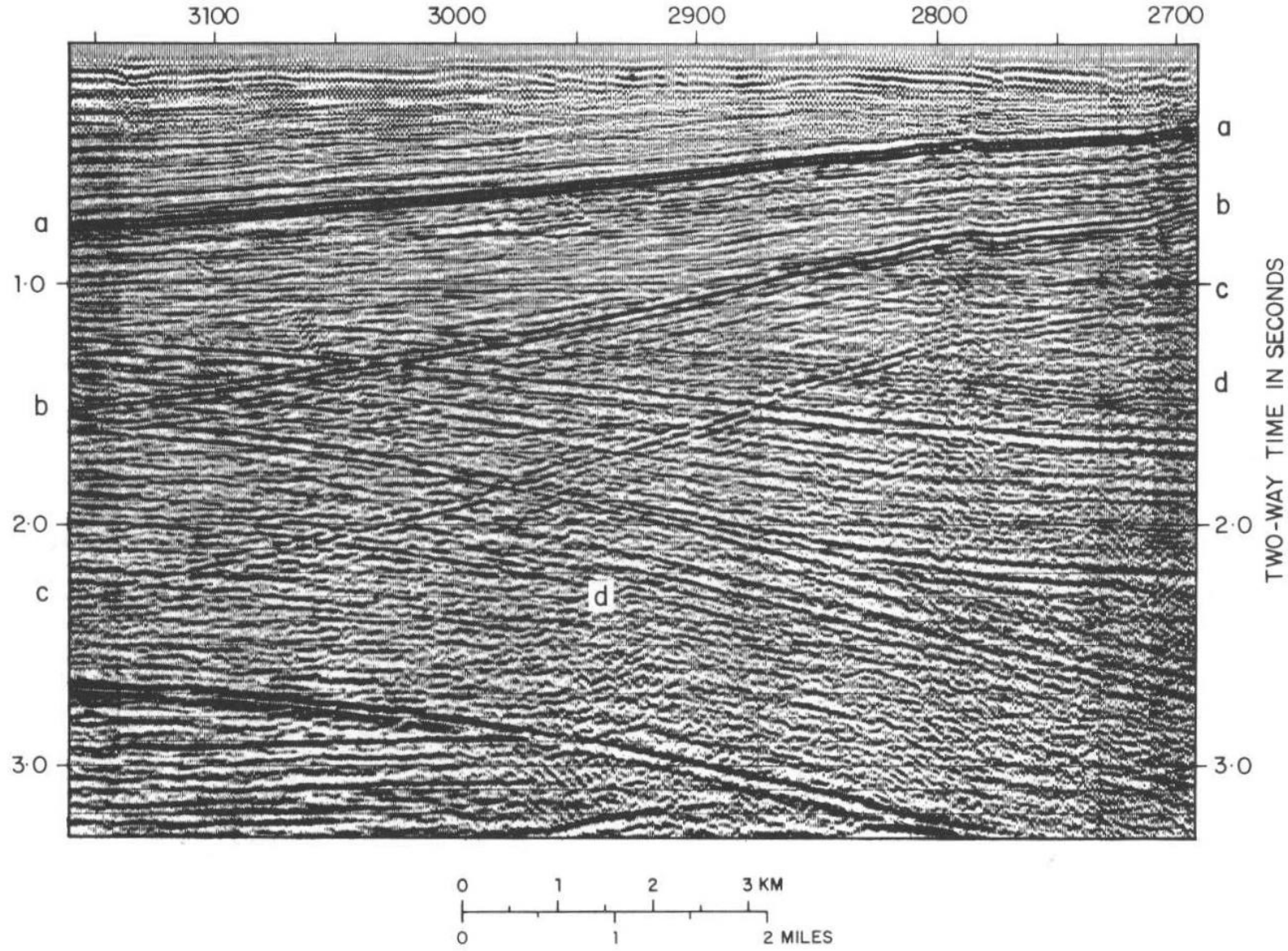

FIGURE 3.14 *Seismic section showing dipping simple multiples from reflection* a. *Three bounces of the multiples,* b, c, *and* d *can be seen. The dip of each successive multiple increases by an amount equal to the dip of the primary reflection* a. *Courtesy Merlin Profilers Ltd.*

Diffraction

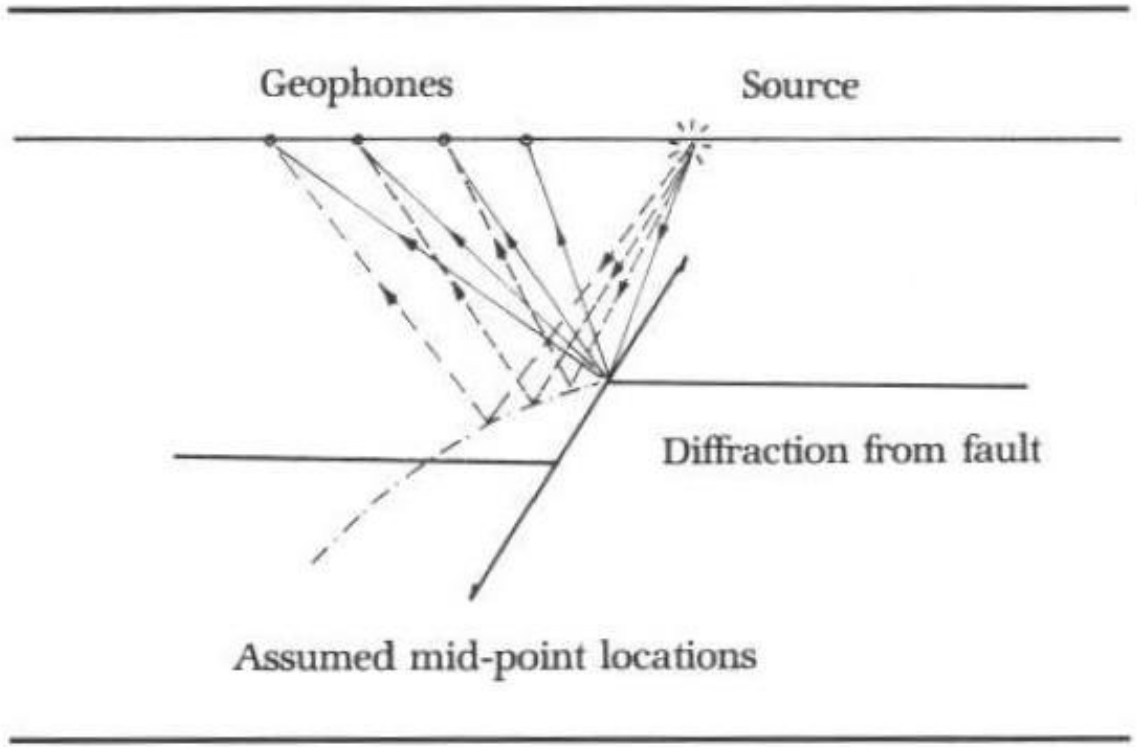

FIGURE 3.16 *Sketch showing a diffraction from a fault. The hyperbolic form of diffractions arises from the assumption made by the CMP method that reflections arise from mid-point locations between the source and geophone.*

of diffraction at its apex. Tracing the apex of diffraction can be a useful method to help locate a fault plane on unmigrated seismic sections for horizontal velocity structures. Fault planes can be found by joining successive diffraction apexes (fig. 3.17). Generally, however, diffractions are troublesome and detract from the appearance of the section. They can be removed by migration techniques, which restore the raypaths back to their proper subsurface positions. The diffraction is collapsed back to a point. Diffractions arising from off the line of section may not be properly migrated and remain as remnant diffractions after migration.

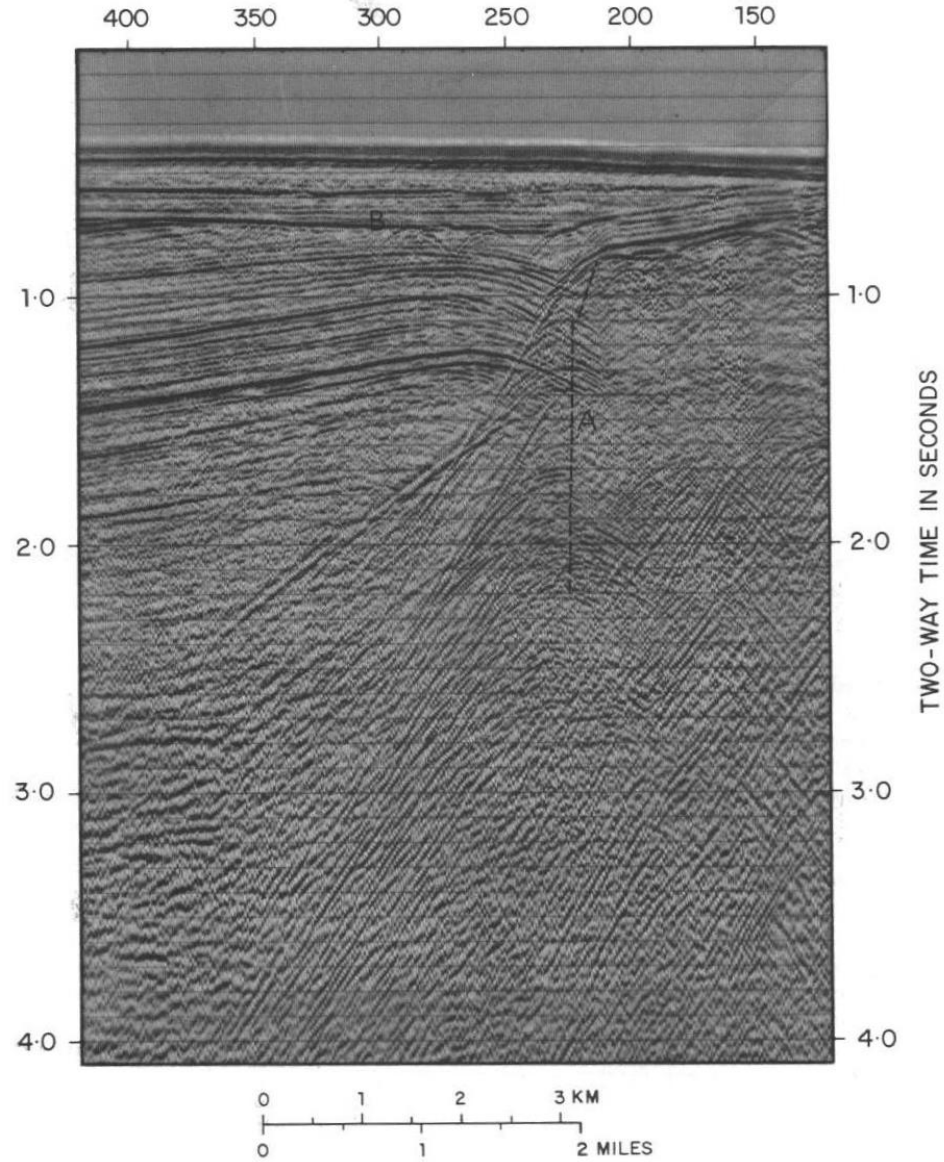

FIGURE 3.17 *Seismic section showing diffractions from a near-vertical fault plane* (A). *Diffractions can be useful. The fault plane can be located by joining the diffraction apexes. Other diffractions are from small faults affecting a flat-lying reflector* (B). *Courtesy Norsk Hydro.*

Seismic Migration

Migration is the process whence reflectors are places in their true reflection subsurface position and collapses diffractions to a point.
On unmigrated stacked sections, reflections are always plotted below the mid-point, which is only correct for horizontal layers.

Actual Seismic path

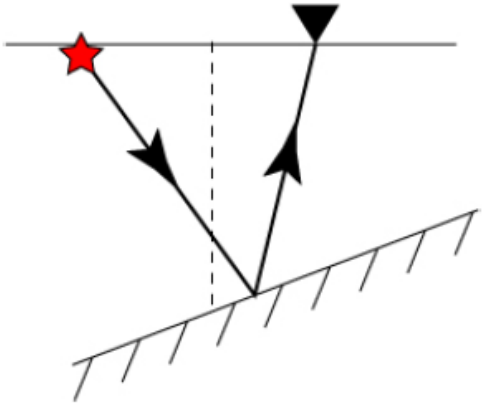

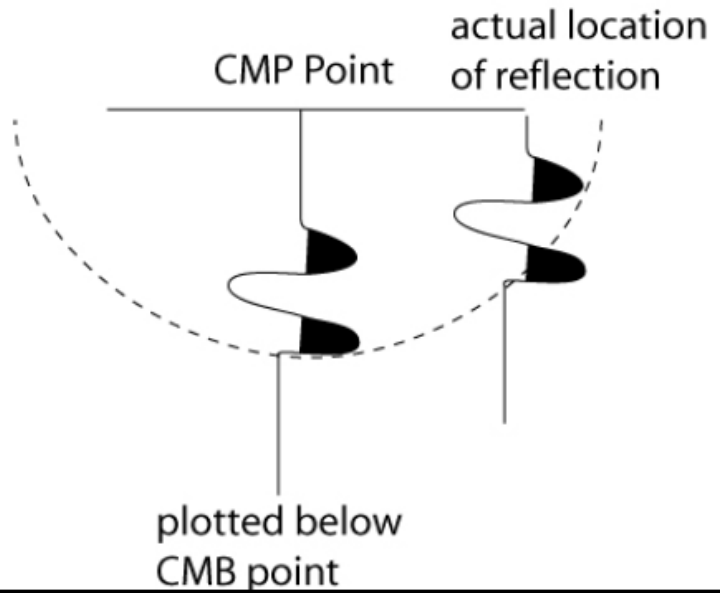

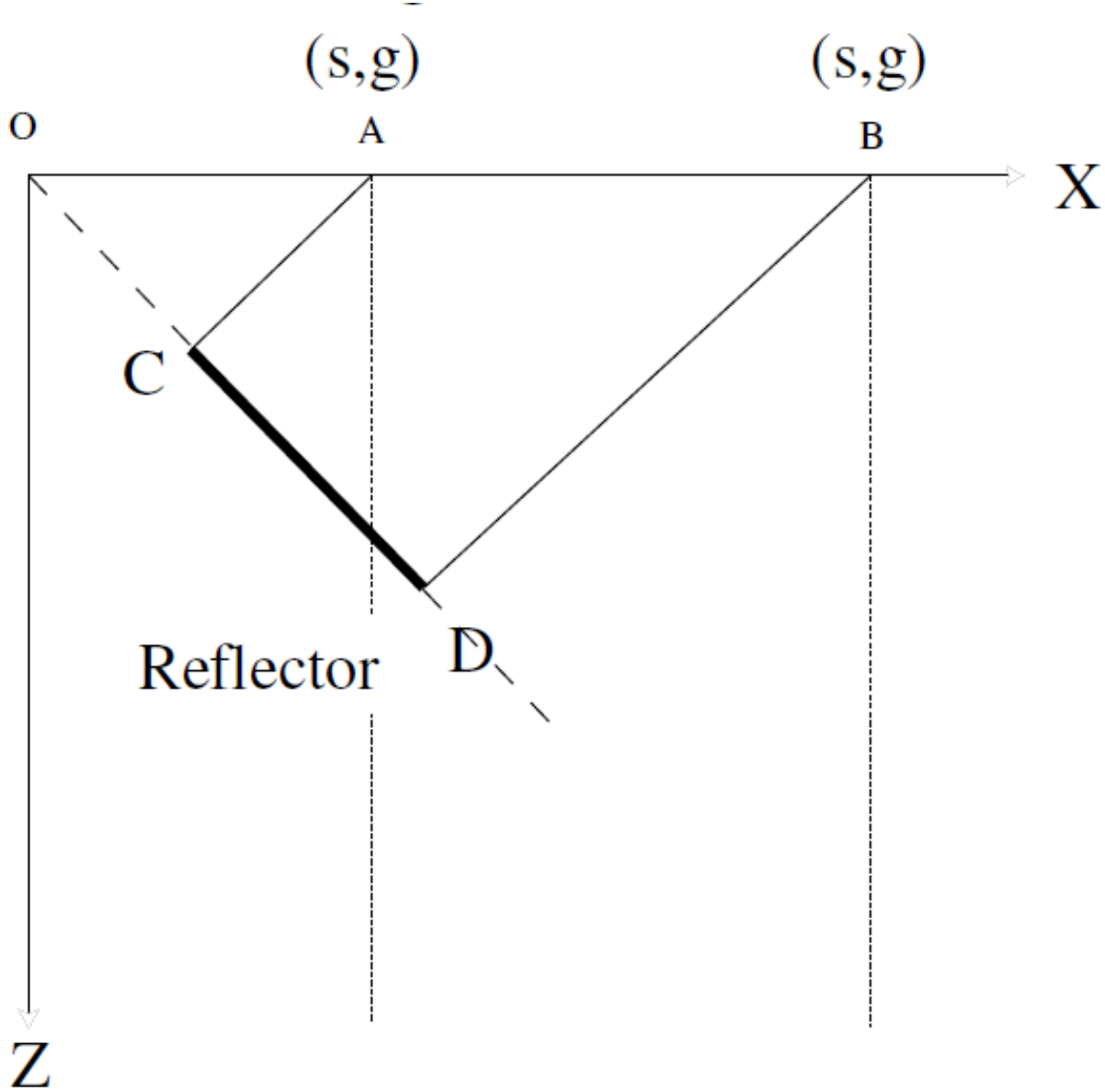
(s,g)
(s,g)
O
A
B
X
C
Reflector
D
Z

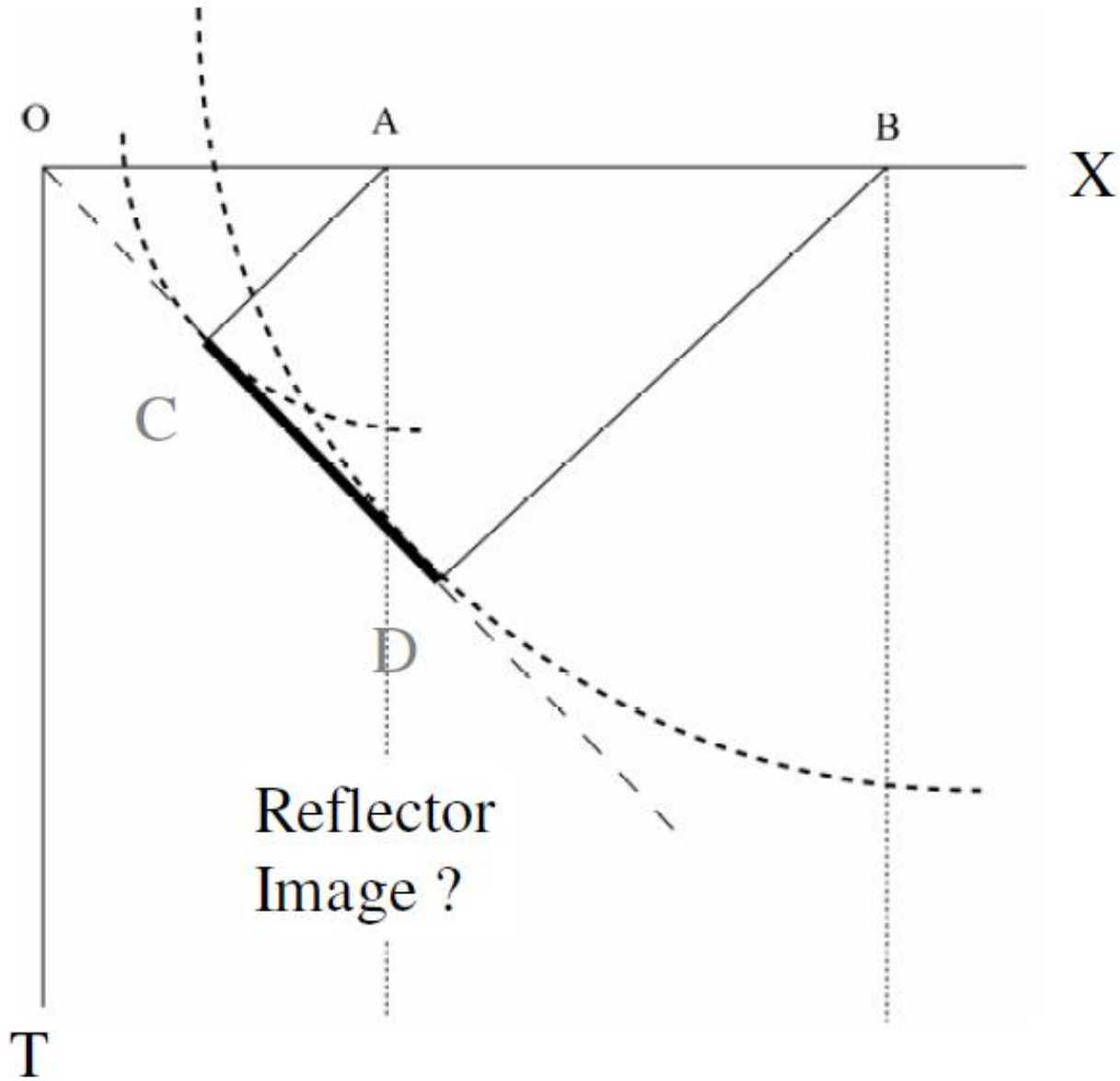
O
A
B
X
C
D
Reflector
Image ?
T

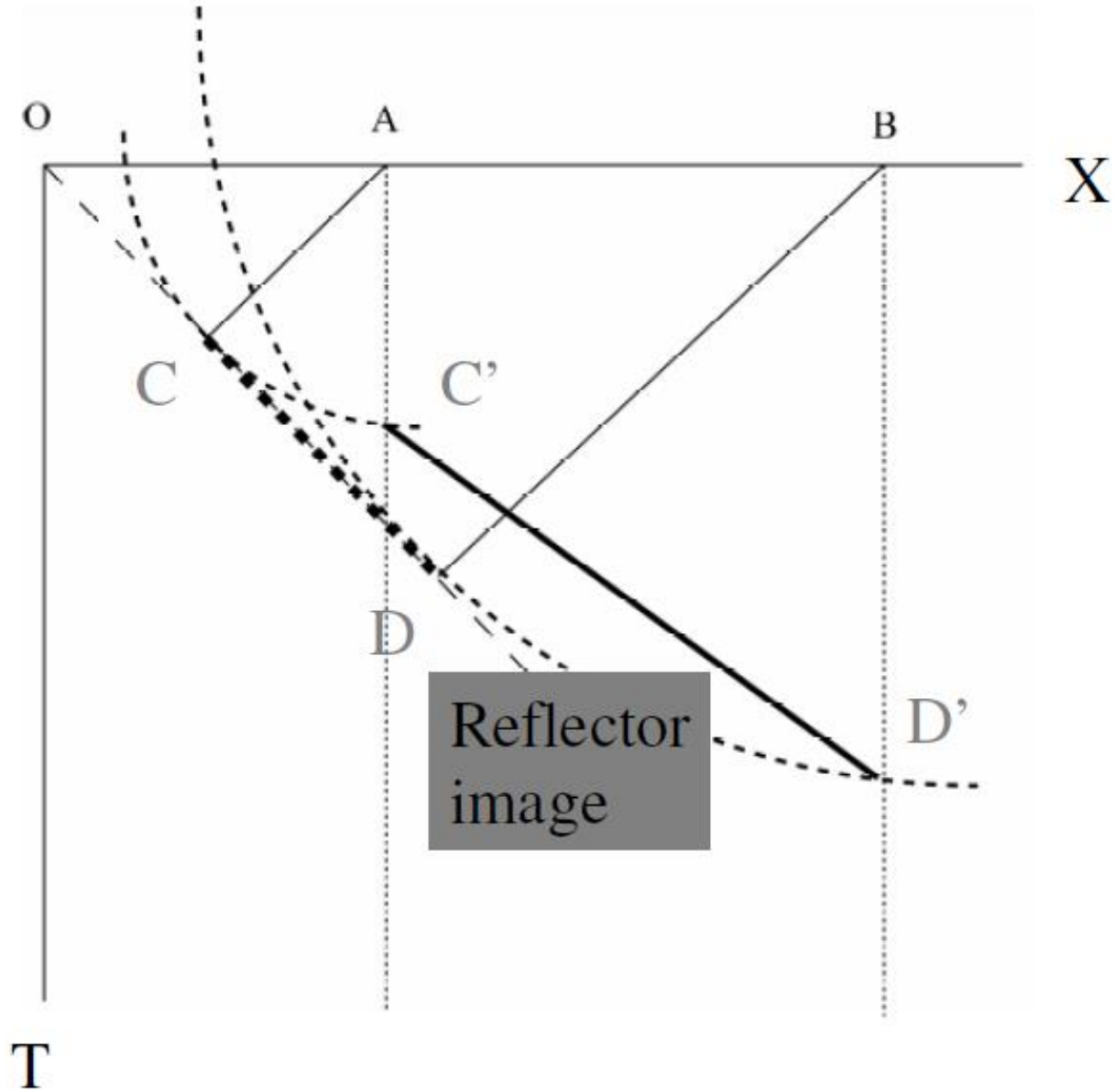
O
A
B
X
C
C'
D
Reflector
image
D'
T

FIGURE 3.22 *The effect of migration.* (a) *Before migration.* (b) *After migration. Migration increases reflection dip, moves the reflection updip, and shortens the reflection length.*

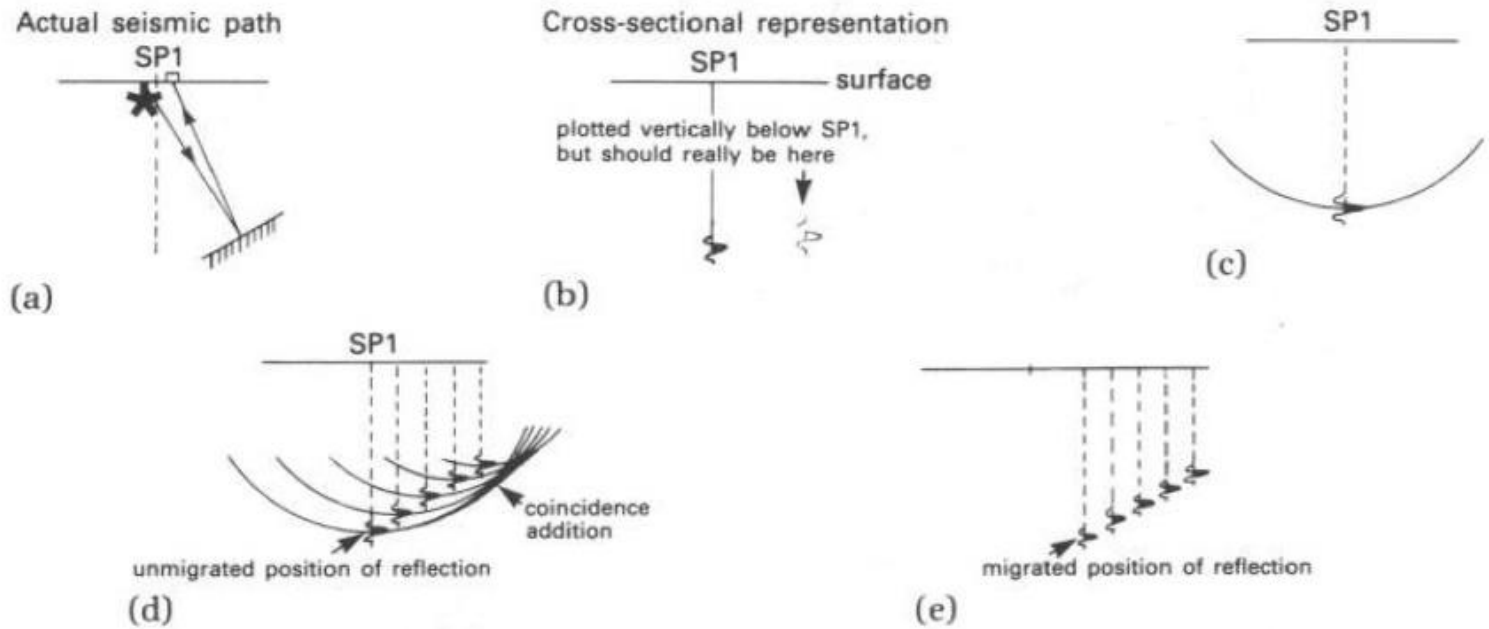

FIGURE 3.23 *A simple view of the process of migration. See text discussion. Reprinted by permission of IHRDC Press from Anstey, 1980a, fig. 4, p. 8.*

Consequences

- The dip angle of the reflector in the geologic section is greater than in the time section.

→ thus, migration steepens reflectors.

- The length of the reflector as seen in the geologic section, is shorter than in the time section

→ thus, migration shortens reflectors.

- Migration moves the reflector in the up dip direction.

MIGRATION

Pre-stack - expensive as moving a lot of ray paths,
but produces sharpest images

Post-stack - normal migration routine

Time migration - robust for minor errors in velocity

Depth migration - unstable if choose the wrong velocity

Dipping Reflectors and Migration

brought together in a CMP gather (fig. 3.20b). Dip produces reflections that have apparent dips less than the dip of the reflectors; apparent lengths greater than the actual lengths of the reflectors; and apparent locations deeper than, and downdip from the reflectors. On true dip lines, the sample points lie in the plane of the section (fig. 3.21a); but on a true strike line, although the reflectors will appear to be horizontal, the actual sampled points are located off-line (fig. 3.21b). The sampled points in sections along the apparent dip are also out of the plane of section. The closer the line is orientated to the true dip, the closer the sampled points will lie to the plane of the section. The amount of distortion increases with dip, depth, and velocity.

To counteract dip effects, seismic sections are frequently migrated—a process that attempts to move the assumed subsurface data points updip to their true subsurface locations (fig. 3.22). The effect of the migration is to steepen the dip and shorten the length of the reflection. Diffraction curves collapse to a point that lies at the apex of the diffraction hyperbola.

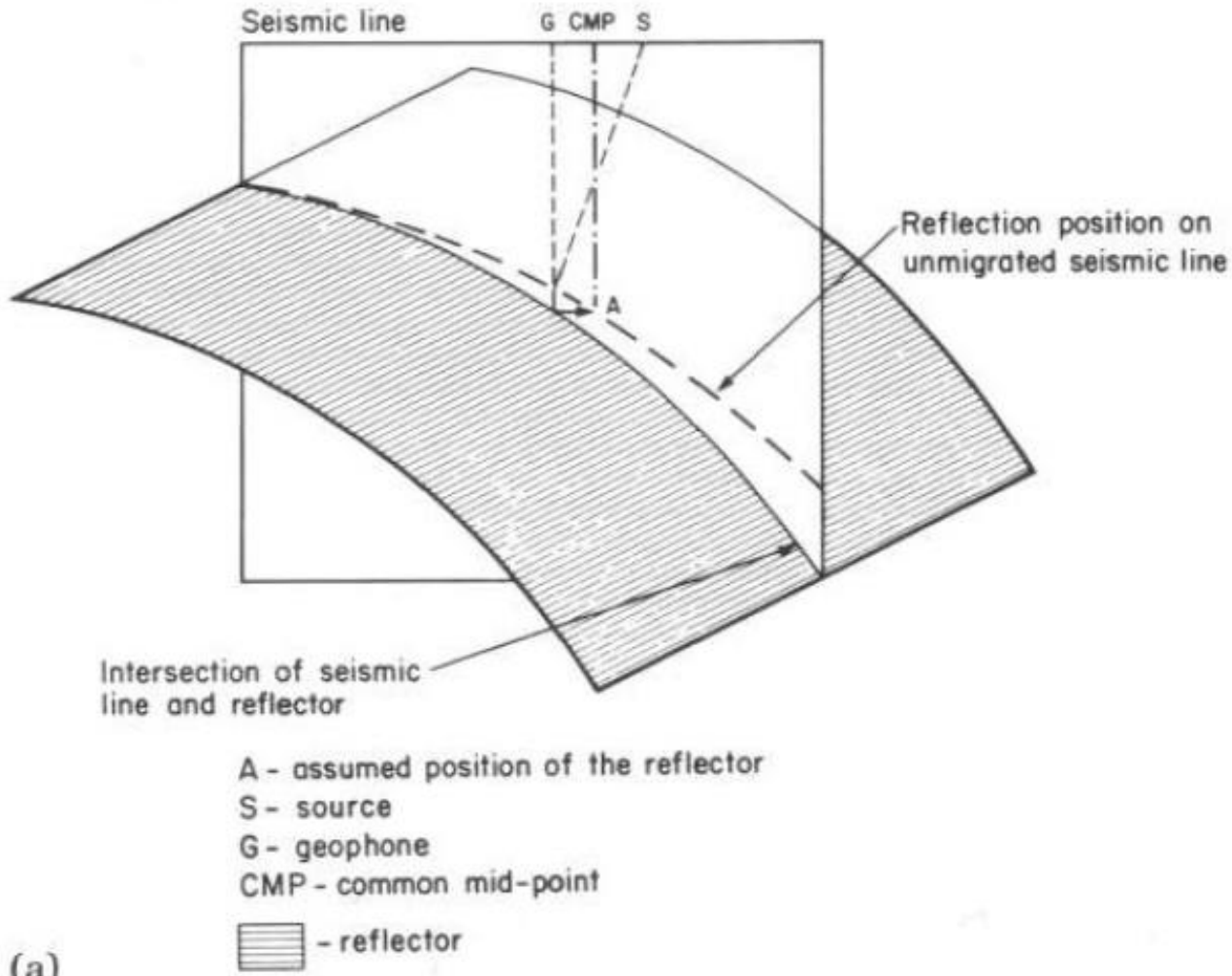
Seismic line
G CMP S
Reflection position on unmigrated seismic line
A
Intersection of seismic line and reflector
A - assumed position of the reflector
S - source
G - geophone
CMP - common mid-point
- reflector

(a)

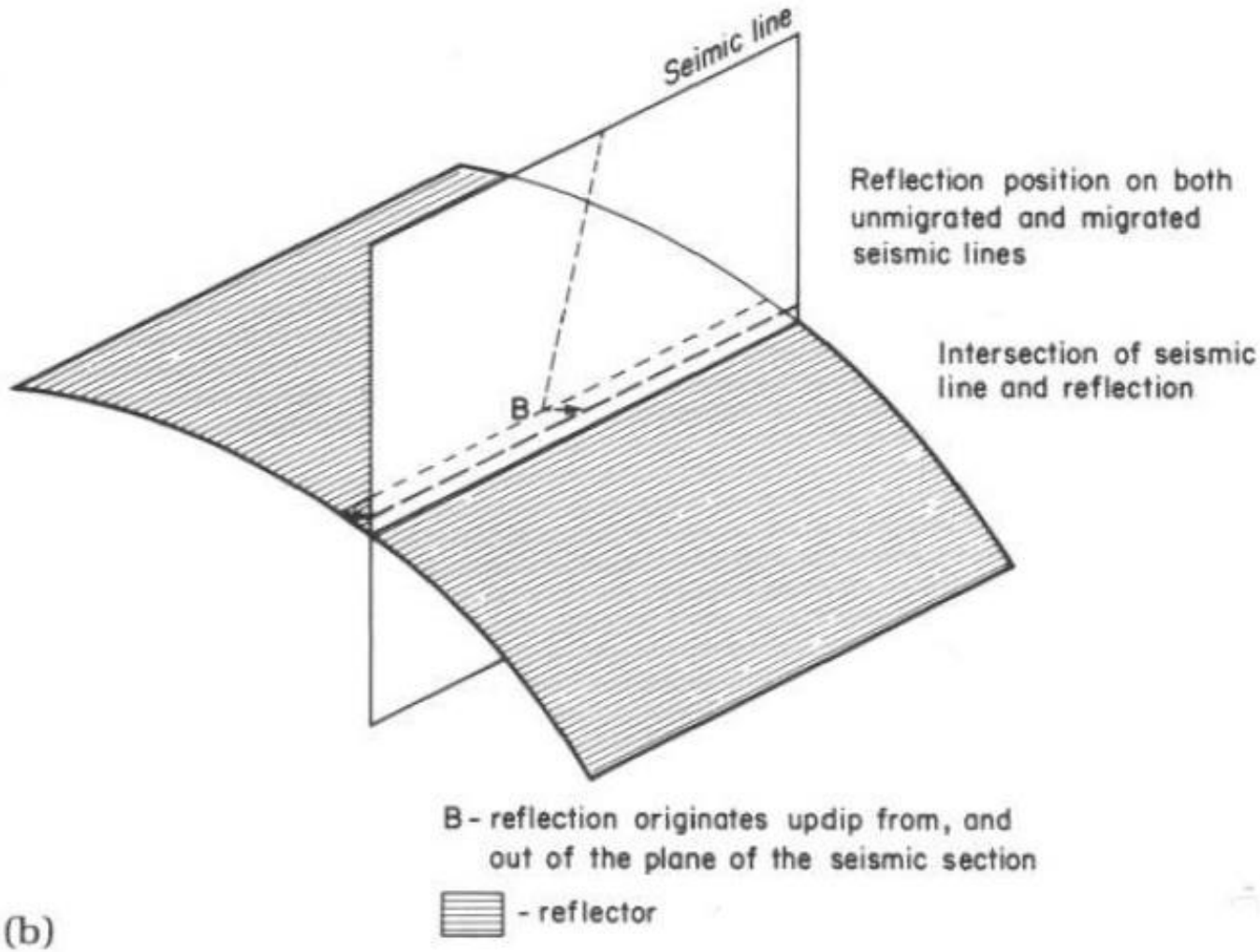
Seimic line
Reflection position on both unmigrated and migrated seismic lines
Intersection of seismic line and reflection
B
B - reflection originates updip from, and out of the plane of the seismic section
- reflector

(b)

Although numerous migration techniques have been developed, three methods are generally applied to data after it has been stacked: Kirchhoff migration, wave-equation or finite-difference migration, and the frequency-domain technique (fig. 3.24). The common idea

The Kirchhoff method migrates the data by searching for diffractions and moving all energy along the diffraction curve to its apex. This method migrates steep dips well, but does not work so well with noisy data. Noise tends to be organized after migration into characteristic syncline-like reflections (fig. 3.24c).

The wave-equation or finite-difference method uses the wave field observed at the surface to calculate the wave field at various levels. Sheriff (1982) gives a clear non-mathematical description of the method. The method has good performance with low signal/noise ratio. It is adaptable to horizontal velocity gradients, but has difficulty with steeper dips (fig. 3.24b).

Frequency-domain migration, of which there are several variants, transforms the data into a frequency versus wave-number domain. This migration uses an exact operator solution of the wave equation, and then transforms the data back. The method is less demanding of computer time than the other two; has good performance with steep dips, but exaggerates errors caused by poor velocity gradients; and is unable to cope with horizontal velocity gradients.

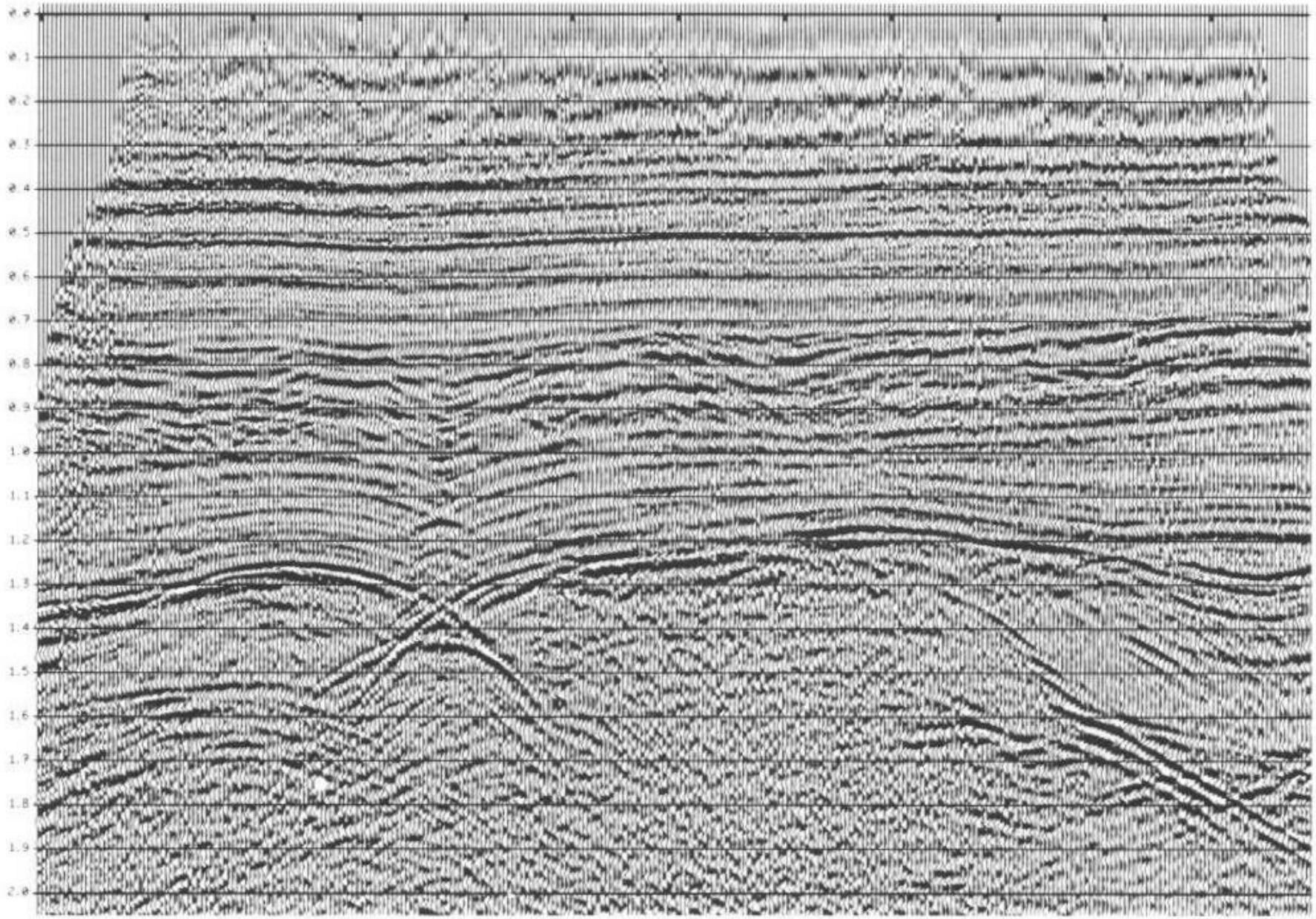

(a)

(a) *Stacked section.* (

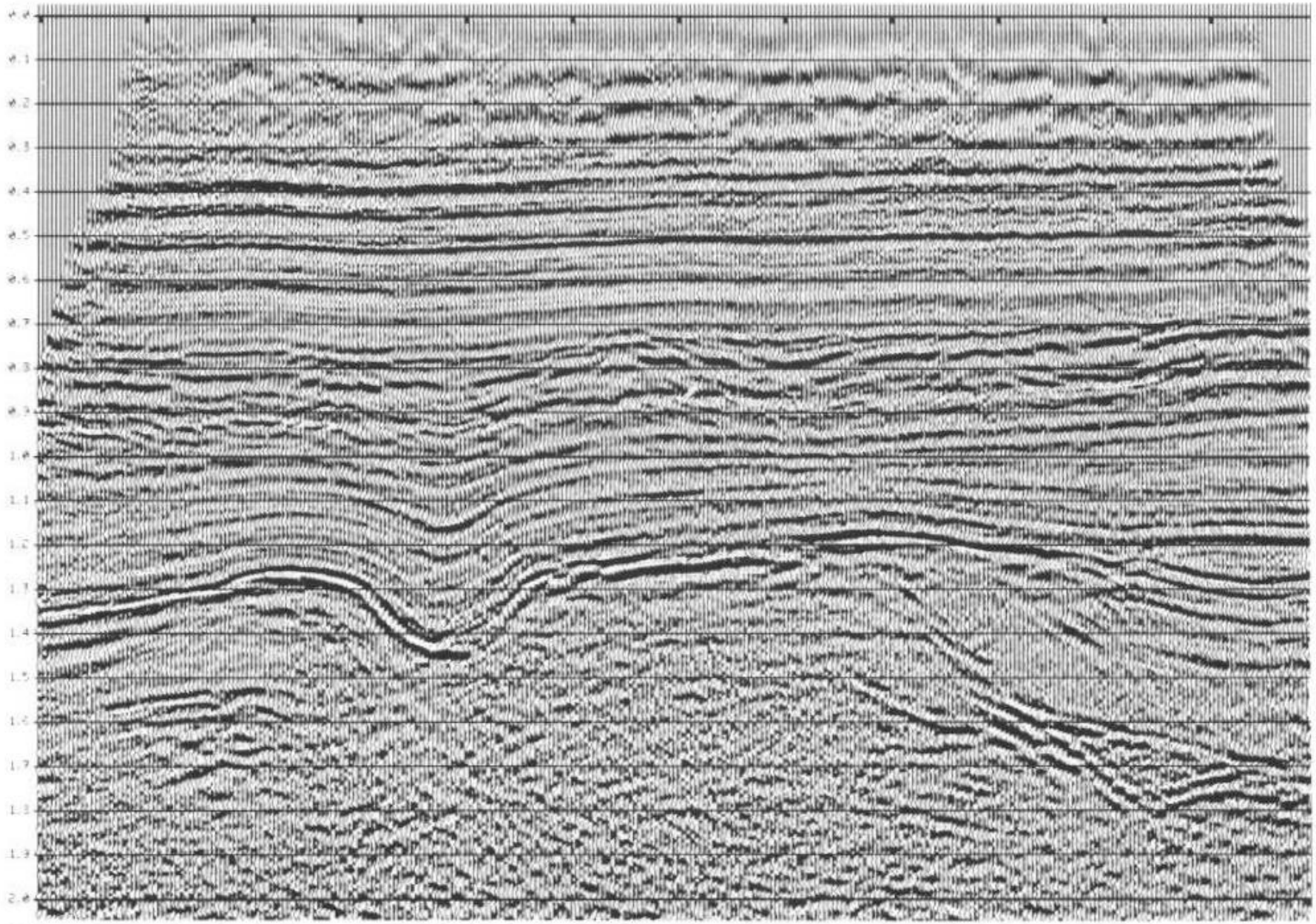

(b)

(b) *Finite-difference migration.*

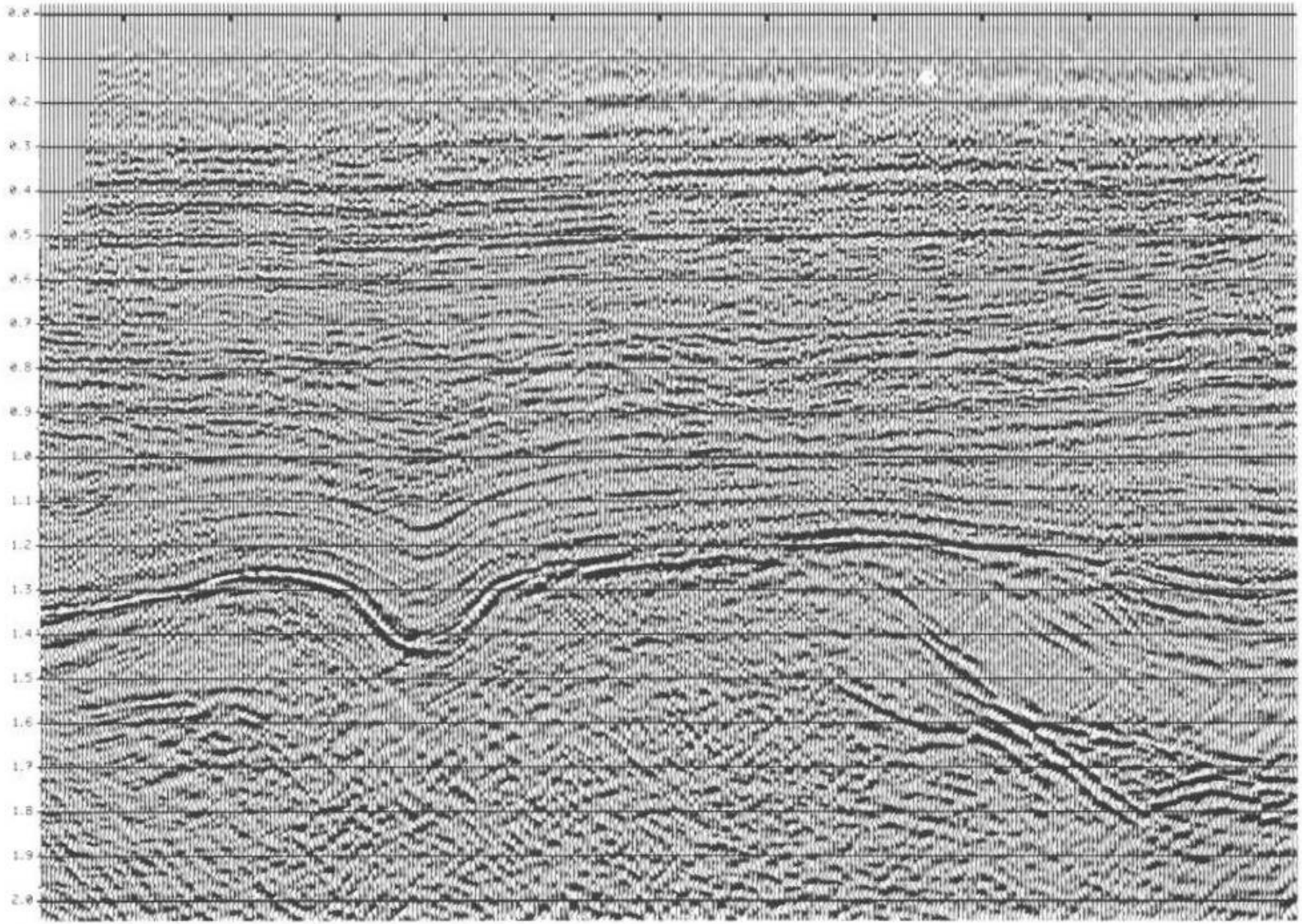

(c)

(c) *Kirchhoff-summation migration.*

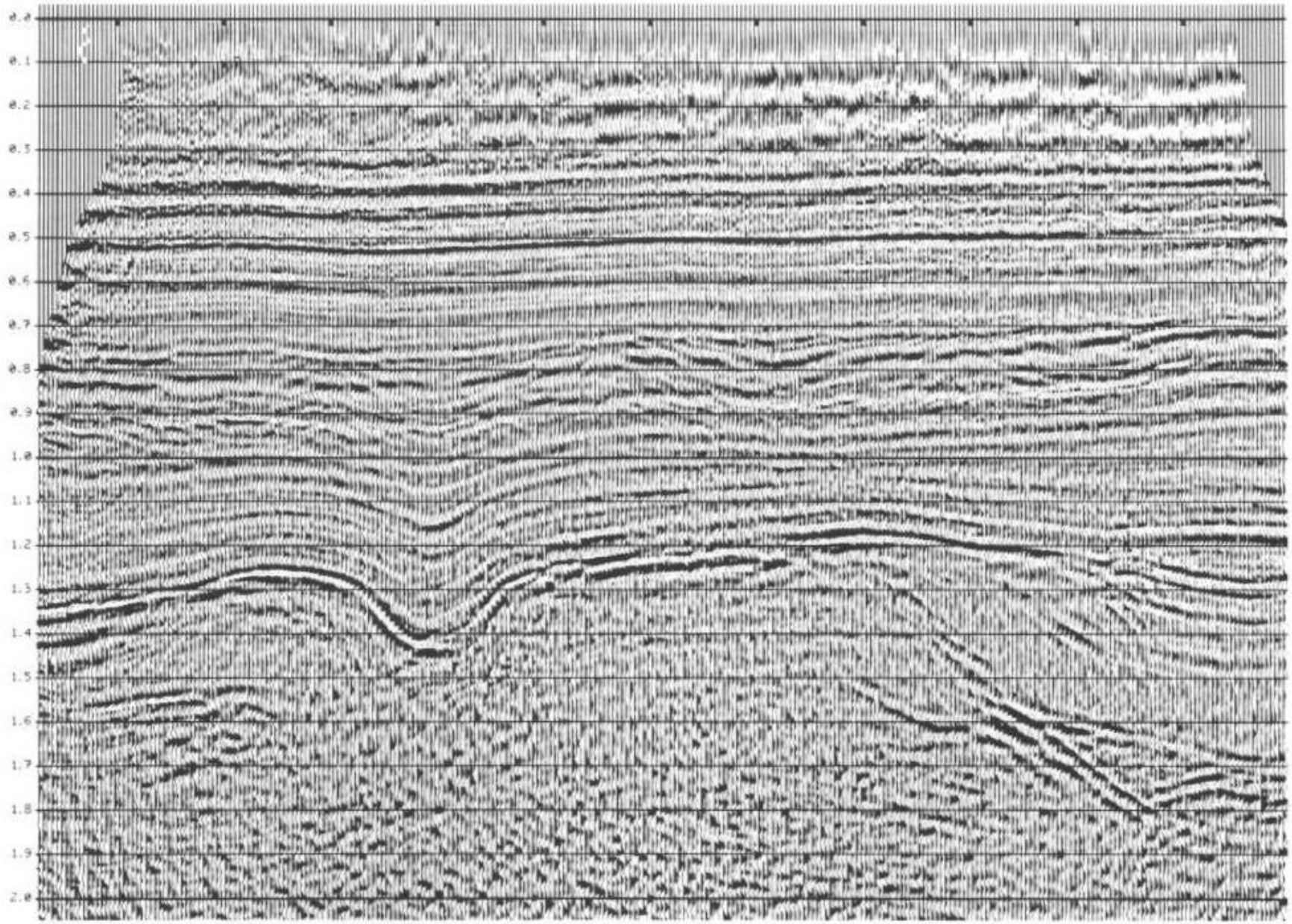

(d)

(d) *Frequency/wavenumber*

tions. After migration, anticlines become narrower because their flanks move inward and synclines become broader because their flanks move outward. However, the migration will have no effect on strike lines where reflection will appear to be horizontal and the actual subsurface data points are off-line. Similarly, the fold axes are not moved, because they are areas of near horizontal dip unaffected by migration.

Anticlines

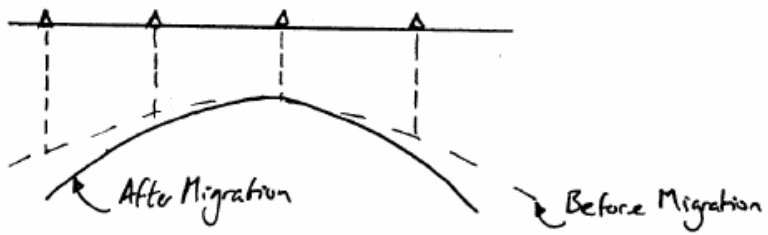

Reflections move updip and steepen during migration. Therefore anticlines look smaller in migrated sections.

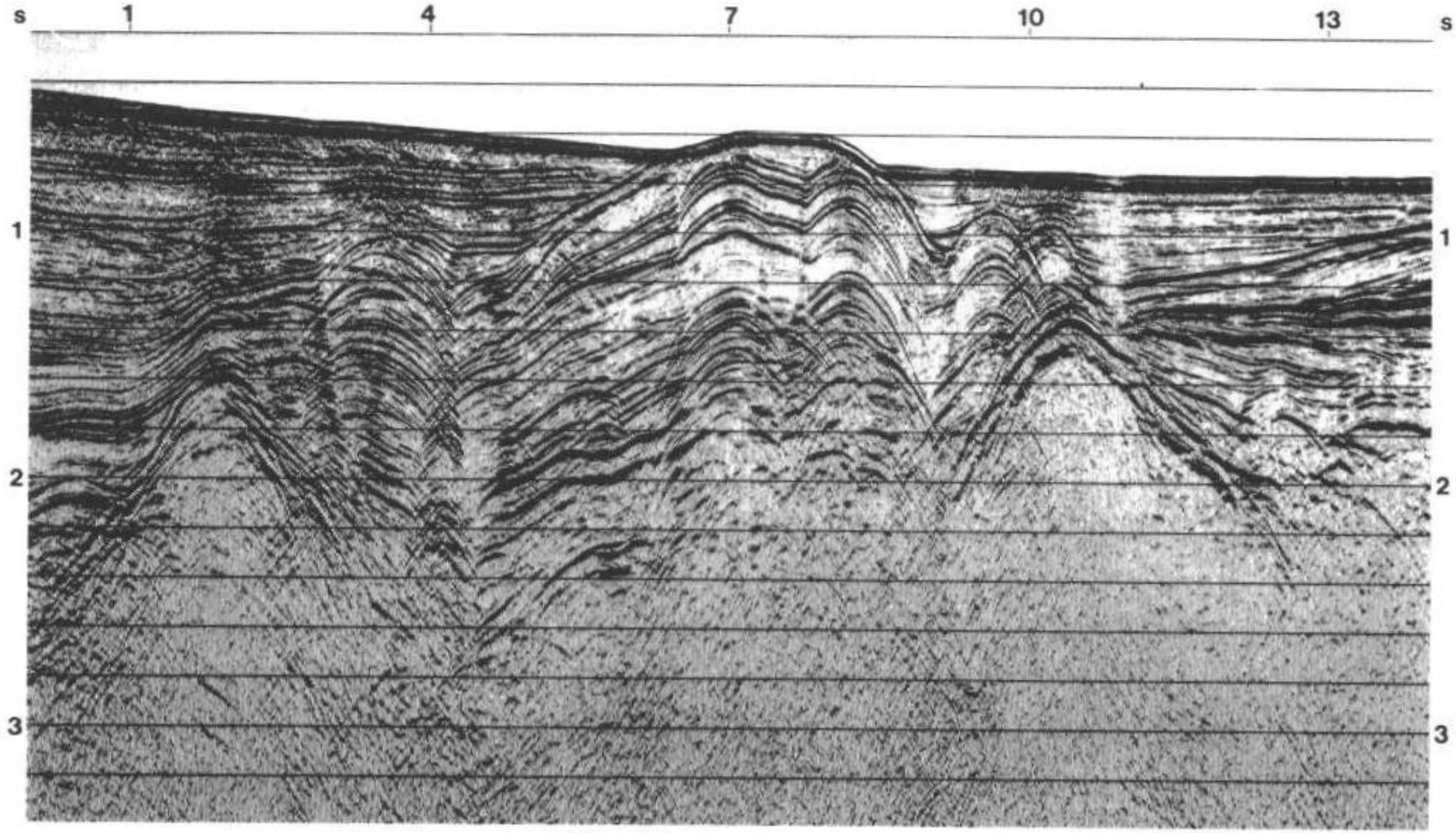

(a)

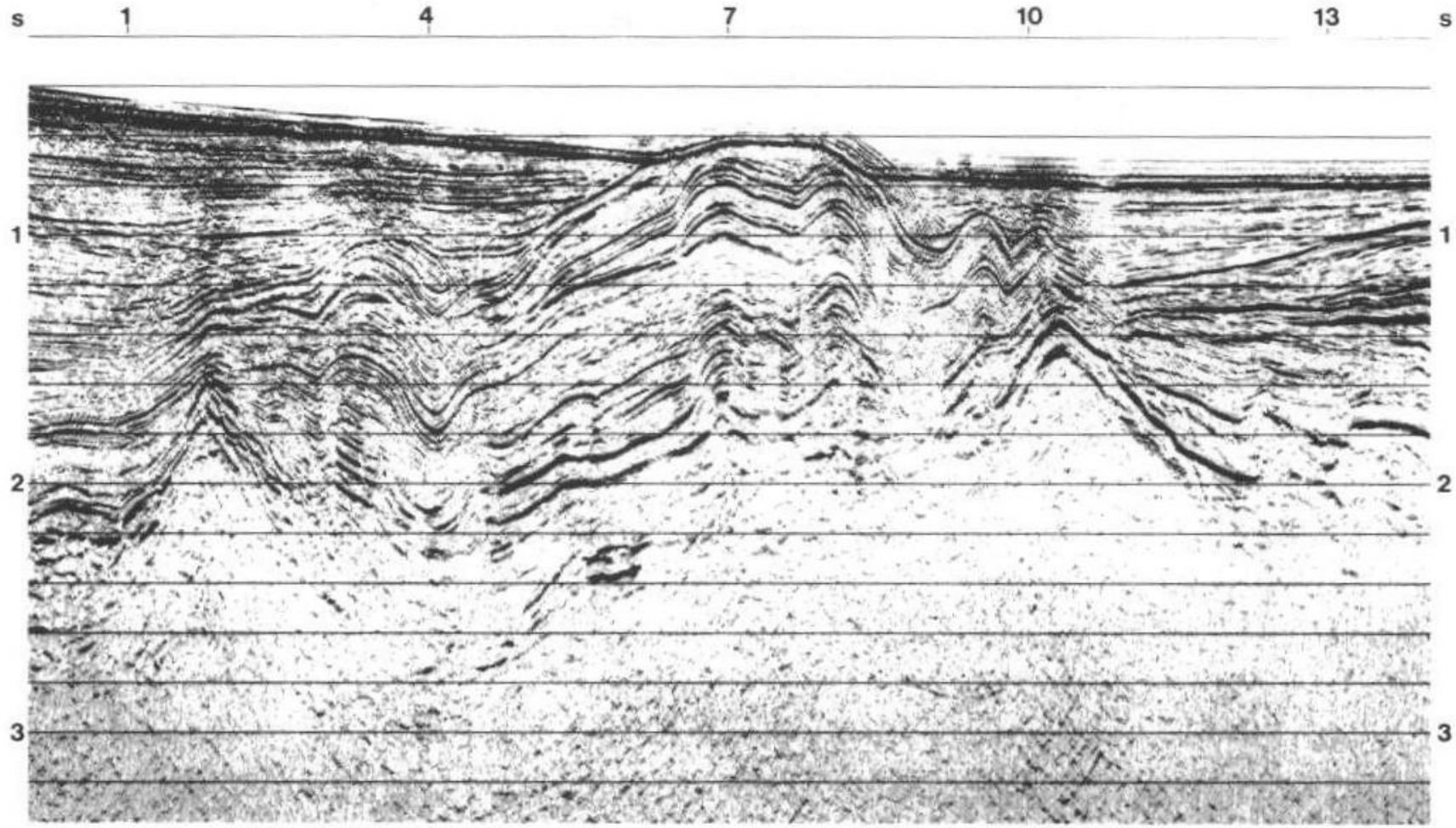

(b)

FIGURE 3.25 *Seismic example of anticlines and synclines: A complex folded structure from the Santa Barbara Channel, offshore California.* (a) *Stacked time section. Reflector dips do not exceed about 25°. Horizontal scale in mues.* (b) *Kirchhoff-summation migration. The migration has steepened dips, narrowed anticlines, broadened synclines, and has resolved some problem areas where there are cross-reflectors on the stacked time section (e.g., in the synclinal axis below the 4-mile point). Courtesy Western Geophysical.*

Diffraction curve migration

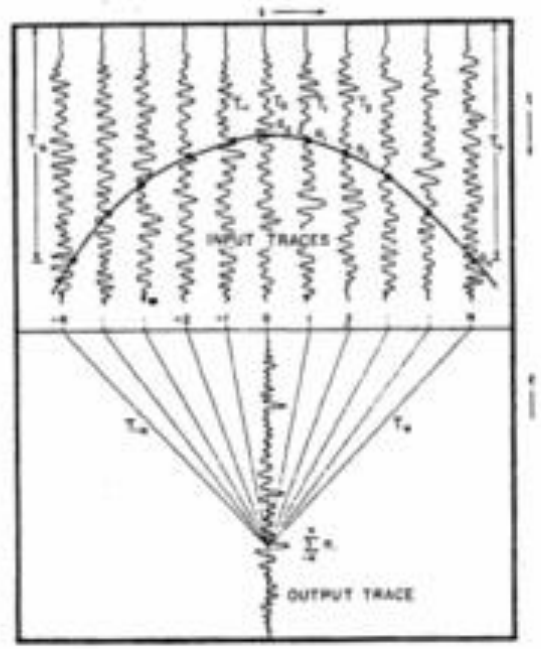

b

Illustrating the difference in philosophy between the wave front (*a*) and diffraction curve (*b*) methods of migration. In (*a*) a single trace amplitude is distributed over the proper wave front. In (*b*) many traces are sampled at the times appropriate for a single scatterer and added to give a single output trace amplitude. [Alber Schneider (1971). Reprinted with permission from Geophysics.]

due to a focusing effect. If the syncline is steep and narrow and deep in the seismic section, another effect occurs. The synclinal axis can become a buried focus for the sound waves, which brings the reflections together at a point still in the subsurface (fig. 3.26). There are now three possible reflection paths for a surface generated seismic wave. One from the axial region of the syncline, and additional reflections from the steep flanks. These three raypaths will give rise to three apparent reflectors. The two reflectors originating from the flanks will be underlain by a third curved reflector which looks like a deeper anticline (fig. 3.26). This buried-focus effect produces a bow-tie configuration, which can be unraveled by migration (fig. 3.27).

Figure 3.28 shows the beneficial effects of migration on a section that is not characterized by high dips. Note especially how dipping reflections have been moved updip, their dip has been increased, diffractions are collapsed, fault terminations sharpened, and the sections generally cleaned up. The differences can be important for the interpretation. For example, in the unmigrated version of the seismic line in figure 3.28, two dipping reflections between 1.8 and 2.1 s, below *B*, could be interpreted to have been overthrust by the flatter overlying reflections to the right. However, the migrated version of the section clearly shows the structural relationship between the two sets of reflectors to be a normal fault.

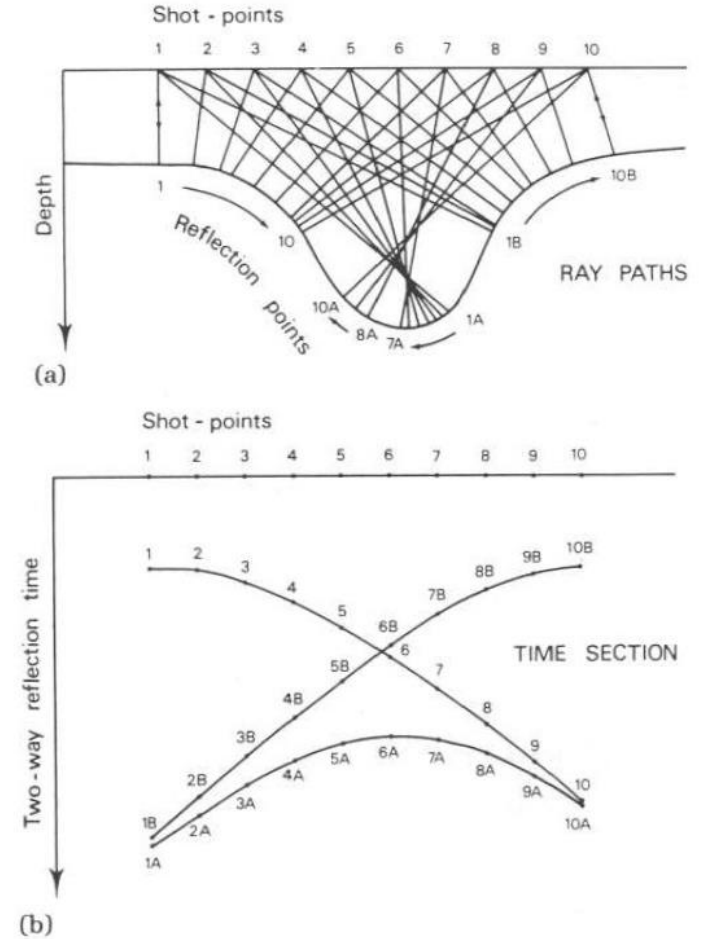

FIGURE 3.26 *The buried-focus or bow-tie effect.* (a) *Geological model showing a reflector with a curvature greater than that of the wavefront. This causes the reflector to be focused below the surface. As a consequence, rays emanating from each of the source locations 1–5 are reflected at up to three different points, all at normal incidence, on the synclinal reflector.* (b) *Schematic seismic section showing the complex pattern of the three reflector curves that resemble the outline of a bow-tie. Reprinted by permission of Graham & Trotman Ltd., London, from* Introduction to Seismic Interpretation, *McQuillin, Bacon, and Barclay, 1979.*

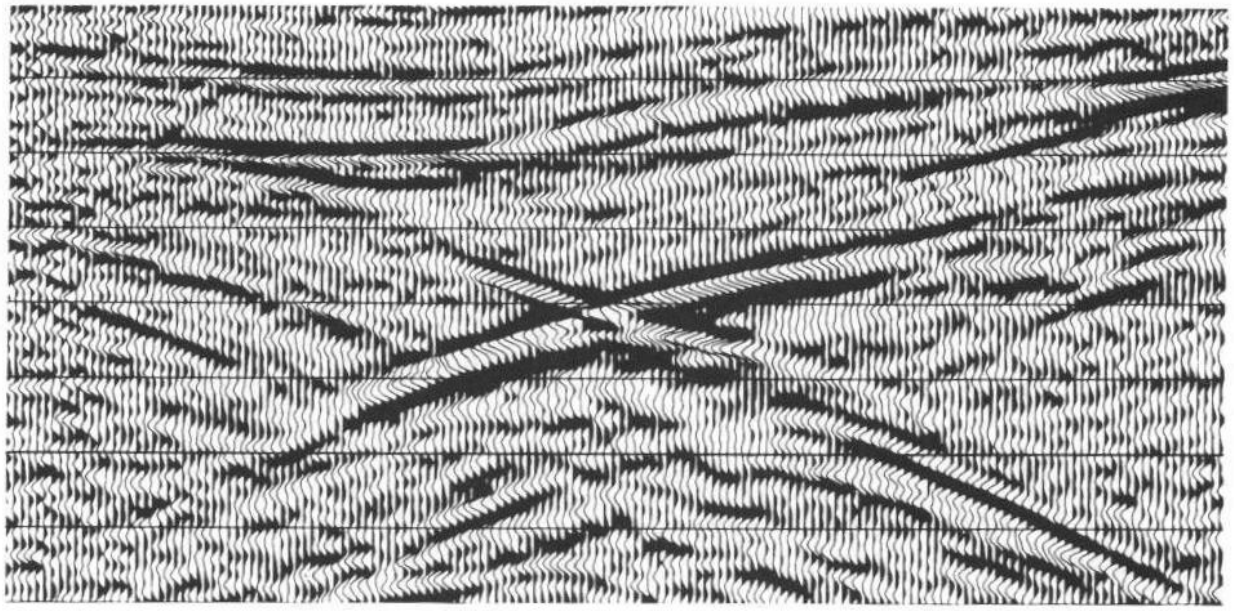

(a)

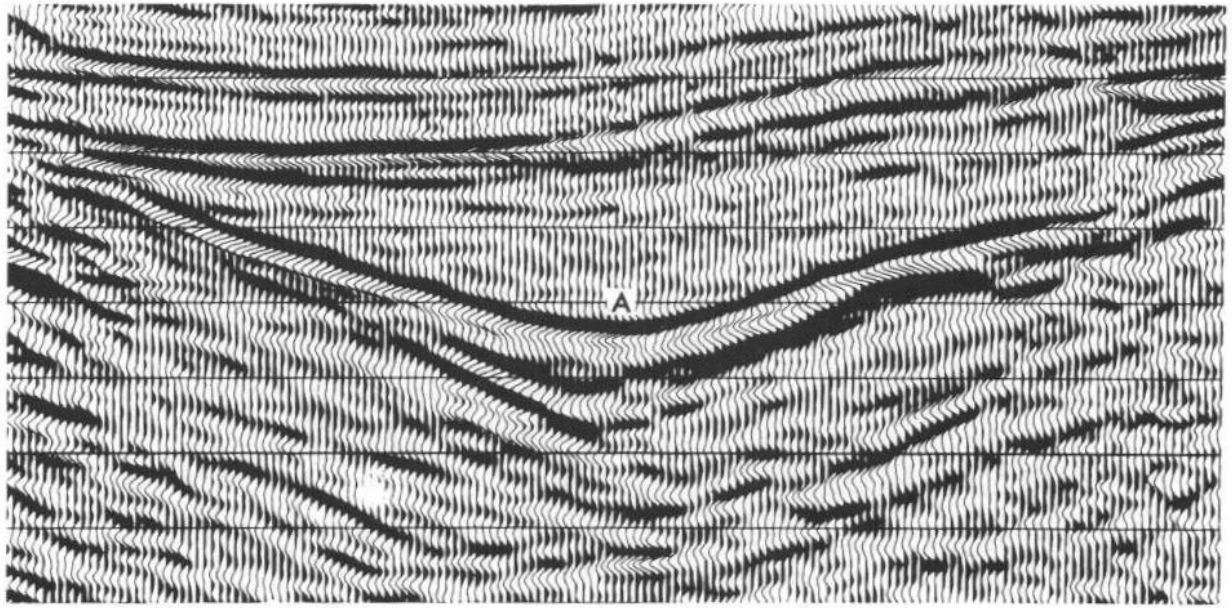

(b)

FIGURE 3.27 *Seismic examples of a buried focus.* (a) *Stacked section showing the bow-tie effect.* (b) *Migrated section, revealing the true synclinal shape of the reflector. Courtesy Norsk Hydro.*

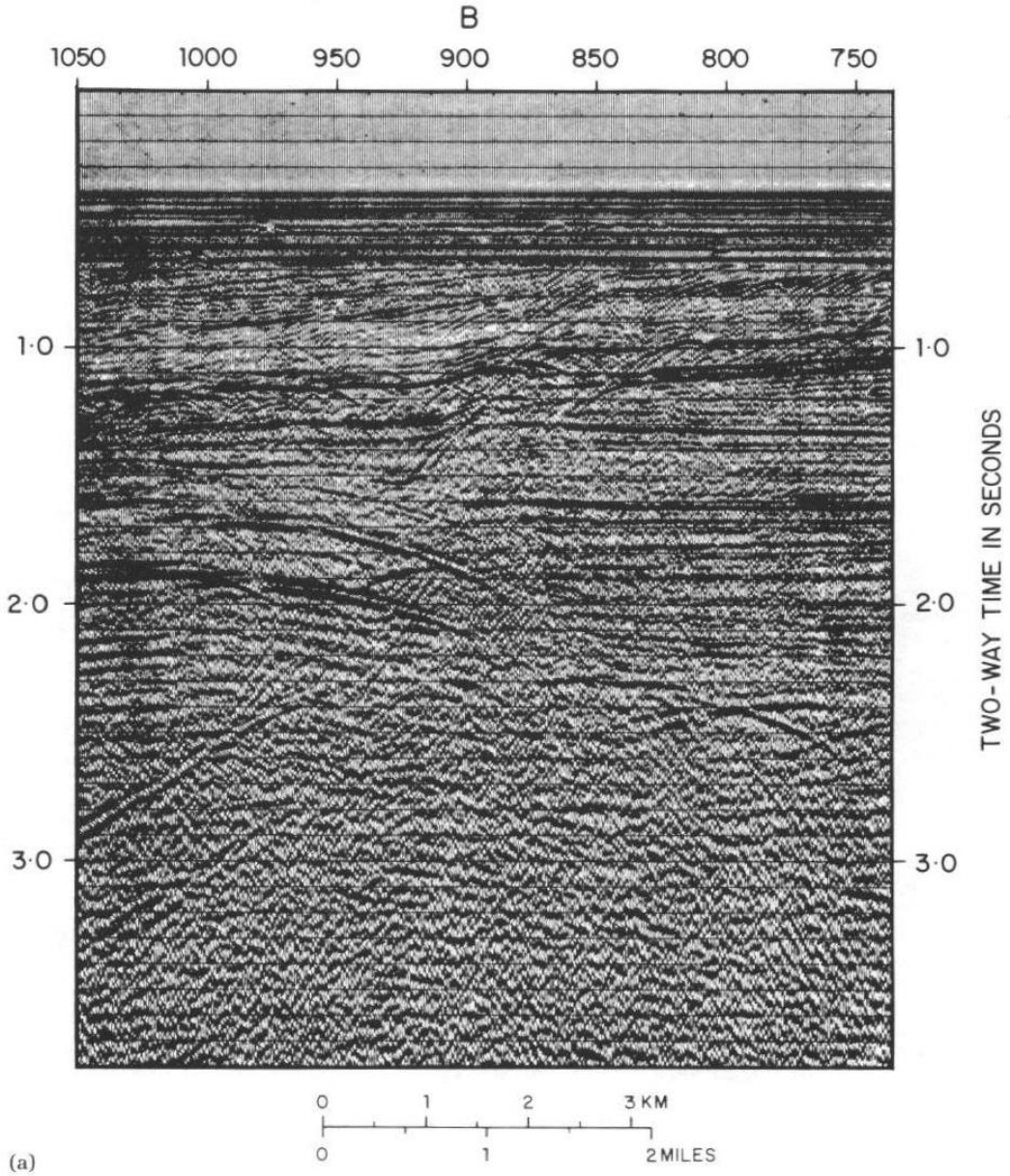

FIGURE 3.28 *Examples of stacked and migrated seismic sections.* (a) *Stacked section.* (b) *Migrated section. Courtesy Norsk Hydro.*

Apparent Thinning Downdip

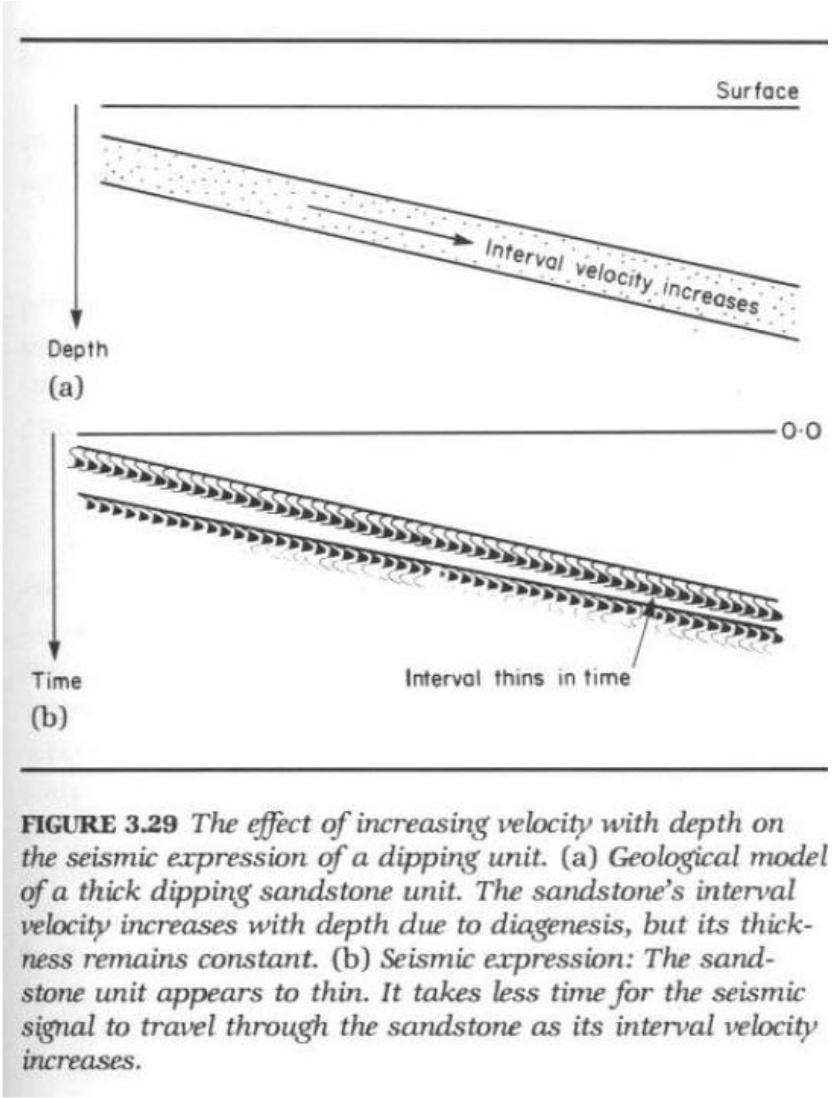

FIGURE 3.29 *The effect of increasing velocity with depth on the seismic expression of a dipping unit.* (a) *Geological model of a thick dipping sandstone unit. The sandstone's interval velocity increases with depth due to diagenesis, but its thickness remains constant.* (b) *Seismic expression: The sandstone unit appears to thin. It takes less time for the seismic signal to travel through the sandstone as its interval velocity increases.*

Apparent Thinning Across Fault

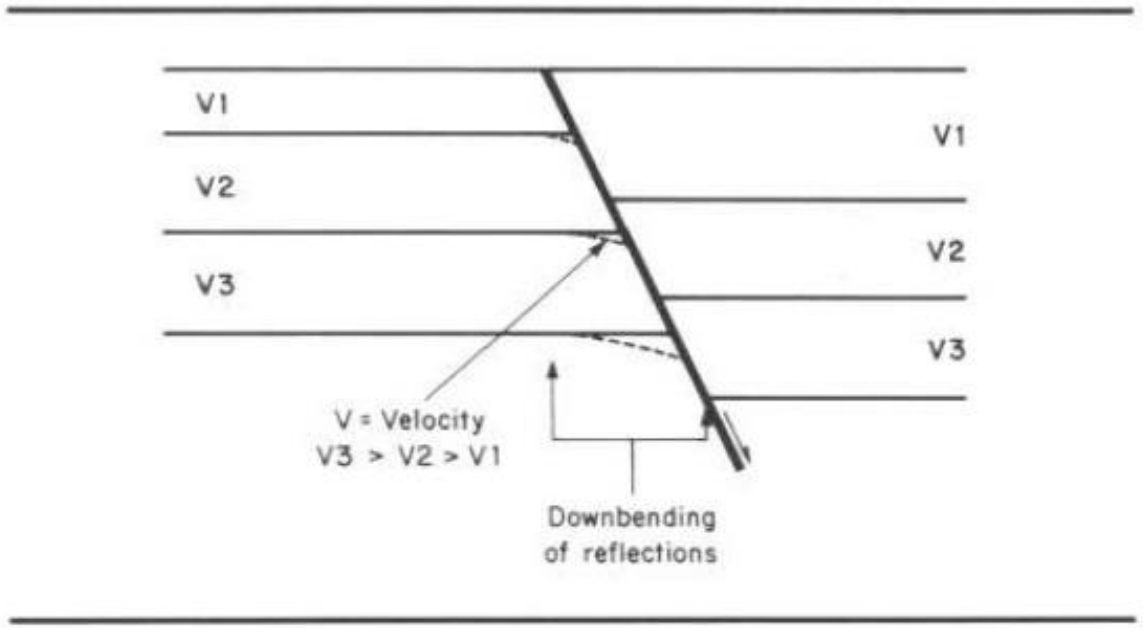

FIGURE 3.30 *Downbending of reflections into a fault. This can occur when low-velocity material is faulted by a dipping fault. In the zone beneath the fault plane, downbending of reflections can occur due to the lower velocities (and, therefore, longer traveltimes) in lower-velocity downthrown rocks.*

Apparent Rollover into Fault

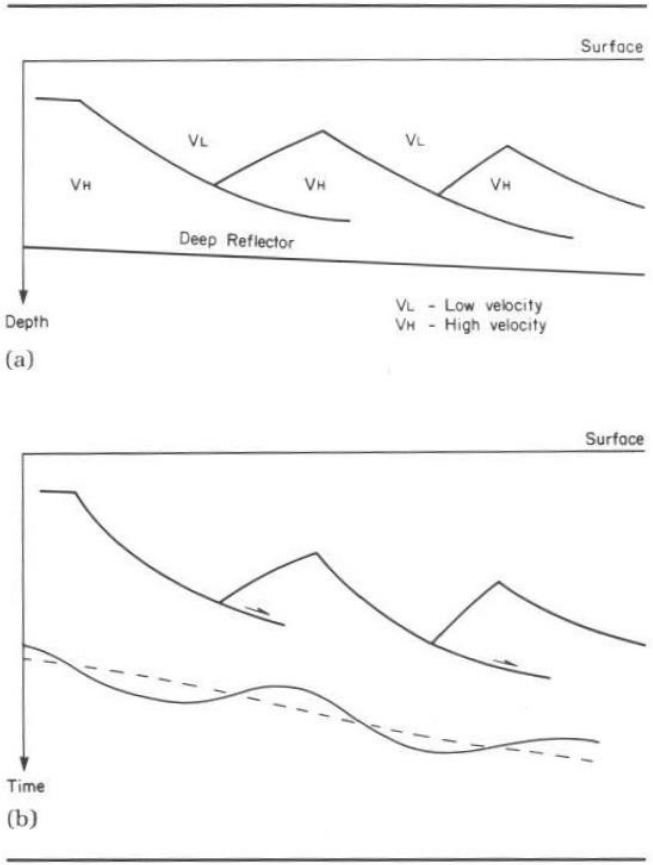

FIGURE 3.31 *Velocity anomalies beneath detached listric-normal faults.* (a) *Geological model showing a set of detached listric-normal faults and associated tilted fault blocks. The faults are underlain by a planar dipping reflector.* (b) *Seismic expression showing velocity pull-up beneath the tilted fault blocks and velocity push-down beneath the intervals of thick low-velocity infill. As a general rule, beware of deeper reflections that mimic the structure of shallower reflections.*

Velocity Anomalies Associated with Salt

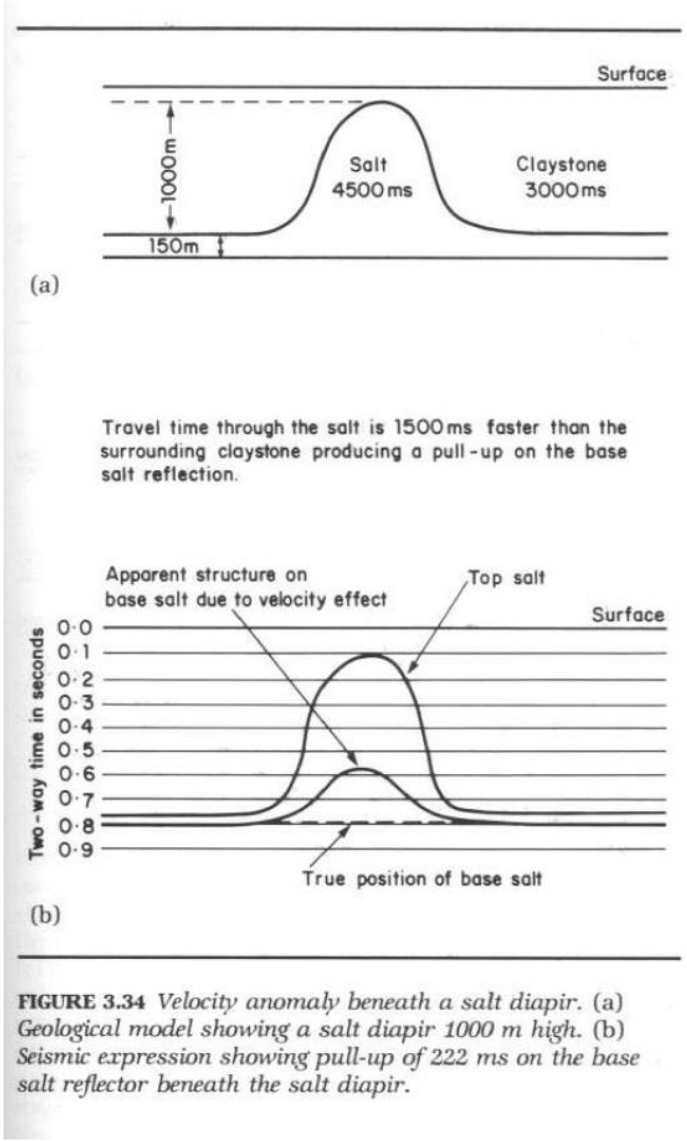

FIGURE 3.34 *Velocity anomaly beneath a salt diapir.* (a) *Geological model showing a salt diapir 1000 m high.* (b) *Seismic expression showing pull-up of 222 ms on the base salt reflector beneath the salt diapir.*

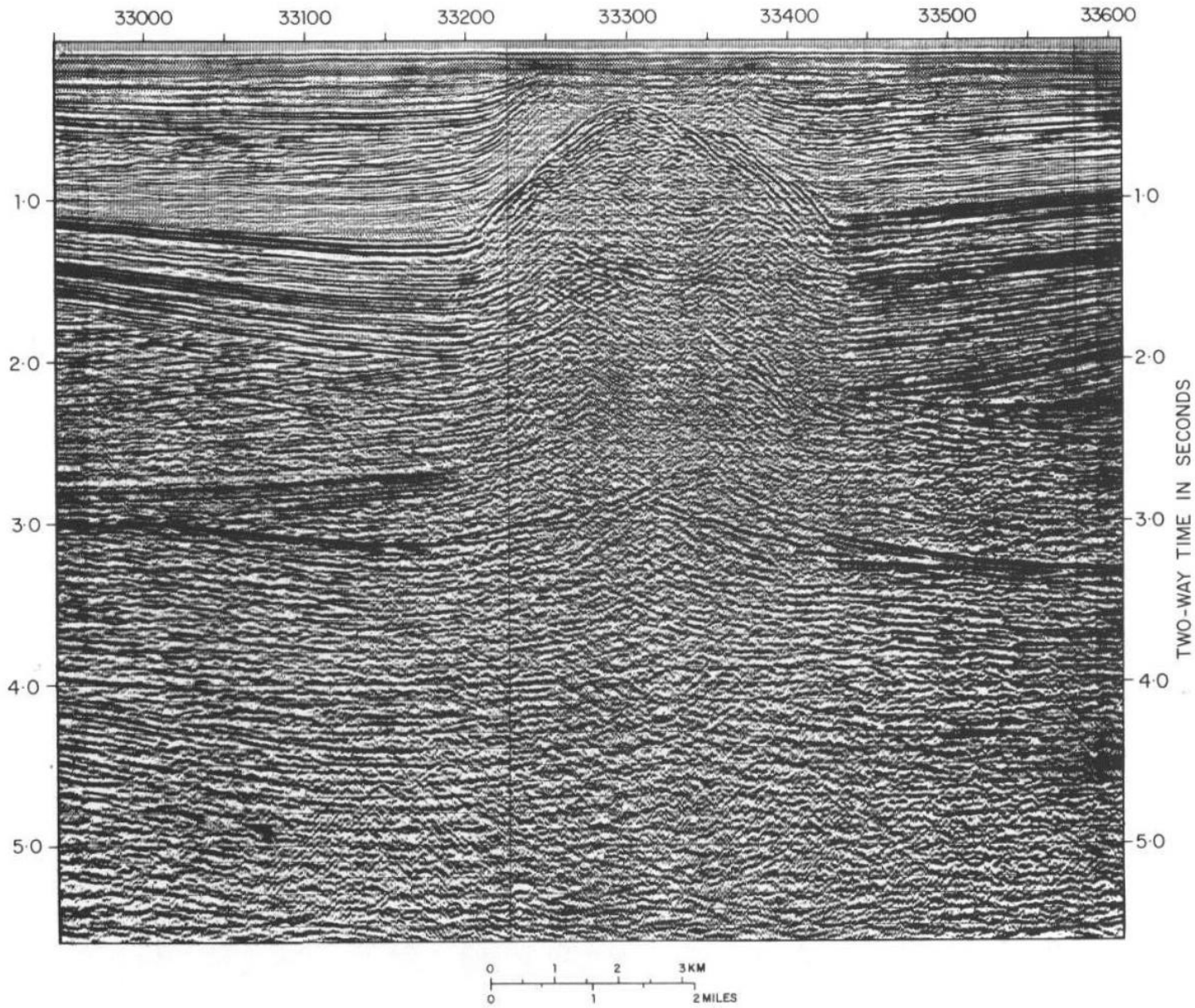

FIGURE 3.33 *Seismic section across a salt diapir. Courtesy Merlin Profilers Ltd.*

sufficient velocity information is available, the degree of pull-up can be used to estimate the salt's thickness and so locate its top. The pull-up can be used as an approximate guide to predict the time of the top salt layer where this cannot be seen clearly on the seismic section.

Chapter 4

Geology and Seismic Section

a biased eye. It can only detect lithological boundaries if the acoustic impedance changes across the boundary; and the change must be above the threshold limit of the seismic system. So, at best, the seismic system detects only

The information gap between what we observe in the seismic section, and what the geology most probably is, has to be filled by the interpreter. The knowledge required for this is twofold. Firstly, the interpreter must be able to identify and eliminate all events relating to noise. Secondly, the interpreter must employ considerable geological skill, including knowledge of sedimentology, stratigraphy, structural geology, etc., to convert the seismic image into a plausible geological reality. Geological

tionship to other reflections. Understanding the link between geology and seismic sections is thus a twofold problem. First, we must establish the significance of the individual reflection and second, establish the significance of the relationship of reflections to each other.

THE INDIVIDUAL REFLECTION

Individual reflections have several measurable and descriptive properties that can be related to geology. The attributes most easily linked to, and diagnostic of, lithology are reflection amplitude, polarity, continuity, and spacing or frequency. Caution should always be used when analyzing reflection characteristics, since both processing and noise can create potential pitfalls.

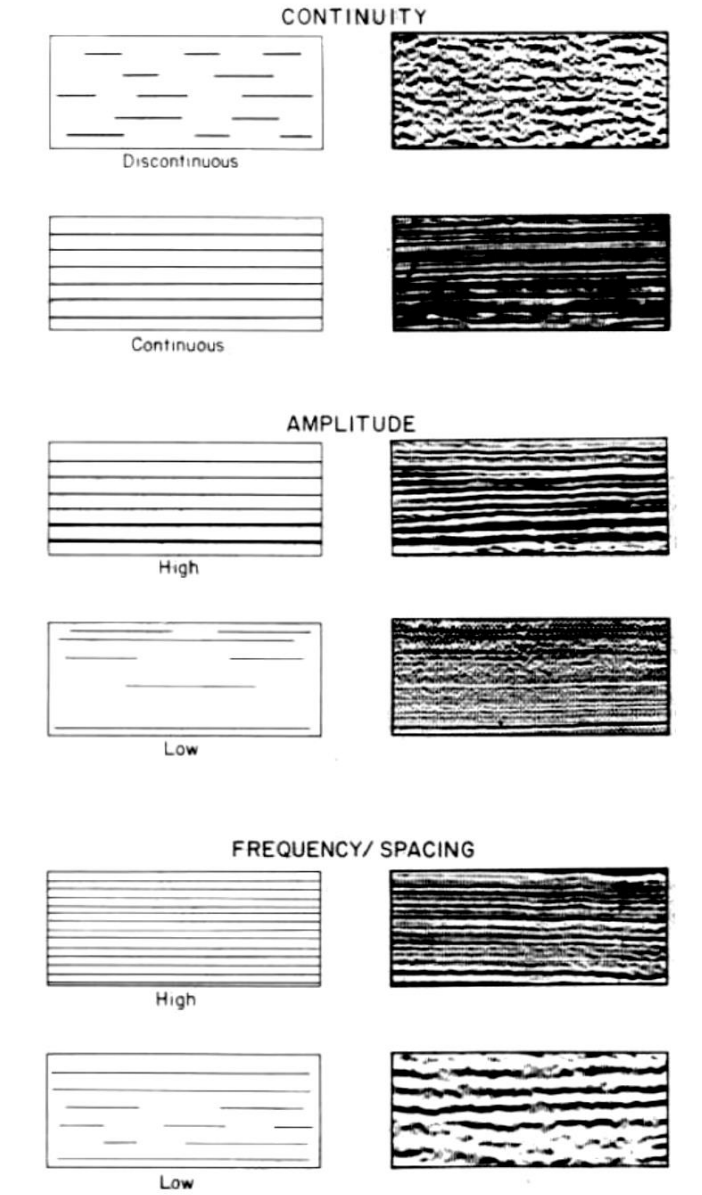

FIGURE 4.1 *Reflection attributes: continuity, amplitude, frequency/spacing.*

REFLECTION AMPLITUDE

Amplitude is the height of a seismic reflection peak (or trough) and is dependent on the reflection coefficient, but this direct relationship may be lost during processing. Frequently, amplitudes on seismic sections are balanced during processing to produce what is thought to be more easily interpretable sections. Usually, however, this makes it difficult and in many instances no longer possible to determine the relative strengths of reflection coefficients. However, where amplitudes can be differentiated, the qualifying terms of high, medium, and low are used (fig. 4.1). Vertical changes in amplitude can be used to help locate unconformities, whereas lateral changes can be used to help distinguish seismic facies. Great caution must be exercised, however, as interference patterns from tuning, multiples, etc., are responsible for many amplitude changes observed in seismic sections.

REFLECTION POLARITY

Reflection polarity can often be determined from onlap relationships on processed minimum-phase sections, or from the maximum amplitude from zero-phase sections (sees figs. 7.10 and 7.13). Polarity in combination with amplitude may provide a good guide to the likely lithologies causing a reflection. For example, in a shallow young sequence, such as the Tertiary of the U.S. Gulf Coast, a porous sand overlain by clay should produce a medium- to high-amplitude reflection with a negative reflection coefficient; a clay overlying a limestone almost always produces a high-amplitude reflection with a positive reflection coefficient, etc.

REFLECTION CONTINUITY

Reflection continuity describes the lateral persistence of a reflection. A discontinuous reflection is one where an alignment is obvious but the continuous parts of the reflection are separated by gaps. The gaps may be as small as two or three traces. A continuous reflection maintains its character for an appreciable distance (say several kilometers or miles). Continuity is graded from very continuous to very discontinuous (fig. 4.1). Continuity can be interpreted in geological terms as lateral changes in acoustic impedance and hence in lithology. Discontinuous reflectors are, thus, characteristic of environments where rapid lateral facies change is the rule (e.g., fluvial, alluvial environments). Continuous reflectors are characteristic of depositional environments where uniform conditions are laterally extensive (e.g., deep-water environments).

Potential pitfalls also arise from disruption of reflections by noise, such as, multiples, migration arcs, diffractions, sideswipe. Usually these coherent type of disruptions can be recognized by drawing a line (real or imaginary) connecting discontinuities. If the line is straight or hyperbolic, the discontinuity is probably not real. A more serious pitfall can arise when continuity is deliberately enhanced during processing (fig. 4.2). For seismic stratigraphic work, processing that has forced continuity into a section is a great disadvantage; unfortunately, it is done all too frequently.

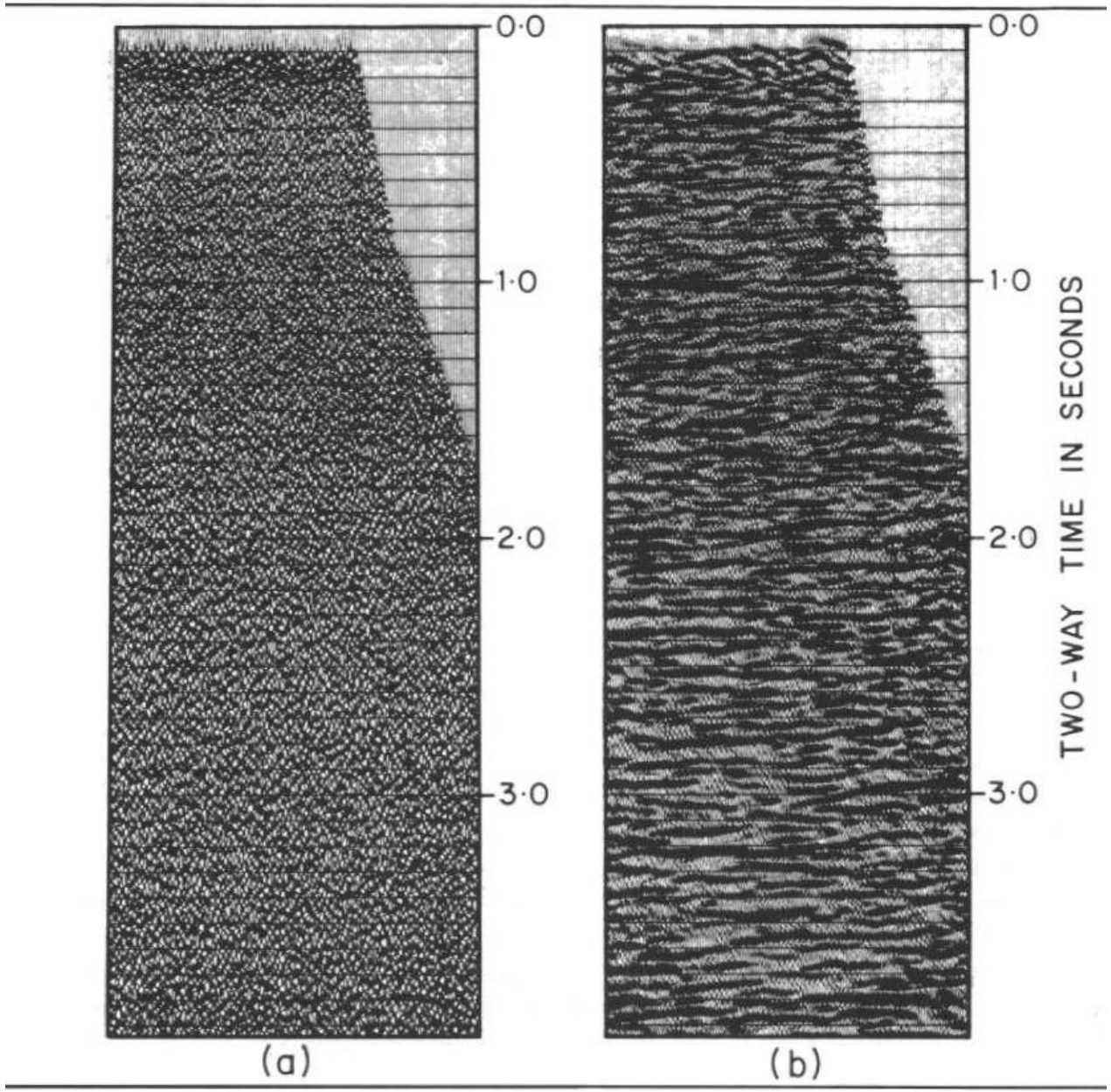

FIGURE 4.2 *Random reflections with continuity enhancement.* (a) *A stacked section from a common shotpoint gather of synthetically made seismic traces using a random-number generator. The data has zero signal-to-noise ratio and all reflection alignments are apparent and not real.* (b) *Section (a) after further processing to enhance continuity. The process effectively forces alignments into the data. The apparent improvement is entirely false, and this type of processing is a potential enemy of the interpreter. Reprinted by permission of the AAPG from Howard and Danbom, 1983.*

REFLECTION SPACING OR FREQUENCY

Reflection spacing or frequency describes the number of reflections per unit time (fig. 4.1). It is affected by both interference effects and the frequency of the seismic signal. The former effects can be interpreted in terms of bed (reflector spacing), and imparts character to the seismic section. Figure 7.17, in chapter 7, shows a characteristic reflector spacing that gives an interval a character that can be correlated easily across faults. Vertical changes in reflector spacing can be used as a guide to locating boundaries between depositional sequences, but should not be used (if possible) as the sole criterion. Lateral changes in spacing can be used to infer facies change. However, lateral change in spacing or character is very susceptible to noise and structuring. Multiples can often produce false increases in reflection spacing. The gradual loss of higher frequencies with depth in a seismic section has a marked effect on reflector spacing. The dominant frequency over an interval can be estimated by measuring the reflection spacing (fig. 2.15).

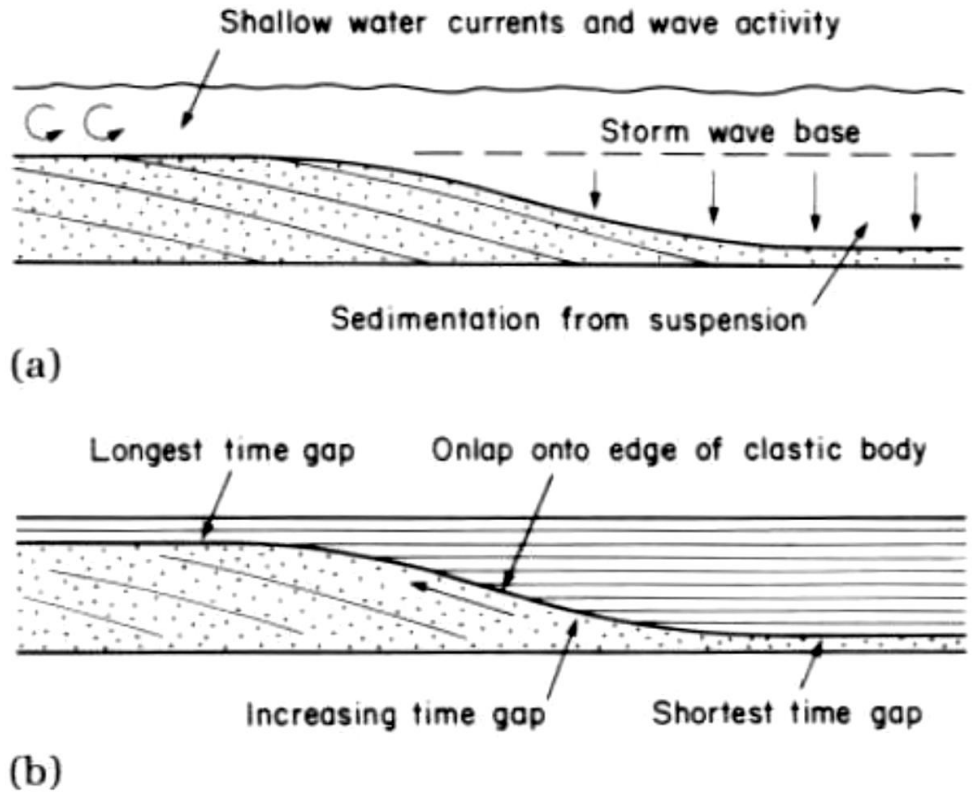

FIGURE 4.5 *Sketches showing how the shape of a clastic body can influence subsequent sedimentation.*

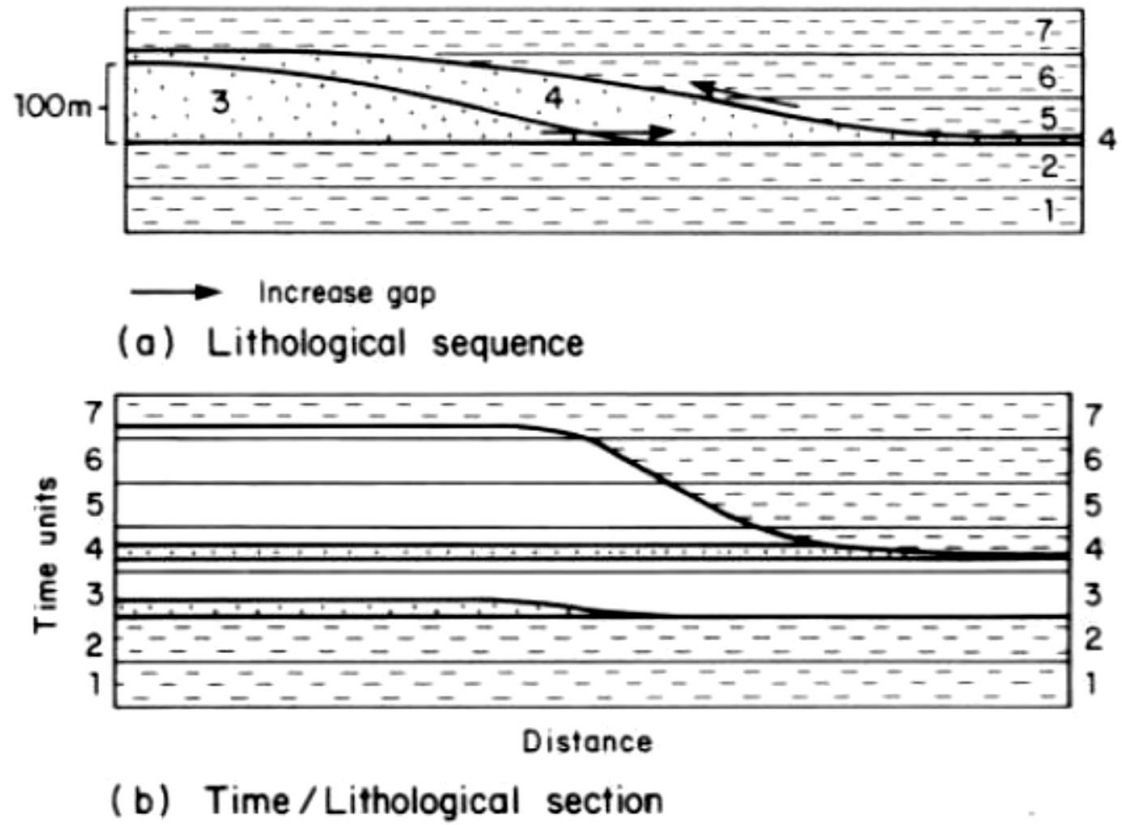

FIGURE 4.6 *Inferred time relationships between sand- and clay-sized grain deposits in a deep-water depositional environment.* (a) *Thickness relationships.* (b) *Time relationships.*

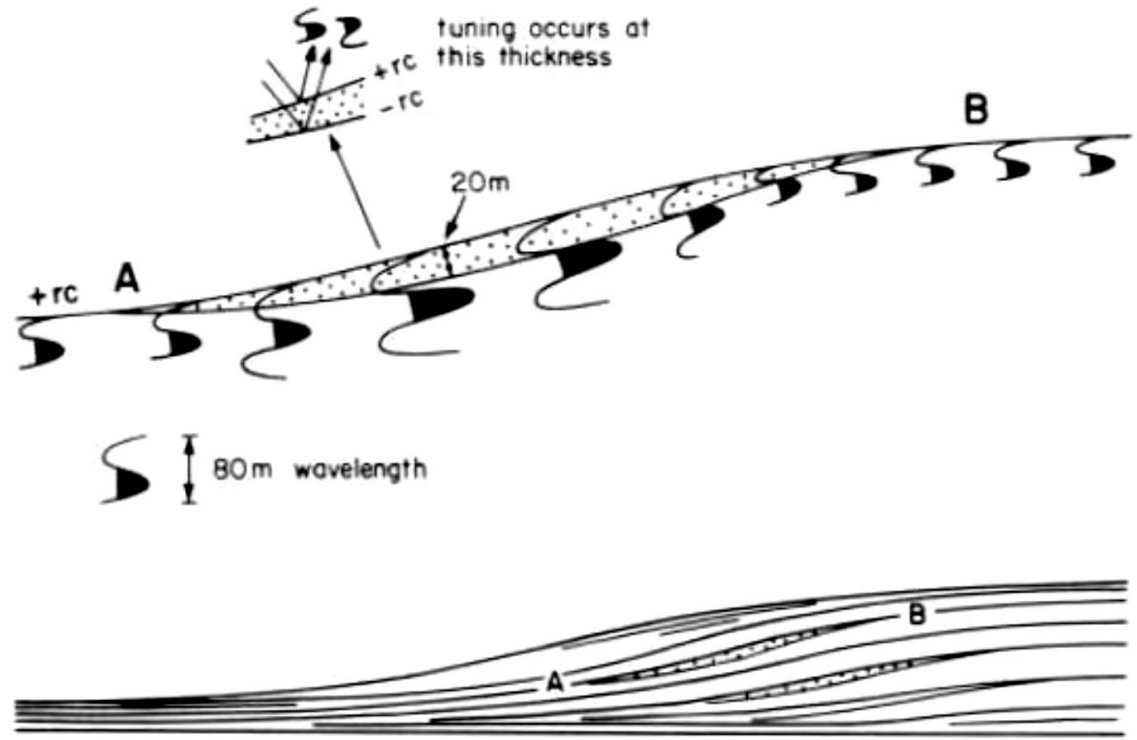

FIGURE 4.9 *Seismic response of clastic units in a shallow-water prograding sequence. Within the range of typical seismic frequencies and interval velocities, most individual shallow-water clastic units must be thinner than the half-wavelength limit for no interference between reflections from the unit's top and base.*

1. Seismic reflections tend to be generated from upper and lower surfaces of units and tend to follow a mixture of gaps and time lines. If internal structure is present (e.g., large scale clinoforms), reflections from both the top and base will both follow unconformities.
2. Reflections follow lithological boundaries but not facies boundaries. Lateral facies change usually results in a change of amplitude, waveform or spacing, and continuity.
3. Where thick clastic units form a submarine fan type of deposit in deep-water depositional settings, reflections from upper surfaces and internal structures follow gaps. Reflections from the base of turbiditic clastic intervals may approximate time lines.
4. In shallow-water clastic environments, most individual units are so thin that they fall between the quarter-wavelength tuning thickness and the limit typically required to produce a reflection (about 1/30 wavelength). Such reflections will vary only in amplitude as thickness changes.
5. In argillaceous sequences, reflections result primarily from interference and approximately parallel time lines.

Seismic Stratigraphy

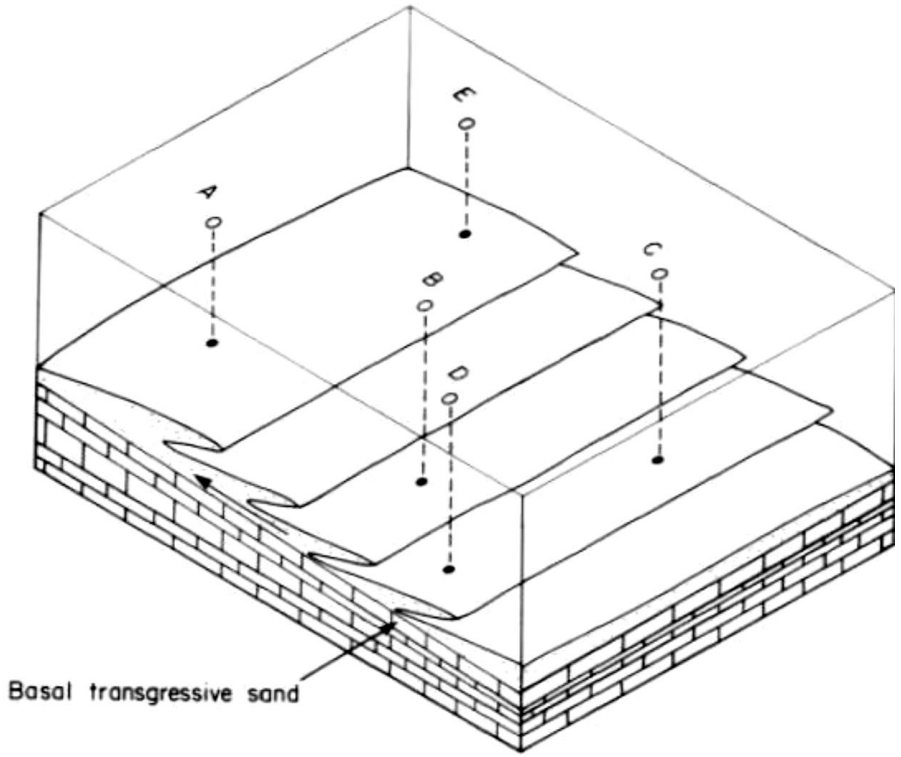

FIGURE 4.12 *Block diagram showing a series of onlapping basal sands. Only wells drilling sands of the same age should be correlated; for example,* A *and* E, *but not* A *and* D.

TABLE 4.1 *Terminology proposed by Exxon explorationists to describe reflection terminations, reflection configurations, and geometry of seismic facies*

Reflection terminations (at sequence boundaries)	Reflection configurations (within sequences)	External forms (of sequences and seismic facies units)
Lapout	Principal stratal configuration	Sheet
Baselap	Parallel	Sheet drape
Onlap	Subparallel	Wedge
Downlap	Divergent	Bank
Toplap	Prograding clinoforms	Lens
Truncation	Sigmoid	Mound
Erosional	Oblique	Fill
Structural	Complex sigmoid-oblique	
Concordance	Shingled	
(no termination)	Hummocky clinoform	
	Chaotic	
	Reflection-free	
	Modifying terms	
	Even — Hummocky	
	Wavy — Lenticular	
	Regular — Disrupted	
	Irregular — Contorted	
	Uniform — Variable	

NOTE: Reprinted by permission of the AAPG from Mitchum, R. M., Vail, P. R., and Thompson, S., 1977, The depositional sequence as a basic unit for stratigraphic analysis, *in* Payton, C. E., Seismic stratigraphy—applications to hydrocarbon exploration: Am. Assoc. Pet. Geol. Mem. 26.

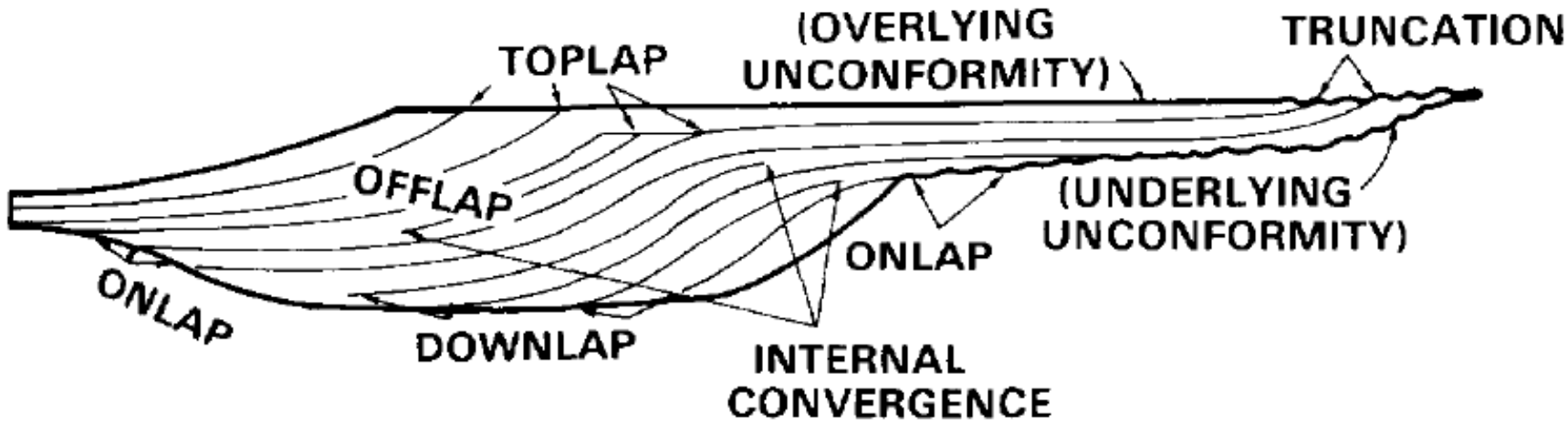

FIG. 1—Seismic stratigraphic reflection terminations within idealized seismic sequence.

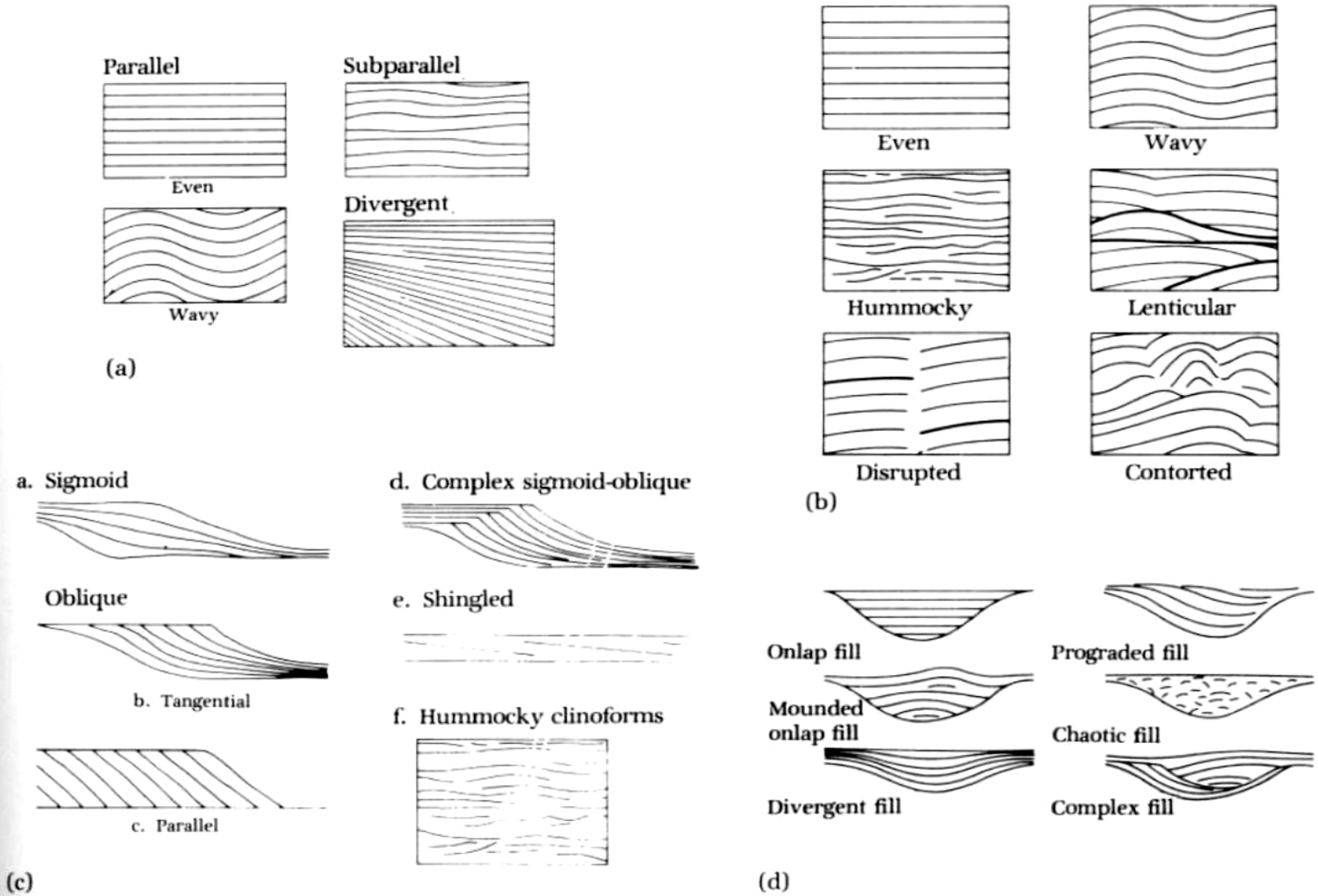

FIGURE 4.15 *Examples of diagnostic reflection configurations.* (a) *Parallel, subparallel, and divergent seismic configurations.* (b) *Modifying seismic reflection configurations.* (c) *Seismic reflection patterns interpreted as prograding clinoforms.* (d) *Fill seismic facies units. Reprinted by permission of the AAPG from Mitchum, Vail, and Sangree, 1977, figs. 4, 6, 11, 15, pp. 123, 125, 130, 133.*

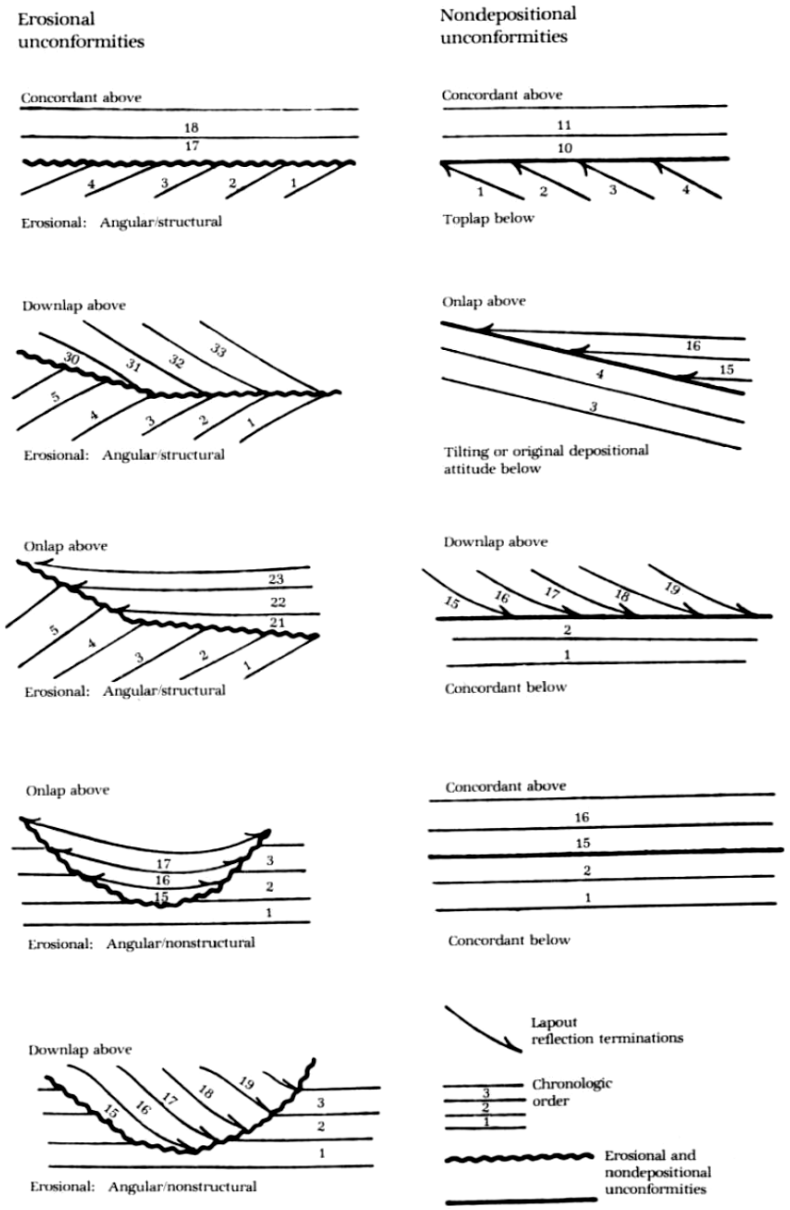

FIGURE 4.16 *Seismic reflection configurations that define unconformities. Reprinted by permission of the AAPG from Brown and Fisher, 1980, fig. 46, p. 82.*

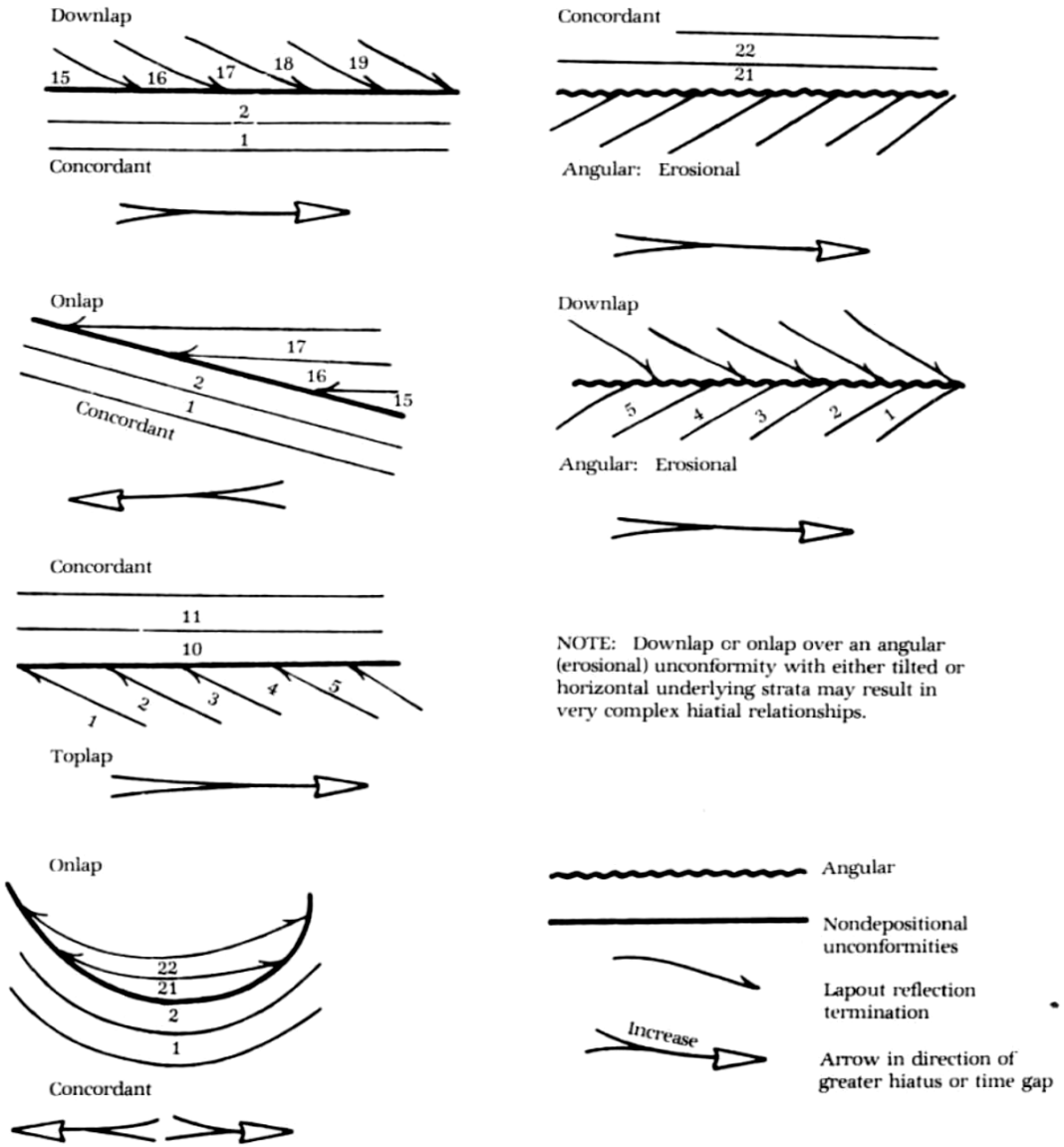

FIGURE 4.17 *Inferring the relative magnitude of a hiatus using seismic-reflection configurations. Reprinted by permission of the AAPG from Brown and Fisher, 1980, fig. 47, p. 83.*

stratigraphic formations, which are based on lithostratigraphy and are commonly time diachronous.

Seismic interpretation using these concepts has become

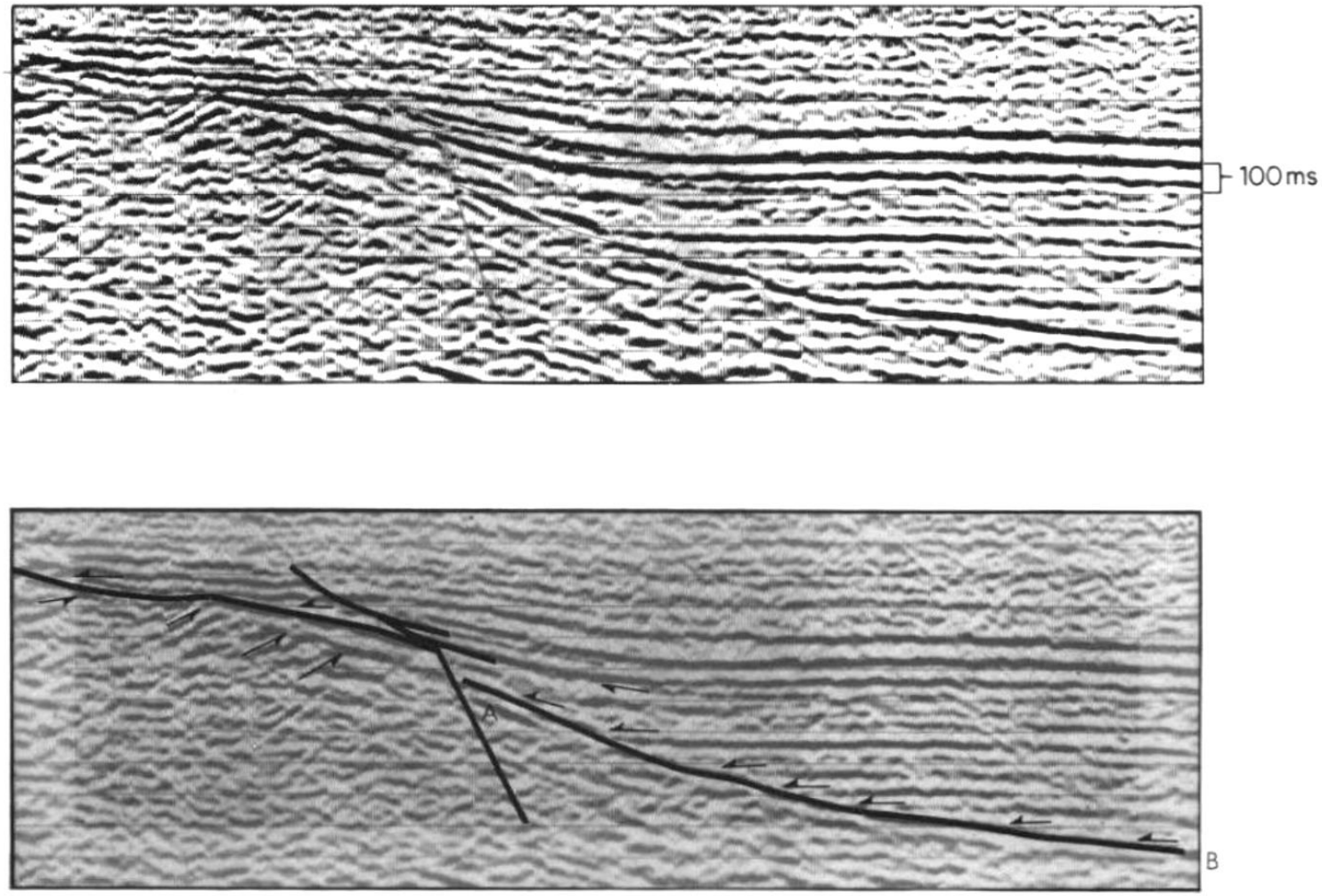

FIGURE 4.18 *Seismic section showing onlap onto a inclined surface. The code shown in figure 7.4 has been used to mark the reflector terminations. Note the possible small-scale, detached, listric, normal fault with associated reverse drag within the onlapping sequence. Courtesy Norsk Hydro.*

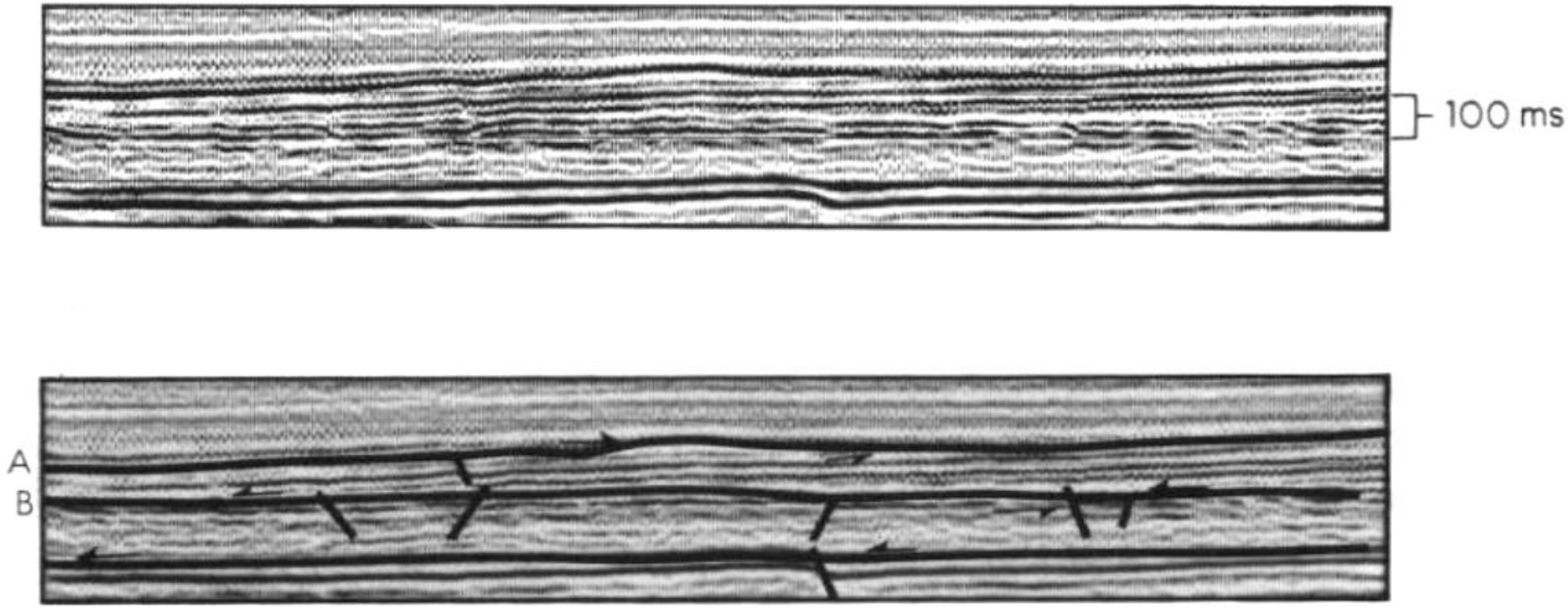

FIGURE 4.19 *Seismic section showing two sequence boundaries,* A *and* B, *with an intervening depositional sequence exhibiting downlap onto* B *and truncation or toplap against* A. *Courtesy Merlin Profilers Ltd.*

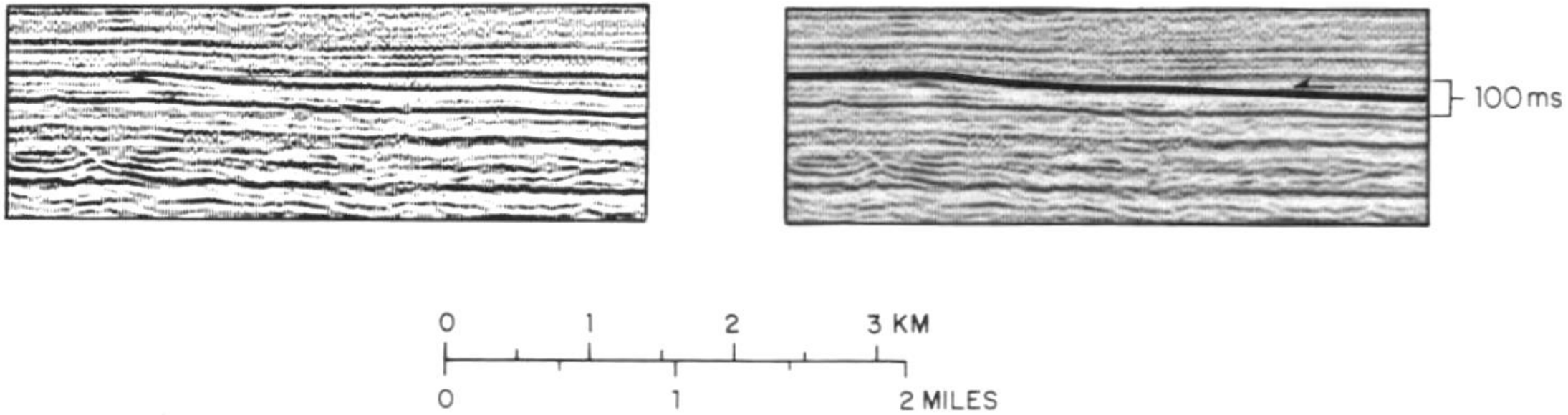

FIGURE 4.20 *Seismic section showing subtle low-angle onlap. Courtesy Merlin Profilers Ltd.*

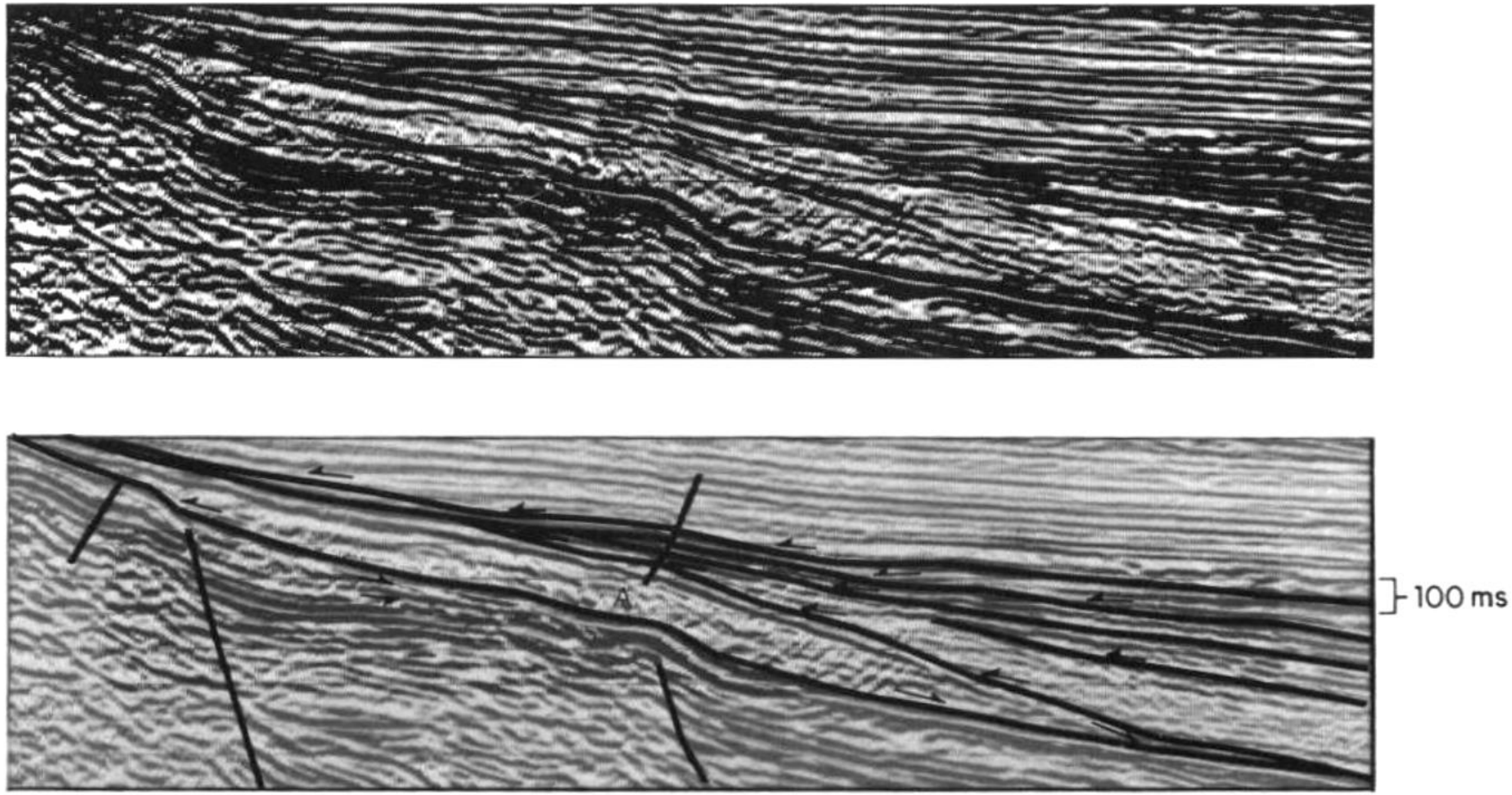

FIGURE 4.21 *Seismic section showing a downlapping sequence* A, *onlapped by a sequence exhibiting complex internal reflection configuration. Courtesy Merlin Profilers Ltd.*

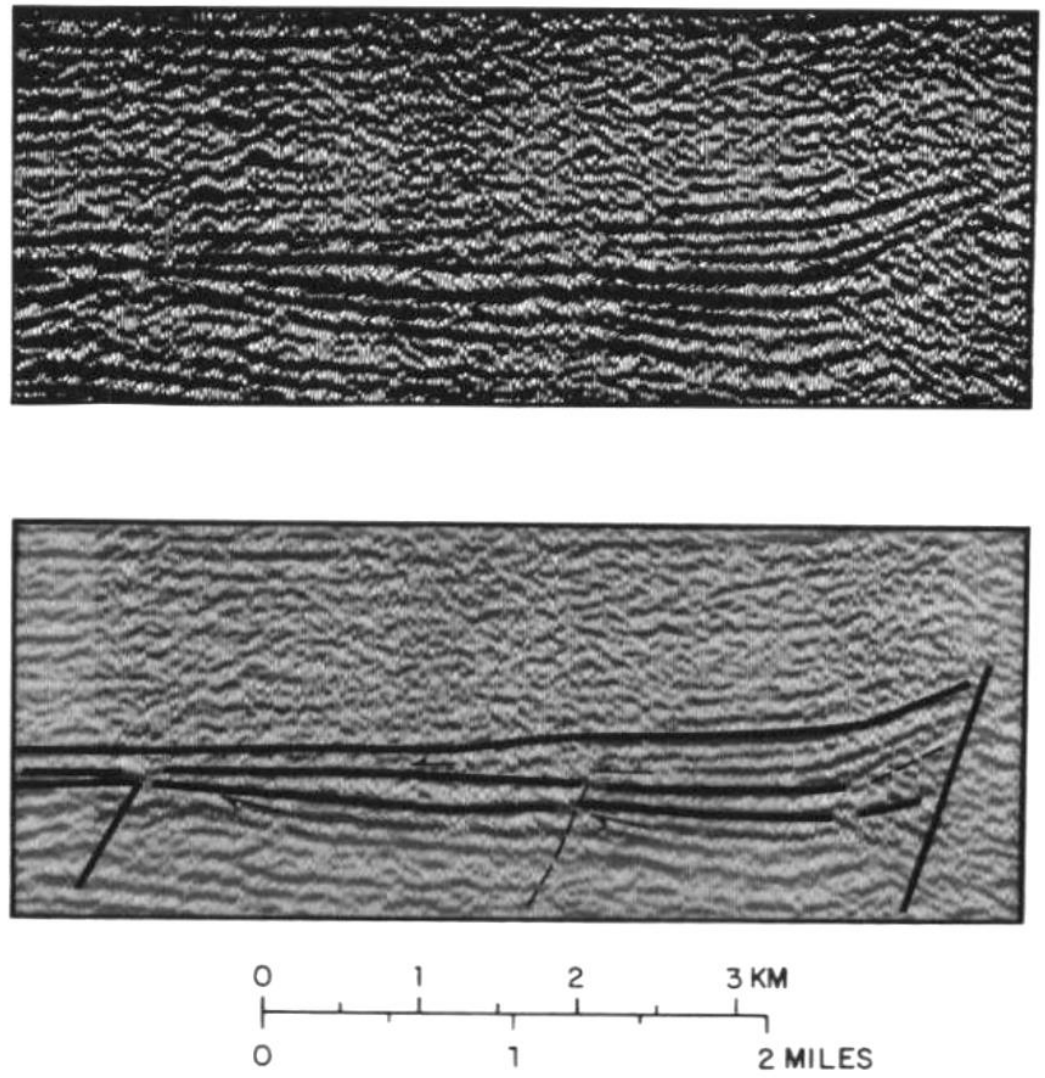

FIGURE 4.22 *Seismic section showing a prograding wedge, developed along a fault scarp, downlapping onto an underlying sequence boundary. Courtesy Norsk Hydro.*

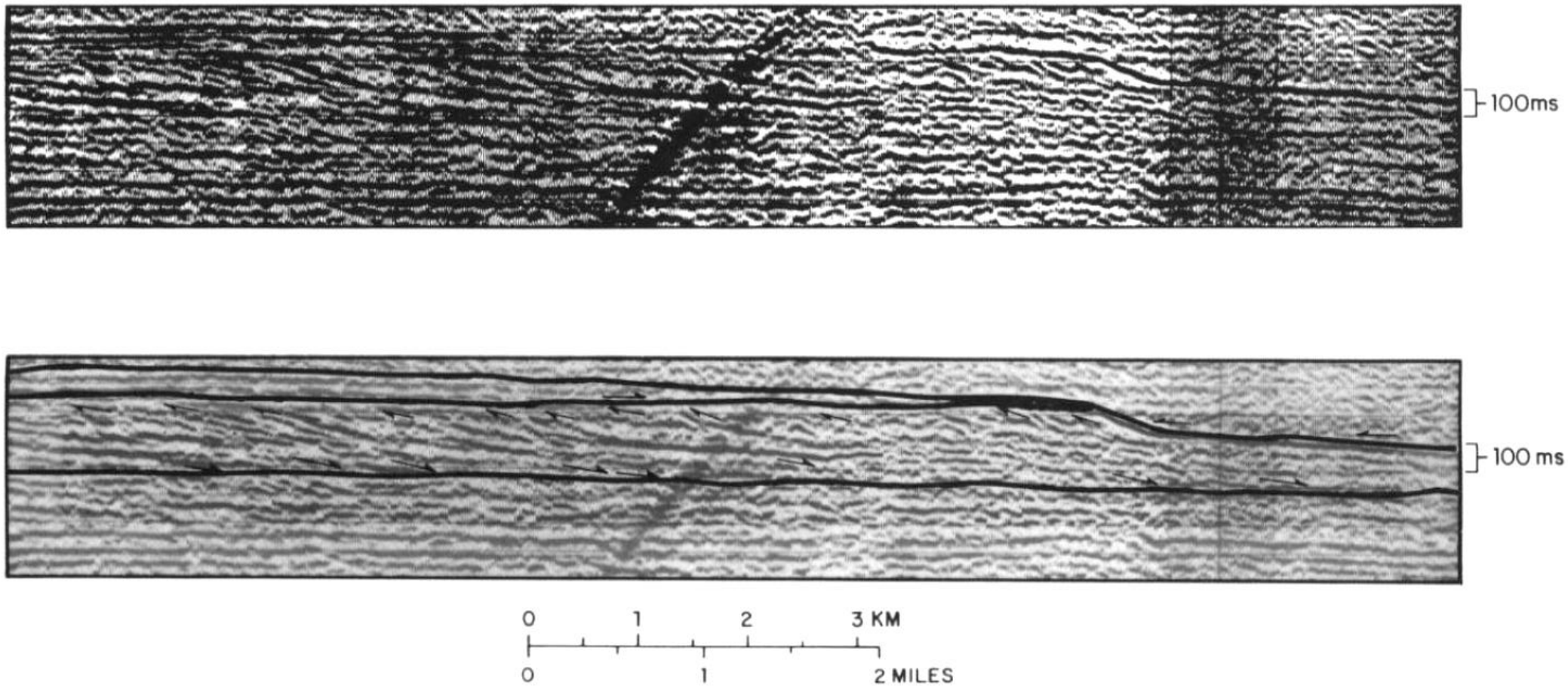

FIGURE 4.23 *Seismic example of a prograding sequence showing toplap, baselap, sigmoidal clinoform pattern, and onlap onto the foreset edge of the sequence. Courtesy Saga Petroleum*

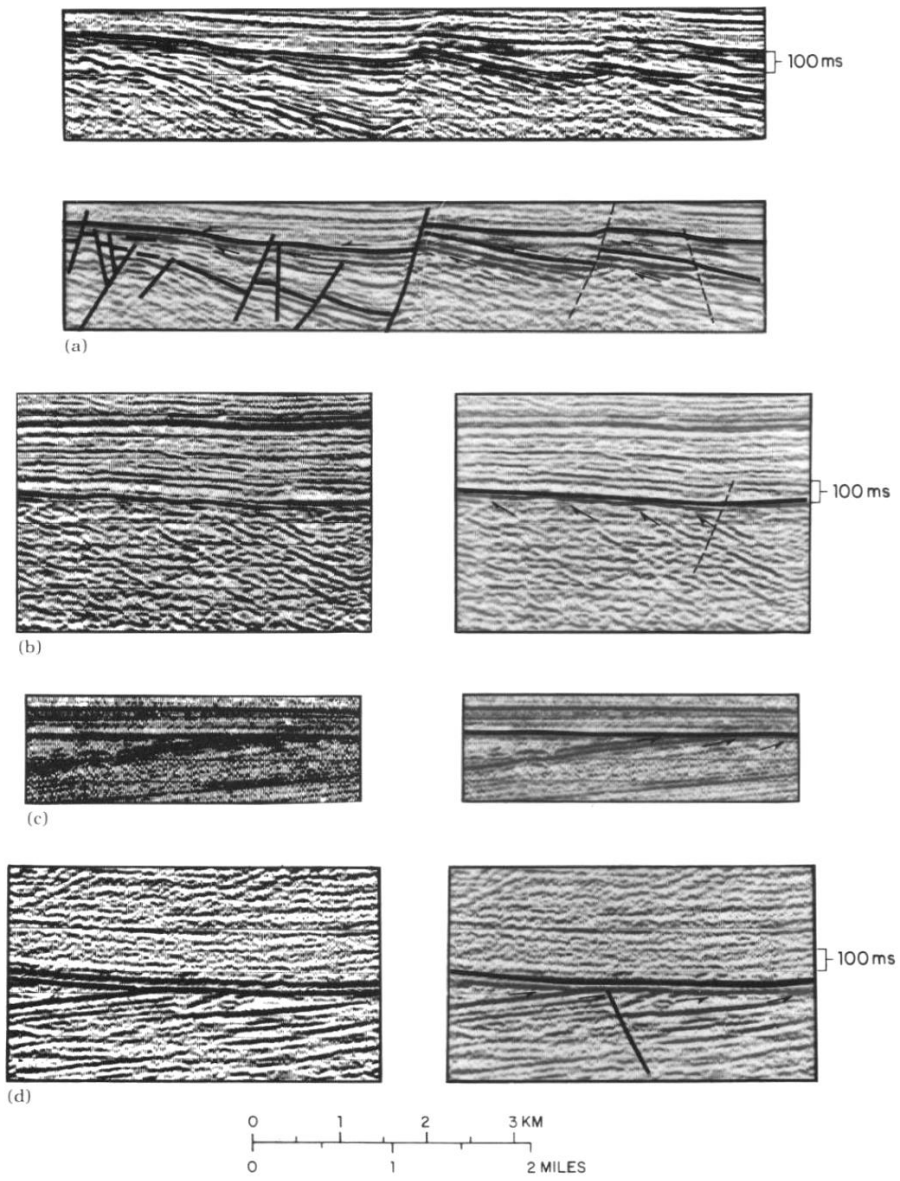

FIGURE 4.24 *Seismic examples of erosional truncation.* a, b, *and* d, *courtesy Merlin Profilers Ltd.;* c, *courtesy Norsk Hydro.*

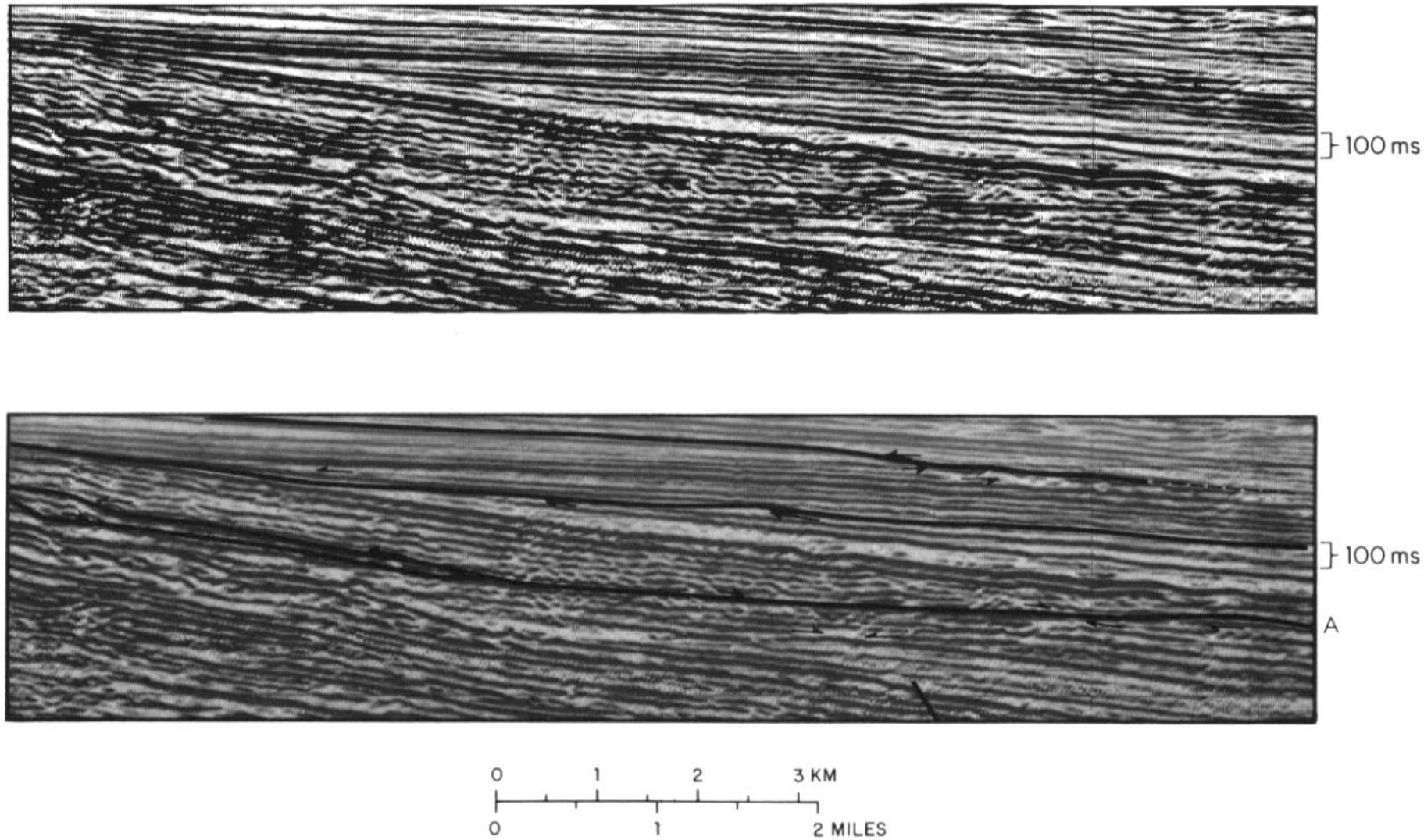

FIGURE 4.25 *Seismic example showing onlap and truncation associated with an inclined sequence boundary A. Courtesy Merlin Profilers Ltd.*

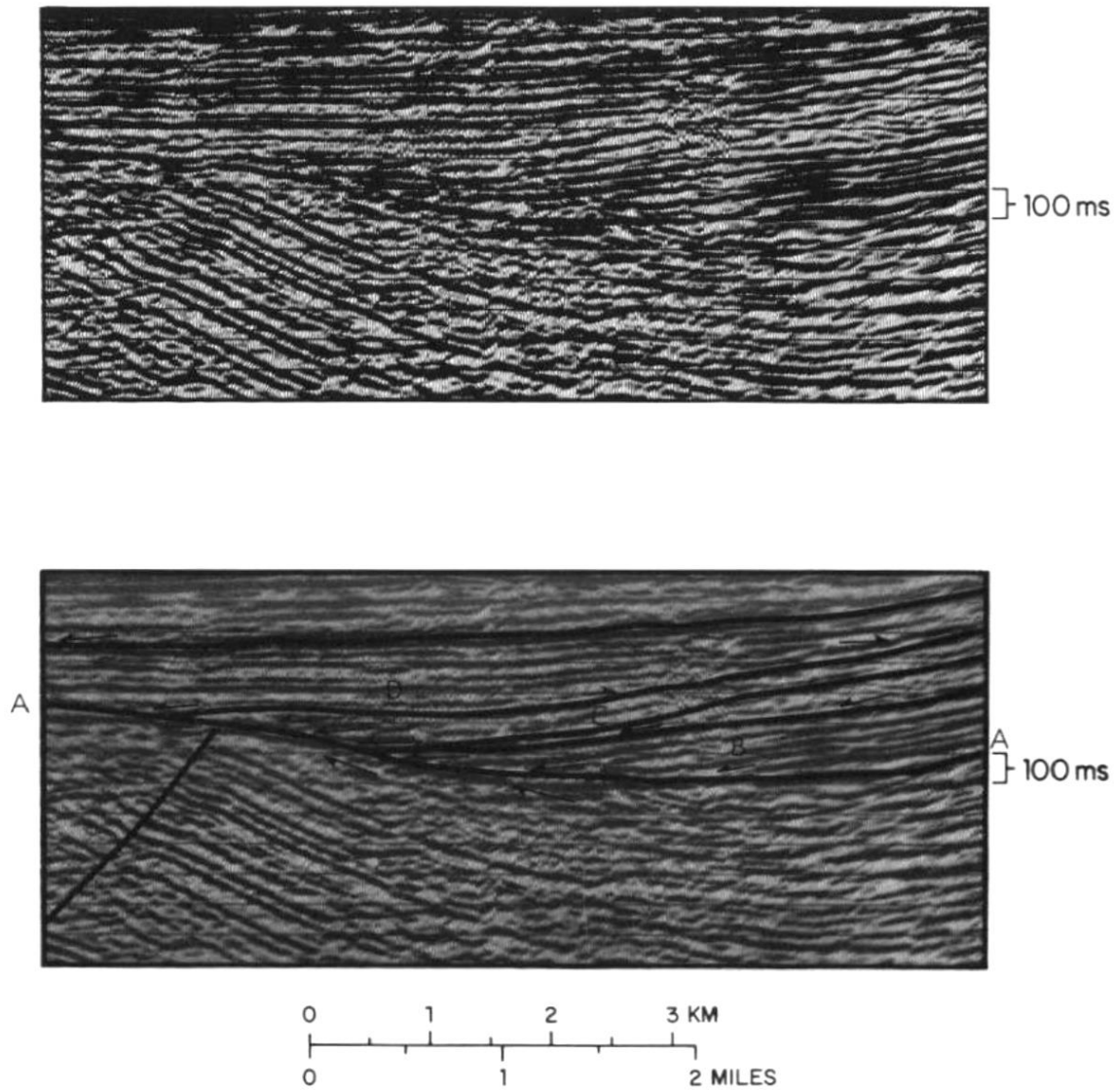

FIGURE 4.26 *Seismic example showing a subcrop sequence truncated beneath an unconformity* A, *which is downlapped by sequences* B *and* C. *Sequence* C *is onlapped from the left by sequence* D. *Courtesy Merlin Profilers Ltd.*

TABLE 4.2 *Seismic reflection parameters used in seismic stratigraphy, and their geological significance*

Seismic facies parameters	Geologic interpretation
Reflection configuration	Bedding patterns Depositional processes Erosion and paleotopography Fluid contacts
Reflection continuity	Bedding continuity Depositional processes
Reflection amplitude	Velocity-density contrast Bed spacing Fluid content
Reflection frequency	Bed thickness Fluid content
Interval velocity	Estimation of lithology Estimation of porosity Fluid content
External form and areal association of seismic facies units	Gross depositional environment Sediment source Geologic setting

NOTE: Reprinted by permission of the AAPG from Mitchum, R. M., Vail, P. R., and Thompson, S., 1977, The depositional sequence as a basic unit for stratigraphic analysis, *in* Payton, C. E., Seismic stratigraphy—applications to hydrocarbon exploration: Am. Assoc. Pet. Geol. Mem. 26.

TABLE 4.3 *Summary of seismic facies characterized by parallel and divergent reflection configurations*

Properties of seismic facies	Depositional environments/Settings			
	Shelf/Platform	Delta platform: DELTA FRONT/DELTA PLAIN	Alluvial plain/ Distal fan delta	Basinal plain
Reflection configuration	Parallel/slightly divergent; highly divergent near rare growth faults	Parallel/slightly divergent on shelf; highly divergent near growth faults in deep-water deltas	Parallel, generally grades basinward into delta plain or into shelf/platform facies	Parallel/slightly divergent; may grade laterally into divergent fills or mounds
Lithofacies and composition	Alternating neritic limestone and shale; rare sandstone; undaform deposits	Shallow marine delta front sandstone/shale grading upward into subaerial delta plain shale, coal, sandstone channels; prodelta facies excluded except where toplap is absent; undaform deposits	Meanderbelt and channel-fill sandstone and floodbasin mudstone; marine reworked fan delta sandstones/profan shale; undaform deposits	Alternating hemipelagic clays and siltstone; calcareous and terrigenous composition; fondoform deposits
Geometry and structure	Sheetlike to wedge-shaped or tabular; very stable setting; uniform subsidence	Sheetlike to wedge-shaped or tabular on shelf-prismatic to lenticular basinward of subjacent shelf edge with growth faults and roll-over anticlines; relatively stable, uniform subsidence on shelf; rapid subsidence and faulting in deep-water delta	Sheetlike to wedge-shaped (individually elongate ribbons or lobes), commonly tilted and eroded	Sheetlike to wedge-shaped; may be slightly wavy or draped over subjacent mounds; generally stable to uniform subsidence; may grade laterally into active structural areas
Lateral relationships	May grade landward into coastal facies and basinward into shelf-margin carbonate facies; local carbonate mounds	May grade landward into alluvial systems and basinward into prodelta/slope clinoforms (on shelf) or growth-faulted prodelta/slope facies (deep-water setting)	Grade landward into reflection-free, high sandstone facies; alluvial facies grade basinward into upper delta plain; fan delta facies grade basinward into shelf/platform or into slope clinoforms	Commonly grades shelfward into mounded turbidites, or slope clinoforms; may grade laterally into deep-water mounds or fills
Nature of upper/lower boundaries	Concordant, coastal onlap and/or baselap over upper surface; upper surface may be eroded by submarine canyons; basal surface concordant, low-angle baselap or (rare) toplapped by subjacent clinoforms	Normally concordant at top but may be rarely onlapped or baselapped; upper surface may be eroded by submarine canyons; basal surface generally toplapped by prodelta/slope clinoforms (on shelf); rarely concordant with prodelta on shelf but common in deep-water, roll-over anticlines	Upper surface may be onlapped by coastal facies; top may be angular unconformity; base in generally concordant; fan deltas rarely overlie clinoforms (toplap)	Generally concordant at top and base; may onlap eroded slope clinoforms or eroded mounds; upper surface rarely eroded
Amplitude	High	High in delta front and coal/lignite or marine transgressive facies within delta plain; low/moderate in most delta plain and in prodelta where in continuity with delta front	Variable—low/high	Low to moderate
Continuity	High	High in delta front, coal/lignite and marine transgressive facies; low/moderate in remainder of delta plain and prodelta where in lateral continuity with delta front	Discontinuous; continuity decreases landward	High
Frequency (cycle breadth)	Broad or moderate; little variability	Variable; broader in delta front; coal/lignite and marine transgressive facies moderate; narrower in other delta plain and prodelta where in continuity with delta front	Variable; generally narrower cycles than shelf/platform	Generally narrower than shelf/platform; commonly very uniform breadth throughout

SOURCE: Adapted from Vail, P. R., Todd, R. G., and Sangree, J. B., 1977, Chronostratigraphic significance of seismic reflections, *in* C. E. Payton, Seismic stratigraphy—applications to hydrocarbon exploration: Am. Assoc. Pet. Geol. Mem. 26, 160–168.

TABLE 4.4 *Summary of seismic facies characterized by progradational reflection configurations*

Properties of seismic facies	Depositional environments/Settings	
	Slope: **ASSOCIATED WITH PROGRADING SHELF/PLATFORM**	Prodelta/Slope: **ASSOCIATED WITH PROGRADING SHELF DELTA OR SHELF-MARGIN DELTA; OR** Slope: **ASSOCIATED WITH PROGRADING NERITIC SHELF SUPPLIED PERIODICALLY BY SHELF DELTA/FAN DELTA**
Reflection configuration	Sigmoid clinoforms Progradational in dip profile; parallel to disrupted and mounded in strike profile	Oblique clinoforms Progradational in dip profile; hummocky, progradational to mounded in strike profile; mounds more common in deep-water slope than in prodelta/slope on shelf
Lithofacies and composition	Hemipelagic slope facies in upper/mid-clinoform; submarine fans common in lower clinoform; generally calcareous clay, silt and some sand (base of clinoform); clinoform deposited in deep water beyond shelf edge	*On shelf:* prodelta (upper) and shallow slope facies (mid-clinoform and lower clinoform); deposited on submerged shelf; composition generally terrigenous clay, silt and sand; sand concentrated in submarine fans at base of clinoform *Beyond shelf edge:* (1) prodelta and deep-water slope associated with shelf-margin delta; may be growth-faulted; clay, silt and sand (in basal submarine fans); and (2) deep-water slope associated with prograding neritic shelf supplied periodically by shelf deltas/fan deltas; clay, silt and sand (in basal submarine fans)
Geometry and structure	Lens-shaped slope system; poorly defined individual submarine fans and point sources; strike profile may intersect facies to define parallel to slightly mounded configurations; rarely affected by growth faults; represents low rate of sedimentation under relatively uniform sea level rise and/or subsidence rate	Complex fan geometry with apices at shelf-edge point sources; each submarine fan resembles a bisected cone; total slope system lens- to wedge-shaped; strike profiles intersect fans or cones to display complex mounds; seismic facies deposited rapidly relative to subsidence and/or sea level rise; highly unstable slopes associated with deep-water deltas (growth faults, roll-over anticlines)
Lateral relationships	Grades updip through shelf/platform edge facies into parallel/divergent shelf/platform (undaform) reflections; may grade downdip into basinal plain (fondoform) or mound/drape seismic facies; grades along strike to similar facies; may change landward to oblique facies	Terminates updip against base of delta platform or shelf/platform (undaform) facies and may grade downdip into basinal plain (fondoform), or mound/drape facies; may change basinward into sigmoid facies; grade along strike into mounded facies and locally submarine canyon-fill facies
Nature of upper/lower boundaries	Generally concordant at top and downlap (baselap) terminations at base; upper surface of outer or distal sigmoids may be eroded by submarine erosion and submarine canyons; eroded surface commonly onlapped by continental rise facies	Toplap termination at top and downlap (baselap) termination at base; may contain local or minor submarine erosion/onlap sequences; outer or distal oblique clinoforms commonly eroded by submarine erosion and submarine canyon cutting; eroded surface generally onlapped by continental rise facies
Amplitude	Moderate to high; uniform	Moderate to high in upper clinoform; moderate to low in lower clinoform; highly variable
Continuity	Generally continuous	Generally continuous in upper clinoform; discontinuous in mid-clinoform and lower clinoform; may exhibit better continuity near base
Frequency (cycle breadth)	Broadest in mid-clinoform where beds thickest; uniform along strike	Broadest at top and generally decreases downdip as beds thin; variable along strike

SOURCE: Adapted from Vail, P. R., Todd, R. G., and Sangree, J. B., 1977, Chronostratigraphic significance of seismic reflections, *in* C. E. Payton, Seismic stratigraphy—applications to hydrocarbon exploration: Am. Assoc. Pet. Geol. Mem. 26, 160–168.

TABLE 4.5 *Summary of seismic facies characterized by mounded and draped reflection configuration*

Properties of seismic facies	Depositional environments/Settings		
	Reefs and banks: **SHELF/PLATFORM MARGIN, BACK SHELF PATCH REEFS AND PINNACLE/BARRIER REEFS**	Submarine canyon and lower slope: **PROXIMAL TURBIDITIES, SLUMPED CLASTICS**	Hemipelagic clastics: **PROXIMAL BASIN AND LOWER SLOPE**
Reflection configuration	Mounded, chaotic, or reflector-free; pull-up or pull-down common	Mounded; complex and variable	Parallel; mirrors underlying surface
Lithofacies and composition	Shallow-water carbonate biogenic buildups; may or may not exhibit reef-forming framework	Sand and shale submarine fans; complex gravity-failure fans or mounds; turbidity flow; other grain flows, submarine landslides/debris flows; clinoform/fondoform deposits	Terrigenous and calcareous clays (commonly alternating); pelagic oozes; deposition from suspension plumes and nepheloid clouds; fondoform deposits
Geometry and structure	Elongate lens-shaped (shelf/platform edge and barrier reefs); elongate to subcircular lens-shaped (patch and pinnacle reefs/banks); form on stable structural elements	Irregular fan-shaped to mounded geometry; common but not restricted to unstable basins	Sheet to blanket geometry exhibiting drape over underlying surface; common in deep, subsiding basins
Lateral relationships	Shelf/platform edge facies grade updip into parallel/divergent shelf/platform facies; grade downdip into talus and sigmoid clinoform facies; patch reef/bank facies grade updip and downdip into parallel/divergent shelf/platform facies; pinnacle and barrier facies grade downdip into talus clinoforms and to basinal plain (fondoform) facies	May grade shelfward into progradational clinoforms (normally oblique), canyon onlap fill, or pinch out against eroded slope; may grade basinward and laterally into basinal plain (fondoform); onlap fills or drapes	Commonly grades laterally or basinward into basinal plain (fondoform) facies; may grade shelfward into submarine canyon onlap fill; may onlap eroded slope
Nature of upper/lower boundaries	Upper surface concordant or may be onlapped by flank reflections; basal surface concordant, baselapping, or may overlie clinoform toplap; pull-up or pull-down of basal surface common	Upper surface commonly erosional and onlapped, baselapped, or concordant (with drape); basal surface irregularly baselapping; may appear concordant (low resolution), or may onlap (mounded onlap fill)	Upper surface commonly concordant, but may be onlapped or baselapped; basal surface generally concordant but may onlap eroded mound or slope
Amplitude	High along boundaries; may be moderate to low internally; commonly reflector-free	Variable; generally low; some higher internal amplitudes may be thin hemipelagic drapes	Low to moderate; some high-amplitude reflections (well defined on high-frequency, shallow data)
Continuity	High along boundaries; internally discontinuous to reflector-free	Discontinuous to chaotic	High
Frequency (cycle breadth)	Broad; cycle may diverge into massively bedded buildup	Highly variable; commonly narrow	Narrow, uniform

SOURCE: Adapted from Vail, P. R., Todd, R. G., and Sangree, J. B., 1977, Chronostratigraphic significance of seismic reflections, *in* C. E. Payton, Seismic stratigraphy—applications to hydrocarbon exploration: Am. Assoc. Pet. Geol. Mem. 26, 160–168.

TABLE 4.6 *Summary of seismic facies characterized by onlap and fill reflection configurations*

	Depositional environments/Settings			
Properties of seismic facies	Coastal (paralic) onlap facies	Continental rise: **SLOPE-FRONT FILL AND ONLAP CLASTICS**	Submarine canyon-fill deposits	Other deep-water fill deposits: **MOUNDED, CHAOTIC, STRUCTURALLY ACTIVE BASINS**
Reflection configuration	Parallel; coastal onlap	Parallel/divergent; platform or shelfward onlap	Parallel/divergent; landward and lateral onlap	Parallel/divergent; chaotic, mounded onlap
Lithofacies and composition	Delta/alluvial plain and medial fan delta sands and shales; supratidal clastic/carbonate facies; rarely beach/shoreface clastic facies	Sand and shale deposited in submarine fans by turbidity flows; hemipelagic terrigenous/calcareous clays; distal pelagic oozes	Sand and shale deposited by turbidity flow in submarine fans near base; hemipelagic and neritic shale/calcareous clays in middle and upper sequence, respectively; locally may contain coarse proximal turbidites	Sand and shale deposited by turbidity flow in submarine fans; hemipelagic terrigenous/calcareous clays; pelagic oozes; locally proximal turbidites
Geometry and structure	Sheetlike or tabular; uniform subsidence during deposition; periodic tilting and erosion; deposited near basinal hinge-line during subsidence and/or sea level rise	Wedge-shaped lens; may be fan-shaped or lobate in plan view; slow subsidence	Elongate; lens-shaped in transverse section; may bifurcate updip; pinches out updip; slow subsidence	Variable lens-shaped; commonly irregular; reflects bathymetric configuration of structural depression; slow to rapid subsidence
Lateral relationships	Pinches out landward; grades basinward into lower delta plain, distal fan-delta, or shelf/platform facies; may grade laterally into marine embayment facies	Pinches out updip; grades basinward into basinal plain or hemipelagic drape facies; continuous laterally for tens of kilometers	Pinches out updip and laterally; grades downdip into continental rise mounded turbidites, or large submarine fans	Pinches out in every direction
Nature of upper/lower boundaries	Upper surface commonly tilted, eroded, and onlapped by similar deposits; base of facies onlaps unconformity, commonly angular	Upper surface commonly baselapped by prograding clinoforms; basal surface onlaps updip against eroded slope (and commonly outer shelf); may show baselap basinward against mounds or bathymetric highs	Upper surface may be concordant with overlying shelf or platform reflections or commonly baselapped by prograding prodelta and slope facies; basal surface onlaps updip and laterally; baselap onto basin floor rarely observed	Upper surface may be concordant with hemipelagic drape or baselapped by prograding clinoforms; basal surface onlaps in all directions
Amplitude	Variable; locally high but normally low to moderate	Variable; hemipelagic facies moderate to high; clastics low to moderate	Variable; generally low to moderate	Variable; generally low to moderate
Continuity	Low in clastics; higher in carbonate facies; decreases landward	Moderate to high; continuous reflections in response to hemipelagic facies	Variable; generally low to moderate	Variable; poor in chaotic or mounded fill; high in low-density turbidites and hemipelagics
Frequency (cycle breadth)	Variable; generally moderate to narrow	Narrow; uniform	Variable but generally narrow	Variable; commonly narrow; may increase breadth toward axis of fill

SOURCE: Adapted from Vail, P. R., Todd, R. G., and Sangree, J. B., 1977, Chronostratigraphic significance of seismic reflections, *in* C. E. Payton, Seismic stratigraphy—applications to hydrocarbon exploration: Am. Assoc. Pet. Geol. Mem. 26, 160–168.

Recognizing Lithology

CLAYS AND SILTS

Clays and silts include sediments settled from suspension, whatever the depositional environment. Such sediments tend to be thin bedded and produce closely spaced reflections (relative to other reflection spacings for a particular seismic section) (fig. 4.29). If the depositional area is extensive, the reflections generally show moderate to good continuity. Amplitude tends to be moderate to poor, but is very dependent on bed spacing (interference effects) and lithology. Divergent reflection patterns are diagnostic of fine-grained sediments, as they indicate deposition under conditions where subsidence and sedimentation rates are of similar magnitude.

Not uncommonly, acoustic-impedance contrasts are so low that the interval appears reflection free (fig. 4.29a). Alternatively, destructive interference by beds of a thickness $\frac{1}{30}$ wavelength or less, can also produce reflection-free intervals. Chaotic reflection patterns can result from deep-sea current activity or slumping, and from flowage due to loading, elevated pore pressure, or slope instability (fig. 4.29).

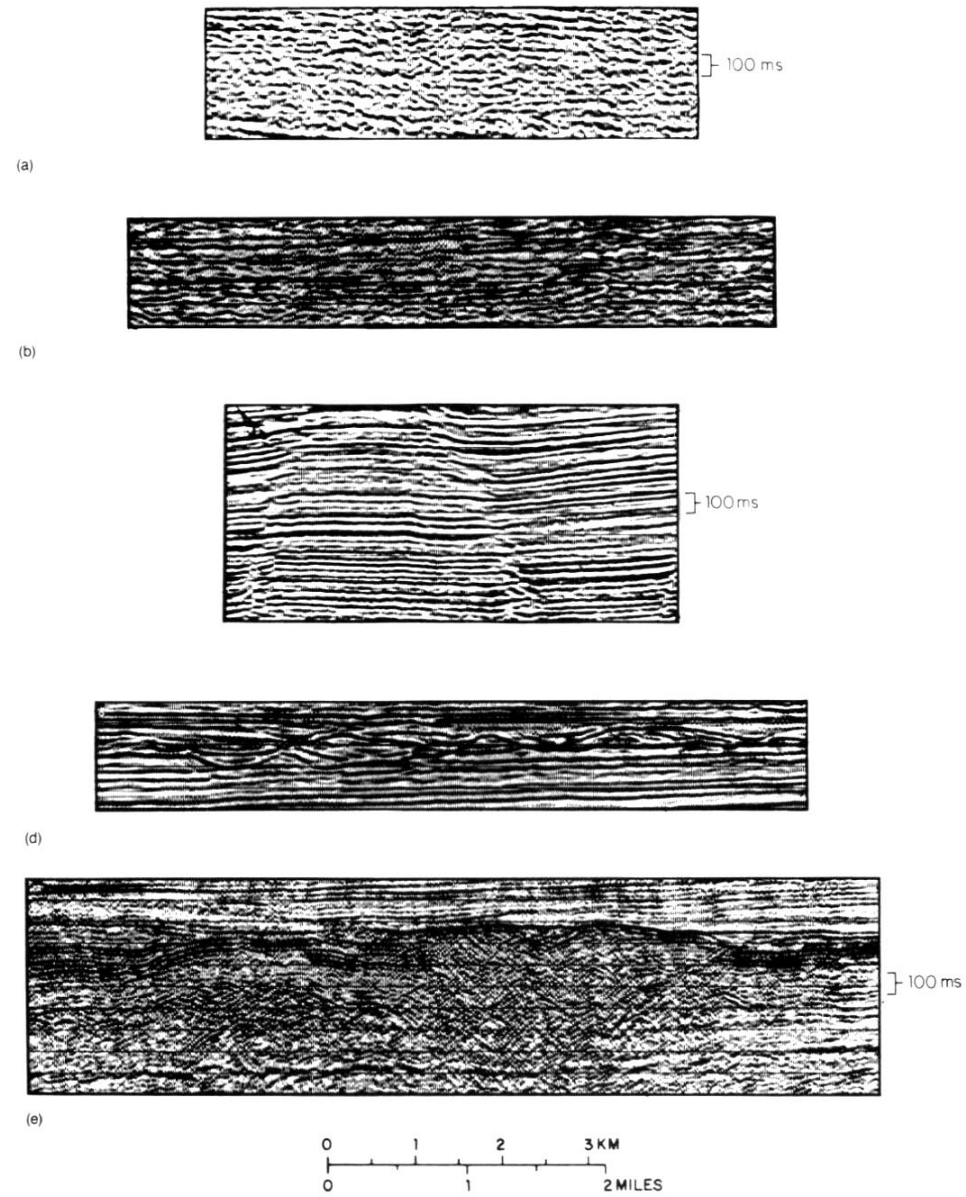

FIGURE 4.29 *Seismic examples of fine-grained sediments.* a *and* e, *courtesy Norsk Hydro;* b, c, *and* d, *courtesy Merlin Profilers Ltd.*

CLASTICS

Clastics are the group of lithologies that every interpreter would like to be able to identify with certainty, but they appear in a great variety of thicknesses, shape, and lateral extent. They are deposited in all environments. Sangree and Widmier (1977) discuss seismic criteria from the interpretation of clastic facies and Anstey (1980b) devotes a short book to the topic.

Interval velocity is not a good indicator (fig. 4.3). The depositional setting is usually the best guide; and here we rely heavily on configuration, internal structure, and facies association. Assuming that the deposits are thick enough to be resolved, deeper-water clastic facies can be characterized by mounded configurations and/or sheet-like forms. Because of their high accumulation rates, clastics have the ability to modify the topography of the basin floor and thus influence the deposition of succeeding sediments. Figures 4.30b and 4.30c show examples of what are interpreted to be mounded clastic facies.

In shallow-water depositional settings, individual clastic units tend to be thin, often below the thinnest required for seismic resolution, and their presence has to be

inferred from depositional setting and amplitude variations (see, e.g., fig. 4.28). As a generalization, Sangree and Widmier (1977) suggest that oblique progradational sequences are more sand prone than sequences with sigmoidal internal structure. Figure 4.31 shows a part of the edge of a thick (>400 m) shallow-water clastic complex that has a sheet-like form and gently inclined clinoforms. The complex has a tapered edge that is onlapped by basinal shales. In a shallow-water environment, internal structure may be the product not only of depositional processes but also of erosional or reworking processes. Figure 4.30d shows part of the same clastic complex; and, although the interval is about 400 m thick, internal reflections are entirely lacking and seismic character here is totally nondiagnostic.

More typical, however, is the case in figure 4.31a, a seismic section across part of the giant Oseberg field, offshore Norway, where the clastic target interval lacks any diagnostic features. The reservoir interval, middle Jurassic Brent Gp. sandy sequence, although more than 100 m thick, has a sheet-like external form, and is too thin to produce seismic features diagnostic of its clastic nature.

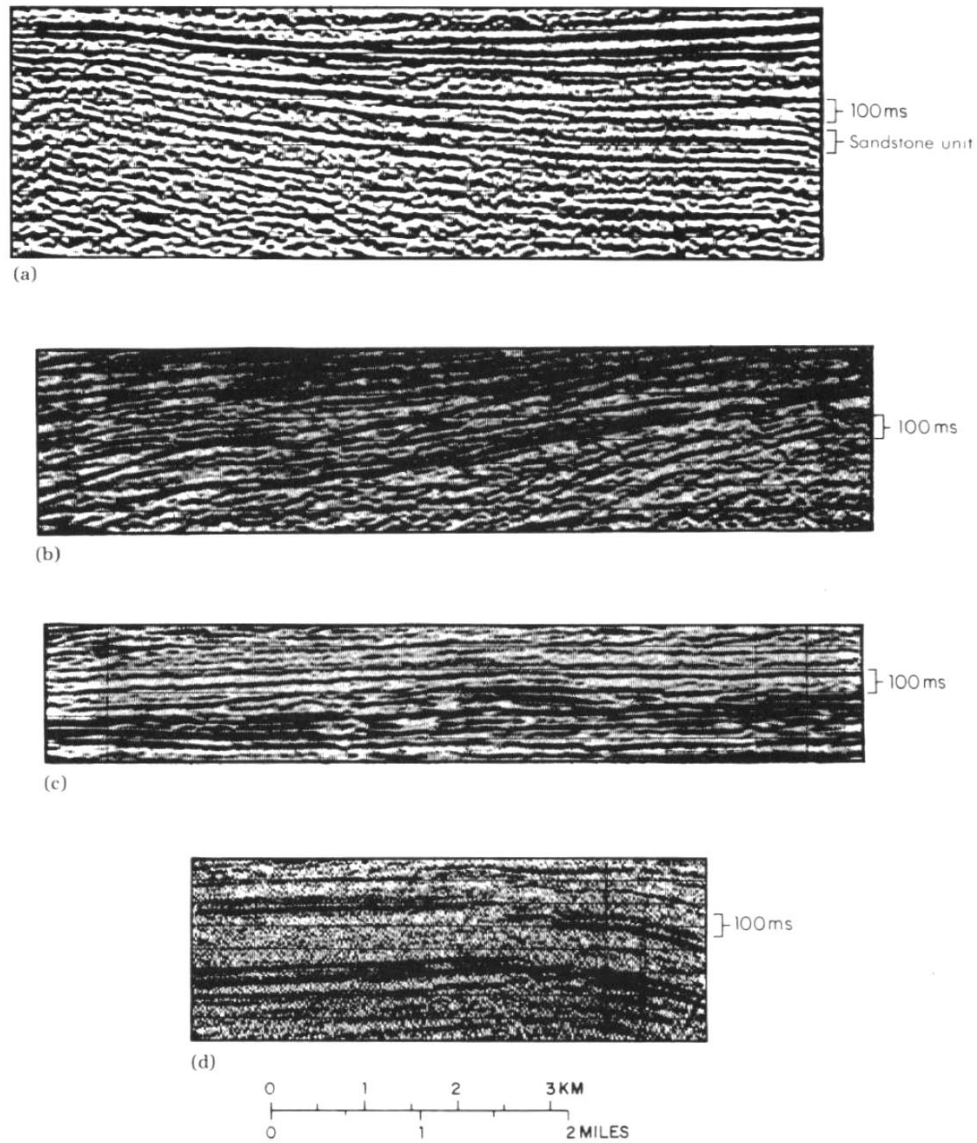

FIGURE 4.30 *Seismic examples of clastic facies.* a *and* d, *courtesy Norsk Hydro;* b *and* c, *courtesy Merlin Profilers Ltd.*

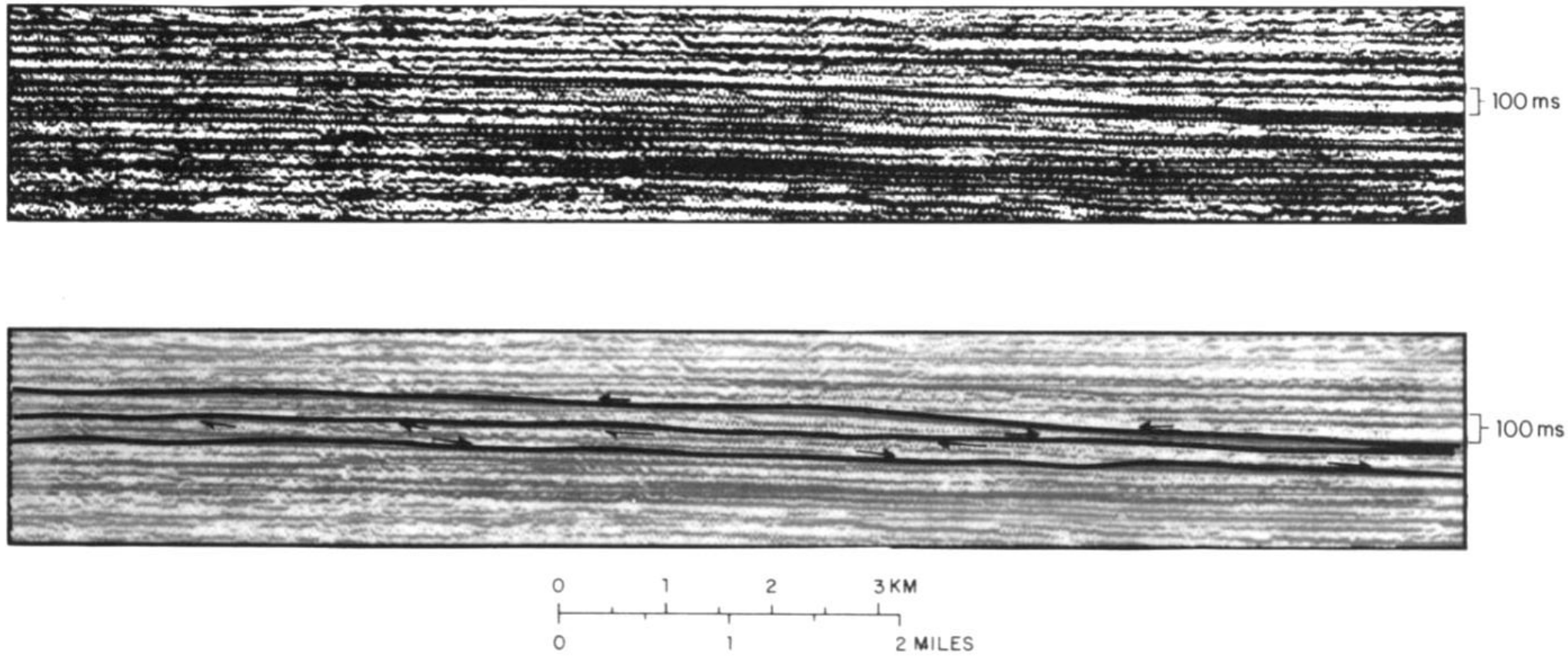

FIGURE 4.31 *Seismic section across a major shallow-marine clastic complex. The tapered profile is typical of clastic deposits. Courtesy Norsk Hydro.*

CARBONATES

Normally, reflections from the top boundary of a carbonate unit have a large positive reflection coefficient because carbonates usually have high velocity and density compared to other common sedimentary rocks. Only in cases where the carbonates are very porous or fractured are reflection coefficients of upper boundaries likely to be negative. The usually high interval velocity introduces a potential resolution problem. Not only do thick sequences appear thin in time on seismic sections due to high velocities but the minimum thickness required for adequate vertical resolution can be quite high. Interval velocities

From a seismic viewpoint, carbonates can be conveniently divided into three groups:

1. Sheet-like deposits: These are often extremely extensive laterally and consist of fine-grained carbonate particles or calcareous microfossils deposited from suspension (e.g., micritic limestones, chalk, calcareous claystones, etc.). These deposits show characteristics similar to those of other fine-grained deposits but can usually be recognized by their high amplitudes, good continuity, and—if thick enough—by high interval velocities, which are rarely less than 3500 m/s. Mistaking volcanic ash or tuff beds for carbonates is a potential interpretation pitfall. Tuff beds have high interval velocities and are laterally extensive, producing a seismic response similar to that of bedded carbonates.

2. Bioclastic deposits: Consisting of sand-sized carbonate grains transported and deposited by high-energy currents, these will have the same form and depositional setting as other noncarbonate clastics. Bioclastics may possibly be identified by their expected higher interval velocity and higher reflection amplitudes. Other considerations, such as the paleogeography and other recognizable associated lithologies may aid an identification. In many cases, however, it may be impossible to differentiate between bioclastics and noncarbonate clastics.
3. Buildups, reefs, biotherms, banks, mounds, etc.: This type of deposit has a large biological element comprising the skeletal remains of living organisms. These deposits are usually characterized by shape and high interval velocity. Figure 4.32 shows reflection configuration criteria for recognizing carbonate buildup on seismic profiles. Bubb and Hatlelid (1977) subdivided carbonate buildups into four major types (fig. 4.33):
   i. Barrier buildups—tending to be linear with relatively deep water on both sides during deposition.
   ii. Pinnacle buildups—roughly equidimensional features surrounded by deep water during deposition.
   iii. Shelf margin buildups—linear features with deep water on one side and shallow water on the other.
   iv. Patch buildups—usually formed in shallow water, either in close proximity to shelf margins, or over broad, shallow seas.

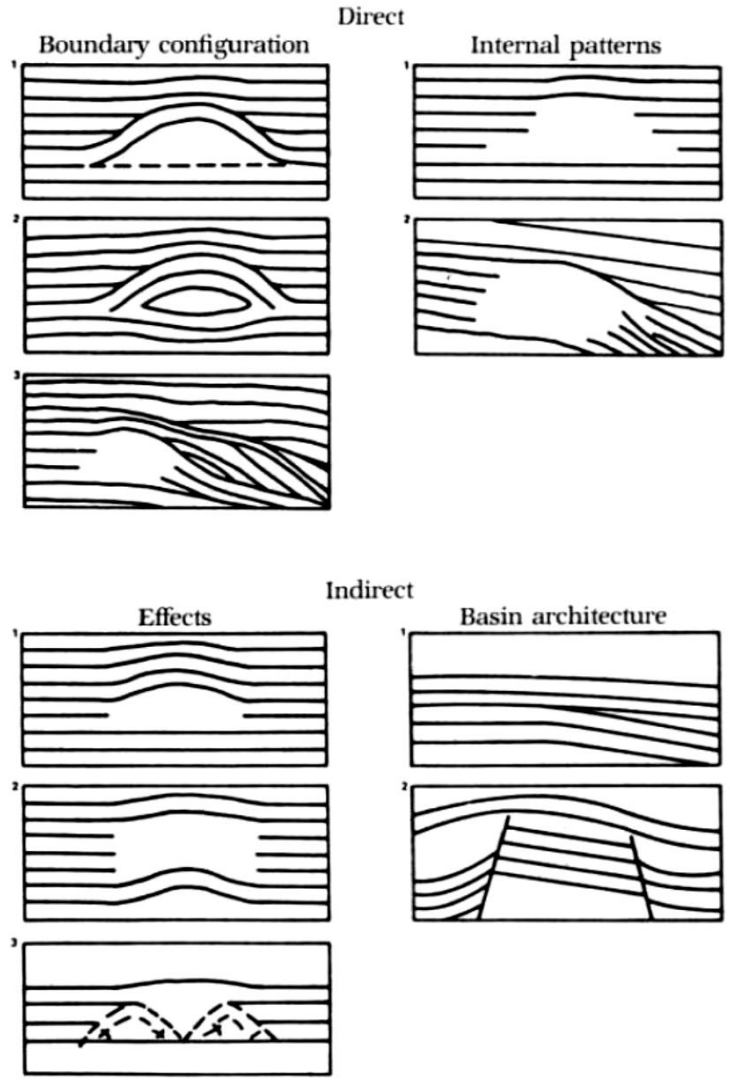

FIGURE 4.32 *Carbonates: Examples of diagnostic reflection configurations. Reprinted by permission of the AAPG from Bubb and Hatlelid, 1977, fig. 3, p. 188.*

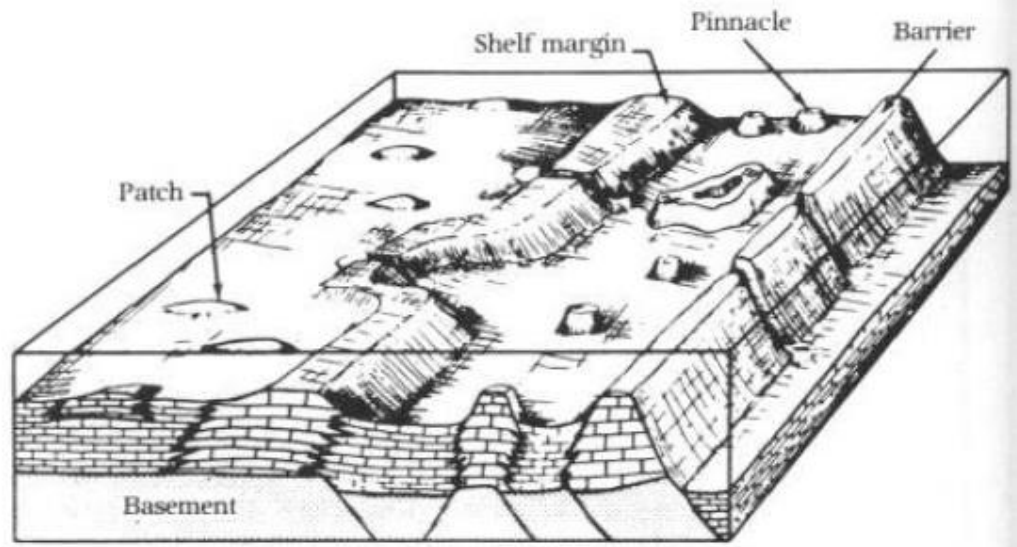

FIGURE 4.33 *Types of carbonate buildups most easily recognizable using seismic data. Reprinted by permission of the AAPG from Bubb and Hatlelid, 1977, fig. 1, p. 186.*

Figure 4.34 shows a carbonate shelf buildup from the Aptian/Albian of Rodessa-Mooringsport Fm. of central Louisiana. The back shelf margin to the north consists of an interbedded sequence of limestone and shales, with a seismic response of parallel high-frequency, low-amplitude reflections. The shelf margin buildup consisting of high-energy porous deposits, has poorly developed interval reflections. The basinal area to the south, consisting of fine-grained calcareous deposits, is characterized by downlap and lateral amplitude variations. Figure 4.35 shows a seismic profile through an Upper Jurassic patch buildup or reef in the Smackover of the U.S. Gulf Coast. The reef, 30–40 m thick, with a lateral extent of several square kilometers, is associated with a dim spot on the Smackover reflection.

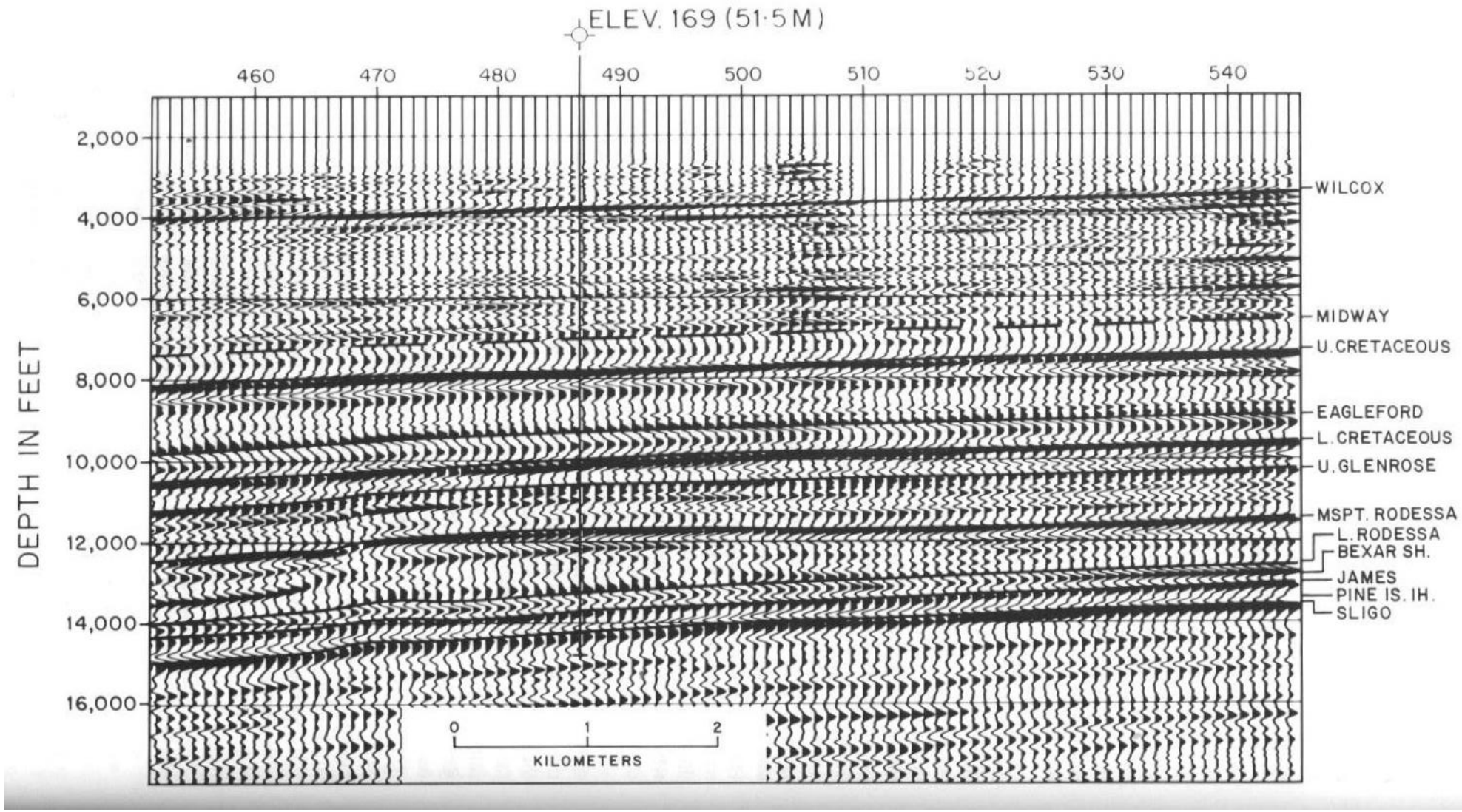
ELEV. 169 (51·5 M)
460
470
480
490
500
510
520
530
540
2,000
4,000
6,000
8,000
10,000
12,000
14,000
16,000
DEPTH IN FEET
WILCOX
MIDWAY
U. CRETACEOUS
EAGLEFORD
L. CRETACEOUS
U. GLENROSE
MSPT. RODESSA
L. RODESSA
BEXAR SH.
JAMES
PINE IS. IH.
SLIGO
0
1
2
KILOMETERS

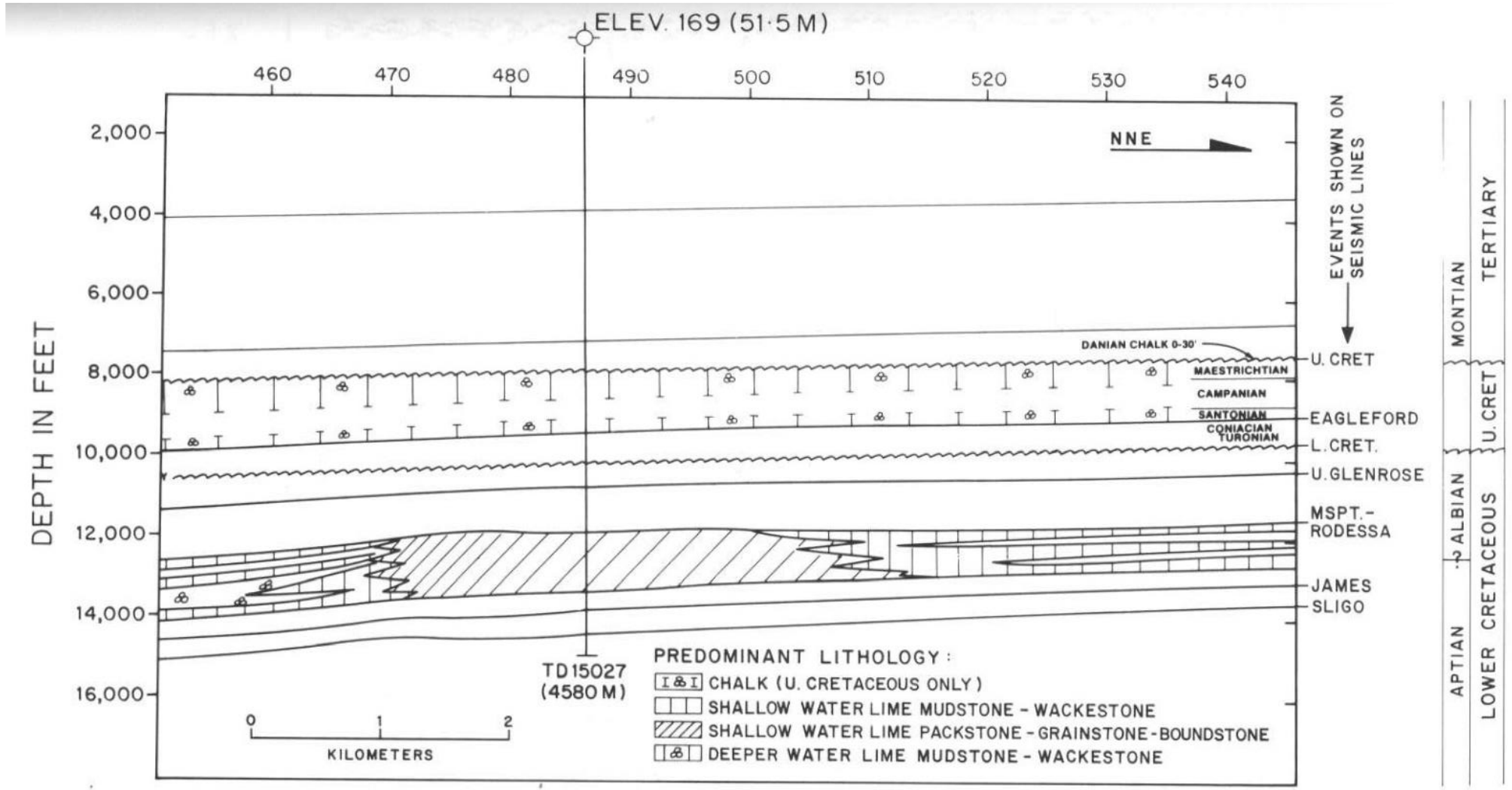

FIGURE 4.34 *Seismic and geological cross-sections across the Cretaceous carbonate shelf, Central Louisiana. Reprinted by permission of the AAPG from Phelps and Roripaugh, 1983.*

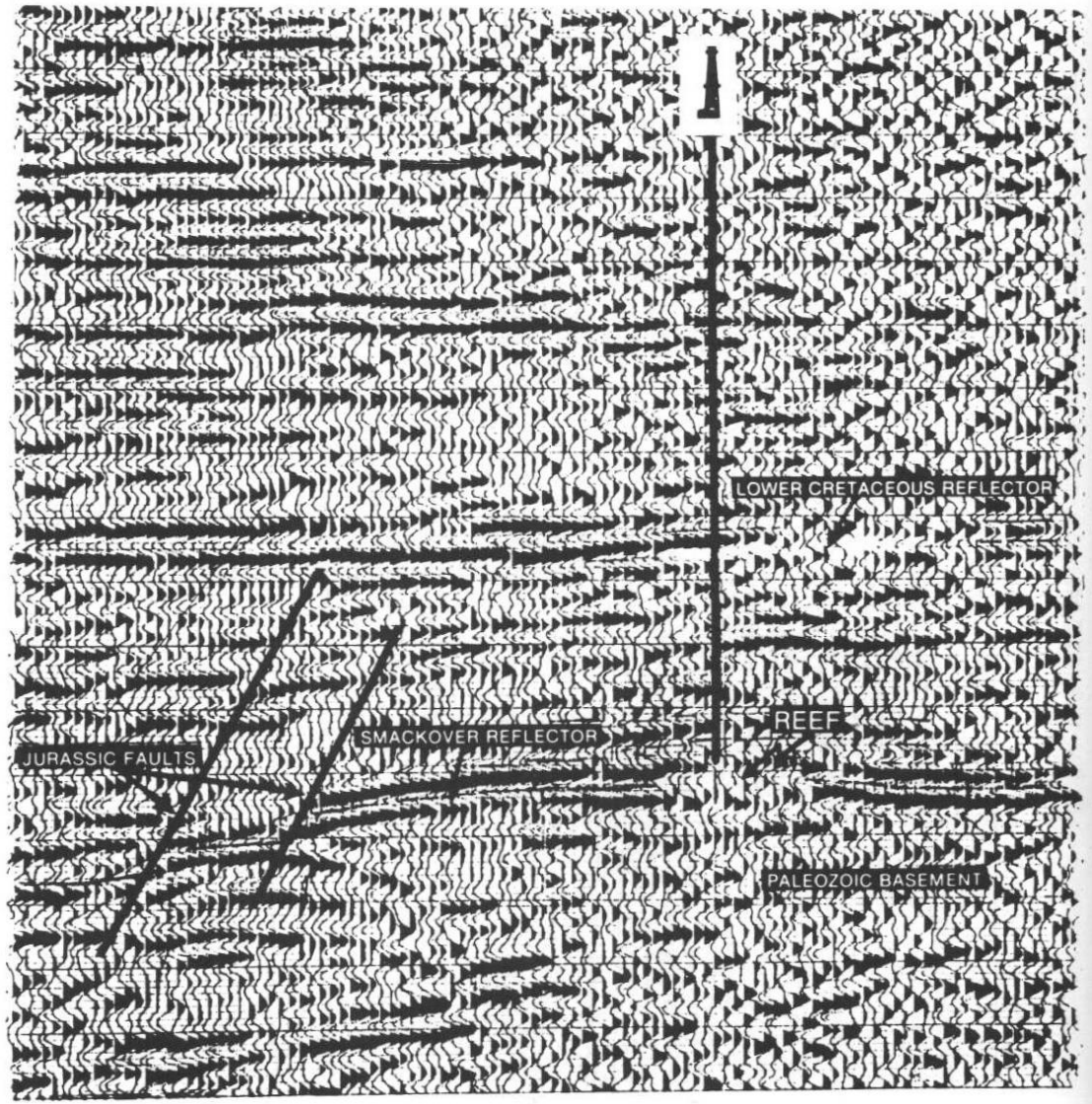

FIGURE 4.35 *Seismic section across porous Upper Jurassic Smackover reef section, U.S. Gulf Coast. The reef is indicated by a dim spot on the Smackover reflection. Reprinted by permission of the AAPG from Baria et al., 1982, fig. 29, p. 1479.*

A grid of good seismic data, often with special processing and always with meticulous interpretation, is required to define the shape and depositional environment of carbonate buildups. The (often) relative small size of the buildups compared to vertical and horizontal resolution limits is always a potential problem (see, for example, figs. 4.36 and 4.37). Indirect methods, using for example, velocity pull-up or push-down effects beneath a buildup, or differential compaction of overlying layers, can sometimes be used to overcome the problem (see figs. 8.22 and 8.23).

The loss of reflection amplitude often associated with reefs is not always a good indication of lower acoustic impedance and high porosity. Nath (1975) describes how defocusing, by dispersion of the seismic signal from the coastal areas of Silurian pinnacle reefs in Michigan, causes dim spots on the unmigrated seismic sections, due to the convex shape of the surface. The apparent fall in reflection coefficient, in these cases, is entirely geometric and not necessarily related to increased porosity.

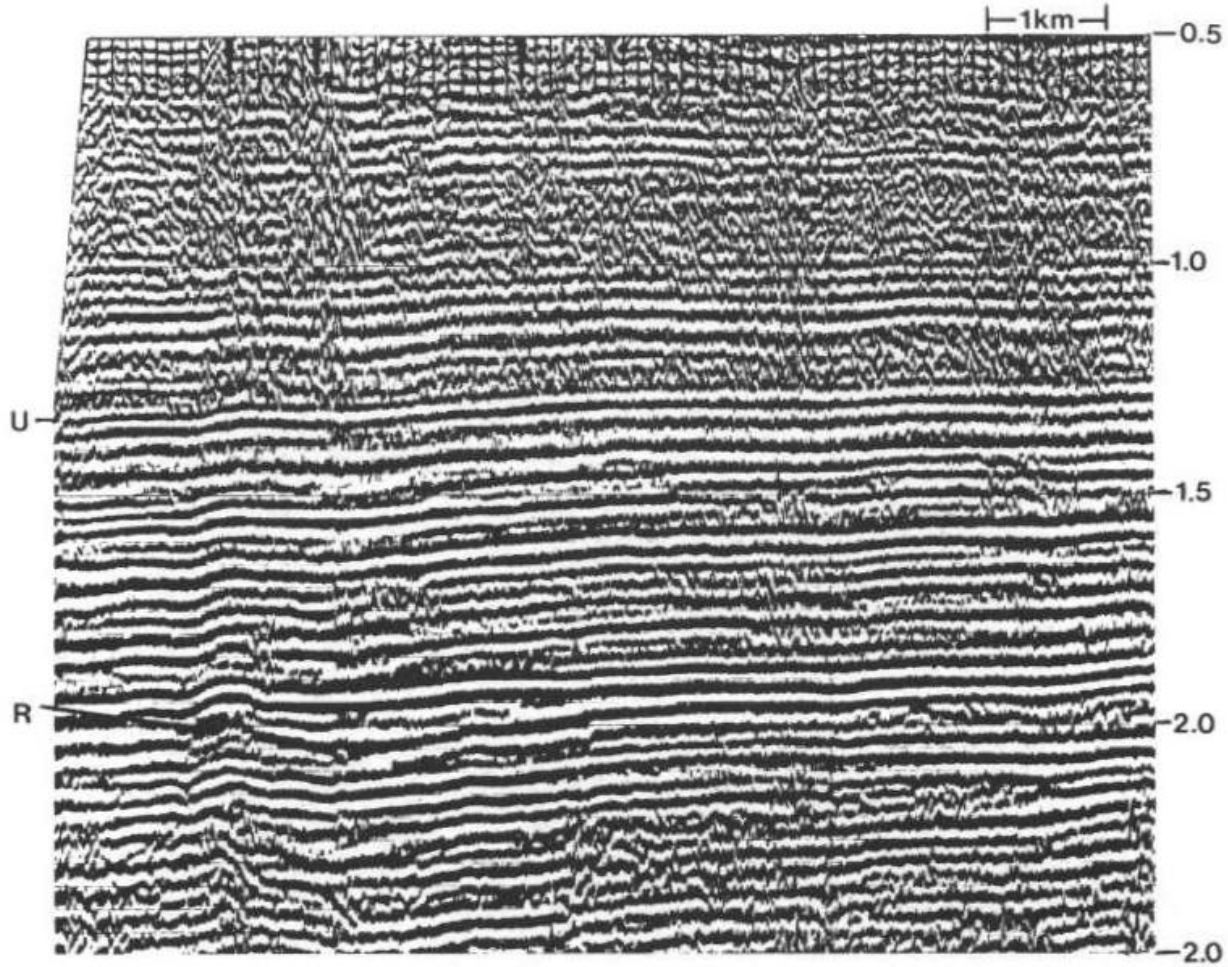

FIGURE 4.36 *Phase section over a reef in Western Canada, R = reef. Note the differential compaction over the reef and velocity pull-up below. The differential compact effects can still be seen to affect unconformity U. Courtesy Seiscom Delta.*

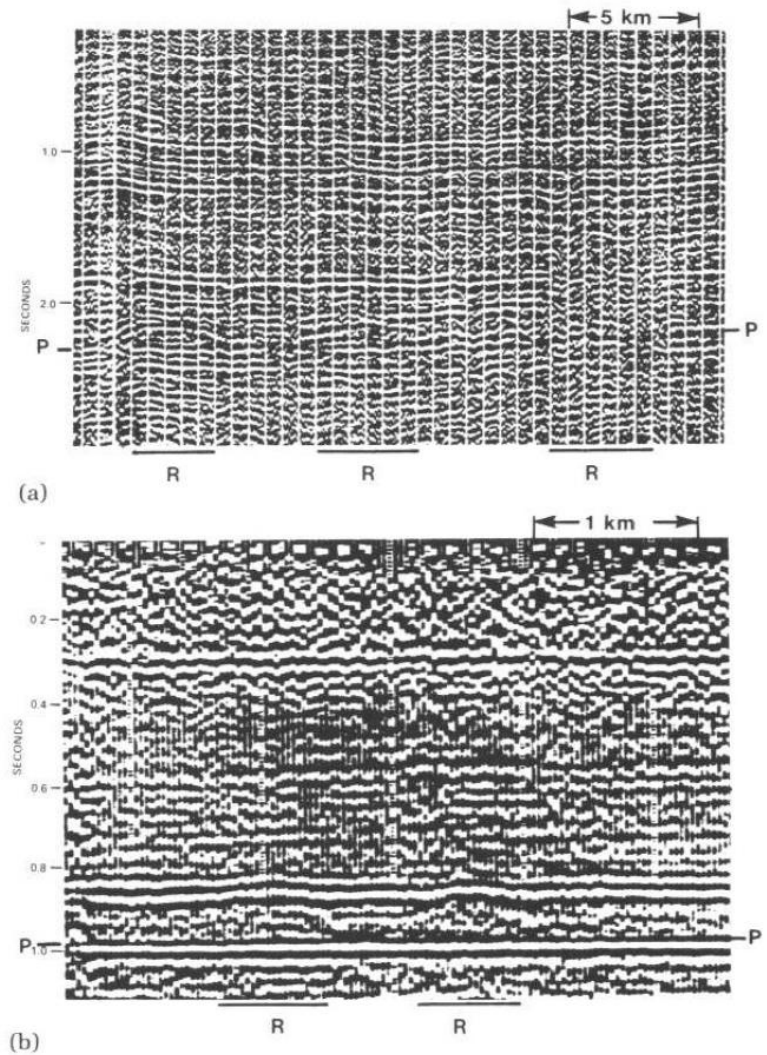

FIGURE 4.37 *Patch reefs. The platform on which the reefs grew is labeled* P *and the reefs are labeled* R. (a) *Three African reefs, the one on the right having grown appreciably higher than the two on the left.* (b) *Two small Canadian reefs. Reprinted by permission of the AAPG from Bubb and Hatlelid, 1977, figs. 8, 10, pp. 193, 195.*

SALT

Salt (see fig. 4.38) and associated evaporites are quite common in many sedimentary sequences. Salt has a low density (2.2 gm/cm^3), lower than that of most other commonly occurring sediments. When deposited in sufficiently thick layers, it becomes inherently unstable if it is buried; and a density inversion between the overburden and salt is achieved. In such circumstances, salt flowage is initiated and passes through three widely recognized stages of pillowing, diapirism, and postdiapirism. Bishop (1978) discusses the complex interaction between depositional history of the surrounding sediments and growth of the salt structure. Controversy surrounds the question of whether the dominant processes in development of a salt diapir involve intrusion or extrusion of the salt.

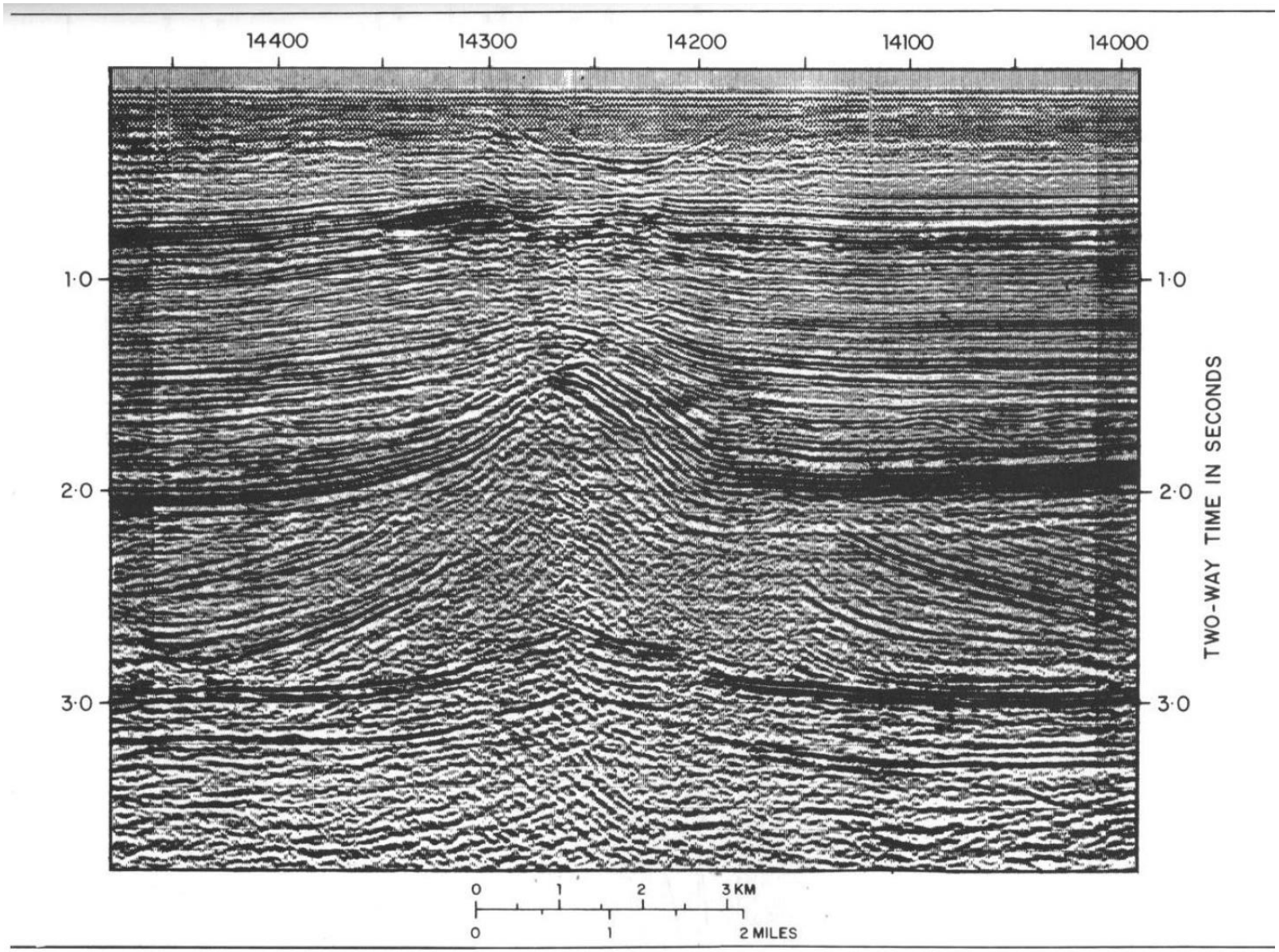

FIGURE 4.38 *Seismic section across a salt diapir. Courtesy Merlin Profilers Ltd.*

GROWTH STAGE	UPLIFTED AREA	WITHDRAWAL BASIN
Pillow Not to scale 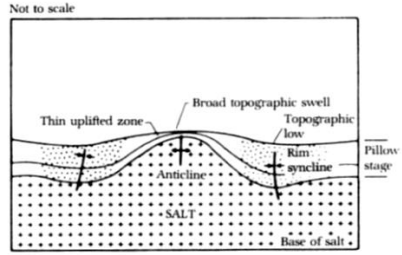 Primary peripheral sink	Geometry Sediments above pillow are thin over broad, equidimensional to elongate area. Maximum thinning over crest. Area extends 100 to 400 km² (40 to 150 mi²), depending on size of pillow. Percentage thinning, 10 to 100%. Facies Thin, sand-poor, fluvial-deltaic deposits over crest of pillow include interchannel and interdeltaic facies. Erosion common. Carbonate deposits on crest would include reef, reef-associated, and high-energy facies.	Geometry Sediments are overthickened in broad to elongate primary peripheral sink, generally located on updip side of salt pillow. Axial trace of sink parallels axial trace of elongate uplift, generally separated by 10 to 20 km (6 to 12 mi). Sink attains 300 km² (120 mi²) in extent, depending on size of pillow. Percentage thickening, 10 to 30%. Recognition of primary peripheral sink may be hindered by interference of nearby salt structures. Facies Thick, sand-rich, fluvial-deltaic deposits in primary peripheral sink include channel axes and deltaic depocenters. Aggradation common in topographically low area of sink. Carbonate deposits in sink would include low-energy facies caused by increase in water depth.
Diapir Not to scale 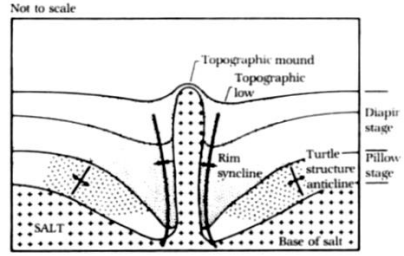 Secondary peripheral sink	Geometry Strata largely absent above dome. An 8 to 50 km² (3 to 20 mi²) area around diapir is thinned, depending on size and dip on flanks of dome. Facies Facies immediately over dome crest not preserved because of piercing by diapir of all but the youngest strata. Sand bodies commonly pinch out against dome flanks.	Geometry Sediments are thickened up to 215% in secondary peripheral sink. Sinks up to 1,000 km² (390 mi²) in extent are equidimensional to elongate, and they preferentially surround single or multiple domes; several sinks flank domes; percentage thickening ranges from 50 to 215%. Facies Expanded section of marine facies dominates, including limestones, chalks, and mudstones; generally sink is filled with deeper water low-energy facies caused by increased water depth. Elevated saddles between withdrawal basins are favored sites of reef growth and accumulated high-energy carbonate deposits.
Postdiapir Not to scale 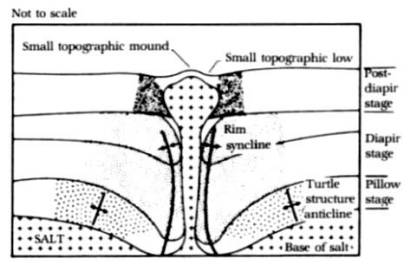 Tertiary peripheral sink	Geometry Strata thin or absent in small 10 to 50 km² (4 to 20 mi²) area over crest and adjacent to dome; area depends on size of dome and dip of flanks. Facies Facies and strata over crest of dome not preserved in places of complete piercement. Modern analogs have interchannel and interdeltaic facies in uplifted area. Mounds above dome include thin sands. Carbonate strata would include reef or high-energy deposits; erosion common.	Geometry Sediments within 20 to 200 km² (8 to 80 mi²) tertiary peripheral sink are thickened 0 to 40%, commonly by < 30 m (100 ft). Axial trace of elongate to equidimensional sink surrounds or flanks a single dome, or connects a series of domes. Facies Modern analogs have channel axes in sink. Aggradation of thick sands common in subsiding sink. Carbonate strata would include low-energy facies.

FIGURE 4.39 *Schematic stages of dome growth and variations in associated strata above and around salt structures. Reprinted by permission of the AAPG from Seni and Jackson, 1983, fig. 4, p. 1223.*

Pillow stage: Syndepositional thinning of sediments over the pillow crests and flanks, developed in response to the pillow's growth, is the most diagnostic feature of this stage. Only minor thickening usually develops into the primary rim syncline.

Diapir stage: Withdrawal of the salt into the growing diapir leads to a collapse of the flanking sequence that thinned toward the original pillow. A secondary rim syncline, its axis immediately adjacent to the diapir's edge, develops above the collapsed area. The secondary rim syncline is usually more extensive than the primary rim syncline and also accumulates a thicker sequence. The thickened sequence in the primary rim syncline is usually outside of the collapsed zone and, in interdomal locations, undergoes passive structural reversal from synclines to anticlines, the "turtle structures" of Trusheim (1960).

Postdiapir stage: During this stage, diapirs stay at or near the sediment surface (assuming there is sufficient salt for continued movement) despite continued subsidence. A small, often subtle, tertiary rim syncline flanks the diapir.

dissolution of salt (fig. 4.40). Jenyon (1984) discusses the formation of collapse features above salt structures and seismic criteria for their recognition. Potentially, dissolution can occur in deeply buried salt structures by salt-undersaturated water deep in the subsurface being brought into contact with the salt. Increasing brine density causes gravitational flow and removal of salt (Anderson and Kirkland, 1980). Alternatively, in the shallow section, meteoric waters can come into contact with a shallow diapir or salt layer and cause dissolution. Shale diapirs would not normally be expected to exhibit collapse features. Care must be taken, however, to distinguish true collapse features due to dissolution—from crestal faulting that typically occurs in competent units due to extension—above any type of anticlinal feature.

Interpretation problems can arise in mapping salt-diapir flanks, a common location of potential traps.

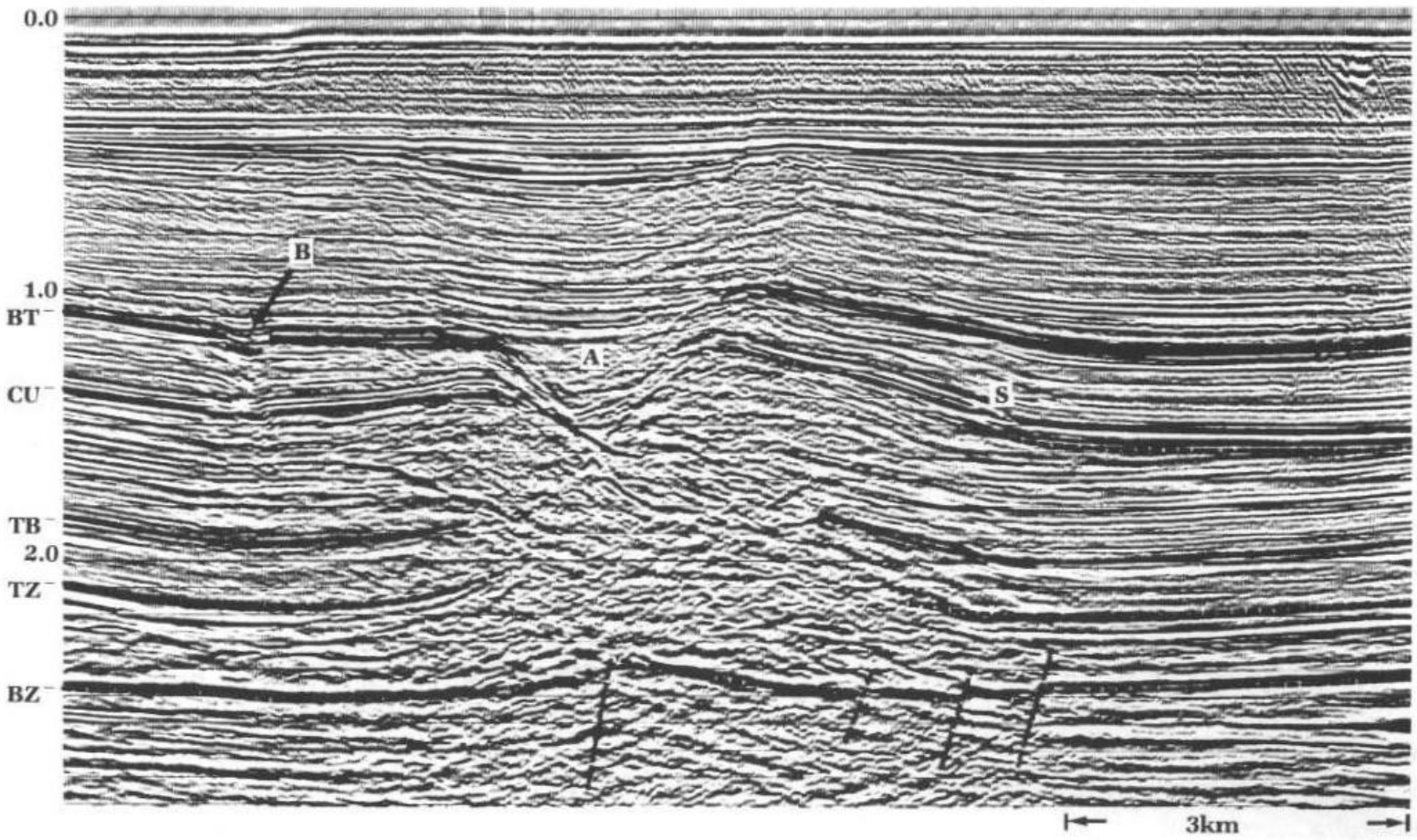

FIGURE 4.40 *Migrated seismic section across a salt diapir and associated collapse feature* (A). BT–CU, *Upper Cretaceous chalk;* TZ, *top Zechstein salt;* BZ, *base Zechstein salt. Reprinted from Jenyon, M. K., MARINE AND PETROLEUM GEOLOGY, 1984, fig. 3, p. 30, by permission of the publishers, Butterworth & Co. (Publishers) Ltd.* ©.

$$\text{salt thickness} = \frac{t \text{ pull-up} \times V_L \times V_S}{2(V_S - V_L)},$$

where

t pull-up = observed pull-up,
V_L = velocity in adjacent lithology,
V_S = velocity salt.

BASEMENT

There are two definitions of basement rocks; igneous or metamorphic crystalline rocks; or economic basement, indurated low-porosity, sedimentary rocks that have no reservoir potential. Neither type of "basement" necessarily has a unique reflection character.

Figure 4.42a shows an example of shallow crystalline basement. Beneath the strong top-basement reflection (positive reflection coefficient) the seismic record is reflection free and seemingly dead. Figure 4.42b shows crystalline basement outcropping at the sea floor. The strong internal reflections are multiples. The "ringing" multiples in figure 3.11 are developed in crystalline basement. Crystalline basement usually produces a largely reflection-free seismic response, and so care must be taken that crystalline basement is not confused with other lithologies that can produce a similar response; for example, salt and shale diapirs, basalt flows, igneous intrusions, etc. When deeply buried, crystalline basement becomes more difficult to identify. The top crystalline basement should have a positive reflection coefficient when overlain by practically any sedimentary rock; but weathering of the upper few tens of meters may not only reduce the reflection coefficient but may also produce potential reservoir properties.

The crystalline basement in figures 4.42a and 4.42b is free of internal primary reflections. The presence of internal reflections, however, does not preclude the possibility of crystalline basement. Weathering can produce reflections, as can internal layering or structural zones within the basement (fig. 4.42c). If good internal reflections are developed, crystalline basement may possibly be identified by its high-interval velocity.

Economic basement is more difficult to define, because its definition is subjective. As a generalization, low-porosity indurated rocks will be characterized by weak discontinuous reflections and poor data quality. Weak reflections with poor continuity will be common, because, although the actual acoustic-impedance values would be high, acoustic-impedance contrasts would be small.

Structural closure involving either type of basement can never be immediately downgraded and disregarded. P'an (1982) describes oil and gas fields with basement rock reservoirs from many different basins, for example, the near billion-barrel La Paz field, Venezuela, the fields of the Central Kansas Uplift, etc. Basement reservoirs are characterized by thick reservoir intervals; and, although porosity and permeability are usually highly variable, production rates are typically high and reserves large.

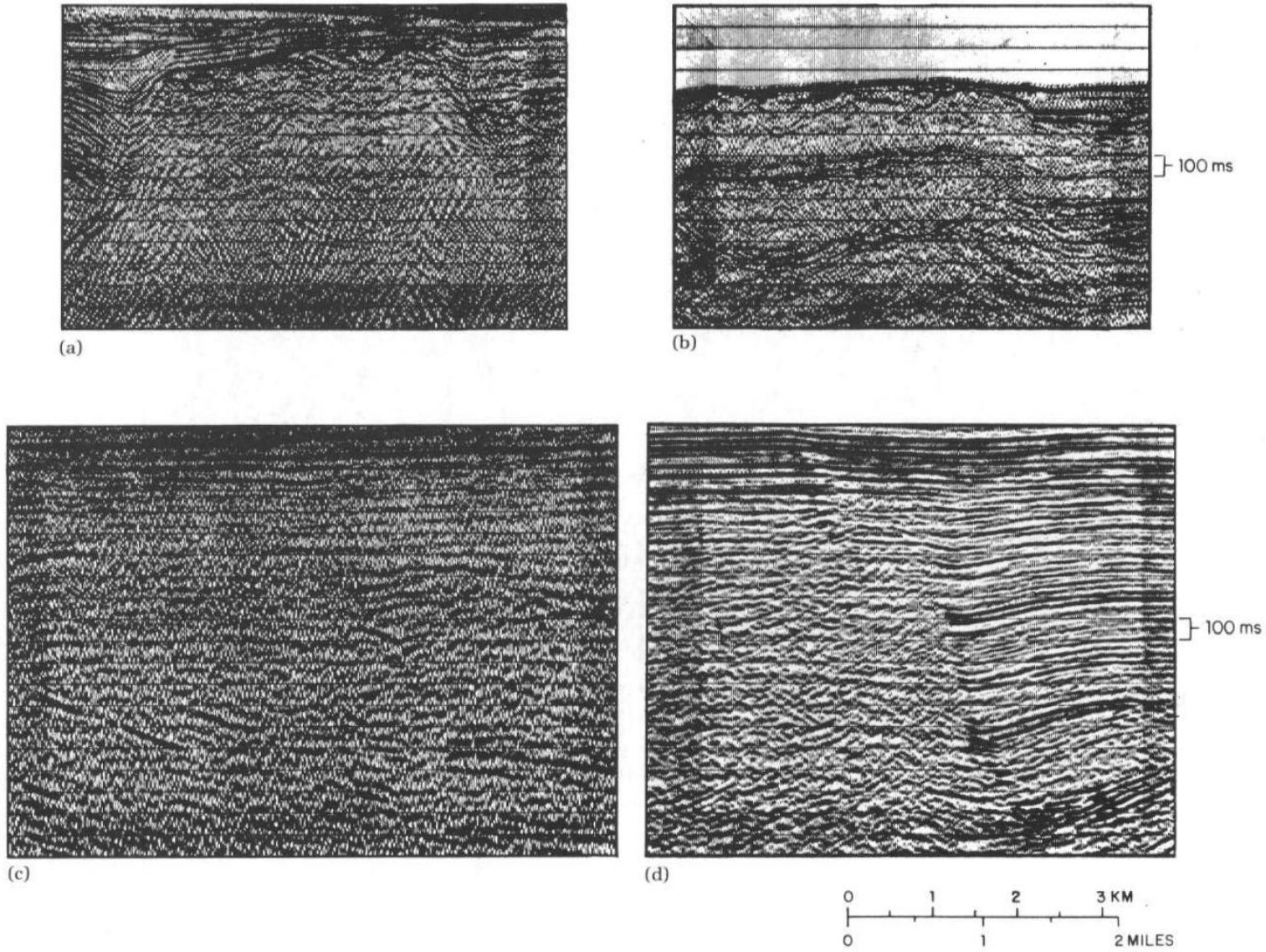

FIGURE 4.42 *Examples of the seismic expression of crystalline basement.* a *and* c, *courtesy Statoil;* b, *courtesy Norsk Hydro;* d, *courtesy Merlin Profilers Ltd.*

IGNEOUS AND VOLCANIC ROCKS

When overlain by practically all sedimentary lithologies, igneous and volcanic rocks, including intrusive and extrusive rocks, are characterized by high-interval velocities, positive reflection coefficients, and high-amplitude reflections. Very poor data quality is not uncommon. Gravity and magnetics can be invaluable aids to seismic data in identifying igneous and volcanic rocks. On the basis of their geometry, intrusive igneous rocks can be grouped into major bodies—for example, laccoliths and batholiths, dikes (near vertical intrusions); and sills (laterally extensive sheets).

Large intrusive bodies generally produce seismically dead intervals. The intrusive nature of the body may be evident from upturning of the adjacent sediments. Igneous intrusives will not show the secondary rim syncline characteristic of salt or mud diapirs. If, however, only the upper part of a deep salt diapir is visible it could prove difficult to separate the two possibilities seismically. Figure 4.43 shows a seismic profile through the mafic intrusion, known as the Great Stone Dome, 100 km E of New Jersey in the center of the Baltimore Canyon Basin. The igneous stock was intruded into, and deformed, a sequence of shallow-water marine sandstones and shales. The effects of the intrusion, rather than the intrusion itself, are the main features of the seismic section. Uplift and disruption associated with the intrusion are evident up to 16 km away. Differential compaction has caused structuring of the overlying Cretaceous and Tertiary sediments (Crutcher, 1983).

Dikes are more difficult to recognize, as the reflection seismic section is unsuited to imaging near-vertical features. In addition, the lateral extent of dikes is generally not great and may be below the Fresnel-zone size for horizontal resolution in many cases. Linear dikes are perhaps most easily recognized on unmigrated sections, where it may be possible to follow the course of a dike by mapping diffractions from its top through a seismic grid.

Frequently, dikes and sills occur together (fig. 4.44).

Sills are igneous bodies intruded laterally into rock sequences and are more easily identified, or at least produce a more pronounced effect in the seismic. Sills can be very laterally extensive, covering thousands of square kilometers. More commonly, individual sills are less extensive, with areas of a few tens of square kilometers. Sills can produce a seismic expression very similar to that of carbonates or evaporites. If thick enough, a sill may, perhaps, be identified by high-interval velocities. The best criterion for the recognition of sills is to observe discordant reflector relationships that demonstrate the intrusive nature of the sill (fig. 4.45).

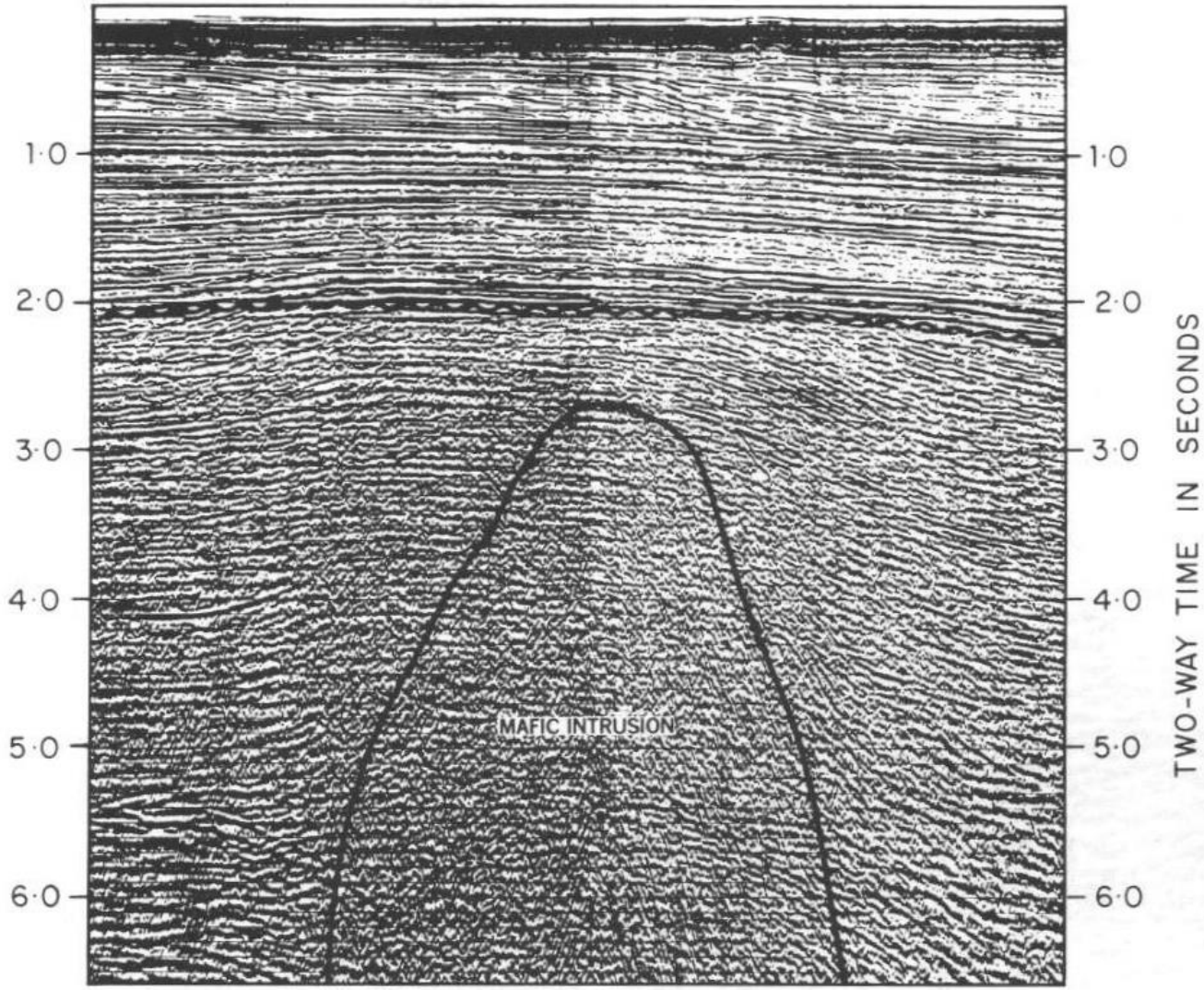

FIGURE 4.43 *Seismic section across the Great Stone Dome mafic intrusion in the Baltimore Canyon Trough off the U.S. east coast. Reprinted by permission of the AAPG from Crutcher, 1983.*

tion across the Paleocene Erlend Complex, N of the Shetland Islands in the North Atlantic. The form of the volcano can be seen clearly in the profile, with reflections

Volcanic rocks are, by definition, extrusive and form three main groups: lavas, tuffs (airborne deposits), and water-deposited volcanic deposits. Lavas can be up to thousands of meters thick and may be difficult to differentiate seismically from intrusive igneous rocks, but they may be expected to show some relationship to a volcanic center or fissure system. Figure 4.46 shows a seismic section across the Paleocene Erlend Complex, N of the Shetland Islands in the North Atlantic. The form of the volcano can be seen clearly in the profile, with reflections from the lava flows dipping radially outwards, at up to 20°, from a central volcanic vent. The vent is roughly circular in plan, with a diameter of about 2 km and a depth of 300–400 m. Drilling results show the basalts to have unusually low interval velocities of around 3500 m/s, which Gatliff et al. (1984) interpret to be probably due to the lava pile having been built up by the extrusion of thin flows, each in turn being weathered before burial by the next lava flow. In the absence of a central vent or gravity data, a seismic interpretation of the volcano in figure 4.46 could be difficult. Not only are the interval velocities uncharacteristically low for typical lavas, but the clinoform prograding pattern of the radially outward-dipping lava flows could be mistaken for a prograding sedimentary sequence in situations where it was not possible to demonstrate the overall shape of the feature, for example, with a widely spaced seismic grid.

FIGURE 4.44 *Seismic expression of an igneous plug with branching sills. Reprinted by permission of IHRDC Press from Badley and Anstey, 1984.*

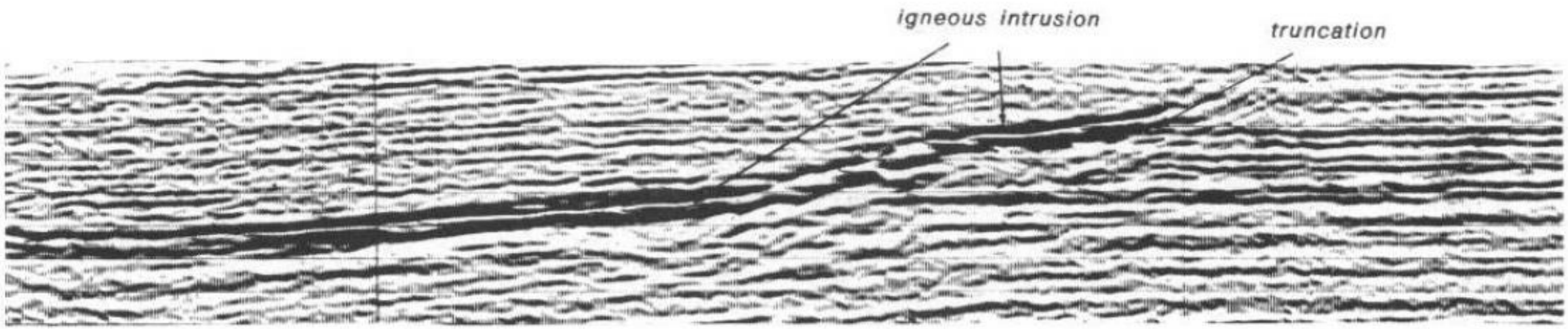

FIGURE 4.45 *Seismic expression of a sill. Note the diagnostic discordant nature of the high-amplitude reflections. Courtesy Merlin Profilers Ltd.*

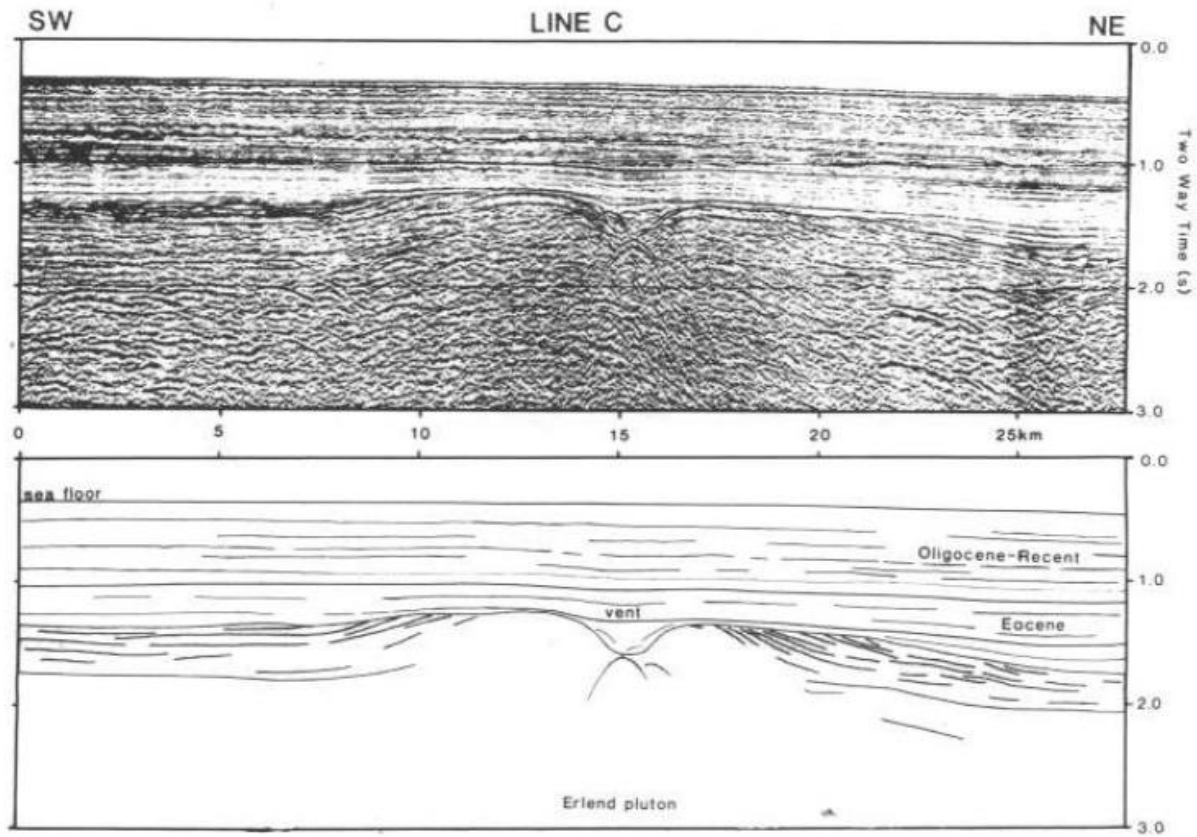

FIGURE 4.46 *Seismic section across the Ereland Paleocene Volcanic Complex, north of the Shetland Islands in the North Atlantic. The form of the volcano can be seen clearly as can reflections from radially outward dipping lava flows. Reprinted by permission of The Geological Society of London from Gatliff et al., 1984, fig. 4 part C.*

porous sands. In a typical sand-claystone sequence, the claystone-to-sand reflection is ordinarily positive and of medium strength for water- or oil-saturated sands of poor porosity. The reflection becomes weak or nonexistent with higher porosity. If the sand is very porous and contains gas, the reflection will have a strong negative reflec-

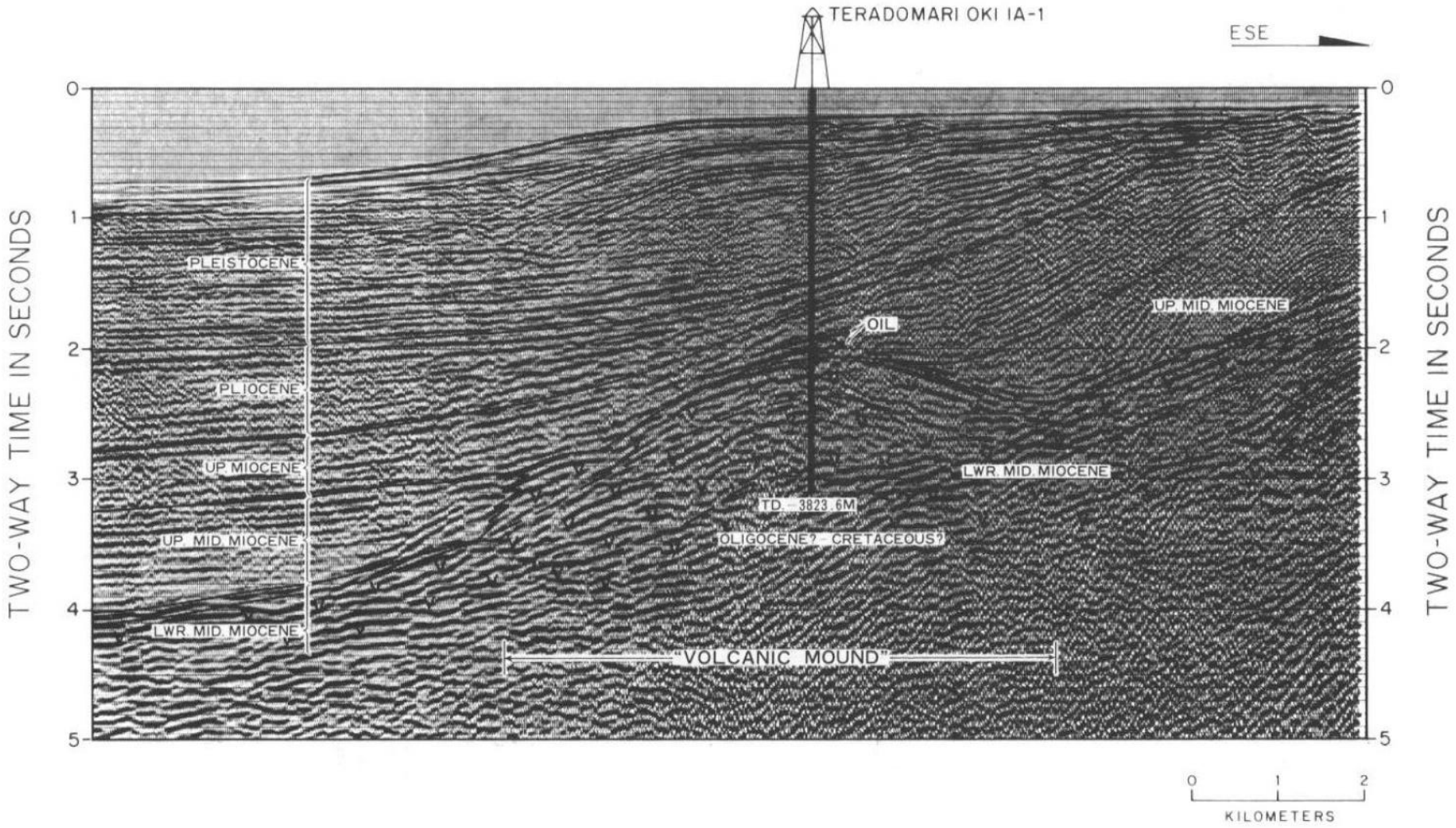

FIGURE 4.47 *Seismic section across a Middle Miocene volcanic mound, Sea of Japan. Reprinted by permission of the AAPG from Suzuki, 1983.*

Reflection associated with Hydrocarbon and Diagenetic Effects

Gas

The presence of gas in a reservoir often produces a detectable suite of responses in the seismic record; and it is obviously very important for the interpreter to be able to recognize these gas effects. Discussed below are the main criteria for recognizing the presence of gas on a seismic section.

Acoustic-Impedance Effects. The way in which a reservoir responds to the presence of gas depends on the acoustic impedance of the gas-filled portion of the reservoir, the water-filled reservoir, and the cap rock; and the thickness of the gas-filled interval. If the gas column is thick enough and there is an acoustic-impedance contrast between the gas-/oil- or the gas-/water-filled portions of a reservoir, a

reflection commonly called a *flat spot* will result. As a rule of thumb, flat spots are likely to be found in porous sandstones or carbonates down to about 2.5 km. Below this depth the effect of gas on velocity is less marked and the chance of getting a good reflection from a gas contrast is reduced. Flat spots will always have positive reflection coefficients, appearing as a trough on seismic sections displayed with SEG normal polarity or a peak on reverse polarity sections (fig. 4.48). Although gas contacts are usually horizontal in depth, they do not always appear horizontal in time due to the push-down effect of the lower velocity in the gas interval (fig. 2.8).

Flat spots are perhaps the best indication of gas, although other diagnostic acoustic-impedance changes between the cap rock and gas-bearing reservoir affect the amplitude and polarity of the top-reservoir reflection. Amplitude anomalies fall into two groups:

1. Anomalies of very high amplitude, commonly termed *bright spots*, and
2. Anomalies of very low amplitude, commonly termed *dim spots*.

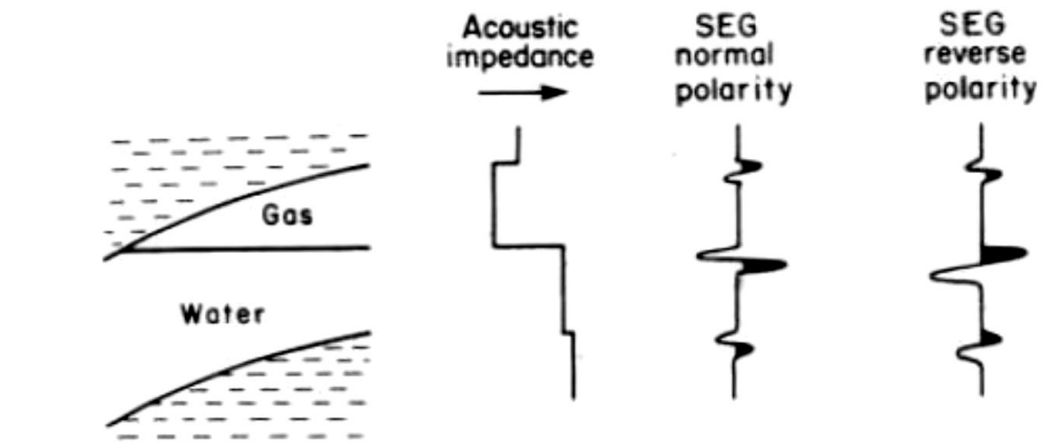

FIGURE 4.48 *The effect of gas on acoustic impedance and seismic response for normal- and reverse-polarity wavelets.*

porous sands. In a typical sand-claystone sequence, the claystone-to-sand reflection is ordinarily positive and of medium strength for water- or oil-saturated sands of poor porosity. The reflection becomes weak or nonexistent with higher porosity. If the sand is very porous and contains gas, the reflection will have a strong negative reflection coefficient—a bright spot (fig. 4.49). While bright spots due to gas are usually associated with porous sands, dim spots due to a reduced reflection coefficient of the top-reservoir reflector are more common with less porous or well-compacted sands and carbonate reservoirs. In these cases the claystone/compacted-sand or claystone/carbonate would usually have a strong positive reflection coefficient. Gas in the reservoir reduces the reflection coefficient, causing the top-reservoir reflector to lose amplitude and dim (fig. 4.50). Amplitude anomalies are sometimes accompanied by corresponding polarity changes. These polarity effects are summarized in figure 4.51. A polarity reversal of the top-reservoir reflector at the gas-oil or gas-water contact is a common feature of bright spots.

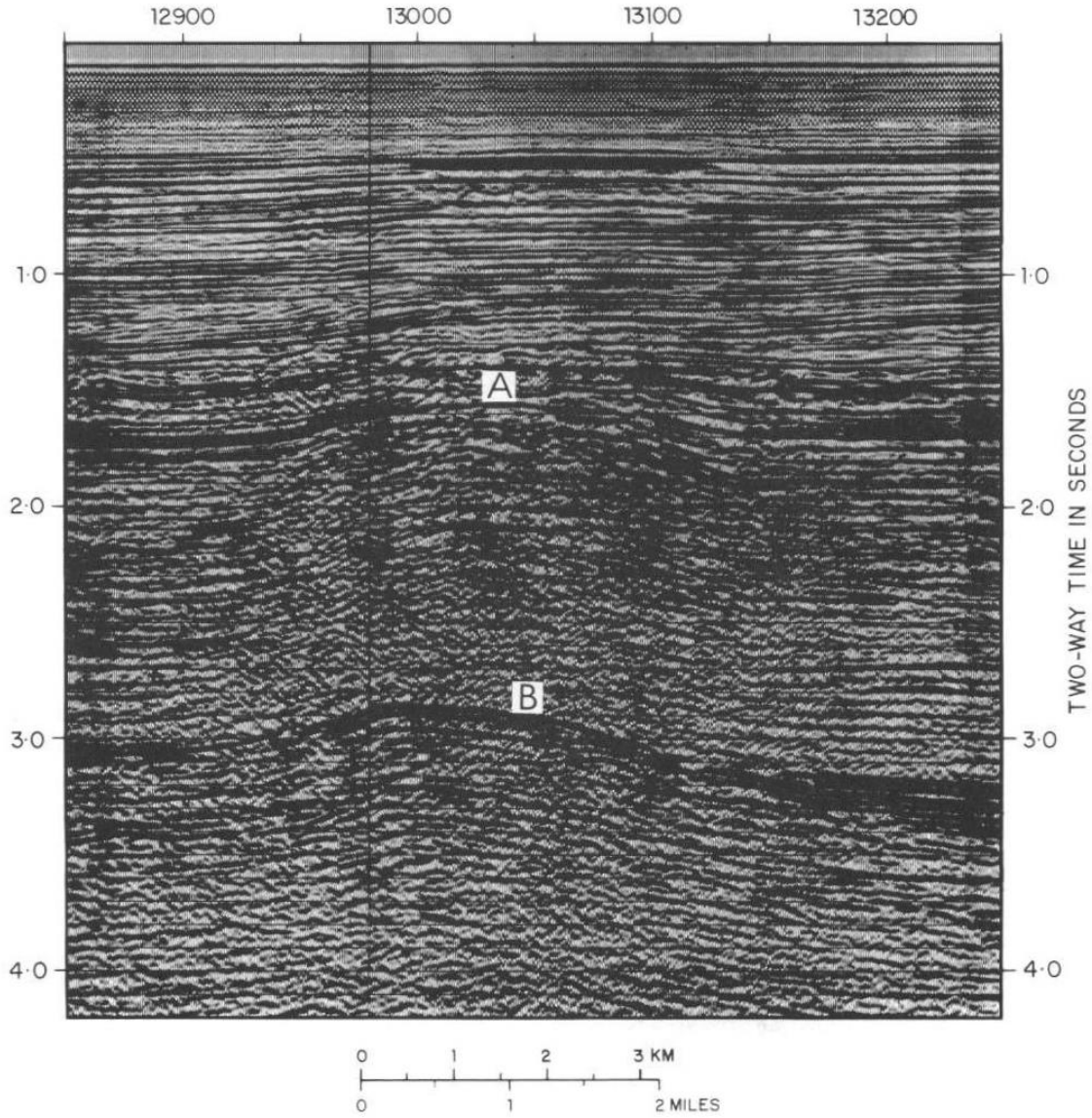

FIGURE 4.49 *Bright spot in a shallow-gas sand above a deeper salt structure. Courtesy Merlin Profilers Ltd.*

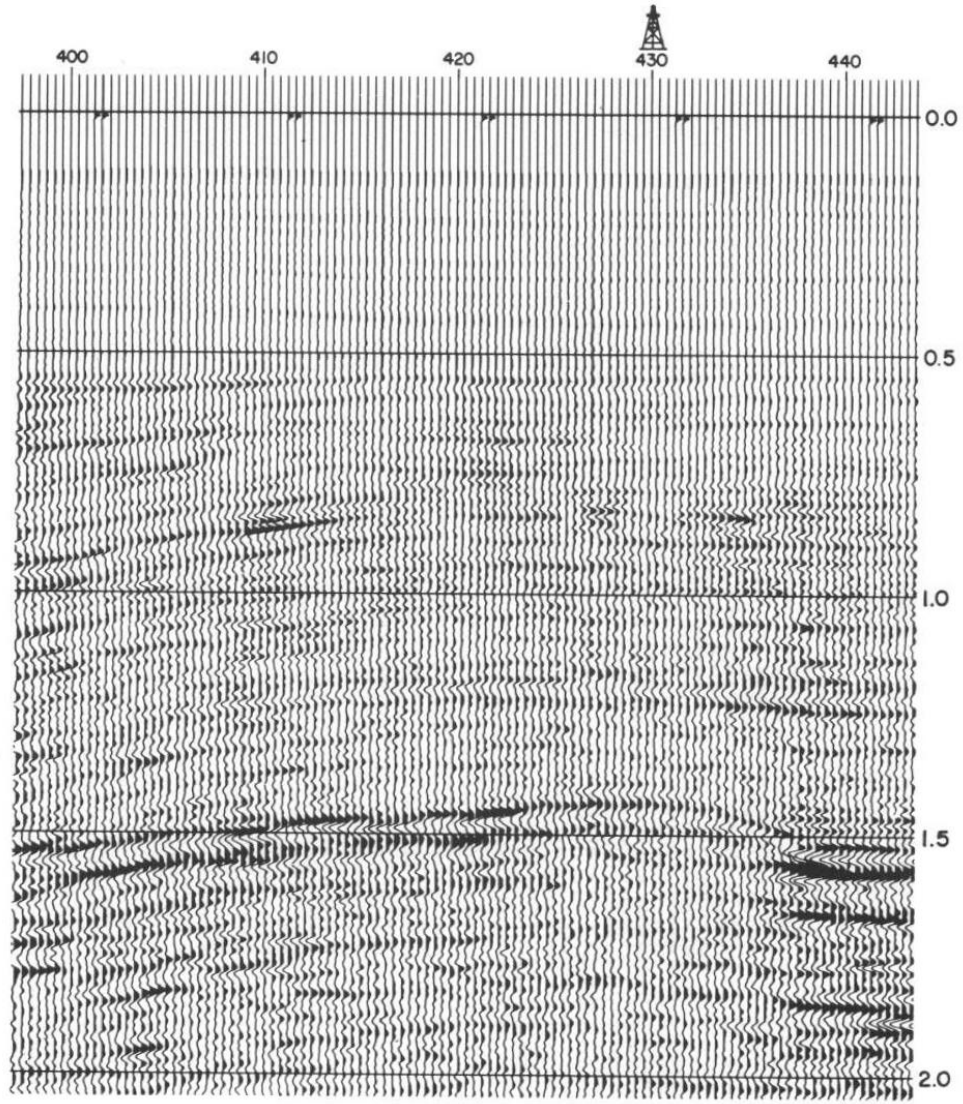

FIGURE 4.50 *Dim spot associated with a gas-bearing porous carbonate overlain by interbedded sands and shales. Reprinted by permission of Teledyne Exploration Company from Barry and Shugart, 1973.*

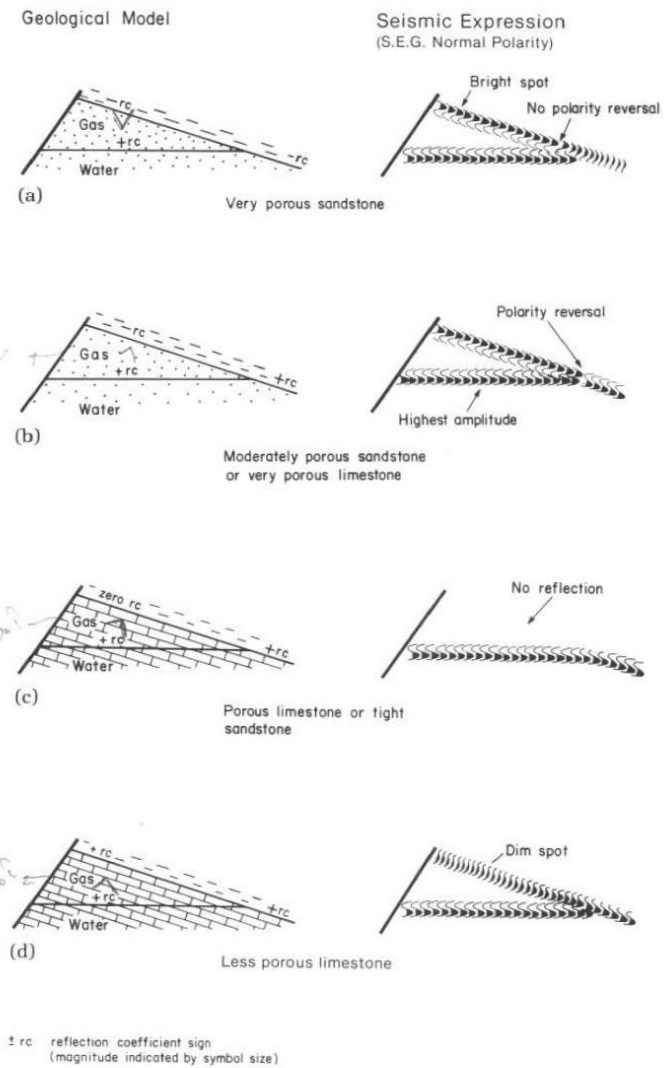

FIGURE 4.51 *Effect of different reservoir properties on the seismic response to the presence of gas. In the example, the reservoir is overlain by relatively low-acoustic-impedance shale.* (a) *Reservoir of porous sand with lower acoustic impedance than the shale.* (b) *Moderately porous sand with slightly greater acoustic impedance than the shale.* (c) *A porous limestone or low-porosity sandstone with greater acoustic impedance than the shale.* (d) *A less porous limestone with much higher acoustic impedance than the shale.*

Velocity Effects. If the gas column is sufficiently thick, a push-down may be observed on underlying reflectors (fig. 2.8). The differential velocity required to produce a push-down can provide a check on the possible gas column. If the interval velocity is unreasonable, for example, 1000 m/s (3300 ft/s), then something is wrong and the effect cannot be caused by gas alone.

Other Effects. A frequency loss is sometimes observed beneath bright spots. This has been attributed to greater absorption of the seismic wave within gas-bearing as opposed to water-bearing intervals. This absorption selectively depletes the signal of higher frequencies. Both amplitude decrease and increase are sometimes associated with bright spots. Actually, anticipated transmission losses through a gas-saturated reservoir are so low as to be scarcely measurable. Amplitude decrease both above and below a bright spot may be due to automatic gain effects—a processing step to balance amplitude across a seismic section—and merely a response to the extra high amplitude of the bright spot. An amplitude increase beneath a bright spot is most likely due to increased signal levels associated with multiples of the bright spot. However, if a shadow is obvious only below, and not above, a bright spot, it could be caused by transmission losses through multiple gas reservoirs.

Diffractions are developed where there is a significant lateral contrast in acoustic impedance and are often seen at the edges of bright spots. They will not be expected in cases where the thickness of the gas interval decreases gradually. "Gas chimneys" or "gas clouds"—poor data zones above gas-bearing structures—are quite common and can be very characteristic (fig. 4.52). Poor data zones are thought to be caused by scattering of seismic energy by escaped gas penetrating the cap rock above a gas reservoir. Gas leakage into the cap rock can occur through a variety of mechanisms (e.g., leakage along fault planes; fractures; or overpressure exceeding the mechanical strength of the seal rocks. Although gas chimneys provide an easy way of locating possible gas-bearing structures, they also have a negative side. If a gas field is found beneath a gas chimney, pity the poor interpreter who must prepare reservoir maps from the seismic record. Usually, data quality beneath gas chimneys is quite deplorable.

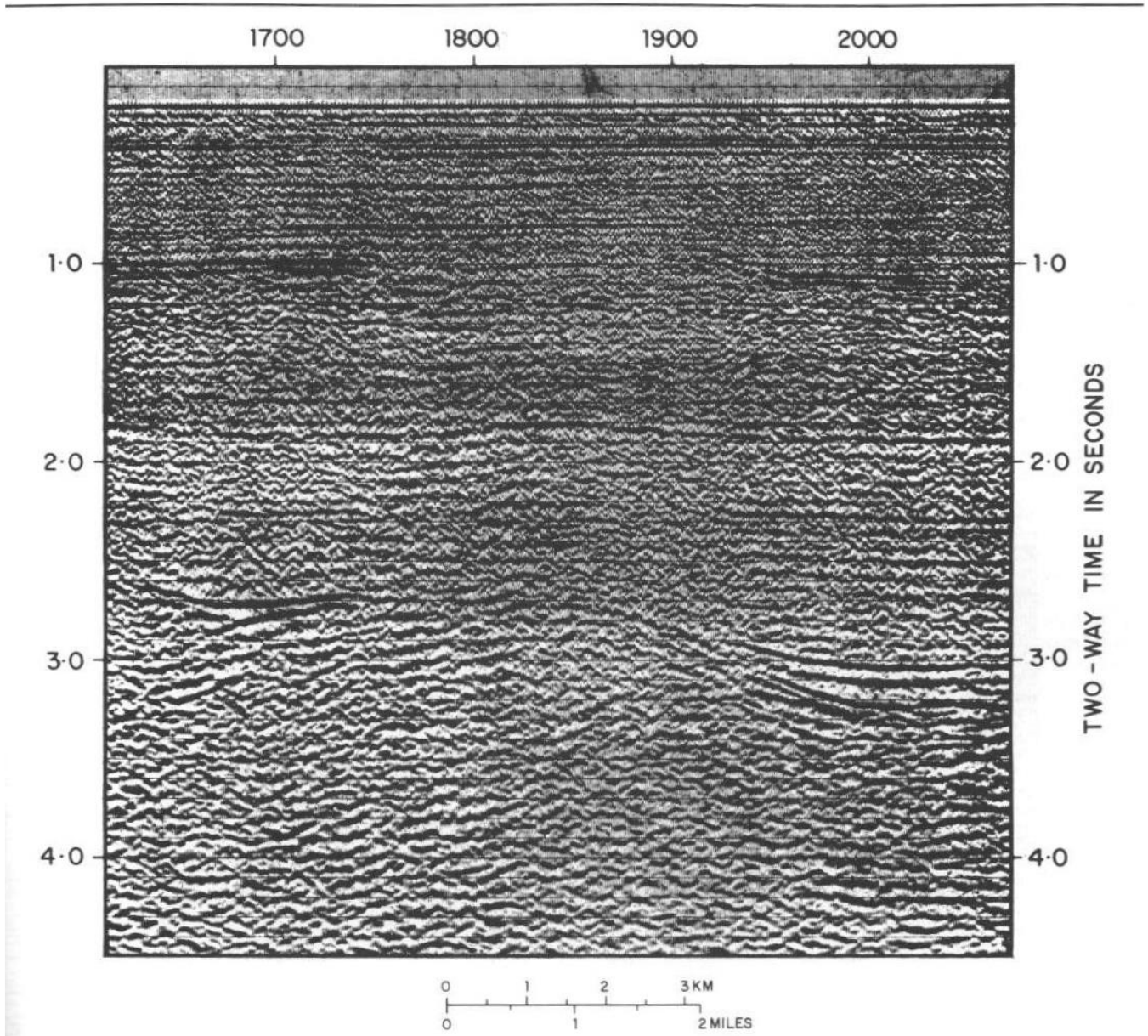

FIGURE 4.52 *Gas-chimney effect above the gas-bearing 34/10 alpha structure, offshore Norway. Courtesy Norsk Hydro.*

Pitfalls

1. Gas saturation: Unfortunately, it only takes a gas saturation of about 5% to produce a detectable amplitude anomaly in a porous sand (Domenico 1973). The maximum velocity decrease occurs at a gas saturation of about 20%. Sands with such low gas saturations, while generating the amplitude effects, would flow only water if tested by a well.

2. Amplitude anomalies: Not all bright spots are caused by gas. Carbonates, igneous intrusions, thinning beds at tuning thickness, can all produce anomalously high reflection coefficients (fig. 4.53). In the case of carbonates, igneous intrusions and other rocks with high acoustic impedance, the reflection coefficient would be positive (gas should produce a strong negative reflection coefficient) and detectable on a polarity display. However, a tuning-thickness amplitude anomaly, associated with a thinning unit of porous sand could have both high amplitude and a negative reflection coefficient. Coal beds can also generate high-amplitude but negative-polarity reflections. Obviously care should be taken in assessing amplitude anomalies.

3. Flat spots caused by diagenetic effects: These are discussed in the following.

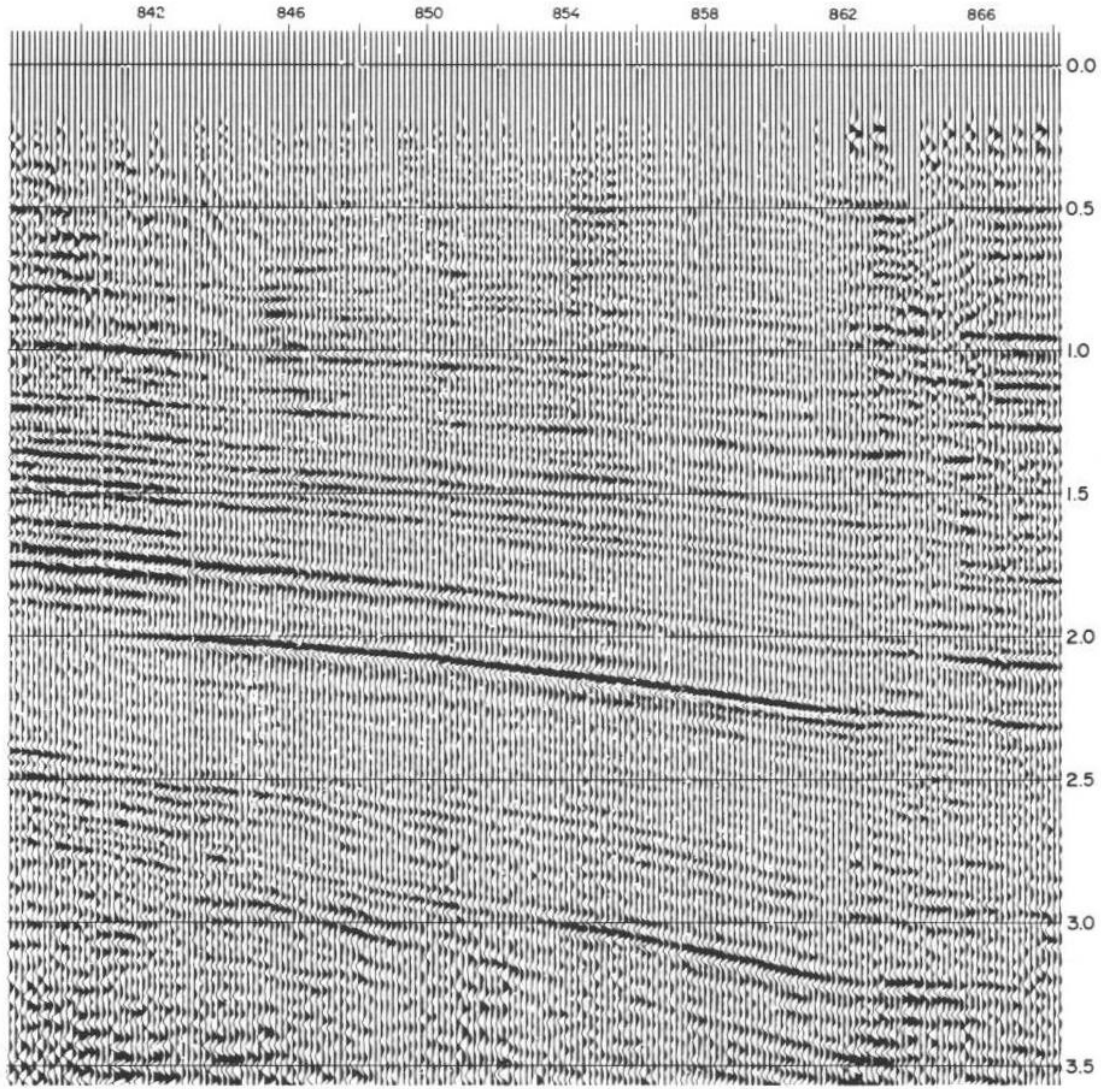

FIGURE 4.53 *Amplitude anomaly generated by a carbonate unit within a comparatively low-velocity sand/shale sequence. The bright spot is not related to hydrocarbons. Reprinted by permission of Teledyne Exploration Company from Barry and Shugart, 1973.*

oil

The presence of oil should have no measurable effect in the seismic record; it should, at best, produce a slight reduction in acoustic impedance. Substituting oil for water has only a relatively small effect on velocity and density. Flat spots are reported at the oil-water contacts of some fields. Meckel and Nath (1977) show a synthetic seismic section across the North Sea Brent Field with a flat spot developed at the oil/water contact. Flat spots associated with oil are not always directly attributable to the effect of oil on the seismic system, but with the inhibiting effect of hydrocarbons on the diagenetic reservoir growth of cementing minerals in the reservoir (Hancock and Taylor, 1978). A number of fields within the North Sea Province show this effect: within the hydrocarbon-bearing intervals the sands are relatively uncemented, but beneath the oil/water contact the sands are well cemented by kaolinite and/or illite (De'Ath and Schuyleman, 1981). The effects of cementation on the acoustic impedance can be large enough to produce a reflection at the oil/water contact. It must be a pleasant surprise to drill a flat spot, expecting gas, and find oil instead.

Gas Hydrates

Under appropriate conditions water saturated with natural gas can freeze. Instead of crystallizing in the usual hexagonal crystal lattice, the ice crystallizes into a cubic form, which traps gas molecules in voids within the crystal lattice. Gas hydrates are stable only over a limited range of pressure and temperature and their thickness is largely determined by water depth and the geothermal gradient within the gas hydrate-bearing sediment (fig. 4.54). As a general rule the greater the water depth the thicker the potential gas hydrate-bearing interval. MacLeod (1982) discusses the factors controlling the occurrence of gas hydrates. Because the reflections from the base gas hydrate tend to follow the sea-floor topography they are sometimes called bottom-simulating reflections or BSRs. Gas hydrates are important for the interpreter because the contrast in acoustic impedance between the gas hydrate and underlying sediments can produce a reflection (fig. 4.55). Gas hydrates increase both velocity and density of the host sediments, and the associated reflection at the base of the hydrate layer has a strong negative reflection coefficient. Interbedded multiples, sideswipe reflections, reflections from slump surfaces, and unconformities can mimic gas-hydrate reflections. Additionally, it is possible to confuse anomalous reflections from the diagenetic boundary with hydrate reflections.

Gas hydrates have yet to be exploited commercially. In fact, their main interest may not be as a source of hydrocarbons but as the seal to gas accumulations trapped below the hydrate layer.

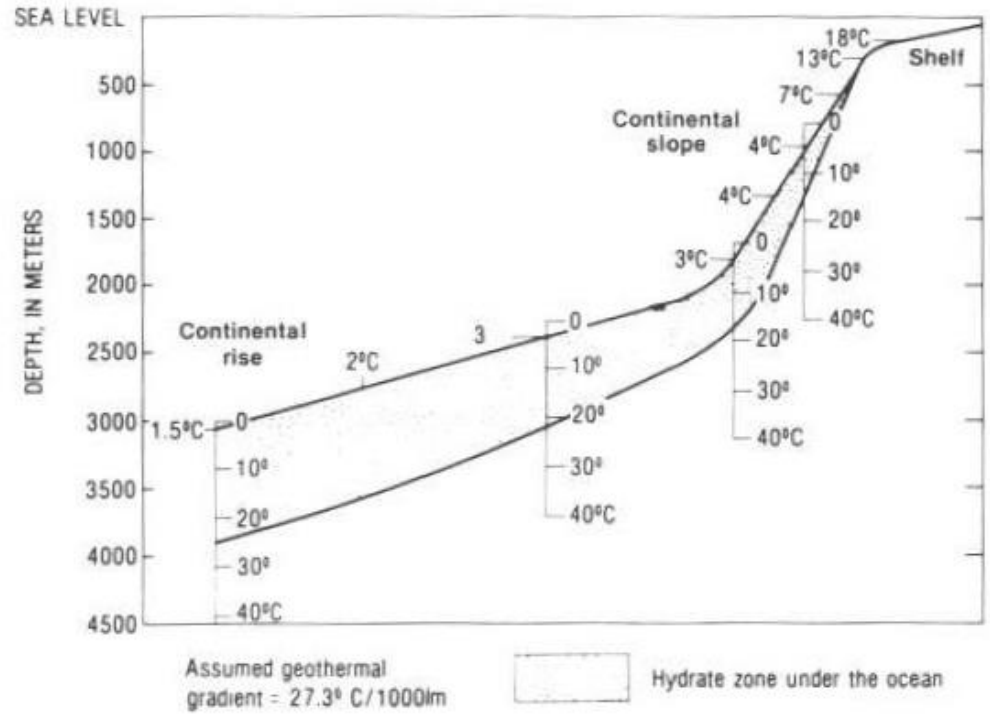

FIGURE 4.54 *Idealized section that shows the zone of gas hydrate stability for outer continental margins. Stippled area is potential region of gas hydrate formation where pressure and temperature conditions are correct for hydrate stability, assuming an adequate methane supply. The following assumptions apply: (1) geothermal gradient of 27.3°C/km; (2) lithostatic and hydrostatic pressure gradients of 0.1 atm/m; and (3) bottom-water temperature range from 1.5 to 18°C depending on water depth. Reprinted by permission of the AAPG from Kvenvolden and Barnard, 1982.*

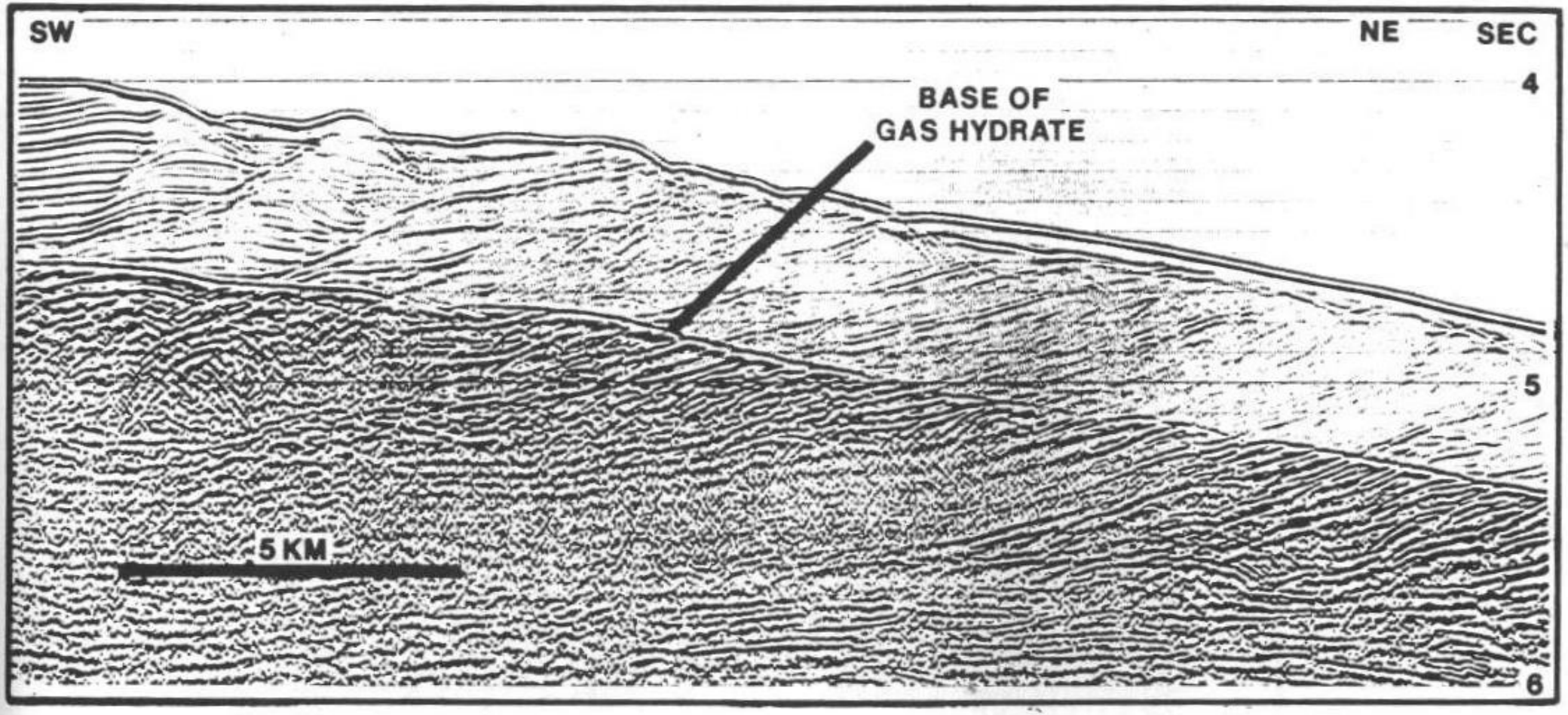

FIGURE 4.55 *Seismic section from the eastern flank of the Blake Outer Ridge. The reflection at the base of the gas hydrate follows the sea-floor bathymetry and crosscuts dipping reflections. The lower amplitude of reflections above the gas hydrate may be the result of reduced acoustic-impedance contrasts in the presence of the gas hydrate. Reprinted by permission of the AAPG from Shipley et al., 1979.*

Diagenetic Effects

The potential of diagenesis effects to produce reflections has already been described in connection with oil/water contacts. The diagenesis of fine-grained silica-rich sediments, also, may cause an acoustic-impedance boundary. Hein et al. (1978) showed that the dissolution and precipitation of diatom frustules (the silicous cell walls of microscopic single-celled plants) involved a change from opal-A to opal-CT. The change causes a marked porosity reduction, which results in increases in both density and velocity. These increases can produce a detectable acoustic-impedance contrast. Since the change from opal-A to opal-CT is dependent on burial depth, the resulting reflection tends to parallel the sea floor and is another type of BSR. Opal-CT eventually changes to quartz, and the associated diagenesis front may also form a reflection.

The opal-A to opal-CT diagenesis changes are depth dependent, they should, therefore, migrate gradually upward through the sequence with time and burial. Below the migrating front, diagenesis could account for the commonly observed reduced reflection amplitude and coherency often seen below BSRs. Hammond and Gaither (1983) show examples of BSRs from the Bering Sea Shelf. Potential interpretation pitfalls are possible where a BSR intersects other reflectors at an angle, opening the way for its incorrect interpretation as a sequence boundary or even a flat spot (fig. 4.56). In this case it may be extremely difficult to determine that the reflection comes from a BSR. The configuration could show the features associated with a gas accumulation, for example, a flat spot, polarity reversal and edge diffractions, etc.

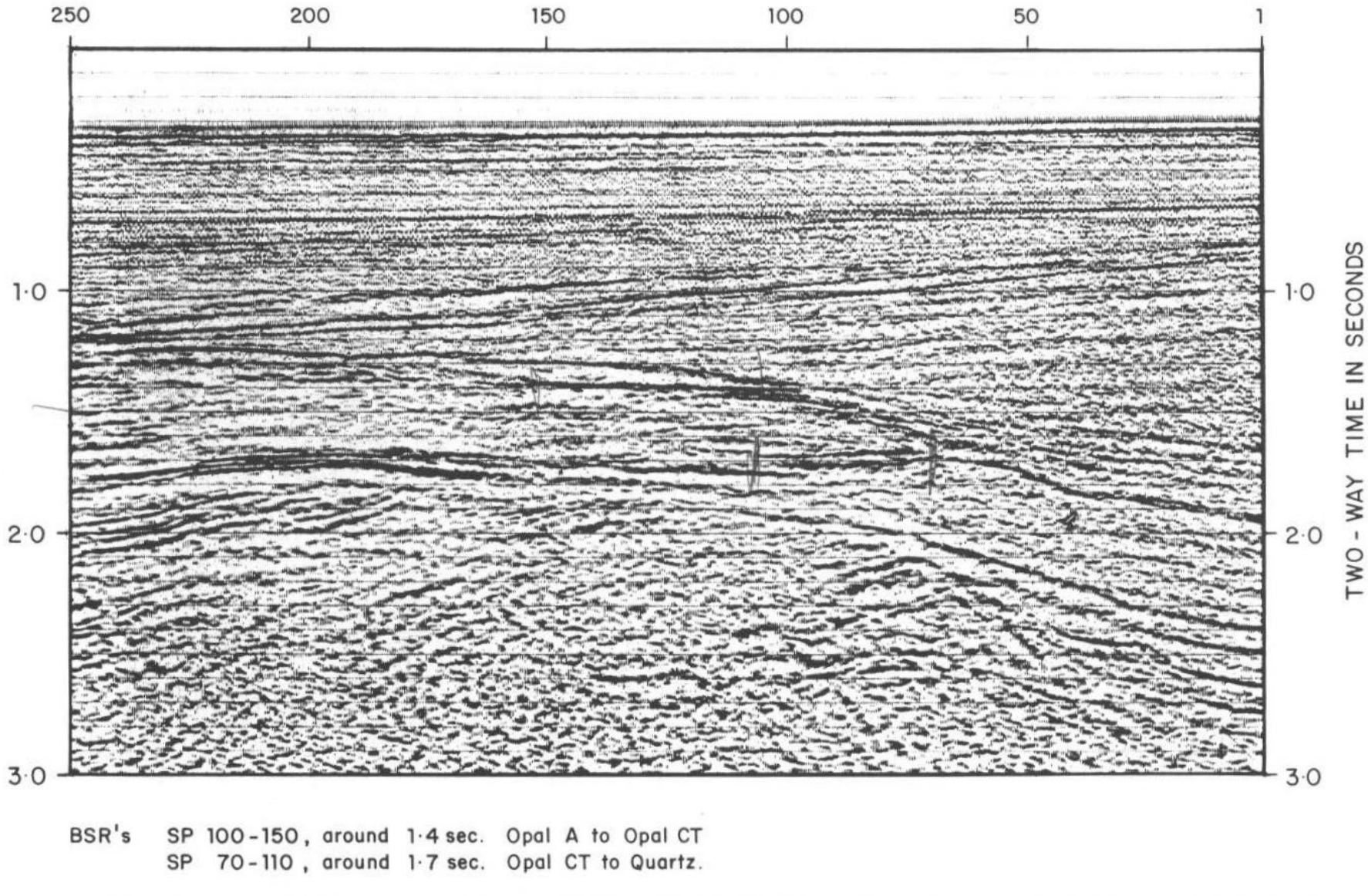

FIGURE 4.56 *Bottom-simulating reflections: Reflections from an opal-A to opal-CT diagenetic front around 1.45 s between shotpoints 100–150 and an opal-CT to quartz diagenetic front around 1.7 s between shotpoints 70–100. Courtesy Norsk Hydro.*

Chapter 5
Structural Feature